Reduced syngas-based chemical kinetics mechanisms for dual fuel engine combustion applications

Nearchos Stylianidis

A thesis submitted in partial fulfilment

Of the requirements of The University of Northumbria at Newcastle

For the degree of

Doctor of Philosophy

Research undertaken in the

School of Engineering and Environment

March 2019

Abstract

The interest in sustainable and environmental friendly fuels such as syngas and their use in dual fuel engine applications, has intensified the research for an accurate and reduced chemical kinetics mechanism. The chemical kinetics mechanism should be applicable to simulate not only multicomponent syngas combustion but also NOx formation and the co-oxidation between the primary fuel (premixed syngas) and the pilot injected diesel based fuel. For the diesel based fuel n-heptane was used as a surrogate due to the fact that it has similar physical and chemical characteristics with the diesel and identical rate of heat release (ROHR). Despite the development of various chemical kinetics mechanisms for the simulation of syngas combustion and n-heptane oxidation, a robust and reduced chemical kinetics mechanism that includes full syngas and NOx chemistry and n-heptane chemistry remains elusive. Therefore, this thesis aimed to develop a reduced and robust chemical kinetics mechanism for multicomponent syngas combustion, NOx formation and syngas/n-heptane co-oxidation.

This study is separated into three main sections: a) The development of a reduced syngas mechanism, b) development of a reduced syngas/NOx mechanism and c) development of a reduced n-heptane/syngas/NOx mechanism.

The first section is the construction of a robust reduced chemical kinetics mechanism for multicomponent syngas combustion. Important chemical reactions were investigated by using sensitivity analysis and their rate constants were updated. By using sensitivity analysis, it was shown that the reactivity of syngas mixtures is governed by H_2 and CO chemistry for H_2 concentrations lower than 50% vol and mostly by H_2 chemistry for H_2 concentrations higher than 50% vol. Reactions responsible for the decomposition of H_2O_2 and the formation of high reactive OH species, found to play a key role in the combustion process during high pressure conditions and therefore their rate constants were updated. The constructed mechanism was validated against experimental results and simulated data obtained by using other well-validated chemical kinetics mechanisms, in terms of ignition delay and LFS. Finally, the new mechanism was implemented in a multidimensional CFD simulation for the prediction of syngas combustion in a micro-pilot-ignited supercharged dual-fuel engine. Results from the CFD were compared against experiments. However, while mixtures with H_2 concentration > 50% vol used, the reactivity of the mixture increased due to the faster formation of OH and therefore some modification were adopted in the new mechanism in order to improve its accuracy. Modification such as the adaptation of new rate constants on important hydrogen

reactions and the removal of reactions with very low sensitivity factor. At the end, a two-part mechanism was constructed for low and high H_2 concentrations.

The second section of this thesis was the optimization of the reduced mechanism for low H_2 content proposed in Part 1, by updating the rate constants of important hydrogen reactions that were found to be very sensitive during high pressure conditions (10, 20 and 30 atm) and by incorporating a 12 reaction NOx pathway. The NOx sub-mechanism was selected after different NOx models available in the literature were tested and validated. The new reduced syngas/NOx mechanism was validated against experimental data as well as the simulated results by using other chemical kinetics mechanisms from the literature, in terms of LFS, ignition delay time, and NO concentration profiles, and showed very low error in all of the conditions. For LFS simulations the calculated absolute grand mean error for the developed mechanism was lower than 2%, for ignition delay times lower than 5% and for NOx formation profiles lower than 5%. Finally, similar to the first part of this study, the new mechanism was used in a multidimensional CFD simulation to predict the combustion of syngas in a micro-pilot-ignited supercharged dual-fuel engine.

The final section of this research was the construction of a reduced n-heptane/syngas/NOx mechanism for modelling n-heptane/syngas co-oxidation, syngas combustion and NOx formation in a micro pilot-ignited dual fuel engine. For the construction of the reduced chemical kinetics mechanism, a comprehensive mechanism for n-heptane oxidation was reduced by using necessity analysis and was coupled with the reduced syngas/NOx mechanism developed in Part 2. The reduced mechanism consists of 276 reactions and was validated against experimental measurements for different fuel types obtained from the literature and numerical results by using other well validated mechanisms in terms of ignition delay time, LFS and NO concentration profiles. Moreover, a multidimensional CFD analysis was conducted for the prediction of syngas combustion in a micro-pilot-ignited supercharged dual-fuel engine. The reduced mechanism simulates accurately the experimental in-cylinder pressure and ROHR for all conditions except from the cases where 100% hydrogen was used.

Preface

Publications from this PhD research

1) Stylianidis, N., Azimov, U., Maheri, A., Tomita, E. and Kawahara, N., 2017. Chemical kinetics and CFD analysis of supercharged micro-pilot ignited dual-fuel engine combustion of syngas. *Fuel*, *203*, pp.591-606.
2) Azimov, U., Stylianidis, N., Kawahara, N. and Tomita, E., 2017. Characterisation of DME-HCCI combustion cycles for formaldehyde and hydroxyl UV–vis absorption. *Fuel*, *210*, pp.578-591.
3) Stylianidis, N., Azimov, U., A chemical kinetics analysis of syngas combustion using a reduced chemical kinetic mechanism.1ST International Research Conference on Sustainable Energy, Engineering, Materials and Environment (SEEME), Newcastle upon Tyne, UK, 2017
4) Stylianidis, N., Azimov, U., Kawahara, N. and Tomita, E., 2017. *Chemical Kinetics and Computational Fluid-Dynamics Analysis of H 2/CO/CO 2/CH 4 Syngas Combustion and NOx Formation in a Micro-Pilot-Ignited Supercharged Dual Fuel Engine* (No. 2017-24-0027). SAE Technical Paper.
5) Stylianidis, N., Azimov, U., Reduced chemical kinetics mechanism for syngas combustion and NOx formation. Internal Combustion Engines, Institution of Mechanical Engineers, Birmingham. UK. 2017.

Acknowledgments

First of all, I want to thank my supervisor Dr. Ulugbek Azimov who was abundantly helpful during the last three years. He has been patient with me since the first day of this PhD and has offered me invaluable support and assistance.

I would also like to thank my family for their unconditional support, and for their understanding throughout the duration of my studies, first at the University of Leicester for my Bachelor degree and then at the University of Northumbria for my Masters degree and then for this PhD degree. They always believed in me, even when I did not believe in myself.

Finally, yet importantly, I would like to thank all my friends that stood by my side throughout the three year period of this PhD. Without their support, my dissertation would not have been possible and complete.

Abbreviations

ATDC	*After Top Dead Centre*
BMG	*Biomass Gas*
BP	*British Petroleum*
BTDC	*Before Top Dead Centre*
CAD	*Computer Aided Design*
CFD	*Computational Fluid Dynamics*
CI	*Compression Ignition*
COG	*Coke Oven Gas*
CPU	*Central Processing Unit*
CSP	*Computational Singular Perturbation*
CV	*Constant Volume*
DARS	*Digital Analysis of Reactive Systems*
DI	*Direct Injection*
DRG	*Direct Relation Graph*
EBU	*Eddy Break Up Model*
EGR	*Exhaust Gas Recirculation*
EU	*European Union*
HCCI	*Homogeneous Charge Compression Ignition*
GRI Mech. 3.0	*Gas Research Institute Mechanism 3.0*
HV	*Heating Value*
ICE	*Internal Combustion Engine*
ILDM	*Intrinsic Low Dimensional Manifolds*
IVC	*Intake Valve Closure*
LFS	*Laminar Flame Speed*
LLNL	*Lawrence Livermore National Laboratory*
LOI	*Level Of Importance*
LTC	*Low Temperature Coefficient*
NASA	*National Aeronautics and Space Administration*
NIST	*National Institute of Standards and Technology*
NTC	*Negative Temperature Coefficient*
PISO	*Pressure-implicit with Splitting of Operators*
PIVC	*Pressure at Valve Closure*
PREMIER	*Premixed Mixture Ignition in the End Gas Region*
RCCI	*Reactivity Controlled Compression Ignition*
RCM	*Rapid Compression Machine*
ROHR	*Rate Of Heat Release*
SI	*Spark Ignition*
TDC	*Top Dead Centre*
TIVC	*Temperature at Intake Valve Closure*
UK	*United Kingdom*
UNN-1	*University of Northumbria at Newcastle One*
UNN-2	*University of Northumbria at Newcastle Two (Final mechanism)*
USA	*United Stated of America*
WWII	*World War two*
0D	*Zero Dimensional*
1D	*One Dimensional*
3D	*Three Dimensional*

List of Symbols

A	*Pre-exponential factor*
A_{ebu}	*Exponential factor of EBU model*
A_h	*Exponential factors for high pressure limit*
A_l	*Exponential factors for low pressure limit*
A_{ar}	*Arbitrary chosen parameter*
B_{ebu}	*Temperature coefficient of EBU model*
B_i	*Necessity coefficient*
B_{R1} , B_{R2}	*Landau-Teller constant*
CA	*Crank angle*
C_{bI}	*Droplets empirical coefficient for bag break up mode*
c_i	*Concentration of the species*
$c\,_{ij}^{o}$	*Flow rate of atom during the consumption of species*
C_{k1}, C_{k2}, C_{k3} *and* C_{k4}	*Turbulent coefficients.*
$Cs1$	*Droplet empirical coefficient for striping break up mode*
c_{sp}	*Specific heat of each species*
c_p	*Heat capacity at constant pressure*
D_b	*stable droplet diameter*
D_d	*Instantaneous droplet diameter*
D_{LJ}	*Lennard-Jones collision diameter*
D_{im}	*Molecular diffusivity of species*
D_i^T	*Thermal diffusion coefficient*
E_h	*Activation energy of the reaction at high pressures*
E_l	*Activation energy of the reaction at low pressures*
E	*Activation energy of the reaction*
F	*Rate of deformation*
$F_{i,j}$	*Diffusion flux component*
$F_{i,j}^{o}$	*The net flow rate for each species and atom*
f_{ij}^{o}	*Flow rate of the atom during the formation of species*
f_r	*Radiation factor (the fraction of volume between the high temperature burned gas and the lower temperature unburned gas)*
G	*Number of datasets considered for a combustion parameter*
g	Characteristic coefficient of the SRI form reaction
$H_{Enthalpy}$	*Final enthalpy of each species*
h_i	*Specific enthalpy of species i*
h_k^0	*Enthalpy during the standard state*
i	*Current species*
I_i	*Redundancy index*
$\bar{J}_k$	*Mass diffusive flux vector of the* k^{th} *species*
j_i	*Diffusion flux*
k	*Chemical reaction*
k_{ebu}	*EBU rate coefficient*

k_{eR}	*Equilibrium rate constant*
k_{fR}	*Forward rate constant*
k_h	*High pressure limit reaction rate*
k_l	*Low pressure limit reaction rate*
k_{rR}	*Backward rate constant*
$\|M\|$	*Molar concentration of the mixture*
m_{fuel}	*Mass of the fuel*
$m_{fuel\,st}$	*Stoichiometric mass of the fuel*
m_{ox}	*Mass of the oxidizer*
$m_{ox\,st}$	*Stoichiometric mass of the oxidizer*
n	*Temperature exponent*
n_F	*Temperature exponent of the fuel*
n_j^o	*Number of atoms*
N_i	*Necessity of species*
N_o	*Number of atoms*
n_P	*Temperature exponent of the product*
N_R	*Number of reactions*
n_{Rk}' *and* n_{Rk}''	*Stoichiometric coefficients*
N_s	*Number of species*
N_d	*Number of datasets considered in a simulation*
N_p	*Number of data points for a case*
o	*Atom*
P	*Pressure (zero and one dimensional simulation : bar, three dimensional simulations : kPa)*
P_{pl}	*Polarizability*
P^r	*Reduced pressure*
Q_i	*Necessity of the species*
q_{rad}	*Radiative heat transfer*
R	*Gas constant*
Re_d	*Reynolds number of the droplet*
R_F	*Consumption rate of the fuel*
r_k	*Reaction k rate*
$[R_k]$	*Species concentration*
$S_{A_{ar},i}{}^S$	*Species sensitivity*
$S_{Entropy}$	*Final entropy of each species*
s_i	*Momentum source component*
S_i	*Production rate of species*
S_{ij}	*Mean velocity strain rate*
s_k^0	*Entropy during the standard state*
SL_{MAX}	*Maximum laminar flame speed*
s_m	*Mass source component*
s_O	*Initial fuel to air ratio*
s_P	*Product to fuel ratio*

t	*Characteristic time*
T_0	*Temperature of the surrounding species*
T	*Temperature*
u	*Gas velocity*
$\overline{u_f}$	*Fluid velocity factor*
u_i	*Diffusion velocity*
u_{iabs}	*Absolute velocity of the fluid*
$\bar{u}$	*Fluid velocity vector*
$u'_{i,k}$	*Stoichiometric coefficient of the reactants*
$u''_{j,k}$	*Products stoichiometric coefficient*
v'_{Rk} *and* v_{Rk}''	*Exponential factors of the concentration*
We	*Weber number*
W_i	*Molecular weight*
W_k	*Molecular weight of species k*
x	*Distance from the surface of the burner*
x_i	*Cartesian coordinate*
$Y_{exp.ij}$	*Value of the experimental results of the jth data point in the ith set of data*
Y_F	*Mass fraction of the fuel*
Y_i	*Mass fraction of species i*
Y_k	*Mass fraction of species k*
Y_N	*Mass fraction of the Nth species*
Y_O	*Initial mass fraction*
Y_P	*Mass fraction of the product*
$Y_{sim,ij}$	*Value of the simulated results of the jth data point in ith set of data*
z	*Characteristic coefficient of the pressure dependent reactions*
Z_{rot}	*Rotational relaxation collision number*
	Greek Symbols
α	*Planck's constant*
α_{kR}	*Third body efficiency of species k*
β_h	*Temperature exponent factor at high pressure*
β_l	*Temperature exponent factor at low pressure*
$\delta_1..\delta_7$	*Thermodynamic coefficients of each species included in the mechanism*
Δ	*Turbulence normal forces*
Δ_B	*Turbulence buoyancy forces*
$\Delta n^o_{k_f}$	*Total number of atoms*
Δ_{NL}	*Turbulence non-linear forces*
$\overline{E_\iota}$	*Absolute error of each individual case*
$\bar{\bar{\varepsilon}}$	*Absolute overall mean error*
ε	*Turbulence dissipation rate*

$\Theta_{inj.}$	*Injection angle*
λ	*Thermal conductivity*
μ	*dipole moment*
μ_i	*Turbulence viscosity*
ρ	*Density*
ρ_k	*Density of the kth species*
σ	*Stefan Boltzmann constant*
σ_k	*Turbulent Prandtl number*
σ_d	*Surface tension coefficient*
τ_b	*Break-up process time scale*
τ_{ij}	*Stress tensor component*
ϕ	*Equivalence ratio*
$\bar{\bar{\Psi}}$	*Absolute grand mean error*
$\psi_{A_{ar}}$	*Vectors of unknowns*
ω_i	*Production rate of species i*
ω_{k_f}	*Reaction k rate*
ω_{kmolar}	*Molar rate of production of the kth species*

Table of Contents

Abstract 1
Preface 3
Acknowledgments 4
Abbreviations 5
List of Symbols 6
Table of Contents 10
List of Figures 13
List of Tables 21
Chapter 1: Introduction 22
1.1 Background 22
1.2 Aim of this research 25
1.3 Contribution to knowledge 26
1.4 Thesis structure 27
Chapter 2: Literature review 28
2.1 Technological development of gaseous fuels 28
2.2 Syngas fuels 30
2.2.1 Gasification process 30
2.3 Syngas in internal combustion engines 32
2.3.1 Syngas in dual-fuel IC engines 33
2.4 Combustion chemistry of syngas 36
2.4.1 Chemical Kinetics Mechanisms 39
2.5 Mechanism reduction 49
2.6 Summary 54
Chapter 3: Numerical models and analytical methodologies used for modelling in-cylinder combustion 56
3.1 0D and 1D simulations 57
3.1.1 Ignition delay time 57
3.1.2 LFS 58
3.1.3 Sensitivity analysis 60
3.1.4 Flow analysis 61
3.1.5 Necessity analysis 62
3.1.6 NOx formation 63
3.2 Multidimensional CFD simulations 67

3.2.1 Experimental set-up 68
3.2.2 Reacting flows governing equations 69
3.2.3 Chemical kinetics 71
3.2.4 Turbulence modelling 76
3.2.5 Spray model 78
3.2.6 Engine cylinder geometry 81
3.3 Error analysis 83
3.4 Fuel mixtures used in this study 84
Chapter 4: Development of a reduced chemical kinetics mechanism for syngas combustion in a micro-pilot ignited dual-fuel engine 87
4.1 Development of the syngas kinetics mechanism 87
4.1.1 Sensitivity analysis 89
4.1.2 Ignition delay time 97
4.1.3 Flame speed 102
4.2 Results and discussion 107
4.2.1 Mechanism validation for CFD combustion analysis 107
4.2.2 Chemical kinetics mechanism for syngas with high H_2 content 110
4.2.3 In-cylinder 3D combustion analysis 117
4.3 Summary 121
Chapter 5: Development of an updated chemical kinetics mechanism for syngas combustion and NOx formation in a micro pilot ignited dual fuel engine. 123
5.1.1 Selection of the NOx sub-mechanism 123
5.1 Chemical kinetics mechanism 127
5.1.2 Chemical detail analysis during syngas combustion 127
5.2 Mechanism validation and results discussion 136
5.2.1 LFS 136
5.2.2 Ignition delay time 139
5.2.3 NOx formation profiles 141
5.2.4 Absolute Grand mean error analysis 145
5.2.5 Multidimensional CFD analysis 147
5.3 Summary 151
Chapter 6: Development of a reduced n-heptane/syngas/NOx mechanism for syngas combustion, n-heptane/syngas co-oxidation and NOx formation in a micro-pilot ignited dual-fuel engine 153
6.1 N-heptane mechanism 154
6.2 Reduced N-heptane/syngas/NOx mechanism development 160
6.2.1 Reduction 160

6.2.3 Coupling 165
6.3 Validation 185
6.3.1 N-heptane oxidation 185
6.3.2. Syngas combustion 187
6.3.3 NOx formation 200
6.3.4 N-heptane/syngas co-oxidation 203
6.3.5 In-cylinder 3D combustion analysis 210
6.4 Summary 218
Chapter 7: Conclusions and future work 220
7.1 Conclusions 220
7.2 Future work 223
References 225
Appendix A 238
Appendix B 248
Appendix C 255

List of Figures

Figure Caption	Page
Figure 2-1 Historical and projected primary energy consumption in EU. Renewables include biomass and biofuels and gas refer to Natural Gas [30].	29
Figure 2-2 Gasification process flow chart [40].	30
Figure 2-3 A conceptual diagram of a pilot-ignited dual fuel engine	35
Figure 2-4 Characteristic stages of the rate of heat release for combustion in a dual fuel engine.	35
Figure 2-5 N-heptane oxidation diagram [28,100]	47
Figure 2-6 Mechanism Reduction procedure [110]	53
Figure 3-1 Flow chart of the modelling procedure.	56
Figure 3-2 Schematic diagram of the experimental set-up [78]	69
Figure 3-3 Full cylinder (A) and 90o sector cylinder (B) meshes used during the CFD analysis.	82
Figure 3-4 Comparison between the monitoring experimental and simulated cylinder pressures.	82
Figure 4-1 The 13 most sensitive reactions for syngas Fuel 24 Type 1 at 1000K and pressures 10, 30 and 50 bar	90
Figure 4-2 Comparison of ignition delay time for Fuel 24 syngas Types 1-4 obtained with new mechanism with other mechanisms at temperatures 800–1053 K, pressure 2.25 bar and equivalence ratio = 0.63	98-99
Figure 4-3 Comparison of ignition delay time for Fuel 24 syngas Type 1 obtained with new mechanism with other mechanisms at temperatures 800-1053K, pressures 20, 40, 80 bars and equivalence ratio 0.63.	99-100
Figure 4-4 Comparison of ignition delay time for Fuel 24 syngas type 2 obtained with new mechanism with other mechanisms at temperatures 800-1053K, pressures 20, 40, 80 bars and equivalence ratio 0.83	100-101
Figure 4-5 Effect of CO concentration on ignition delay times of syngas mixtures compared with Keromnes et al. [21] mechanism.	101
Figure 4-6 LFS results obtained with new mechanism for a) syngas Fuel 24 Types 1 b)syngas Fuel 34 Type 2 c) syngas Fuel 24 Type 3 and d) syngas Fuel 24 Type 4 at pressures 2.25 Bar and temperature 450 K.	103-104

Figure 4-7 LFS of H_2/CO/CO_2 -35:35:30 fuel mixture at a) pressure 1.01 Bar and temperature 303 K, b) pressure 1.01 Bar and temperature 373 K and c) pressure 3.04 Bar and temperature 373 K. 104-105

Figure 4-8 Calculated LFS of obtained with new mechanism and compared with different kinetic models for a) CH_4 10% / H_2 90% , b)) CH_4 30% / H_2 70% and c)) CH_4 50% / H_2 50% at pressure 1.01 Bar and temperature 298K 105-106

Figure 4-9 Effect of pressure on the LFS obtained with new mechanism for syngas Fuel 24 Type 1 at pressure20 Bar and temperature 450 K, b) pressure 40 Bar and temperature 450 K and c) pressure 80 Bar and temperature 450 K. 106-107

Figure 4-10 Comparison of CFD in-cylinder pressure obtained using the new mechanism with the experimental results from Azimov et al [78] and the simulated results using different chemical kinetics mechanisms for Fuel 24 syngas Types 1-3, equivalence ratio 0.52,0.48 and 0.6 and different timings of fuel micro-pilot injection. 108-109

Figure 4-11 Comparison of CFD in-cylinder pressure obtained using the new mechanism with the experimental measurements obtained from Azimov et al [78], for Fuel 24 syngas Type 4 equivalence ratio 0.6 and Θinj.=3º BTDC 110

Figure 4-12 The most sensitive reaction for modified syngas mechanism at equivalence ratio 0.63, temperature 1000K and pressures 10, 30 and 50 bar. 111

Figure 4-13 Comparison of reaction flows of carbon atoms for syngas Fuel 24 Type 1(H_2 13.7/CO 22.3/ CO_2 16. 8/ CH_4 1.9/ N_2 45 %vol.) and Type 4 (H_2 56.8/CO 5.9/ CO_2 2.2/ CH_4 29.5/ N_2 5.6 %vol.)at 30 bar. Flow values are given in mol/(cm^3 sec) 113

Figure 4-14 Comparison of reaction flows of hydrogen atoms for syngas at temperature 1000 K and pressures 10, 30 and 50 bar. (A) Fuel 24 Type 1(H_2 13.7/CO 22.3/ CO_2 16. 8/ CH_4 1.9/ N_2 45 %vol.), (B) Fuel 24 Type 4 (H_2 56.8/CO 5.9/ CO_2 2.2/ CH_4 29.5/ N_2 5.6 %vol.). Fluxes below 1% of maximum flow have been filtered. Flow values are given in mol/(cm^3 sec). 114

Figure 4-15 Data obtained with modified mechanism for syngas Fuel 24 Type 4 with high H_2 and compared with other kinetic mechanisms. (a) LFS calculated at temperature 450K, pressure 2.25 bar and equivalence ratio 0.4-1.0, and (b) Ignition delay calculated at temperatures 800-1052K, pressure 2.25 bar and equivalence ratio 0.6. 115-116

Figure 4-16 Effect of different reaction rates of H_2O_2 +H=H_2 + HO_2 reaction on 3D CFD in-cylinder pressure during micro-pilot ignited syngas combustion. 116

Figure 4-17 Comparison of experimental and simulated in-cylinder pressures and heat release rates of dual-fuel micro-pilot ignited syngas combustion. Computed 118-120

using 3D-CFD with new kinetic mechanism. (a–b) Fuel 24 Type 1, (c–d) Fuel 24 Type 2, (e–f) Fuel 24 Type 3 and (g–h) Fuel 24 Type 4. PIVC = 225 kPa, TIVC = 330 K

Figure 4-18 Sequential images of dual-fuel micro-pilot ignited syngas combustion and temperature distribution with new kinetics mechanisms for Fuel 24 Type 3, eq. ratio -0.6, Θinj-14ºBTDC, PIVC = 225 - kPa, TIVC = 330 K. 120

Figure 4-19 Sequential images of dual-fuel micro-pilot ignited syngas combustion and OH distribution with new kinetics mechanism for Fuel 24 Type 3, eq. ratio -0.6, Θinj-14ºBTDC, PIVC = 225 - kPa, TIVC = 330 K. . 121

Figure 5-1 Comparison of the calculated NO profiles obtained by using the three NOx sub-models and the experimental results from [177] 126

Figure 5-2 Reaction flows analysis of hydrogen atoms for syngas Fuel mixture 14 Type 1, at temperature 300K and pressures a) 4, b) 10 and c) 16 bar. Fluxes below 1% of maximum flow have been filtered. Flow values are given in mol/(cm3 sec) 128-129

Figure 5-3 The 13 most sensitive reactions from Syngas/NOx mechanism for syngas Fuel 24 Type 1 at 1000K and pressures 10, 30 and 50 bar 130

Figure 5-4 Comparison of different reaction rates for a) R20 and b) R30 133-134

Figure 5-5 Species Sensitivity analysis towards NOx formation using the reduced proposed mechanism in a low calorific syngas-air diffusion flame highlighting the most important species affecting NO formation for Fuel 14 at 0.8 equivalence ratio, preheat temperature 300 K and pressures 4,10 and 16 bars 135

Figure 5-6 Species Sensitivity analysis towards NOx formation using GRI Mech. 3.0 in a low calorific syngas-air diffusion flame highlighting the most important species affecting NO formation Fuel 14 at 0.8 equivalence ratio, preheat temperature 300 K and pressures 4,10 and 16 bars 135

Figure 5-7 Comparison between the measured and calculated LFSs for a) Fuel 8 Type 1, b) Fuel 8 Type 2 and c) Fuel 8 Type 3. 137

Figure 5-8 Comparison between the measured and calculated LFSs for a) Fuel 9 Type 1, b) Fuel 9 Type 2 and c) Fuel 9 Type 3. 138-139

Figure 5-9 Comparison between the measured and calculated ignition delay time for $H_2/CO/O_2/CH_4$/AR fuel mixture at a)P=1.6 bar , b) P=12 bar and c) P=32 bar 140-141

Figure 5-10 Comparison of the calculated NO profiles by using the chemical kinetics mechanisms tested and the experimental measurements obtained from [176] at a)P=1 bar, b)3.05 bar and c) 9.15 bar. 142-143

Figure 5-11 Comparison of the calculated NO profiles by using the chemical kinetics mechanisms tested and the experimental measurements obtained from [13] at a) eq. ratio 0.72, b) eq. ratio 1.03 and c) eq. ratio 1.34. 144-145

Figure 5-12 Comparison of the calculated absolute grand mean error for LFS simulations 146

Figure 5-13 Comparison of the calculated absolute grand mean error for ignition delay time simulations 146

Figure 5-14 Comparison of the calculated absolute grand mean error for NOx formation simulations 147

Figure 5-15 Comparison of experimental and simulated in-cylinder pressure and heat release rate of dual-fuel micro-pilot ignited syngas combustion for Fuel 24 Type 1 at a) equivalence ratio 0.63 and Θ injection 9º BTDC and b) eq. ratio 0.68 and Θ injection 7ºBTDC 149

Figure 5-16 Comparison of experimental and simulated in-cylinder pressure and heat release rate of dual-fuel micro-pilot ignited syngas combustion for Fuel 24 Type 2 at equivalence ratio 0.4 and Θ injection 18º BTDC. 149

Figure 5-17 Comparison of experimental and simulated in-cylinder pressure and heat release rate of dual-fuel micro-pilot ignited syngas combustion for Fuel 24 Type 3 at equivalence ratio 0.6 and Θ injection 14º BTDC 150

Figure 5- 18 Sequential images of dual-fuel micro-pilot ignited syngas combustion with new kinetics mechanisms. Fuel 24 Type 1 eq. ratio 0.63, Θ inj.= 9º BTDC, PIVC = 225 - kPa, TIVC = 330K. 150

Figure 5-19 Sequential images of NO concentration during dual-fuel micro-pilot ignited syngas combustion by using the new kinetics mechanisms. Fuel 24 Type 1 eq. ratio 0.63, Θ inj.= 9º BTDC, PIVC = 225 - kPa, TIVC = 330 K 151

Figure 6-1 Comparison of the simulated ignition delay time by using different n-heptane mechanisms and the experimental results obtained from [179]. 155-156

Figure 6-2 Comparison of the simulated ignition delay time by using different n-heptane mechanisms and the experimental results obtained from [180-183]. 156-157

Figure 6-3 Comparison of the simulated LFS by using different n-heptane mechanisms and the experimental results obtained from [184]. 158-159

Figure 6-4 Comparison of the simulated LFS by using different n-heptane mechanisms and the experimental results obtained from [185]. 159-160

Figure 6-5 Flow chart of mechanism reduction method used in Chapter 6 161

Figure 6-6 History of reduction ratio and necessity factor using necessity analysis method 162

Figure 6-7 Comparison of the calculated ignition delay times for n-heptane/air mixture. Fuel 19 Table 3-3, using the original n-heptane mechanism from Creck modelling group [109], Generation 0, and the constructed skeletal mechanisms, Generations 10,15,22 and 24. 164

Figure 6-8 Comparison of the calculated ignition delay times for H_2/CO/CO_2/CH_4/H_2O/O_2/AR mixture. Fuel 4 Table 3-3, using the original n-heptane mechanism from Creck modelling group [109], Generation 0, and the constructed skeletal mechanisms, Gen10,15,22 and 24. 165

Figure 6-9 Comparison of ignition delay predictions for n-heptane/air mixture (Fuel 19) using a) the original Creck mechanism [109] (Generation 0) b) Generation 22 skeletal mechanism and c) UNN-1 mechanism. 166

Figure 6-10 Comparison of ignition delay predictions for 0.29659% H_2/ 0.29659% CO/ 0.15748% CO_2/ 0.08924% CH_4/ 0.20997% H_2O/ 0.95013% O_2/ 98% AR mixture using a) the original Creck mechanism [109] (Generation 0) b) Generation 22 skeletal mechanism and c) UNN-1 mechanism. 167

Figure 6-11 Ignition delay time sensitivity to major hydrogen based reactions a) ignition delay time of n-heptane/air mixture Fuel 19 b) ignition delay time of syngas mixture Fuel 4. Circles show UNN-1 mechanism, squares show A X 10 and triangles show A X 0.1. 171

Figure 6-12 Ignition delay time sensitivity to major methane based reactions a) ignition delay time of n-heptane/air mixture Fuel 19 b) ignition delay time of syngas mixture Fuel 4. Circles show UNN-1 mechanism, squares show A X 10 and triangles show A X 0.1 172

Figure 6-13 Ignition delay time sensitivity to major n-heptane based reactions a) ignition delay time of n-heptane/air mixture Fuel 19 b) ignition delay time of syngas mixture Fuel 4. Circles show UNN-1 mechanism, squares show A X 10 and triangles show A X 0.1. 173

Figure 6-14 Comparison of the calculated ignition delay time by using UNN-2 mechanism, n-heptane Creck reduced mechanism and the experimental measurements obtained from [186-188] for n-heptane/air mixtures at a)13.5 bar, b)20 bar and c) 55 bar. 186

Figure 6-15 Comparison of the LFS by using UNN-2 mechanism, n-heptane Creck reduced mechanism and GRI Mech. 3.0 for Fuel 24 Type 1 at a) P=20 bar and b) P=40 bar. 188

Figure 6-16 Comparison of the LFS by using UNN-2 mechanism, n-heptane Creck reduced mechanism and GRI Mech. 3.0 for Fuel 24 Type 5 at a) P=20 bar and b) P=40 bar 188-189

Figure 6-17 Comparison of the calculated LFS by using UNN-2 mechanism, GRI Mech. 3.0 and the experimental measurements obtained from [175] for a) H_2/CH_4:20%/80% b) H_2/CH_4:50%/50% and c) H_2/CH_4:90%/10%, Fuel 10 Table 3-3. 190

Figure 6-18 Comparison of the calculated LFS by using UNN-2 mechanism, GRI Mech. 3.0 and the experimental measurements obtained from [173], Fuel 8 for a) $H_2/CO/CH_4$: 47.5%/47.5%/5% b) $H_2/CO/CH_4$: 40%/40%/20% and c) $H_2/CO/CH_4$: 30%/30%/40%. 191-192

Figure 6-19 Comparison of the ignition delay time obtained by using UNN-2 mechanism, n-heptane Creck reduced mechanism [109] and GRI Mech. 3.0 [26] for Fuel 24 Type 1, at a) Eq. ratio 0.2 and P=20 bar, b) Eq. ratio 0.2 and P= 40 bar, c) eq. ratio 0.4 and P= 20 bar and d) Eq. ratio 0.4 and P =40 bar. 193-194

Figure 6-20 Comparison of the ignition delay time obtained by using UNN-2 mechanism, n-heptane Creck reduced mechanism [109] and GRI Mech. 3.0 [26] for Fuel 24 Type 5, at a) Eq. ratio 0.2 and P=20 bar, b) Eq. ratio 0.2 and P= 40 bar, c) eq. ratio 0.4 and P= 20 bar and d) Eq. ratio 0.4 and P =40 bar. 194-195

Figure 6-21 Comparison of the calculated ignition delay time by using UNN-2 mechanism, GRI Mech. 3.0 [26] and the experimental measurements obtained from [11] for Fuel 3 Type 3 H_2/CH_4:80%/20% at a)5 atm b)10 atm and c)20 atm. 196

Figure 6-22 Comparison of the calculated ignition delay time by using UNN-2 mechanism, GRI Mech. 3.0 [26] and the experimental measurements obtained from [11] for Fuel 3 Type 4 H_2/CH_4:20%/80% at a)5 bar b)10 bar and c)20 bar. 197

Figure 6-23 Comparison of the calculated ignition delay time by using UNN-2 mechanism, GRI Mech. 3.0 [26] and the experimental measurements obtained from [171] for $H_2/CO/CO_2$:33%/67/0% ,Fuel 5 Type 1, at a) eq. ratio 0.3 b) eq. ratio 1.0 and c) eq. ratio 1.5. 198-199

Figure 6-24 Comparison of the calculated ignition delay time by using UNN-2 mechanism, GRI Mech. 3.0 [26] and the experimental measurements obtained 199-200

from [171] for H_2/CO/CO_2:35%/35%/30% ,Fuel 5 Type 2, at a) eq. ratio 0.3 b) eq. ratio 1.0 and c) eq. ratio 1.5.

Figure 6-25 Comparison of the simulated NO concentration profiles by using UNN-2 mechanism, GRI Mech. 3.0 [26] and the experimental measurements obtained from [13] for Fuel 13 Table 3-3, at pressure 1 atm, temperature 300 K and equivalence ratios a) 0.71 b) 1.03 and c) 1.34. 201-202

Figure 6-26 Comparison of the simulated NO concentration profiles by using UNN-2 mechanism, GRI Mech. 3.0 [26] and the experimental measurements obtained from [177] for a) Fuel 13 Type1, b)Fuel 13 Type 2 and c) Fuel 13 Type 3(see Table 3-3) at pressure 1 .01 bar, temperature 300 K and equivalence ratio 0.71 202-203

Figure 6-27 Comparison of the simulated ignition delay times by using UNN-2 mechanism, Creck reduced mechanism [109] and Chalmers mechanism [251] for Fuel 22 Type 1 H_2/C_7H_{16}:20%/80% at a) P= 55 bar and eq. ratio 1.0 b)P=30 bar and equivalence ratio 2 and c) P=55 bar and equivalence ratio 2. 204-205

Figure 6-28 Comparison of the simulated ignition delay times by using UNN-2 mechanism, Creck reduced mechanism [109] and Chalmers mechanism [251] for Fuel 22 Type 2 H_2/C_7H_{16}:80%/20% at a) P= 55 bar and eq. ratio 1.0 b)P=30 bar and equivalence ratio 2 and c) P=55 bar and equivalence ratio 2. 205-206

Figure 6-29 Comparison of the simulated ignition delay times by using UNN-2 mechanism, Creck reduced mechanism [109] and Chalmers mechanism [251] for Fuel 23 Type 1, CH_4/C_7H_{16}:20%/80% ,at a) P= 55 bar and eq. ratio 0.5 b) P=30 bar and equivalence ratio 1 and c) P=55 bar and equivalence ratio 1. 207

Figure 6-30 Comparison of the simulated ignition delay times by using UNN-2 mechanism, Creck reduced mechanism [109] and Chalmers mechanism [251] for Fuel 23 Type 2, CH_4/C_7H_{16}:80%/20% at a) P= 55 bar and eq. ratio 0.5 b) P=30 bar and equivalence ratio 1 and c) P=55 bar and equivalence ratio 1. 208

Figure 6-31Comparison of the simulated ignition delay times by using UNN-2 mechanism, Creck reduced mechanism [109] and Chalmers mechanism [251] for Fuel 23 Type 3, CH_4/C_7H_{16}:95%/5%, at a) P= 55 bar and eq. ratio 0.5 b) P=30 bar and equivalence ratio 1 and c) P=55 bar and equivalence ratio 1. 209

Figure 6-32 Comparison of experimental and simulated in-cylinder pressure and heat release rate of dual-fuel micro-pilot ignited syngas combustion for Fuel 24 Type 1, Table 3-3 211-212

Figure 6-33 Comparison of experimental and simulated in-cylinder pressure and heat release rate of dual-fuel micro-pilot ignited syngas combustion for Fuel 24 Type 2, Table 3-3 212

Figure 6-34 Comparison of experimental and simulated in-cylinder pressure and heat release rate of dual-fuel micro-pilot ignited syngas combustion for Fuel 24 Type 3, Table 3-3. 213

Figure 6-35 Comparison of experimental and simulated in-cylinder pressure and heat release rate of dual-fuel micro-pilot ignited syngas combustion for Fuel 24 Type 5, Table 3-3 213-214

Figure 6-36 Comparison of experimental and simulated in-cylinder pressure and heat release rate of dual-fuel micro-pilot ignited syngas combustion for Fuel 24 Type 6, Table 3-3. 214

Figure 6-37 Comparison of experimental and simulated in-cylinder pressure and heat release rate of dual-fuel micro-pilot ignited syngas combustion for Fuel 24 Type 7, Table 3-3. 215

Figure 6-38 Comparison of the simulated ignition delay times by using UNN-2 mechanism, GRI Mech. 3.0 [26], O Conaire mechanism [195] and Li mechanism [232] for Fuel 24 Type 7 at a) P= 20 bar and eq. ratio 0.2 and b)P=40 bar and equivalence ratio 0.2. 215-216

Figure 6-39 Comparison of the simulated ignition delay times by using UNN-2 mechanism, GRI Mech. 3.0 [26] , O Conaire mechanism [195] and Li mechanism [232] for Fuel 24 Type 7 at a) P= 20 bar and eq. ratio 0.4 and b)P=40 bar and equivalence ratio 0.4. 216

Figure 6-40 Comparison of the simulated LFS by using UNN-2 mechanism, GRI Mech. 3.0 [26], O Conaire mechanism [195] and Li mechanism [232] for Fuel 24 Type 7 at a) P= 20 bar and T=450 K and b)P=40 bar and T= 450 K 217

Figure 6-41 Sequential images of dual-fuel micro-pilot ignited syngas combustion with new kinetics mechanism. Fuel 24 Type 3 eq. ratio 0.8, Θinj = 8º BTDC 218

Figure 6-42 Sequential images of dual-fuel micro-pilot ignited syngas combustion with new kinetics mechanism. Fuel 24 Type 6 eq. ratio 0.6, Θinj 17.5º BTDC. 218

List of Tables

Table Caption	Page
Table 1-1 Effect of biomass type	31
Table 2-2 Effect of gasifying agent	32
Table 2-3 Different Detail Mechanisms that were used in this thesis	51
Table 3-1 Engine specifications	68
Table 3-2 Coefficients of the Standard high Reynolds $k-\varepsilon$ model	78
Table 3-3 Fuel mixtures used in this study	85
Table 4-1 Reduced syngas mechanism constructed in Chapter 4 (A units cal-cm-sec-K, E units cal/mol).	88
Table 4- 2 Comparison of the CPU time and the number of reactions of the mechanism developed in Chapter 4 with other well-validated mechanisms	109
Table 4-3 Reaction rate constants for reaction $H_2O_2+H=H_2+HO_2$ proposed by different authors (A units cal-cm-sec-K, E units cal/mol).	116
Table 5-1 Reduced syngas/NOx mechanism constructed in Chapter 5 (A units cal-cm-sec-K, E units cal/mol).	132
Table 5-2 Comparison of the experimental and simulated maximum in cylinder pressure (Max P) and the crank angle when the maximum pressure reached.	148
Table 5-3 Comparison of the CPU time and the number of reactions of the mechanism developed in Chapter 5 with other well-validated mechanisms	151
Table 6-1 N-heptane mechanisms used in Chapter 6	154
Table 6-2 Overall mean error and number of reactions of each skeletal mechanism	164
Table 6-3 Modified n-heptane based reactions (A units cal-cm-sec-K, E units cal/mol)	170
Table 6-4 The reduced n-heptane/syngas/NOx mechanism (UNN-2) developed in Chapter 6 (A units cal-cm-sec-K, E units cal/mol)	174-185

Chapter 1: Introduction

1.1 Background

The environmental problems due to the harmful exhaust gas emissions from the combustion of fossil fuels coupled with the reduction of fossil fuel supplies are causing worldwide interest in the use of renewable and environmentally friendly fuels. By using sustainable and environmentally friendly fuels, the targets are the reduction of harmful exhaust gas emissions without negative effects on the efficiency of the engine and the replacement of traditional fossil fuels. A possible solution is by using synthesized gases (syngas) as a fuel. Syngas is a sustainable and environmentally friendly fuel as it is produced by the gasification of feedstock or coal and produces lower amount of harmful emissions during its combustion in comparison with the traditional fossil fuels. Syngas consists of different components such as H_2/CO/CH_4/CO_2 and N_2 [1, 2]. The proportion of each component included in the syngas depends mainly on the gasification procedure and the type of feedstock or biomass that was used to produce it [3]. For example, by using Indian coal and oxygen as gasifying agent the syngas composition is 15.3 %mole H_2, 60.1%mole CO, 0.003% mole CO_2 0.192 %mole H_2O, 0.23 %mole CH_4 and 0.8 %mole N_2. While on the other hand by using Rice Husk and oxygen as gasifying agent the syngas composition is 36.5 %mole H_2, 21.8%mole CO, 20.2% mole CO_2 19.9 %mole H_2O , 0.6 %mole CH_4 and 0.4 %mole N_2 [4].

As it can be observed, syngas mixtures consist mainly of large amounts of H_2 and CO. The effects of the amount of H_2 and CO included in the mixture on the combustion process and NOx emissions have been investigated by many authors [5-8]. According to Shudo et al [9], mixtures of H_2 and CO have high antiknock behaviour, while they emit low unburned hydrocarbons, CO and NOx during their combustion. Therefore, they concluded that such mixtures could serve as fuels for internal combustion engines for the replacement of traditional fossil fuels [9, 10]. Zhang et al [11], showed that the addition of H_2 in a methane based syngas fuel, increases the reactivity of the mixture and results in the mitigation of NOx and CO emissions [11]. Other studies, [12-14] suggested that by increasing the hydrogen concentration under stoichiometric conditions, results in higher combustion temperatures and higher NOx emissions. Therefore, such mixtures are more appropriate for lean-burn applications (equivalence ratio < 1.0), because of the excess air which will keep the combustion temperatures at moderated levels and the NOx emissions low [12, 13].

Different combustion technologies were developed in order to overlap the efficiency and emissions problems. The homogeneous charge compression ignition engine (HCCI) is a promising solution to achieve high efficiency and at the same time lower exhaust gas emissions [15]. However, the main problem of HCCI engines is related with the combustion control [16]. Due to the higher ignition temperature of syngas fuels, in comparison with the traditional fossil fuels such as diesel, a secondary fuel is required that will trigger the combustion process and ignite the primary premixed syngas fuel. A promising solution is by using pilot ignited dual fuel engines [17]. In this engine, the combustion of the lean premixed syngas blend is initiated by the auto-ignition of a small quantity of pilot diesel based fuel that is injected into the combustion chamber before top dead centre (TDC) [18, 19].

Dual fuel engines have been used for a wide range of applications, such as in power production plans, and they are mainly used for the combustion of gaseous fuels. Most commonly, they are diesel engines that have been modified and can achieve very low levels of emissions.

The composition of the gaseous fuels as well as the behaviour of the individual chemical components included in the syngas, towards the temperature and pressure variations are critical factors affecting the combustion process and NOx formation. Therefore, analysis and understanding of the chemical kinetics that occur during syngas combustion is a necessary process. However, the understanding of the chemical kinetics that occur during syngas combustion is a difficult and complex procedure due the appearance of different gases that react differently at different operational conditions. Moreover, the complexity involved in analysing the combustion chemistry in dual fuel engines is increased even more by the injection of the diesel based fuel via the pilot. The complexity to analyse the combustion chemistry in detail during syngas combustion, offers a considerable challenge to researchers to develop an accurate, robust and computationally efficient chemical kinetics mechanism, applicable for the simulation of the multi-component syngas combustion, the co-oxidation of the pilot injected diesel base fuel and the syngas and NOx formation.

Chemical kinetics mechanisms are essential tools for the design and the development of new optimised ICE. They are used in computational fluid dynamics (CFD) simulations and coupled with turbulence sub models, for accurate analysis of the combustion chemistry and its interactions with the turbulence. Because syngas fuels consist mainly of H_2/CO, the chemical kinetics mechanisms that were developed during the past years were mainly focused on simulating the combustion of pure H_2 or H_2/CO syngas mixtures [20-23]. However, as stated

by Glarborg et al [24] and later by Mathieu et al [25], simple H_2/CO mixtures are not fully adequate to represent real syngas fuels, since CH_4 has a significant influence on the combustion process. Therefore, CH_4 chemistry should be included in the chemical kinetics mechanism. Moreover, for the investigation of NOx formation during syngas combustion, an accurate and robust NOx chemical kinetics mechanism should be coupled with the syngas mechanism.

In contrast to the number of chemical kinetics mechanisms developed for the simulation of H_2/CO syngas mixtures, only a few mechanisms can be found that are suitable for the simulation of multicomponent syngas combustion. Azimov et al [2] performed a multidimensional analysis of $CH_4/CO_2/CO/H_2$ syngas combustion in a micro pilot ignited dual fuel engine using a constructed chemical kinetic mechanism. The constructed mechanism was validated against experimental results for specific syngas mixtures, showing a good agreement. However, the proposed model did not contain NOx chemistry, which is necessary for the calculation of NO formation. GRI Mech. 3.0 [26], is a well validated and detailed chemical kinetics mechanism that consists of 351 reactions and contains full H_2, CO and CH_4 chemistry, as well as detailed NOx chemistry. However, GRI Mech. 3.0 was mainly constructed for the simulations of natural gas (CH_4>80%) and therefore it has a significant uncertainty while simulating multicomponent syngas fuels.

On the other hand, different chemical kinetics mechanisms have been developed for the simulation of n-heptane oxidation. It is well known that large hydrocarbons have a complicated temperature dependence as they have a two stage, low and high temperature oxidation. Therefore, the chemical kinetics mechanisms for large hydrocarbons (such as n-heptane) required a very large number of species and reactions in order to accurately simulate their oxidation during the low, negative temperature coefficient (NTC), and high temperature regions. For example, the detailed updated mechanism for heptane oxidation, proposed by Lawrence Livermore National Laboratory (LLNL)[27], consists of 2526 reactions and 540 species. It is understandable then that mechanisms of such size need very high computational time for a complete simulation.

Despite the development of different chemical kinetics mechanisms for the simulation of individual n-heptane oxidation and syngas combustion, there is a clear need for a robust and computational efficient chemical kinetics mechanism that will be able to simulate syngas/n-heptane co-oxidation, syngas combustion and NOx formation. Recently, Ra et al [28], developed a reduced n-heptane/syngas mechanism that consists of 312 reactions for the

simulation of n-heptane/syngas combustion in an RCCI engine. However, the proposed mechanism does not include either methane or NOx chemical pathways.

1.2 Aim of this research

By following the literature search, this thesis is aimed at understanding the combustion chemistry during multicomponent syngas combustion and to develop a reduced, robust and computational efficient n-heptane/syngas/NOx mechanism for the simulation of syngas combustion, NOx formation and n-heptane/syngas co-oxidation. In order to achieve that, this thesis was separated into three stages/objectives:

1) Development of a reduced chemical kinetics mechanism for the simulation of multicomponent syngas combustion in a micro pilot ignited dual fuel engine. A detail chemical analysis of the combustion process must be conducted for the identification of important reactions affecting the reactivity of the mixture at different combustion conditions and by using different fuel mixtures. The mechanism will be validated against experimental and simulated results, by using other well validated mechanisms, in terms of laminar flame speed and ignition delay time. Finally, the new mechanism will be implemented in multidimensional CFD simulations for the prediction of the syngas combustion in micro pilot dual fuel engine.

2) Development of an updated reduced chemical kinetics mechanism for syngas combustion and NOx formation in a micro-pilot ignited dual fuel engine. By using a testing procedure, different NOx sub-model will be tested and validated against experimental results for NOx formation. The most accurate and computational efficient model will be adopted and coupled with the syngas mechanism developed in objective 1. A detail analysis of the reactions and the species affecting NOx formation and syngas combustion must be conducted for the identification of the important reactions and the optimization of their rate constants in order to reduce the uncertainty and the errors. For the validation procedure, the new reduced syngas/NOx mechanism will be validated against experimental results and simulated data, using well validated mechanisms developed by other authors, in terms of laminar flame speed, ignition delay time and NOx formation profiles. Finally, similarly to the syngas mechanism developed in Part 1, the syngas/ NOx mechanism will be implemented in multidimensional CFD simulations for the prediction of syngas combustion in micro pilot ignited dual fuel engine.

3)The final objective of this research is the development of a reduced n-heptane/syngas/NOx chemical kinetics mechanism for the simulation of syngas combustion, NOx formation and the

co-oxidation between n-heptane and syngas in a micro-pilot ignited dual fuel engine. Different reduced, skeletal and detailed mechanisms for n-heptane oxidation will be collected from the literature and tested against experimental results. The most accurate mechanism will be reduced via necessity analysis based on sizing and accuracy requirements, and a new skeletal mechanism will be generated. The generated skeletal mechanism will then be coupled with the syngas/NOx mechanism (Part 2) and will be validated against experimental results in terms of ignition delay time, laminar flame speed and NOx concentration profiles not only by using syngas fuels but also for pure n-heptane and n-heptane/syngas mixtures. Finally, similarly to the previous two developed mechanisms, the n-heptane/syngas/NOx mechanism will be implemented in multidimensional CFD for the simulation of syngas combustion and n-heptane/syngas co-oxidation in micro pilot ignited dual fuel engine.

1.3 Contribution to knowledge

To date, despite the development of various chemical kinetics mechanisms for the simulation of syngas combustion and n-heptane oxidation, a robust and reduced chemical kinetics mechanism that includes full syngas and NOx chemistry and n-heptane chemistry remains elusive

Therefore, during this thesis, a reduced and robust syngas-based chemical kinetics mechanism for dual fuel engine combustion applications was developed. The mechanism can be used in not only zero and one-dimensional simulations for the investigation of the combustion chemistry, but it can be implemented in multidimensional CFD simulations for the analysis of the combustion process including the effect of turbulence. The final mechanism includes full syngas chemistry (H_2, CH_4, CO, CO_2 and N_2), NOx chemistry and n-heptane chemistry.

The capabilities of the mechanism in addition to its small size offer to researchers and manufacturers a comprehensive, robust and computational efficient tool that can be used for the analysis of the combustion chemistry (syngas combustion and the co-oxidation between syngas and n-heptane), the interactions between the species, and the formation of NOx emissions.

1.4 Thesis structure

This thesis is separated into seven chapters:

Chapter 1 is the introduction of this thesis.

Chapter 2 is an overview of the current literature related to syngas fuels, their application in dual fuel engines and the current status of the chemical kinetics mechanisms for syngas combustion and the techniques that were used for the reduction of detailed mechanisms.

Chapter 3 discusses the methodologies that were followed for the modelling of the combustion chemistry and the reduction techniques that were used for the mechanism reduction and the analysis of the combustion chemistry. Moreover, all of the available experimental data obtained from the literature related to syngas combustion, and used for the validation of the developed mechanisms, were summarized and categorized.

In Chapter 4, a reduced chemical kinetics mechanism of syngas combustion in a micro pilot ignited dual fuel engine was developed. Important chemical reactions affecting the combustion process were identified by conducting a sensitivity analysis study and their rate constants were updated. Moreover, important reactions that influence the reactivity of the mixture at high-pressure, low temperature conditions were imported. Two mechanisms were developed (low and high H_2 content) and validated against experimental measurements.

The mechanism that was constructed in Chapter 4 for low H_2 content was further optimized in Chapter 5 by incorporating a 12-reaction NOx pathway and by updating the rate constants of important hydrogen reactions that were found to be very sensitive during high pressure conditions.

In Chapter 6, a reduced chemical kinetics mechanism for n-heptane oxidation, n-heptane/syngas co-oxidation, syngas combustion and NOx formation was constructed and validated against various experimental results presented in Chapter 3.

Finally, in Chapter 7, the findings and the conclusions from this research are summarized and recommendations for future work are discussed.

Chapter 2: Literature review

In the last century, the consumption of energy worldwide has been increased by a factor of seventeen, while the harmful CO_2, NOx and SO_2 emissions produced from the combustion of fossil fuels have resulted in severe and serious pollution of the atmosphere and the environment [29]. For example, in Europe, CO_2 emissions levels increased by 2.5% in 2017 in comparison with 2016, while for the same period in Asia the emissions levels increased by 2.3% [30]. Moreover, if the consumption of fossil fuels continues at its current rate, 93 million barrels per day , petroleum resources are estimated to be depleted in less than 50 years [31].

A sector that is directly related with the environmental pollution and the reduction of fossil fuels is the transport sector, as it is a major consumer of petroleum fuels such as diesel, gasoline etc. For example, according to recent researches, in 2017 the petroleum products accounted for about 95% of the total transportation sector energy use worldwide [31].

In order to address the problems related with the fossil fuels reduction and environmental pollution, governments of the leading countries such as USA, have created different research programmes, which are focused on the development of concepts such as renewable resources, green energy and eco-friendly processes. These programmes focus on investigating the potential of using biomass for the production of synthesized gasses (syngas), which then can be used for heat and power generation via the combustion process or they can be further converted into transportation fuels and other high-value chemicals [32].

2.1 Technological development of gaseous fuels

The history of the gaseous fuels is not recent and starts from the early 18^{th} century [33]. At the beginning, gases were used as fuels for lighting purposes and more specifically for lighting the streets [33] and house lighting [34]. In the automotive sector, this technology was initially adopted in 1923 by Georges Impert, who produced a wood gas generator that was applied in mobile applications [35]. This technology was used for the mass production of wood-gas vehicles during WWII with more than a million of such vehicles produced [36, 37]. By the end of the 1940s and the end of WWII, petrol became the dominant fuel in the transportation sector. That led to the reduction and the elimination of these gas-fuel cars from the market.

Since then, the flammable gasses have only been used in stationary power generation systems. Moreover, coal, which was used as the primary fuel in gas power plants, has been characterized as one of the most environmentally pollutant fuels due to the production of high amounts of

harmful CO_2 and NO during its combustion. Therefore, the governments of the leading countries, such as the USA and UK, draw stringent laws and regulations in order to reduce the use of coal and other solid fuels [38]. A possible solution for the reduction of the polluting emissions is the use of gaseous fuels that are produced by the gasification of feedstock or coal. These gaseous fuels are called synthesized gasses (syngas) because they consist of different chemical components such as H_2, CO, CO_2, CH_4 and N_2. In general the amount of each component included in the syngas mixture varies between 5-50%vol for H_2, 10-60%vol for CO, 10-35%vol for CO_2, 0.5-10%vol for CH_4 and 5-60%vol for N_2 [39], and depends mainly on the gasification process that was followed for its production and the type of feedstock that was used. However, the effects of both parameters on syngas composition are analysed in detail in Section 2.2.

According to BP Energy outlook for 2018 [30] ,for the EU in 2040 the carbon emissions are estimated to be over 35% lower than in 2016. This is mainly due to the higher use of non-fossil fuels and renewables, while on the other hand the use of carbon-based fuels and fossil fuels reduced significantly. The primary energy consumption for EU from the time-period between 1970 until 2040 is presented in Figure 2-1. According to the figure it can be seen that the use of coal based and fossil oil fuels is reduced gradually while on the other hand the use of renewable fuels (such as biofuels, biomass) and gaseous fuels increased [30].

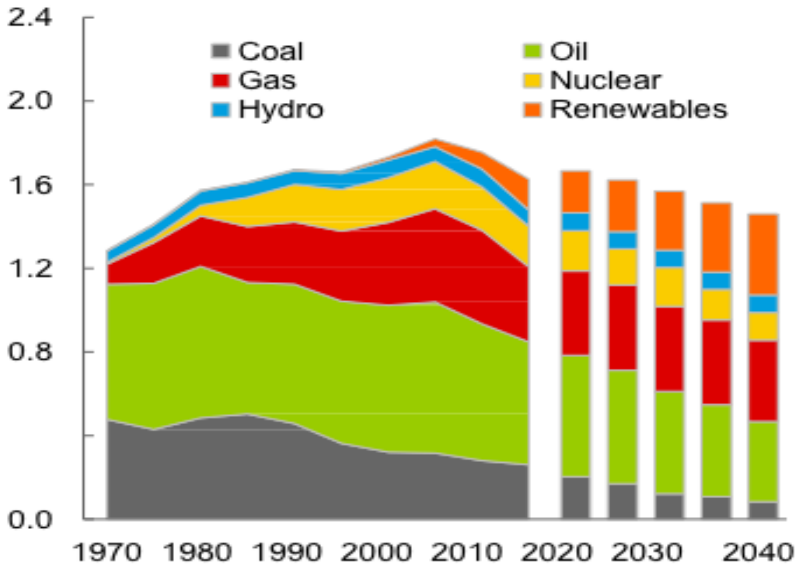

Figure 2-1 Historical and projected primary energy consumption in EU. Renewables include biomass and biofuels and gas refer to Natural Gas [30].

2.2 Syngas fuels

For the production of syngas from natural feedstock such as rice husk, pine, nutshell, crops etc., a thermochemical gasification procedure has to be followed. The end of product will be a gaseous fuel who consisting predominately of 30-60% hydrogen and variables amounts of other chemical components such as 20-60% CO, 3-10% CO_2 and 3-10% CH_4.

2.2.1 Gasification process

Among the available technologies that are used for the conversion of solid feedstock to gas, the gasification process is characterized as the most energy efficient and reliable method. Gasification is a thermochemical conversion process in which the carbonaceous material is converted into a gaseous product (syngas) that mainly consists of H_2 and CO and lower amounts of CH_4, CO_2, N_2 and H_2O [40]. In order for the gasification to be performed, a gasifying agent is used (for example pure oxygen, air or steam) at a temperature range between 500 and 1400 ^oC and at elevated pressures up to 33 bar [40, 41] . Moreover, according to [40], the moisture content of the biomass plays a critical role on the gasification process. The authors mentioned that by using feedstock with moisture content in the range of 25-60% directly in the gasifier will result in high amounts of energy losses in the overall process. Therefore they made the conclusion that feedstock needs to be dried or preheated to low moisture content (between 10% and 20%) before to be used into the gasifier [40]. The gasification process is separated in 4 different steps: 1)the drying of the feedstock, 2) the de-volatilization of the biomass particles (production of vapours and char), 3) the cracking and reforming of the volatiles and 4) the gasification of the char. The char gasification and the reforming reactions are enhanced by steam atmosphere in order to produce more light gases such as CO, CO_2 and H_2 [42]. All of the steps of the gasification process are presented in Figure 2-2.

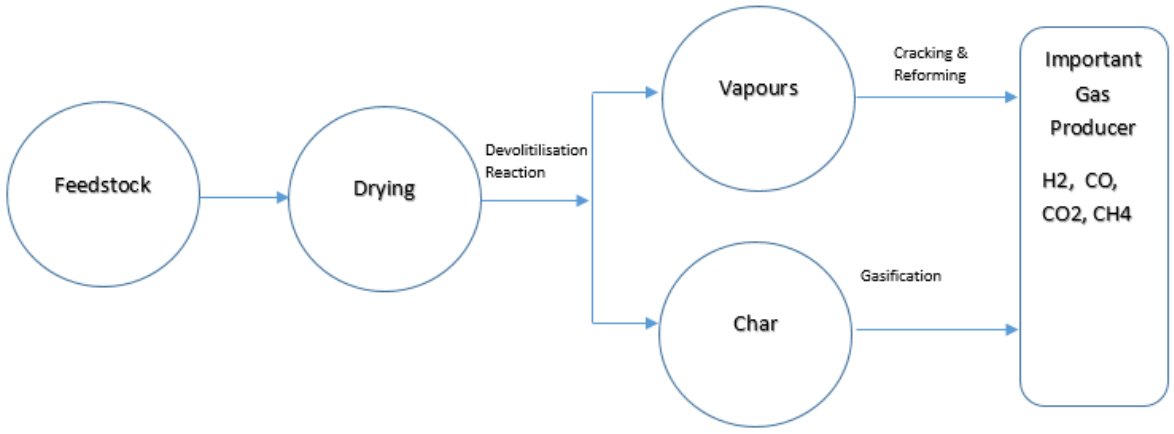

Figure 2-2 Gasification process flow chart [40].

The produced gasses characterized as intermediate energy carriers, can be used for the heat and power generation via the combustion process or they can be further converted into transportation fuels and other high-value chemicals (for example formaldehyde) by using chemical conversion processes such as fermentation [43, 44].

The quality of the produced syngas and its composition depend on the gasification procedure (more specifically the gasifying agent) and the type of feedstock that was used for its production. Table 2-1 and Table 2-2 show two comparisons performed by Couto et al [39] in order to investigate the effects of the biomass type and gasifying agent on syngas, respectively. According to Table 2-1, by using different types of feedstock, the syngas composition as well as the heating value changed. For example, by using pine, H_2, CO and CH_4 concentrations are $5.269x10^{-3}$ mol/kg, $7.22\ x10^{-3}$ mol/kg and $2.72\ x10^{-3}$ mol/kg respectively while the heat value is the highest from all, 14.68 MJ/m^3. On the other hand by using rice husk, H_2 is $2.36\ x10^{-3}$ mol/kg, CO is $6.51\ x10^{-3}$ mol/kg and CH_4 is $2.09\ x10^{-3}$ mol/kg, while the heat value is the lowest ,11.11 MJ/m^3[39].

Table 2-1 Effect of biomass type

Feedstock	H_2 (mol/kg)	CO (mol/kg)	CO_2 (mol/kg)	CH_4 (mol/kg)	$C2H_2$ (mol/kg)	C_2H_4 (mol/kg)	C_2H_6 (mol/kg)	HV (MJ/m^3)	Ref
Rice husk	$2.36\ x10^{-3}$	$6.51\ x10^{-3}$	$70177\ x10^{-3}$	$2.09\ x10^{-3}$	$6.2x10^{-5}$	$7.6x10^{-4}$	$1.1x10^{-4}$	11.11	[45]
Nut shell	$4.855\ x10^{-3}$	$7.88\ x10^{-3}$	$4.477\ x10^{-3}$	$2.93\ x10^{-3}$	$4.9x10^{-5}$	$6.1x10^{-4}$	$2.1x10^{-4}$	14.55	[45]
Pine	$5.269\ x10^{-3}$	$7.22\ x10^{-3}$	$5.005\ x10^{-3}$	$2.72\ x10^{-3}$	$1.2x10^{-4}$	$8.1x10^{-4}$	$1.7x10^{-3}$	14.68	[45]
Eucalyptus	$2.75\ x10^{-3}$	$7.12\ x10^{-3}$	$3.80\ x10^{-3}$	$3.16\ x10^{-3}$	$2.6x10^{-5}$	$5.5x10^{-4}$	$1.5x10^{-4}$	13.41	[45]
Vine Pruning	$1.04\ x10^{-3}$	$2.378\ x10^{-3}$	-	$6.41\ x10^{-3}$	$1.99\ x10^{-3}$	$1.21\ x10^{-3}$	$1.21\ x10^{-3}$	11.41	[39]
Cherry stone	$6.39\ x10^{-3}$	$6.68\ x10^{-3}$	-	$3.71\ x10^{-3}$	$1.03\ x10^{-3}$	$1.73\ x10^{-3}$	$1.73\ x10^{-3}$	-	[46]

For the effect of the gasifying agent, Table 2-2, it can be seen that by using air as gasifying agent, the concentrations of H_2 and CO as well as the heating value are lower than if using oxygen, 17 %vol, 21% vol and 5.7 MJ/m^3 respectively. Moreover, by using O_2 as a gasyfing agent, the concentration of H_2 and CO, included in the produced gas, increased remarkably and that leads to a significant increase in the heating value, 10.4 MJ/m^3. Finally, by using steam a significant increase in the amount of CH_4 (7%vol) and the heating value (14.68 MJ/m^3) can be observed [39].

Table 2-2 Effect of gasifying agent

Agent	H2 (%vol, dry base)	CO (%vol, dry base)	CO2 (%vol, dry base)	CH4 (%vol, dry base)	N2 (%vol, dry base)	HV (MJ/m^3)	Ref
Air	17	21	13	1	48	5.7	[39]
O2	32	48	15	2	3	10.4	[39]
Steam	52	23	18	7	-	14.68	[39]

It is clear that a variety of syngas fuels with different compositions and heating values could be produced, each one with its own combustion characteristics. Furthermore, each individual species included in the syngas mixture has different thermochemical characteristics, such as the dissociation energy, and reacts differently at different temperatures. For example, according to [47, 48] , at 298 K the average bond dissociation energy of H_2 (H−H) is 436.002 kJ/mol, of N_2 (N≡N) is 945.3 kJ/mol, of CO_2 (C=O) is 732.2 kJ/mol and of CH_4 is 413 kJ/mol. Moreover, for dual fuel applications, the effect of the diesel-base fuel, such as n-heptane, must be taken into account. N-heptane has a dissociation energy of 389 kJ/mol while injecting high amounts of n-heptane (more than 3 g/cycle) results in the co-oxidation with the premixed syngas fuel and that has a significant effect on the combustion process. More details about dual fuel engines and the use of n-heptane as surrogate for diesel can be found in the next Section of this thesis, Section 2.3.1.

Due to the appearance of different gases that have different physical and chemical characteristics and react differently at different temperatures and pressures, the analysis of the combustion chemistry and the investigation of the interactions between the species during syngas combustion is a very difficult and complicated procedure. However, understanding of the physical and chemical characteristics of such mixtures and the effects of the gas composition on the combustion process and emissions is a necessary procedure that needs to be followed.

2.3 Syngas in internal combustion engines

In order to analyse the advantages and disadvantages of using syngas, it is very important to understand their application in internal combustion engines. Two different types of engines can be found in the market; mobile and stationary [49, 50]. Both types are separated into internal (ICE) and external combustion types depending on their application. Mobile type engines are only internal combustion while stationary engines can be both internal and external combustion. This research will focus on ICEs as they are one of the most vital technological advancements related to power Generation [51, 52]. The advantages of ICEs are that they have

a flexible application in non-moving and moving machineries, their capital cost is low, they have good part-load performance, their operating efficiency is high, they are safer during their use in comparison with other combustion technologies and they are more reliable [34, 50].

The idea of using syngas in ICEs, attracts the attention of different research groups due to the fact that it's believed to be very promising and economically competitive in comparison with natural gas [53]. Two different types of ICEs are used for the combustion of syngas fuels a) the spark-ignition (SI) and more specifically the naturally aspirated carbureted and port injection types and the direct injection (DI) type, and b) the dual fuel compression ignition (CI) engines [33].

For the carbureted and port injection SI engines, the fuel and air are mixed prior of the combustion chamber and therefore the volumetric efficiency of the engine is reduced. Moreover, they have higher fuel consumption in comparison with the direct injection SI engines as their pumping and heat losses are higher [54]. Consequently, the syngas fuelled carbureted and port-injection SI engines have lower theoretical power output than those of natural gas and gasoline [55]. By using direct injection SI engines, the air and fuel are mixed inside the combustion chamber and therefore, there is no restriction in the air amount aspirated into the chamber. This results in the engine power output of direct injection systems to be higher than that of port injection systems [56].

2.3.1 Syngas in dual-fuel IC engines

This research is mainly focused on syngas combustion in pilot-ignited dual fuel engine applications. As already highlighted, syngas is considered to be an alternative fuel for fossil fuels, producing lower emissions during its combustion at a lower cost and resulting in higher engine performance. However, the self-ignition temperature of syngas is very high (> 500^{o} C) and therefore it cannot be autoignited by compression ignition (CI) in an internal combustion modified diesel engine [5, 18]. A possible solution to this problem is the use of dual fuelling, where a surrogate fuel of diesel, such as n-heptane, with lower self-ignition temperature is injected as a pilot fuel to initiate the combustion of the primary syngas fuel, which is already premixed with air in the combustion chamber [57-59]. A conceptual diagram of a dual fuel CI engine is presented in Figure 2-3.

Surrogate fuels are usually used for the representation of current transportation fuels, such as diesel. A surrogate fuel is defined as a fuel that consists of low number of pure compounds

whose characteristics are similar to the characteristics of the target fuel, such as the diesel fuel. A surrogate fuel is necessary to represent the chemical and physical characteristics of the diesel, in order to reproduce accurately the vaporization, injection and mixing processes that occur prior of the ignition in dual fuel engines. Thus, important physiochemical parameters such as the molecular structure, ignition behavior, soot propensity, viscosity, density, surface tension and volatility need to be taken into consideration.

Surrogate fuels are usually used in computational analysis allowing the accurate and less complex simulation of the combustion process while on the other hand they are used in experimental studies for the testing of the combustion characteristics of different target fuels in different experimental devices [60]. According to Donkerbroek et al [61], for conventional diesel combustion, both diesel and n-heptane show identical physical and chemical characteristics and have similar ROHR. Therefore, they concluded that n-heptane can be used as a diesel surrogate fuel. Following the findings from Donkerbroek et al [77], it was decided that n-heptane could be used in this thesis as the diesel-based fuel that is injected in the combustion chamber for the ignition of the primary premixed syngas fuel in dual-fuel combustion applications.

For dual fuel combustion applications, n-heptane is only used for the initiation of the pilot ignition of syngas. While injected in very small amounts via a micro-pilot, n-heptane is completely consumed during the ignition of the syngas and therefore the combustion proceeds without any n-heptane. This is because by injecting only 1.2 mg/cycle of n-heptane, the contribution of the total ROHR is negligible as it provides only 2% of the total energy value in the cylinder [2]. According to previous studies [62, 63], when n-heptane is injected via micro-pilot, the ROHR profiles are not affected due to the n-heptane, and only a low level of smoke was observed. This statement is opposite to what has been found when a higher amount of n-heptane is used, as in [57]. For the rest of this thesis, n-heptane was used as a surrogate for diesel.

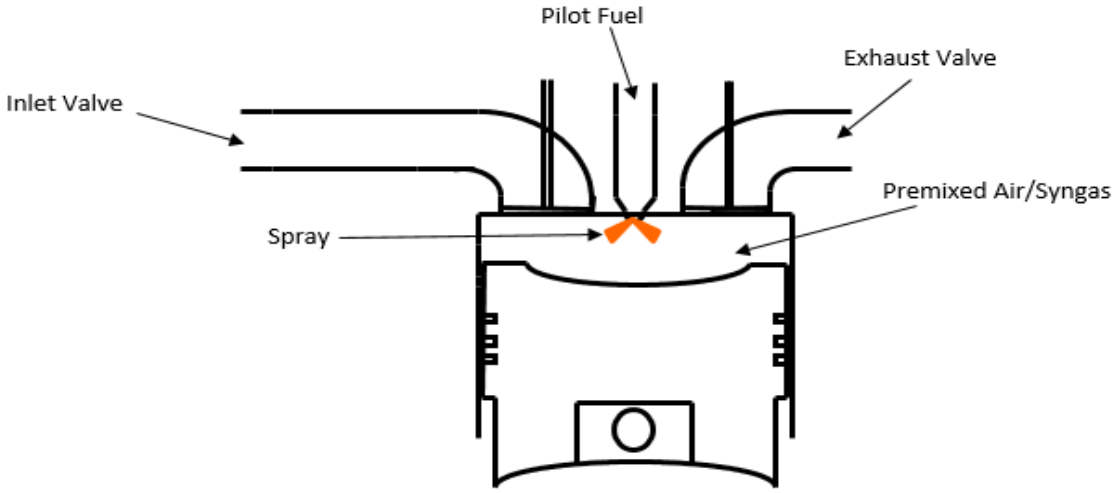

Figure 2-3. A conceptual diagram of a pilot-ignited dual fuel engine

In dual-fuel engines, syngas combustion consists of four different stages; the first stage (1) is the ignition delay time of the injected diesel base fuel, the second (2) is the autoignition and the combustion of the diesel base fuel, the third (3) is the ignition and the combustion of the primary premixed syngas fuel and the last stage (4) is the diffusion combustion stage that starts at the end of the syngas fuel combustion [64, 65]. The four-stage process is presented in Figure 2-4. The diesel injection time is 12° CA BTDC and TDC is at 0° CA.

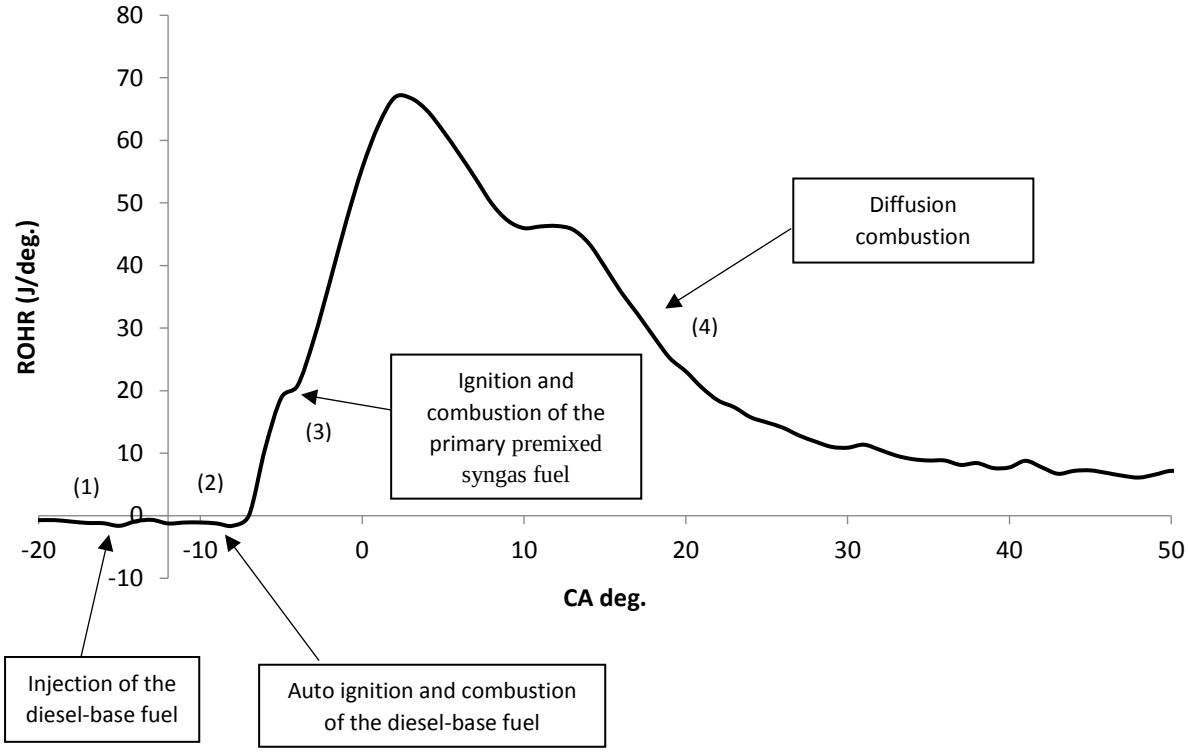

Figure 2-4 Characteristic stages of the rate of heat release for combustion in a dual fuel engine.

2.4 Combustion chemistry of syngas

The combustion chemistry during syngas combustion is directly related with the in-cylinder pressure and temperature. During the 1970s, researchers mainly focused on high temperature and low pressure in-cylinder conditions [5]. However, during the last decades, the desire to reduce the harmful emissions and improve the efficiency of the engine (HCCI engines) led to a shift towards high pressure and low temperature in-cylinder conditions [66, 67]. This is because syngas fuels produced from the gasification of solid feedstock contain high amounts of H_2, which in high temperature conditions will lead to higher NOx emissions [68].

NOx is a collective term for NO and NO_2 species and is formed by the chemical reaction of nitrogen and oxygen. Formation of thermal NOx, prompt NOx and fuel NOx are the major pathways where the nitrogen and oxygen are combined for the formation of NOx [69-71]. First thermal NOx is formed from the reaction between the nitrogen that exists in the air and the oxygen radicals. This NOx formation type is triggered under high temperature conditions (above 1500 K) and is directly related to the temperature: the higher the temperature, the higher the rate of formation of the thermal NOx. Prompt NOx is formed especially at fuel rich conditions at the flame front due to the chemical reaction between the molecular nitrogen and the hydrocarbon radicals Finally, fuel NOx is formed by the interaction between the nitrogen included in the fuel and the oxygen of the combustion air [69]. Each one of those NOx formation types is presented in detail in Chapter 3, Section 3.1.6.

For each one of the three NOx formation types, the NOx formation rate is directly related with the in-cylinder temperature and the fuel properties such as the type, the composition and the equivalence ratio of the mixture. For example for rich fuels with high hydrogen amount, the formation of NOx is higher due to the formation of more hydrocarbon radicals. The hydrocarbons radicals interact with molecular hydrogen for the formation of Prompt NOx. Moreover, during the combustion of syngas mixtures with high hydrogen content, the formation of high reactive OH radicals is faster. The relationship between OH radicals, the in-cylinder temperature and the combustion intensity was investigated in detail by many authors [72-75] showing that the higher the amount of OH radicals formed, the higher the temperature and therefore the higher the intensity of the mixtures. High temperature, especially higher than 1500 K, lead to the fast formation of thermal NOx [69, 76].

As it can be observed, syngas composition and especially the amount of hydrogen included in the fuel mixture has a significant effect on the emissions formation and in the general

combustion process. Therefore, during recent years the effects of the different syngas components, and more specifically the hydrogen concentration, have been studied extensively.

According to Lieuwen [77] and Chaos and Dryer [5], for syngas chemistry, the formation of OH radicals is a key factor and is directly connected with the changes in the temperature and pressure. At low temperature and high-pressure conditions, the dominated kinetic pathways for the formation of OH radicals change from the faster O and H pathways to the slower H_2O_2 and HO_2 pathways. This results in a reduction of the mixtures reactivity and a higher ignition delay time, which is now highly depended on the pressure [5].

Azimov et al [78] investigated how the emissions and performance of a four-stroke single cylinder engine are affected by H_2 and CO_2 syngas contents. The concentration of H_2 varied between 13.7 %vol to 100%vol (pure hydrogen mixture), while the concentration of CO_2 varied between 2.2%vol to 34.0%vol. The ignition of the premixed lean syngas was initiated by using micro pilot injection of diesel-base fuel. The engine was supercharged and operated in a premixed mixture ignition in the end-gas region (PREMIER). For all the tested syngas fuels, PREMIER combustion was observed especially when the pilot diesel amount was very small (1.2 mg/cycle). Under PREMIER combustion mode, the performance of the engine was enhanced, and the efficiency increased. Furthermore, the authors showed that by using higher hydrogen composition, the combustion duration was shorter and that caused an increase in the mean-combustion temperature and the indicated mean effective pressure (IMEP).

Sahoo et al [7], investigated the combustion of H_2/CO syngas mixture on a dual fuel pilot injection CI engine in which diesel was used as the pilot fuel. For the experiments, different load conditions varying from 20-100% were used with an interval of 20%. The authors showed that exergy efficiencies at higher loads were better by using syngas in dual fuel mode than by using diesel fuelling. Furthermore, they made the conclusion that by increasing the hydrogen content in the syngas mixture, the work availability of the dual fuel engine was improved.

The same research team conducted a separated study [8], in order to investigate the combustion of H_2/CO syngas on a dual fuel engine and to analyse the effects of the H_2/CO ratio on important combustion parameters such as the in-cylinder pressure, the exhaust gas temperature, the brake thermal efficiency and the emissions (NOx and CO). The authors confirmed the findings of [6, 7], showing that the higher the hydrogen content in the syngas mixture, the higher is the brake thermal efficiency of the engine. In terms of NOx, the authors showed that

by increasing hydrogen, NOx emissions also increased, while unburned CO emissions increased with the amount of CO included in the mixture.

Roy et al. [62, 63] analysed the effect of hydrogen content and exhaust gas recirculation (EGR) in different syngas types (produced from biomass and coke oven coal) on the emissions levels and the efficiency of a dual-fuel engine. The authors concluded that by using syngas with higher H_2 (>20%), the power of the engine increased by 12%.

Finally, Tomita et al. [12] investigated the combustion characteristics of a supercharged syngas engine with micro-pilot ignition. The authors showed that by increasing the syngas H2 content, on the one hand, the lean limit of the mixture increased and the engine operated with higher efficiency and more stable combustion, while on the other hand, the combustion temperature increased as the mixture became richer and the produced NOx emissions were higher in comparison with leaner mixtures. Therefore, they made the conclusion that lean mixtures are more suitable for use in internal combustion engines because of the excess air which will keep the combustion temperature at moderated levels and will keep the NOx emissions low [2, 12].

By considering the findings from the literature search, it is understandable that a chain reaction process is created between the in-cylinder pressure and temperature variations, the hydrogen chemistry, NOx formation and the performance of the engine. However, despite the fact that basic syngas mixtures including only H_2 and CO have been studied extensively, they are not representative of real syngas mixtures produced from the gasification of different types of feedstock [25]. This is because realistic syngas mixtures do not contain only H_2 and CO but they consists of various amounts of H_2, CO, CH_4, CO_2 and N_2, as already shown in previous paragraphs [41, 79, 80]. As highlighted by Glaborg et al [24], each gas should be taken into account, even in trace amounts, due to the fact that each gas can drastically affect the oxidation of the syngas fuel and therefore the reactivity of the mixture.

Only a few experimental studies are available that investigate the effect of the different syngas components, especially CH_4, on syngas combustion and NOx formation. Mathieu et al [25] performed an experimental shock tube study to investigate the ignition of syngas mixture representative of a syngas produced from biomass (0.09%mol CH_4/ 0.296%mol CO/ 0.157%mol CO_2 / 0.3%mol H_2 / 0.2%mol H2O/ 0.95%mol O2 / 98%mol AR). The authors showed that the addition of CH_4 increases the ignition delay time, while the addition of CO has a negligible effect on the combustion process. Therefore, they concluded that simple H_2/CO mixtures are not fully adequate to represent real syngas fuels, since CH_4 has an important

influence on the combustion process. Watson et al [13], conducted a comparative study of syngas consisting of $CH_4/CO_2/CO/H_2$ and pure methane fuels (e.g. natural gas), in order to investigate the formation of NOx. The authors concluded that at lean equivalence ratios (> 1.0), the syngas fuels produce significantly lower emissions than fuels containing only methane.

Gersen et al [81], performed an experimental investigation of $H_2/CO/CH_4$ syngas combustion using a rapid compression machine at equivalence ratios of 0.5 and 1.0, pressures of 20 to 80 bar and a temperature range of 900-1100 K. The authors investigated the effect of H_2, CH_4 and CO on the ignition delay time by varying their mole fractions (%mol) between 0 % and 100% for CH_4 and N_2 and 0 % and 50% for CO. They made the statement that CO had negligible effect on the combustion process, while increasing H_2 increased the reactivity of the mixture and therefore the ignition delay time reduced. Moreover, they showed that by increasing CH_4 drastically reduced the reactivity of the mixture and the ignition delay time increased at all of the tested conditions.

By summarizing the results from the literature, it can be observed that hydrogen has a major role in syngas combustion and NOx formation and is directly related to the in-cylinder pressure and temperature variations [82]. However, syngas fuels are not consisted only by H_2 but also from other gases, as already highlighted and shown in this thesis.

Each component included in the syngas mixtures, even in trace amount, affects the reactivity of the mixture and the combustion process, yielding various effects on the ignition delay time, the combustion intensity and the emissions formation. Therefore, it is important for all of the components included in the syngas mixtures to be taken into account, otherwise by ignoring species that promote or inhibit the ignition may lead to catastrophic consequences and failure of the engine.

2.4.1 Chemical Kinetics Mechanisms

From the numerical point of view, it is very difficult to investigate and analyse in detail the combustion chemistry and the interactions among the species that take part during the combustion process. The complexity to analyse in detail the combustion process, in addition to the wide range of syngas fuels available, offers a considerable challenge to researchers to develop an accurate, robust and computationally efficient chemical kinetics mechanism applicable for the simulation of the combustion process with different syngas compositions.

Chemical kinetics mechanisms are essential tools for the design and the development of new optimised IC engines. The accurate simulation of the combustion chemistry and the reacting

flows during syngas combustion is the base for the designing of new combustors. The chemical kinetics mechanisms are used for the prediction of important combustion characteristics like the ignition delay time, the laminar flame speed and NOx emissions and they are implemented in computational fluid dynamics (CFD) simulations and coupled with turbulence sub models for the accurate analysis of the combustion chemistry and its interactions with the turbulence.

Syngas

Because syngas fuels consist mainly of 5-50%vol H_2 and 10-60%vol CO, in previous years, the chemical kinetics mechanisms that were developed, for the investigation of important combustion parameters during syngas combustion, were mainly focus on hydrogen and carbon chemistry without considering the effects of the other syngas components, for example CH_4 [82].

Sun et al [20], investigated the laminar flame speed at high pressures and developed a chemical kinetics mechanism for modelling the combustion of H_2/CO mixtures. The authors highlighted the importance of the reaction rate constants and thermal properties for the accuracy and the performance of the mechanism. More specifically, the authors emphasized on the importance of reaction $CO+HO_2=CO_2+OH$ and they updated the rate constant of the specific reaction to minimize the uncertainty level. However, the rate constants were adopted for specific range of conditions (for ignition delay time the mechanism was tested for ignition temperatures up to 1020 K) and therefore at higher temperatures the mechanism shows significant level of error. Moreover, NOx chemical kinetics pathways are not presented in the proposed mechanism and therefore cannot be used for the investigation of the formation of important species such as NO and NO_2.

Saxena and Williams [83] developed a chemical kinetics mechanism for the combustion of H_2/CO mixtures. The authors revised the rate parameters of elementary steps related to hydrogen from [84-87], they removed the initiation step of hydrogen (reaction $H_2+O_2=2OH$), and finally they modified the three-body recombination rates and they adopted an initiation step for CO. The proposed mechanism was validated against experimental results for autoignition times and burning velocities showing very good agreement and relatively low deviation (> 5%). However, for hydrogen counterflow diffusion-flame extinction experiments, the calculated strain rate by using the proposed mechanism deviates significantly from the experimental results. As stated by the authors this deviation is related with the transport properties of the hydrogen and helium based species included in the mechanism. The transport properties were constructed based on a previous version of the mechanism and therefore need to be updated in order to produce more accurate results.

On another research study, Li et al. [88], updated the detailed CH_3OH mechanism of Held and Dryer [89], by using new reaction rate correlations and thermochemical properties for OH, HO_2 and CO_2OH species. Experimental data involving CH_2O, H_2 and CO as initial fuels were used for validation purposes. The authors suggested that the rate correlations for the reactions responsible for the formation of CO, CO_2 and H_2, are very important for the accurate reproduction of the experimental results at high temperatures. However, the updated mechanism was validated only against experimental results for moderated pressures (up to 9.6 atm). As already highlighted in this thesis, during the recent years there is a shift to high pressures/low temperature combustion conditions and therefore more extensive validation of the proposed updated model required at such ultra-boost conditions.

Only few mechanisms can be found that were developed and tested at high pressure/intermediate temperature conditions. Frassoldati et al. [23] investigated numerically and experimentally the combustion characteristics, the flame structure and the NOx and soot emissions of different CO/H_2 syngas mixtures at high pressure and intermediate to high temperatures conditions. The authors proposed a detail chemical kinetics mechanisms that includes full chemical NOx reaction pathways. The detailed mechanism was validated against a range of experimental results in terms of ignition delay time and laminar flame speed, especially at high pressure conditions, showing low level of deviation (> 5%). However, for real syngas mixtures the effect of the impurities created by the different components included in the mixture such as CH_4 and CO should be taken into account as it affects directly NOx formation and the combustion process. Due to the fact that the reactions rates included in the proposed detailed mechanism were constructed based on the combustion of H_2/CO, they are not fully adequate to accurately simulate real syngas fuels. Implementation of methane chemistry in the proposed model will change the thermochemical stability of the mechanism and new improved rate constants of the reactions should be used. Moreover, a main disadvantage of the proposed mechanism is the number of reactions. The mechanism consists of 173 reactions, has a high level of complexity and requires high computational time while used in multidimensional CFD simulation.

Recently, Keromnes et al. [21] studied the combustion and oxidation of hydrogen and syngas mixtures ($H_2/CO/CO_2/N_2$) at elevated pressures. They developed a new chemical kinetics mechanism, which consists of 51 reactions. The constructed mechanism was validated in terms of ignition delay time, flame speed and species concentration profiles for pressures up to 70 bar, temperature range between 900-2500K and different equivalence ratios (0.1-4). The authors, highlighted the importance of reactions $H+O_2+M=HO_2+M$, $H_2O_2+M=2OH+M$ and

$H_2O_2+H=H_2=HO_2$ on the combustion process during low to intermediate temperatures while for high temperatures they concluded that reaction $H+O_2=O+OH$ has the highest level of importance. All of these reactions are related with the formation and the consumption of high reactive OH radicals, that, in turn, are directly affected by the in-cylinder temperature changes. During low temperatures, the major chemical pathways responsible for the formation of OH are the slower H_2O_2 and HO_2 pathways while during high temperatures the faster O and H are the most important. However, real syngas fuels are not consisted only from H_2 and CO but from varying amount of other gases such as CH_4, CO_2 and N_2. Each of these components reacts differently at different temperatures and affects the formation of OH radicals. For example, reaction $CH_4 + OH = CH_3 + H_2O$ is responsible for the consumption of OH especially at high temperature conditions while reaction $CH_3 + O_2 = CH_2O + OH$ is responsible for the formation of OH at high temperature conditions. Both of these reactions directly affect the formation or the consumption rate of high reactive OH radicals and are essential parts of chemical kinetics mechanisms for methane oxidation. Methane is a critical factor included in multicomponent syngas fuels and a robust and accurate chemical kinetics mechanism for syngas combustion should include methane chemistry. Therefore, it can be said that a major disadvantage of the mechanism proposed by Keromnes et al [21] is the absence of methane chemistry that does not allow the mechanism to be used for the simulation of multicomponent syngas combustion, but is restricted only for H_2/CO mixtures.

By summarizing the findings from the literature review about the chemical kinetics mechanisms, it can be seen that despite the fact that different chemical kinetics mechanisms were developed for the simulation of H_2/CO syngas combustion, only a few mechanisms were developed that incorporate methane chemistry and therefore are applicable for the simulation of multicomponent syngas combustion.

Azimov et al [2] performed a multidimensional CFD study and developed a reduced syngas mechanism for the simulation of multicomponent syngas combustion in a dual fuel engine.

The authors incorporated methane chemistry in the proposed mechanism by adding the 9 reactions chemical pathway for CH_4 chemistry proposed by Li et al [90]. The developed reduced mechanism was then implemented in multidimensional CFD simulations and compared against experimental results. Four different syngas mixtures were used for validation purposes:

a) H_2 13.7 %vol, CO 22.3%vol, CH_4 1.9%vol, CO_2 16.8%vol and N_2 45.3%vol
b) H_2 20.0%vol, CO 22.3%vol, CH_4 1.9%vol, CO_2 16.8%vol and N_2 39.0%vol
c) H_2 13.7%vol, CO 22.3%vol, CH_4 1.9%vol, CO_2 23.0%vol and N_2 39.1%vol

d) H_2 56.8%vol, CO 5.9%vol, CH_4 29.5%vol, CO_2 2.2%vol and N_2 5.6%vol.

For all of the mixtures, the developed model shows good correlation for equivalence ratios lower than 0.7. However, for equivalence ratios higher than 0.7 the proposed mechanism shows a significant deviation from the experimental data. Moreover, the developed mechanism was tested only against experimental results for in-cylinder pressure and ROHR, therefore further validation required against experimental measurements for laminar flame speed and ignition delay time for various fuel mixtures in order to ensure the accuracy of the mechanism.

Other mechanisms were developed for the simulation of natural gas but were also used for the simulation of multicomponent syngas fuels. One such mechanism is the detail GRI Mech. 3.0 [26], which includes full hydrogen, carbon and methane chemistry as well as detailed thermal and prompt NOx and Soot pathways. However, GRI Mech. 3.0 [26], was originally constructed for the simulation of natural gas combustion at high temperatures and low to medium pressures. Natural gas consists of 60-90%vol CH_4 and 40-10% vol H_2, and therefore the mechanism has a significant level of uncertainty while used for the simulation of multicomponent syngas fuels with variable amount of different gases.

NOx

For a comprehensive and complete syngas chemical kinetics mechanism, the implementation of a NOx sub-mechanism, applicable to simulate accurately the effects of the different gases and the combustion parameters on NOx formation is a necessary procedure.

However, the appearance of different combustible and non-combustible gases in the syngas that react differently with the temperature and affecting differently the formation of NOx, make the implementation of a NOx sub-mechanism a difficult and complex procedure. Only few detail mechanisms can be found that include full syngas and NOx chemistry.

Glaborg et al [91], performed an experimental and theoretical study for the detailed analysis of NOx formation on moist CO oxidation under post flame conditions (pressure 1 atm and temperature range 800-1400 K). The authors measured the concentrations of NO, NO_2, CO_2 and CO and used them for the development and validation of the NOx chemical kinetics mechanism. Moreover, the rate constants for NOx reactions were adopted from Tsang and Herron [92]. The developed model was in general in good agreement with the experimental results (general error lower than 10%). The authors made the conclusions that the presence of NO_2 and NO indeed has a significant impact on the consumption of CO at low temperatures ($T<1400$ K) through three major pathways: 1) At low NO concentrations, HO_2 radicals have been converted to OH radicals via reaction $NO+HO_2=NO_2+OH$ and that enhanced the

consumption of CO, 2) The catalysis of the chain-carrier recombination, increases the consumption of CO and 3) NO_2 was reacted as a scavenger of reactive radicals. However, at higher temperatures (T>1400 K), NO_2 showed an adverse effect than during low temperatures, and enhance the formation of reactive radicals [93].

Konnov et al [94, 95], developed a detailed H/N/O chemical kinetics mechanism for the investigation of the production rate of NO during the combustion of fuel lean, stoichiometric and fuel rich H_2/air mixtures in well-stirred reactors a temperatures between 1500-2200 K. The authors used steady state assumptions for the development of explicit expressions that used for the prediction of the instantaneous NO formation rate in a hydrogen flame. Moreover, the authors proposed a new possible chemical route for the formation of NO during fuel-rich hydrogen combustion. This route includes a sequence of chemical reactions related to N_2H_3 radicals and NNH chemistry. Recently, the authors updated the previous detailed model by implementing new NCN chemistry kinetic pathways applicable for the analysis of prompt – NO formation.

Dayma and Dagaut [96] investigated numerically and experimentally the oxidation of a diluted hydrogen system by using various concentrations of NO ($_XNO$ 220-250 ppm) and NO_2 ($_XNO_2$ 65-70 ppm) , at pressures 1-10 atm, temperatures between 700-1150 K and equivalence ratio 1.0. The authors developed a detailed model that was in a good matching with their data (lower that 8% uncertainty). According to the results from the numerical and experimental investigation, the authors concluded that the effects of NO and NO_2 on hydrogen oxidation can be attributed to : 1) unreactive radicals such as HO_2 are converted into OH highly reactive radicals via the reaction $NO+HO_2=NO_2+OH$ which in turn will be consumed via reaction $H_2+OH=H_2O+H$ promoting hydrogen oxidation, and 2) the generation of NO and high reactive OH via the reaction $NO_2+H-NO+OH$.

Rasmussen et al [97], proposed a detailed kinetic model for the analysis of the combustion of homogeneous $CO/H_2/O_2/NOx$ mixtures in laminar flow reactor at pressures 20-100 atm, temperatures between 600-900 K, eq.ratio 0.63 and ratios between NO/NO_2 : 36/113 ppm, 126/26 ppm and 145/6 ppm. Numerical results using the proposed model were compared with experimental data, reproducing well the formation and consumption of CO, CO2, NO_2, NO_2 and O_2 during the oxidation of $H_2/CO/O_2/NOx$ at high pressures. However, the model trends to over-predict the ignition delay time of syngas combustion.

As it can be observed from the literature, despite the fact that different mechanisms for NOx formation at different operational conditions have been developed, no mechanism was developed applicable to simulate accurately the effect of all of the syngas components (including CH_4) on NOx formation for a broad range of initial conditions, including high pressure/low temperature conditions. Only GRI Mech. 3.0 [26] that was analysed in the previous paragraph includes full methane, hydrogen and NOx chemical pathways. However, as it was mentioned earlier, it was developed for the simulation of natural gas and therefore the mechanism shows considerable uncertainty when used for the analysis of multicomponent syngas combustion.

Furthermore, different reduced NOx sub-models have been developed for the analysis of NOx formation. These sub-models are reduced versions of detailed models and can be implemented in syngas mechanisms as sub-mechanisms for the investigation of NOx formation. Such model is the 12 reaction sub-mechanism proposed by Pan et al [98] that was constructed based on the thermal NOx formation and therefore includes the full 3-step Zeldovich thermal model and important reactions affecting the formation of NOx at high temperatures. A second NOx sub-model, was proposed by Takeshi et al [99] and includes 19 reactions. The authors analysed the importance of HCN, CH and C_2H_2 on NOx prompt formation especially under fuel rich conditions. The authors concluded that implementation of the prompt chemical pathway allows more accurate analysis of soot emissions and therefore, they updated the model proposed by Pan et al [98] by incorporating important CH and HCN and NH_2 based reactions.

However, it has to be mentioned that the reduced NOx sub-models are usually less accurate than the detailed models due to the low number of reactions and species, while further optimization and upgrade of the reaction rate constants is required when implemented and coupled with syngas mechanisms. This is because the implementation of the NOx sub-models into the syngas chemical kinetics mechanism may affect the thermal and chemical stability of the model. Therefore, detail chemical analysis and validation are required before coupling such a model with multicomponent syngas mechanisms.

N-heptane

For the simulations of multicomponent syngas combustion for dual fuel engine applications, the effect of the diesel based fuel must be considered. The pyrolysis, partial oxidation and the combustion process of heavy hydrocarbons fuels such as n-heptane, is a complex chain radical process with a complicated temperature dependence, involving a very large number of reactions with hundreds of molecular and intermediate species. Therefore, in order to analyse

and understand the complex low and high temperature oxidation phenomena, it is very important to understand the different classes of primary propagation reactions that are involved in the oxidation process. Since the high and low temperature oxidation process of n-alkanes is similar with n-heptane, the different classes of primary propagation reactions during the high and low temperature oxidation are the same. The detailed mechanisms are based on 10 different classes of primary propagation reactions of alkyl radicals R* [75]:

Class 1: Alkyl radicals isomerization

Class 2: Alkyl radicals b-decomposition

Class 3: Formation of a conjugate alkene and HO_2* from the O_2 H-abstraction

Class 4: Formation of peroxy radicals (ROO*) from the addition of O_2 on R*

Class 5: Internal isomerization between hydroperoxyalkyl radicals (*QOOH) and peroxt radical (ROO*)

Class 6: Formation of aldehydes and small alkenes from the decomposition of *QOOH

Class 7: Formation of conjugate alkenes and HO_2* from the decomposition of *QOOH

Class 8: Formation of OH* and o-etherocycles from the decomposition of QOOH*

Class 9: Formation of hydroperoxyalkyl peroxy radicals (*OOQOOH) from the addition of O_2 on *QOOH

Class 10: Formation of ketohydroperoxides (OQOOH) from the decomposition of *OOQOOH

The flux diagram of the fuel RH oxidation, including the 10 different classes of primary propagation reactions of alkyl radicals, is shown in Figure 2-5. A double arrow used when isomerization takes place in the reaction step. For high temperature reaction pathways, the dashed line box was used, while the dash-dotted line box was used for low temperature reaction pathways. In the flux diagram, RH shows the fuel, R*, R'*, R"* , Q and Q' show the alkyl radicals, S, S' and S" are olefins, Sc and Sc* are the conjugate olefin of the fuel and its radical respectively. Finally, P1 and P2 are the decomposition products of the olefins [28, 100].

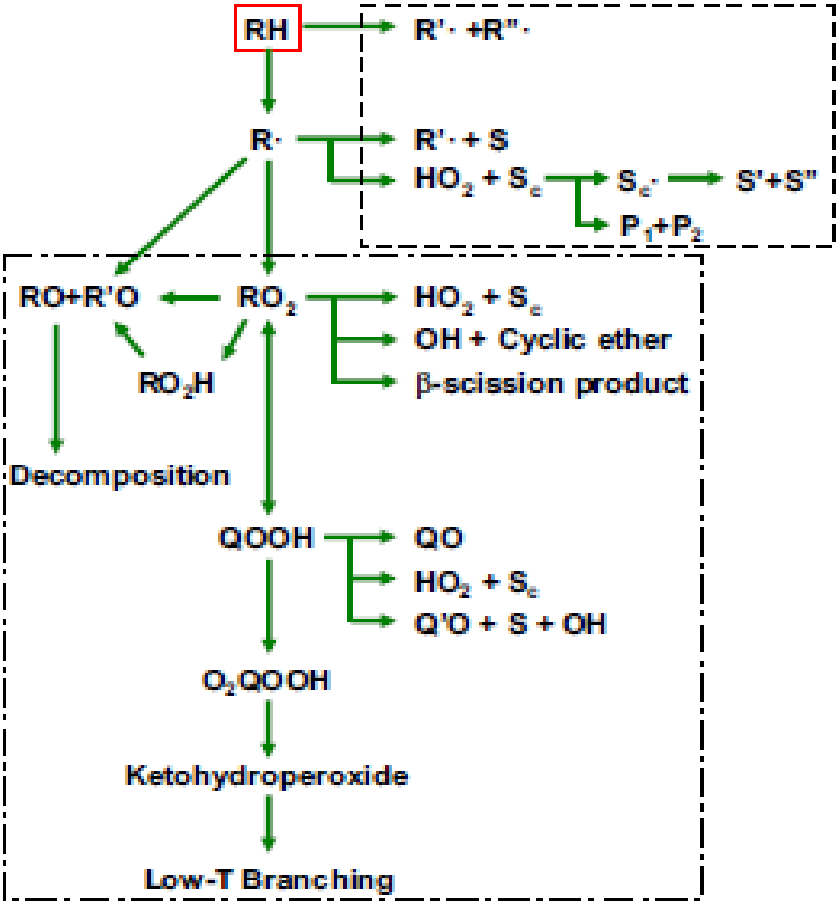

Figure 2-5 N-heptane oxidation diagram [28,100]

The oxidation of n-heptane has been the subject of numerous theoretical investigations. Different detail mechanisms have been developed for the simulation of n-heptane oxidation including low and high temperature oxidation and negative temperature coefficient (NTC) event. Curran et al [101, 102], performed a numerical investigation of n-heptane and iso-octane oxidation and developed a comprehensive detailed chemical kinetics mechanism for n-heptane oxidation. The n-heptane mechanism contains 2539 reactions and 560 species and was tested by comparing the simulated results with various experimental results. The mechanism captures accurately the low and high temperature oxidation of n-heptane, implying that the mechanism includes all of the important reactions and the associated reaction rates required for the accurate representation of n-heptane oxidation. Moreover, Mehl et al [27], proposed a new version of the detailed n-heptane mechanism proposed by LLNL laboratory [103]. The authors revised the mechanism by updating the reaction rates of HO_2/CH_3O_2 abstraction reactions and the reaction rates of the alkyl and alkoxy radical reactions. Finally, they incorporated a large block of reactions in order to improve the performance of the mechanism to simulate the low

temperature oxidation of unsaturated fuels such as hexenes and pentenes. The final mechanism includes 2526 reactions and 540 species and was validated against a wide range of experimental results in terms of ignition delay times and laminar flame speed.

Furthermore, Ranzi et al [104] proposed a reduced chemical kinetics mechanism for n-heptane oxidation. The proposed mechanism includes 1738 reaction and 106 species and was constructed based on the overall lumped mechanism POLIMNI_1212. The authors validated the proposed model against experimental measurements and simulated results by using the detailed model. The reduced mechanism showed a good level of similarity with the experimental results (lowest than 10% error) and captures accurately the low and high temperature oxidation of n-heptane as well as the NTC event.

By following the literature, it is obvious that n-heptane mechanisms are complex and contain large number of reactions and species. Mechanisms of such size require very high computational time for a complete simulation, while on the other hand it is very difficult to be implemented in CFD simulations due to the high complexity. Therefore, different studies have been performed and different reduced mechanisms have been developed for the oxidation of surrogates of conventional engine fuels such n-heptane. Seshadri et al [105] developed a reduced chemical kinetics mechanism for n-heptane. The mechanism consists of 6 overall steps. 23 species and 34 reactions and was used for the calculation of the burning velocities of premixed n-heptane flames. Tanaka et al [106] developed a reduced mechanism for the combustion of n-heptane in rapid compression engine. The model consists of 32 species and 44 reactions and incorporates full low temperature oxidation chemical pathways that were suggested in different comprehensive models [101]. However, the reduced model lacks of intermediate chemical pathways that are necessary for the accurate simulation of the NTC event. Moreover, the mechanism models the reactions from alkylketoperoxide to CO as a single irreversible reaction due to the absence of species with carbon number 2 to 5. Despite the fact that the model shows a good agreement with experimental results for ignition delay times using RCM, it shows a significant deviation with the measured ignition delay times obtained from shock tube experiments. The deviation between the experimental and simulated results is probably due to the oversimplification of the model and the absence of intermediate chemical pathways [100].

Recently, Ra et al [28] developed a reduced n-heptane/syngas mechanism for RCCI engine applications. The reduced mechanism was based on the detail mechanism proposed by Lawrence Livermore National Laboratory (LLNL) [103], and consists of 81 species and 312 reactions. The authors implemented syngas mechanism as a sub-mechanism and focused on

the co-oxidation reaction pathways of n-heptane and syngas. The reduced mechanism was validated against numerical and experimental results in terms of ignition delay times for n-heptane/syngas mixtures showing a good level of accuracy at all of the conditions. Finally the reduced model was implemented in a multidimensional CFD simulation for the analysis of the diesel fuel spray. Experimental measurements for in-cylinder pressure and heat release rate were used for the validation of the reduced mechanism. The proposed model showed high level of accuracy with calculated error between the simulated and experimental results below 8%. However, a main drawback of the proposed model is the fact that it does not include either methane or NOx chemical pathways that are necessary for the simulation of real syngas mixtures and the analysis of the emissions formation.

2.5 Mechanism reduction

A chemical kinetics mechanism consists of different species, with their associated transport and thermal properties, and elementary chemical reactions with their associated rate constants. Detailed analysis of the thermal and transport data files can be found in Chapter 3 Section 3.2.3. An elementary reaction that is included in the mechanism specifies the reactants, the products and the associated rate constants. For elementary reactions the general expression of the rate constant (k_{fR})is given by the standard Arrhenius equation:

$$k_{fR} = A_R T^{\mathrm{n}} \exp\left(-\frac{\mathrm{E}}{RT}\right) \tag{2.1}$$

where A_R is the pre-exponential factor, n is the temperature exponent and E is the activation energy of the reaction, while R is the universal gas constant [107]. The backward rate constant k_{rR} can be calculated then by the deviation between the forward rate constant k_{fR} and the equilibrium rate constant k_{eR} :

$$k_{rR} = \frac{k_{fR}}{k_{eR}} \tag{2-2}$$

Where the equilibrium rate constant k_{eR} is calculated by:

$$k_{eR} = \left(\frac{P_{1atm}}{RT}\right) \sum_{k=1}^{..} (n_{rk}" - n_{rk'}) \quad \exp\{\frac{1}{R} \left(\sum_{k=1}^{N} (n_{Rk}" - n'_{Rk})(s_k^0 - \frac{h_k^0}{T}) \right) \} \tag{2-3}$$

in which s_k^0 (J/K) and h_k^0 (J/K) are the entropy and the enthalpy during standard state and atmospheric pressure, P_{1bar}, conditions [107].

However, it has to be noted that even if the reaction rate of all of the reactions included in the mechanism is based on the original Arrhenius equation (Equation 2.1), different types of reactions can be found in a chemical kinetics mechanisms such as :

-Standard form

-Three body reaction

-Pressure dependence

-Landau Teller reaction.

Each one of the reaction types as well as the mathematical modelling behind the Arrhenius rate equation are described in detail in the numerical models and analytical methodologies chapter, Chapter 3, Section 3.2.3 of this thesis.

The number of reactions and species included in the mechanism depends mainly on the fuel mixture and the experimental conditions. For example, for the simulation of hydrogen combustion, the detailed San Diego mechanism [108] includes 268 reactions and 57 species. By assuming that multicomponent syngas mixtures include not only H_2 and CO but also CH_4, CO_2, N_2, it is understandable that a chemical kinetics mechanism for syngas combustion requires higher number of reactions and species. An example is the detailed GRI Mech. 3.0 [26] mechanism that includes 351 reaction and 180 species. The mechanism includes full H_2, CH_4, CO, CO_2 and N_2 chemistry as well as NOx chemistry.

Moreover, for large hydrocarbons fuels such as n-heptane, the number of reactions included in the mechanism increased significantly. As already explained in Section 2.4, the oxidation of large hydrocarbons is separated in three main stages: a) Low temperature, b) NTC and c) high temperature oxidation. In each one of the three stages, the combustion chemistry is driven by different chain branching stems including different reactions and species. One of the most famous and well validated detailed chemical kinetics mechanisms used for the simulation of the oxidation of large hydrocarbons, was developed by the Lawrence Livermore National Laboratory [103] . The detailed mechanism includes 2526 reactions and 540 species.

During this research, different detailed mechanisms have been used for validation and reduction purposes. A list of the detailed mechanisms used in this thesis is presented in Table 2-3

Table 2-3 Different detailed mechanisms that were used in this thesis

Mechanism	Description	No. of reactions	No. of species	Reference	Website
GRI Mech. 3.0	Syngas/ Natural gas	351	180	[26]	http://combustion.berkeley.edu/gri-mech/
LLNL Mech.	N-heptane	2526	540	[27,103]	https://combustion.llnl.gov/mechanisms/alkanes/n-heptane-detailed-mechanism-version-3
Frassoldati Mech.	H_2/CO and NOx	173	32	[76]	http://creckmodeling.chem.polimi.it/menu-kinetics/menu-kinetics-detailed-mechanisms/menu-kinetics-h2-co-mechanism
Creck Modelling Group Mech.	N-heptane	1738	106	[109]	http://creckmodeling.chem.polimi.it/menu-kinetics/menu-kinetics-reduced-mechanisms/menu-kinetics-reduced-n-heptane

Despite the fact that the detailed mechanisms have a great level of accuracy, they usually become unmanageable and require high computational time while used in multidimensional CFD simulations due to their large size.

Therefore, in order to reduce the size of the mechanisms but at the same time to retain the required level of accuracy, a two-stage reduction procedure must be followed. The first stage is the skeletal reduction by using different hand-made and numerical reduction techniques.

For hand-made reduction techniques, the reduced mechanisms can be achieved by hand on the basis of the experience and the knowledge of the user [110]. However, such mechanisms are often developed for a restricted or narrow range of conditions and therefore cannot be used accurately for the simulation of various combustion conditions, for example different temperatures, pressures or equivalence ratios. Therefore, it is beneficial to use general numerical reduction methods that will automatically reduce the mechanisms based on the physical quantities related with the species or reactions included in the mechanism.

Numerical reduction methods are usually implemented in different software such as DARS [111] and Chemkin [112] or they can be developed by using mathematical software such as Matlab [113]. Different numerical reduction techniques that are often used by researchers are; the reaction flow analysis [114], sensitivity analysis [115], necessity analysis [116] and direct relation graph (DRG) [117, 118]

For each numerical reduction technique, a set of selection criteria can be used based on different combustion parameters. Through the identification of the set of selection criteria, the

species or reactions that play a minor role in the combustion process could be identified and eliminated from the mechanism, reducing its size [110].

The new reduced size mechanism that was developed from the first reduction stage is called skeletal mechanism and is validated against experimental and simulated results by using the original mechanism in order to ensure its accuracy.

The second reduction stage includes further reduction or optimization of the skeletal mechanism by using different time-scale separation methods. By using these time-scale separation methods, the reactions time and the life-time of the species included in the mechanism are calculated and compared with the time required for different physical processes to be triggered such as the diffusion and the turbulence or the life-time of other reactions. Thus, some reactions can be considered as being fast or short-lived and can be eliminated or their rate constants can be updated. Such time-scale separation methods are:

a) The level of importance (LOI) analysis, concerns the species chemical lifetime, or a function of its lifetime, as a selection criterion. Species with the lowest lifetime, usually, are attached with the lowest level of importance and can be assumed redundant [119].
b) The computational singular perturbation analysis (CSP), in which the set of differential equations that govern the system is rewritten and a new set of basic vectors is used. The new vectors are then used to describe the fast and the slow sub domains of the skeletal mechanism and they contain a linear combination of the reaction rates that involved in the original detail mechanism. The problem will be then converted to one of an eigenvalue problem and the fast "sub-domains" which includes fast, short-live species can be identified and removed or updated [120].
c) The intrinsic low dimensional manifolds technique (ILDM) in which attractive manifolds for the chemical kinetics are involved in the mechanism. According to Maas et al [121] and Schmidt et al [122], the attractive manifolds are equilibrium solution spaces in which the fast reactions relax towards and the slow reactions are moving within. The time-scales of the reactions included in these manifolds can then be calculated and therefore a time separation of the fast chemical processes can be achieved [121]. The fast and short-lived reactions can then be identified and optimized or removed from the mechanism.

While the mechanism has been further reduced by using the time-separation methods, is finally validated against experimental results in order to ensure its accuracy level. A schematic overview of the general reduction process (including the first and second reduction stages) can be found in Figure 2-6. The starting step is the detailed chemical kinetics mechanism that was validated against experimental results, showing a high level of accuracy. Then, the first reduction stage is conducted in which the detailed mechanism is reduced by using numerical reduction techniques and a skeletal mechanism is generated. Finally, the second reduction stage is followed and the generated skeletal mechanism is validated or further reduced by using time scale separation methods.

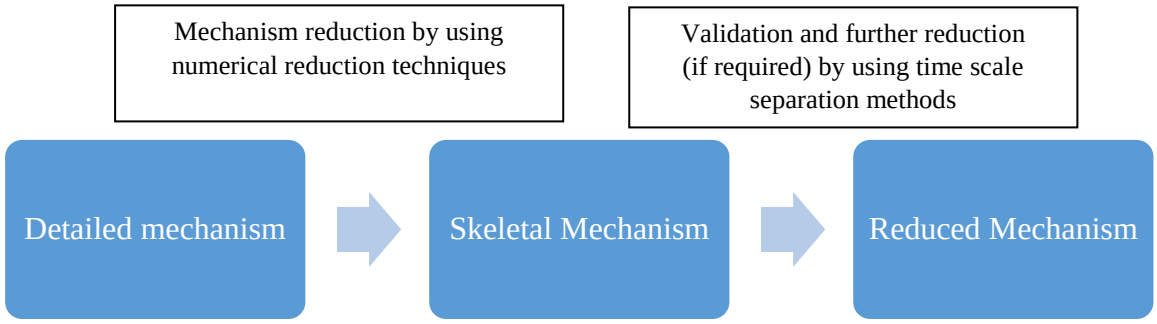

Figure 2-6 Mechanism Reduction procedure [110]

During this research study three different computational techniques were used for the mechanism reduction and the analysis of the combustion chemistry. First, sensitivity analysis was used for the identification of the most sensitive (important) species/reactions during high pressure conditions. Then, reaction flow analysis was conducted for the investigation of the importance of the reaction paths in the mechanism under high pressure conditions. Species with the lowest calculated net flow are eliminated from the mechanism. Finally, necessity analysis was used for the elimination of the less necessary species and the development of the skeletal mechanism. Necessity analysis is an advanced hybrid reduction method that uses both sensitivity analysis and flow analysis techniques for the identification of the species and reactions that are most necessary for the consumption or the formation of user-set important species/targets. Species with the lowest necessity factor can be removed from the mechanism. A detail description of each reduction technique that was used during this project, including the mathematical equations, can be found in Chapter 3.

2.6 Summary

In this chapter, literature information regarding syngas production, the application of syngas in dual fuel engines, the combustion chemistry of syngas and the numerical modelling of syngas combustion are described. Syngas is produced by the gasification of natural feedstock or coal and consists of different components such as H_2/CO/CH_4/CO_2 and N_2. The proportion of each component included in the syngas depends mainly on the gasification procedure and the type of feedstock or biomass that was used for tis production. For example by using O_2 as a gasyfing agent, the produced gas includes high concentration of H_2 and CO while on the other hand by using steam the concentration of CH_4 included in the syngas increased significantly. The produced syngas can be used as fuel for heat and power production or it can be further used and converted ,via a chemical conversion process, for example fermentation, into transportation fuels and other chemicals.

Despite the fact that different types of internal combustion engines can be found in the market, this thesis is mainly focused on syngas combustion in pilot-ignited dual fuel engine applications. In this type of engine, a surrogate diesel based fuel is used for the combustion initiation and the autoignition of the primary premixed syngas fuel. This is because syngas has high ignition temperature and therefore a secondary diesel based fuel with lower autoignition temperature is required in order to increase the in-cylinder temperature and finally to ignite the syngas. N-heptane was found to have similar physical and chemical characteristics with diesel and therefore was used as a surrogate for the diesel fuel in the rest of this thesis. However, the amount of n-heptane that is injected in the cylinder plays a critical role on the combustion process and the formation of emissions and therefore should be controlled by using micro-pilot.

Due to the fact that syngas mixture consists of different components that react differently at different conditions, different experimental studies have been conducted for the investigation of the effects of those components on syngas combustion and NOx formation. According to the literature, by using rich mixtures, the combustion temperature is higher in comparison with lean mixtures and that results in higher NOx emissions. Therefore, it can be concluded that lean mixtures are more suitable for use in internal combustion engines.

From the numerical point of view, different chemical kinetics mechanisms have been developed for the simulation of H_2/CO syngas combustion but only few detailed mechanisms include not only H_2 and CO but also CH_4 and NOx chemistry. Moreover, for the simulation of syngas combustion in dual fuel engines, n-heptane chemistry should be included as the co-oxidation between syngas and n-heptane plays a major role on the combustion process.

Standalone n-heptane mechanisms include a high number of reactions and therefore it is very difficult and time ineffective to be implemented in multidimensional CFD simulations for the analysis of the combustion chemistry and its interactions with the turbulence.

For the reduction of the detailed mechanisms, a two stage reduction procedure is used by researchers: 1) First a skeletal reduction procedure is followed by using different hand-made and numerical reduction techniques and 2) The skeletal mechanism is further reduced or optimized by using different time-scale separation methods. Finally, the reduced mechanism is validated against experimental results in order to ensure its accuracy level. However, the user (researcher or manufacturer) must be careful due the fact that elimination of important reactions may reduce the accuracy level of the mechanism.

By summarizing the conclusions from the literature review, it can be concluded that, the analysis of the combustion chemistry of syngas in dual fuel engines is a difficult and complicated procedure as it includes different chemical components that react different at different operational conditions and affect significantly the formation of NOx. Moreover, it can be concluded that despite the fact that different mechanisms for H_2/CO syngas combustion can be found in the literature, the development of a reduced accurate and robust chemical kinetics mechanism that will be able to be implemented in multidimensional CFD simulations for the analysis of syngas combustion, NOx formation and n-heptane/syngas co-oxidation remains elusive.

Chapter 3: Numerical models and analytical methodologies used for modelling in-cylinder combustion

During this research, the modelling of the combustion process and the investigation of the combustion chemistry have been achieved by following a two-stage modelling procedure. Firstly, zero (0D) and one (1D) dimensional simulations were conducted for the analysis of important combustion characteristics (LFS, ignition delay time and the concentration of important NOx species), the analysis of the combustion chemistry and the reduction of the chemical kinetics mechanisms.

Next, a multidimensional CFD analysis was conducted for the simulation of multicomponent syngas combustion in a supercharged micro-pilot ignited dual-fuel engine. Numerical results by using the developed mechanisms were compared with experimental measurements. The flow chart of the modelling procedure followed during this research for the development of the reduced mechanisms is presented in Figure 3-1.

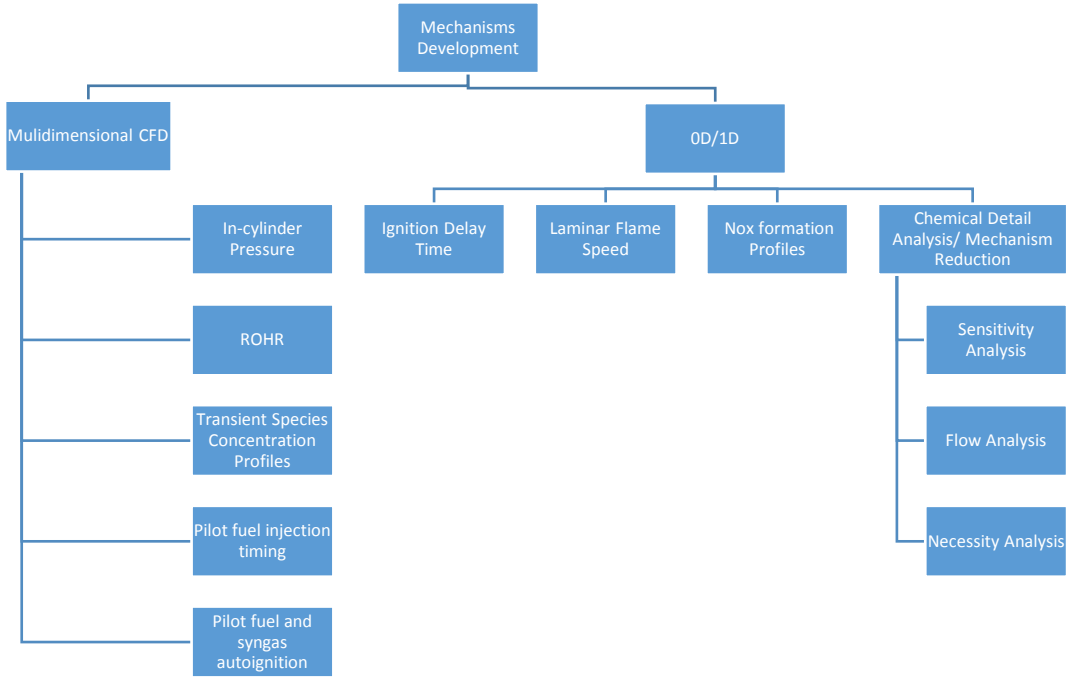

Figure 3-1 Flow chart of the modelling procedure.

This chapter aims to introduce the important combustion parameters such as the LFS, ignition delay time and NO formation and analyse the mathematical background of each of these parameters. Additionally, a detail description of the experimental set-up, the engine geometry and the mathematical models used for the spray modelling, the turbulence model, the mass and species flow rate and momentum conversation equations and the chemical reaction flow

governing equations that were used during the CFD analysis are presented. Finally, all of the fuel mixtures that were collected from the literature and used in this research are summarized and presented.

3.1 0D and 1D simulations

Zero and one-dimensional chemical kinetic analyses were performed using the Digital Analysis of Reaction Systems (DARS) [123]. DARS enables the detailed analysis of the combustion chemistry, focusing on internal combustion engines. For this research study, important combustion parameters such as the flame speed, the ignition delay time and NO concentration profiles were simulated by using different combustion models implemented in DARS such as the HCCI engine model, the rapid compression machine model (RCM), the constant volume (CV) and freely propagating flame model. Additionally, the combustion chemistry was analysed by using the reacting flow and sensitivity analysis methods, while the mechanism reduction was achieved by using necessity analysis method.

3.1.1 Ignition delay time

In internal combustion engines, the ignition delay is defined as the time difference between the start of the fuel injection and the initiation of the combustion. This time period is affected by physical factors such as the vaporization and the atomization of the fuel and the mixing between the air and the fuel. Additionally, it is affected by chemical factors such as the low temperature and pre-combustion reactions that are activated prior to the combustion and during the fuel injection into the combustion chamber [124]. The combustion initiation is usually characterized by a rapid increase of the in-cylinder pressure tracers and an increase in the concentration of OH radicals. OH, is highly sensitive to the temperatures variations, the higher the temperature the higher is the concentration of the OH radicals and therefore the more intense is the combustion. Due to this direct relationship between the temperature and the OH concentration, many researchers characterized OH as a marker of the temperature rise and the ignition occurrence [66, 125]. Therefore, during such studies, ignition delay times were calculated based on the slope of the pressure tracers or based on the maximum slope of the OH concentration [126, 127].

Experimental studies related to ignition delay times were mostly performed by using shock tubes experimental apparatus at pressures 1-49 atm and temperature range 950-1950 K [128]. For the simulation of the experimental ignition delay times obtained by using shock tubes, the ignition delay times were simulated by using a constant volume reactor incorporated in DARS

software and assuming adiabatic conditions [129]. By changing the experimental apparatus from shock tube to constant volume, may result in inaccuracies and errors during the calculation of the ignition delay times. However, for ignition delay times lower than 1ms, the effect of the constant volume can be assumed to be negligible [130].

Moreover, the performance of the developed mechanisms to simulate the ignition delay time in an HCCI was investigated by comparing the simulated results obtained by using the developed mechanisms with the numerical results obtained by using other well-validated mechanisms available in the literature. This is because of the absence of experimental data related to ignition delay times using HCCI engines. For the simulations, the HCCI reactor module incorporated in DARS was used. For DARS HCCI analysis the simulation was run for 265 crank-angle degrees (CA°) while the intake-valve closure (IVC) time was 135 CA° before top dead centre (BTDC). The gas mixture pressure and temperature at IVC were 225 kPa and 450 K, respectively.

3.1.2 LFS

One of the most important parameters used by researchers for the investigation and the analysis of the combustion process is the LFS. The importance of the LFS lies in the fact that it serves as the basis for the turbulent combustion and is directly related with the mixture reactivity, intensity, exothermicity and diffusivity. Additionally, many researchers have studied LFS in order to understand the spatial distribution of the flame and to analyse phenomena such as the blow off and the propensity of the fuel to flashback [131, 132].

In this thesis, LFS was used as a validation parameter for the developed chemical kinetics mechanisms. For the simulations of the LFS, the one-dimensional freely propagating module incorporated in DARS was used [133]. For the laminar flame simulations, the laminar flame propagated front is assumed to travel perpendicular to a z-axis. The mixture of fuel and oxidant is travelling towards the z-direction while the burned mixture propagates at z->+00 and the unburned mixture at z->-00 direction. In order to understand the LFS behaviour, it is important to understand first the mathematical correlations and more specifically the species and energy conservation equations behind it. First, the general continuity equation (Equation 3.1) is used as a base which represents the overall mass conservation equation. Then the species conservation equation (Equation 3.2) describes the mass fraction changing rate of the species *i* in the flow field because of the production rate ω_i and the diffusion *ji* over the field zone. Finally, the energy conservation equation (Equation 3.3) is defined by the general assumption

that the total energy in the system is not changed. According to Equation 3.3, the changing rate of the heat that is transported by the gas convection is equal to: a) the heat transfer because of the conductivity (term 1 (A) on the right side of the Equation 3.3), b) the rate of change because of the enthalpy release during the species production (term 2 (B) on the right side of the Equation 3.3), c) the thermodiffusion (term 3 (C) on the right side of the Equation 3.3) and d) the radiation (term 4 (D) in the right side of the Equation 3.3) [133].

The continuity (overall mass conservation) Equation:

$$\frac{d(pu)}{dz} = 0 \qquad [\text{kg}/(\text{m}^3.\text{s})] \qquad (3.1)$$

The species conservation Equation:

$$pu\left(\frac{dY_i}{dz}\right) = -\left(\frac{dj_i}{dz}\right) + \omega_i \qquad [\text{kg}/(\text{m}^3.\text{s})] \qquad (3.2)$$

The energy conservation Equation:

$$puc_p\left(\frac{dT}{dz}\right) = \underbrace{\left(\frac{d}{dz}\right)\left(\lambda\left(\frac{dT}{dz}\right)\right)}_{A} \underbrace{-\sum_{i=1}^{N_s} h_i\omega_i}_{B} \underbrace{-\sum_{i=1}^{N_s} c_p j_i \frac{dT}{dz}}_{C} \underbrace{-4\alpha\sigma(T^4 - T_0^4)Vf_r}_{D} \qquad [\text{J}/(\text{m}^3.\text{s})] \qquad (3.3)$$

where the density is symbolized by ρ, the gas velocity component is u, the mass fraction of species i is Y_i, $j_i$is the diffusion flux, u_i is the diffusion velocity, ω_i=$Wi\Sigma vi$ is the production rate of species i where W_i is the molecular weight, c_p is the heat capacity at constant pressure, λ is the thermal conductivity, h_i is the specific enthalpy of species i and $N_s$is the number of species. α is Planck's constant, σ the Stefan Boltzmann constant, T_0 the temperature of the surroundings and f_r is the fraction of volume between the high temperature burned gas and the lower temperature unburned and is called the radiation factor.

The radiation and thermal diffusion factors were highlighted by previous studies [21, 134, 135] as very important for the accuracy of the LFS simulations. Keromnes et al. [21] showed that the exclusion of the radiation and thermal diffusion factors from the simulations increase the calculated LFS by 8% for a stoichiometric mixture. Therefore, during this research it was decided that both of these factors will be included in all of the simulations.

Moreover, the convergence parameter in DARS was adjusted so that the convergent solution could be obtained by using 400 grid points. Finally, the initial and boundary conditions used for the simulations were taken directly from the experimental measurements, allowing a direct comparison between the simulated and experimental results.

3.1.3 Sensitivity analysis

Sensitivity analysis is one of the most common methods used by researchers for the investigation of the chemical combustion, the identification of the most important species/reactions during the combustion process and the reduction of the chemical kinetics mechanisms. During sensitivity analysis the changes in a quantity of interest (species/reactions) resulting from the changes in the controlling parameters are investigated. By using DARS, the sensitivities are transported through the mechanism and each species or reaction is rated based on its own importance to consume or produce other important species. Mathematically, the species sensitivity towards a chosen parameter, A_{ar}, is calculated by the summation of the reactions sensitivities in which the species takes part [111]:

$$S_{A_{ar},i}{}^{S} = \frac{\partial \psi_{A_{ar}}}{\partial c_i} \approx \sum_{k=1}^{N_r} \frac{\partial \psi_{A_{ar}}}{\partial r_k} \frac{\partial r_k}{\partial c_i} \tag{3.4}$$

in which, $S_{A_{ar},i}{}^{S}$ is the sensitivity of the arbitrary chosen parameter A_{ar}, in the vectors of unknowns $\psi_{A_{ar}}$, towards species i. The final sensitivity of the species or reaction can then be calculated by the differentiation of the last term of Equation 3.4. The final mathematical expression of the species sensitivity analysis is given by:

$$S_{A_{ar},i}{}^{S} = \left[\sum_{k=1}^{N_r} \frac{\partial \psi_{A_{ar}}}{\partial r_k} \times \frac{u'_{i,k}}{c_i} r_k\right] \tag{3.5}$$

in which $u'_{i,k}$ is the stoichiometric coefficient of the species i in the reaction k, c_i is the species i concentration and r_k is the reaction k rate.

As it was stated earlier the accumulation (formation or consumption) of radicals has a direct relationship with the sensitivity factor of each reaction [136]. Reactions that are responsible for the fast consumption of radicals are assigned with a negative sensitivity factor while reactions that are responsible for the formation of radicals are assigned a positive sensitivity factor. However, it has to be mentioned that despite the fact that some reactions are responsible for the consumption of radicals and have negative sensitivity factor, they may be responsible for the formation of other high reactive species and therefore to increase the reactivity of the mixture. For example, reactions $H_2O_2+M=OH+OH+M$ and $H_2O_2+H=H_2+HO_2$ who, on the one

hand, are responsible for the fast consumption of H_2O_2 and HO_2 radicals respectively and therefore they have negative sensitivity factor, but on the other hand are responsible for the formation of high reactive OH species and therefore increase the reactivity of the mixture.

Moreover, a redundancy index is assigned for each species. The redundancy index of each individual species shows how important the specific species is to the changes of the selected parameter in relation with the other species included in the mechanism [110]. The redundancy index, I_i, is calculated by:

$$I_i = \frac{{S_{Ar,i}}^S}{\max\limits_{k=1,N_S}({S^S}_{Ar,k})} \tag{3.6}$$

Species with high redundancy index are characterized as redundant and can be eliminated from the mechanism during the reduction process.

3.1.4 Flow analysis

Reaction flow analysis investigates the importance of the reaction paths in the mechanism under the conditions specified by the user. During flow analysis, the transfer rate of important atomic species, such as C, O, H and N, is calculated. The backward and forward reactions are analysed separately in order to capture the reaction pairs, which have a high flow of atoms in both directions, but the net flow may be low [110, 111].

Two main flow parameters were used for the investigation of the backward and forward reactions. The flow f_{ij}^o, of atom *o* during the formation of species *i* from species *j*, Equation 3.7, and the flow c_{ij}^o, of atom *o* during the consumption of species *i* and *j*, Equation 3.8.

$$f_{ij}^o = \sum_{k_f=1}^{N_R}(r_{k_f}\, \mathrm{u'_{j,k_f}}\, \mathrm{u''_{i,k_f}})\, \frac{n_i^o}{\Delta n_{k_f}^a} \tag{3.7}$$

$$c_{ij}^o = \sum_{k_b=1}^{N_R}(r_{k_b}\, \mathrm{u''_{j,k_b}}\, \mathrm{u'_{i,k_b}})\, \frac{n_j^o}{\Delta n_{k_b}^a} \tag{3.8}$$

Where r_{k_f} is the reactions *k* rate, $u'_{j,k}$ and $u''_{j,k}$ are the reactants and products stoichiometric coefficients in reaction *k*. The subscript *f* represents the forward and *b* the backward reactions. n_j^o is the number of atoms and is normalized to the total number of atoms transported in the reaction, $\Delta n_{k_f}^o = \sum_{i=1}^{N_s} u'_{i,k_f}\, n_i^o$.

Finally, the net flow $F_{i,j}^{o}$ for each species and atom is calculated by:

$$F_{i,j}^{o} = \int_{t=t_0}^{t_1} f_{ij}^{o}\, dt - \int_{t=t_0}^{t_1} c_{ij}^{o}\, dt \tag{3.9}$$

The higher the calculated net flow is between two species, the more important are the species to the mechanism. Species with relatively low net flow can be assumed redundant and can be removed from the mechanism, as they are not significantly affecting the formation or the consumption of other species.

3.1.5 Necessity analysis

During this thesis, the necessity analysis reduction method was used for the reduction of the n-heptane mechanism which was then coupled with the syngas/NOx mechanism for the construction of the final reduced n-heptane/syngas/NOx mechanism, see Chapter 7. Necessity analysis is a hybrid reduction method that combines both sensitivity analysis and flow analysis methods in order to find the species and reactions that are most necessary (important) for the consumption or the formation of user-set important species/targets [116, 137]. The species with the lower necessity factor (redundant species) were identified by the simultaneous use of both reaction flow and sensitivity analysis methods.

First, the species with high sensitivity factors that are necessary and significantly affect the combustion process were identified via the sensitivity analysis method. Then, the transfer rates of important atoms such as H, O, N and C between the species in the reaction mechanism are calculated by using the reaction flow analysis. Both the mathematical correlations and the numerical equations used for the calculation of the sensitivity factor and the atoms flow were described in detail in the previous Sections 3.1.3 and 3.1.4.

By the combination of sensitivity and flow analysis methods a necessity factor is calculated based on the importance of the species itself on forming and consuming important species and from the flow of atoms to and from the important species in the mechanism [116, 137]. The necessity *N* of species *i* is calculated by:

$$N_i = \max(I_j\, f_{ij}^{o}, I_j c_{ij}^{o}, I_i; j = \{1, N_S\}, o = \{1, N_o\}\,) \tag{3.10}$$

Where the first value of *Ni* is calculated further by:

$$N_{i,0} = \max\left(\frac{{s_{j,i}}^{S}}{\max\limits_{k=1,N_S}\left({s^S}_{j,k}\right)}, B_i\right) \tag{3.11}$$

$S_{j,i}{}^{S}$ is the sensitivity of species j to species i and $S_{j,k}{}^{S}$ is the sensitivity of species j to species k. N_s and N_o are the total number of species and atoms respectively, k denotes a species and B_i takes on the value 1 or 0 if species i is set as a necessary species by the user or not. $f_{i,j}^{o}$ is the weighted flow of atoms from species j to species i and $c_{i,j}^{o}$ is the weighted consumption of atoms from species i to species j . Both are calculated through flow analysis. Finally, $S_{j,I}^{S}$ and $S_{j,k}^{S}$ contain the information of how sensitive the species j is towards i and k respectively and is calculated by the sensitivity analysis method. Once necessity analysis is over, a necessity factor is calculated for each individual species in the mechanism based on its own importance regarding a specific combustion parameter. In that case, the combustion parameter was temperature. The necessity factor varies between 0 and 1. The closer it is to 1, the more important is the species, while the closer it is to zero, the lowest is the importance of the species and it can therefore be eliminated from the mechanism. The reduction, then, is performed manually by the user based on the attached necessity factor.

3.1.6 NOx formation

One of the main characteristics of syngas fuels are the low NOx emissions that are produced during their combustion. By using the term NOx, researchers usually refer to the amount of NO and NO_2 species that are included in the NOx. NO is the dominant species during NOx formation while NO_2 appears in much lower amount. Other nitrogen oxides such as N_2O, N_2O_4 and N_2O_5 are also formed in negligible amounts during NOx formation [138, 139].

Due to the fact that environmental pollution caused by exhaust gas emissions is seen as a major problem nowadays, the formation and consumption of NOx during the combustion in IC engines has been studied extensively during recent years. Different experimental studies can be found that have investigated the effect of individual syngas components on the amount of NO and NO_2 formed, highlighting the effect of the CH_4 and H_2 addition on the reduction of NOx [69, 140, 141]. Asgari et al. [140], investigated the NOx formation in post-flame gases from syngas/air combustion at atmospheric pressures. The authors showed that for H_2/CO mixtures, increasing the equivalence ratio from lean to stoichiometric (0.5 to 1.0) results in the reduction of NO_2 concentration while NO concentration increased. Van Huynh et al. [69] investigated the combustion of syngas and NOx emissions at different gasification conditions utilizing oxygen-enriched-air and steam. They observed that NOx emissions were lower when lean fuel mixture (equivalence ratio < 0.5) was used and the heat release rate decreased. Moreover, Choudhuri et al [141] analysed the combustion characteristics of hydrogen-natural

gas hybrid fuels. The authors changed the concentration of natural gas included in the mixture between 0-35 %vol in order to calculate and compare the influence of natural gas addition on NOx emissions. They showed that by increasing the concentration of natural gas in the mixture the flame luminosity and the flame length also increased, while NO and NOx emissions decreased monotonically with the increase in natural gas. By summarized the results obtained from different experimental studies it can be concluded that increasing the concentration of H_2, results in an increase of NOx emissions. However, more experimental studies needed for a complete understanding of the effect of the general syngas mixture (not individual component included in the syngas mixtures such as H_2 and CH_4) on NOx.

From the numerical prospectus, NOx formation is divided in three different formation types, as already highlighted in the literature review section. Each type includes different chemical kinetics pathways applicable for the simulation of NOx formation at specific conditions. The first type is thermal NOx, the second the prompt NOx and the third one the Fuel NOx formation type.

Thermal NOx formation

Thermal NOx formation describes the interaction between the O_2 and the N_2 that exist in the combustion air in order to form NOx. This process is temperature depended as it requires very high temperatures (above 1500 K) to be triggered and therefore is characterized as non-linear [142]. This is because in–cylinder local areas may have higher than average temperatures, which results in higher amounts of NOx than that produced in the rest of the cylinder. Additionally, the amount of NOx produced during the thermal NOx formation process is also affected by other factors such as the residence time, which is a description of the time-period that the combustion gas has very high temperatures [143, 144]. At temperatures below 1500 K, the characteristic residence time in typical gas turbine combustors is lower in comparison with the residence time for temperatures above 1500 K [145, 146]. Therefore the produced thermal NOx at low temperatures (<1500 K) / low residence time is significantly lower than for high temperature (>1500 K) / high residence time conditions [145, 146].

In order to model the thermal NOx formation process, a three-stage chemical kinetics mechanism was used. The mechanism is called the Zeldovich mechanism and is written in the form of equilibrium reactions:

$$N_2+O=NO+N \quad (3.12)$$

$$N+O_2=NO+O \quad (3.13)$$

$$N+OH=NO+H \quad (3.14)$$

Among the three reactions, reaction 3.12 determines the rate of the thermal NOx formation as it requires very high temperatures to be triggered [147]. This is because of the strong triple bond in the N_2 molecule that requires a high amount of thermal energy to break. Usually, the minimum temperature required for this reaction to be activated is around 1400 K while the produced NO reaches its maximum at temperatures over 1900 K [148, 149].

Fuel NOx formation

Fuel NOx formation describes the process where oxygen included in the combustion air interacts with the nitrogen included in the fuel mixture to form NOx. The amount of bound nitrogen included in the gaseous fuels, especially in syngas, is much lower than the amount of bound nitrogen included in coal or oil [150]. Therefore, the amount of NOx produced during syngas combustion is lower compared to the NOx emissions produced by using other types of fuels [149, 151]. In contrast to the thermal NOx formation type, fuel NOx formation type does not have a specific chemical kinetics pathway to model the fuel/NOx formation process as it depends on the fuel type (gaseous or liquid) and the mixture's composition. However, it can be represented by the two general equation:

$$N_{fuel} + OH \Leftrightarrow NO + X \quad (3.15)$$

$$N_{fuel} + NO \Leftrightarrow N_2 + X \quad (3.16)$$

Where N_{fuel} represents the nitrogen oxidation species that are formed during the combustion of the specific fuel and X symbolizes the reaction products that depend on the fuel and the oxidants. In general, Reaction 3.15, describes the formation of NO during the consumption of high reactive OH radicals, while Reaction 3.16 is responsible for the formation of N_2 and the consumption of NO [144,146].

Prompt NOx formation

The last NOx formation type is called Prompt NOx formation. During this process the radical hydrocarbon fragments that are produced during the fuel combustion, interact with the molecular nitrogen (N_2) that exceeds in the combustion air for the formation of transition substances which then will be oxidized (reaction with the oxygen included in the combustion air) for the formation of NOx [148]. The prompt NOx formation process can be described by:

$$CH + N_2 = HCN + N \quad (3.17)$$

$$N+O_2=NO+O \quad (3.18)$$

$$HCN+OH=CN+H_2O \quad (3.19)$$

$$CN+O_2=NO+CO \quad (3.20)$$

Where the radical hydrocarbon fragments, for example CH react with N_2 for the formation of transition substances (for example HCN) and atomic nitrogen (N). The atomic nitrogen will be then oxidized for the formation of NO, Equation 3.18, while the transition substances will be further decomposed, Equation 3.19, and finally oxidized for the formation of NO, Equation 3.20.

The amount of NOx that is formed during that process has a relatively weak temperature dependence and a very short lifetime of only several microseconds [152]. Moreover, the contribution to NOx emission from this formation type is very important in systems that use fuel-rich mixtures and produce very fuel-rich flames, for example staged combustion systems. While for utility furnaces that use lean mixtures the contribution of prompt NOx to the total NOx is very low in comparison with fuel NOx type [153].

Similar with the fuel NOx formation type, the chemical kinetics sub mechanism that is used to model the prompt NOx formation depends on the fuel mixture that will be used and the combustion conditions.

NOx modelling

As can be clearly understood, modelling NOx formation is a complicated and difficult three-stage procedure that depends on different factors such as the in-cylinder temperature variations, the turbulence, the fuel mixture composition and the time-period that the combustion gas has very high temperatures. Therefore, a robust and accurate NOx chemical kinetics mechanism should include the most important reactions for each one of the three formation types and additionally, the rate constants of the reactions should be adjusted in order to minimize the risk of errors due to the temperature dependence.

During this research, a 12 reaction step NOx model proposed by [98] was tested and adopted into the reduced syngas mechanism. The NOx sub-mechanism includes the full three-step Zeldovich sub-model as well as important reactions required for modelling prompt and fuel NOx formation processes [154]. The 12 reaction step NOx mechanism that was used in this thesis can be found in Chapter 5, Table 5-1.

The performance of the chemical kinetics mechanisms in terms of NOx prediction was evaluated by using experimental results from the literature, obtained by using flat flame burner

and jet wall stagnation flame experiments. Similar to the LFS simulations, the one-dimensional freely propagating module available in DARS, was used. The mole fractions of NO are then calculated along the axial distance of the burner, allowing a direct comparison with the experimental data. Radiation factor and thermal diffusion are included in all of the simulations and, similar to the LFS calculations, the convergence parameters were adjusted so that at least 400 grid points were used, in order to ensure the accuracy of the simulations.

3.2 Multidimensional CFD simulations

For the multidimensional CFD simulations, STAR-CD V.4.2 software was used [107]. In order to formulate and resolve complex gas-phase chemistry problems, STAR-CD was linked with thermodynamic and transport databases of CHEMKIN. The thermodynamic properties of the computational cells were incorporated in CHEMKIN database, which in turn resolves complex chemistry equations and returns the new thermochemical properties of the species [112]. By obtaining the new calculated thermodynamic information for all the computational cells, different sub-models were activated for the calculation of the flow rate between the cells, the heat transfer and mass transfer. Reynolds averaged equations were used to incorporate the turbulence, the chemistry and the n-heptane liquid spray models into the CFD. More specifically, a high Reynolds $k-\varepsilon$ model was used for the turbulence description by using a standard wall function. For an accurate and detailed analysis of the combustion process, the model is based on the experimental specifications. Cylinder wall and cylinder head temperatures were set to 450 K, while the piston surface temperature was set to 500 K. PISO algorithm was implemented into the model for the transient flow calculation. The properties of the fuel atomization were calculated by using the well-known Reitz-Diwakar model [155, 156]. It is worth mentioning here, that due to the complexities in coupling the turbulent flame speed sub model with the complex chemistry, no laminar flamelet model was incorporated in the CFD simulations. The flame velocity was calculated by using the thermochemical and transport properties of the species included in the mechanism. Engine specifications including initial parameters, geometry mesh dimensions, injection timing and combustion initial parameters such as the temperature and pressure at IVC were taken directly from the experimental apparatus, allowing for an accurate and direct comparison with the experimental data.

During that section, the experimental set-up that was used, the geometric mesh of the cylinder and the set of mathematical modelling equations that were employed in the STAR-CD for the thermofluids analysis and the calculation of the fluid flow, heat and mass transfer and the complex chemical kinetics were analysed.

3.2.1 Experimental set-up

The multidimensional CFD simulations were performed for the simulation of syngas combustion in a in a water- cooled four-stroke single-cylinder engine with two intake and two exhaust valves [62]. In this engine, a small amount of diesel-base pilot fuel is injected into the combustion cylinder prior the top dead centre (TDC), and autoignited due to the in-cylinder temperatures. The autoignition of a small quantity of diesel pilot fuel increases the in-cylinder temperatures and ignites the primary premixed syngas fuel. In order to ensure that only small amount of diesel-base fuel was injected, a commercial solenoid-type injector was modified. Modifications including the replacement of the seven-hole nozzle of the commercial injector by one with four holes, each 0.1 mm in diameter. The duration and the injection time of the diesel-base fuel were controlled through an injector driver which transferred signals to the injector. Furthermore, a common-rail injection system was used to supply to the injector at a constant injection pressure of 80 MPa. The amount of injected pilot diesel-base fuel was between 1.2 mg/cycle and 3.0 mg/cycle. The simulations began from the intake valve closure at 135^{o} CA BTDC and were carried until 130^{o} CA after top dead centre (ATDC). The experimental engine specifications used in this study are presented in Table 3-1 and a schematic diagram of the experimental system is presented in Figure 3-2.

Table 3-1 Engine specifications

Engine type	4-stroke, single cylinder water cooled
Bore × Stroke	96 × 108 mm
Swept volume	781.7 cm^3
Compression ratio	16
Combustion system	Dual-fuel, direct injection
Combustion chamber	Shallow dish
Engine speed	1000 rpm
Intake valve closure (IVC)	135 deg. BTDC
Initial pressure at IVC	225 kPa
Initial temperature at IVC	330 K
Injection system	Common-rail
Nozzle hole × diameter	4 × 0.10 mm
Pilot fuel injection pressure	80 MPa
Pilot fuel injection quantity	1.2 -3 mg/cycle
Equivalence ratio	Variable

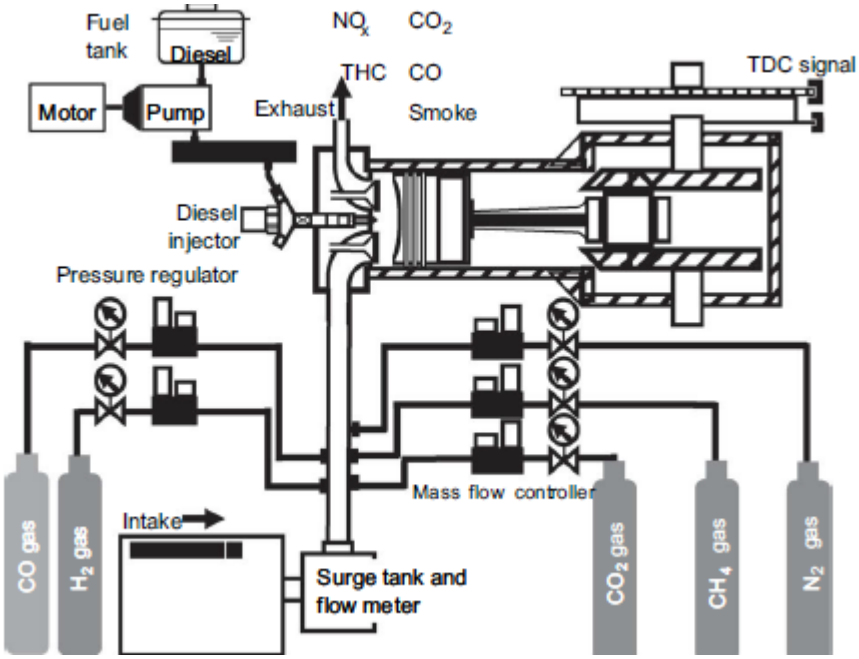

Figure 3-2 Schematic diagram of the experimental set-up [78]

3.2.2 Reacting flows governing equations

For the description of the chemical reacting flow, mathematical equations were used for their formulation. Equations such as the conservation equations for the mass, the momentum, the energy and the chemical species coupled with the thermodynamic relationships [157-159]. By using chemical kinetics mechanisms, the enthalpy of the reaction is used as a coupling factor between the chemical species concentrations and the energy equation. Moreover, the conservation equations are made up from a set of ordinary or partial differential equations for species and energy with the time and space as independent variables. The governing conservation equations that were used during the multidimensional CFD simulations are described in the sections below.

Mass and momentum conservation

The Navier-Stokes equations (mass and momentum conservations equations) were used for compressible and incompressible fluid flow. Mass conservation (Equation 3.21) and momentum conservation (Equation 3.22) are described by [160]:

$$\frac{\partial \rho}{\partial t} + \frac{\partial}{\partial x_j}(\rho u_{iabs}) = s_m \tag{3.21}$$

$$\frac{\partial \rho\, u_i}{\partial t} + \frac{\partial}{\partial x_j}\left(\rho u_{iabs} - \tau_{ij}\right) = -\frac{\partial \rho}{\partial x_i} + s_i \tag{3.22}$$

Where t is the time, x_i is the Cartesian coordinate (i=1,2,3), u_{iabs} is the component of the absolute velocity of the fluid in the direction x_i, ρ is the density, τ_{ij} is the components of the stress tensor, s_m is the mass source and finally s_i is the momentum source components.

Species conservation

Despite the fact that Equation 3.21, defines the conservation of mass in a fluid flow, it does not include any distinction for the chemical species included in the flow. However, the mass conservation of each individual species included in the mixture is very important, especially for chemically reacting flow systems consisting of multicomponent syngas mixture,. For an individual species, the mass fraction is calculated by:

$$Y_k = \frac{\rho_k}{\rho} \tag{3.23}$$

Where Y_k is the k^{th} species mass fractions, the total density of the fluid is ρ and the mass density of the k^{th} species symbolized by ρ_k. Moreover, it is important to mention here that the summation of the mass fractions for all of the species included is 1 ($\sum_{k=1}^{k} Y_k = 1$) and the summation of the mass density for all of the species is the total density ρ ($\sum_{k=1}^{k} \rho_k = \rho$) [159].

The species mass conservation equation, Equation 3.23, can then be used for the description of the chemical composition of a gaseous mixture in a differential element. The molecular convection and diffusion as well as the homogeneous reactions are affecting the mass conservation of the k^{th} species as shown in Equation 3.24.

$$\rho \frac{\partial Y_k}{\partial t} + \rho \bar{u} \,.\nabla Y_k = \omega_{k_f} \dot{W_k} - \nabla \bar{J}_k \tag{3.24}$$

Where t is the time, ρ is the density of the fluid, the fluid velocity vector is $\bar{u}$, $\bar{J}_k$ is the mass diffusive flux vector of the k^{th} species, the molar rate of production of the k^{th} species is symbolized by ω_{k_f} and the k^{th} species molecular weight is W_k

According to Equation 3.20, the changes in the mass fraction of a chemical species (k^{th} species) in a differential element, $\rho \frac{\partial Y_k}{\partial t}$, plus the effect of the convection on the species mass concentration $\rho \bar{u} \,.\nabla Y_k$, is equal to the chemical reactions effects on the k^{th} species mass concentration $\omega_k W_k$ minus the effects of the molecular diffusivity on the mass concentration of the species, $\nabla \bar{J}_k$ [159].

Energy conservation

For reacting flow systems, the thermal energy conservation equation is used for the description of the temperature profile of the chemical reacting flow, which has a great influence on the molecular diffusion, the convection and in the chemical reaction. The energy conservation equation is described by:

$$\rho c_p \frac{\partial T}{\partial t} + \rho c_p \bar{u} \,.\nabla \mathrm{T} = \nabla \,.(\lambda \nabla \mathrm{t}) - \rho \sum_{k=1}^{k} c_{p,k} Y_k \bar{u}.\nabla \mathrm{T} - \sum_{k=1}^{k} h_k \omega_k W_k + q_{rad} \qquad (3.25)$$

Where the constant pressure heat capacity of the k^{th} species is symbolized by c_p, λ is the thermal conductivity, the fluid velocity vector of the k^{th} species is $\bar{u}$, the formation enthalpy of the k^{th} species is h_k and q_{rad} is the radiative heat transfer [159].

3.2.3 Chemical kinetics

From the mathematical point of view, the analysis of the reacting flows during the combustion process is a difficult and complicated procedure that is affected mainly by the complex chemical kinetics that requires the solution of different differential equations related with the mass fractions of the species that are coupled non-linearly via the reaction rate laws. Pre-tabulated kinetically controlled reaction models implemented in CFD have several limitations such as the number of allowable reversible and irreversible reactions or the simplicity of the reaction rate expressions. These models are applicable for the simulation of relatively simple reaction systems. However, in reality the combustion chemistry is not a simple procedure and includes a high number of reactions and species. Therefore, a robust and accurate chemical kinetics mechanism should include a relatively high number of species and reactions in order to be accurate. During this research, the complex chemistry model incorporated in STAR-CD software was used to simulate the combustion chemistry.

Complex chemistry model

By using the complex chemistry model, chemical kinetics mechanisms which have a high number of reactions and species can be used in the simulations. One limitation of the complex chemistry model is that no other sub-model, for example flamelet model, ignition model or NOx model can be coupled. This is because the combustion process is driven mostly by the reaction rate of the chemical reactions and the species conservation equations.

The transport equations for the mass fraction of the species included in the mechanism is given by:

$$\frac{\partial}{\partial t}(pY_i) + \frac{\partial}{\partial x_j}\left(p\, u_j Y_i - F_{i,j}\right) = S_i \qquad (3.26)$$

where $F_{i,j}$ is the diffusion flux component calculated by:

$$F_{i,j} = \frac{m_t}{\sigma_{i,j}} \frac{\partial Y_i}{\partial x_j} + pD_{im} \frac{\partial Y_i}{\partial x_j} + \frac{D_i^T}{T} \frac{\partial T}{\partial x_j} \quad (3.27)$$

in which D_i^T is the thermal diffusion coefficient, S_i is the production rate, D_{im} the molecular diffusivity of species *i* in the mixture and *i=1…N(or N-1)*, where *N* is the total number of species. It is important to be mentioned here that the molecular diffusivity is different for each individual species included in the mechanism. By resolving the transport equations for *N-1* species, the mass fraction for the *Nth* species is calculated from:

$$Y_N = 1 - \sum_{i-1}^{N-1} Y_i \quad (3.28)$$

For a reversible reaction containing *N* chemical species, the general form is expressed by:

$$\sum_{k=1}^{N} (n_{Rk}{}' R_k Y_{Rk}') = \sum_{k=1}^{N} (n_{Rk}'' R_k T_{Rk}'') \quad , \quad R = 1, \dots, N_R \quad (3.29)$$

And the production rate is calculated by:

$$S_i = M_i \sum_{R=1}^{N_R} \left[(n_{Ri}'' - n_{Ri}') \left(k_{fR} \prod_{k=1}^{N} [R_k]^{v_{Rk}'} - k_{rR} \prod_{k=1}^{N} [R_k]^{v_{Rk}''} \right) \right] \quad (3.30)$$

where the total number of reactions in the system is N_R, the species concentration in moles is $[R_k]$, the stoichiometric coefficients are $n_{Rk}{}'$ and $n_{Rk}{}''$, the concentration exponential factors are $v_{Rk}{}'$, and $v_{Rk}{}''$ and finally the forward rate constant k_{fR} and the backward rate constant k_{rR} [107].

Chemical reactions and combustion

In the chemical kinetics mechanism, different types of reactions may be found. Although all of the reaction rate calculations are based on the standard Arrhenius rate equation, each type of reaction requires a different modified Arrhenius rate expression for its reaction rate calculation. The standard Arrhenius rate equation has been described in detail in Chapter 2, Section 2.5 of this thesis. Therefore, all of the different modified Arrhenius rate expressions for the reactions included in the chemical kinetics mechanisms are described in this section.

Three-body reaction

This type of reaction is included in the mechanism if "third body" species are needed in a reaction. By adding third body species in the reaction mechanism the rate of production S_i, Equation 3.26, has to be multiplied by the concentration factor given by:

$$\sum_{k=1}^{N} \alpha_{kR} |R_k| \quad (3.31)$$

Where α_{kR} is the third body efficiency of species k in reaction R.

For three body reactions in the mechanisms, the third body inert molecule that is required to stabilize the reaction's excited product by collision is refer as M. For example, reaction H_2O_2+M=OH+OH+M. The inert molecule (M) actually removes the excess energy from the excited product and dissipates it as heat.

Pressure-dependent reaction

The in-cylinder pressure is one of the main factors affecting the combustion process and therefore, is directly related with the combustion chemistry. Chemical kinetics reactions that are activated during the combustion process react differently at different pressure conditions. In order to express this pressure dependence, chemical kinetic data for both low and high pressure conditions should be included into the mechanism for each pressure-depended reaction. Then the reaction rate of the chemical kinetics reaction, at a pressure between the low and high pressure limits, is calculated based on the two limiting factors. Three different types of reaction formulation can be used in the mechanism; a) the Liendemann form, b) the TROE form and c) the SRI form.

During the Lindemann form the low and high pressure limit values, k_l and k_h, are given by using the standard Arrhenius rate equations:

$$k_l = A_l T^{\beta_l} \exp\left(-\frac{E_l}{ER}\right) \tag{3.32}$$

$$k_h = A_h T^{\beta_h} \exp\left(-\frac{E_h}{ER}\right) \tag{3.33}$$

Where A_l and A_h are the exponential factors used for the low and high pressure limits respectively and β_l and β_h are the temperature exponent factors at low and high pressure limit respectively.

For each reaction, the rate constant at any pressure is then calculated by:

$$k = k_h \left(\frac{P^r}{1+P^r}\right) \tag{3.34}$$

Where P^r is the reduced pressure which is given by:

$$P^r = \frac{k_l |M|}{k_h} \tag{3.35}$$

Where $|M|$ is the mixture concentration. It is important to mention here that if the pressure depended reaction is also a third body reaction, then the third body efficiency effect will be included in the calculation of the reaction rate.

For pressure depended reactions that use the TROE form, the reaction rate at any pressure is given by:

$$k_h = k_h \left(\frac{P_r}{1+P_r}\right) F \tag{3.36}$$

Where P^r is calculated similarly to Lindemann form from Equation 3.35, while F is calculated by

$$\log F = \left[1 + \left(\frac{logP_r + t_1}{t_2 - 0.14(logP_r + t_1)}\right)^2\right]^{-1} \log F_z \tag{3.37}$$

Where t_1 and t_2 are the characteristic times and $F_z = (1 - z)\exp\left(-\frac{T}{z}\right) + z\exp\left(-\frac{T}{z}\right) + \exp\left(-\frac{z^2}{T}\right)$. z is the characteristic coefficient of the pressure dependent reactions.

The final form of pressure-depended reaction is called SRI form. During SRI form the reaction rate constant of each pressure depended reaction is calculated by [107]:

$$k = k_h \left(\frac{P_r}{1+P_r}\right) F \tag{3.38}$$

Where F is calculated by :

$$F = [g\, exo\, \left(-\frac{g}{t}\right) + \exp\left(-\frac{T}{g}\right)]^{F_g}\, dt^g \tag{3.39}$$

And F_g by

$$F_g = \frac{1}{1+(logP_r)^2} \tag{3.40}$$

Where g is the characteristic coefficient of the SRI form reaction and is defined in the reaction mechanism by the user based on the in-cylinder pressure conditions.

Landau-Teller reaction

The last form of reaction that is included in the mechanism is the Landau –Teller reaction. By using that reaction form the reaction rate constant is calculated by:

$$k_{fr} - A_R T^{\beta_R} \exp\left[-\frac{E_R}{RT} + \frac{B_{R1}}{T^{\frac{1}{3}}} + \frac{B_{R2}}{T^{\frac{2}{3}}}\right] \quad (3.41)$$

Where B_{R1} and B_{R2} are the Landau-Teller constants. When both constants are zero the reaction rate constant is calculated by the simple Arrhenius rate Equation.

As it can be seen, a comprehensive and detailed list of chemical reactions and their reaction rates must be included in the chemical kinetics mechanism for the accurate prediction of the ignition behaviour, the NOx formation and the combustion characteristics (e.g. pressure, ROHR and flame characteristics). This is the reason why a chemical kinetics mechanism must be developed carefully with specific attention on the reduction procedure so that elimination of species or reactions that may affect the accuracy of the simulations is avoided and to ensure that all of the reactions with the correct form are included. It is important to mention here, that for turbulent combustion, an eddy break up based reaction could be included in the mechanism and the rate constant calculated by the standard eddy break up model. That type of reaction is implemented for the spray modelling and n-heptane chemistry and is analysed in detail in Chapter 3, section 3.2.5.

Thermodynamic and transport properties of the species

For all of the individual species included in the syngas mixtures used during this thesis as well as the individual species included in the developed mechanisms, their decomposition rates as well as the reaction rates are included as thermal and transport files in Appendix A Table A1 and Table A-2 respectively. The thermal file includes the coefficients of each species included in the mechanism that were used for the calculation of specific heats ,standard state enthalpies and standard state entropies as a function of temperature for each species included in the mechanism [112]. Two different temperatures used for each species (min and max) and seven different coefficients for each temperature used. Thus, for each species, 14 coefficients are used. The final specific heat *(c_{sp})* enthalpy (H_{Enthalpy}) and entropy *($S_{Entropy}$)* for each species are calculated by:

$$c_{sp}(T) = R[\delta_1 + \delta_2 T + \delta_3 T^2 + \delta_4 T^3 + \delta_5 T^4] \quad (3.42)$$

$$H_{Enthalpy}(T) = RT\left[\delta_1 + \frac{\delta_2}{2}T + \frac{\delta_3}{3}T^2 + \frac{\delta_4}{4}T^3 + \frac{\delta_5}{5}T^4 + \frac{\delta_6}{T}\right] \quad (3.43)$$

$$S_{Entropy}(T) = R\left[\delta_1 lnT + \delta_2 T + \frac{\delta_3}{2}T^2 + \frac{\delta_4}{3}T^3 + \frac{\delta_5}{4}T^4 + \delta_7\right] \quad (3.44)$$

In which R is the gas constant and T is the temperature. Furthermore, the thermodynamic database includes the name of the species, its elemental makeup and the temperatures in which the fits are valid. For accuracy reasons, all of the thermodynamic properties of the species have been taken from the NASA chemical database [161] and are similar to the thermodynamic data used in CHEMKIN [112].

For the transport properties of each species, a transport data file is presented in Appendix A Table A-2. The transport database includes important molecular properties for each individual species such as [162]:

1) Its geometrical configuration. An index showing if the molecule has a monoatomic, non-linear or linear configuration. For monoatomic, an index value of 0 is used. For non-linear an index 2 is given. Finally, for linear an index 1 is given.
2) The Lennard-Jones potential well depth ε/k_B in Kelvins
3) The Lennard-Jones collision diameter, D_{LJ} in Angstroms
4) The dipole moment, μ in Debye. Note: a Debye is $10^{-18}\ cm^{3/2}\ erg^{½}$
5) The polarizability P_{pl} in cubic Angstroms
6) And the rotational relaxation collision number Z_{rot}.

Similar to the data file the transport properties of each species have been taken directly from NASA chemical database[161].

3.2.4 Turbulence modelling

Turbulence was implemented into the CFD simulations by using the standard high-Reynolds number $k-\varepsilon$ model. This model is appropriate to fully model the turbulence of the compressible and incompressible in-cylinder flows as well as the buoyance effects. A set of transport equations were used for the calculations of the turbulence kinetic energy and the turbulence dissipation rate.

Turbulence kinetic energy

By using the standard high-Reynolds number $k-\varepsilon$ model the turbulence kinetic energy is given by:

$$\frac{\partial}{\partial t}(\rho k)+\frac{\partial}{\partial x_j}\left[\rho u_j k-\left(\mu_i+\frac{\mu_i}{\sigma_k}\right)\frac{\partial k}{\partial x_j}\right]=\mu_i(\Delta+\Delta_B)-\rho\varepsilon$$
$$-\frac{2}{3}\left(\mu_i\frac{\partial u_i}{\partial x_i}+\rho k\right)\frac{\partial u_i}{\partial x_i}+\mu_i\Delta_{NL} \qquad (3.45)$$

Where

$$\Delta=S_{ij}\frac{\partial u_i}{\partial x_j} \qquad (3.46)$$

$$\Delta_B=-\frac{\rho}{\sigma_{k,i}}\frac{1}{\rho}\frac{\partial \rho}{\partial x_i} \qquad (3.47)$$

$$\Delta_{NL}=-\frac{\rho}{\mu_i}\overline{u_i'u_j'}\frac{\partial u_i}{\partial x_j}-\left[\Delta-\frac{2}{3}\left(\frac{\partial u_i}{\partial x_i}+\frac{\rho k}{\mu_i}\right)\frac{\partial u_i}{\partial x_j}\right] \qquad (3.48)$$

Where for linear models $\Delta_{NL}=0$ and the turbulent Prandtl number is σ_k. The turbulent generation by shear and normal stress and buoyancy forces is given by the first term on the right hand side of Equation 3.45 ($\mu_i(\Delta+\Delta_B)$). The viscous dissipation by the second term ($-\rho\varepsilon$) and the amplification or attenuation due to compressibility effects by the third term $-\frac{2}{3}\left(\mu_i\frac{\partial u_i}{\partial x_i}+\rho k\right)\frac{\partial u_i}{\partial x_i}$. The final term on the right side of Equation 3.45, ($\mu_i\Delta_{NL}$) describes the non-linear contributions.

Turbulence dissipation rate

The turbulent dissipation rate is calculated through:

$$\frac{\partial}{\partial t}(\rho\varepsilon)+\frac{\partial}{\partial x_j}\left[\rho u_j\varepsilon-\left(\mu+\frac{\mu_t}{\sigma_k}\right)\frac{\partial \varepsilon}{\partial x_j}\right]=\overbrace{C_{k1}\frac{\varepsilon}{k}\left[\mu_i\Delta-\frac{2}{3}\left(\mu_i\frac{\partial u_i}{\partial x_i}+\rho k\right)\frac{\partial u_i}{\partial x_i}\right]}^{\text{A}}+$$
$$\underbrace{C_{k3}\frac{\varepsilon}{k}\mu_i\Delta_B}_{\text{B}}-\underbrace{C_{k2}\,\rho\frac{\varepsilon^2}{k}}_{\text{C}}+\underbrace{C_{k4}\rho\varepsilon\frac{\partial u_i}{\partial x_i}}_{\text{D}}+\underbrace{C_{k1}\frac{\varepsilon}{k}\mu_i\Delta_{NL}}_{\text{E}} \qquad (3.49)$$

Where the turbulent Prandtl number is symbolized by $\sigma_k$andC_{k1}, C_{k2}, C_{k3} and C_{k4} are the turbulent coefficients. The values of these coefficients are pre-tabulated into the program and they are given in Table 3-2. Moreover, the production of dissipation due to linear stresses and dilatation/compression effects is given by the term one (A) in the right side of Equation 3.49, $C_{k1}\frac{\varepsilon}{k}\left[\mu_i\Delta-\frac{2}{3}\left(\mu_i\frac{\partial u_i}{\partial x_i}+\rho k\right)\frac{\partial u_i}{\partial x_i}\right]$. The second term (B) in the right side of the Equation 3.49 (

$C_{k3}\frac{\varepsilon}{k}\mu_i \Delta_B$) is the contribution to the production dissipation because of the buoyancy, term number three(C) in the right side of the Equation 3.49, $-C_{k2}\,\rho\frac{\varepsilon^2}{k}$) is the dissipation destruction, the fourth term (D) in the right side of the Equation 3.49 ($C_{k4}\rho\varepsilon\frac{\partial u_i}{\partial x_i}$)is the contribution due to the temporal mean density changes and finally, the last term number five (E) in the right side of the Equation 3.49, ($C_{k1}\frac{\varepsilon}{k}\mu_i \Delta_{NL}$) is the contribution due to non-linear stresses.

Table 3-2 Coefficients of the Standard high Reynolds $k-\varepsilon$ model

σ_k	C_{k1}	C_{k2}	C_{k3}	C_{k4}	k	E
1.0	1.44	1.92	0.0 or 0.44	-0.33	0.419	9.0

3.2.5 Spray model

For the spray model the Langrangian model, implemented n STAR CD, (Dispersed multi-phase flow model) was used. For cases in which the number of droplets is relatively small, mass, momentum and energy conservation equations can be used for each element. However, when the number of droplets is high (like this study), a statistical approach is used. In this approach, elements (droplets) with the same properties are grouped into parcels [107]. The total population is represented by a finite number of parcels.

However, the interfacial forces induced by the droplets motion to the continuous phase, relative to the in-cylinder air, may result in unstable behaviour of the droplets. Therefore, a break up model is required to determine the rate of change of the size of the droplets. During this study, the Reitz Diwakar model was used [155, 156]. In this model, the break-up of the droplets due to the aerodynamic forces affecting them, occurs by one of the following two modes [107, 163, 164]:

1) 'Bag break-up' mode, in which the droplet is expanded in the low-pressure wake region due to the influences of the non-uniform pressure field around it, and, eventually, when the surface tension forces are overcome, it integrates.
2) 'Striping break-up' mode, in which the liquid is removed, stripped or sheared from the surface of the droplet.

In each of these two cases, theoretical studies have provided a criterion for the onset of break-up and concurrently estimations for the break-up process time scale, τ_b and the stable droplet diameter, D_b . This allows the calculation of the break-up rate by [107, 163]:

$$\frac{dD_d}{dt} = -\frac{D_d - D_{d,stable}}{\tau_b} \quad (3.50)$$

where D_d is the instantaneous droplet diameter.

Moreover, the time scales and the criteria for each one of the two modes are:

'Bag break-up' mode

During this mode, a critical value of the Weber number, We, is used for the determination of the instability:

$$We \equiv \frac{\rho|u-u_d|^2 D_d}{2\sigma_d} \geq C_{bI} \quad (3.51)$$

in which C_{bI} is the empirical coefficient and its value ranges between 3.6 to 8.4 [155, 156]. During this research, a value of C_{bI} =6 was used. Moreover, σ_d is the coefficient of the surface tension and the stable droplet size , D_d, is one that satisfies the equality in Equation 3.47.

Furthermore, the characteristic time is calculated by:

$$\tau_b = \frac{C_{b2}\,\rho_d^{\frac{1}{2}}\,D_d^{\frac{3}{2}}}{4\sigma_d^{\frac{1}{2}}} \quad (3.52)$$

where $C_{b2} = \pi$.

'**Striping break-up' mode**

For ''Striping break-up' mode, the criterion used for the onset of break-up is given by:

$$\frac{We}{\sqrt{Re_d}} \geq C_{sI} \quad (3.53)$$

in which Re_d is the Reynolds number of the droplet, and *Cs1* is the empirical coefficient with a value of 0.5 [155, 156].

For this mode the characteristic time is given by:

$$\tau_b = \frac{C_{s2}}{2}\left(\frac{\rho_d}{\rho}\right)^{\frac{1}{2}}\frac{D_d}{|u-u_d|} \quad (3.54)$$

in which the empirical coefficient C_{s2} is in the range of 2 to 20, u is the instantaneous fluid velocity and $u_d$is the instantaneous droplet velocity [155, 156].

Turbulence-controlled eddy brake up model (EBU)

For representation of the mixing turbulent chemical reaction, the eddy break up (EBU) model proposed by Magnussen was used [165]. The model was initially constructed for combustion applications and follows two basic assumptions:

1) A single step irreversible reaction is implemented into the chemical kinetics mechanism which involves the fuel (F), the oxidant (O), the products (P) and possible background inert species.
2) The time scale of the reaction is very small so that the rate-controlling mechanism of the reaction can be controlled by the turbulent macromixing.

The consumption rate of the fuel R_F is calculated by:

$$R_F = -\frac{\rho\varepsilon}{k} A_{ebu} \min\left[Y_F, \frac{Y_O}{S_O}, B_{ebu}\frac{Y_P}{S_P}\right] \qquad \text{kg/m}^3\text{s} \qquad (3.55)$$

Where *R* and *P* are the reactant and product respectively, coefficient k takes a value between $1 \leq k \leq 10$. A_{ebu} and B_{ebu} are the empirical coefficients of the model. Moreover, the first two terms in the brackets of Equation 3.55 determine the local rate controlling mass fraction, while the third term is used as a reaction inhibitor when the temperature is very low. The micro-mixing time scale is taken to be k/ε, which is the dissipation time scale [107].

In this study, for the simulations of the pilot-injected diesel spray, the ignition and the turbulent mixing representation, C_7H_{16} chemistry was incorporate in the developed mechanisms by using the global single-step reaction, $C_7H_{16} + 11O_2 = 7CO_2 + 8H_2O$, based on an eddy breakup (EBU) mixing representation and by specifying the reaction parameters of EBU [107]. As mentioned earlier, by using the single step reaction based on the EBU, the time scale of the reaction is very small (activation energy is zero) and therefore, n-heptane is ignited almost immediately. The ignition of n-heptane leads to the creation of a small zone of very high temperature that is sufficient to ignite the premixed syngas fuel. The modelling of pilot-injection n-heptane spray and ignition by using only the single step reaction based on the EBU, can be used accurately in situations when the injected diesel base fuel is very small. For conditions in which the amount of the injected diesel base fuel is higher, the single reaction based on the EBU has to be coupled with the appropriate chemical kinetics mechanism. The reason for that is because when micro-pilot injection is used, the ROHR profiles do not include

any changes due to the pilot diesel fuel combustion and the soot formation level is undetectable [62, 63]. However, when the amount of pilot-injected diesel base fuel is high, the total ROHR is significantly affected and the thermodynamic stability of the combustion changes due to the impurities created from the mixing of the diesel spray with the primary premixed syngas fuel [57].

For the mechanisms developed in Chapters 4 and 5, the amount of injected diesel fuel used was 1.2 mg/cycle, which proved to have a negligible effect on the total ROHR [61-63]. Therefore, only the single global reaction was used for the simulations of the pilot-injected diesel spray, the ignition and the turbulent mixing representation. The reaction is implemented into the mechanisms as R1 and can be found in all of the developed mechanisms in Table 4-1, Chapter 4 for the syngas mechanism, in Table 5-1, Chapter 5 for the syngas/NOx mechanism and in Table 6-4, Chapter 6 for the syngas/NOx/n-heptane mechanism. However, it is important to be mentioned here that the final mechanism proposed in Chapter 6 was validated against experimental results by using a higher amount of injected diesel-base fuel (3.0 mg/cycle). Therefore, in order to take into account the effect of the impurities created by n-heptane ignition and the co-oxidation with the premixed syngas fuel, a combination of both the single-step global reaction based on the EBU mixing representation model and the n-heptane chemistry incorporated into the developed mechanism was used. First, for the n-heptane injection and the initial ignition, the single-step global reaction based on the EBU mixing was used. Then, the low and high temperature oxidation of the remaining amount of n-heptane during the combustion process and the co-oxidation with the premixed syngas fuel were simulated using the developed chemical kinetics mechanism.

3.2.6 Engine cylinder geometry

The cylinder mesh used for the CFD analysis was constructed using the CAD sub-model incorporated in STARCCM+ [166]. A full cylinder moving mesh was first constructed including 53,024 cells. However, in order to reduce the computational time of the simulations, a 90° moving-sector mesh of 13,256 cells with cyclic boundaries was used to represent a bowl-in-piston configuration that was representative of the experimental single-cylinder pilot-ignited dual-fuel engine [62]. The grid size of the meshes was chosen to be between 0.5-2.0 mm with a time step of 0.1 CA°. However, the cell-size distribution within the computation domain of the full mesh is different from the cell-size distribution of the sector mesh, as can be seen from Figure 3-3. In order to investigate the accuracy level of the constructed meshes,

both were tested against the experimental motoring in-cylinder pressure histories. The comparison between the motoring experimental and simulated in-cylinder pressure histories is presented in Figure 3-4. According to this figure, both meshes show good correlation with the experimental measurements. Therefore, it was decided to use the sector mesh for all of the multidimensional CFD simulations.

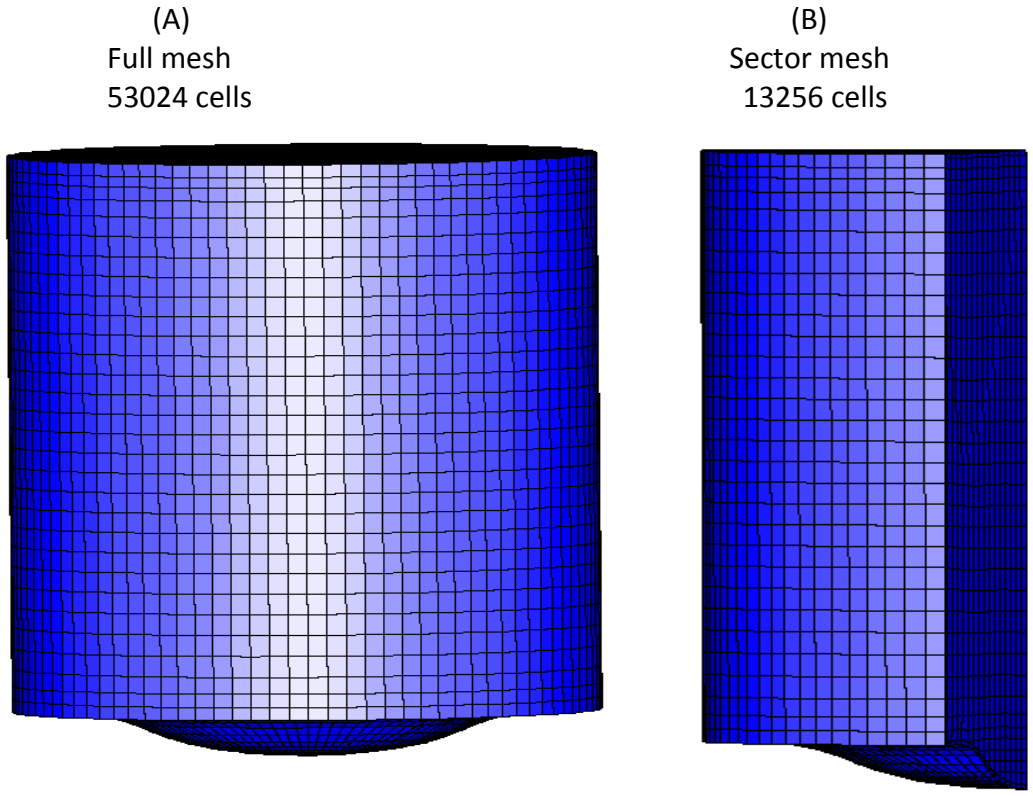

Figure 3-3 Full cylinder (A) and 90° sector cylinder (B) meshes used during the CFD analysis.

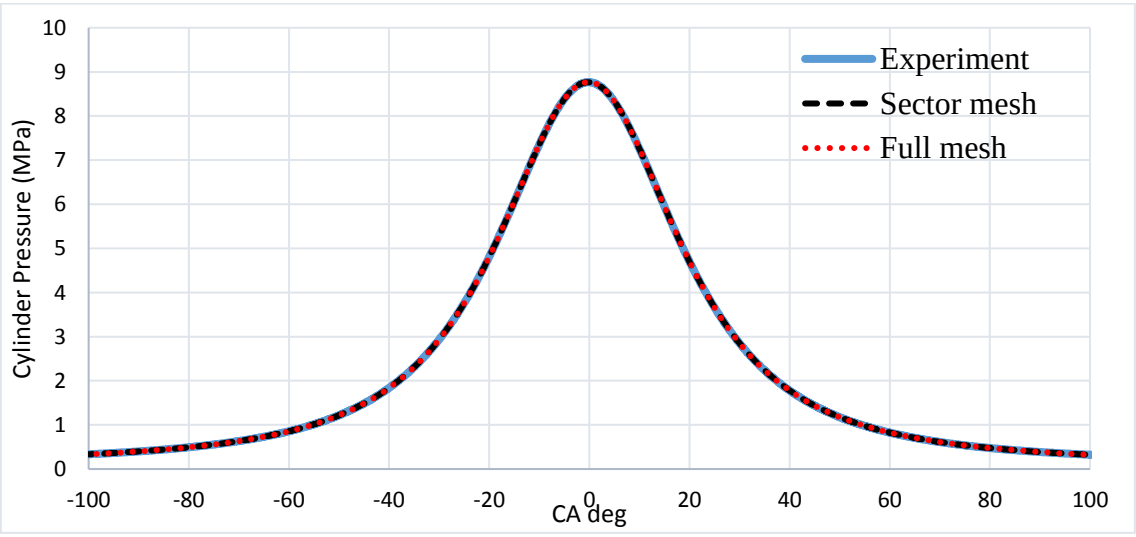

Figure 3-4 Comparison between the monitoring experimental and simulated cylinder pressures.

3.3 Error analysis

For the development of the reduced syngas/NOx mechanism, presented in Chapter 5, different NOx sub-mechanisms were tested and validated against experimental results and the most accurate and computational efficient was chosen and added to the syngas mechanism. The accuracy of the tested mechanisms was based on the deviation (%) between the experimental and simulated results. The deviation between the simulated and experimental results was calculated by conducting an error analysis study. Furthermore, an error analysis study was also conducted for all of the 0D and 1D simulations performed in Chapter 5 and allowable error limits were set in order to ensure the accuracy of the developed syngas/NOx mechanism. Despite the fact that other researchers used 10% to15% allowable error limit for all of the tested combustion parameters [130, 167], during this study the error limit that was used for LFS is 2%, for ignition delay time is 5 % and for the NOx calculations is 5%. The reason why lower error limits were used during this study in comparison with other researcher studies, was because various chemical kinetics mechanisms were already developed during the past years performing very well under specific conditions and having relatively low errors. Therefore, it was necessary to reduce the error limit in order to ensure that the developed mechanisms perform better than the already developed mechanisms and can cover a variety of experimental conditions with better accuracy.

Finally, during the reduction of the comprehensive n-heptane mechanism, presented in Chapter 7, an error analysis was conducted for the calculation of the deviation (%) between the original n-heptane mechanism and the latest Generation skeletal mechanisms. The calculated deviation (%) was used as a loop stopping criterion.

Three different error values were used during this study; The absolute error values of each individual case $\bar{E}_\iota$,the overall mean error, $\bar{\bar{\varepsilon}}$, and the grand mean error , $\bar{\bar{\Psi}}$. The following objective functions were used for the error calculations:

$$\bar{E}_\iota = \frac{1}{N_p}\sum_{j=1}^{N_p}\left|\frac{(Y_{sim,ij}-Y_{exp.ij})}{Y_{exp.ij}}\right| \times 100\% \tag{3.56}$$

$$\bar{\bar{\varepsilon}} = \frac{1}{N_d}\sum_{i=1}^{N_d}\bar{E}_\iota \tag{3.57}$$

$$\bar{\bar{\Psi}} = \frac{1}{G}\sum_{i=1}^{G}\bar{E}_\iota \tag{3.58}$$

Where, N_d is the number of data sets, N_p is the number of data points in the *ith* data set, and G is the number of datasets considered in a case. $Y_{sim,ij}$ is the simulated results of the *jth* data

point in *ith* set of data and $Y_{exp.ij}$ is the experimental results of the *jth* data point in the *ith* set of data [130, 167, 168].

3.4 Fuel mixtures used in this study

During this research a variety of different fuel mixtures were used for the investigation of n-heptane oxidation, syngas combustion, NOx formation during syngas combustion and n-heptane/syngas co-oxidation. Syngas fuels consist of different combustible (H_2,CO_2 and CH_4) and non-combustible gasses (CO and N_2). As it was already described in detail in Chapter 2 of this thesis, the concentration of each gas included in the syngas mixture depends on the type of feedstock or coal that was used and the gasification process that was followed for its production. More specifically, it depends on the gasifying agent that was used. For example, by using air as gasifying agent the produced syngas fuel will be a low calorific gas with varying proportions of H_2, CO, CO_2, CH_4 and N_2 and with a heating value between 4 to 7 MJ/Nm^3. On the other hand by using steam or oxygen as gasifying agent, the produced syngas will be a medium calorific value gas, consisting of varying proportions of H_2, CO and CH_4 and a heating value between 10-28 MJ/Nm^3 [38, 169, 170].

Therefore, similar fuels but with different composition were used in order to cover a variety of syngas mixtures with different compositions at different engine conditions. For all of the tested mixtures, different initial conditions, such as initial pressure, temperature and equivalence ratio, were used in order to investigate the performance of the mechanism on simulating a variety of mixtures at different combustion conditions. The equivalence ratio (ϕ) is defined as the ratio of the actual fuel to the oxidizer (in that case air) ratio to the stoichiometric fuel to oxidizer ratio and is given by :

$$\phi = \frac{actual\ fuel\ to\ oxidizer\ ratio}{stoichiometric\ fuel\ to\ oxidizer\ ratio} = \frac{(m_{fuel}/m_{ox})}{(m_{fuel\ st}/m_{ox\ st})} \tag{3.56}$$

All of the fuel mixtures that were used during this study are summarized in Table 3-3, including the range of equivalence ratios, initial pressure and temperature and the modelling approach that was used for the simulation. All of the data described in Table 3-3 are used in the following chapters of this thesis for comparison and validation of the developed mechanisms. For reasons of simplicity and because the experimental data presented in Table 3-3 have been used not only for one comparison but in each chapter, it was decided as this table, with all of the fuels placed in the methodology chapter. Therefore, for the rest of this thesis for all of the comparisons, all of the fuels are referring to Table 3.-3

The term AR in the composition of some of the fuel mixtures is refer to argon. Moreover, in all of the mixtures oxidizer is air (71% N_2 and 29% $O_{2)}$, this is the reason why is not appeared in the actual mixture composition. The only exception is for Fuel 13 (Table 3-3) in which the authors [193] measured the profiles of nitric oxide concentration at atmospheric pressures, in premixed hydrogen-oxygen-nitrogen flames by using a gas sampling that has 19% O_2 and 81% N_2.

Table 3-3 Fuel mixtures used in this study

No.	Fuel Mixture	Composition (%vol)		Equivalence ratio (ϕ)	Initial P	Initial T	Model	Ref.
Syngas Mixtures								
1	$H_2/CO/CO_2/N_2$	Type1	6.25/6.25/6.25/81.25	1.0	1 atm	914-1068 K	Constant Volume	[21]
		Type2	3.125/9.375/6.25/81.25					
		Type3	1.25/11.25/6.25/81.25					
2	$H_2/CO/CH_4/O_2/AR$	0.406/0.406/0.075/1.113/98.0		0.5	1.6/12/32 atm	1010-1920 K	Constant Volume	[25]
3	H_2/CH_4	Type1	60/40	0.5	5/10/20 atm	1050-1850 K	Constant Volume	[11]
		Type2	40/60					
		Type3	80/20					
		Type4	20/80					
4	$H_2/CO/CO_2/CH_4/H_2O/AR$	0.29659/0.29659/0.15748/0.08924/0.20997/0.95013/98.0		0.5	1.6/12/32 atm	1075-2220 K	Constant Volume	[25]
5	$H_2/CO/CO_2$	Type 1	33/67/0.0	0.3,1.0,1.5	1 atm	1041-1250 K	Constant Volume	[171]
		Type2	35/35/30					
6	$H_2/CO/CO_2$	35/35/30		0.4-1	1-3 atm	303-373 K	LFS	[172]
7	H_2/CH_4	Type1	90/10	0.4-1.2	1 atm	298 K	LFS	[130]
		Type2	70/30					
		Type3	50/50					
8	$H_2/CO/CH_4$	Type1	47.5/47.5/5	0.2-2.5	1 atm	295 K	LFS	[173]
		Type2	40/40/20					
		Type3	30/30/40					
9	$H_2/CO/CH_4/CO_2$	Type 1	54/11/25/10	0.4-0.9	1 atm	298 K	LFS	[174]
		Type2	60/10/0.0/30					
		Type3	32/58/0.0/10					
10	H_2/CH_4	Type1	20/80	0.4-2.2	1 atm	298 K	LFS	[175]
		Type2	50/50					
		Type3	90/10					
11	$H_2/CO/CO_2/N_2/CH_4$	16.99/20.58/11.84/47.67/2.8		0.8	1,3.05, 9.15atm	300 K	Premixed Laminar Flame-NOx	[176]
12	$H_2/CO/CO_2/CH_4$	37.5/37.5/20/5.0		0.71/1.03/1.34	1 atm	300 K	Premixed Laminar flame NOx	[13]
13	$H_2/O_2/N_2$	Type1	2H2+1.4O2+5.3N2	0.71	1 atm	300 K	Premixed Laminar flame NOx	[177]
		Type2	2H2+1.4O2+4.6N2					
		Type3	2H2+1.4O2+6.1N2					
14	$H_2/CO/CO_2/N_2/CH_4$	20/20/12/46/2		0.8	4,10,16 bar	300 K	Counter-flow /Species Sensitivity	[178]
N-Heptane Mixtures								

15	N-heptane/air	100% n-heptane			0.5-2	6.5-42 atm	650-1333 K	Constant Volume	[179]
16	N-heptane/air	100% n-heptane			0.5-1	40 bar	680-1282 K	Constant Volume	[180-183]
17	N-heptane/air	100% n-heptane			0.7-1.3	1 atm	298-358 K	LFS	[184]
18	N-heptane/air	100% n-heptane			0.5-1.6	1 atm	298-398 K	LFS	[185]
19	N-heptane/air	100% n-heptane			1.0	13.5,38 bar	729-1450 K	Constant Volume	[186]
20	N-heptane/air	100% n-heptane			1.0	20 bar	750-1430 K	Constant Volume	[187]
21	N-heptane/air	100% n-heptane			1.0	20 -55 bar	813-1250 K	Constant Volume	[188]
N-heptane/Syngas Mixtures									
22	n-heptane/H_2	Type 1	20/80		1 , 2	30 , 55 atm	800-1400 K	Constant Volume	[189]
		Type2	80/20						
23	n-heptane/CH_4	Type1	20/80		0.5-1	30,55 atm	800-1400 K	Constant Volume	
		Type2	80/20						
		Type3	5/95						
CFD									
24	H_2/CO/CO_2/CH_4/N_2	Type1	13.7/22.3/16.8/1.9/45.3	BMG	0.1-1	225 Kpa	298 K	CFD	[78]
		Type2	20.0/22.3/16.8/1.9/39.0	BMG					
		Type3	13.7/22.3/23.0/1.9/39.1	BMG					
		Type4	56.8/5.9/2.2/29.5/5.6	COG					
		Type5	56.8/22.3/16.8/1.9/39.1	COG					
		Type6	13.7/22.3/34.0/1.9/28.1	BMG					
		Type7	H_2 only (100%)	Hydrogen					

Chapter 4: Development of a reduced chemical kinetics mechanism for syngas combustion in a micro-pilot ignited dual-fuel engine

As already highlighted in Chapter 2 there is a need of a reduced, robust and computational efficient mechanism for the simulation of multicomponent syngas (including CH_4) combustion. Moreover, the reduced mechanism should be able to be implemented in multidimensional CFD simulations, capturing accurately the interactions between the turbulent fluid dynamics and the combustion chemistry in IC engines.

Therefore, in this chapter, a reduced and robust chemical kinetics mechanism for multicomponent syngas combustion in a dual fuel micro pilot ignited engine was developed. For the development of the new reduced mechanism a reduced mechanism proposed by Azimov et al [2] was optimized by updating the rate constants of important hydrogen reactions identified from sensitivity analysis and by incorporating reactions found to be important under high-pressure, low-temperature conditions. The developed syngas chemical kinetics mechanism was validated by comparing ignition delay, in-cylinder pressure, temperature and LFS predictions against corresponding experimental and simulated data obtained by using the most commonly used chemical kinetics mechanisms developed by other researchers. Finally, the developed mechanism was used in CFD analysis to predict in-cylinder combustion of syngas and results were compared with experimental data. The work presented in this Chapter was published in Fuel and can be found in [190].

4.1 Development of the syngas kinetics mechanism

During this study a CFD compatible, syngas chemical kinetics mechanism was developed shown in Table 4-1which can simulate dual-fuel engine combustion at various engine conditions. The mechanism was compared with H_2/CO syngas mechanisms developed and validated against experiments by other authors (Keromnes et al. [21], Frassoldati et al. [191] and GRI Mech. 3.0 [26]). To consider CH_4 component in the syngas composition, the nine-step reduced mechanism for CH_4 autoignition proposed by Li et al. [90] was used to add methane chemistry to H_2/CO reactions. To simulate the pilot-injected diesel spray and ignition, C_7H_{16} chemistry was added in the proposed mechanism by using the single-step global reaction, $C_7H_{16} + 11O_2 = 7CO_2 + 8H_2O$, based on an eddy break up (EBU) mixing representation by specifying the EBU reaction parameters.

Table 4-1 Reduced syngas mechanism constructed in Chapter 4 (A units cal-cm-sec-K, E units cal/mol).

	Reactions	***A***	***n***	***E***	**Ref.**
	n-Heptane Reaction EBU				
R1	$C_7H_{16}+11O_2=7CO_2+8H_2O$	0.	0.	0.	[148]
	/EBU/ 4. 0. 1 0.				
R2	$CH_4+O_2=CH_3+HO_2$	3.98E13	0.0	56855.5	[90]
R3	$CH_4+HO_2=CH_3+H_2O_2$	0.964E11	0.0	24629.4	[90]
R4	$CH_4+OH=CH_3+H_2O$	1.60E07	1.83	2771.1	[192]
R5	$CH_3+O_2=CH_2O+OH$	3.30E11	0.0	8934.4	[90]
R6	$CH_2O+OH=HCO+H_2O$	3.90E10	0.0	406.1	[90]
R7	$CO+O(+M)=CO_2(+M)$	9.04E12	0.89	3800.0	[191]
	/LOW / 0.2070E27 -3.340 7610.0 /M/ H_2O/12.00/ H_2/2.00/ CO/1.50/ CO_2/2.00/ AR/0.50/				
R8	$CO+OH=CO_2+H$	0.9600E12	0.14	7352.0	[191]
R9	$CO+OH=CO_2+H$	0.7320E11	-1.00	-16.0	[191]
R10	$CO+HO_2=CO_2+OH$	0.1200E18	0.00	17000.0	[191]
R11	$CO+H_2O=CO_2+H_2$	0.2000E9	0.00	38000.0	[191]
R12	$HCO(+M)=CO+H(+M)$	0.3000E14	0.03	23000.0	[191]
	/M/ H_2O/5.00/ CO_2/3.00/ H_2/1.90/ CO/1.90/				
R13	$HCO+O=CO_2+H$	0.3000E14	0.00	0.0	[191]
R14	$HCO+H=H_2+CO$	0.1000E13	0.00	0.0	[191]
R15	$HCO+OH=H_2O+CO$	0.5000E14	0.00	0.0	[191]
R16	$HCO+HO_2=H_2O_2+CO$	0.4000E12	0.00	0.0	[191]
R17	$HCO+HO_2=>H+OH+CO_2$	0.3000E14	0.00	0.0	[191]
R18	$O_2+CO=CO_2+O$	0.2530E10	0.00	0.0	[191]
R19	$O_2+HCO=HO_2+CO$	0.1000E15	0.00	47700.0	[191]
R20	$OH+OH(+M)=H_2O_2(+M)$	0.7400E14	-0.370	0.0	[191]
	/LOW / 0.2300E19 -0.900 -1700.0 /TROE/ 0.7346 94.00 1756.0 5182.0 /M/ H_2/2.00 /H_2O/6.00/ CO/1.50/ CO_2/2.00/ AR/0.70/				
R21	$H+O_2=OH+O$	3.52E16	-0.7	17061.4	[193]
R22	$H_2+O=OH+H$	5.06E4	2.67	6287.6	[194]
R23	$H_2+OH=H2O+H$	1.17E9	1.3	0.0	[194]
R24	$H+O_2(+M)=>HO_2+(M)$	4.6E12	0.4	0.0	[21]
	/LOW / 1.737E19 -1.23 0.0 /M/ AR/0.0/ H_2/1.3/ H_2O/10.0/ CO/1.9/ CO_2/3.8/				
R25	$H+H+(M)=>H_2+(M)$	1.30E18	-1	0.0	[193]
	/M/ H_2/2.5/ H_2O/12.0/ CO/1.9 /CO_2/3.8/ AR/0.5/				
R26	$H+OH(+M)=>H_2O(+M)$	4.00E22	-2	0.0	[193]
	/M/ H_2/2.5/ H_2O/12.0/ CO/1.9/ CO_2/3.8/ AR/0.38/				
R27	$HO_2+H=>OH+OH$	7.08E13	0.0	298.8	[195]
R28	$HO_2+H=H_2+O_2$	1.66E13	0.0	821.8	[21]
R29	$HO_2+OH=H_2O+O_2$	2.89E13	0.0	-496.9	[73]
R30	$HO_2+HO_2=H_2O_2+O_2$	1.300E11	0.00	-1.630E03	[21]
Additional reactions for biomass feedstock derived gas (low H2 concentration)					
R29b	$HO_2+OH=H_2O+O_2$	2.456E13	0.0	-4.970	[21]

R31	$H_2O_2+H=H_2+HO_2$	7.7E12	0.0	3755	[73]
R32	$O+H_2O=OH+OH$	2.97E06	2.02	1.340E04	[21]
Reaction constants for coke-oven feedstock derived gas (high H2 concentration)					
R31	$H_2O_2+H=H_2+HO_2$	1.21E07	0.0	5200	[196]

4.1.1 Sensitivity analysis

In order to investigate the important reactions affecting syngas combustion and the reactivity of the mixture under high pressures (10,30 and 50 bar), medium to high temperatures (100K) and lean mixture conditions (equivalence ratio < 1.0), a sensitivity analysis study was conducted. Sensitivity analysis was performed for Fuel mixture 24 Type 1 (Table 3-3), at temperature 1000 K, equivalence ratio 0.63 and pressure 10, 30 and 50 bar. The specific temperature (1000 K) was selected because we wanted to investigate which reactions are important under high-pressure/low temperature conditions similar to ultra-boost combustion. Therefore 1000 K was decided to be used while three different high pressures were selected, 10, 30 and 50 bar. Moreover, it is important to be mentioned here that because the experimental measurements that were used for multidimensional CFD analysis, cover a range of equivalence ratios lower than 1.0, and because of the statements of other authors [12, 13], that for internal combustion engines, lean mixtures are more suitable to be used, only equivalence ratio 0.63 was used. However, for rich mixture conditions the sensitivity of the reactions may change.

From this sensitivity analysis, a sensitivity factor was calculated for each individual reaction included in the mechanism (total 32) and the 13 most sensitive reactions are shown in Fig 4-1. According to the figure, reactions such as H_2O_2 (+M) = OH + OH (+M), $H_2O_2 + H = H_2 + HO_2$ and $CO + H_2O = CO_2 + H_2$ have high negative sensitivity factor while reactions such as $H_2+OH=H_2O+H$, $H_2 + O = OH + H$, $O_2 + CO = CO_2 + O$, $CH_3+O_2=CH_2O+OH$ and $CH_4 + OH= CH_3 + H_2O$ have high positive sensitivity factor.

As already described in Chapter 3, section 3.1.3, reactions with positive sensitivity factor are responsible for the fast formation of radicals, while reactions with negative sensitivity factor are responsible for the fast consumption of radicals. However, it has to be mentioned that reactions H_2O_2 (+M) = OH + OH(+M) and $H_2O_2 + H = H_2 + HO_2$ found to have a negative sensitivity factor especially at high pressures due to the fact that are responsible for the fast consumption of H_2O_2 and HO_2 respectively. However, both of these reactions, despite the fact that they are responsible for the fast consumption of radicals, they contribute to the increasing of the mixtures reactivity due to the fact that they responsible also for the formation of high reactive OH.

All of the reactions highlighted from the sensitivity analysis are described in detail below. For each reaction, the Arrhenius rate equation is used for the calculation of its reaction rate constant. The rate constant shows how fast the reaction proceeds (moles/sec), not whether it is spontaneous. The higher the temperature, the higher the reaction rate. Detail information about Arrhenius rate equation can be found in chapter 2 and chapter 3 of this thesis. However, it is important to be mentioned here that the rate constants for all of the reactions used in this thesis are constructed by other authors for a certain range of temperatures and fuel conditions. For example Sutherland et al [194] calculated the reaction rate constants for different reactions at different pressures and temperatures covering the range of the experimental in-cylinder temperatures and pressures. The best rate constant for each reaction that express with high accuracy the temperature dependence at all of the tested temperatures was then chosen and used. Thus, for a certain range of temperatures and pressures only one rate constant is used for each reaction included in the mechanism. The accuracy of the rate constants for all of the reactions was tested by validating the mechanism against experimental and numerical data not only by performing zero and one dimensional simulations (laminar flame speed and ignition delay time) but by also conducting a multidimensional CFD analysis for the simulation of syngas combustion in micro pilot ignited dual-fuel engine.

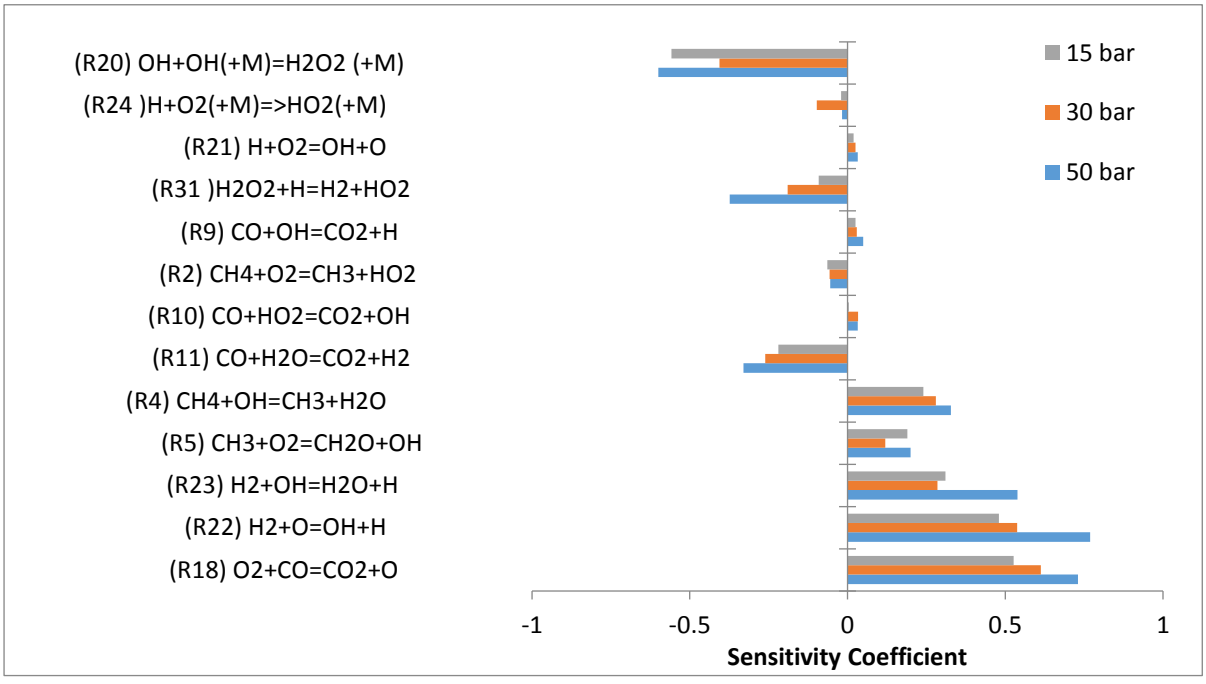

Figure 4-1 The 13 most sensitive reactions for syngas Fuel 24 Type 1 at 1000K and pressures 10, 30 and 50 bar

(R20) H_2O_2 (+M) = OH+OH (+M)

The dissociation of H_2O_2 radicals is characterized by many researchers as the central kinetic feature in the operation of HCCI engines, or the key factor for the abnormal combustion

phenomena, such as engine knock, in SI engines [196, 197]. This is because the decomposition of H_2O_2 via R20 gives access for secondary reactions and forms very reactive OH radicals [198]. Other studies showed that at higher pressures, H_2O_2 concentration increases during $H_2O_2(+M) = OH + OH(+M)$ reaction [2]. This is because at high pressure conditions, the mixture concentration is high, including enhanced third-body efficiencies M, and that leads to a sufficient concentration of less reactive HO_2 radicals and in turn to the formation of H_2O_2. At low to medium temperatures, the characteristic reaction time of H_2/CO mixtures is longer and that leads to the reduction of the reaction's sensitivity, as shown by Chaos et al [5]. Moreover, according to the authors, this reduction in reaction sensitivity causes the H_2O_2 concentration to increase. It was also shown that as the equivalence ratio increased, the H_2O_2/OH ratio decreased and the higher syngas initial H_2 concentration provides an enhanced chain-initiation process through $H_2 + O_2=OH + OH$ or $H_2 + O_2 =H +HO_2$ reactions, ensuring the occurrence of subsequent chain-branching reactions along with an increase in the OH concentration.

Two different studies have been conducted for the investigation and the generation of low-pressure limit and high pressure limit rate constants for R20. First Hong et al. [75], investigated R20 by using a laser absorption diagnostic for H_2O and OH [74, 75] at 1.8 atm pressure. Their results were in agreement with a previous study by Kappel et al. [198], although they have lower experimental uncertainty. They suggested a new lower pressure limit rate constant for R20 based on the work of Frassoldati et al [191], and a high pressure limit rate constant from a different study conducted by Sellevag et al [199]. The second study, conducted by Troe et al. [200], suggests new pressure dependent rate constants by performing a theoretical study based on experimental data.

During a study by Keromnes et al [21], the performance of both rate constants proposed by Hong et al [75] and Troe et al [200] were investigated. The authors analysed the accuracy of the rate constants proposed by Hong et al and Troe et al by comparing both rate constants with experimental results at a range of pressures (10-50 bar) and by analysing the sensitivity of each set of rate constants on the pressure changes. They concluded that at pressures between 20 and 40 bar, the rate constants of R20 from both authors (Hong et al [75] and Troe et al [200]) present a steeper fall-of behaviour while for pressures 15 bar and 50 bar, a normal trend was observed and the sensitivity of R20 increased by increasing the pressure. This is an explanation also for the unusual behaviour of R20 towards pressure at 30 bar, observed in Figure 4-1. Moreover, the authors concluded that the uncertainty level of both rate constants is identical at low to intermediate pressures but at high pressures the rate constant proposed by Hong et al [75], is closer to the experimental results. Therefore, in this thesis, the rate constant proposed

first by Frassoldati et al [191] and then used by Hong et al. [75], have been used due to the lower level of experimental uncertainty.

(R24) $H + O_2 (+M) \rightarrow HO_2 (+M)$

R24 has a key role in hydrogen combustion and is responsible for the reactivity at low temperatures [21]. Therefore, the temperature and pressure dependence of the chain propagation reaction R24 has been studied extensively by many researchers [73] . Fernandes et al. [201], proposed pressure and temperature dependent rate constants for a temperature range between 300– 900 K and a pressure range between 1.5 and 900 bars. The authors have tried to extend the temperature and pressure range by using the unimolecular rate theory. However, at temperature ranges from 1000 to 1200 K, the mixture reactivity decreased significantly, while the ignition delay time increased. This is because of the low pressure limit rate constant which uses argon as a bath gas. Bates et al.[202] studied the pressure and temperature dependence of R24 at temperature ranges from 1020 to 1260 K and pressure ranges from 10 to 50 bars by using argon. They proposed a low pressure limit rate constant that was in a good agreement with the experimental data. Finally, during a new study by Keromnes et al. [21] , a ‘‘hybrid’’ expression of rate constant was used by combining the high pressure limit rate constants proposed by Fernandes et al. [201] (exponential frequency factor A = 4.6E12 cal-cm-sec-K and activation energy E 0 .00 cal/mol) and the low pressure limit rate constant proposed by Bates et al. [202] (exponential frequency factor A = 1.73E19 cal-cm-sec-K and activation energy E =0.00 cal/mol). The new hybrid rate constants showed a good agreement with the experimental data at all temperature and pressure ranges. Therefore, in this study, the new rate constants proposed by Keromnes et al. [21] were adopted.

(R21) $H + O_2 = OH + O$

R21 is one of the most important reactions in the syngas chemical reaction mechanism. Lot of researchers [21, 203-205] studied R21 due to its importance on the domination/control of the oxidation of different fuels at temperatures above 1000 K. All of the research studies related with R21 [21,203-205], concluded that this reaction has a strong temperature dependency that may lead to high level of uncertainty [21]. This is the reason why it was decided as the temperature dependency of R21 to be examined based on the findings of other authors and the best rate constants to be chosen and adopted in the developed mechanism.

Because of its sensitivity, the rate constants used in different mechanisms vary. For example, the rate constants proposed by Pirraglia et al. [203] were adopted by Muller et al. [204] and Oconnair et al.[195], in order to reproduce more accurate explosion limits at temperatures between 680–900 K. Keromnes et al. [21] used a rate constant proposed by Hong et al. [205],

which has 10% uncertainty at temperature ranges from 1100 to 3370 K. Furthermore, Fernandez-Galisteo et al [193] used a modified version of the rate constants proposed by Saxena et al [83] for a temperature range from 1000 -2000K, for the investigation of hydrogen-air premixed flames. The authors showed that by using the new rate constants, the mechanism provides good predictions of hydrogen air lean flame burning velocities at all of the tested conditions. Therefore, during this study the rate constant from Fernandez-Galisteo et al.[193] was adopted.

(R31) $H_2O_2 + H = H_2 + HO_2$

This reaction is very important under low temperature (close to 1000K) and high pressure conditions (20-30 bar) [21]. The consumption of one HO_2 radical leads to the production of one H2O2 molecule, which in turn via R20 will be consumed for the formation of two high reactive OH radicals [21]. Therefore, it can be said that R31 is responsible for the increase of the reactivity. Due to its high sensitivity, this reaction has been studied in detail by many authors in order to find the best rate constants [73]. Different rate constants result in different ignition delay times, as shown by Keromnes et al. [21]. For example, at 50 bar and 1000 K the ignition delay times obtained by Baulch et al. [206] were by a factor of 3 different than those obtained by Tsang et al. [207]. This is because the authors used different rate constant (i.e activation energy, exponential and frequency factors) to express the temperature dependence of this reaction. More specifically, the activation energy that was used by Tsang et al was 4005 cal/mol and the exponential/frequency factor was $8.0x10^{-}11$ cal-cm-sec-K, while for Baulch et al [206] the activation energy was 7850 cal/mol and the exponential/frequency factor $1.31x10^{2}$ cal-cm-sec-K.

During a study by Ellingson et al. [208], the rate constants are calculated by using the canonical variational transition state theory. The calculated ignition delay times from Ellingson's approach were in a good agreement with those of Mittal et al. [209]. Furthermore, Konnov et al [73] proposed a new rate constant for reaction $H_2O_2 + H = H_2 + HO_2$ which is based on a the rate constant proposed by Baulch et al. [206]. The authors, re-evaluated $H_2O_2 + H = H_2 + HO_2$ rate constant and increased the uncertainty factor to 3 in order to reduce the deviation from the experimental ignition delay times especially at temperature range 800-1200 K and pressures 25 -50 bar. In this work, the rate constant recommended by Konnov et al [73] was adopted with an exponential factor A = 7.7E12, which lies within the stated level of uncertainty, in order to get the best agreement of the proposed mechanism with the experimental data and with the ignition delay times from other existing mechanisms.

(R9) $CO + OH = CO_2 + H$

According to Li et al. [88], the LFS and the mixture reactivity are sensitive to R9 [210]. Moreover, Frassoldati et al[191] investigated the importance of R9 at temperatures between 2285 K and 2635 K. The authors concluded that the formation of CO_2 is very sensitive to R9 especially at temperature 2285 K and that the oxidation of CO through R9 is faster than other terminating chain reactions such as reaction $CO+O+M=CO_2+M$. In order to control the formation of CO_2 and reduce the uncertainty of the mechanism, the authors proposed new rate constant for R9 based on the rate constant proposed Davis et al [211]. By implementing the new rate constant for R9 into their mechanism, the mechanism simulates accurately syngas combustion across a wide range of temperatures (500 to 3000 K) and has significant low uncertainty (lower than 5%). Therefore, in order to obtain the best agreement with the experimental data and the LFS measurements the reaction constants proposed by Frassoldati et al. [191] were used in this study.

(R4) $CH_4 + OH = CH_3 + H_2O$

This reaction is responsible for the consumption of CH_4 and the formation of CH_3 radicals. Different rate constants have been proposed in the literature and used in different chemical reaction mechanisms. The rate constant used for GRI Mech 3.0 [26] was based on the Cohen's Transition State Theory and validated against experimental data [212]. Baulch et al. [213] also proposed a new rate constant based on the study of Madronich and Felder [214] with an extended temperature range from 250 to 2500 K. Srinivasan et al. [215], on the other hand, proposed a new non-Arrhenius expression for a temperature range between 195 and 2025 K.

Li and Williams et al [192], used a new rate constant for R4 and they validated their mechanism against experimental results showing a good level of accuracy (>5%).Therefore it was decided as the rate constant proposed by Li and Williams et al [192] to be adopted in the new developed mechanism.

(R5) $CH_3 + O_2 = CH_2O + OH$

One of the most important reactions in the CH_4 oxidation responsible for the accurate prediction of methane ignition delay time is R5 [216]. The formation of formaldehyde and high reactive OH is a key intermediate in the combustion of syngas and natural gas fuels [217]. The importance of this reaction has forced researchers to investigate in detail the temperature and pressure dependence of R5 and propose different rate constants. For example, for a range of temperatures 800-1100 K the rate constant used in the San Diego mechanism [108] is higher by a factor of forty-two than the rate constant used in GRI Mech 3.0 [26]. For the same range of temperatures, the rate constant proposed by Srinivasan et al. [218], is one order of magnitude

lower than the rate constant suggested by Herbon et al.[219]. Furthermore, Li et al [90], proposed new rate constants for R5, for the prediction of methane auto ignition and knocking phenomena in dual fuel engines. The authors showed that by adopting the new rate constant into their mechanism, the mechanism predicts accurately the experimental in-cylinder pressure during non-knocking and knocking conditions for equivalence ratios between 0.5 and 1.5, temperature range between 800K and 1200 K and pressures from 50 to 150 bar. The rate constant proposed by Li et al [90]was also adopted by Maghbouli et al [220] for the simulation of knocking combustion in diesel-natural gas dual fuel engine, and by Gharehghani et al [221] for the reproduction of syngas combustion and knock in dual fuel gas/diesel compression ignition engine. Both studies concluded that by implementing the rate constant proposed by Li et a l[90] for R9, the deviation between the numerical and experimental results reduced significantly (lower than 15%). Therefore, during this study, the rate constant proposed by Li et al[90] was adopted in the developed mechanism.

(R22) $H_2 + O = OH + H$

The consumption and the production of hydrogen radicals play a key role on the ignition delay times and the LFS and in general are very important for the in-cylinder combustion. Therefore, reactions, which are responsible for the production of hydrogen radicals, have been investigated in depth by different researchers in order to find the most accurate rate constant during low and high temperature and pressure conditions. R22 is responsible for the production of H and OH radicals. The production of OH radicals leads to the initiation of reaction R23 which will be discussed in the next paragraph. According to a review by Baulch et al. [222], the most accurate rate constant for R22 was proposed by Sutherland et al. [194]. The expression from Sutherland is compared with the measurements from Natarajan and Roth [223] at temperatures ranging from 1713 to 3532 K, with Davidson and Handson [224] validating at ranges from 2120 to2750 K and finally tested by Javoy et al. [225] at temperatures 2690 to3360 K. For all of these temperature ranges, the expression proposed by Sutherland showed a very good agreement with the measurements. Therefore, during this study the rate constants proposed by Sutherland [194] were adopted in the developed mechanism.

(R23) $H_2 + OH = H_2O + H$

The production of OH radicals from R22, triggers R23. The reaction between H_2 and OH radicals leads to the conversion of OH to H atoms. LFS and ignition delay times are also very sensitive to this reaction [226]. Many researchers investigated the rate constants and proposed a value to accurately predict the sensitivity of this reaction to the temperature changes. For temperature ranges between 300 and 2500 K, Baulch et al. [222] proposed a new rate constant

which was used also by Konnov [227]. However, a second research by Baulch et al. [206] based on the work of Michael et al. [228] and Oldenborg et al. [229], showed that R23 is very sensitive to temperature changes. At 300 K, the uncertainty factor of R23 was 1.2 increasing to 2 at a temperature of 2500 K [206]. Therefore, a new rate constant has been proposed by Baulch et al. [206] in order to satisfy the uncertainty of R23 at different temperatures. Furthermore, Sutherland et al [194] measured experimentally, by using two independent experimental methods (flash photolysis-shock tube (FP-ST) technique and atomic resonance absorption spectroscopy), the rate constants for R23 for temperatures ranging from 504 to 2485 K. The new rate constant proposed by Sutherland et al [194],was later adopted by Fernandez-Galisteo et al [193] , and was validated against experimental measurements showing high level of accuracy. Therefore, during this study the rate constant proposed by Sutherland et al. [194] was adopted.

(R18) $O_2 + CO = CO_2 + O$

According to a research by Saxena et al. [83], although reaction 18 does not affect the laminar burning velocities, it is very important for the ignition initiation and the ignition delay times, especially at lower hydrogen content. This reaction is therefore an essential reaction and is added to the mechanisms by using the rate constant from Frassoldati et al. [191].

(R10) $CO + HO2 = CO_2 + OH$

This reaction is initiated during high pressure conditions or during the initial stages of the oxidation of hydrocarbons in which the concentrations of HO_2 are high [88]. Therefore, at high pressure conditions, reaction $CO + HO_2 = CO_2 + OH$ is very important for the accurate simulation of the CO oxidation and should be incorporated in the kinetics mechanisms [230]. It is very important during high pressures and shows the higher sensitivity factor from all of the reactions of the CO subsystems [231]. In order to reduce the uncertainty related with R10, the rate constants proposed by Frassoldati et al. [191] were used.

(R29) $OH + HO_2 = H_2O + O_2$

A recent study by Keromnes et al. [21] showed that R29 is very sensitive to the fuel-lean flames. Many theoretical and experimental studies have been conducted in order to analyse the dependency of the reaction rate constants on the temperature [208, 232, 233]. However, at temperatures around 1250 K, unusual temperature dependence is observed, which leads to a non-Arrhenius behaviour and creates a deep minimum for the calculated rate constant [21, 73, 198]. This makes the reproduction of the temperature dependence very difficult and creates a high level of uncertainties [73, 234]. Recent investigations by Hong et al. [235] and Burke et al. [236], showed that R29 has a weak temperature dependence but they also concluded that

future work is required to ensure the accuracy of the rate constants at temperatures between 900 and 1200 K. In this study it was decided to use a duplicate R31 by adopting the reaction rate proposed initially by Keyser et al [237] and modified by Keromnes et al [21] for lower temperature ranges, while for higher temperatures the rate constant proposed by Konnov et al [73] was used.

4.1.2 Ignition delay time

Ignition delay time simulations were performed using RCM model in DARS and by using different fuel mixtures and initial conditions. However, due to the fact that for Fuel 24 Types 1, 2 and 3 (Table 3.3) experimental results were available only for 3D CFD, the developed reduced mechanism was compared only against numerical results by using different tested a mechanisms proposed by other authors such as Keromnes et al. [21], Frassoldati et al. [191] and GRI Mech 3.0 [26]. The chemical kinetics mechanism obtained from the literature were already tested by other authors showing high level of accuracy and therefore it was decided to be used as validation point for the developed reduced mechanism.

Ignition delay time obtained using the new mechanism was compared with that obtained by Keromnes et al. [21], Frassoldati et al. [191] and GRI Mech 3.0 [26] for Fuel mixture 24 Type 1, 2, 3 and 4 (see Table 3-3) at T = 800–1053 K, P = 2.25 bar and equivalence ratio = 0.63. The specific temperature range (800-1053 K) was chosen because the main temperature range in which the rate constants for all of the reactions implemented in the developed mechanism, tested by other authors was between 800-1100K. Furthermore, similar equivalence ratio (0.63) and similar in cylinder pressure were used for all of the tested fuel mixtures. The purpose of this comparison was the investigation of the performance of the mechanism in simulating different fuel mixtures at similar initial engine conditions by comparing with already validated and tested chemical kinetics mechanisms from the literature.

Fig. 4-2 shows that the ignition delay time for the new mechanism matches very well with those obtained using different tested mechanisms in the broad range of temperatures, for all syngas types investigated in this paper. Furthermore, the mechanisms capture accurately the effect of the temperature on the ignition delay time: the higher is the temperature the lower is the ignition delay time. This is because at by using higher temperatures, the ignition temperature of the fuel is reached faster and that has as a results the fuel to be ignited faster.

Figs. 4-3 and 4-4 show the ignition delay times for new mechanism at high pressures (20, 40 and 80 bars). Analysis was performed for Fuel 24 Type 1 at temperature range 800–1053 K and equivalence ratio = 0.63, and Fuel 24 Type 2 at temperature range 800–1053 K and

equivalence ratio = 0.83. However, it is very important to be mentioned here that although the equivalence ratio was different, the results were obtained for two different mixture compositions and therefore the effect of the equivalence ratio cannot be investigated. The effect of equivalence ratio on the ignition delay time was set as a future task and can be performed when data for similar fuel mixture compositions but different equivalence ratios will be available. The results obtained using the new mechanism were in a good agreement with the ignition delay times obtained using the Frassoldati et al. [191] and Keromnes et al. [21] mechanisms and in exceptionally good agreement with ignition delay times obtained using the GRI Mech 3.0 [26] mechanism.

The ignition delay times using Fuel mixture 1 Type 1, 2 and 3 defined in Table 3-3 from the University of Connecticut were also used for the comparison. The study was performed under stoichiometric conditions with 50%, 25% and 10% H_2 in the H_2/CO fuel mixtures at the end-of-compression temperature range of 914–1068 K, using the new mechanism and the mechanism reported by Keromnes et al. [21]. The authors [21] validated their proposed mechanism against the experimental results obtained from the university of Connecticut for H2/CO mixtures showing a good agreement with error lower than 5%. Therefore, the simulated results of Keromnes et al were used and compared with the developed reduced mechanism. Results in Fig. 4-5 show the inhibiting effect of CO on the ignition delay times of syngas, which increase with increasing the concentration of CO in the syngas. The new mechanism captures this inhibiting effect very well and its predictions are in a good agreement.

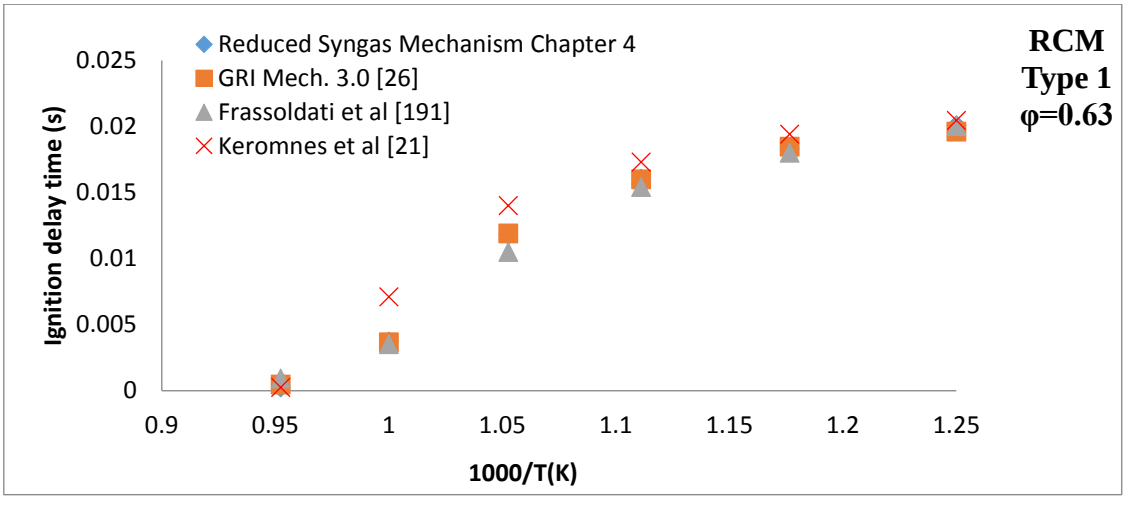

a)

Figure 4-2 Comparison of ignition delay time for Fuel 24 syngas Types 1-4 obtained with new mechanism with other mechanisms at temperatures 800–1053 K, pressure 2.25 bar and equivalence ratio = 0.63

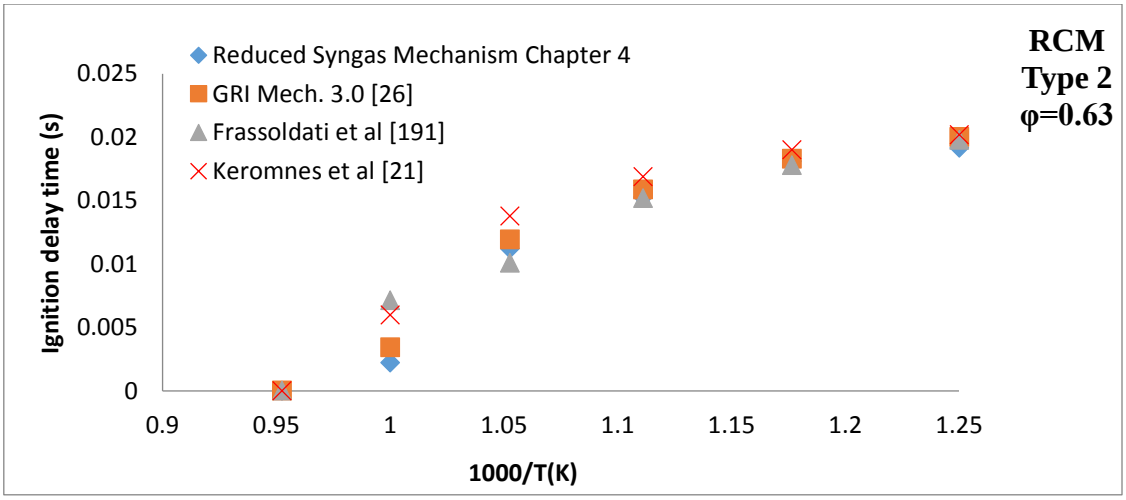

b

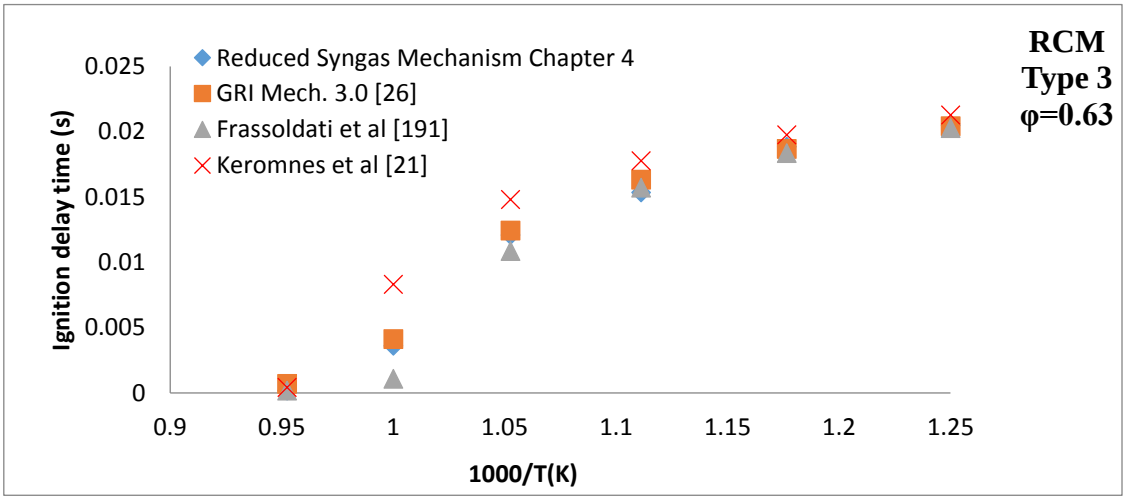

c)

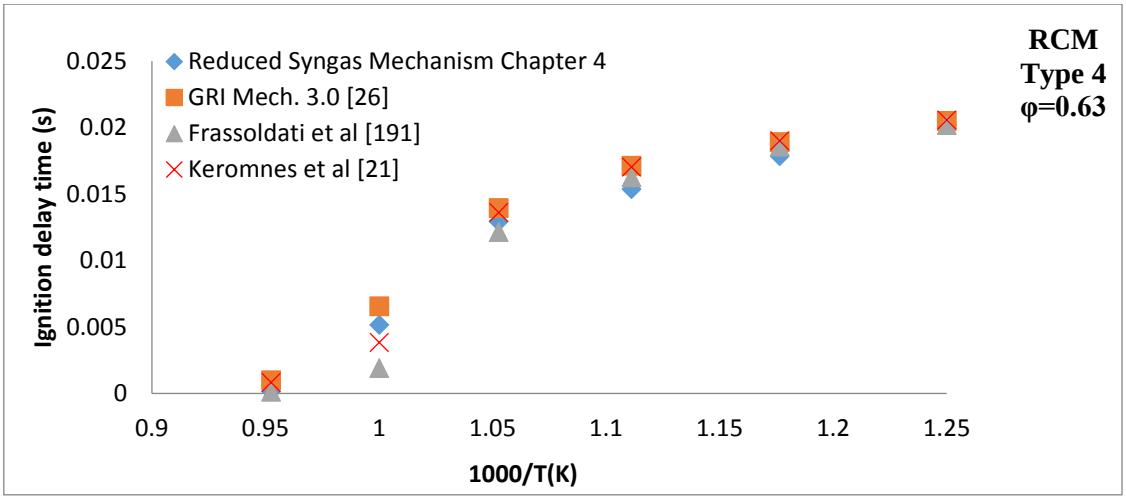

d)

Figure 4-2 (cont.) Comparison of ignition delay time for Fuel 24 syngas Types 1-4 obtained with new mechanism with other mechanisms at temperatures 800–1053 K, pressure 2.25 bar and equivalence ratio = 0.63

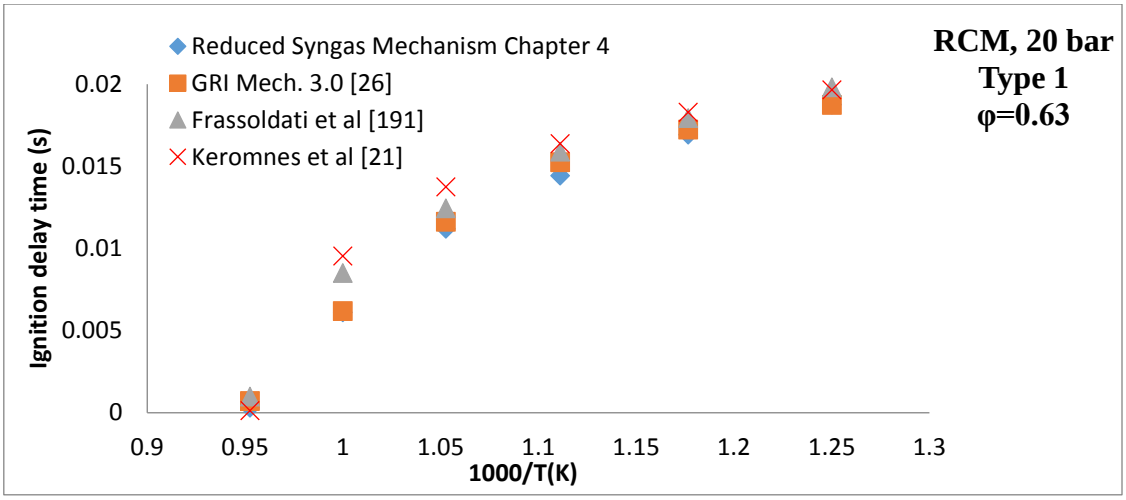

a)

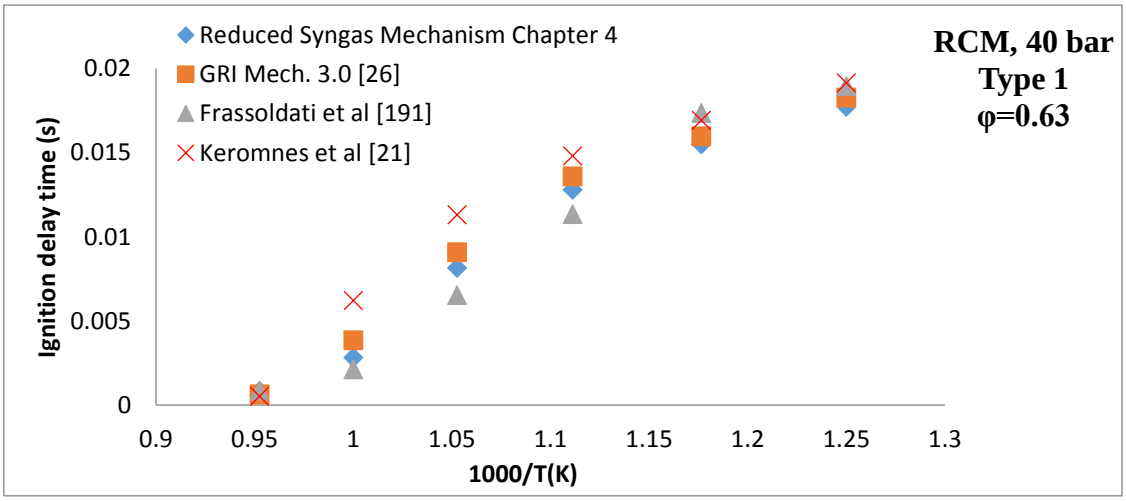

b)

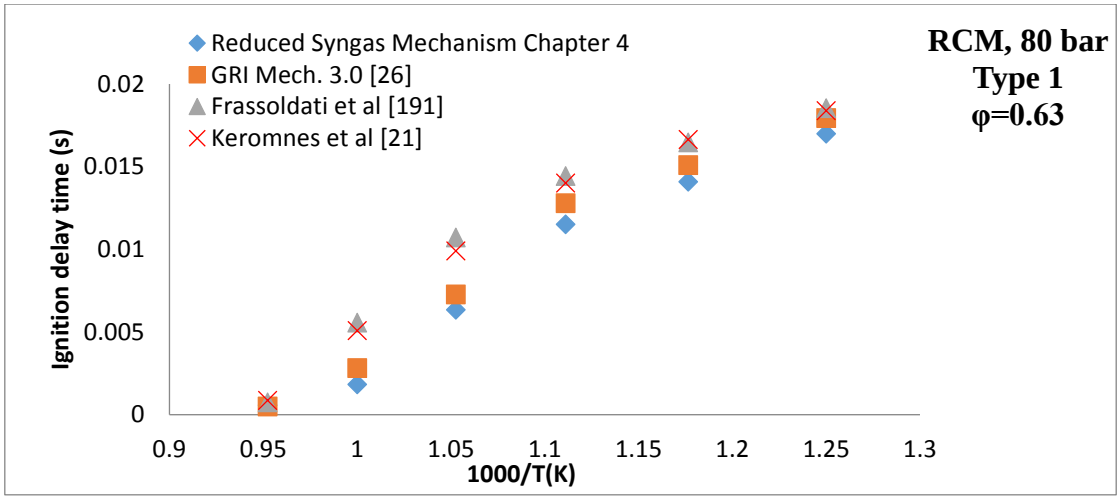

c)

Figure 4-3 Comparison of ignition delay time for Fuel 24 syngas Type 1 obtained with new mechanism with other mechanisms at temperatures 800-1053K, pressures 20, 40, 80 bars and equivalence ratio 0.63.

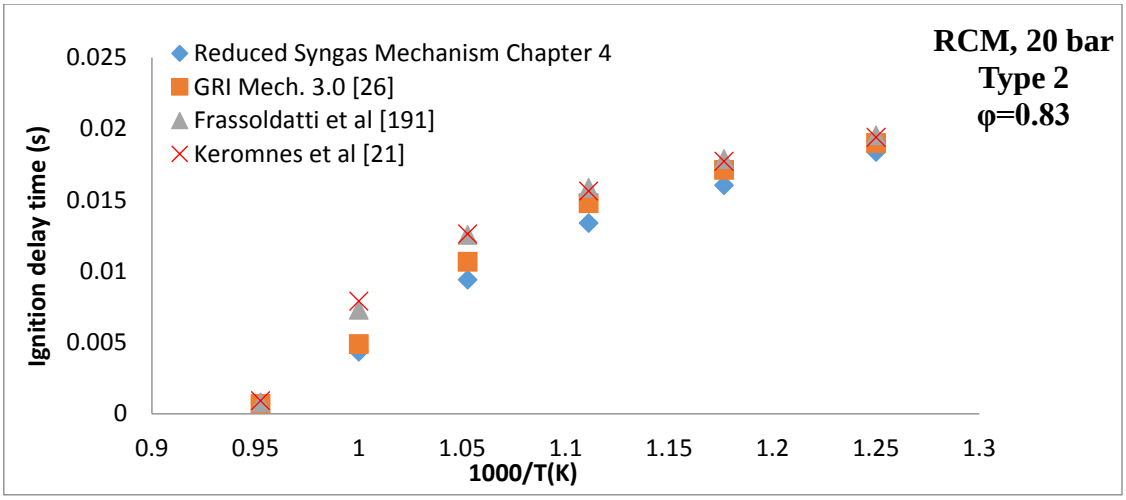

a)

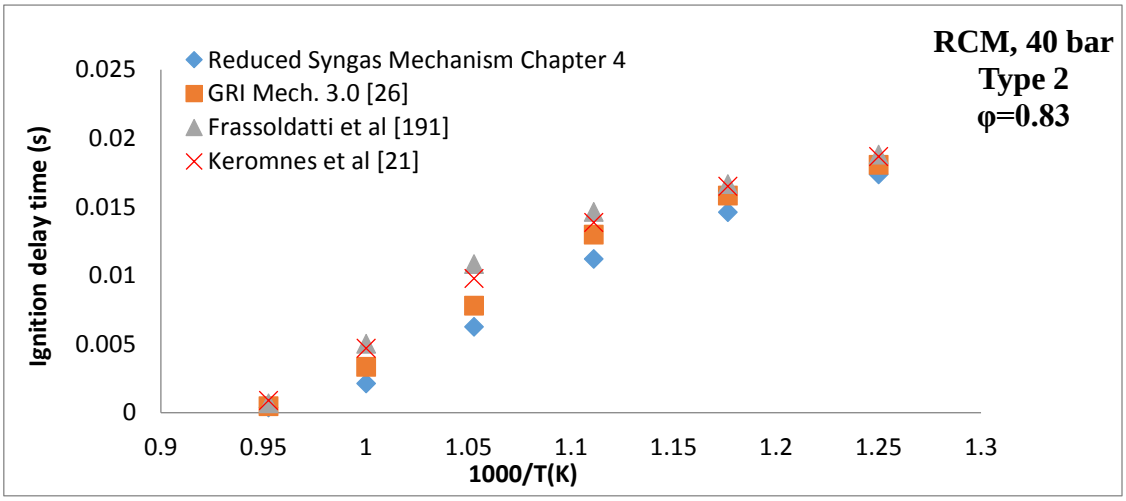

b)

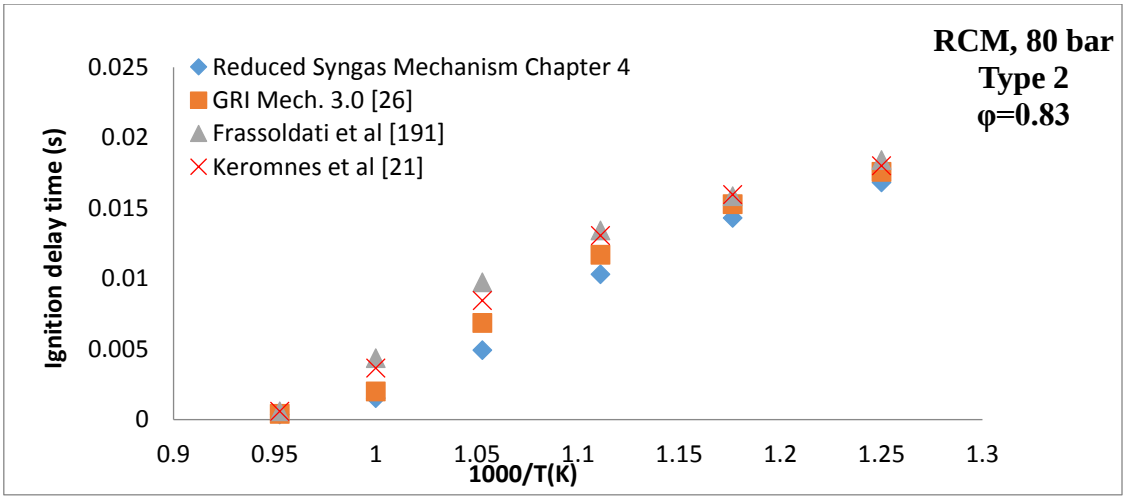

c)

Figure 4-4 Comparison of ignition delay time for Fuel 24 syngas type 2 obtained with new mechanism with other mechanisms at temperatures 800-1053K, pressures 20, 40, 80 bars and equivalence ratio 0.83.

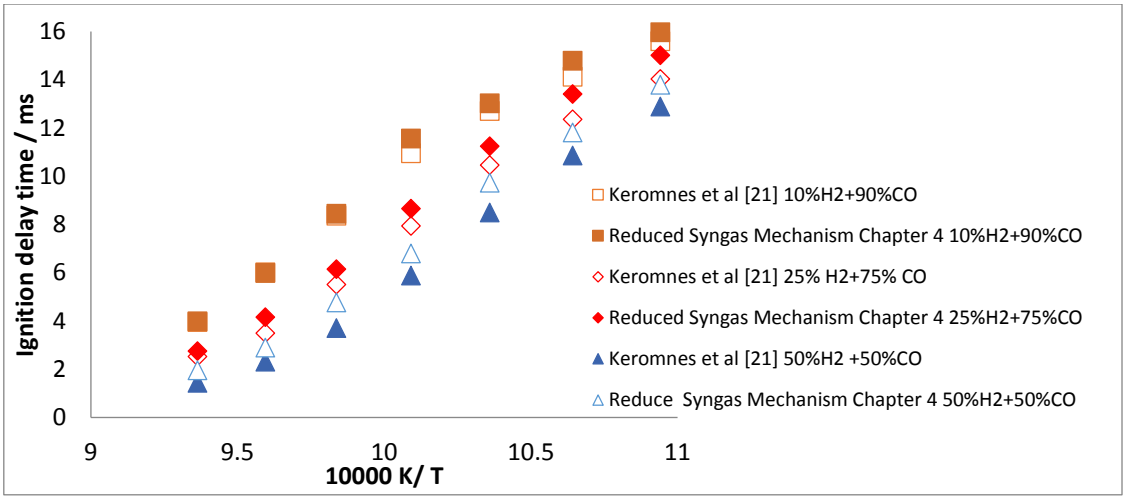

Figure 4-5 Effect of CO concentration on ignition delay times of syngas mixtures compared with Keromnes et al. [21] mechanism.

4.1.3 Flame speed

The flame speed analysis was performed to compare the LFS (LFS) obtained using the new mechanism with that of Keromnes et al. [21], Frassoldati et al. [191] and GRI Mech 3.0 [26]. Fig. 4-6 shows that for Fuel 24 syngas Types 1–4 over a range of equivalence ratios, the new mechanism showed an identical trend in LFS as the one obtained using the above mentioned mechanisms. For Fuel 24 syngas Type 4, the GRI Mech 3.0 mechanism slightly over predicted the LFS. This is due to the high H_2 concentration in the Type 4 syngas. GRI Mech 3.0 was developed to simulate mainly natural gas combustion and was not designed to predict the oxidation of fuel with high H_2 content. Figure 4-6 also shows that the LFS for syngas Fuel 24 Type 2 is slightly higher due to higher H2 concentration compared to syngas Types 1 and 3.

The new mechanism was also used for the simulation of LFS for $H_2/CO/CO_2$ mixture and was compared with the experimental data of Hu et al. [172] and predictions from the different kinetics models [21, 26, 191] over a range of equivalence ratios= 0.4–1.0. Fig. 4-7 shows the flame speed calculated using the chemical kinetics mechanisms for $H_2/CO/CO_2$ – 35:35:30 mixture, Fuel 6 (Table 3-3), at different pressures and temperatures. The new mechanism performed remarkably well at predicting the LFS across all the equivalence ratios investigated by Hu et al. [172].

In this study, the LFS of H_2/ CH_4 at a range of CH_4 ratios and equivalence ratios was also considered, to evaluate the new mechanism. Fig. 4-8 shows the LFS for various H_2:CH_4 ratios, Fuel 7 Types 1, 2 and 3, at T = 298 K and P = 1.01 bar (1 atm) and equivalence ratio ranging from 0.4 to 1.2. For H_2/CH_4 mixtures, the LFS results obtained with the new mechanism exhibit the best agreement with the laminar speed data obtained using Keromnes et al. [21] and the GRI Mech 3.0 [26] mechanisms. Moreover, the developed mechanism captures accurately the

effect of the methane concentration included in the mixture on the maximum LFS; The higher is the concentration of methane in the mixture, the lower is the reactivity of the mixture and therefore the lower is the LFS. This is highlighted by the comparison of the maximum LFS for 10%vol CH_4, Figure 4-8 a, approximately 250 cm/s and the maximum LFS for CH_4 50%vol, Figure 4-8 c, approximately 150 cm/s.

LFS was also evaluated at high pressures.(P = 20 , 40 and 80 bar). Fig. 4-9 shows that for Fuel 24 Type 1, at P = 20 and 40 bar the laminar speed data obtained using the new mechanism matches well with those obtained using the GRI Mech 3.0 mechanism, showing slight deviation from the LFS obtained using Keromnes et al. [21] and Frassoldati et al. [191] mechanisms. However, this difference gradually disappears at lower equivalence ratio levels, those usually used in dual-fuel engine combustion. At high pressure of 80 bar the LFS data matches well for all tested mechanisms and equivalence ratios.

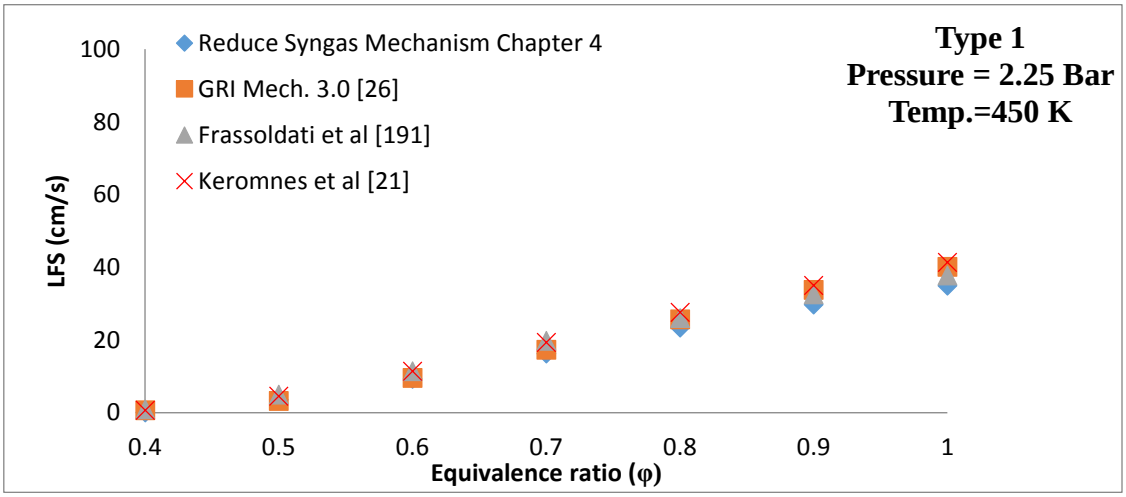

a)

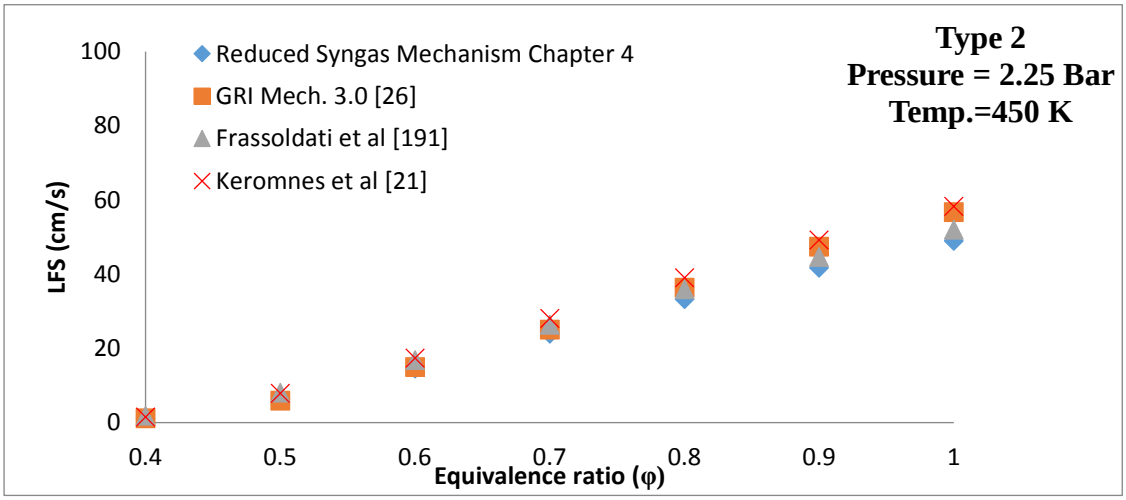

b)

Figure 4-6 LFS results obtained with new mechanism for a) syngas Fuel 24 Types 1 (13.7/22.3/16.8/1.9/45.3 %vol) b) syngas Fuel 24 Type 2(20.0/22.3/16.8/1.9/39.0 %vol) c) syngas Fuel 24 Type 313.7/22.3/23.0/1.9/39.1 %vol) and d) syngas Fuel 24 Type 4 (56.8/5.9/2.2/29.5/5.6 %vol) at pressures 2.25 Bar and temperature 450 K

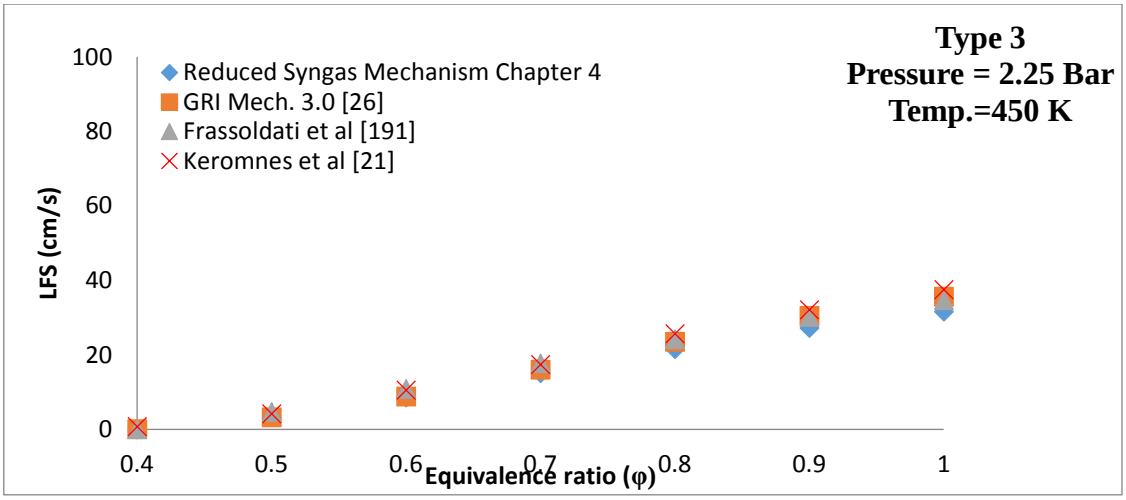

c)

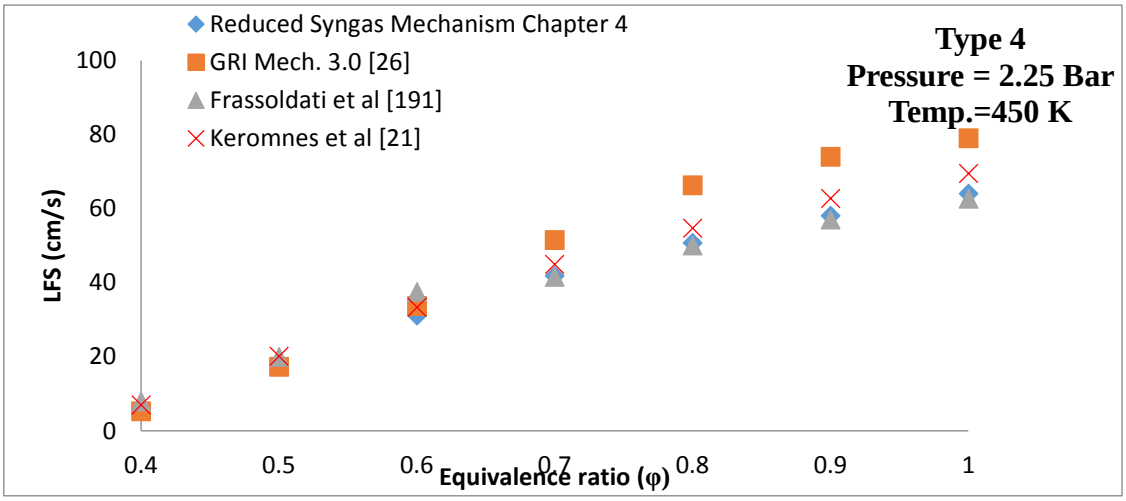

d)

Figure 4-6 (cont.) LFS results obtained with new mechanism for a) syngas Fuel 24 Types 1 (13.7/22.3/16.8/1.9/45.3 %vol) b) syngas Fuel 24 Type 2(20.0/22.3/16.8/1.9/39.0 %vol) c) syngas Fuel 24 Type 313.7/22.3/23.0/1.9/39.1 %vol) and d) syngas Fuel 24 Type 4 (56.8/5.9/2.2/29.5/5.6 %vol) at pressures 2.25 Bar and temperature 450 K

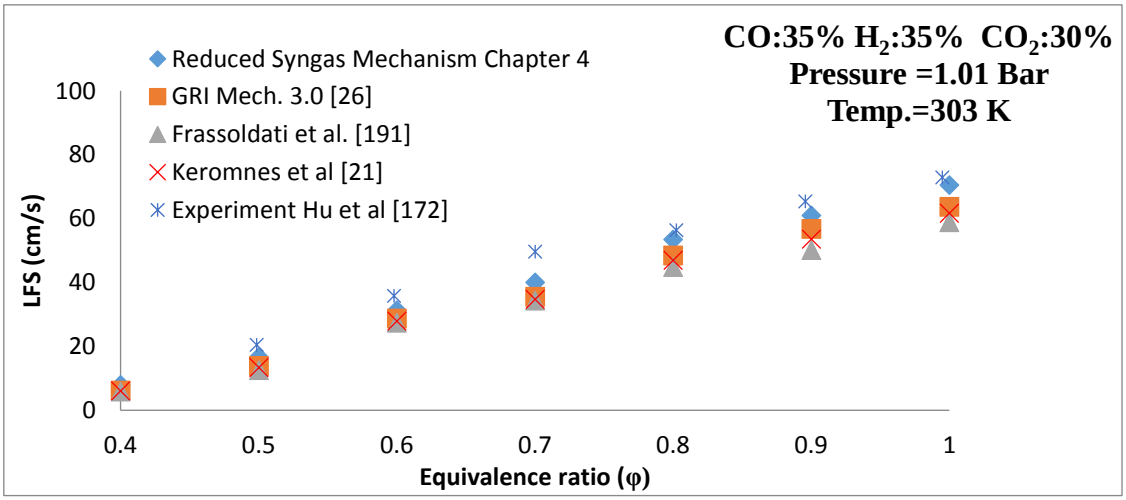

a)

Figure 4-7 LFS of H_2/CO/CO_2 -35:35:30 fuel mixture at a) pressure 1.01 Bar and temperature 303 K, b) pressure 1.01 Bar and temperature 373 K and c) pressure 3.04 Bar and temperature 373 K.

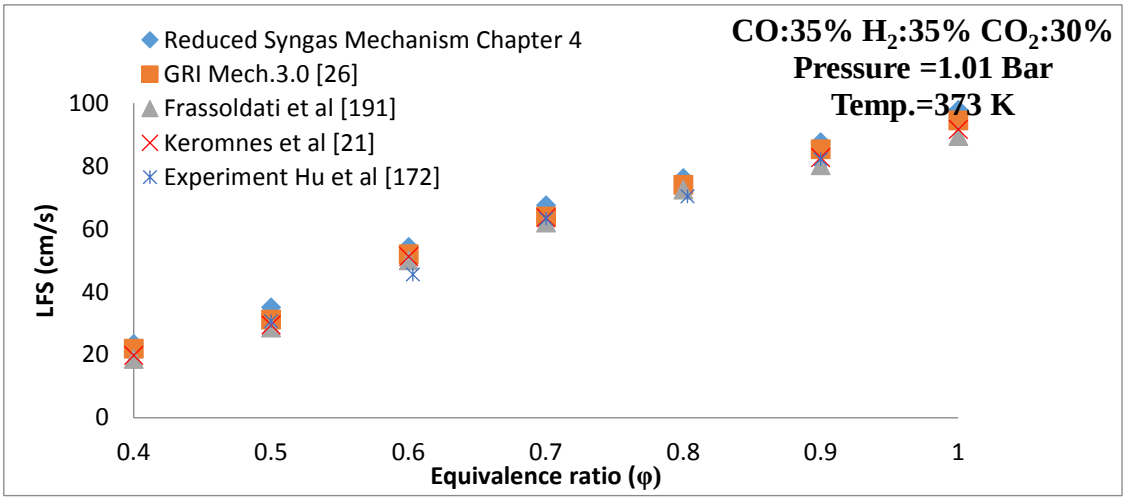

b)

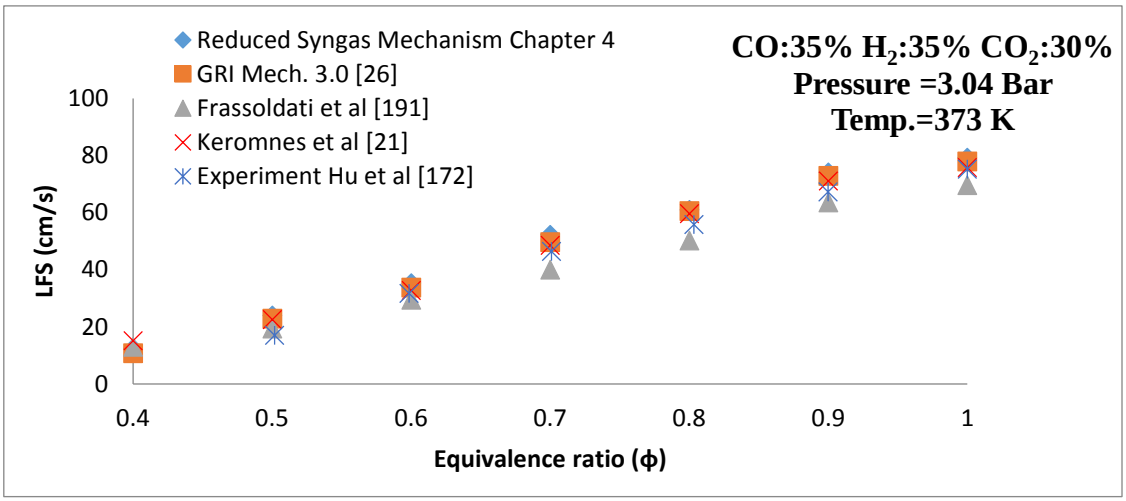

c)

Figure 4-7 (cont.) LFS of H_2/CO/CO_2 -35:35:30 fuel mixture at a) pressure 1.01 Bar and temperature 303 K, b) pressure 1.01 Bar and temperature 373 K and c) pressure 3.04 Bar and temperature 373 K.

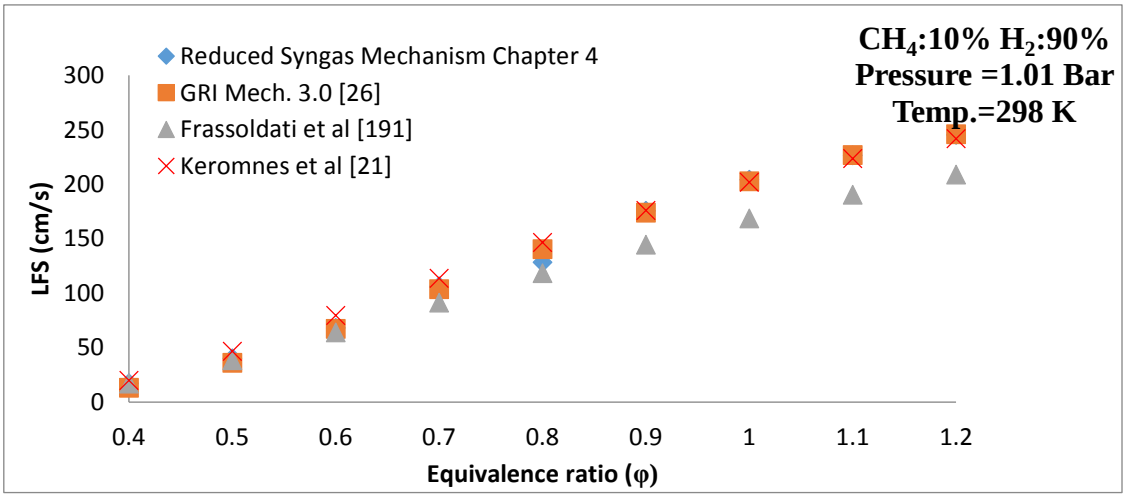

a)

Figure 4-8 Calculated LFS of obtained with new mechanism and compared with different kinetic models for a) CH_4 10% / H_2 90% , b) CH_4 30% / H_2 70% and c) CH_4 50% / H_2 50% at pressure 1.01 Bar and temperature 298K

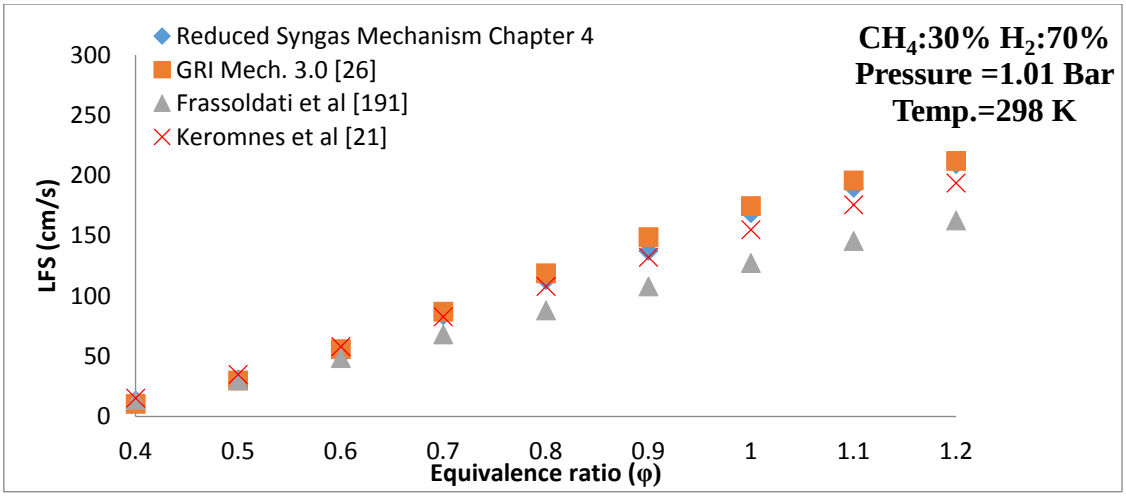

b)

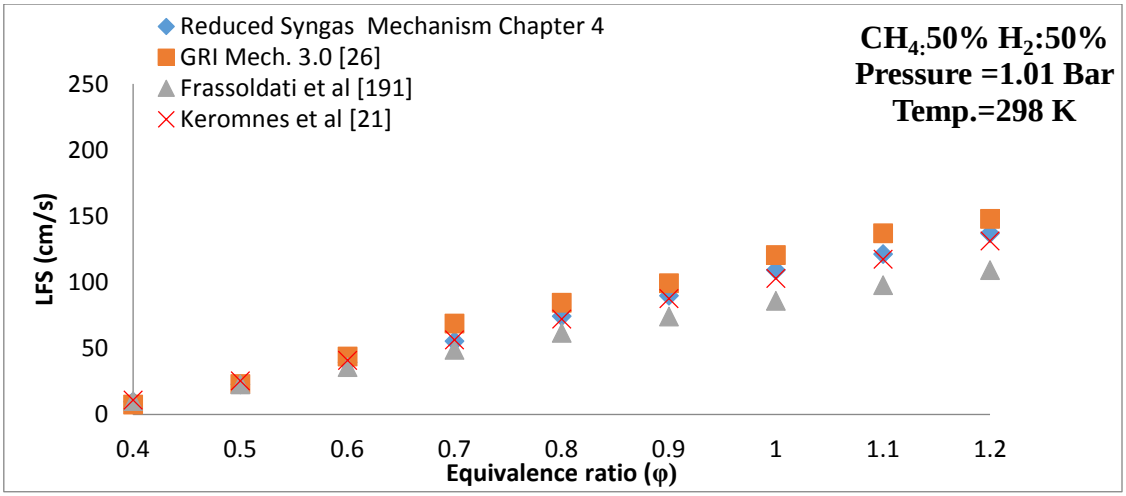

c)

Figure 4-8 (cont.) Calculated LFS of obtained with new mechanism and compared with different kinetic models for a) CH_4 10% / H_2 90% , b) CH_4 30% / H_2 70% and c) CH_4 50% / H_2 50% at pressure 1.01 Bar and temperature 298K

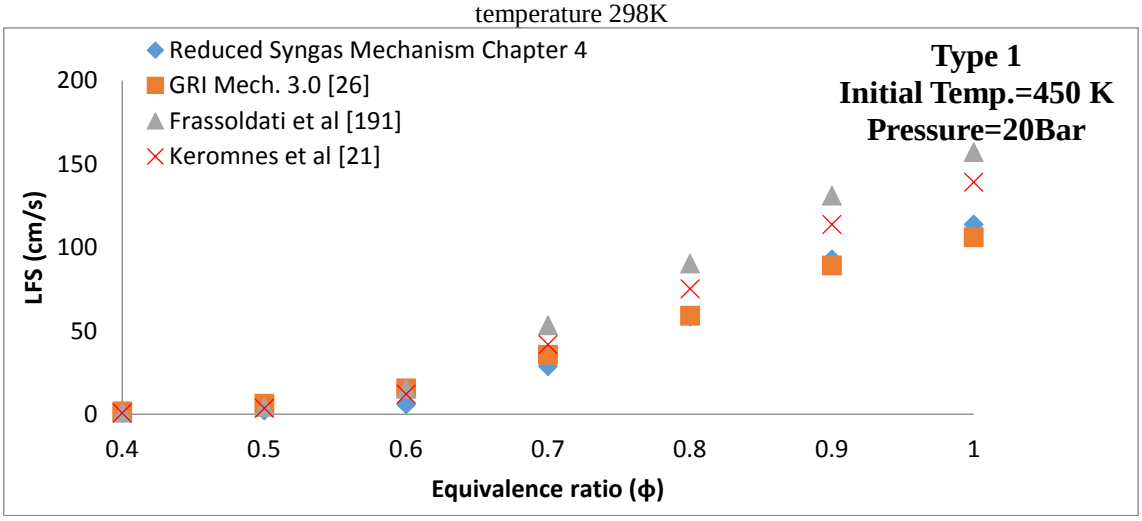

a)

Figure 4-9 Effect of pressure on the LFS obtained with new mechanism for syngas Fuel 24 Type 1(13.7/22.3/16.8/1.9/45.3 %vol) at pressure20 Bar and temperature 450 K, b) pressure 40 Bar and temperature 450 K and c) pressure 80 Bar and temperature 450 K.

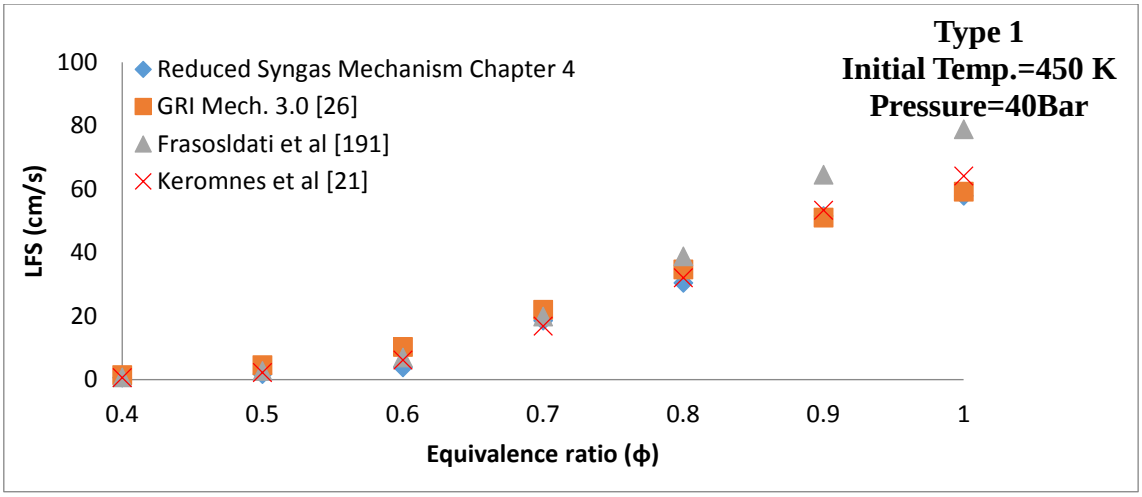

b)

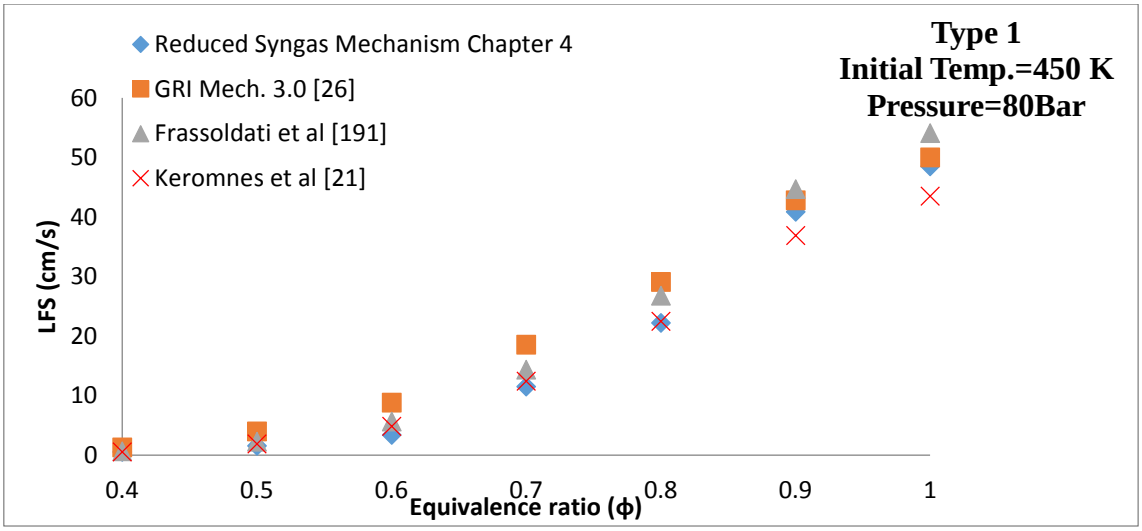

c)

Figure 4-9 (cont.) Effect of pressure on the LFS obtained with new mechanism for syngas Fuel 24 Type 1 (13.7/22.3/16.8/1.9/45.3 %vol) at pressure20 Bar and temperature 450 K, b) pressure 40 Bar and temperature 450 K and c) pressure 80 Bar and temperature 450 K.

4.2 Results and discussion

4.2.1 Mechanism validation for CFD combustion analysis

To validate the mechanism for the engine in-cylinder-like conditions in a dual-fuel engine, the mechanism was used in a multidimensional CFD analysis by applying the pilot injection. Experimental results for CFD were only available for in-cylinder pressure and ROHR. Therefore, validation of the mechanism against experimental results for laminar flame speed, exhaust gas temperature and emissions is consider as a future task when such experimental results will be available. Fig. 4-10 compares the in-cylinder pressure obtained by a new mechanism using CFD code with that of Slavinskaya et al. [238], Keromnes et al. [21], Frassoldatti et al. [191], GRI Mech 3.0 [26] and an engine experiment [78]. Fig. 4-10 shows that new mechanism accurately simulates the engine in-cylinder combustion for syngas with different compositions, Fuel 24 Types 1, 2 and 3, where other syngas mechanisms show very

large deviation from experiments. A similar trend was observed for a range of different equivalence ratios and injection timings. The deviation between the experimental and simulating results especially on the region between 10-50 CA is directly related with the different rate constants of the reactions included in each mechanism. The tested mechanisms were constructed by other authors for the simulation of different mixtures (for example H_2/CO mixtures) and therefore cannot capture accurately syngas combustion. Moreover, the mechanisms compared in Figure 4-10, Slavinskaya et al. [238], Keromnes et al. [21], Frassoldatti et al. [191], GRI Mech 3.0 [26], cannot be reported as original contribution of this research and therefore are not included in detail in this thesis.

Moreover, in order to check the computational efficiency of the mechanism, the CPU time required for a full CFD simulation was calculated and compared with other mechanisms. The CPU time required for a full CFD simulation and the number of reactions of each mechanism implemented into the CFD are presented and compared in Table 4-2. It can be seen that, in addition to the high level of accuracy of the developed mechanism, it requires the lowest CPU time for a full simulation in comparison with other mechanisms and has the lowest number of reactions, which leads to a significant reduction in complexity when the mechanism is used.

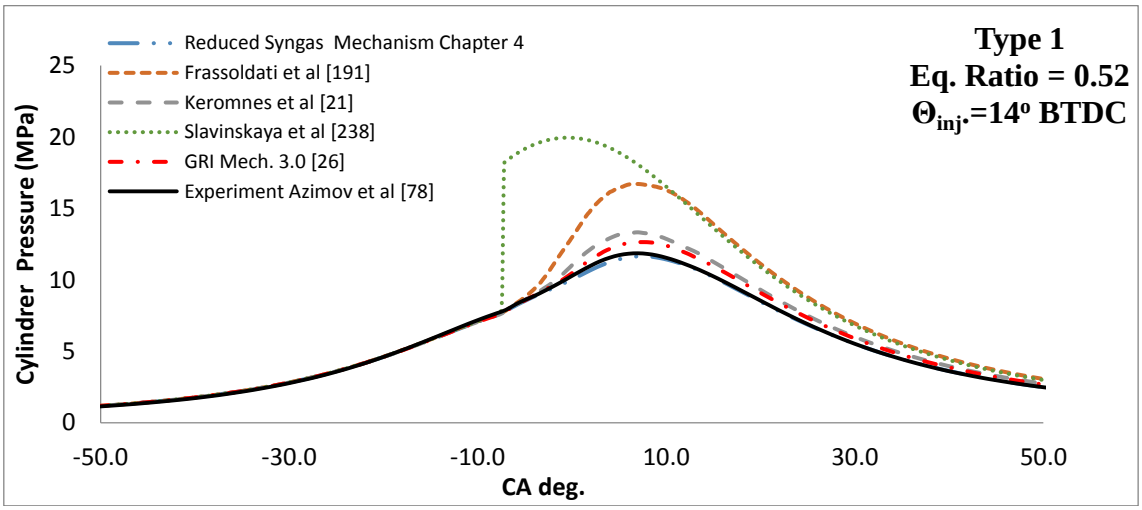

a)

Figure 4-10 Comparison of CFD in-cylinder pressure obtained using the new mechanism with the experimental results from Azimov et al [78] and the simulated results using different chemical kinetics mechanisms for Fuel 24 syngas Types 1-3, equivalence ratio 0.52 ,0.48 and 0.6 and different timings of fuel micro-pilot injection.

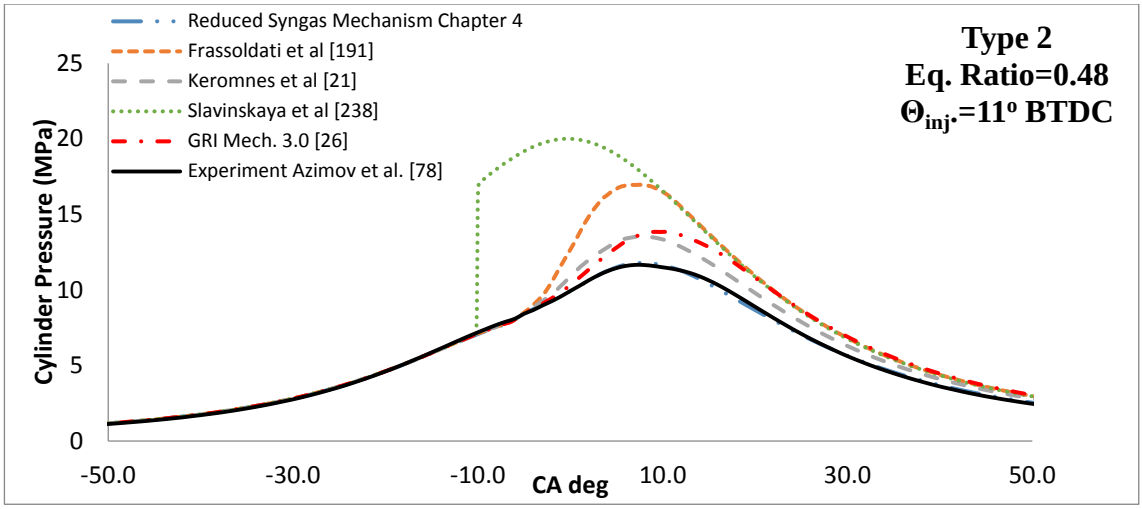

b)

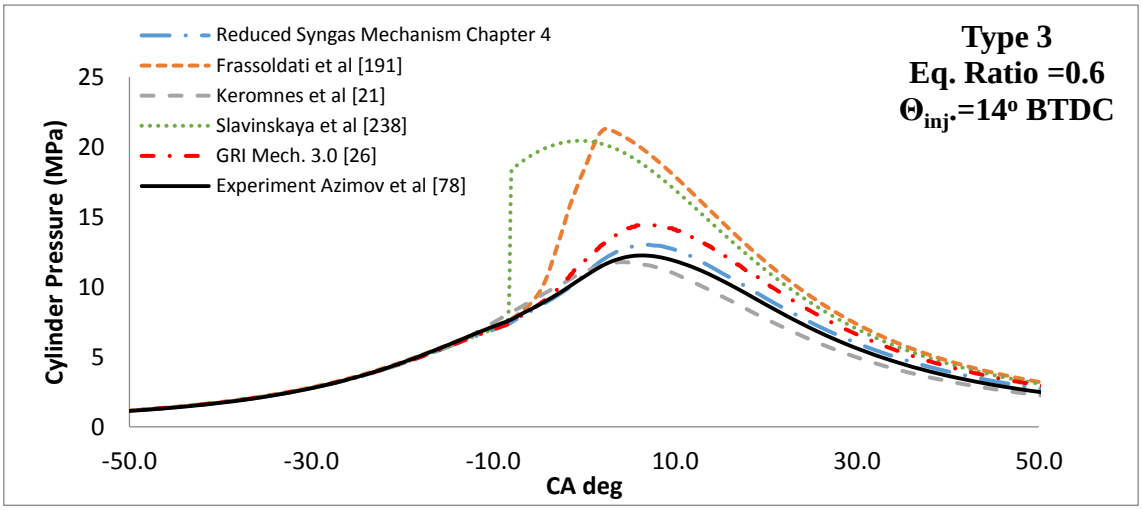

c)

Figure 4-10 (cont.) Comparison of CFD in-cylinder pressure obtained using the new mechanism with the experimental results from Azimov et al [78] and the simulated results using different chemical kinetics mechanisms for Fuel 24 syngas Types 1-3, equivalence ratio 0.52 ,0.48 and 0.6 and different timings of fuel micro-pilot injection.

Table 4- 2 Comparison of the CPU time and the number of reactions of the mechanism developed in Chapter 4 with other well-validated mechanisms

	Chemical Kinetics Mechanisms	Reactions	CPU Time
	Syngas Mechanism		
1	Reduced Syngas Mechanism for low H_2 concentration (Chapter 4)	32	2 hours
2	GRI mech. 3.0. [26]	325	1 day
3	Constructed Mechanism 1 (Frassoldatti et al [191] + CH_4)	173	15 hours
4	Constructed Mechanism 2 (Keromnes et al [21] +CH_4)	40	2.5 hours
5	Slavinskaya et al [238]	28	2 hours

4.2.2 Chemical kinetics mechanism for syngas with high H_2 content

The developed mechanism showed a good match between simulation results and experimental data for Fuel 24 syngas Types 1–3 (biomass solid feedstock) at various equivalence ratios and injection timings. However, with this mechanism the combustion rate was much higher for syngas Fuel 24 Type 4 (coke-oven solid feedstock). The higher combustion rate was due to the higher H_2 concentration (>50%). The comparison between the simulated in-cylinder pressure by using the new developed syngas mechanism and the experimental measurements obtained from Azimov et al [78], for Fuel 24 Type 4, at eq. ratio 0.6 and $\Theta_{inj.}$ 3^{o}BTDC is presented in Figure 4-11.

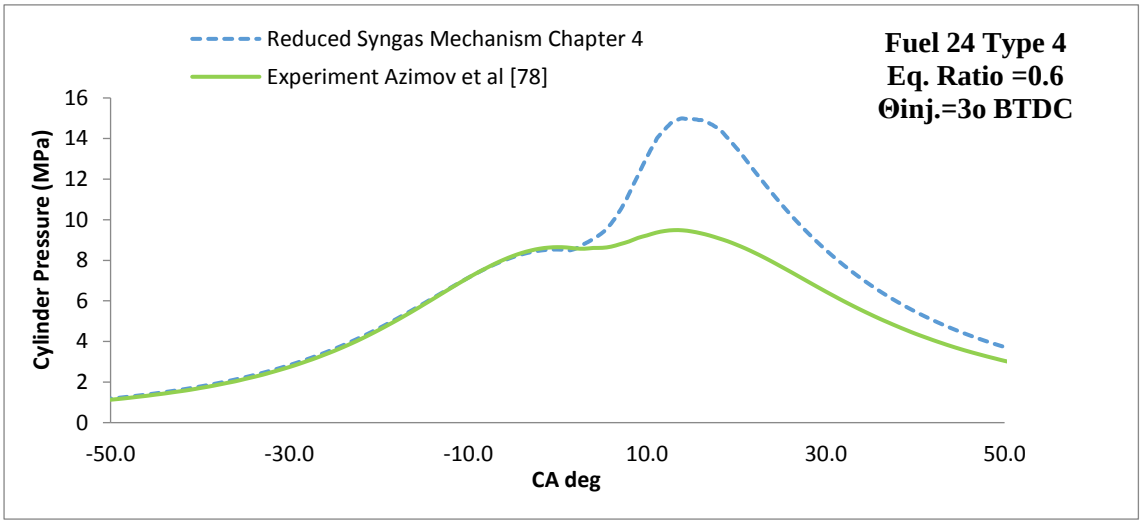

Figure 4-11 .Comparison of CFD in-cylinder pressure obtained using the new mechanism with the experimental measurements obtained from Azimov et al [78], for Fuel 24 syngas Type 4 equivalence ratio 0.6 and Θinj.=3o BTDC

By following the results from the sensitivity analysis presented in Figure 4-1 for syngas mixtures with H_2<20%vol, it was expected that hydrogen based reactions responsible for the formation of OH high reactive radicals such as reactions $H_2O_2 + H = H_2 + HO_2$ and $H_2O_2 (+M) = OH + OH (+M)$ to play a critical role also for syngas mixtures with H_2 <50%vol.

In order to investigate the important reactions affecting syngas combustion when syngas mixtures with high H_2 content are used, a second reaction sensitivity analysis was performed. Reaction sensitivity for syngas mixtures with high H_2, Fuel 24 Type 4, is presented in Figure 4-12. The Figure shows the high sensitivity of $H_2O_2(+M) = OH + OH(+M)$, $H_2O_2 + H = H_2 + HO_2$, and $HO_2 + HO_2 = H_2O_2 + O_2$ reactions and low sensitivity of HO2 + H = OH + OH reaction. It should be noticed that reactions R7, R27 and R30 were not shown as sensitive in Fig. 4-1 when the original mechanism was applied to syngas Fuel 24 Type 1 (H_2-13.7%) and showed strong sensitivity in Fig. 4-12 when the modified mechanism was applied to syngas Fuel 24 Type 4 (H_2-56.8%). A brief description of these three reactions is given below.

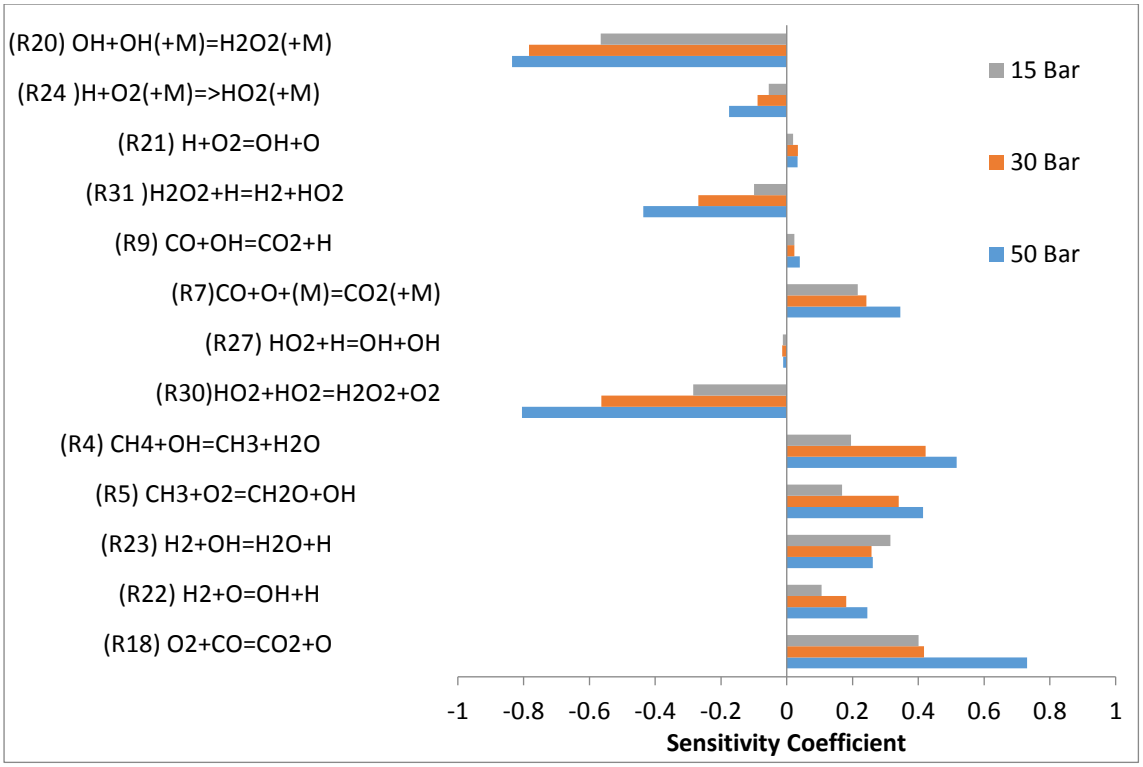

Figure 4-12. The most sensitive reaction for modified syngas mechanism at equivalence ratio 0.63, temperature 1000K and pressures 10, 30 and 50 bar.

(R7) CO + O (+M) = CO_2 (+M)

R7 is responsible for the conversions of CO to CO_2 and is very sensitive at high pressures and high temperatures. In order to estimate accurately the dependence of R7 on the temperature and pressure, low pressure limit rate constants must be used [211]. Frassoldati et al [207], focused on the low pressure limit of R7, and proposed new rate constants that were validated against experimental results. According to the authors, by using the new rate constants the deviation between the numerical and experimental results was lower than 10% , while the pressure dependency of R7 was captured accurately. Therefore, for this research the high and low pressure limit rate constants which were proposed by Frassoldati et al. [191] and validated against experimental data were used.

(R27) HO_2 + H = OH + OH

According to O'Conaire et al. [195], changing the rate constant of R27 has an adverse effect on the results of the flow reactor simulations. They suggested a rate constant for R27 which is within the limits of the experimental data obtained from the NIST database [239], and has a lower uncertainty factor. In this research, the rate constants proposed by O'Conaire [195] were adopted because they are within the limits of the experimental data.

(R30) HO_2 + HO_2 = H_2O_2 + O_2

This reaction is very sensitive during low temperature and high pressure conditions [240]. Both reactions, R30 with R31, contribute to the formation of H_2O_2 which in turn decomposes into

two highly reactive OH radicals through reaction R20. However, it can be said that R30 and R31 are competitors; in which R30 increases the reactivity as it produces two HO_2 radicals while R31 inhibits the reactivity as it produces only one HO_2 radical. Keromnes et al [21] proposed a new set of rate constants for R22. The authors validated the rate constants by comparing with experimental results showing that the rate constants perform remarkably well especially at high pressure conditions. Therefore, the set of rate constants used by Keromnes et al. [21] were chosen for this study.

Comparison of two sensitivity analyses for Fuel 24 Type 1, shown in Fig. 4-1 and for Fuel 24 Type 4, shown in Fig. 4-12, suggest that for Type 1, with lower H_2 content, more carbon-based reactions play an important role in chemical kinetics, whereas, for Type 4 with higher H_2 content, the number of hydrogen-based sensitive reactions prevailed. This is because the hydrogen concentration included in Fuel 24 Type 4 is >50% and therefore hydrogen chemistry became the dominant kinetics pathway in the mechanism and controls the reactivity of the mixture. The decomposition rate of H_2O_2 and the formation rate of OH species are faster and higher amount of OH species are formed resulting in more intense combustion. Therefore, more reactions responsible for the decomposition of H_2O_2 and the formation of OH appeared in the sensitivity analysis in Figure 4-12, having higher sensitivity factor in comparison with the sensitivity analysis of Figure 4-1 for H_2<13.7%.

Figs. 4-13 and 4-14 show the flow of species of carbon and hydrogen in syngas Fuel 24 Type 1 and Type 4. It is important to be mentioned here that for the flow analysis presented in Figures 4-13 and 4-14, fluxes for H below 1% of maximum flow have been filtered. According to Figure 4-13, it can be seen that for carbon atoms of both syngas types, the major paths represent the high-temperature hydrocarbon oxidation of CH_4 through CH_3 and further oxidation of CH_3 to CH_2O. Moreover according to Figure 4-14, the flow analysis for hydrogen species at lower H_2 content of syngas Fuel 24 Type 1, shows an identical trend at pressures of 10, 30 and 50 bar with the flow analysis of syngas Fuel 24 Type 4, H_2>50%vol. The flow rates between the species increased by increasing the pressure. For example for Fuel 24 Type 1 Figure 4-14 A, the forward flow rate from OH to H_2O species at 10 bar is 7480 mol/(cm^3 sec) while at 50 bar increased to 809994 mol/(cm^3 sec). Similar trend can be observed also for Fuel 24 Type 4 Figure 4-14 B, in which the forward flow rate from OH to H_2O_2 is 20438 mol/(cm^3 sec) at 10 bar and increased to 2453580 mol/(cm^3 sec) at 50 bar.

Moreover, when Fuel 24 Type 4 (H_2 > 50 %vol) used, the flow rate between the species and especially between H_2O_2 to OH (backward and forward flow rate) is much higher than when

Fuel 24 Type 1 (H_2 < 20 %vol). For example, at pressure 50 bar the flow rate from OH to H_2O_2 for Fuel 24 Type 4 is 276595 mol/(cm^3 sec) while for Fuel 24 Type 1 is 109015 mol/(cm^3 sec). This indicates that for higher H_2, hydrogen chemistry is more dominant and the formation of OH species is faster in comparison to lower hydrogen concentrations, increasing the reactivity of the mixture.

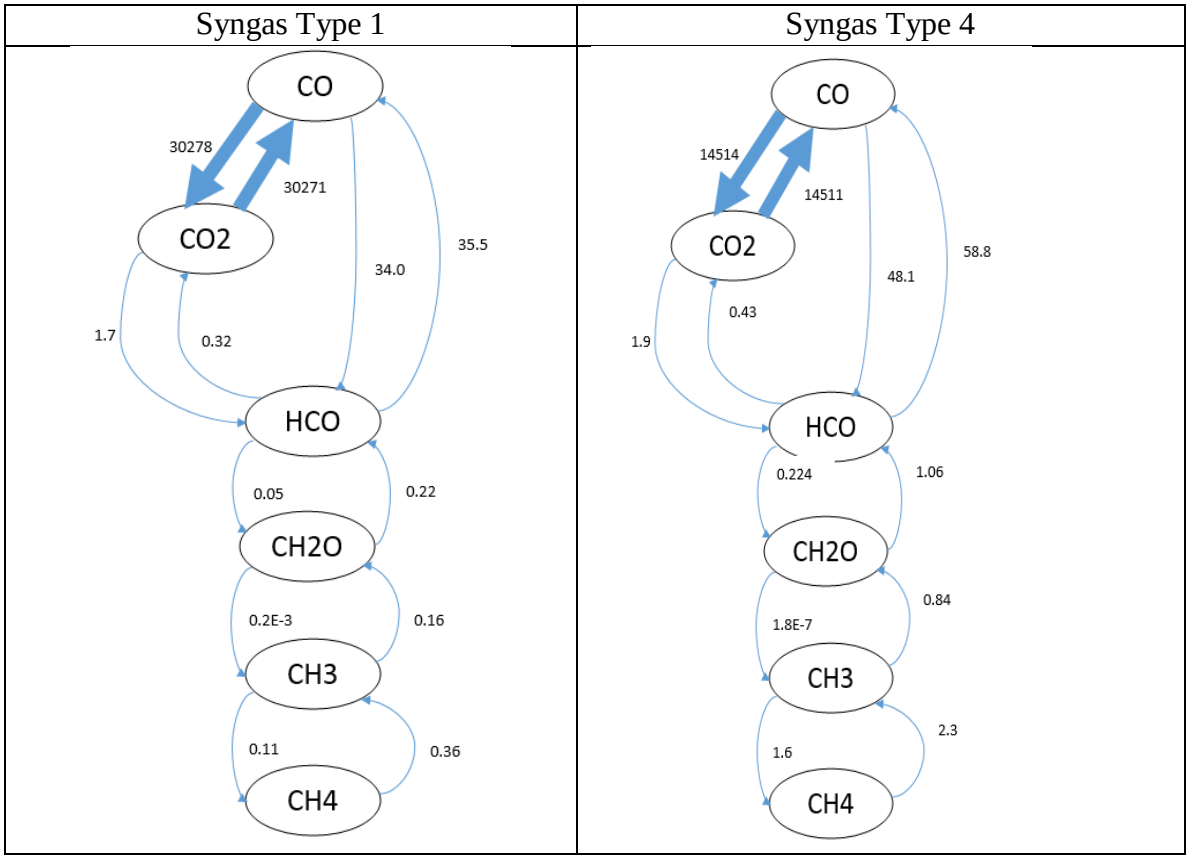

Figure 4-13 Comparison of reaction flows of carbon atoms for syngas Fuel 24 Type 1(H_2 13.7/CO 22.3/ CO_2 16. 8/ CH_4 1.9/ N_2 45 %vol.) and Type 4 (H_2 56.8/CO 5.9/ CO_2 2.2/ CH_4 29.5/ N_2 5.6 %vol.)at 30 bar. Flow values are given in mol/(cm3 sec).

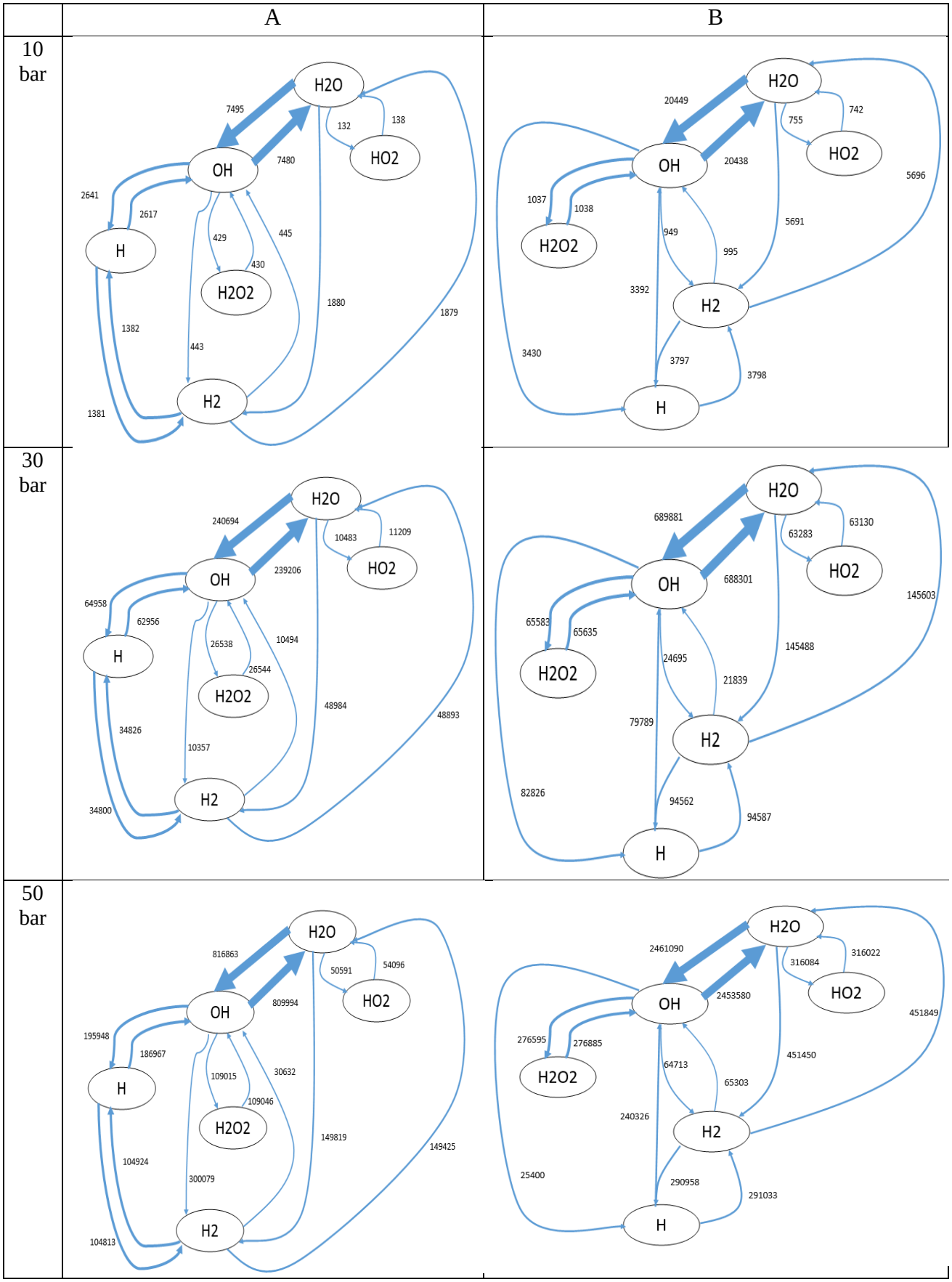

Figure 4-14. Comparison of reaction flows of hydrogen atoms for syngas at temperature 1000 K and pressures 10, 30 and 50 bar. (A) Fuel 24 Type 1(H_2 13.7/CO 22.3/ CO_2 16. 8/ CH_4 1.9/ N_2 45 %vol.), (B) Fuel 24 Type 4 (H_2 56.8/CO 5.9/ CO_2 2.2/ CH_4 29.5/ N_2 5.6 %vol.). Fluxes below 1% of maximum flow have been filtered. Flow values are given in mol/(cm3 sec).

Ignition delay time and LFS obtained using the modified mechanism were compared with those obtained using Keromnes et al. [21], Frassoldatti et al. [191], GRI Mech 3.0 [26]. Fig. 4-15 shows that the modified mechanism used to simulate syngas with a high H_2 concentration, Fuel 24 Type 4, accurately predicted ignition delay and LFS. Moreover the mechanism captures accurately the effects of the equivalence ratio on laminar flame speed and the temperature on ignition delay time; The higher is the equivalence ratio, the richer is the mixture and therefore the higher is the intensity of the combustion and the laminar flame speed. On the other hand, the higher is the temperature the lower is the ignition delay time of the mixture.

To estimate the effect of different rate constants on the in-cylinder heat production and pressure rise, the mechanism was tested by running 3D CFD analyses with reaction rate constants proposed by different authors, see Table 4-3. Fig. 4-16 shows in-cylinder pressure CFD results for syngas composition of Fuel 24 Type 4. H_2O_2 +H=H_2 + HO_2 reaction constants proposed by Hong et al. [196] and adjusted power factor n = 0.0 showed the closest match with experimental data and therefore were adopted in the new modified mechanism for high hydrogen concentrations .

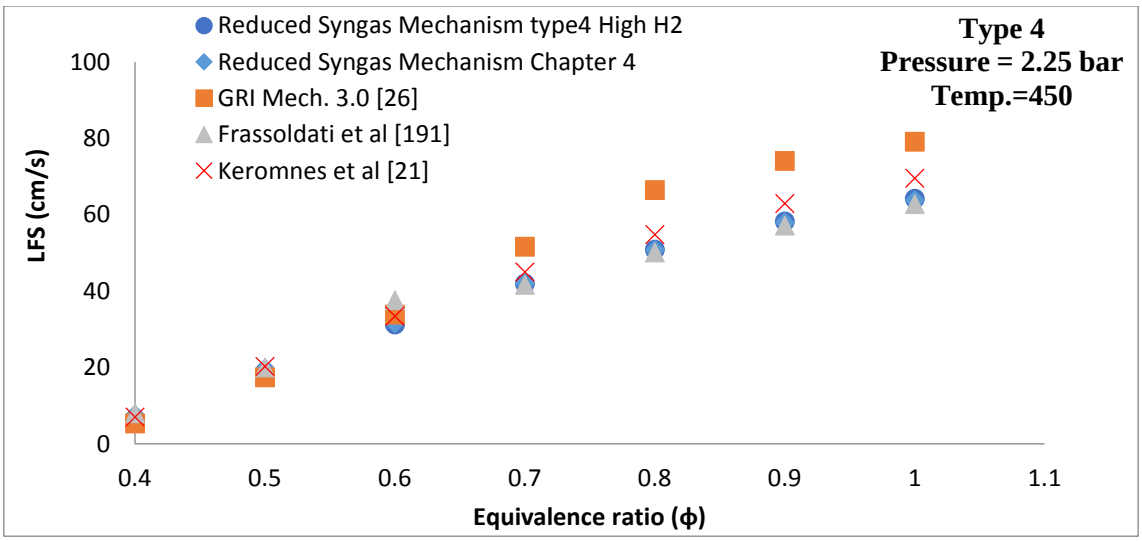

a)

Figure 4-15. Data obtained with modified mechanism for syngas Fuel 24 Type 4 with high H2 and compared with other kinetic mechanisms. (a) LFS calculated at temperature 450K, pressure 2.25 bar and equivalence ratio 0.4-1.0, and (b) Ignition delay calculated at temperatures 800-1052K, pressure 2.25 bar and equivalence ratio 0.6.

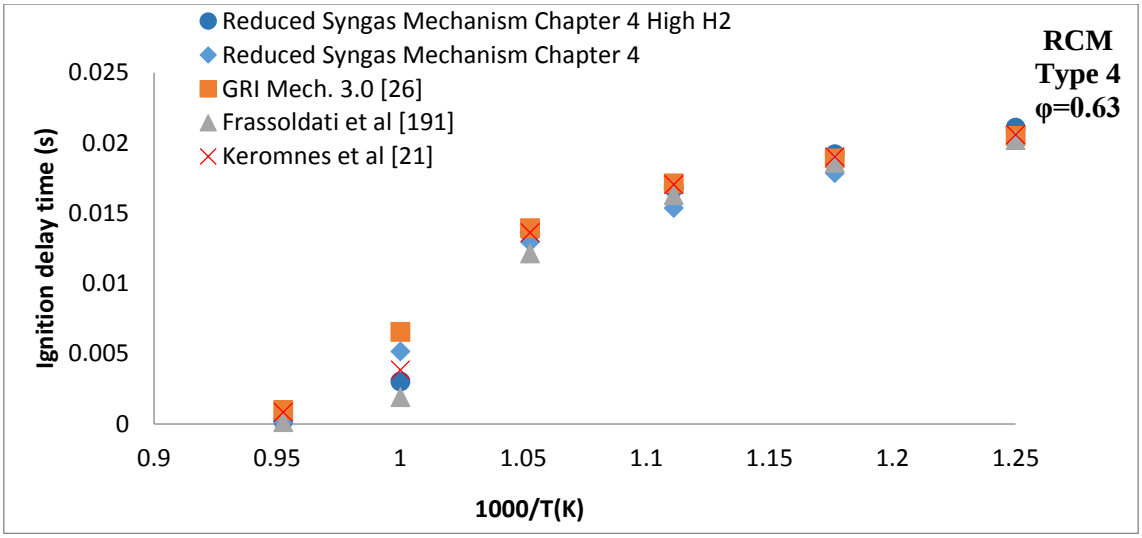

b)

Figure 4-15 (cont.). Data obtained with modified mechanism for syngas Fuel 24 Type 4 with high H2 and compared with other kinetic mechanisms. (a) LFS calculated at temperature 450K, pressure 2.25 bar and equivalence ratio 0.4-1.0, and (b) Ignition delay calculated at temperatures 800-1052K, pressure 2.25 bar and equivalence ratio 0.6.

Table 4-3 Reaction rate constants for reaction $H_2O_2+H=H_2+HO_2$ proposed by different authors (A units cal-cm-sec-K, E units cal/mol).

	A	**n**	**E_A**	**Ref.**
Keromnes et al	2.150E10	1.00	6000	[21]
Frassoldati et al	6.03E10	0.0	7950	[191]
Hong et al	1.21E07	0.0	5200	[196]
Konnov et al	1.7E12	0.00	3755	[73]
GRI mech.3.0	1.21E07	2.0	5200	[26]

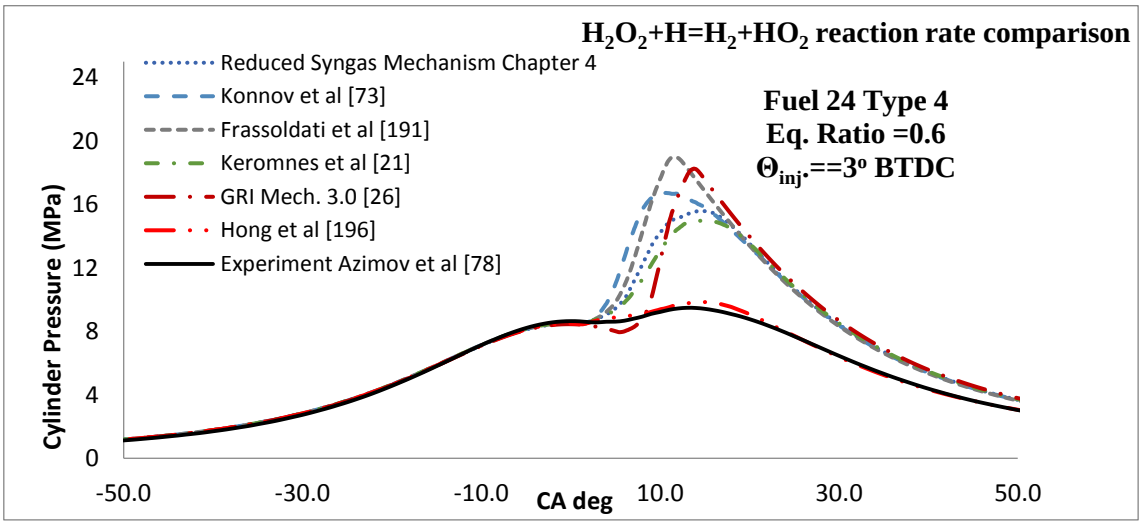

Figure 4-16 Effect of different reaction rates of H_2O_2 +H=H_2 + HO_2 reaction on 3D CFD in-cylinder pressure during micro-pilot ignited syngas combustion.

4.2.3 In-cylinder 3D combustion analysis

To validate the new mechanism shown in Table 4-1, for the in-cylinder-like conditions in a dual-fuel engine, an analysis was performed by applying a micro-pilot injection using the coupled CFD and developed syngas chemical kinetics mechanism. The pressure and ROHR plots shown in Fig. 4-17 for different types of syngas, Fuel 24 Types 1, 2, 3 and 4, at various equivalence ratios and injection timings. Conditions a-b, c-d and e-f were simulated using the new chemical kinetics mechanism, and conditions g-h were simulated using the modified mechanism with constants for reaction R31 adopted from Hong et al. [196] with adjusted power factor n = 0.0.

It can be seen that the developed reduced mechanism reproduces accurately all of the stages of the combustion process at all of the conditions tested. The first stage includes the injection and the ignition of the n-heptane, following by the second stage that is the ignition of the premixed syngas fuel due to the high in-cylinder temperature. The third and final stage includes the diffusion/combustion.

Moreover, experimental data for laminar flame speed are not available. However, in terms of laminar flame speed, the mechanism was compared against experimental results from the literature as well as simulated data by using well-validated mechanisms from other authors and high accuracy was demonstrated. Therefore, it was decided as crank angle resolved in-cylinder spray and temperature distribution and the crank angle resolved in-cylinder spray and OH distribution to be plotted in order to directly investigate flame propagation and OH formation during the combustion process

For further analysis, the crank angle resolved in-cylinder spray and temperature distribution for syngas Fuel 24 Type 4 eq. ratio 0.6 is presented in Fig. 4-18. The images show in detail the combustion process: First, n-heptane is injected via the micro-pilot following by further ignition and combustion of the premixed syngas. The maximum in-cylinder spatial temperature reached about 2200 K and it is seen that the flame front propagates towards the cylinder wall gradually consuming the unburned in-cylinder mixture and then fully burning the fuel.

Moreover, in order to examine the relationship between the temperature and OH concentration, the crank angle resolved in-cylinder spray and OH distribution for syngas Fuel 24 Type 3 eq. ratio 0.6, is presented in Figure 4-19. The images highlight the relationship between the in-cylinder temperature and the concentration of OH: The higher is the temperature, the higher is the concentration of OH. Again, this is an indicator of the importance of hydrogen and more

specifically OH high reactive species for the intensity and the reactivity of the combustion. The higher is the concentration of OH radical species, the more intense is the combustion.

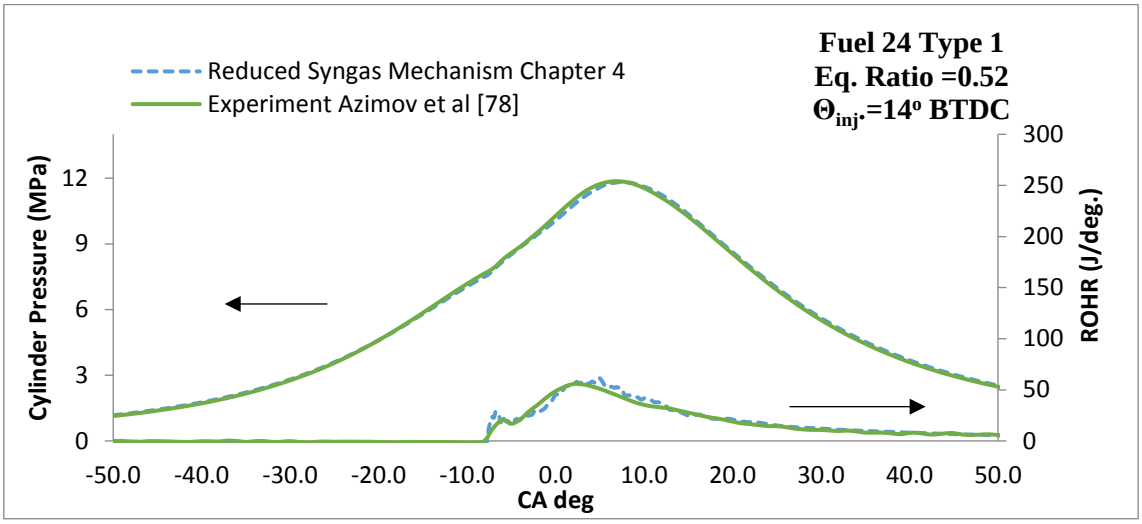

a).

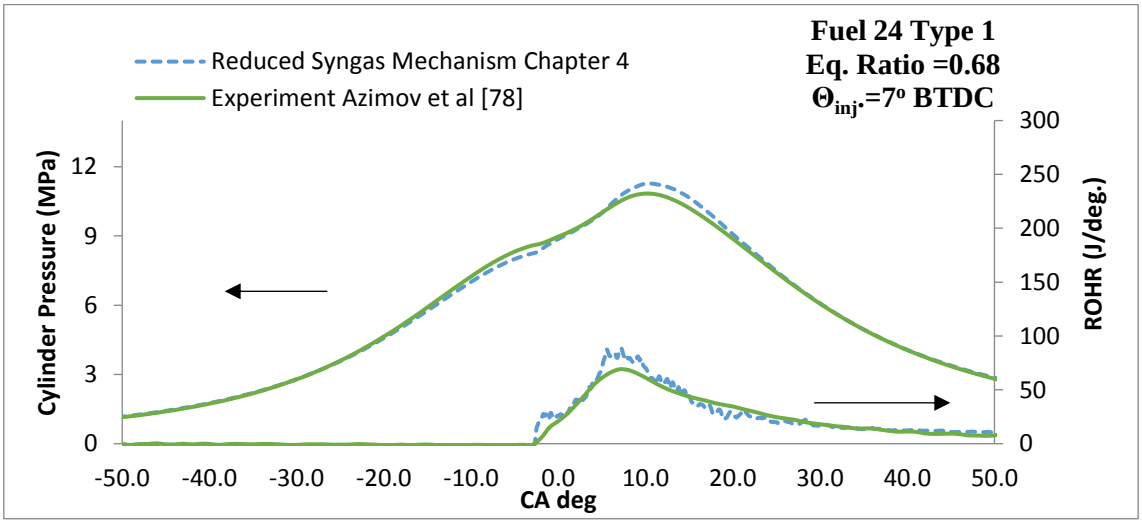

b)

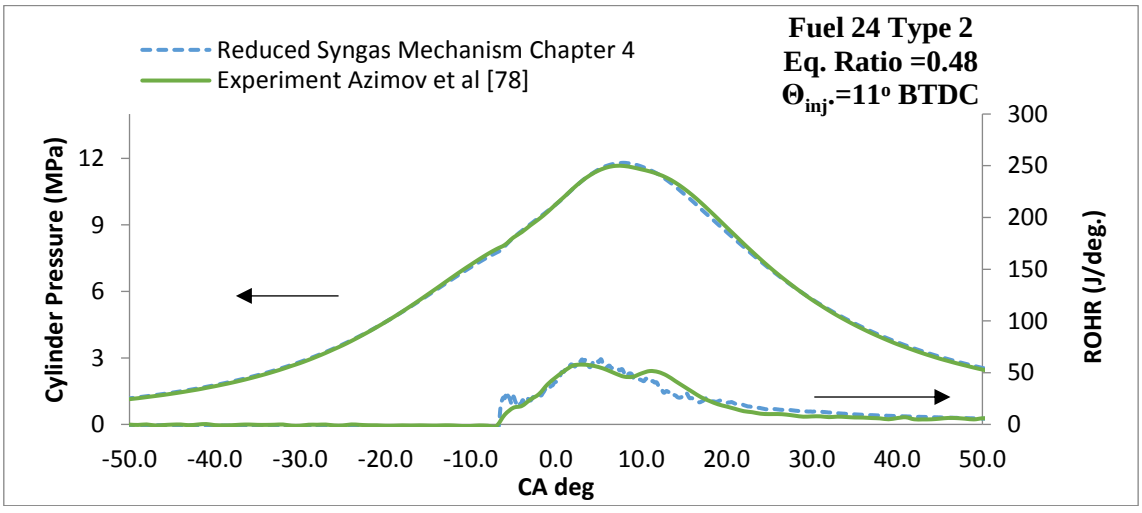

c)

Figure 4-17 Comparison of experimental and simulated in-cylinder pressures and heat release rates of dual-fuel micro-pilot ignited syngas combustion. Computed using 3D-CFD with new kinetic mechanism. (a–b) Fuel 24 Type 1, (c–d) Fuel 24 Type 2, (e–f) Fuel 24 Type 3 and (g–h) Fuel 24 Type 4. PIVC = 225 kPa, TIVC = 330 K

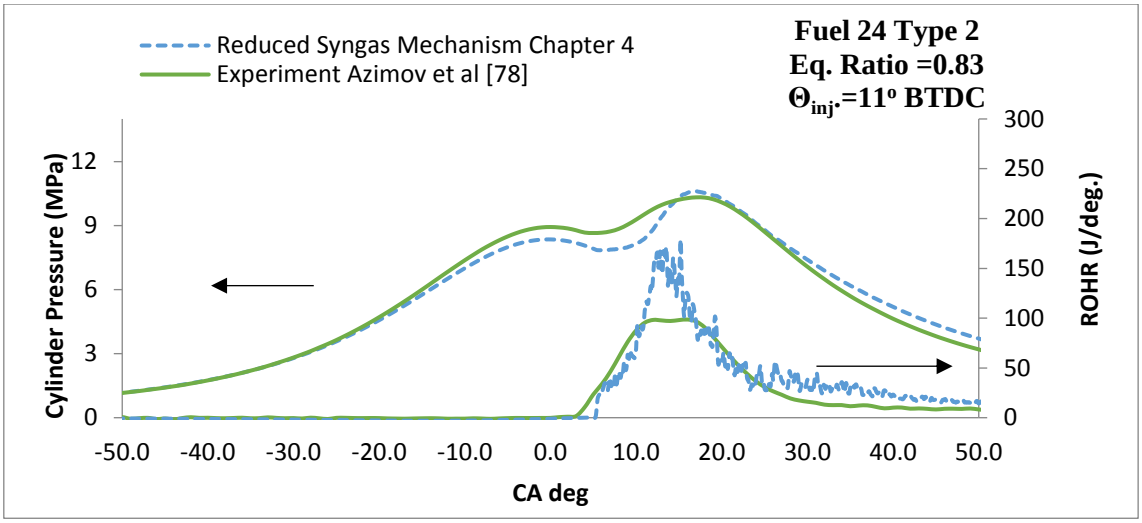

d)

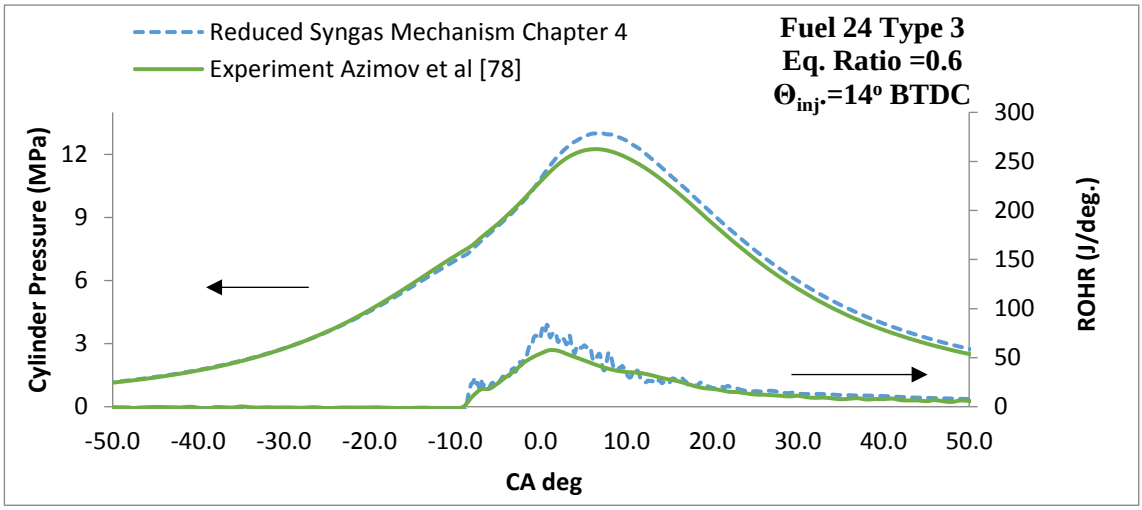

e)

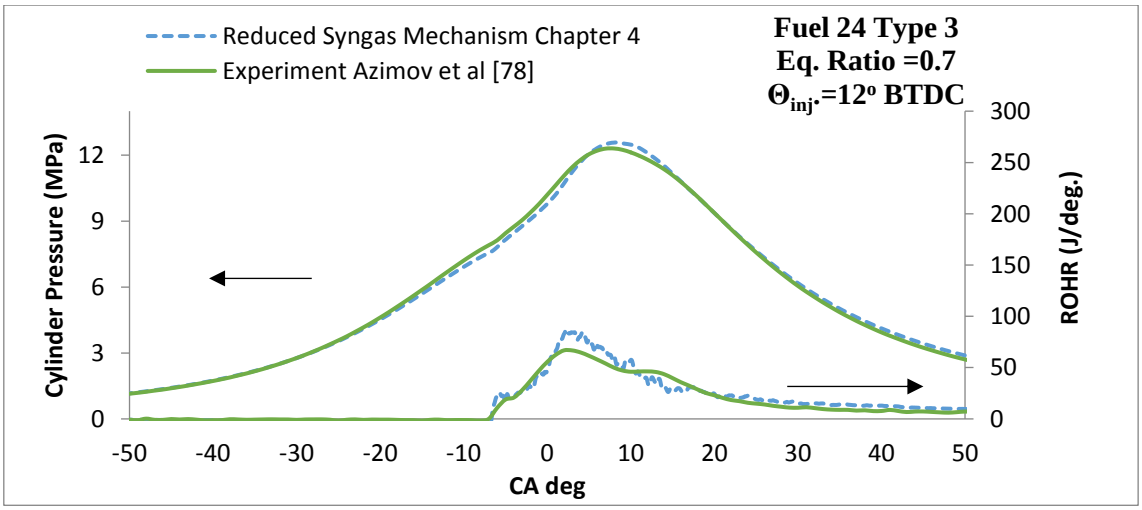

f)

Figure 4-17 (cont.) Comparison of experimental and simulated in-cylinder pressures and heat release rates of dual-fuel micro-pilot ignited syngas combustion. Computed using 3D-CFD with new kinetic mechanism. (a–b) Fuel 24 Type 1, (c–d) Fuel 24 Type 2, (e–f) Fuel 24 Type 3 and (g–h) Fuel 24 Type 4. PIVC = 225 kPa, TIVC = 330 K.

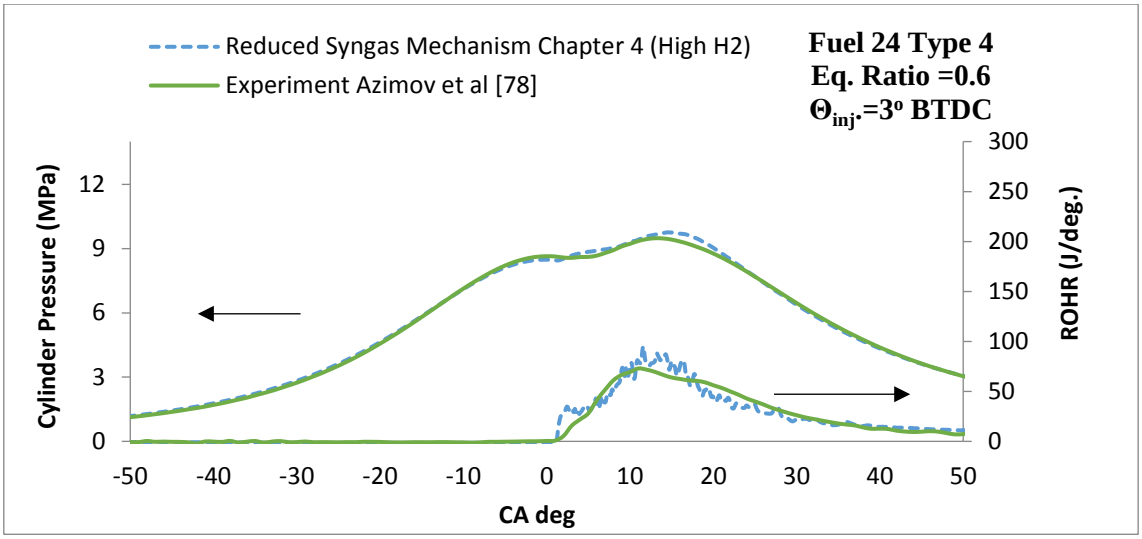

g)

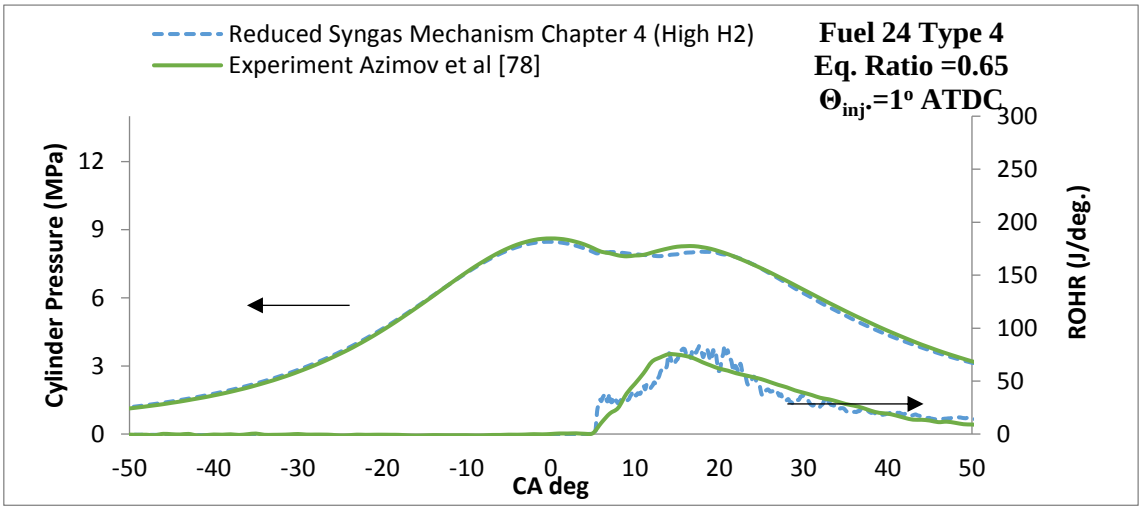

h)

Figure 4-17 (cont.) Comparison of experimental and simulated in-cylinder pressures and heat release rates of dual-fuel micro-pilot ignited syngas combustion. Computed using 3D-CFD with new kinetic mechanism. (a–b) Fuel 24 Type 1, (c–d) Fuel 24 Type 2, (e–f) Fuel 24 Type 3 and (g–h) Fuel 24 Type 4. PIVC = 225 kPa, TIVC = 330 K.

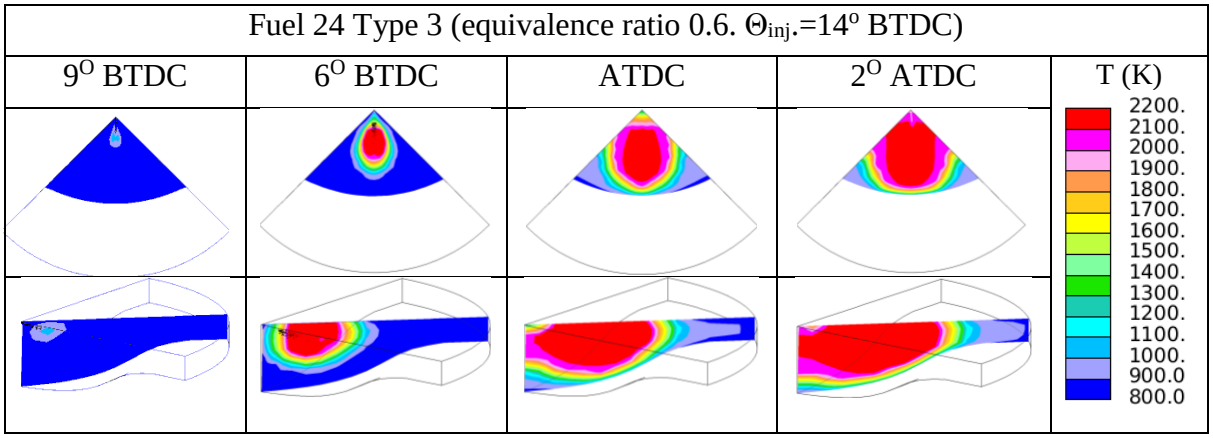

Figure 4-18 Sequential images of dual-fuel micro-pilot ignited syngas combustion and temperature distribution with new kinetics mechanisms for Fuel 24 Type 3, eq. ratio -0.6, Θinj-14BTDC, PIVC = 225 - kPa, TIVC = 330 K.

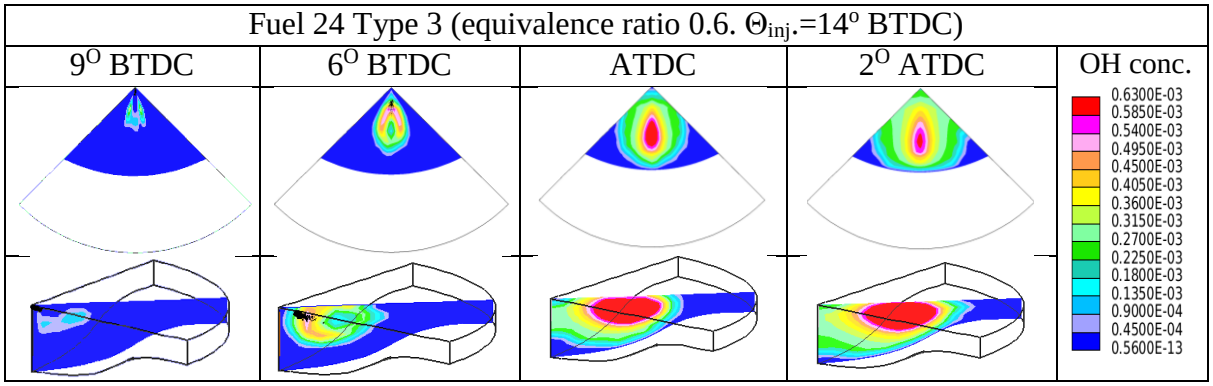

Figure 4-19 Sequential images of dual-fuel micro-pilot ignited syngas combustion and OH distribution with new kinetics mechanism for Fuel 24 Type 3, eq. ratio -0.6, Θinj-14BTDC, PIVC = 225 - kPa, TIVC = 330 K. .

4.3 Summary

In this chapter, a new CFD-compatible syngas chemical kinetics mechanism was developed based on the flow and reaction sensitivity analysis and CFD simulations. The developed syngas mechanism was implemented in a multidimensional CFD simulation for the prediction of syngas combustion in a supercharged dual-fuel engine. The results were compared with experimental data of combustion and syngas chemical kinetics mechanisms developed by other researchers. Ignition delay time and LFS results predicted by using the new mechanism are in a very good agreement with those obtained by using other validated syngas mechanisms. Moreover, the new mechanism captures accurately the effect of CO and CH_4 concentration included in the mixtures; the higher CO concentration, the higher is the ignition delay time while the higher is the amount of CH_4 in the mixture the lower is the LFS.

Sensitivity analysis showed that the reactivity of syngas mixtures was found to be governed by hydrogen and CO chemistry for H_2 concentrations lower than 50% and mostly by hydrogen chemistry for H_2 concentrations higher than 50%. In the mechanism validation, particular emphasis was placed on predicting the combustion under high pressure conditions. For high H_2 concentration in syngas under high pressure, the reactions $HO_2 + HO_2 = H_2O_2 + O_2$ and $H_2O_2 + H = H_2 + HO_2$ were found to play an important role affecting the in-cylinder combustion rate and heat production. The rate constants for the $H_2O_2 + H = H_2 + HO_2$ reaction showed strong sensitivity to high pressure ignition times and had considerable uncertainty. To accurately simulate syngas derived from coke oven feedstock with high H_2 concentration, some modifications to a new mechanism were introduced. In particular, constants for reaction R31 were adopted from Hong et al. [196] with adjusted power factor n = 0.0 and reactions $HO_2 + OH = H_2O + O_2$ and $O + H_2O = OH + OH$ were excluded from the mechanism. These reactions did not appear in the list of the most sensitive reactions. In fact, they are not contributing to the further chain branching and chain propagation where H radical presence is required.

Finally, the new developed mechanism was used in CFD analysis to predict in-cylinder combustion of syngas and results were compared with experimental data. The new mechanism predicted the in-cylinder combustion very well for both biomass and coke-oven syngas in a micro-pilot ignited supercharged dual-fuel engine and accurately reproduced the in-cylinder pressure and heat-release rate data for different equivalence ratios, and injection timings.

Chapter 5: Development of an updated chemical kinetics mechanism for syngas combustion and NOx formation in a micro pilot ignited dual fuel engine.

As already stated and analysed in the literature review, Chapter 3, syngas fuels are expected to produce lower NOx emissions during the combustion process and this is one of the primary reasons why they are tending to replace fossil fuels such as diesel and gasoline. Therefore, for a robust, comprehensive and accurate syngas chemical kinetics mechanism, NOx chemistry is a very important part that should be included in the mechanism. Only a few detailed mechanisms already exist that include full syngas and NOx chemistry. The detailed GRI Mech. 3.0 [26] was constructed for the simulation of natural gas mixtures with CH_4 composition higher than 80% and includes detail CH_4 and NOx chemical pathways in addition to H_2/CO chemistry. Moreover, the detailed mechanism proposed by Frassoldati et al. [23], consists of 275 reactions including full H_2/CO chemistry as well as NOx chemistry. However, both of these mechanisms consist of a high number of reactions and species and therefore require high computational time for a complete CFD simulation. The computational efficiency is very important, especially for the calculation of turbulent combustion.

As can be easily understood, there is a need for a robust, comprehensive and reduced syngas/NOx chemical kinetics mechanism that would be applicable for the simulation of not only syngas combustion but also NOx formation.

Therefore, during this chapter the reduced chemical kinetics mechanism developed in Chapter 4, for the simulation of H_2/CO/CO_2/CH_4 syngas combustion in a micro-pilot-ignited supercharged dual fuel engine, was optimized by incorporating a 12-step reaction NOx pathway and by updating the rate constants of important hydrogen reactions that were found to be very sensitive during high pressure conditions. The new reduced mechanism was validated against experimental data as well as the simulated results by using well-validated chemical kinetic mechanisms from the literature, in terms of LFSs, ignition delay time, rate of heat release (ROHR), in-cylinder pressure and NO mole fractions. The work presented in this Chapter was published in [241].

5.1.1 Selection of the NOx sub-mechanism

For the selection of the most suitable NOx model for incorporation into the reduced syngas mechanism, three different NOx models found in the literature were compared against

experimental results. The first model is a 12 reaction sub-mechanism proposed by Pan et al. [98] that includes a full 3 step Zeldovich reaction model and the most important reactions regarding thermal NOx. The second NOx model, was proposed by Takeshi et al. [99] and includes 19 reactions. The authors highlight the importance of CH and HCN radicals and especially their role in the connection between the N group and CxHy group. They concluded that under fuel rich conditions the prompt formation pathway of the N group is very important and leads to soot and to the formation of C_2H_2. Therefore, they upgraded the 12 reaction NOx model proposed by Pan et al. [98] by adding an extended sub-model, which consists of 7 important reactions with HCN, CH and NH_2 species. The final NOx sub-mechanism that was tested, was proposed by Miller et al. [242], and is a super extended version of the original Zeldovich model. The authors suggested an optimized version of the Zeldovich model applicable for the simulation of NOx at elevated temperatures and pressures. The super-extended Zeldovich model consists of 67 reactions.

Two basic criteria were set for the model selection; 1) the deviation between the calculated and experimental results to be within the pre-set error limit of 5% and 2) the selected model must be computational efficient. The lower the number of reactions and species included in the mechanism, the more time efficient it is. For the testing of the NOx sub-models and the comparison with experimental measurements, NO concentration profiles along the axial direction from the surface of the burner were used as quantitative measurements. The simulations were performed by using the premixed laminar flame configurations in DARS. Experimental measurements obtained from [177] for NOx concentration profiles for different premixed nitrogen-hydrogen-oxygen fuel compositions were used for the comparison. The authors measured the NOx concentration profiles in premixed hydrogen-oxygen-nitrogen flames by using a gas sampling that has O2/N2 ratio 19/81% at pressure 1 bar.Three different mixtures were used (Fuel 13 Table 3-3) .: a) $2H_2+1.4O_2+5.3N_2$, b) $2H_2+1.4O_2+4.6N_2$ and c) $2H_2+1.4O_2+6.1N_2$ [243]. All of the simulations were conducted at pressure 1 bar, initial temperature 300 K and eq. ratio 0.71. The comparison between the calculated and experimental results for NO concentration profiles along distance from the surface of the burner (X) are presented in Figure 5-1a for Fuel 13 Type 1, Figure 5-1b for Fuel 13 Type 2 and Figure 5-1c for Fuel 13 Type 3. According to Figure 5-1, the super-extended mechanism over-predicts the experimental results at all of the tested fuel mixtures. On the other hand, the constructed mechanisms using the 12 reactions NOx model and the 19 reactions model show an identical trend at all of the tested conditions and they are in a good agreement with the experimental

results. This indicates that at lean conditions, the 12 reactions step model performs remarkably well even without the 7 prompt NOx reactions that are included in the Takeshi model. Moreover, the deviation between the numerical and experimental results was also calculated using the error analysis method introduced in Chapter 3.

For Figure 5-1 a (Fuel 13 Type 1), the overall mean error for the 12 reactions step model proposed by Pan et al [98] is 3.8% , for Takeshi model [99] is 4.0% and for the Super-Extended model [242] is 13.5%. For the Fuel 13 Type 2, Figure 5-1 b, again the 12 reactions step model has the lowest overall mean error (2.4%) and is followed by Takeshi model (3.0%). On the other hand, the overall mean error for the Super- Extended model is relatively high, in comparison with the rest of the mechanisms, 8.1%. Finally for Fuel 13 Type 3 , Figure 5-1 c, the trend regarding the overall mean errors for the three mechanisms is similar to Fuel 13 Types 1 and 2. The 12 reactions step model and Takeshi sub-model have similar calculated overall mean errors, 2.2 % and 3.0% respectively, while the Super-Extended model deviates from the experimental results and has an overall error of 47.1%. The deviation between the Super-Extended model and the experimental results, is related to the calibration procedure that was used for the development of the mechanism. According to the authors [242], the model was calibrated and developed based on certain conditions (equivalence ratio >1.2) and therefore shows high sensitivity when used for different conditions.

Moreover, in order to analyse even more the differences between the mechanisms and choose the best one, the grand mean errors of each mechanism (12 reactions NOx model [98], Takeshi sub-model [99] and Super-Extended Model [242]) were calculated and compared. By using the 12-reaction NOx sub-model the grand mean error is 2.8%, for the Takeshi sub-model is 3.3% and finally for the Super-Extended model the grand mean error is 22.9%. By considering the two basic criteria that were pre-set for the selection of the NOx model, it was decided to select the 12-reaction NOx sub-mechanism for implementation into the reduced syngas mechanism.

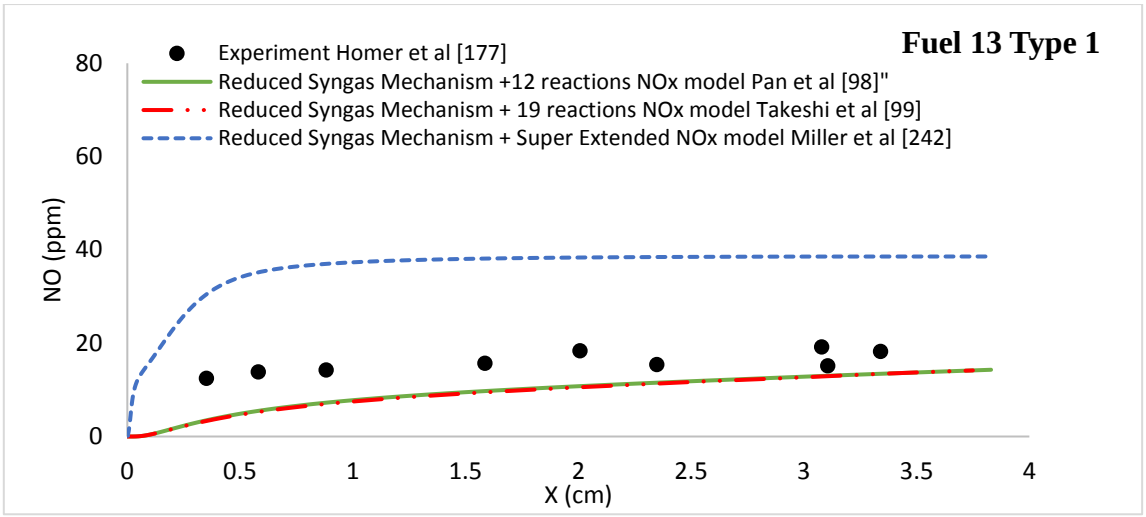

a)

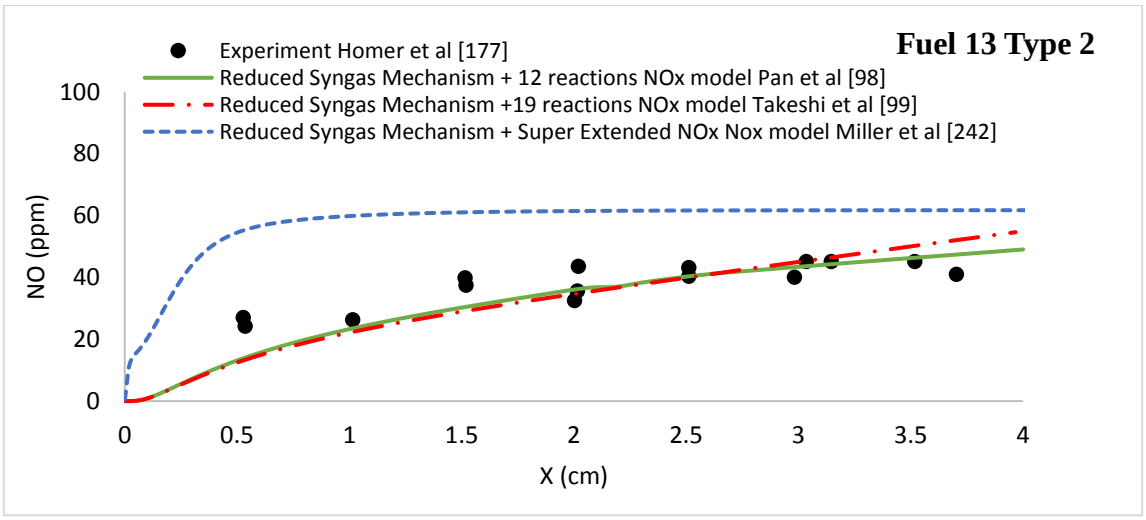

b)

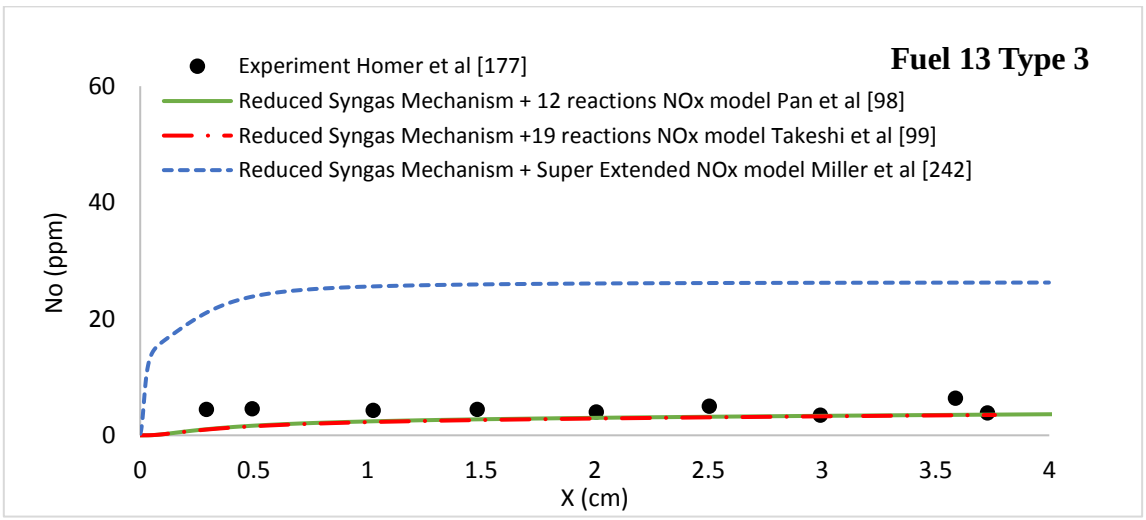

c)

Figure 5-1 Comparison of the calculated NO profiles obtained by using the three NOx sub-models and the experimental results from [177]

5.1 Chemical kinetics mechanism

5.1.2 Chemical detail analysis during syngas combustion

Implementing the 12 reaction NOx mechanism into the syngas mechanism changed its thermal stability. Therefore, a chemical detail analysis was performed to analyse the combustion chemistry and investigate the most important reactions affecting syngas combustion. The combustion chemistry was investigated by following a three stage procedure. First, reaction flow analysis was conducted for the identification of the important species that have the highest flow rate and therefore are affecting the combustion process. Then, reaction sensitivity was performed for the identification of the important reactions affecting syngas combustion. Finally, different reaction rate constants, obtained from the literature for each one of the important reactions highlighted from the sensitivity analysis, were tested against experimental results and the best were chosen and adopted in the mechanism.

Flow analysis

Reaction flow analysis was performed for Fuel mixture 14, tested by Sahu et al. [178], see Table 3-3, at 0.8 equivalence ratio, pre-heat temperature 300 K and pressures of 4, 10 and 16 bar. It is important to be mentioned that the reason why those pressures have been chosen is because the investigation of the species behavior at low, medium and high pressure is critical for the understanding of the combustion chemistry. Therefore, flow analysis was conducted at 4 bar (low pressure) , 10 bar (med pressure) and 16 bar (high pressure). Fluxes for H below 1% of maximum flow have been filtered. The flow analysis for hydrogen species at pressures of 4, 10 and 16 bar are presented in Figure 5-2a, b and c respectively.

According to reaction flow analysis at all of the pressures, hydrogen based species such as HO_2, H_2O, OH and H_2 have the higher flow rates and therefore can be characterized as the driving species of the combustion. Moreover, species such as CH_4 and CH_3 should not be ignored as they show a relatively high flow flux at all of the conditions. The high flow rate of methane based species is an indicator that CH_4 affects the combustion process even in low amounts.

Moreover, according to the flow analysis in Figure 5-2, the higher is the pressure and therefore the more intense is the combustion, the higher is the flow rate, especially between hydrogen-based species. For example, for pressure 4 bar the flow path between OH and H (towards H) is 310 mol/(cm^3 sec) while for 10 and 16 bar the flow rates are 4800 and 5500 mol/(cm^3 sec) respectively. This is because the formation or the consumption of hydrogen-based species is more intense at higher temperature and pressure conditions. In particular, the formation of OH

is directly related with the combustion intensity and the in-cylinder conditions during the combustion; the higher is the temperature and the pressure (more intense is the combustion), the higher is the concentration of OH radicals. This is the primary reason why many researchers use the maximum concentration of OH radicals as an indicator of the combustion initiation.

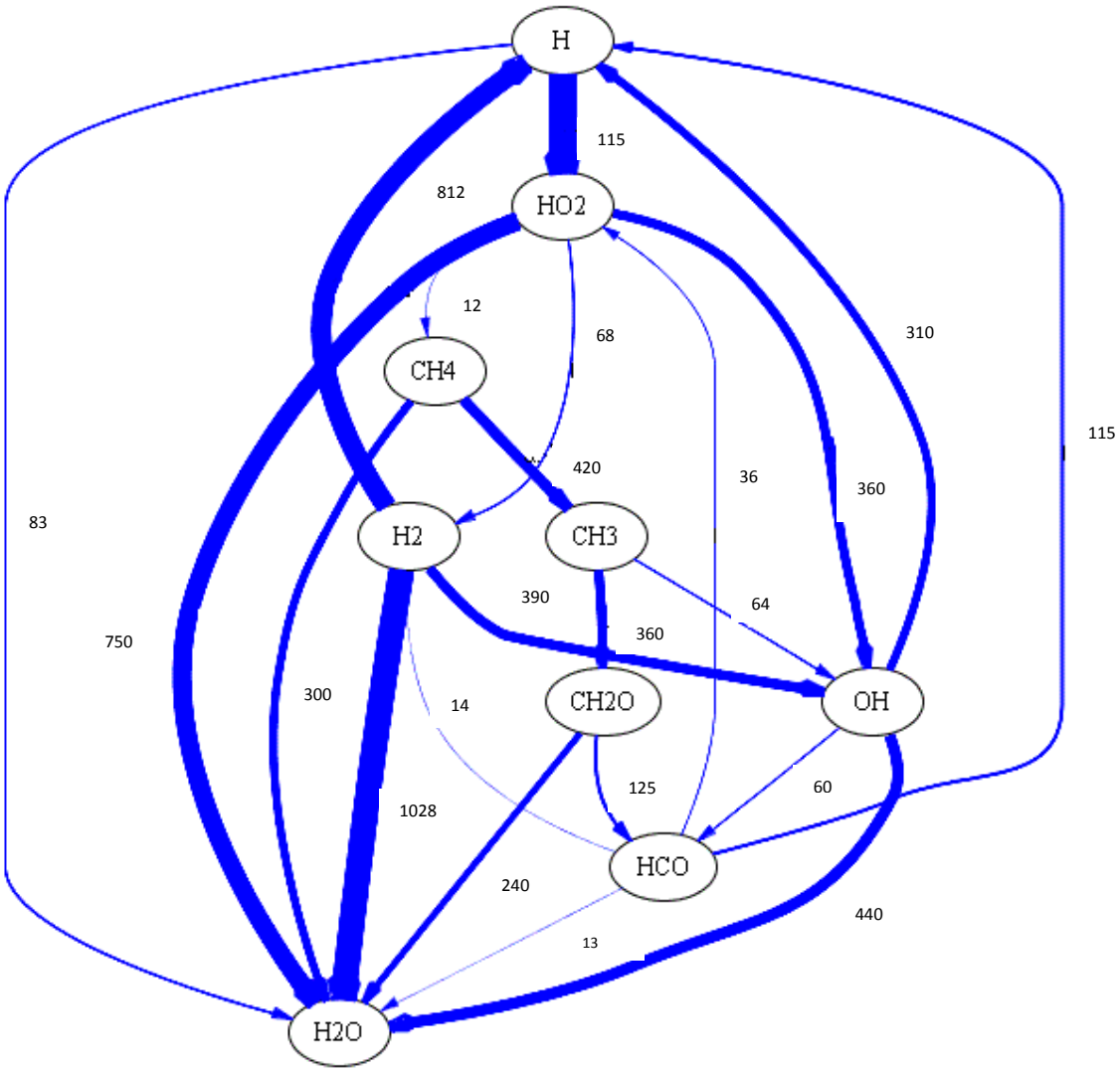

Figure 5-2. Reaction flows analysis of hydrogen atoms for syngas Fuel mixture 14 Type 1, at temperature 300K and pressures a) 4, b) 10 and c) 16 bar. Fluxes below 1% of maximum flow have been filtered. Flow values are given in mol/(cm^3 sec)

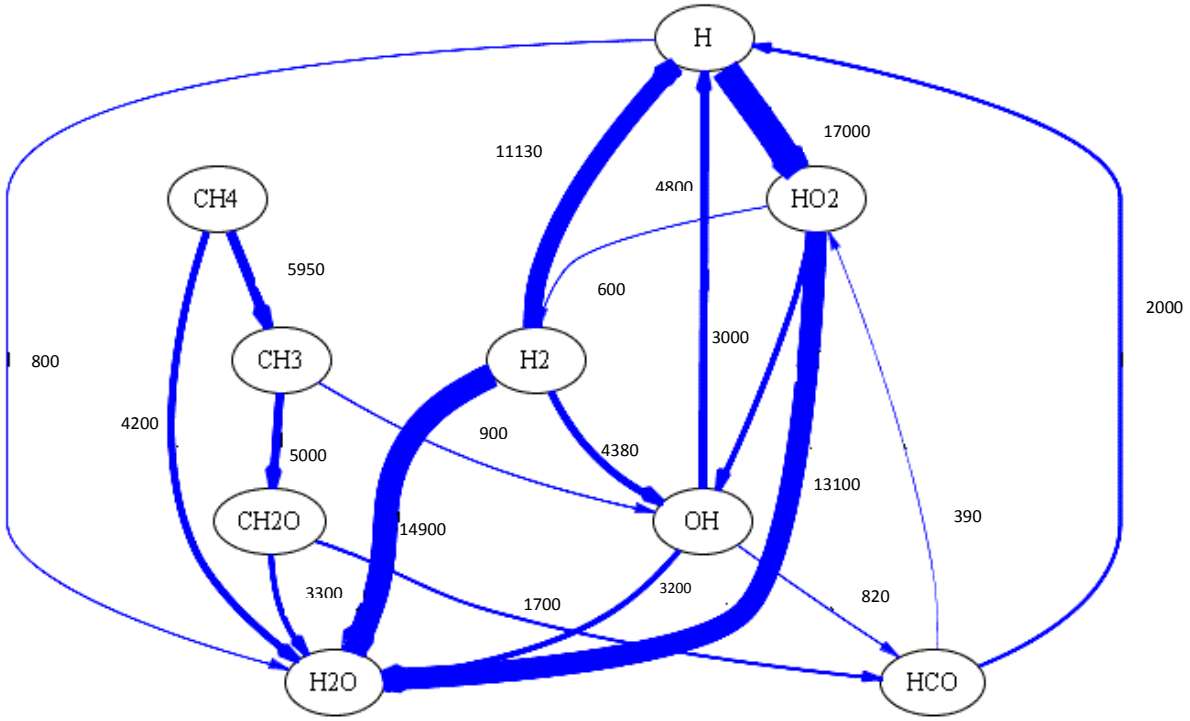

b)

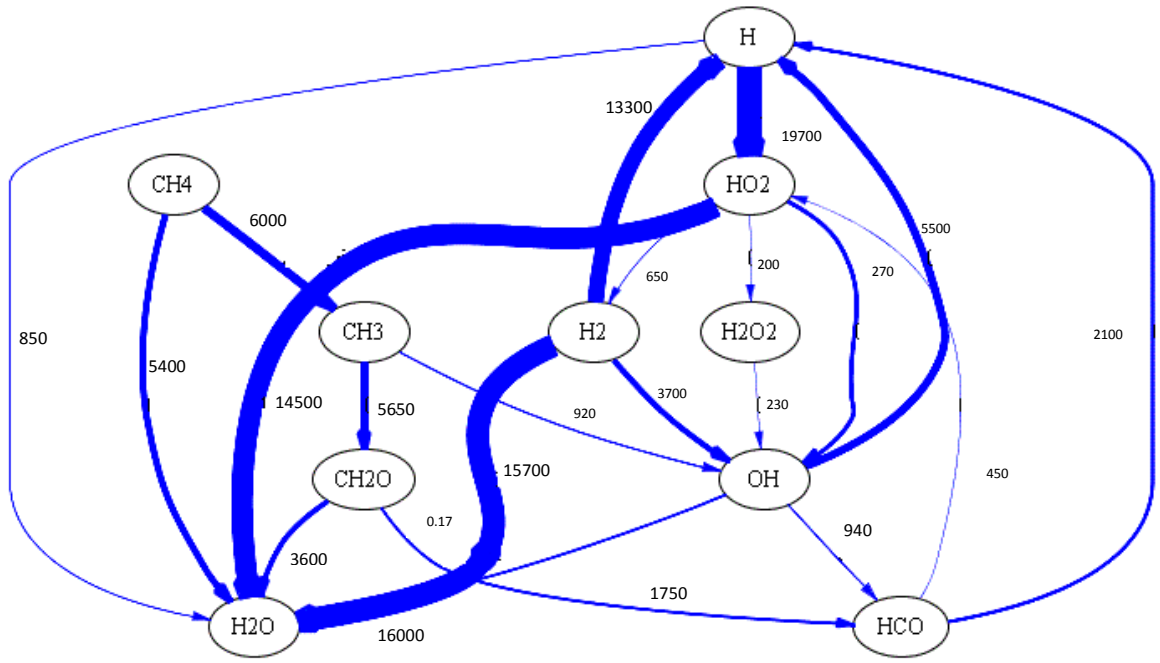

c)

Figure 5-2. (cont.) Reaction flows analysis of hydrogen atoms for syngas Fuel mixture 14 Type 1, at temperature 300K and pressures a) 4, b) 10 and c) 16 bar. Fluxes below 1% of maximum flow have been filtered. Flow values are given in mol/(cm^3 sec)

Reaction sensitivity analysis

The importance of the reactions included in the mechanism, on syngas combustion, was investigated by conducting a reaction sensitivity study. Sensitivity analysis was performed for syngas Fuel 24 Type 1 at temperature 1000 K, equivalence ratio 0.63 and pressures of 10, 30 and 50 bar. The reason why 1000 K was chosen is because the scope of this analysis was the investigation of the effect of the implementation of the NOx sub-mechanism on syngas reactions and the stability of the mechanism during syngas combustion. According to [244] at 1000 K, thermal NOx formation is on the initial formation stage and syngas chemistry is still the dominant chemical pathway of the mechanism. Each individual reaction included in the chemical kinetics mechanism was marked with a sensitivity factor, showing how important the reaction is on forming or consuming other species during syngas combustion. However, for reasons of simplicity, only the thirteen most sensitive reactions are presented in Figure 5-3. The findings from the reaction sensitivity analysis are similar to the findings observed from the reaction sensitivity study of the syngas mechanism in Chapter 4, see Figure 4-1. According to Figure 5-3, as it was expected, hydrogen based reactions have the highest sensitivity factors at high pressure conditions. Moreover, the important carbon and methane based reactions show a relatively high sensitivity factor. More specifically, reactions such as $H_2O_2(+M)=OH+OH(+M)$, $H_2O_2+H=H_2+HO_2$ and $CO+H_2O=CO_2+H_2$ were found to have high negative sensitivity factor, while reactions such as $H_2+O=OH+H$, $H_2+OH=H2O+H$, $O_2+CO=CO_2+O$ and $CH_4+OH=CH_3+H_2$ were found to have high positive sensitivity factor.

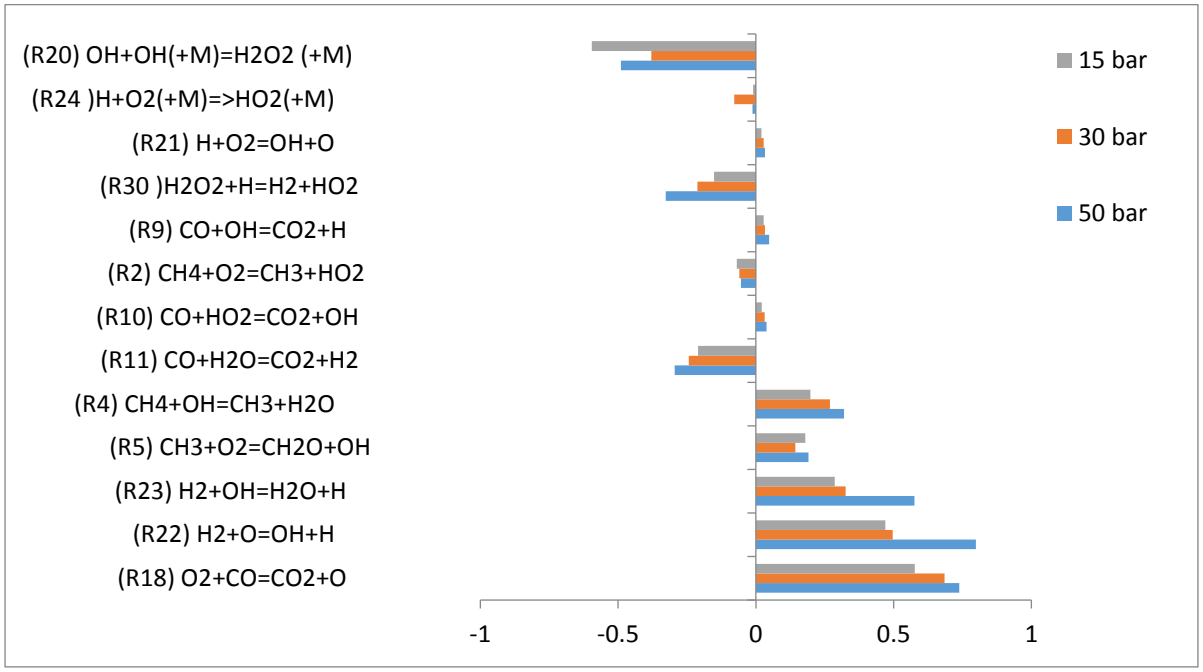

Figure 5-3 The 13 most sensitive reactions from Syngas/NOx mechanism for syngas Fuel 24 Type 1 at 1000K and pressures 10, 30 and 50 bar

Reaction rate constants optimization

By summarizing the results from both flow analysis and sensitivity analysis methods, during high pressure conditions, syngas combustion is driven mostly by hydrogen based reactions. Therefore, specific attention was given to the two reactions that were found to be very sensitive to pressure changes and contribute to an increase in syngas reactivity: (R20) H_2O_2 (+M) =OH+OH (+M) and (R30) $H_2O_2+H=H_2+HO_2$. Both of the reactions were analysed in detail in Chapter 4 due to their importance on affecting syngas combustion, especially for fuel mixtures with high H_2 content at high pressure conditions. R20 is characterized as the central kinetic feature in the operation of the engine and it directly affects the reactivity of the mixture due to the formation of high reactive OH radicals. The formation of OH radical species will increase the reactivity of the mixture and will in turn affect important combustion parameters such as the flame speed and ignition delay. R30, was the reaction that was found to have the highest level of uncertainty, especially during low temperature/high pressure conditions and was modified in Chapter 4 for the simulation of high H_2 mixtures. It is responsible for the formation of H_2O_2 which in turn will be decomposed via R20 to produce highly reactive OH. Therefore, it can be said that it indirectly affects the reactivity of the mixture.

Because of the importance of these reactions, it was decided to test different rate constants for both, in order to find the one with the lowest uncertainty and best match with the experimental results. The experimental measurements from Lapalme et al. [173] for LFS were used as quantitative measurements to test the rate constants for both reactions. The authors measured the experimental LFS of $H_2/CO/CH_4$ syngas mixture at pressure 1.01 bar , temperature 295 K and equivalence ratios between 0.7 and 1.65. For simplicity reasons, only Fuel 8 Type 1 was used (see Table 3-3). The comparison between the different rate constants for reactions R20 and R30 and the experimental data can be found in Figure 5-4. For reaction 30, the rate constant proposed by Konnov et al. [73], gave the best match with the experimental results and has a low uncertainty factor and therefore has been adopted in the proposed mechanism. On the other hand, for R20 the rate constant proposed by Li et al. [232] shows the best agreement between the simulated and experimental data and therefore was chosen for that mechanism. The final reduced syngas/NOx mechanism can be found in Table 5-1

Table 5-1. Reduced syngas/NOx mechanism constructed in Chapter 5 (A units cal-cm-sec-K, E units cal/mol).

	Reactions	***A***	***n***	***E***	***Ref.***
	n-Heptane Reaction EBU				
R1	$C_7H_{16}+11O_2=7CO_2+8H_2O$	0.	0.	0.	[148]
	/EBU/ 4. 0. 1 0.				
R2	$CH_4+O_2=CH_3+HO_2$	3.98E13	0.0	56855.5	[90]
R3	$CH_4+HO_2=CH_3+H_2O_2$	0.964E11	0.0	24629.4	[90]
R4	$CH_4+OH=CH_3+H_2O$	1.60E07	1.83	2771.1	[192]
R5	$CH_3+O_2=CH_2O+OH$	3.30E11	0.0	8934.4	[90]
R6	$CH_2O+OH=HCO+H_2O$	3.90E10	0.0	406.1	[90]
R7	$CO+O(+M)=CO_2(+M)$	9.04E12	0.89	3800.0	[191]
	/LOW / 0.2070E27 -3.340 7610.0 /M/ H_2O/12.00/ H_2/2.00/ CO/1.50/ CO_2/2.00/ AR/0.50/				
R8	$CO+OH=CO_2+H$	0.9600E12	0.14	7352.0	[191]
R9	$CO+OH=CO_2+H$	0.7320E11	-1.00	-16.0	[191]
R10	$CO+HO_2=CO_2+OH$	0.1200E18	0.00	17000.0	[191]
R11	$CO+H_2O=CO_2+H_2$	0.2000E9	0.00	38000.0	[191]
R12	$HCO(+M)=CO+H(+M)$	0.3000E14	0.03	23000.0	[191]
	/M/ H_2O/5.00/ CO_2/3.00/ H_2/1.90/ CO/1.90/				
R13	$HCO+O=CO_2+H$	0.3000E14	0.00	0.0	[191]
R14	$HCO+H=H_2+CO$	0.1000E13	0.00	0.0	[191]
R15	$HCO+OH=H_2O+CO$	0.5000E14	0.00	0.0	[191]
R16	$HCO+HO_2=H_2O_2+CO$	0.4000E12	0.00	0.0	[191]
R17	$HCO+HO_2=>H+OH+CO_2$	0.3000E14	0.00	0.0	[191]
R18	$O_2+CO=CO_2+O$	0.2530E10	0.00	0.0	[191]
R19	$O_2+HCO=HO_2+CO$	0.1000E15	0.00	47700.0	[191]
R20	$OH+OH(+M)=H_2O_2(+M)$	2.951E14	0.00	4.843E04	[232]
	/LOW / 1.202E17 0.0 4.55E04 /TROE/ 0.5 1E-30 1E30 /M/ H_2/2.5 /H_2O/12.00/ CO/1.90/ CO_2/3.80/ AR/0.64/				
R21	$H+O_2=OH+O$	3.52E16	-0.7	17061.4	[193]
R22	$H_2+O=OH+H$	5.06E4	2.67	6287.6	[194]
R23	$H_2+OH=H_2O+H$	1.17E9	1.3	0.0	[194]
R24	$H+O_2(+M)=>HO_2+(M)$	4.6E12	0.4	0.0	[21]
	/LOW / 1.737E19 -1.23 0.0 /M/ AR/0.0/ H_2/1.3/ H_2O/10.0/ CO/1.9/ CO_2/3.8/				
R25	$H+H+(M)=>H_2+(M)$	1.30E18	-1	0.0	[193]
	/M/ H_2/2.5/ H_2O/12.0/ CO/1.9 /CO_2/3.8/ AR/0.5/				
R26	$H+OH(+M)=>H_2O(+M)$	3.5E22	-2	0.0	[21]
	/M/ H_2/0.73/ H_2O/3.65/ AR/0.38/				
R27	$HO_2+H=>OH+OH$	7.08E13	0.0	298.8	[195]
R28	$HO_2+H=H_2+O_2$	1.66E13	0.0	821.8	[21]
R29 (a)	$HO_2+OH=H_2O+O_2$	2.89E13	0.0	-496.9	[73]
R29 (b)	$HO_2+OH=H_2O+O_2$	2.456E13	0.0	-4.970	[21]

R30	$H_2O_2+H=H_2+HO_2$	1.7E12	0.0	3755	[73]
R31	$HO_2+HO_2=H_2O_2+O_2$	1.300E11	0.00	-1.630E03	[21]
R32	$O+H_2O=OH+OH$	2.97E06	2.02	1.340E04	[21]
NOx mechanism					
R33	$N+NO=N_2+O$	3.5E13	0.0	330.0	[154]
R34	$N+O_2=NO+O$	2.65E12	0.0	6400	[154]
R35	$N+OH=NO+H$	7.3E13	0.0	1120	[154]
R36	$N_2O+O=N_2+O_2$	1.4E12	0.0	10810	[26]
R37	$N_2O+O=2NO$	2.9E13	0.0	23150	[26]
R38	$N_2O+H=N_2+OH$	4.4E14	0.0	18880	[154]
R39	$N_2O+OH=N_2+HO_2$	2.0E12	0.0	21060	[26]
R40	$N_2O(+M)=N_2+O(+M)$	1.3E11	0.0	59620	[154]
	/LOW/ 6.2E14 0.0 56100 /M/ H_2/2.0/ H_2O/6.0/ CH_4=2.0/ CO/1.5/ CO2/2.0/				
R41	$HO_2+NO=NO_2+OH$	2.11E12	0.0	-480.0	[26]
R42	$NO+O(+M)=NO_2(+M)$	1.06E20	-1.41	0.0	[26]
	/M/ H_2/2.0/ H_2O/6.0/ CH_4/2.0/ CO/1.5/ CO_2/2.0/				
R43	$NO_2+O=NO+O_2$	3.9E12	0.0	-240.0	[26]
R44	$NO_2+H=NO+OH$	1.32E14	0.0	360.0	[26]

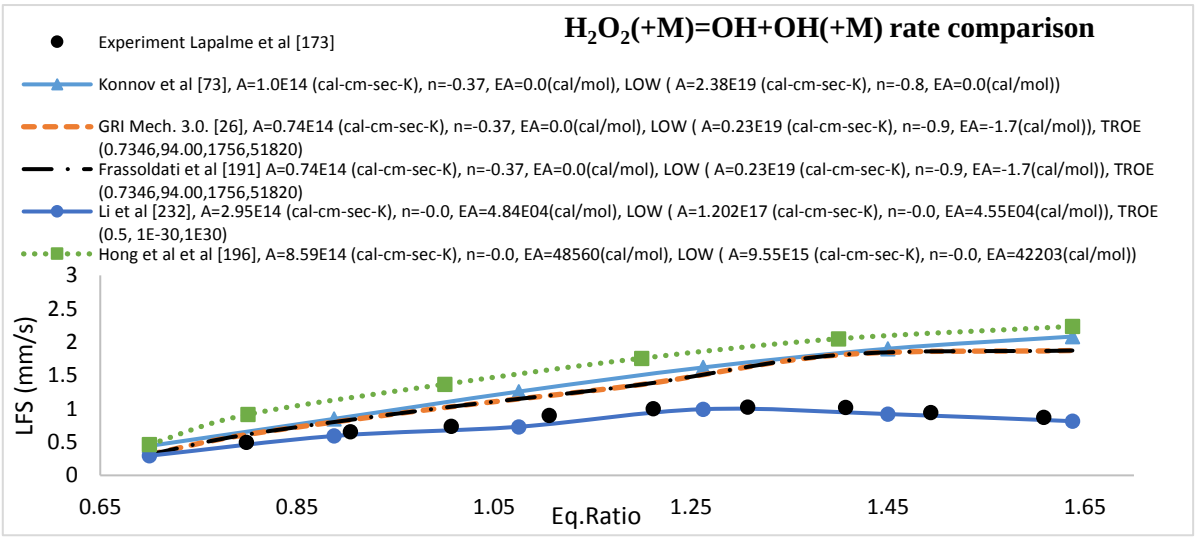

a)

Figure 5-4 Comparison of different reaction rates for a) R20 and b) R30

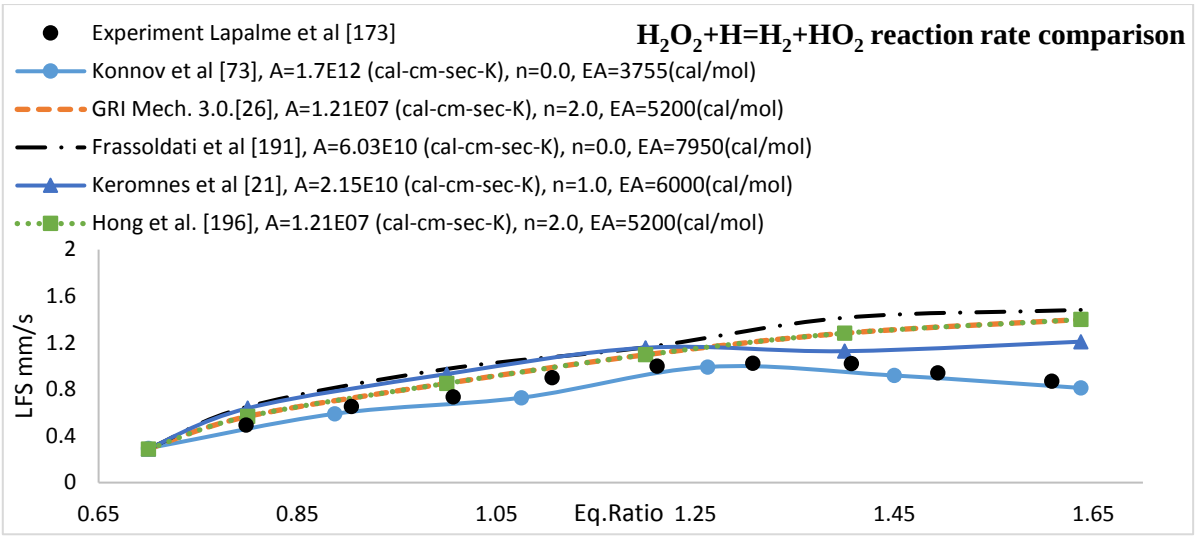

b)

Figure 5-4 (cont.) Comparison of different reaction rates for a) R20 and b) R30

Species sensitivity analysis towards NOx

As already highlighted, the addition of NOx chemistry affects the chemical stability of the mechanism and more specifically the chemical interactions between the species included in the mechanism. Therefore, it is very important to investigate the most important species that play a critical role in NOx formation and consumption. For the purposes of that study, species sensitivity analysis has been performed for Fuel 14 tested by Sahu et al. [178], see Table 3-3, in a low calorific syngas-air diffusion flame at 0.8 equivalence ratio, preheat temperature 300 K and pressures of 4, 10 and 16 bar. Similar to flow analysis, those three pressures were chosen because it was critical to understand which species are affecting most the formation of NOx at low, medium and high pressures. Moreover, by using 0.8 equivalence ratio the temperature inside the combustion chamber reached 1600 K. According to [244], at such temperature (1600 K) the formation rate of thermal NOx is very high and therefore a detail analysis of the sensitivity of the species included in the mechanism towards NOx formation could be obtained. The species sensitivity analysis towards NOx is presented in Figure 5-5. As it was expected, hydrogen, oxygen and nitrogen based species play an important role in the NOx formation. Additionally, carbon based species such as CO and CO_2 show relatively high sensitivity coefficients and should be taken into account. However, the presence of CH_4, as one of the most important species affecting NOx, shows that CH_4 is indeed affecting NOx formation even in trace amounts and should not be ignored.

Moreover, species sensitivity analysis was also conducted for the detail GRI Mech 3.0 [26] in order to compare the sensitivity results with the results obtained using the proposed mechanism, see Figure 5-6. By comparing the species sensitivity analyses using both the

reduced mechanism and GRI Mech. 3.0, it can be said that their general trend is similar. Hydrogen and nitrogen based species have very high sensitivity factors and can be characterized as the driving forces of NOx formation while carbon based and methane based reactions are also found to play a critical role.

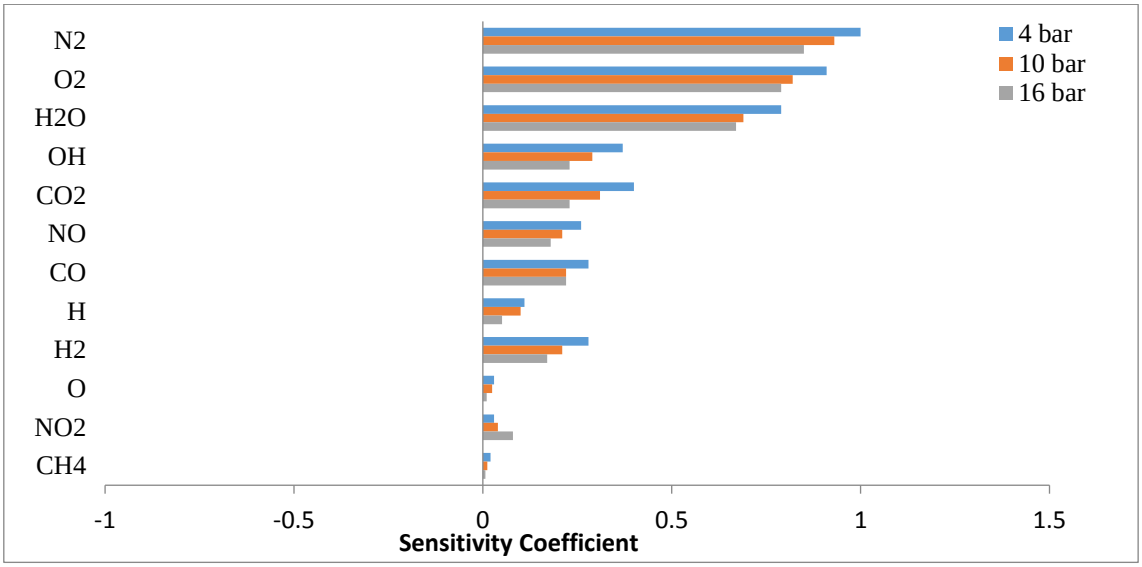

Figure 5-5 Species Sensitivity analysis towards NOx formation using the reduced proposed mechanism in a low calorific syngas-air diffusion flame highlighting the most important species affecting NO formation for Fuel 14 at 0.8 equivalence ratio, preheat temperature 300 K and pressures 4,10 and 16 bars

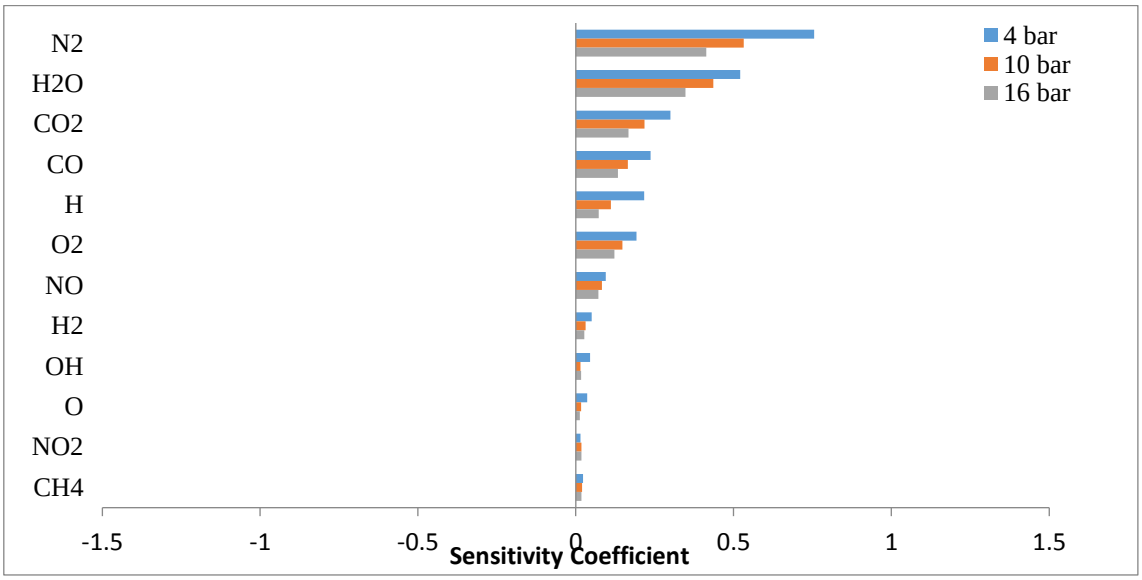

Figure 5-6 Species Sensitivity analysis towards NOx formation using GRI Mech. 3.0 in a low calorific syngas-air diffusion flame highlighting the most important species affecting NO formation Fuel 14 at 0.8 equivalence ratio, preheat temperature 300 K and pressures 4,10 and 16 bars

5.2 Mechanism validation and results discussion

The developed reduced syngas/NOx mechanism was validated against experimental measurements as well as calculated results by using three chemical kinetics mechanisms available in the literature (Keromnes et al. [21], Frassoldati et al. [191] and GRI Mech 3.0 [26]). Similar to Chapter 4, the nine-step reduced mechanism for CH_4 autoignition by Li et al. [90] was used to add methane chemistry to H_2/CO reactions. Moreover, the mechanism proposed by Keromnes et al. [21] does not include NOx chemistry and therefore the 12 step NOx sub-model by Pan et al. [98]was also implemented.

5.2.1 LFS

H_2/CO/CH_4 mixture

Figure 5-7 compares the results of the calculated LFS for three different H_2/CO/CH_4 mixtures, Fuel 8 Type 1, Fuel 8 Type 2 and Fuel 8 Type 3 (see Table 3-3), at atmospheric pressure (1.01 bar), T=295K and equivalence ratio range 0.2-2.5, with the experimental results obtained from Lapalme et al. [173]. The reduced mechanism performs very well at all of the tested conditions and is having a relatively low overall mean error at all of the conditions. The overall absolute mean error for the reduced mechanisms is 0.83% for Fuel 8 Type 1, 3.6% for Fuel 8 Type 2 and 3.2% for Fuel 8 Type 3. Moreover, it captures accurately the effect of CH_4 on the LFS: The maximum LFS (SLmax) is reduced as the CH_4 concentration increases. This is because of the inhibiting effect caused by the higher CH_4 concertation, which reduces the reactivity of the mixture and therefore the LFS [3, 168].

On the other hand, GRI Mech. 3.0 is in a good agreement at lean conditions but deviates from the experimental LFS measurements for eq. ratios >1.3. The absolute overall mean errors for GRI Mech. 3.0 for Fuel 8 Types 1, 2 and 3 are 1.3%, 12.5% and 17.4% respectively. The remaining two mechanisms (Keromnes et al [21] and Frassoldati et al [191]) deviate from the experimental results, especially for the fuel mixtures with high CH_4 (Type 2 and Type 3). More specifically the absolute overall mean errors for Keromnes et al mechanism are 1.54%, 29.3% and 27.9% for Fuel 8 Types 1, 2 and 3 respectively, while Frassoldati et al has 1.9% overall mean error for Fuel 8 Type 1, 33.8% for Fuel 8 Type 2 and 29.9% for Fuel 8 Type 3.

By summarizing the results obtained from the calculation of the absolute overall grand mean error for each mechanism it can be said that the new developed syngas/NOx mechanism has the lowest overall grand mean error for all of the Fuel mixtures (Fuel 8 Types 1,2 and 3) and is followed by GRI Mech. 3.0. The rest of the two mechanisms (Keromnes et al and Frassoldati et al) have a relative high overall mean error especially for Fuel 8 Types 2 and 3.

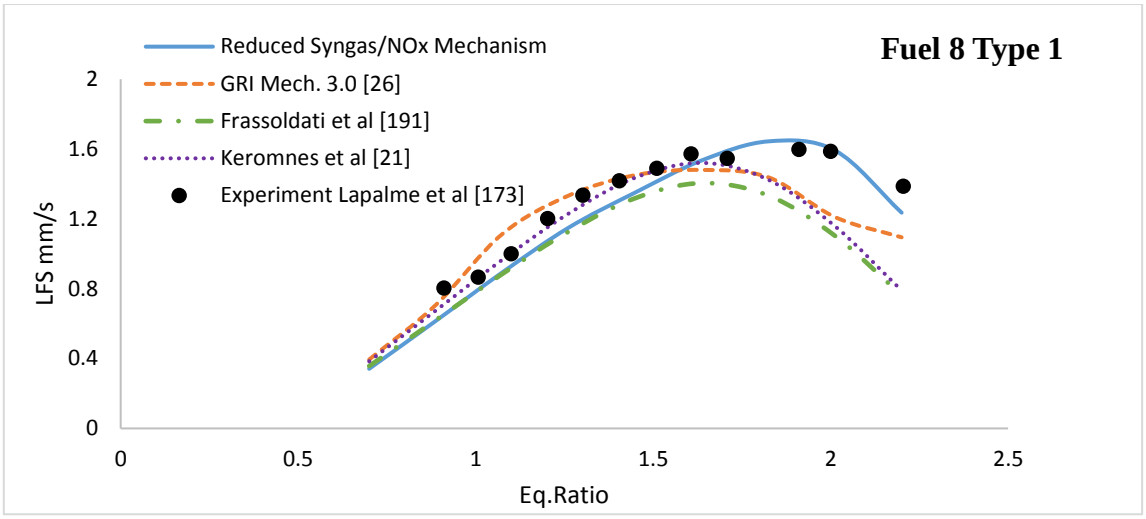

a)

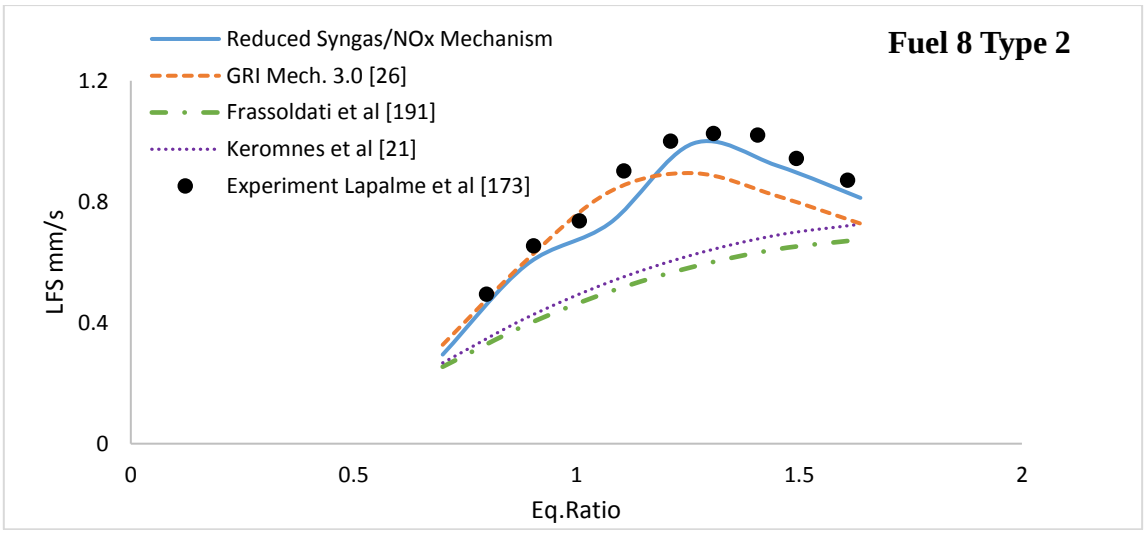

b)

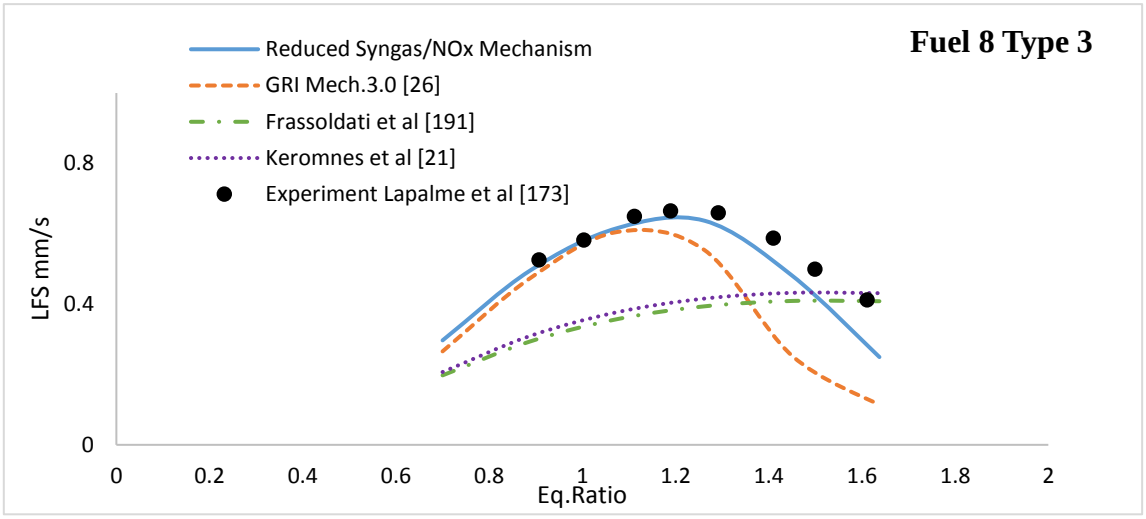

c)

Figure 5-7 Comparison between the measured and calculated LFSs for a) Fuel 8 Type 1, b) Fuel 8 Type 2 and c) Fuel 8 Type 3.

$H_2/CO/CO_2/CH_4$ mixture

The constructed mechanism was also validated against the experimental results obtained by Park et al. [174]. The authors measured experimentally the LFS of $H_2/CO/CO_2/CH_4$ syngas mixture, see Table 3-3 Fuel 9, at pressure 1.01 bar, temperature 298 K and equivalence ratios between 0.4 and 0.9. The comparison between the experimental and simulated results is presented in Figure 5-8. Again, the reduced mechanism is in a good agreement with the experimental results and is having low overall mean error at all of the conditions. For Fuel 9 Type 1 is 0.9%, for Fuel 9 Type 2 is 1.1 % and for Fuel 9 Type 3 is 2.3 %.

GRI Mech. 3.0 shows a good agreement with the experimental results for Fuel 9 Type 1, especially at high equivalence ratios, and for Fuel 9 Type 2. This can be observed also from the calculated absolute overall mean errors for both fuel mixtures, in which GRI Mech. 3.0 has 2.3% error for Fuel 9 Type 1 and 2.5% error for Fuel 9 Type 2. However, for Fuel 9 Type 3, GRI Mech. 3.0 under-predicts the experimental measurements and has an overall mean error of 3.7%. For the mechanism proposed by Keromnes et al.[21], the results for Fuel 9 Type 1 are close to the experimental measurements especially at high equivalence ratios and the calculated absolute overall mean error is 3.2%. On the other hand for Fuel 9 Type 2 and Type 3, the Keromnes et al. mechanism under-predicts the experimental measurements at all of the equivalence ratios and that has as a result relatively high calculated overall mean errors for both Fuel 9 Types 2 and 3, 4.1% and 4.5% respectively.

Finally, the Frassoldati et al. [191] mechanism deviates from the experimental data at all of the tested conditions and has the highest absolute overall mean error for all of the mechanisms at all of the conditions. For Fuel 9 Type 1, the absolute overall mean error is 6.5%, for Fuel 9 Type 2 7.4% and for Fuel 9 Type 3 7.5%.

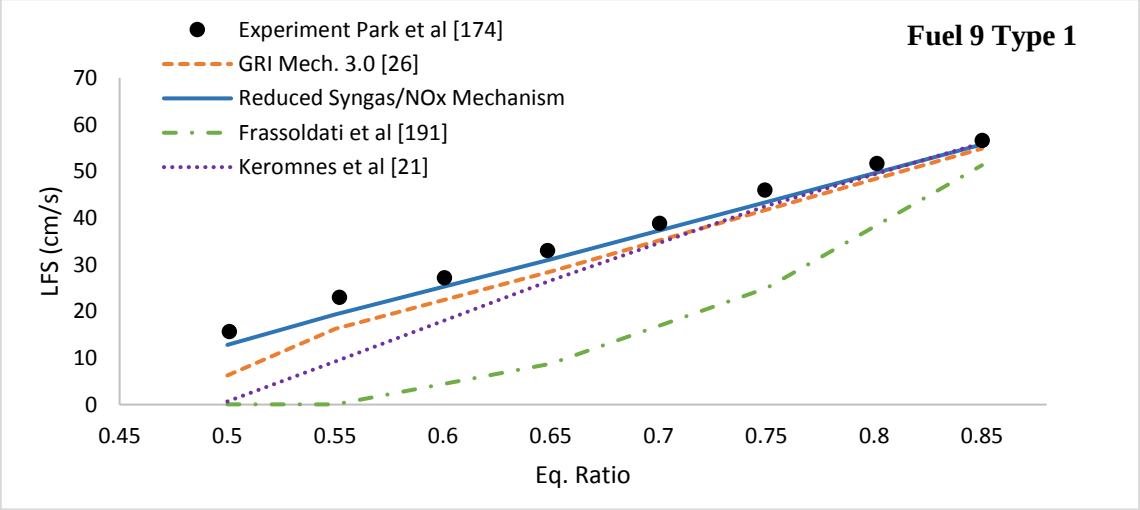

a)

Figure 5-8 Comparison between the measured and calculated LFSs for a) Fuel 9 Type 1, b) Fuel 9 Type 2 and c) Fuel 9 Type 3.

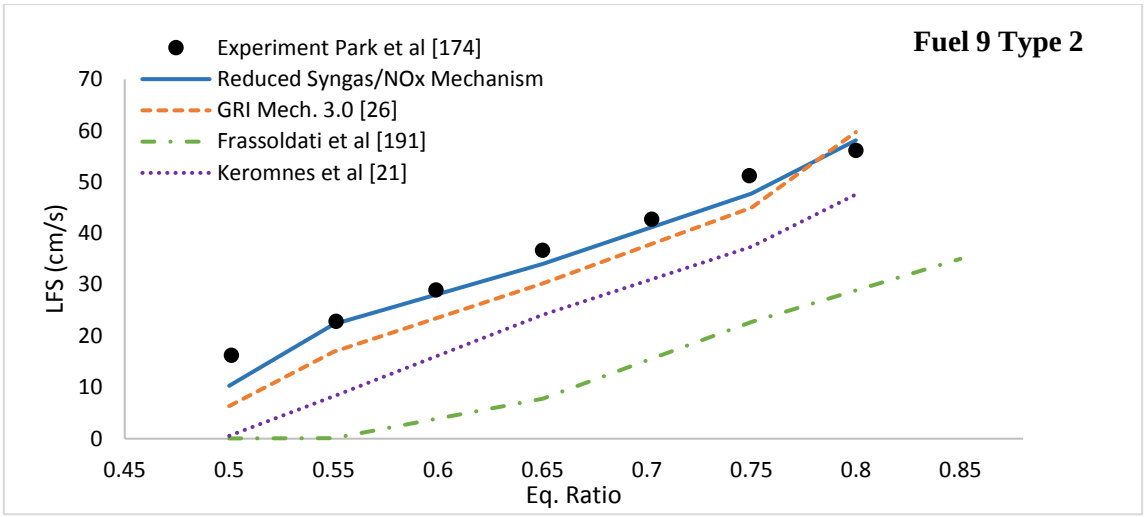

b)

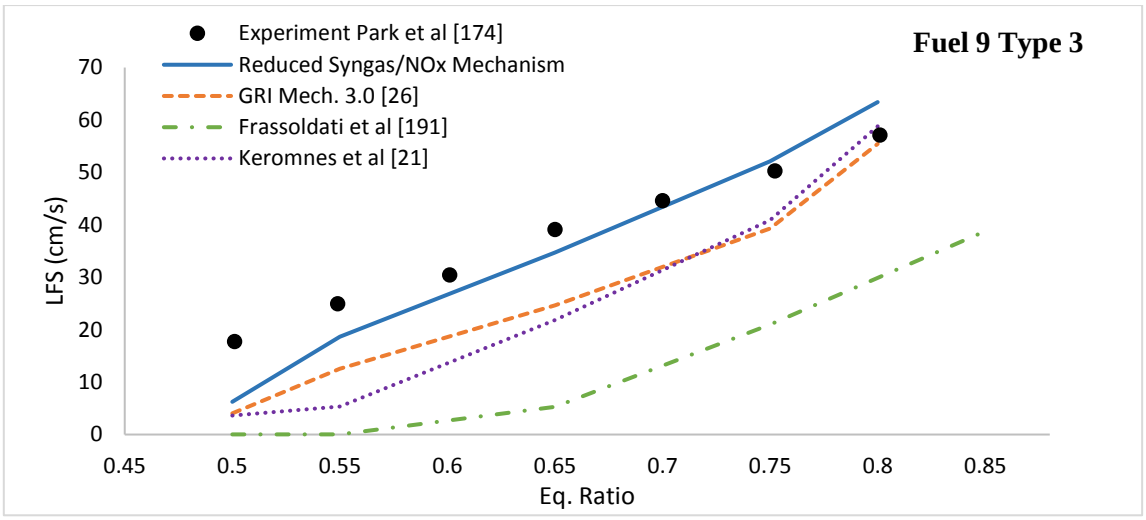

c)

Figure 5-8 (cont.) Comparison between the measured and calculated LFSs for a) Fuel 9 Type 1, b) Fuel 9 Type 2 and c) Fuel 9 Type 3.

5.2.2 Ignition delay time

$H_2/CO/CH_4/O_2/AR$ mixture

To evaluate the performance of the reduced mechanism for predicting the ignition delay time, the experimental measurements from Mathieu et al. [25] for lean H2/CO/CH4/O2/AR mixtures were used, Fuel 2 Table 3-3. The authors measured the ignition delay times using constant equivalence ratio of 0.5 and a range of T=1010-1920 K and P= 1.6, 12 and 32 bar. The experimental and simulated results were compared and are presented in Figure 5-9. The developed reduced mechanism shows a good match at all of the pressures and temperatures tested, and accurately captures the effect of the pressure on the reactivity of the mixture and therefore the ignition delay time: The higher is the pressure the higher is the concentration of the reactants and therefore the higher is the reactivity of the mixture. This results in a lower ignition delay time as the mixture is ignited earlier. The rest of the tested mechanisms deviate from the experimental results at all of the conditions.

For further analysis of the performance of the tested mechanisms, the absolute overall mean errors for each mechanism were calculated. For pressure 1.6 atm, Figure 5-9 a, the new developed syngas/NOx mechanism has the lowest overall grand mean error, 4.4%, followed by Keromnes et al mechanism with 5.1%. For Frassoldati et al and GRI Mech. 3.0 the absolute grand mean errors are relatively high, 9.6% and 19.3% respectively. For 12 atm pressure, only the new developed syngas/NOx mechanism has low absolute overall mean error, 2.5%, while the rest of the mechanisms show a high deviation with the experimental results. For Keromnes et al the absolute overall mean error is 36%, for Frassoldatti et al 40.2% and for GRI Mech.3.0 21.3%. Finally for 32 atm pressure, the new developed mechanism has an absolute overall mean error of 2.7%, Keronmes et 8.4%, Frassoldati et al 6.7% and GRI Mech.3.0 6.1%. By summarizing the findings from the errors comparisons, is it obvious that the new developed syngas/NOx mechanism is more accurate and is having the lowest deviation with the experimental results at all of the conditions.

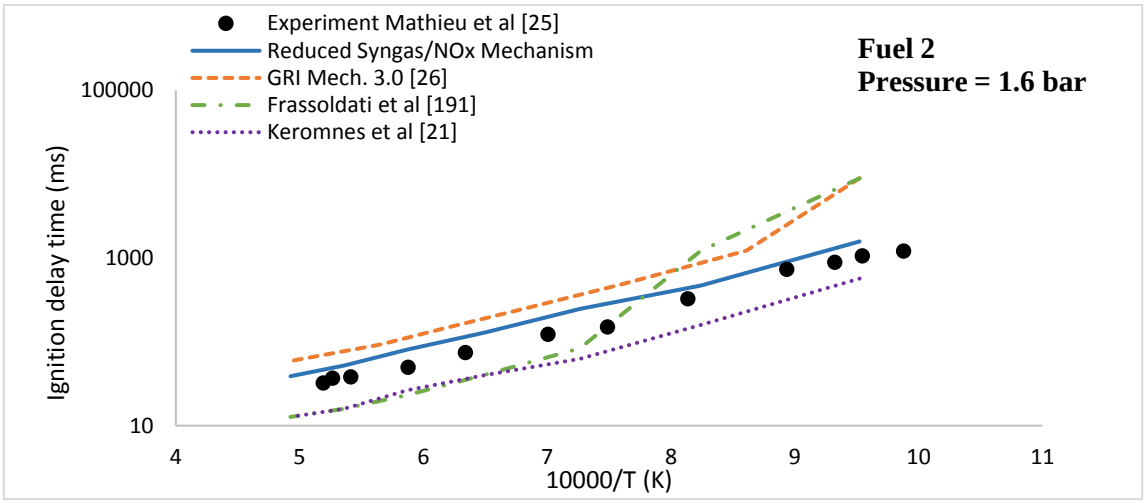

a)

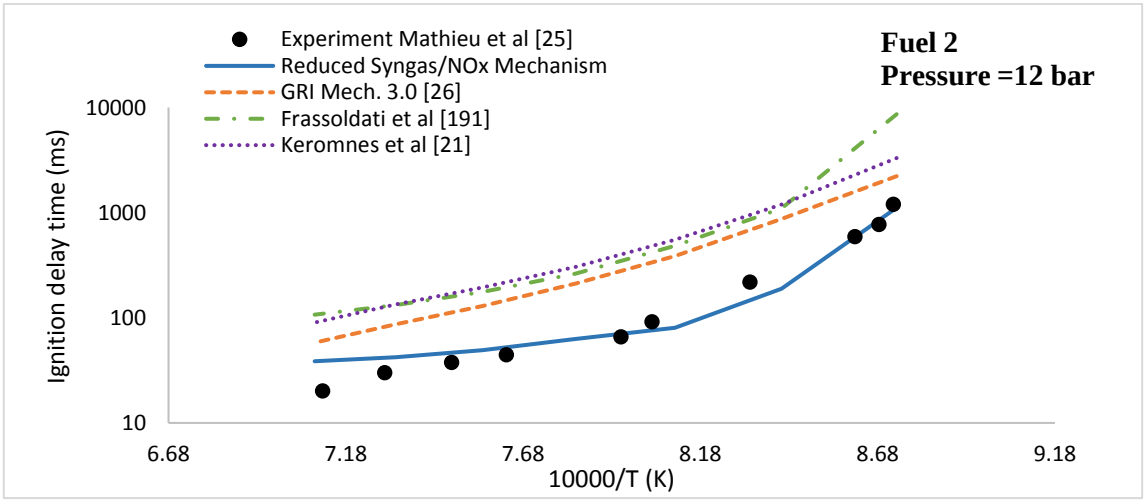

b)

Figure 5-9 Comparison between the measured and calculated ignition delay time for $H_2/CO/O_2/CH_4/AR$ fuel mixture at a)P=1.6 bar , b) P=12 bar and c) P=32 bar

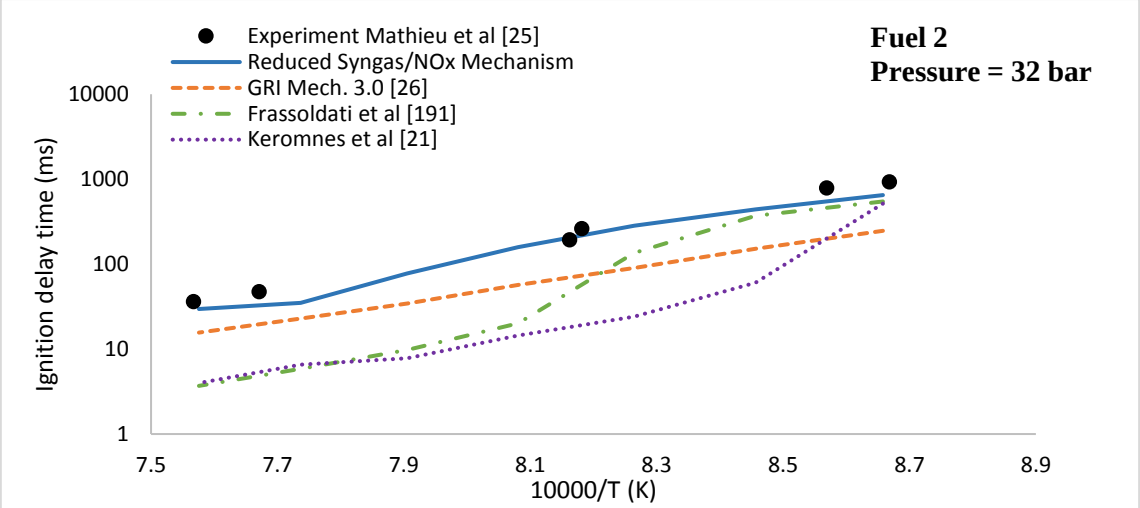

c)

Figure 5-9 (cont.) Comparison between the measured and calculated ignition delay time for $H_2/CO/O_2/CH_4/AR$ fuel mixture at a)P=1.6 bar , b) P=12 bar and c) P=32 bar.

5.2.3 NOx formation profiles

$H_2/CO/CO_2/CH_4/N_2$ mixture

For the purpose of this research, a flat flame burner configuration was chosen. A flat flame burner usually consists of a fine porous metal disk or a buddle of small parallel channels that are contained at the end of the chamber. The gas mixtures (fuel and oxidant) travels upwards through the channels at the top of the burner and finally emerges in uniform velocity distribution across the upper surface of the burner. During the ignition of the fuel mixture, a flat flame is produced across and close to the burner. Usually, this kind of burners are cooled at the circumference and they are design to be operated at different stream velocities [245].

The concentration of NO along the axial direction from the surface of the burner was calculated at three different initial pressures: 1 bar, 3.05 bar and 9.15 bar. The syngas composition consists of 16.99%vol H_2, 20.58%vol CO, 2.8%vol CH_4, 47.67 %vol N_2 and 11.84%vol CO_2 by volume [178] and can be found in Table 3-3, Fuel 11. The simulation results were compared and validated against experimental data from Charlston et al. [176] and presented in Figure 5-10.

According to Charlston et al [176], NO formation depends on the flame front and the pressure. The authors suggested that the majority of NO is formed in axial distance lower than 2mm for all of the pressures tested which is the region of the flame front. Then, NO reaches a plateau and continues with relatively low reduction in the post flame region (burnt gas region). For the effect of the pressure on NO, the authors made the statement that the higher is the pressure, the higher is the NO formation.

The conclusions from Charlston et al are confirmed by the results of Figure 5-10. First it can be seen that at all of the tested pressures, NO increased rapidly at approximately 1mm and reaches a plateau at distance between 1-2 mm. Then, NO continues with relatively low reductions until 10mm.

Moreover, the effect of the pressure is captured very well by the developed mechanism and the mechanism from Frassoldati et al . For both mechanisms at pressure 1 bar, NO reaches a plateau at approximately 1mm with maximum value 2.00E-06 ppm while for pressure 9.15 bar the plateau is reached at 1mm with maximum NO value at 3.00E-06 ppm.

For a detail analysis of the deviation between the experimental and simulated results the absolute overall mean error is calculated for each mechanism tested. For the developed mechanism for pressure 1 bar the error is 3.5%, for 3.05 bar is 1.3% and for 9.15 bar is only 0.46%, while for Frassoldati et al for pressures 1 bar, 3.05 bar and 9.15 bar the calculated errors are 2.3%, 1.4% and 1.0% respectively. On the other hand, Keromnes et al under-predicts the experimental results and has an absolute overall mean error of 8.7% for pressures 1 bar, 8.8% for 3.05 bar and 7.3% for 9.15 bar. Finally, GRI Mech. 3.0 has very high absolute overall mean error for 1 bar pressure, 26.4%, while for 3.05 bar and 9.15 bar the calculated errors are 5.3% and 4.4% respectively.

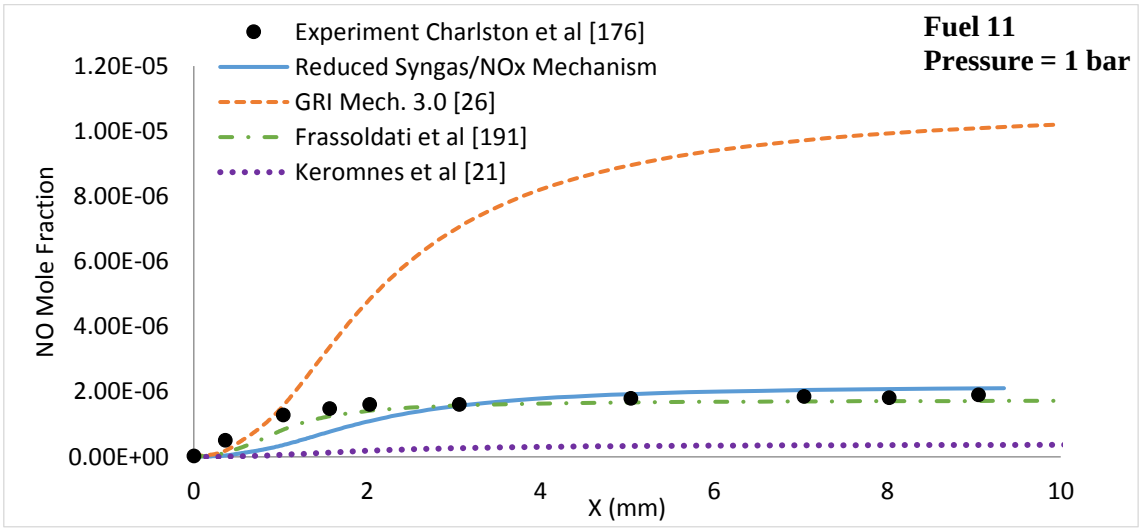

a)

Figure 5-10. Comparison of the calculated NO profiles by using the chemical kinetics mechanisms tested and the experimental measurements obtained from [176] at a)P=1 bar, b)3.05 bar and c) 9.15 bar.

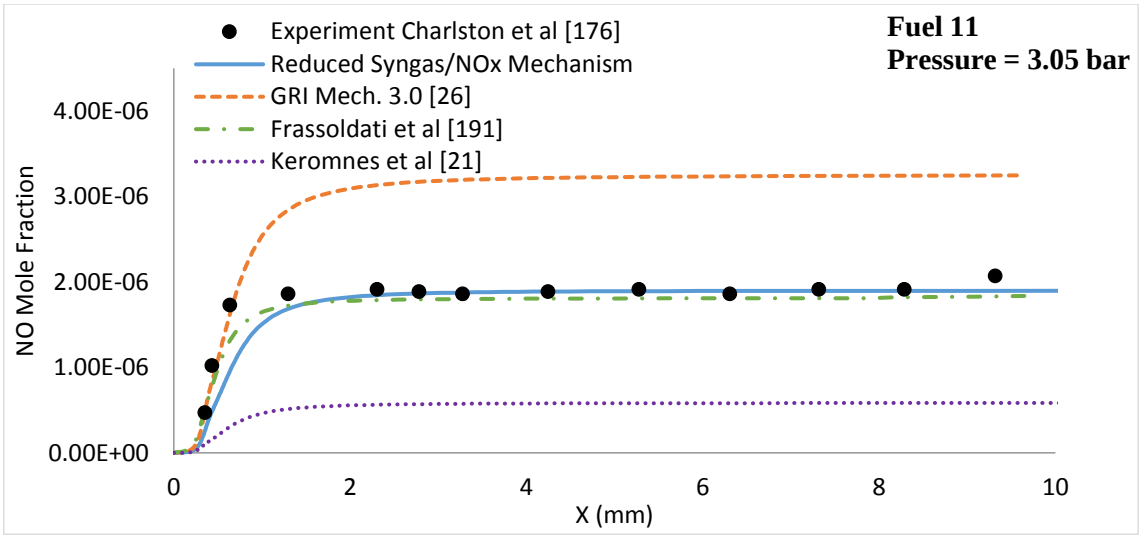

b)

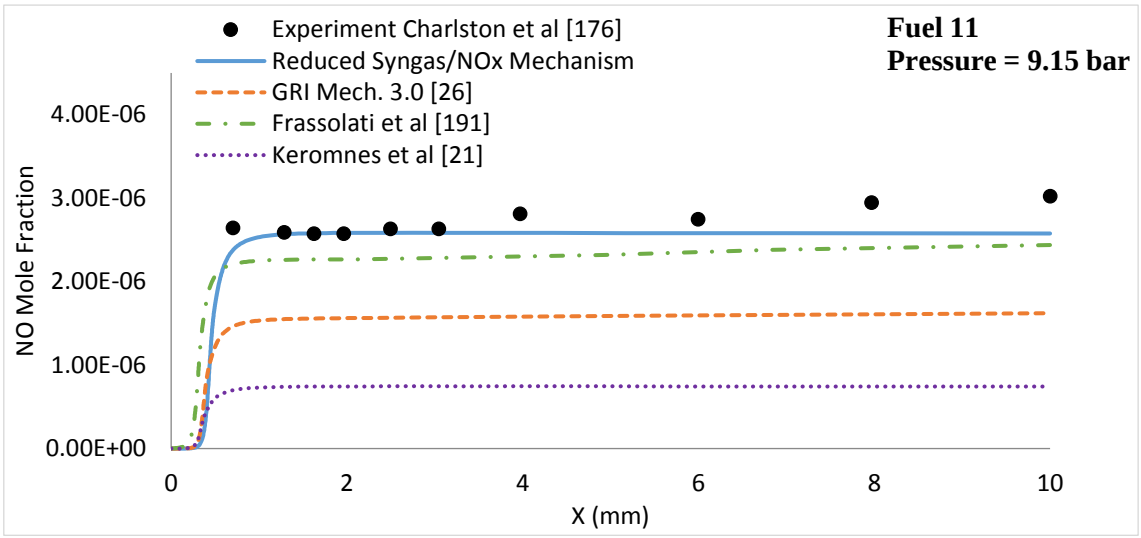

c)

Figure 5-10 (cont.). Comparison of the calculated NO profiles by using the chemical kinetics mechanisms tested and the experimental measurements obtained from [176] at a)P=1 bar, b)3.05 bar and c) 9.15 bar.

$H_2/CH_4/CO/CO_2$ mixture

The performance of the constructed mechanism on predicting NO formation was also evaluated by using the experimental data from Watson et al. [13]. The authors performed an experimental study to analyse the formation of NOx during the combustion of $CH_4/H_2/CO/CO_2$ syngas mixture, Fuel 12 Table 3-3, at atmospheric pressures (1.01 bar), T = 300K and a range of equivalence ratios of 0.7-1.4. The comparison between the experimental measurements of NO profiles along the axial distance of the burner and the simulated results are presented in Figure 5-11.

According to the comparison, the proposed mechanism accurately reproduces the experimental NO measurements and is having low calculated absolute overall mean error at all of the tested conditions. For 0.72 equivalence ratio the error is 5.2%, for 1.03 is 5.9% and for 1.34 is 5.8%.

Moreover, it captures the effect of the equivalence ratio on NO formation: The higher is the equivalence ratio, the richer is the mixture composition and therefore the higher is the NO formation.

For the rest of the mechanisms, Keromnes et al.[21] performs very well at equivalence ratio 1.34 and has an overall mean error of 7.2%. However, the mechanism under-predicts the experimental results at 0.72 and 1.03 equivalence ratios in which the overall mean errors are 25.5% and 50.2% respectively. This is because the mechanism was originally developed by Keromnes et al [21] for the simulation of pure H_2 and H_2/CO mixtures. By implementing CH4 and NOx chemical pathways, the thermal stability of the mechanism changed and that results in an unsteady behavior of the mechanism while simulating multicomponent syngas combustion and NOx. That has as a result the deviation of the experimental results at equivalence ratios 0.72 and 1.03.

On the other hand, Frassoldati et al.[191] has a relatively low overall mean error at 0.72, 7%. However, as the equivalence ratio increased the deviation between the simulated results by using Frassoldati's mechanism and the experimental measurements increased too. At 1.03 equivalence ratio, the absolute overall mean error is 13.8%, while at 1.34 equivalence ratio the error is 32.9%. Finally, GRI Mech. 3.0 [26] deviates from the experimental results at all of the conditions tested and has absolute overall error 60.2% at 0.72 equivalence ratio, 64.2% at 1.03 equivalence ratio and 76% at 1.34 equivalence ratio.

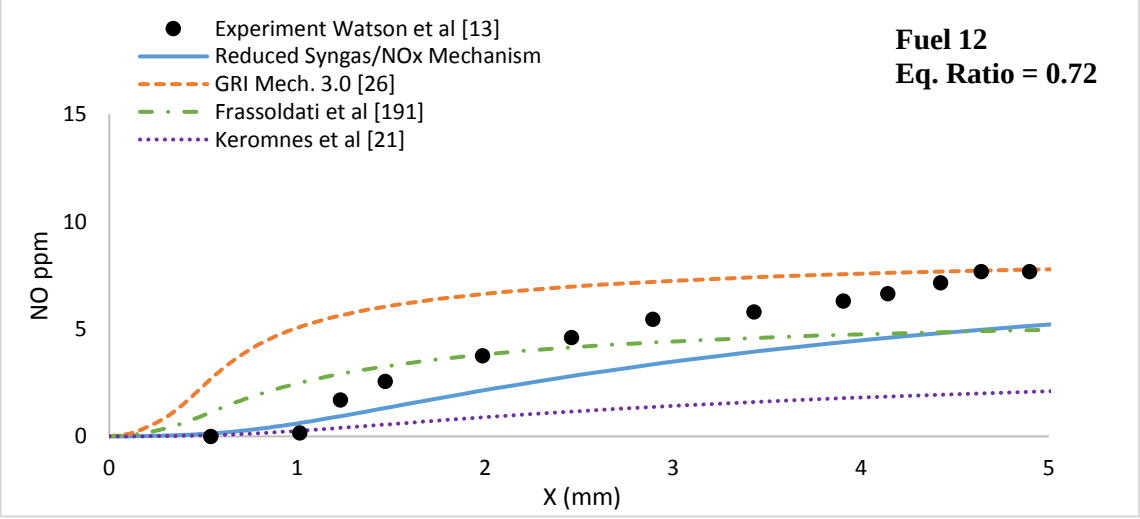

a)

Figure 5-11. Comparison of the calculated NO profiles by using the chemical kinetics mechanisms tested and the experimental measurements obtained from [13] at a) eq. ratio 0.72, b) eq. ratio 1.03 and c) eq. ratio 1.34.

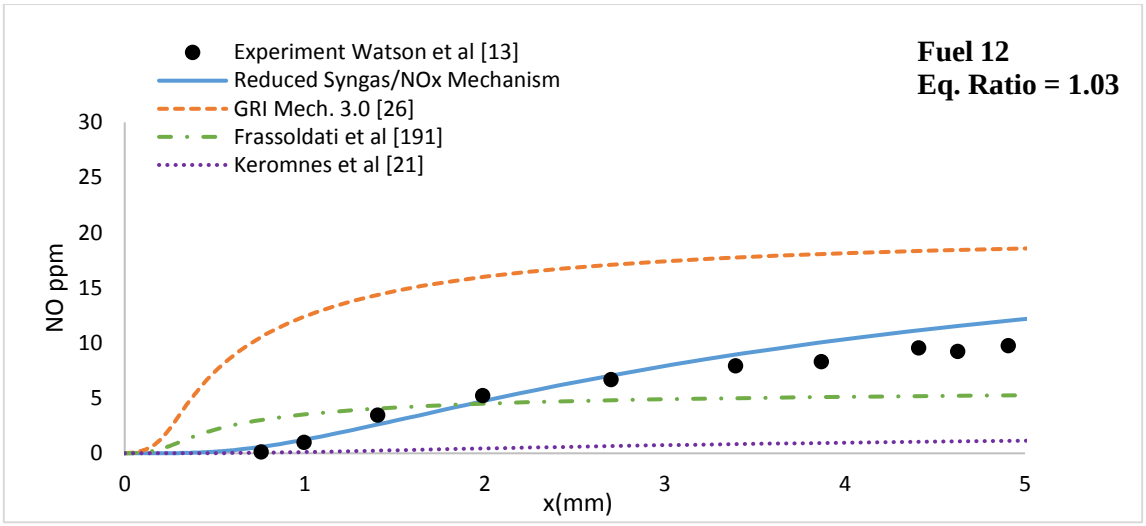

b)

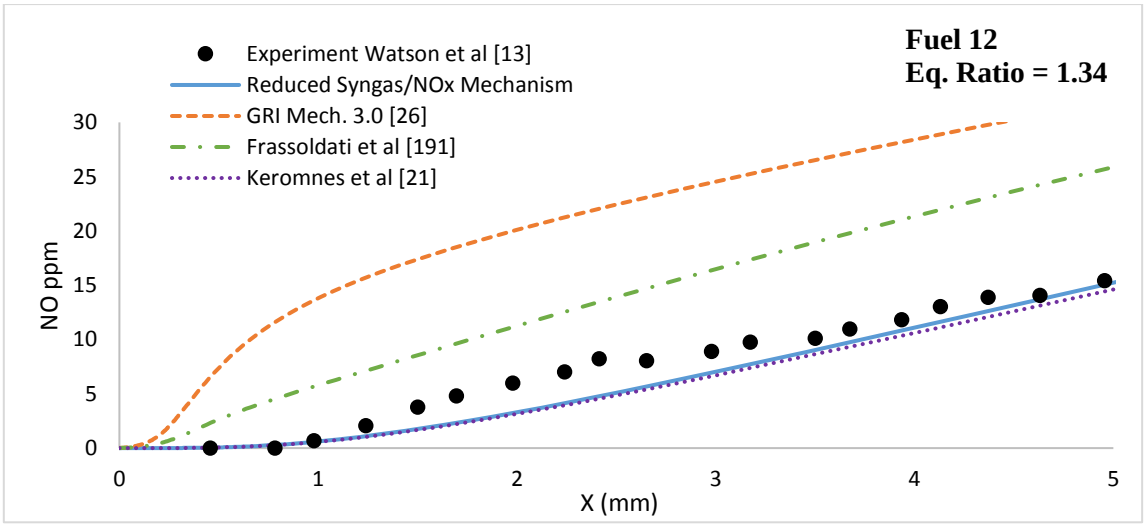

c)

Figure 5-11.(cont.) Comparison of the calculated NO profiles by using the chemical kinetics mechanisms tested and the experimental measurements obtained from [13] at a) eq. ratio 0.74, b) eq. ratio 1.03 and c) eq. ratio 1.34.

5.2.4 Absolute Grand mean error analysis

As it was already described in Chapter 3 Section 3.3, for further analysis of the deviation between the numerical and experimental results, the absolute grand mean error for each mechanism tested in this chapter was calculated for each combustion parameter (LFS, ignition delay and NOx formation profiles). Furthermore, a pre-set error limit was used for each combustion parameter in order to ensure the accuracy level of the mechanisms. Finally, for all of the tested conditions, the calculated individual errors can be found in Appendix B.

LFS

For LFS simulations, the acceptable error limit was set to 2 %. The mechanisms that are inside this error limit are characterized as acceptable for the simulation of the specific experimental data. The calculated grand mean errors for LFS calculations are presented in Figure 5-12. The calculated grand mean error by using the proposed mechanism is ~ 2 % which lies inside the

preset acceptable individual error limit (2%). Moreover, the proposed mechanism has the lowest error value from all of the tested mechanisms.

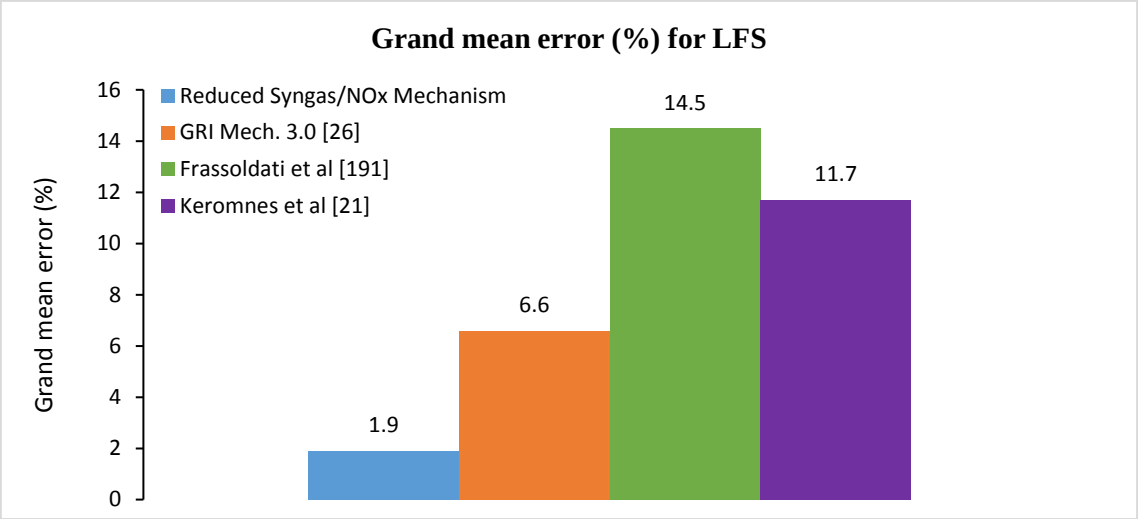

Figure 5-12. Comparison of the calculated absolute grand mean error for LFS simulations

Ignition delay time

For ignition delay time simulations, the acceptable error limit was set to 5 %. The absolute grand mean errors for ignition delay times by using all of the tested mechanisms are compared in Figure 5-13. It can be seen that the calculated absolute grand mean error by using the reduced syngas/NOx mechanism is only ~3.2%which, again is the lowest in comparison with the other tested mechanisms and is inside the acceptable error limit.

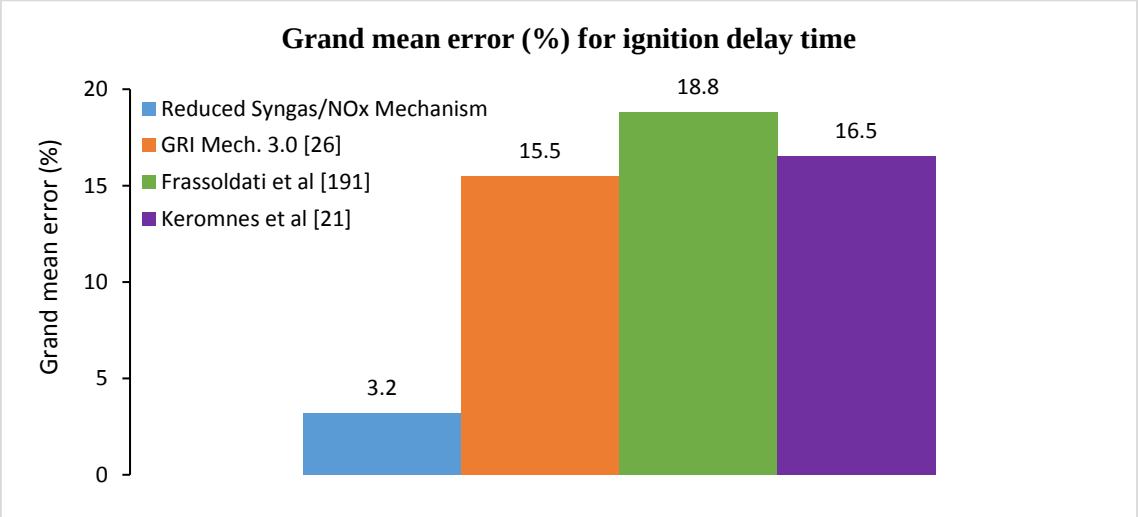

Figure 5-13. Comparison of the calculated absolute grand mean error for ignition delay time simulations

NOx comparison

For NOx formation simulations, the acceptable error limit was set to 5 %. The comparison between the calculated absolute grand mean errors for NOx formation simulation by using the tested mechanisms is presented in Figure 5 -14. According to Figure 5-14,the calculated grand

mean error by using the proposed reduced mechanism is very low (~3.6%) and is inside the preset error limit . Therefore, can be characterized as suitable for the simulation of NOx formation.

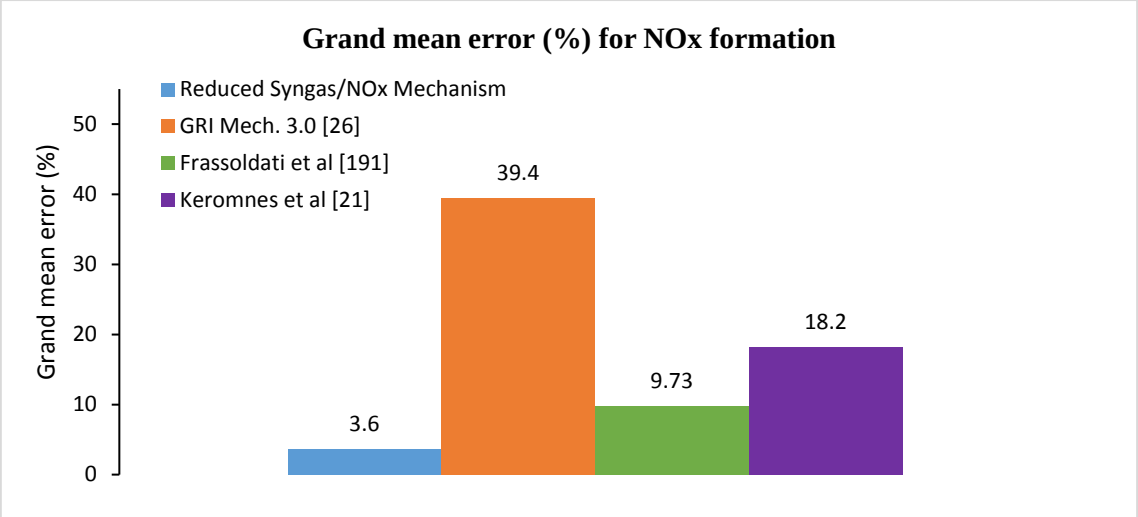

Figure 5-14. Comparison of the calculated absolute grand mean error for NOx formation simulations

By considering all of the results from the error analysis it is obvious that the reduced mechanism shows a high level of accuracy and can be characterized as applicable for the simulation of LFS, ignition delay time and NO mole fractions. In contrast, the rest of the mechanisms tested in this approach show high calculated errors that exceed the pre-set error limit. In conclusion, it can be said that the proposed reduced mechanism offers a robust and computational efficient solution for the accurate simulation of multicomponent syngas combustion and NOx formation.

5.2.5 Multidimensional CFD analysis

Finally, a multidimensional computational fluid dynamics (CFD) analysis was performed to evaluate the combustion of syngas derived from biomass and coke-oven solid feedstock, in a micro-pilot ignited supercharged dual-fuel engine, under lean conditions. Three types of multicomponent syngas mixtures were used for the simulations. Each type of fuel is simulated by using different equivalence ratio and injection times. For Fuel 24 Type 1, the simulations were conducted by using equivalence ratios 0.63 and 0.68 and Θ injection 9° BTDC and 7° BTDC respectively. For Fuel 24 Type2, equivalence ratio of 0.4 and Θ injection 18° BTDC were used. Finally, for Fuel 24 Type 3, the equivalence ratio was 0.6 and the Θ injection was 14° BTDC. All of the fuels are presented in Table 3-3.

The results obtained by using the proposed reduced mechanism and those of Keromnes et al. [21], Frassoldati et al. [191] and GRI Mech 3.0 [26], were compared and validated against the

experimental data from Azimov et al. [78]. The comparison of the experimental in cylinder pressure and ROHR and the simulated data is presented in Figure 5-15 for Fuel 24 Type1, Figure 5-16 for Fuel 24 Type2 and Figure 5-17 for Fuel 24 Type 3. According to the comparison, the proposed reduced mechanism is in a good agreement with the experimental pressure and ROHR at all of the tested conditions. However, in order to investigate in detail the differences between the simulated and experimental results, the maximum in-cylinder pressure (Max P) and the crank angle in which the maximum pressure was reached for each set of simulated and experimental data used for the CFD analysis are presented in Table 5-2. According to the comparison, the difference between the experimental and the calculated Max P by using the reduced syngas/NOx mechanism is 1.1 MPa for Fuel 24 Type 1 eq.ratio 0.63, 1.1 MPa for Fuel 24 Type 1 eq.ratio 0.68, 0.7 MPa for Fuel 24 Type 2 eq.ratio 0.4 and finally, 0.7 MPa for Fuel 24 Type 3 eq.ratio 0.6. Moreover, for all of the conditions, by using the reduced syngas/NOx mechanism, the CA in which the Max P was reached is identical with the experimental results. The in-cylinder pressure tracers, especially the max in cylinder pressure, as well as the time required to reach the maximum in-cylinder pressure are related directly with the ignition delay time, the flame speed and the combustion intensity. The rest of the mechanisms show an over-prediction of the experimental results

Table 5-2 Comparison of the experimental and simulated maximum in cylinder pressure (Max P) and the crank angle when the maximum pressure reached.

	Fuel 24 Type 1 Eq. Ratio = 0.63 $\Theta_{inj.}$= 9º BTDC		**Fuel 24 Type 1 Eq. Ratio = 0.68 $\Theta_{inj.}$= 7º BTDC**		**Fuel 24 Type 2 Eq. Ratio = 0.4 $\Theta_{inj.}$= 18º BTDC**		**Fuel 24 Type 3 Eq. Ratio = 0.6 $\Theta_{inj.}$= 14º BTDC**	
	Max P (MPa)	CA (deg.)	Max P (MPa)	CA (deg.)	Max P (MPa)	CA (deg.)	Max P (MPa)	CA (deg.)
Experiment Azimov et al [78]	11.4	9	10.8	10	12.5	5	12.2	6
Reduced Syngas/NOx Mech.	12.5	9	11.9	10	11.8	5	12.9	6.1
Frassodlati et al [191]	19.5	10.6	19.2	11	16.2	6.9	21.2	5.6
GRI Mech. 3.0 [26]	19.8	8.8	19.7	9.8	15.1	7	14.4	5.7
Keromnes et al [21]	14.6	11	15.26	12.2	11.2	5.5	11.5	6.7

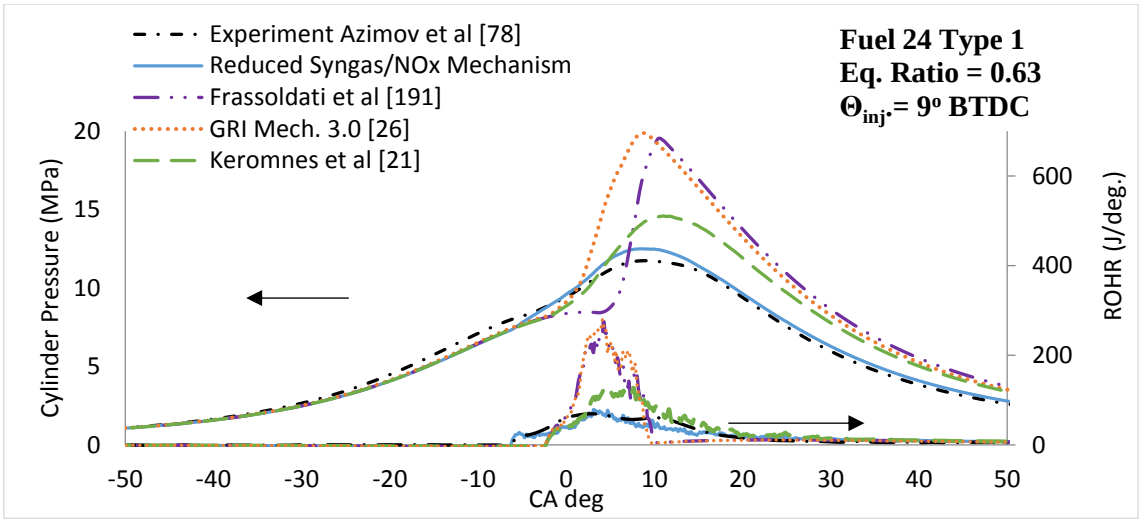

a)

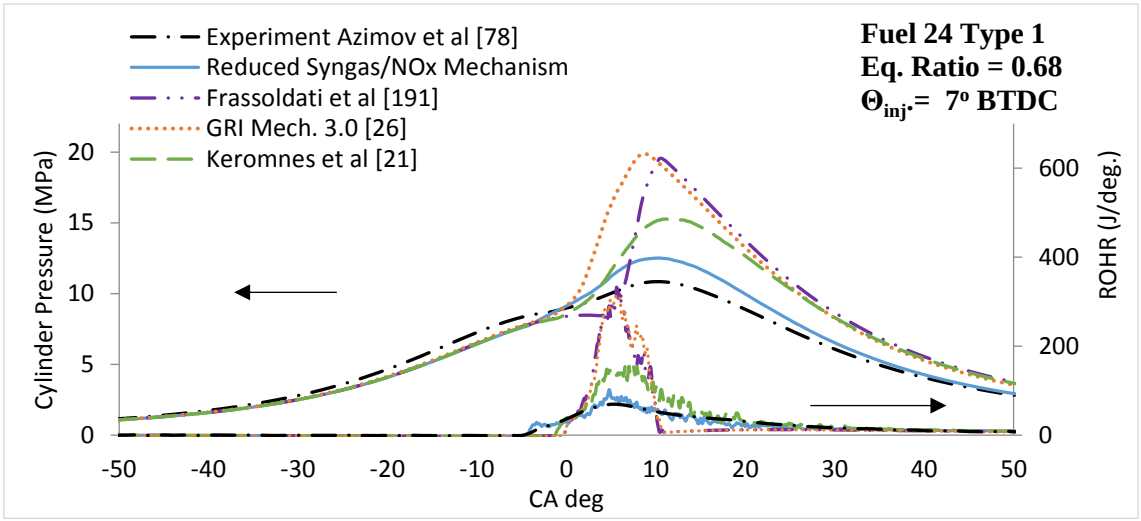

b)

Figure 5-15 Comparison of experimental and simulated in-cylinder pressure and heat release rate of dual-fuel micro-pilot ignited syngas combustion for Fuel 24 Type 1 at a) equivalence ratio 0.63 and Θ injection 9º BTDC and b) eq. ratio 0.68 and Θ injection 7ºBTDC

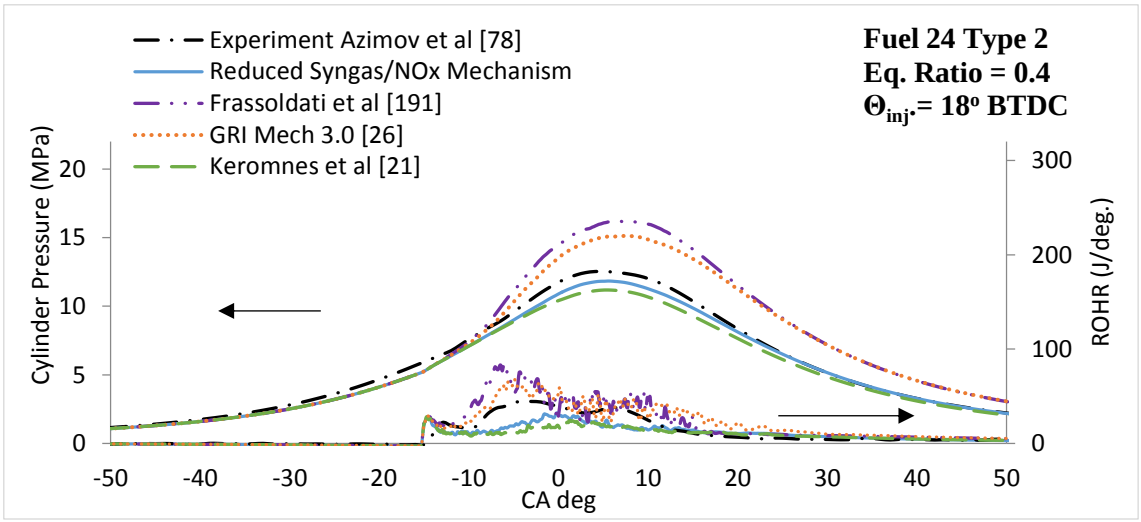

Figure 5-16 Comparison of experimental and simulated in-cylinder pressure and heat release rate of dual-fuel micro-pilot ignited syngas combustion for Fuel 24 Type 2 at equivalence ratio 0.4 and Θ injection 18º BTDC.

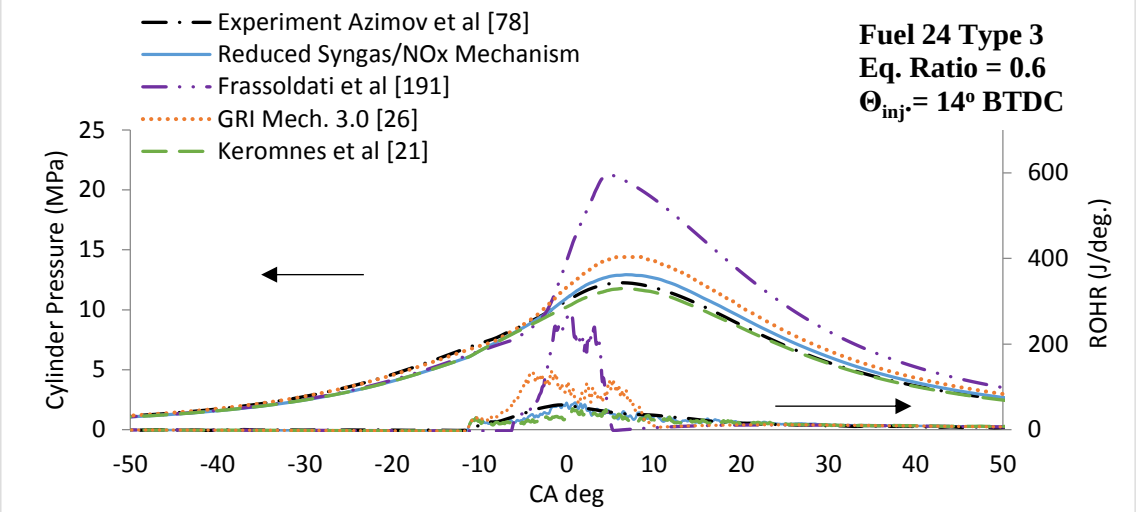

Figure 5-17 Comparison of experimental and simulated in-cylinder pressure and heat release rate of dual-fuel micro-pilot ignited syngas combustion for Fuel 24 Type 3 at equivalence ratio 0.6 and Θ injection 14º BTDC.

For a better understanding of the in-cylinder combustion process, the sequential images of the spray and temperature distribution for Fuel 24 Type 1 (equivalence ratio= 0.63) by using the reduced mechanism are presented in Figure 5-18. The images show micro-pilot injected n-heptane spray development with further ignition and combustion of syngas. The temperature reaches 2200 K while the flame front propagates smoothly towards the walls of the cylinder, consuming the unburned syngas mixture. Furthermore, the sequential images of NO formation for Fuel 24 Type 1 (Equivalence ratio 0.63) are presented in Figure 5-19. As can be seen, NO concentration increases as the temperature is increased and reaches its maximum value during the highest in-cylinder temperature (2200 K).

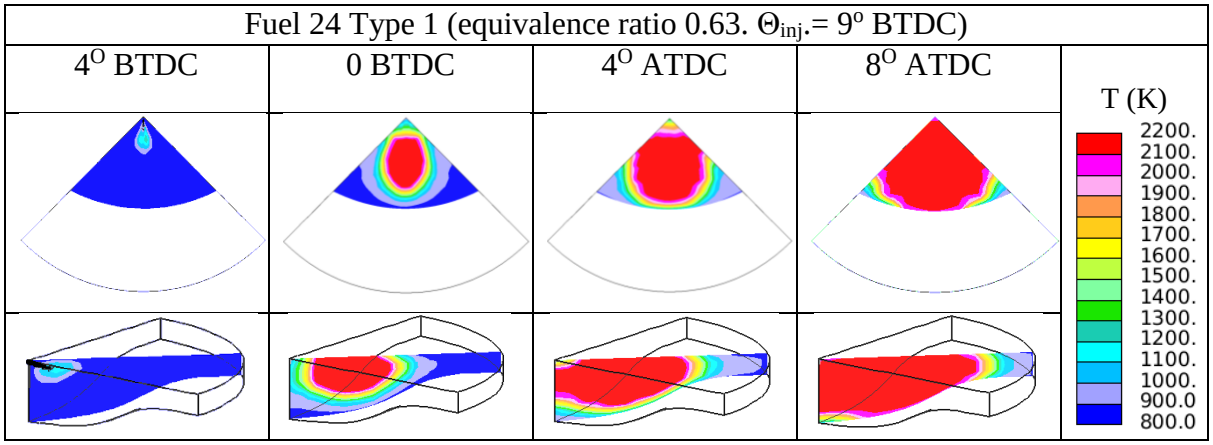

Figure 5- 18.Sequential images of dual-fuel micro-pilot ignited syngas combustion with new kinetics mechanisms. Fuel 24 Type 1 eq. ratio 0.63, Θ inj.= 9o BTDC, PIVC = 225 - kPa, TIVC = 330K.

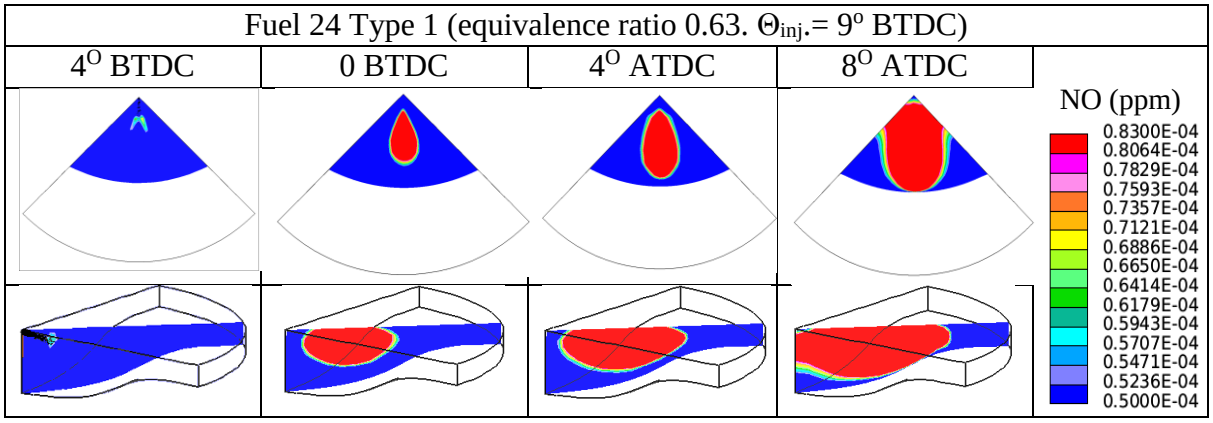

Figure 5-19.Sequential images of NO concentration during dual-fuel micro-pilot ignited syngas combustion by using the new kinetics mechanisms. Fuel 24 Type 1 eq. ratio 0.63, Θ inj.= 9o BTDC, PIVC = 225 - kPa, TIVC = 330 K

In order to check the computational efficiency of the developed mechanism, the CPU time for each one of the chemical kinetics mechanisms used in the multidimensional CFD simulation was calculated. The comparison of the calculated CPU time and number of species for each one of the chemical kinetics mechanisms is presented in Table 5-3. According to the comparison, the developed reduced syngas/NOx mechanism requires the lowest CPU time for a complete CFD simulation, 2.5 hours, and has the lowest number of species, only 44.

Table 5-3 Comparison of the CPU time and the number of reactions of the mechanism developed in Chapter 5 with other well-validated mechanisms

	Chemical Kinetics Mechanisms	**Reactions**	**CPU Time**
	Syngas/NOx mechanism		
1	Reduced Syngas/NOx mechanism (Chapters 5 and 6)	44	2.5 hours
2	Constructed Mechanism 1 (Frassoldatti et al [191] + CH4)	182	16.5 hours
3	Constructed Mechanism 2 (Keromnes et al [21] +12 step NOx sub-mech. +CH4)	52	3 hours
4	GRI mech. 3.0.[26]	325	1 day

5.3 Summary

During this chapter, the reduced chemical kinetics mechanism developed in Chapter 4, for the simulation of $H_2/CO/CO_2/CH_4$ syngas combustion in a micro-pilot-ignited supercharged dual fuel engine, was optimized by incorporating a 12-step reaction NOx pathway and by updating the rate constants of important hydrogen reactions that were found to be very sensitive during high pressure conditions. For the investigation of the important species and reactions affecting syngas combustion, flow analysis and reaction sensitivity studies were conducted. According to the flow and sensitivity analyses, the reactivity of the mixture is mainly affected by hydrogen and carbon based species and reactions. Moreover, R20 and R30 that were also highlighted in Chapter 4, show high sensitivity during high pressure, low temperature conditions and were

optimized by adopting new rate constants. For R20 the constant proposed by Li et al [232] was used, while for R30 the rate constant proposed by Konnov et al [73] was adopted.

Sensitivity analysis was also performed for the investigation of the important species affecting NOx formation. It was found that the formation of NOx is mostly affected by hydrogen-based, nitrogen-based and carbon-based species. Moreover, CH_4 was also highlighted as a sensitive species for NOx formation. This is an indicator that CH_4 plays a very important role not only for NOx formation but also for other important combustion parameters such as LFS and ignition delay time.

The developed syngas/NOx mechanism was then validated against experimental measurements and simulated results by using other well validated mechanisms in terms of LFS, ignition delay time and NO concentration profiles. According to the comparisons, the reduced mechanism accurately simulates the experimental results of the LFS and ignition delay time at all the conditions tested and captures very well the inhibiting effect of CH4 addition on the LFS and the effects of the pressure and temperature on ignition delay. Furthermore, the calculated NO concentrations are in a good agreement with the experimental results for both $H_2/CH_4/CO/CO_2$ and $H_2/CO/CO_2/CH_4/N_2$ mixtures. On the other hand, the results obtained by using GRI mech. 3.0, Frassoldati et al. and Keromnes et al. mechanisms, deviate from the experimental data.

Finally, a multidimensional CFD analysis was performed to evaluate the performance of the reduced mechanism on simulating the in-cylinder pressure, ROHR and NOx formation during syngas combustion in a micro-pilot-ignited supercharged dual fuel engine. According to the comparisons, the calculated in-cylinder pressure and ROHR are in a good agreement with the experimental results for all the three syngas mixtures with different equivalence ratios and injection timings. The rest of the three mechanisms over-predict the experimental ROHR and in-cylinder pressure at all of the conditions tested.

Chapter 6: Development of a reduced n-heptane/syngas/NOx mechanism for syngas combustion, n-heptane/syngas co-oxidation and NOx formation in a micro-pilot ignited dual-fuel engine

As previously mentioned, the ignition temperature of syngas fuels is relatively high and therefore a secondary diesel-based fuel must be used in dual-fuel applications [18]. The diesel-based fuel is injected via a pilot into the cylinder and is then ignited due to the in-cylinder conditions. The ignition of the secondary diesel-based fuel increases the in-cylinder temperature, resulting in the ignition of the primary premixed syngas fuel. After the syngas is ignited, the combustion proceeds without any diesel-based fuel chemistry.

The appearance of different gases in the syngas mixtures, in addition to the effect of the diesel-base fuel, makes the numerical analysis of the in-cylinder combustion very difficult. A robust, computational efficient and universal CFD compatible chemical kinetics mechanism must be developed that would be applicable to simulate, not only the multi-component syngas combustion and NOx formation, but also the co-oxidation of the pilot injected diesel-based fuel and the syngas. During this thesis, n-heptane was used as a surrogate of diesel.

Despite the fact that few mechanisms have been developed for the simulation of n-heptane oxidation and syngas combustion, there is a need for a reduced mechanism that will be able to model n-heptane/syngas co-oxidation and NOx formation. Therefore, during this chapter, a reduced, robust and computational efficient n-heptane/syngas /NOx mechanism was constructed for the simulation of n-heptane/syngas co-oxidation, syngas combustion and NOx formation in a micro-pilot injected dual-fuel engine. For the development of the n-heptane/syngas/NOx mechanism, different steps were followed. First, a comprehensive n-heptane mechanism was reduced by using necessity analysis and a skeletal mechanism was constructed. The skeletal mechanism for n-heptane was then coupled with the reduced syngas/NOx mechanism proposed in Chapter 5. The complete n-heptane/syngas/NOx mechanism was then validated against various experimental results for ignition delay time, LFS and NO concentration profiles for different n-heptane/air, n-heptane/syngas and syngas only mixtures. Finally, a multidimensional CFD analysis was performed for the prediction of syngas combustion and n-heptane/syngas co-oxidation in a micro-pilot ignited supercharged dual-fuel engine. The simulated results were compared with the experimental measurements in terms of in-cylinder pressure and ROHR.

6.1 N-heptane mechanism

In order to find the best and most computational efficient n-heptane mechanism for the reduction and the coupling with the syngas/NOx mechanism, a comprehensive comparison of different n-heptane mechanisms available in the literature was conducted. Four different reduced, skeletal and detailed mechanisms were collected and validated against experimental data for 100% n-heptane fuels in terms of LFS and ignition delay times, see Table 6-1. The four n-heptane mechanisms were validated by using the experimental data for ignition delay times reported in [179-183], Fuel 15 and Fuel 16 Table 3-3, and the measurements for LFSs from [184, 185], Fuel 17 and Fuel 18 Table 3-3. For ignition delay time the comparisons are presented in Figures 6-1 and 6-2.

Table 6-1 N-heptane mechanisms used in Chapter 6.

No.	Mechanism	Reactions	Species	References
1	Creck Reduced mechanism	1790	106	[109]
2	LLNL detailed mechanism	2827	654	[27]
3	Lu et al. Skeletal	842	188	[246, 247]
4	Wisconsin Reduced mechanism	52	29	[248]

Figure 6-1, shows the comparison of the experimental measurements reported by Ciezki and Adomeit [179] and the simulation results by using the tested mechanisms. The authors measured the ignition delay times of 100% n-heptane mixture by using three different equivalence ratios ,0.5,1 and 2, three different pressures, 6.5, 13.5 and 42 bar, and a range of temperature 650-1333 K, Fuel 15. According to the comparison, only Wisconsin's reduced mechanism proposed by [248] deviates from the experimental results, especially at high temperatures. This is because the Wisconsin mechanism was constructed from the reduction of a comprehensive detail mechanism and the authors focused on low temperature oxidation of n-heptane and the negative temperature coefficient region [248]. Therefore, important reactions affecting the performance of the mechanism at high temperatures may missing and that leads to the deviation with the experimental results especially at high temperatures. The rest of the mechanisms show a good agreement with the experimental data at all of the conditions tested. Moreover, the ability of the tested mechanisms to capture the ignition delay times for the oxidation of stoichiometric n-heptane/ air mixtures, Fuel 16, at high pressure 40 bar, temperature range 680-1282 K and equivalence ratios 0.5-1 , was tested by comparing the simulated results with the experimental measurements from [180-183], see Figure 6-2. Similar to the comparison results from Figure 6-1, only Wisconsin's reduced mechanism deviates from the experimental results, especially at intermediate to high temperature conditions due to the fact that it was developed for the simulation of NTC and low temperature oxidation of n-

heptane and therefore important reactions affecting the performance of the mechanism during intermediate and high temperatures are missing. On the other hand, the rest of the mechanisms show a good agreement with the experimental data at all of the conditions.

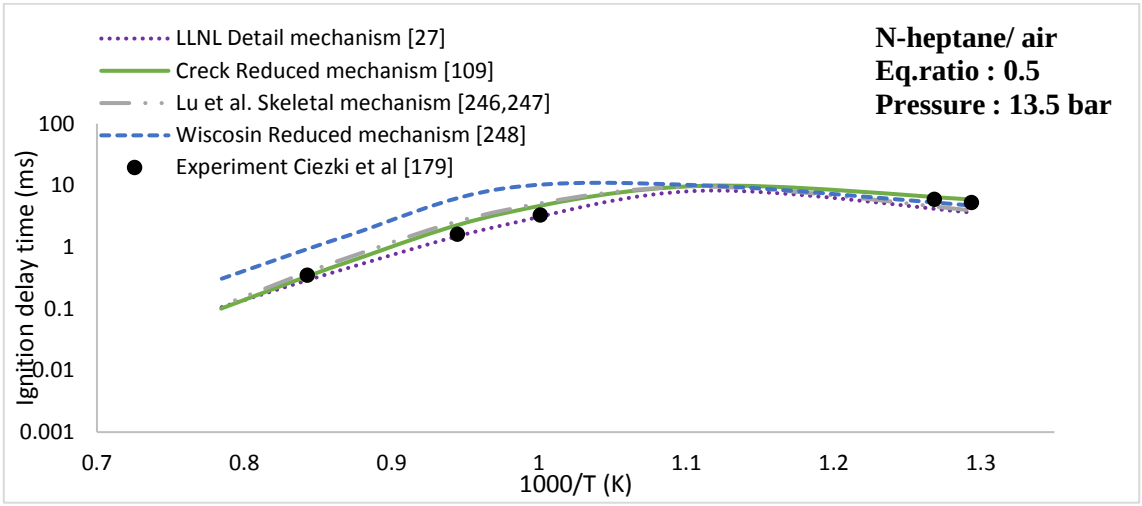

a)

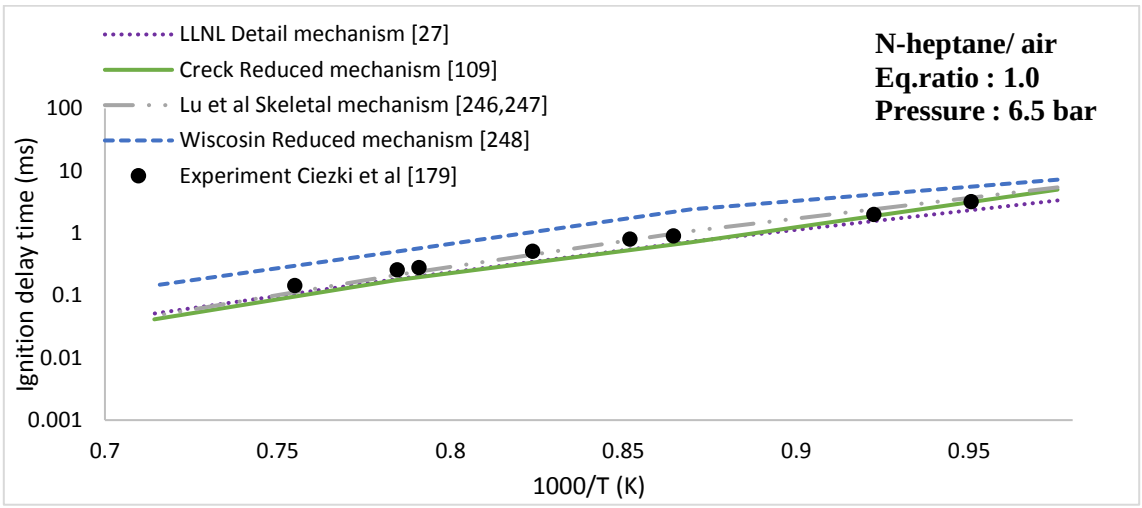

b)

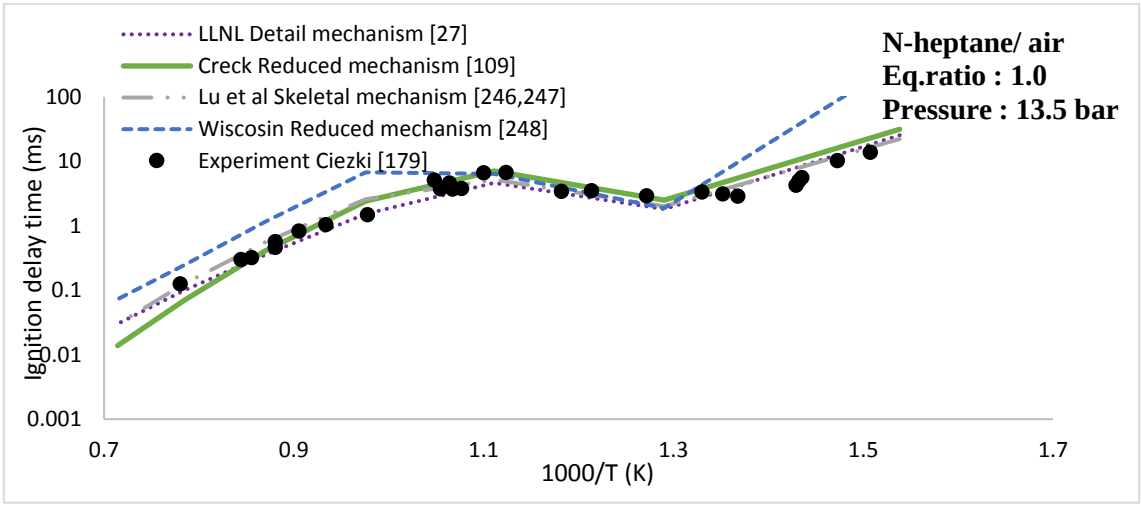

c)

Figure 6-1 Comparison of the simulated ignition delay time by using different n-heptane mechanisms and the experimental results obtained from [179].

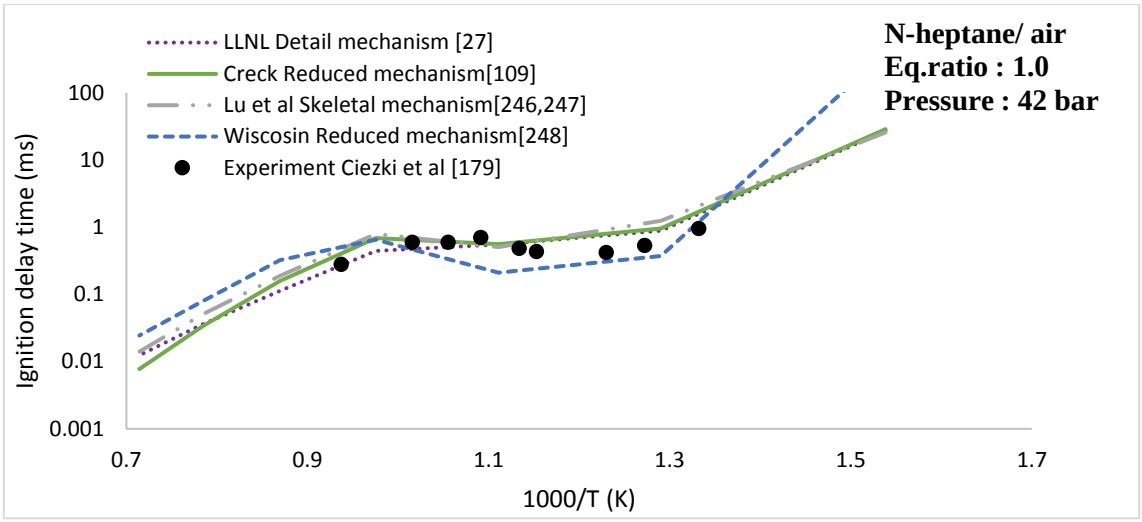

d)

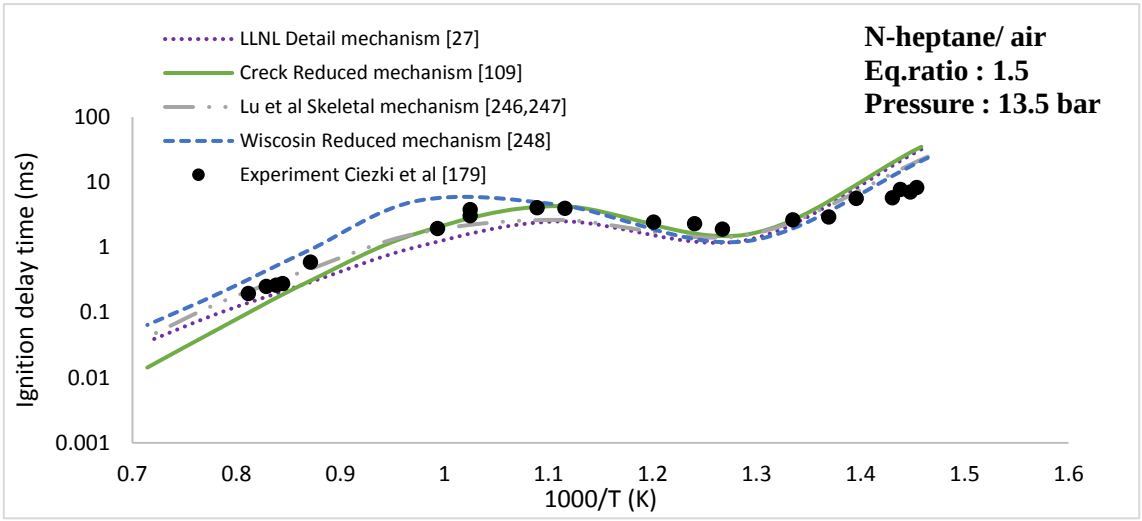

e)

Figure 6-1 (cont.) Comparison of the simulated ignition delay time by using different n-heptane mechanisms and the experimental results obtained from [179].

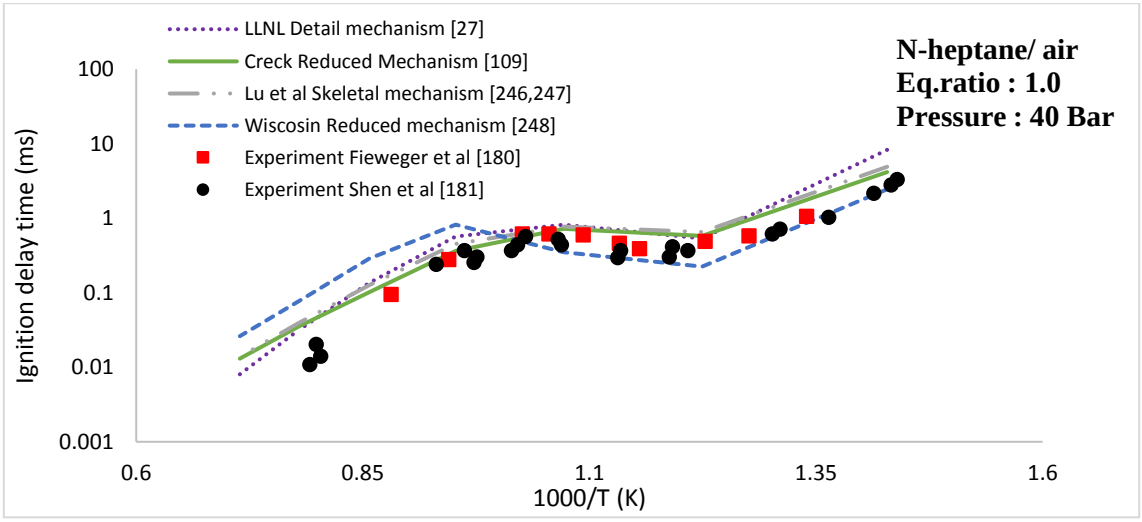

a)

Figure 6-2 Comparison of the simulated ignition delay time by using different n-heptane mechanisms and the experimental results obtained from [180-183].

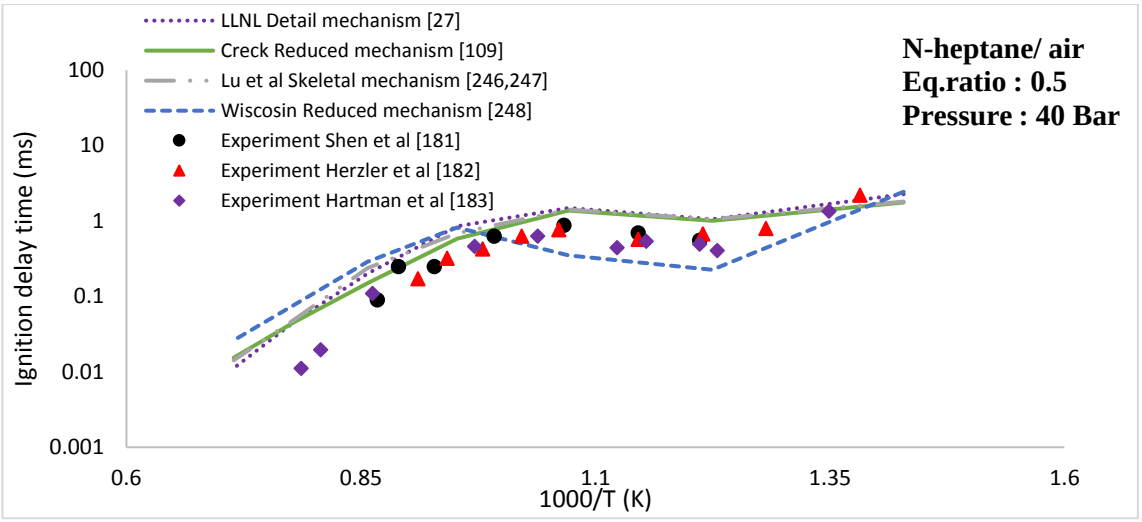

b)

Figure 6-2 (cont.) Comparison of the simulated ignition delay time by using different n-heptane mechanisms and the experimental results obtained from [180-183].

The tested n-heptane mechanisms have also been validated using LFS measurements reported in [184, 185]. Sillenghem et al. [184] used the heat flux method to measure the laminar burning velocities of n-heptane/air mixtures in a flat flame adiabatic burner at a range of equivalence ratios, 0.7-1.3, atmospheric pressure (1.01 bar) and temperatures from 298-358 K Fuel 17 Table 3-3. According to the comparison shown in Figure 6-3, the LFS by using the reduced mechanism from Wisconsin [248] is higher than the experimental results at all of the equivalence ratios and at all of the temperatures tested. Moreover, the skeletal mechanism from Lu et al. [246, 247] shows a good agreement with the experimental results at low equivalence ratios but as the mixture gets richer, the mechanism deviates from the measurements at all of the test temperatures. Only the reduced mechanism from Creck group [109] and the detail LLNL mechanism [27] are in a good agreement with the experimental results at all of the conditions.

The second set of LFS experimental data was obtained from Dirrernberger et al. [185]. The authors measured the adiabatic laminar burning velocities of pure n-heptane mixtures at atmospheric pressures (1.01 bar), temperatures from 298-398 K and equivalence ratios 0.6-1.3. According to the comparison shown in Figure 6-4, the reduced mechanism from Wisconsin [248] deviates from the experimental results at all of the equivalence ratios and temperatures tested. The skeletal mechanism proposed by Lu et al. [246, 247] shows a high deviation with the experimental results, especially at equivalence ratios between 0.9 and 1.4, showing again that at rich fuel mixtures the mechanism has a high level of uncertainty. Finally, the reduced mechanism from Creck modelling group [109] and the detail LLNL [27] mechanism show the closest match with the experimental results at all of the tested conditions.

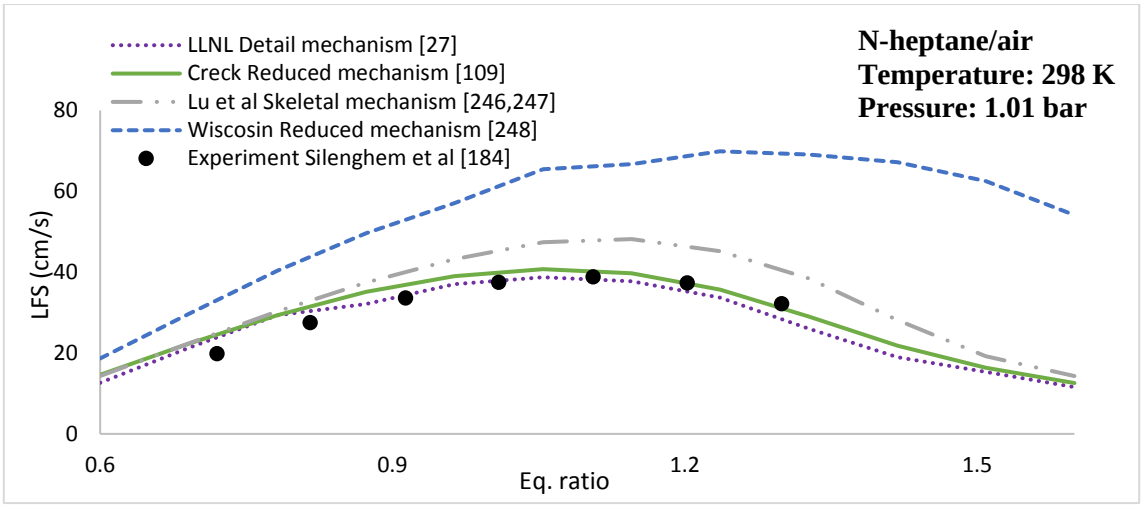

a)

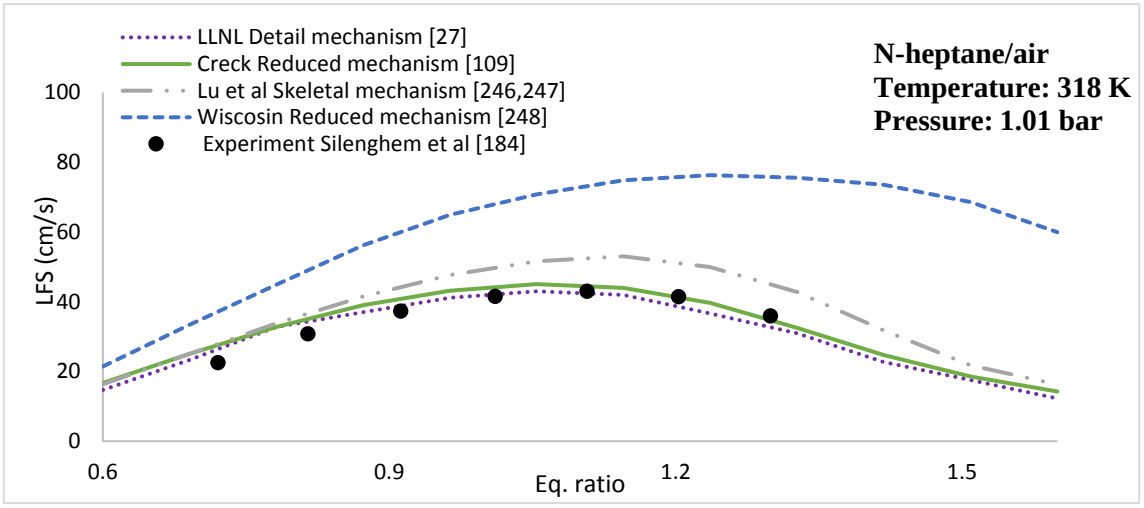

b)

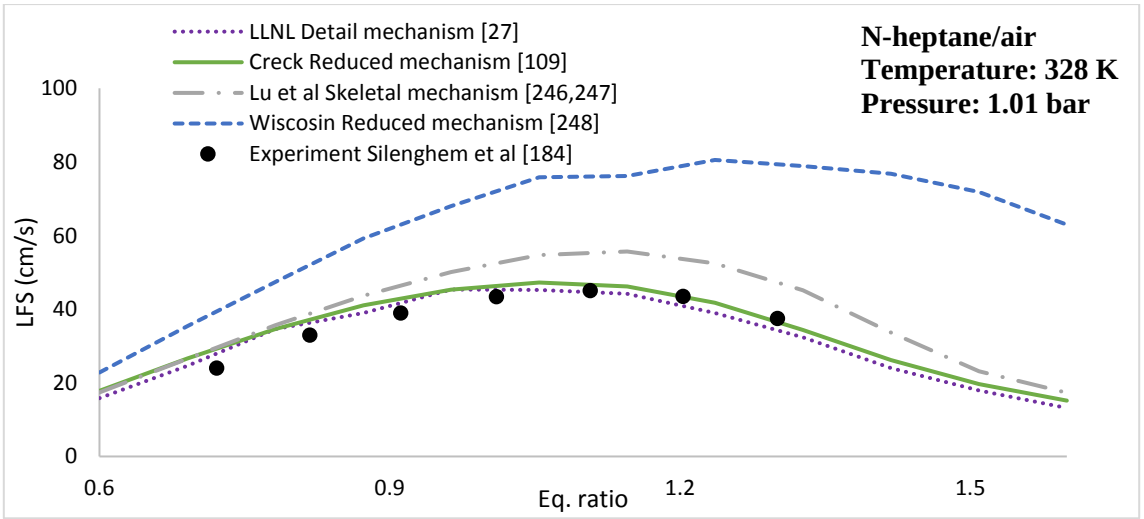

c)

Figure 6-3Comparison of the simulated LFS by using different n-heptane mechanisms and the experimental results obtained from [184].

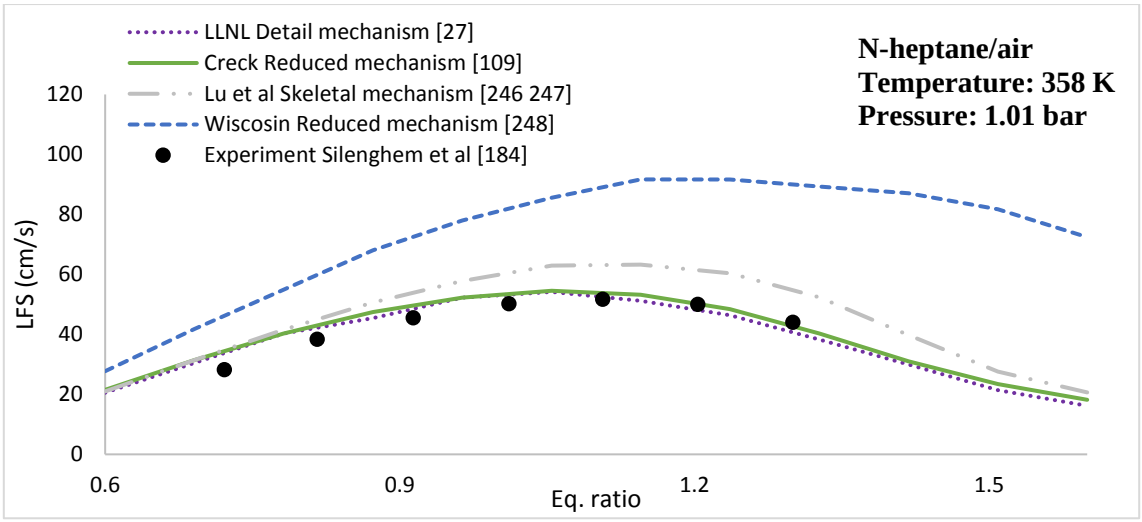

d)

Figure 6-3 (cont.) Comparison of the simulated LFS by using different n-heptane mechanisms and the experimental results obtained from [184].

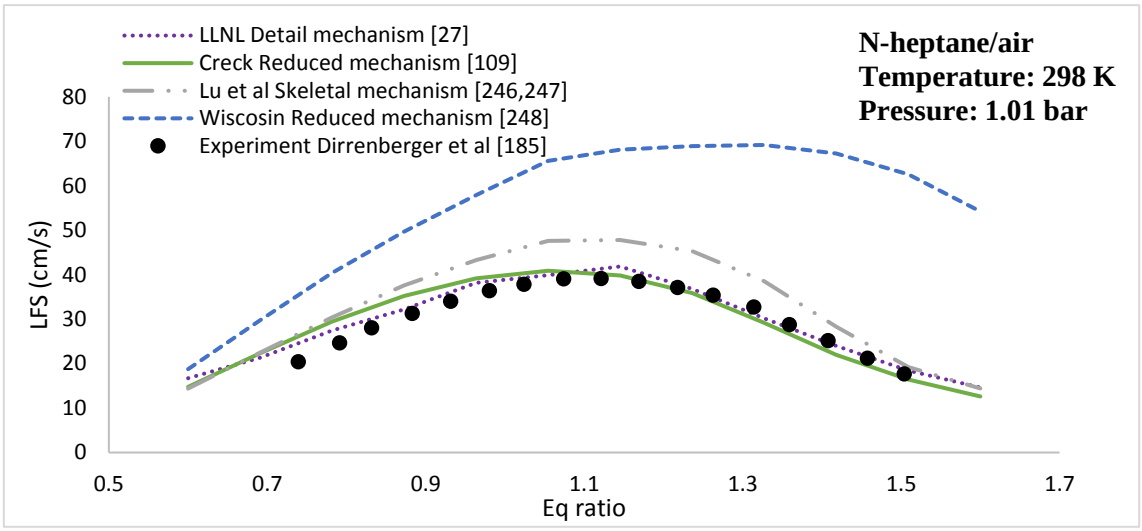

a)

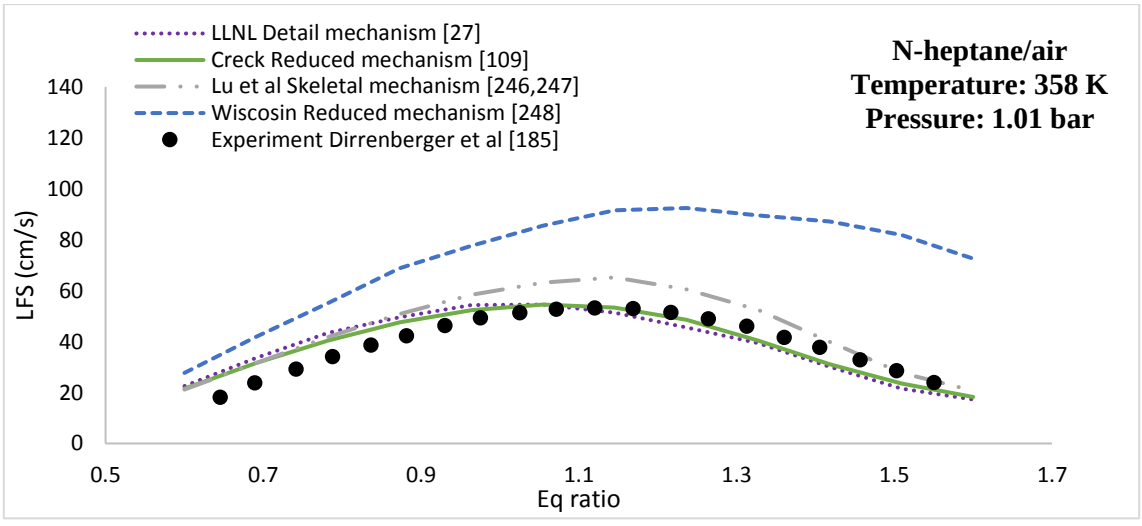

b)

Figure 6-4 Comparison of the simulated LFS by using different n-heptane mechanisms and the experimental results obtained from [185].

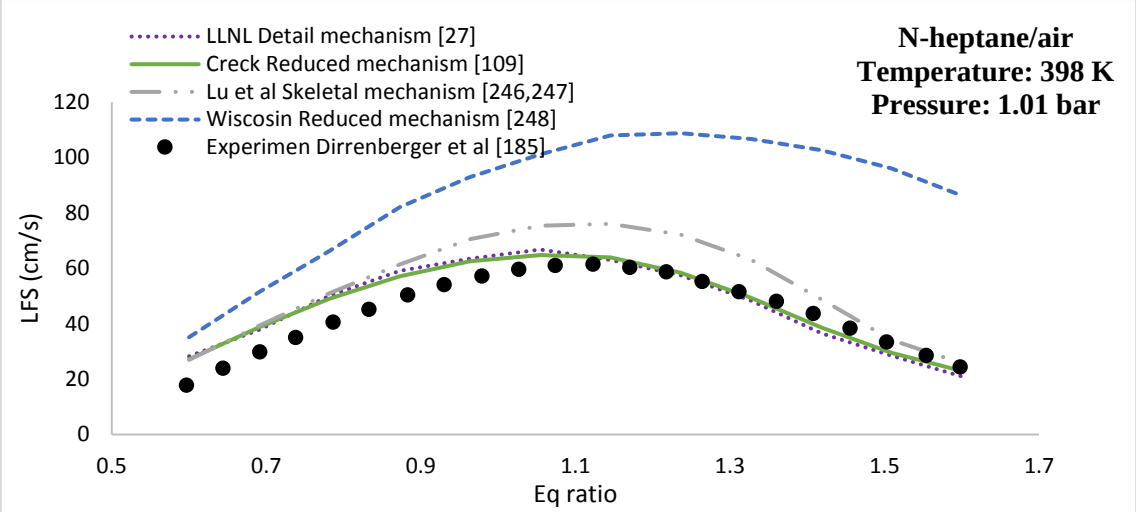

c)

Figure 6-4 (cont.) Comparison of the simulated LFS by using different n-heptane mechanisms and the experimental results obtained from [185].

By summarizing the results of the comparison between the experimental ignition delay times and LFSs with the simulated results, the Wisconsin reduced mechanism shows the highest deviation and therefore was not chosen for further investigations. Moreover, the skeletal mechanism proposed by Lu et al. was excluded due to the deviation with the experimental LFSs at high equivalence ratios.

The detail LLNL mechanism [27] and the reduced mechanism from the Creck modelling group [109] were the only mechanisms that performed very well at all of the tested conditions. However, due to the higher number of reactions and species included in the detail LLNL mechanism, the reduced Creck mechanism was used for the reduction and coupling with the syngas/NOx mechanism developed in Chapter 5.

6.2 Reduced N-heptane/syngas/NOx mechanism development

6.2.1 Reduction

The reduction of the n-heptane mechanism proposed by Creck modelling group [109] was performed by using the necessity analysis method. Necessity analysis is a hybrid reduction tool as it combines both flow analysis and sensitivity analysis reduction methods in order to find the reactions and species that are the most necessary for the consumption or the formation of specific targets [110]. A detailed description of the necessity analysis method was given in Chapter 3.

In order to ensure the accuracy of the reduction process, an iteration loop was used and a generation number was attached on each new skeletal mechanism generated. The loop stops and all the generated skeletal mechanisms collected when the deviation between the original mechanism and the last Generation exceeds 0.5%.

The reduction sampling point for the necessity analysis was set to a stoichiometric n-heptane/air mixture at initial conditions T=800K and P=40 bar. The search-initiating species were N-C_7H_{16}, CO, CO_2, H_2, CH_4 and N_2. The necessity analysis flow chart is presented in Figure 6-5.

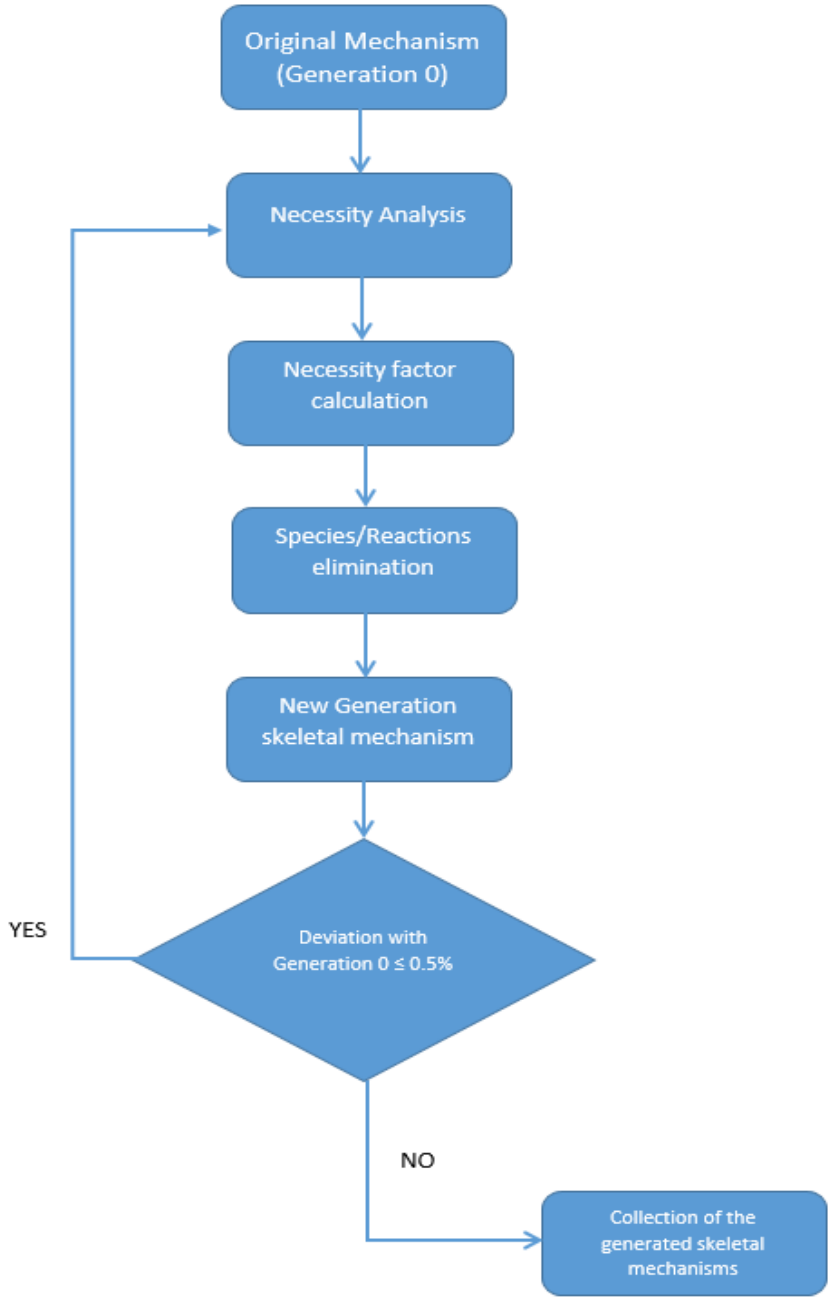

Figure 6-5 Flow chart of mechanism reduction method used in Chapter 6

Increasing the necessity factor reduces the size of the mechanism as the number of reactions is decreased. Therefore, each new Generation skeletal mechanism has lower number of reactions in comparison with the original mechanism and the previous Generation skeletal mechanisms.

This can be seen from the history of the reduction ratio presented in Figure 6-6. According to Figure 6-6, by increasing the Generation number, the reduction ratio and the necessity factor also increased. For example, the necessity factor for Generation 10 is 0.060 and the reduction ratio is 47.0% while for Generation 20 the necessity factor is 0.21 and the reduction ratio is 77.3%. However, the elimination of reactions and species in order to reduce the size of the mechanism, has as a result the reduction of the performance of the skeletal mechanisms and the deviation from the original mechanism (Generation 0), although this deviation also depends on the testing conditions and the fuels that were used for each simulation. During this section, 24 Generations were created and are presented in Appendix C Table C-1.

Moreover, in order to ensure the computational efficiency of the mechanism a second selection criterion was used. Therefore, it was decided as the number of the reactions included in the mechanism should be close to 300. The combination of the two selection criteria ensures the computational efficiency and the accuracy of the mechanism.

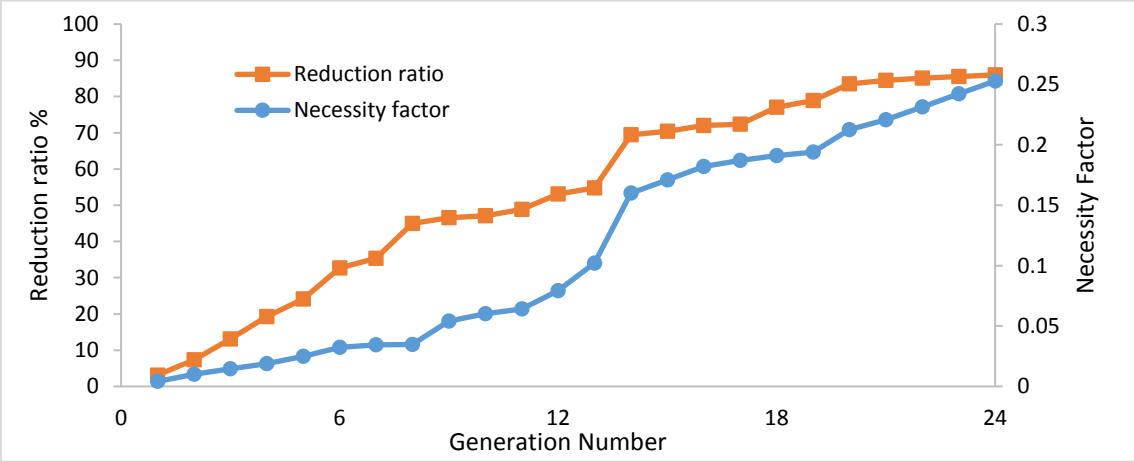

Figure 6-6 History of reduction ratio and necessity factor using necessity analysis method

The comparison between the calculated ignition delay time by using different Generations and the original mechanism is presented in Figure 6-7. The ignition delay time was calculated for stoichiometric n-heptane/air fuel mixture, Fuel 19 Table 3-3, at equivalence ratio 1, pressure 38 bar and a range of temperatures 700-1450 K. Those conditions were chosen because it was critical to evaluate the performance of the new Generation skeletal mechanisms on capturing the ignition delay time at low to high temperatures (simulating accurately the effect of low and high temperature oxidation as well as the NTC), high pressure (38 bar) and equivalence ratio 1.0. The simulations were performed by using the constant volume reactor, implemented in DARS software, and by assuming adiabatic conditions.

Additionally, the effects of the reduction process on the performance of the skeletal mechanisms to simulate syngas combustion were investigated by comparing the simulated ignition delay times for 0.29659%vol H_2/ 0.29659%vol CO/ 0.15748%vol CO_2/ 0.08924%vol CH_4/ 0.20997%vol H_2O/ 0.95013%vol O_2/ 98%vol AR syngas combustion with the original mechanism, Fuel 4 Table 3-3. The simulations were conducted at equivalence ratio 0.5, pressure 12 bar and temperature range 700-1450 K. The comparison is presented in Figure 6-8. It is important to mention here that for reasons of simplicity only Generations 10, 15, 22 and 24 were chosen for comparison.

As shown in Figure 6-7, the simulated ignition delay times by using the 10th and 15th Generation mechanisms are in a good agreement with the original mechanism (Generation 0). As the necessity factor increased and the mechanisms reduced further, the deviation between the skeletal mechanisms and the baseline case increased. This is because of the elimination of important reactions and species that affect the accurate prediction of the n-heptane oxidation. However, it is important to mention that the deviation does not change monotonically. The predicted ignition delay time by using the 22nd Generation mechanism is slightly lower than Generation 0 in the NTC region. On the other hand, by using the 24th Generation, the ignition delay time is slightly higher in the high to intermediate temperature region and over predicts the ignition delay times of the original mechanism (Generation 0) even more in the low temperature region. Additionally, the mechanisms of the 24th Generation and after do not accurately capture the effect of the NTC and the low temperature oxidation. On the other hand, the 22nd Generation mechanism shows a good agreement with Generation 0 at both low and high temperature regions and only slightly under predicts the ignition delay time in the NTC region. For the ignition delay times by using syngas fuel mixture, Figure 6-8, the trend is similar with Figure 7-7. The more extended is the reduction process, the larger is the deviation between the skeletal mechanisms and the original mechanism, Generation 0, especially by using the skeletal mechanisms of the 24th Generation and higher, where the deviation is very large during low to intermediate temperatures. This again indicates that important reactions and species that are affecting both n-heptane oxidation as well as syngas combustion are missing from Generation 24. Reactions such as $NC_7H_{15}+O_2=C_7H_{15}O_2$ who characterized by many authors [28, 100, 249] as a key reaction for n-heptane oxidation during intermediate to low temperatures and reaction $C_7H_{14}+HO_2=C_7H_{14}OOH$ who is responsible for the formation of C_7H_{14} from $C_7H_{14}OOH$ during low temperatures. According to Ra et al [28] the formation of C_7H_{14} from $C_7H_{14}OOH$ slows down the low temperature branching process because the

formation of high reactive $C_7H14OOH$ is intercepted by this reaction. The elimination of that reaction, make all of the heptyl hydroperoxides to react with O_2 for the formation of high amount heptylperocides and their isomers, which in turn enhances the degenerate branching reactions and affects significantly the ignition delay time at low temperatures [28, 100]. The 22nd Generation mechanism on the other hand, shows a good match with Generation 0 and is not affected by the reduction process. For the calculation of the deviation between the skeletal mechanisms and the original mechanism the error analysis method presented in Chapter 3, was used. First the absolute error value ($\overline{E_i}$)at each temperature is calculated and then the overall mean error ($\bar{\bar{\varepsilon}}$). The calculated overall mean error ($\bar{\bar{\varepsilon}}$) and the number of reactions of each skeletal mechanism are presented in Table 6-2.

Table 6-2 Overall mean error and number of reactions of each skeletal mechanism

Skeletal Mechanism	Overall mean error, $\bar{\bar{\varepsilon}}$ (%)		Number of Reactions
	N-heptane	Syngas	
Generation 0 (Original Mech.)	-	-	1791
Generation 10	0.092	0.034	934
Generation 15	0.146	0.091	522
Generation 22	0.290	0.154	264
Generation 24	2.31	0.585	248

The number of reactions incorporated in the 22nd Generation mechanism is 264 and the calculated overall mean error between the skeletal mechanism and the base mechanism is 0.29% for n-heptane and 0.154% for syngas. The number of reactions lies inside the pre-set criterion ($\leq$ 300 reactions), and, additionally, the calculated error is inside the pre-set error limit ($\leq$ 0.5%). Therefore, the 22nd Generation mechanism was chosen for the coupling with the syngas/NOx mechanism.

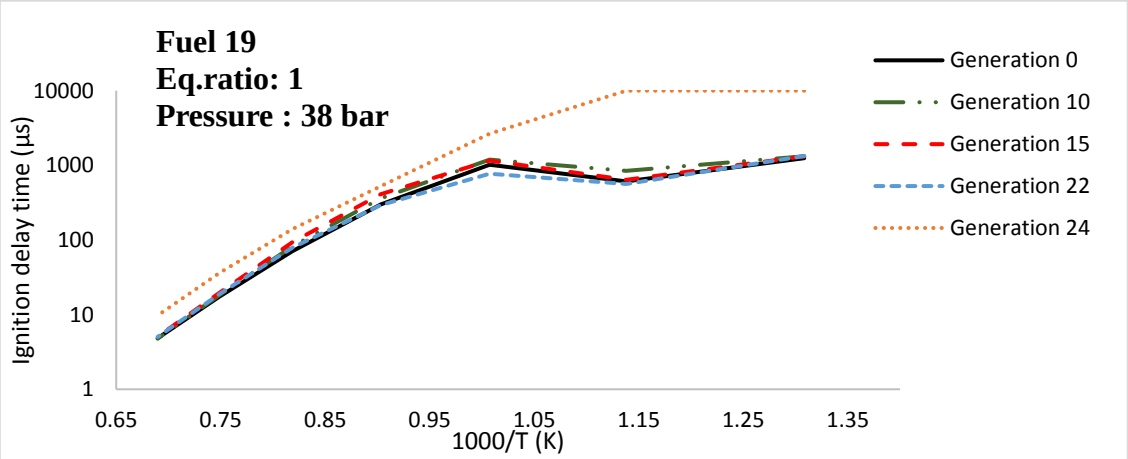

Figure 6-7 Comparison of the calculated ignition delay times for n-heptane/air mixture. Fuel 19 Table 3-3, using the original n-heptane mechanism from Creck modelling group [109], Generation 0, and the constructed skeletal mechanisms, Generations 10,15,22 and 24.

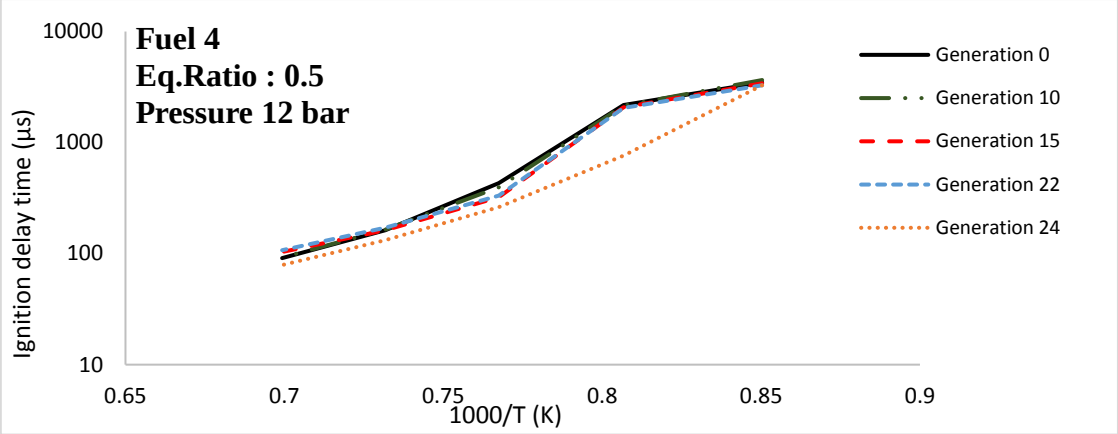

Figure 6-8 Comparison of the calculated ignition delay times for $H_2/CO/CO_2/CH_4/H_2O/O_2/AR$ mixture. Fuel 4 Table 3-3, using the original n-heptane mechanism from Creck modelling group [109], Generation 0, and the constructed skeletal mechanisms, Generations 10,15,22 and 24.

6.2.3 Coupling

For the syngas combustion and NOx formation, the reduced mechanism for syngas/NOx constructed in Chapter 5 was selected for the coupling with the 22nd Generation n-heptane skeletal mechanism. Because the n-heptane skeletal mechanism includes full CH_4, H_2 and CO chemistry, no additional reactions were incorporated during the coupling. However, the rate constants of the syngas reactions included in the reduced syngas/NOx mechanism as well as the NOx sub-mechanism were adopted in the new mechanism. For reasons of simplicity, the new mechanism is called University of Northumbria at Newcastle (UNN-1) mechanism.

By incorporating the reduced syngas/NOx mechanism in the new mechanism, the thermal and chemical stability of the mechanism changed. In order to investigate how the performance of the UNN-1 mechanism is affected, the calculated ignition delay times by using the UNN-1 mechanism for both pure n-heptane and syngas mixtures were compared with the ignition delay times by using the original Generation 0 mechanism and the 22nd Generation skeletal mechanism. For the comparison, two different fuel mixtures at specific initial conditions were used : a) for n-heptane oxidation, it was decided as the mechanisms to be validated at medium pressure (P=13.5 bar) , equivalence ratio 1.0 and a range of temperatures that will cover low and high temperature oxidation as well as the NTC (729-1160 K), and b) for syngas combustion it was decided to validate the mechanism at lean equivalence ratios (0.5), low pressure- close to atmospheric pressure (1.6 bar)- and a range of temperatures that cover low and high temperature oxidation of syngas (1000-2200 K).

First, for stoichiometric n-heptane-air fuel mixture, Fuel 19 Table 3-3, the ignition delay time was calculated at equivalence ratio 1.0, pressure 13.5 bar and a range of temperature 729 K – 1160 K,. The comparison among the three mechanisms is presented in Figure 6-9.

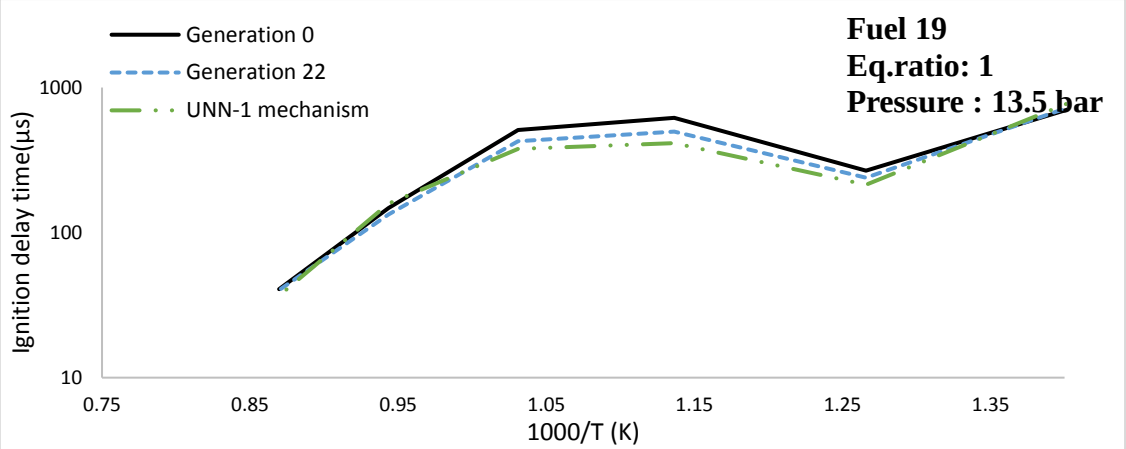

Figure 6-9 Comparison of ignition delay predictions for n-heptane/air mixture (Fuel 19) using a) the original Creck mechanism [109] (Generation 0) b) Generation 22 skeletal mechanism and c) UNN-1 mechanism.

According to Figure 6-9, the UNN-1 mechanism is in a good agreement with the baseline mechanism, Generation 0, during the low and high temperature oxidation of n-heptane. However, it shows a slightly under-prediction of the baseline case (Generation 0) and the skeletal mechanism (Generation 22) in the NTC region. This indicates that the syngas reactions and especially the hydrogen reactions that were modified by changing the rate constants, indeed affect the performance of the mechanism to accurately capture the n-heptane oxidation. On the other hand, for syngas combustion, the ignition delay time for 0.29659% H_2/ 0.29659% CO/ 0.15748% CO_2/ 0.08924% CH_4/ 0.20997% H_2O/ 0.95013% O_2/ 98% AR syngas mixture, Fuel 4 Table 3-3, was used for the comparison. The simulations were conducted at pressure 1.6 bar, equivalence ratio 0.5 and temperature range 1150-2040 K. The comparison is presented in Figure 6-10.

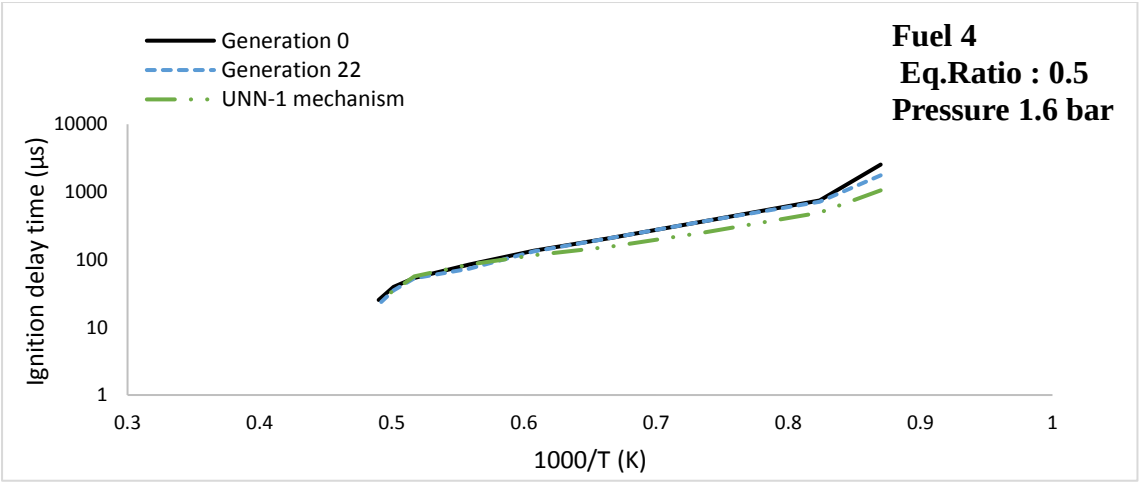

Figure 6-10 Comparison of ignition delay predictions for 0.29659% H_2/ 0.29659% CO/ 0.15748% CO_2/ 0.08924% CH_4/ 0.20997% H_2O/ 0.95013% O_2/ 98% AR mixture using a) the original Creck mechanism [109] (Generation 0) b) Generation 22 skeletal mechanism and c) UNN-1 mechanism.

According to Figure 6-10, the UNN-1 mechanism is in a good agreement with the rest of the mechanisms at intermediate to high temperatures but slightly under-predicts the ignition delay time at low temperatures.It is important to be mentioned here that different initial conditions such as pressure and equivalence ratio as well as different mixture compositions could have been used for the comparison of UNN1 mechanism. However, due to the fact that UNN1 is the intermediate mechanism before the final updated reduced n-heptane/syngas/NOx mechanism and its performance on simulating accurately low and high temperature oxidation as well as NTC event for during n-heptane combustion and syngas oxidation at low temperatures is obvious from the comparisons presented in Figure 6-9 and 6-10, it was decided as various mixtures covering a wide range of initial conditions, to be used for the validation of the final mechanism.

In order to identify the reactions responsible for the deviation and improve the performance of the developed mechanism, the rate constants of important syngas and n-heptane reactions were tested and adjusted. Following the findings of Chapters 4 and 5, important hydrogen based reactions such as OH+OH(+M) =H_2O_2(+M), H+O_2=OH+O, HO_2+OH=>H_2O+O_2 and H_2O_2+H=H_2+HO_2 and important methane based reactions such as CH_4+OH=CH_3+H_2O, CH_4+O_2=CH_3+HO_2 and CH_4+HO_2=CH_3+H_2O_2 were chosen and used for this analysis. Moreover, n-heptane reactions, such as $NC7H_{16}$ + OH = C_7H_{15} + H_2O, NC_7H_{16} + HO_2 = NC_7H_{15} + H_2O_2 and NC_7H_{15} + O_2 = $C_7H_{15}O_2$, that were highlighted by other researchers [28, 249, 250] as important for low temperature oxidation, were used. The effect of each reaction on the ignition delay time of syngas and n-heptane was investigated by using the two different fuel mixtures: a) the stoichiometric n-heptane/air fuel mixture, Fuel 19, at equivalence ratio 1, pressure 38 bar and a range of temperatures 769-1450 K, and b) 0.29659% H_2/ 0.29659% CO/ 0.15748% CO_2/ 0.08924% CH_4/ 0.20997% H_2O/ 0.95013% O_2/ 98% AR , Fuel 4, at pressure 1.6 bar, equivalence ratio 0.7 and temperature range 1070-2220 K.

For the investigation of the n-heptane and syngas ignition delay times sensitivity on specific reactions, a similar procedure with the one suggested by Ra and Reitz et al [100] was used. The authors showed that by varying the pre-exponential factor *A*, is sufficient to demonstrate ignition delay time sensitivities on the reactions rates. Moreover, they suggested that by multiplying the exponential factor *A*, by 0.1 and 10 the sensitivities of the ignition delay time on the specific reactions are successfully demonstrated and there is no need to change activation energy or temperature coefficient. Therefore, in this study the ignition delay time is calculated by using three cases of pre-exponential factor *A* of the reaction of interest; 1) original

value, 2) original value x10 and 3) original value x0.1. The original value is the pre-exponential factor A of the reaction of interest taken directly from the UNN-1 mechanism. The sensitivity of the calculated ignition delay times for n-heptane and syngas fuels on specific syngas and n-heptane reactions is presented in Figure 6-11 for hydrogen based reactions, Figure 6-12 for methane based reactions and Figure 6-13 for n-heptane based reactions.

Hydrogen based reactions

One of the most important reactions affecting not only syngas combustion but also n-heptane oxidation is OH+OH(+M) =H_2O_2(+M). This reaction is highly sensitive, especially during low temperatures and is responsible for the decomposition of H_2O_2 and the formation of two very reactive OH radicals [198]. It can be seen from Figure 6-11 that by changing the exponential factor and therefore the Arrhenius reaction rate, the ignition delay time of n-heptane is affected and reduced, especially at the NTC and low temperature region. The trend is also similar for the syngas ignition delay time. The ignition delay time for syngas shows high sensitivity to that specific reaction during medium to low temperatures.

Reaction H+O_2=OH+O is one of the main chain branching reactions affecting the oxidation of the fuel at temperatures above 1000 K and therefore was chosen for testing [21, 195]. As can be seen from Figure 6-11, the ignition delay time of n-heptane shows very little sensitivity on that specific reaction during low to mid temperatures (approx. 1000 K) and during high temperatures. In contrary, syngas ignition delay time, Figure 12 b, shows very high sensitivity on the chain branching reaction across the full temperature range. By reducing the exponential factor, the ignition delay time increased in comparison with the baseline. In contrary, by increasing the exponential factor, the ignition delay time is reduced, especially at low to intermediate temperatures.

For HO_2+OH=H_2O+O_2, a duplicate reaction was used in the mechanisms developed in Chapters 4 and 5 for low and high temperatures. Therefore, for this analysis the pre-exponentials factors of both reactions (low and high temperatures) were changed. Interestingly, it can be seen in Figure 6-11 that the sensitivity level of n-heptane ignition delay time is higher than syngas ignition delay time. Especially during low temperature and NTC regions, the ignition delay time of n-heptane increased significantly by increasing the exponential factor of the reaction. In contrary, syngas ignition delay time shows lower sensitivity during low temperature combustion and only during high temperature is it affected by the changes in the reaction's rate constant.

Finally, reaction $H_2O_2+H=H_2+HO_2$ is responsible for the consumption of HO_2 radicals and the formation of one H_2O_2 radical, especially during low temperature and high pressure conditions. . According to Figure 6-11, n-heptane ignition delay time is not affected by the modifications in the Arrhenius rate constants of that specific reaction. On the other hand, syngas ignition delay time shows a high sensitivity factor, especially during low to intermediate temperatures.

Methane based reactions

In order to investigate the sensitivity of the n-heptane and syngas ignition delay times on the CH_4 based reactions, the exponential factors of three main reactions, $CH_4+OH=CH_3+H_2O$, $CH_4 + O_2 = CH_3 + HO_2$ and $CH_4+HO_2=CH_3+H_2O_2$, were modified and tested. From Figure 6-12, it can be seen that the ignition delay time of n-heptane is very sensitive at all of the tested methane based reactions, during the NTC and low temperature regions. In contrary, syngas ignition delay time is more sensitive to the reactions during high temperatures combustion.

N-heptane based reactions

$NC_7H_{16}+OH=C_7H_{15}+H_2O$ is responsible for the abstraction of hydrogen and the formation of C_7H_{15} and HO_2. It is very important for the accurate simulation of the NTC and it affects n-heptane oxidation, especially at low to intermediate temperatures. It can be seen from Figure 6-13a, that modifications to the rate constant of the reaction cause significant changes to the predicted ignition delay times during low to intermediate temperatures and NTC regions. Conversely, according to Figure 6-13b, the ignition delay time shows negligible sensitivity on that reaction during syngas combustion.

On the other hand, reaction $NC_7H_{16}+HO_2=C_7H_{15}+H_2O_2$ is responsible for the consumption of HO_2 radicals and it mainly affects the ignition delay time during mid temperature oxidation of n-heptane. According to Figure 6-13a, ignition delay time of n-heptane is sensitive to that reaction during med temperatures and especially during the NTC temperature region. For the ignition delay times when using syngas fuel, Figure 6-13b, the trend is similar with reaction $NC_7H_{16}+OH=C_7H_{15}+H_2O$, in which the modifications on the rate constant of the reaction do not affect the ignition delay time.

Finally, the sensitivity of the ignition delay times on the reaction responsible for the oxygen addition to heptyl radicals, $NC_7H_{15}+O_2=C_7H_{15}O_2$ was studied. Other researchers show that this reaction mainly affects the ignition delay during the NTC temperature region and gives a relative depth on the NTC behavior [28]. According to Figure 6-13a, the n-heptane ignition delay time is relative sensitive to that reaction, not only during the NTC region but also during

low temperature oxidation. On the other hand, during intermediate to high temperatures, the ignition delay time of n-heptane shows relatively low sensitivity to that reaction. Moreover, by changing the rate constant of that reaction, the ignition delay time when using syngas fuel is not affected and the simulated ignition delay times are identical with the baseline case.

By summarizing the results obtained from the comparisons of Figures 6-11, 6-12 and 6-13, it is obvious that n-heptane oxidation and syngas combustion are mostly influenced by the radical branching reactions or radical termination reactions that are related to the formation or the dissociation of high reactive OH. This is because the formation of OH affects the reactivity of the fuel mixture while on the other hand they have a very important position in the hierarchical structure of the reaction mechanism. However, it is important to mention that the rate constants of H_2 and CH_4 based reactions were not adjusted because: a) they are affecting the oxidation pathways of all hydrocarbon fuels as they are placed on the lowest oxidation pathways in the hierarchy of the reaction mechanism and b) the rate constants of those reactions were validated and tested very well against different experimental measurements in order to minimize their uncertainty factor in Chapters 4 and 5. Therefore, it was decided as specific attention to be given to the n-heptane based reactions. The modified n-heptane based reactions including the adjusted rate constants are presented in Table 6-3. Moreover, the final UNN-2 mechanism can be found in Table 6-4. For reasons of simplicity, the final mechanism is called UNN-2 mechanism for the rest of this chapter.

Table 6-3 Modified n-heptane based reactions (A units cal-cm-sec-K, E units cal/mol)

Reaction	Old rate constant			New rate constant		
	A	*n*	*E*	*A*	*n*	*E*
$NC_7H_{16}+OH=C_7H_{15}+H_2O$	4.8E06	2.0	-2259.83	1.80E07	2.0	-2259.83
$NC_7H_{16}+HO_2=C_7H_{15}+H_2O_2$	1.76E05	2.5	14860.00	1.76E04	2.5	14860.00
$NC_7H_{15}+O_2=C_7H_{15}O_2$	2.0E11	0.0	0.0	2.0E12	0.0	0.0

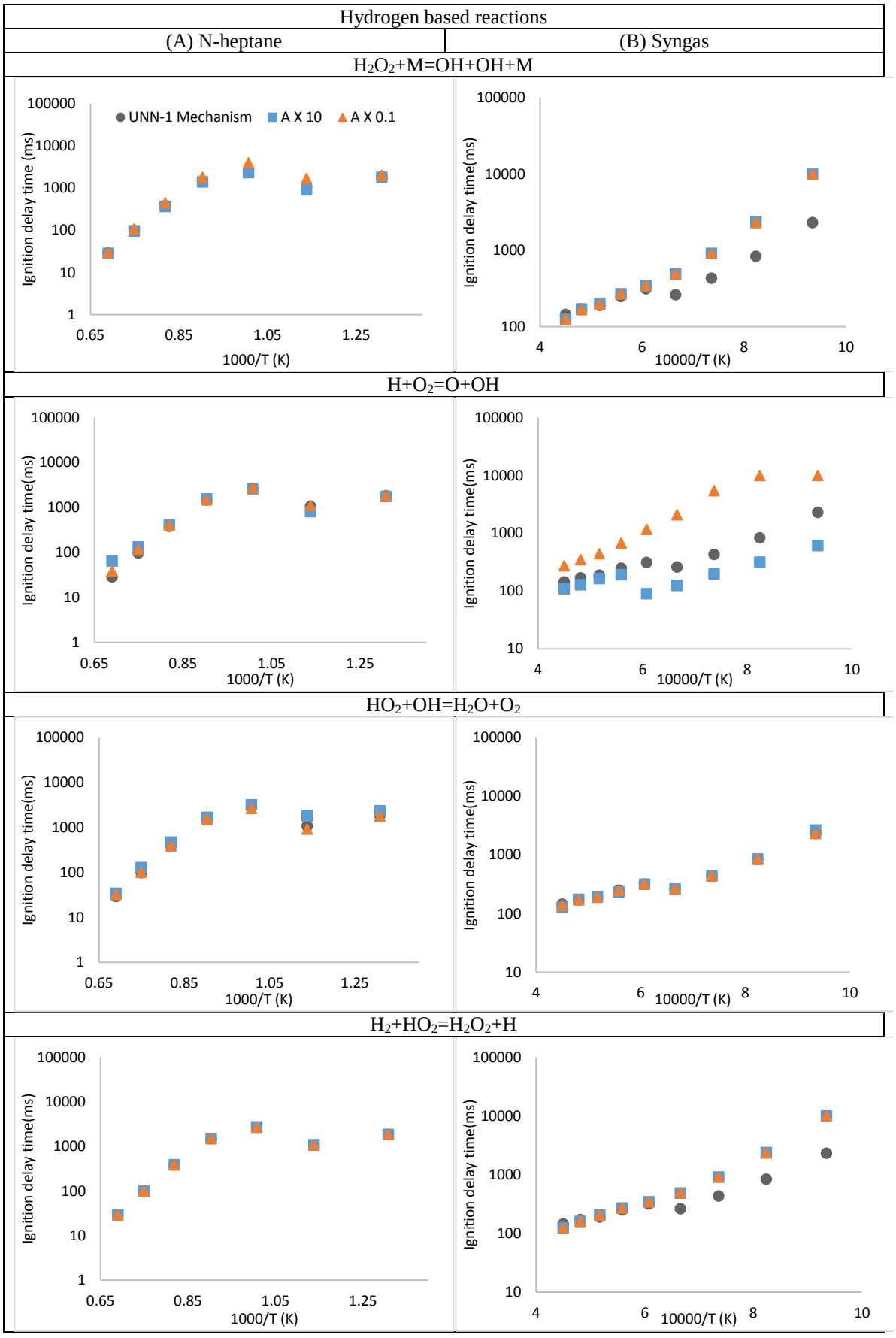

Figure 6-11 Ignition delay time sensitivity to major hydrogen based reactions a) ignition delay time of n-heptane/air mixture Fuel 19 b) ignition delay time of syngas mixture Fuel 4. Circles show UNN-1 mechanism, squares show A X 10 and triangles show A X 0.1.

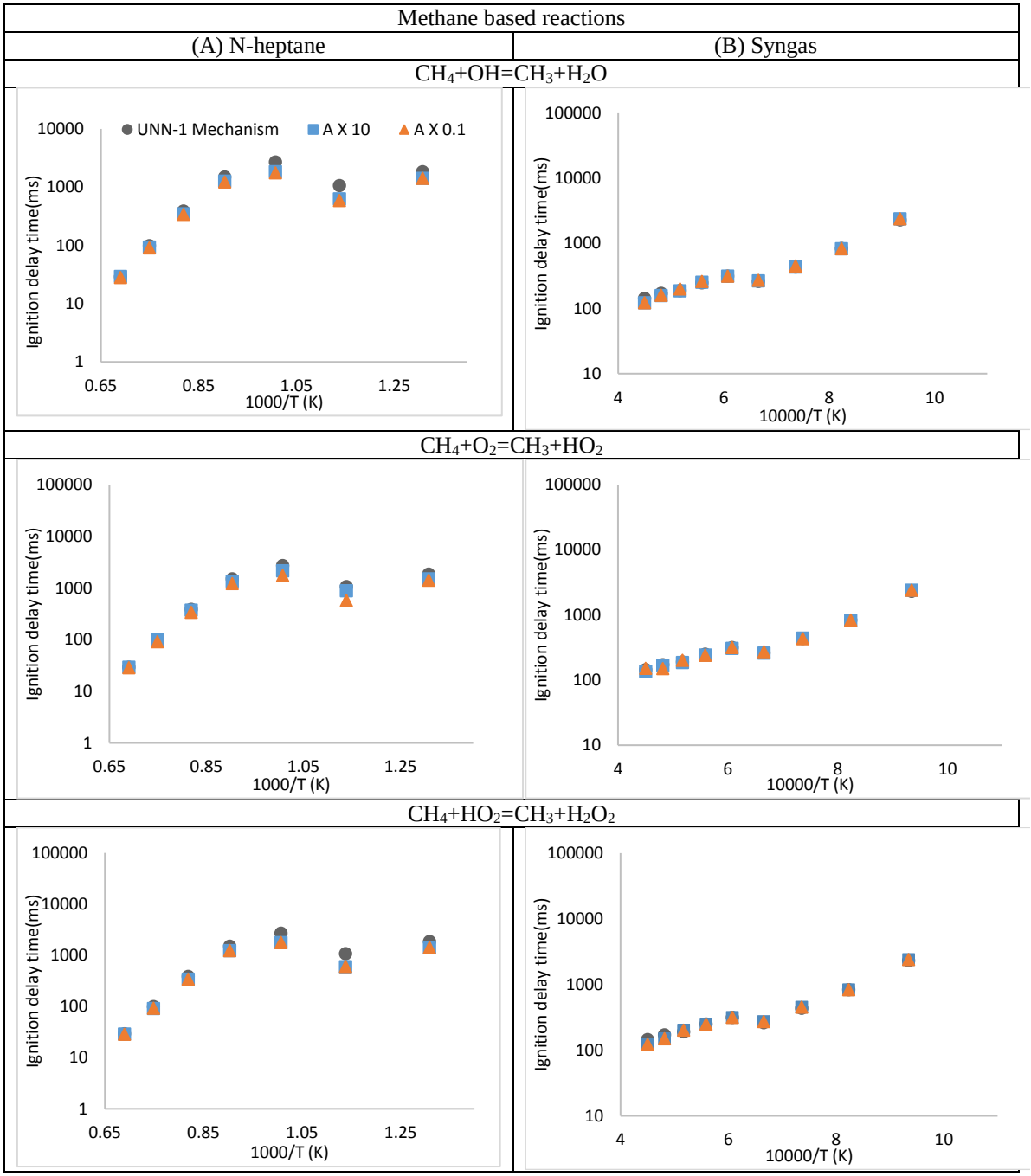

Figure 6-12 Ignition delay time sensitivity to major methane based reactions a) ignition delay time of n-heptane/air mixture Fuel 19 b) ignition delay time of syngas mixture Fuel 4. Circles show UNN-1 mechanism, squares show A X 10 and triangles show A X 0.1

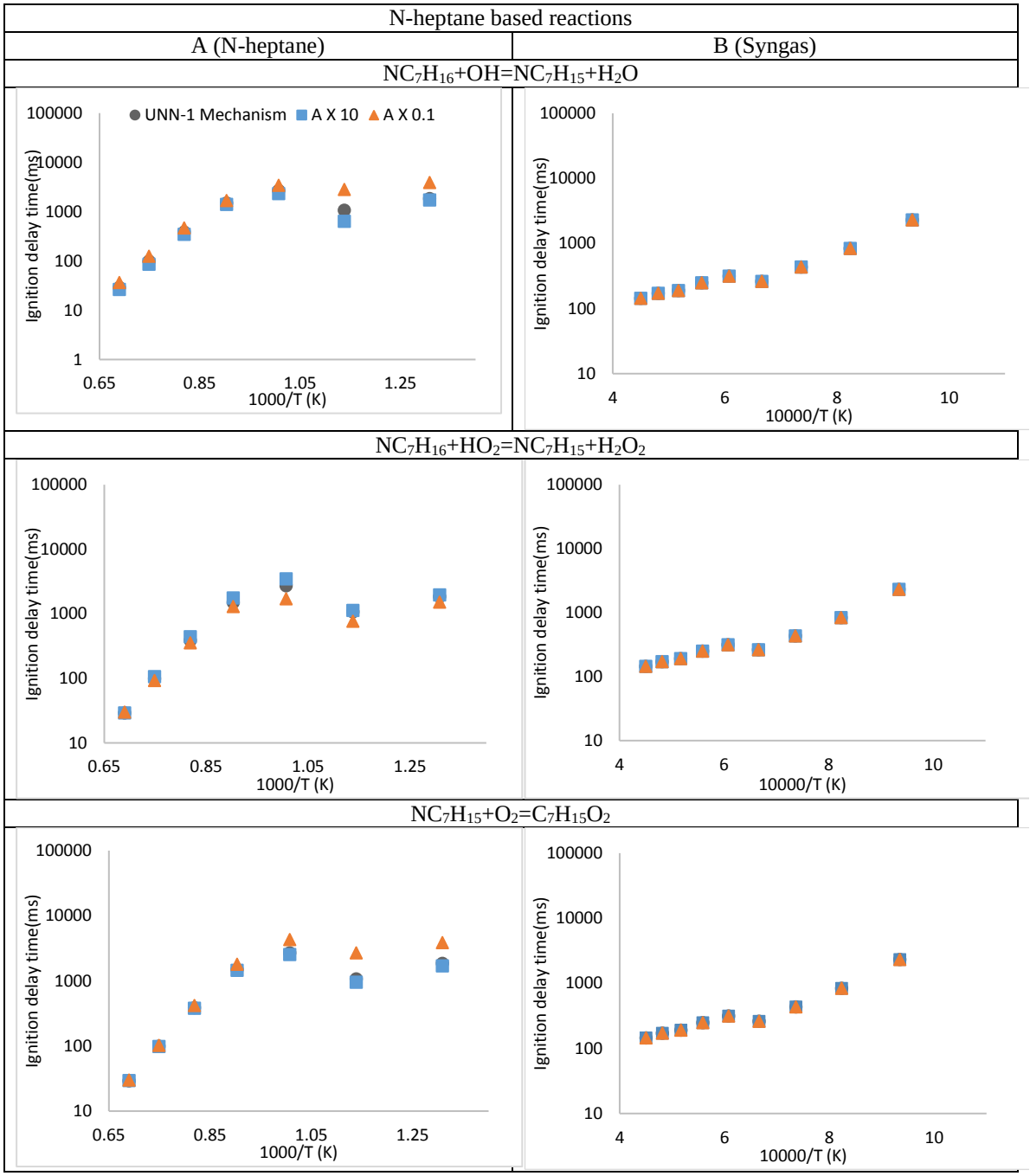

Figure 6-13 Ignition delay time sensitivity to major n-heptane based reactions a) ignition delay time of n-heptane/air mixture Fuel 19 b) ignition delay time of syngas mixture Fuel 4. Circles show UNN-1 mechanism, squares show A X 10 and triangles show A X 0.1.

Table 6-4 The reduced n-heptane/syngas/NOx mechanism (UNN-2) developed in Chapter 6 (A units cal-cm-sec-K, E units cal/mol)

	Reactions	***A***	***n***	***E***	***Ref.***
	n-Heptane Reaction EBU				
R1	$C_7H_{16}+11O_2=7CO_2+8H_2O$	0.	0.	0.	[148]
R2	$H_2+O=OH+H$	5.06E4	2.67	6287.6	[194]
R3	$H+O_2=OH+O$	3.520E16	-0.7	17061.4	[193]
R4	$H+O_2(+M)=HO_2(+M)$	4.6E12	0.4	0.0	[21]
	/LOW /1.737E19 -1.23 0.0/ /M/AR/0.0/ H_2/1.3/ H_2O/10.0/ CO/1.9/ CO_2/3.8/				
R5 (a)	$OH+HO_2=O_2+H_2O$	2.89E13	0.0	-496.9	[73]
R5 (b)	$OH+HO_2=O_2+H_2O$	2.456E13	0.0	-4.97E02	[21]
R6	$HO_2+H=OH+OH$	7.08E13	0.0	293.8	[109]
R7	$O+HO_2=O_2+OH$	3.2500E13	0.0	0.0	[109]
R8	$2OH=H_2O+O$	2.97E06	2.02	1.340E04	[21]
R9	$H+H+M=>H_2+M$	2.2300E14	0.0	96081.00	[109]
	/M/H_2/2.50/ H_2O/12.00/ AR/0.50/ CO/1.90/ CO_2/3.80/				
R10	$H+OH+M=H_2O+M$	4.00E22	-2.0	0.0	[109]
	/M/ H_2/2.5/ H_2O/12.0/ CO/1.9/ CO_2/3.8/ AR/0.38/				
R11	$HO_2+H=>H_2+O_2$	1.66E13	0.0	821.8	[21]
R12	$2HO_2=O_2+H_2O_2$	1.3E11	0.0	-1.63E03	[21]
R13	$2OH(+M)=H_2O_2(+M)$	2.95000E14	0.0	48340	[232]
	/LOW/ 1.20E17 0.0 45550.0/				
	/TROE/ 0.5 1E-30 1E30 /				
	/M/H_2/ 2.00/ H_2O/ 6.00/ CH_4/ 2.00/ CO/ 1.50/ CO_2/ 2.00/ C_2H_6/ 3.00/ AR/ 0.70/ N_2/ 0.90/				
R14	$O_2+CO=CO_2+O$	2.5300E12	0.0	47700	[109]
R15	$O_2+HCO=HO_2+CO$	0.1000E13	0.0	0.0	[109]
R16	$CO+O(+M)=CO_2(+M)$	0.964E11	0.0	3800.0	[191]

	/LOW /0.2070E27 -3.340 7610.0/				
	/M/H_2O/12.00/ H_2/2.00/ CO/1.50/ CO_2/2.00/ AR/0.50/				
R17 (a)	CO+OH=CO_2+H	9.6000E12	0.140	7352.00	[191]
R17 (b)	CO+OH=CO_2+H	7.3200E11	0.030	-16.00	[191]
R18	CO+HO_2=CO_2+OH	3.0000E13	0.0	23000.00	[191]
R19	CO+H_2O=CO_2+H_2	0.2000E12	0.0	38000.0	[191]
R20	C2H4(+M)=H2+C2H2(+M)	8.0000E12	0.44	88770.00	[109]
	/LOW/ 1.58E51 -9.300 97800.0/				
	/TROE/ 0.7345 180.0 1035. 5417./				
	/M/H_2/ 2.00/ H_2O/ 6.00/ CH_4/ 2.00/ CO/ 1.50/ CO_2/ 2.00/ AR/ 0.70/				
R21	H+C_2H_3(+M)=C_2H_4(+M)	6.0800E12	0.270	280.00	[109]
	/LOW/ 1.40E30 -3.860 3320.0/				
	/TROE/ 0.7820 207.5 2663. 6095./				
	/M/ H_2/ 2.00/ H_2O/ 6.00/ CH_4/ 2.00/ CO/ 1.50/ CO_2/ 2.00/ AR/ 0.70/				
R22	2C_2H_3=C_4H_6	1.0000E13	0.0	0.0	[109]
R23	C_2H_2+C_2H_4=C_4H_6	5.0000E10	0.0	28000.00	[109]
R24	H+C_2H_3=H_2+C_2H_2	3.0000E13	0.0	0.0	[109]
R25	H2+C_2H_4=H+C_2H_5	1.0000E14	0.0	65000.00	[109]
R26	2CH_3=>H_2+C_2H_4	5.0000E14	0.0	32000.00	[109]
R27	CH_3+C_2H_3=CH_4+C_2H_2	1.3330E13	0.0	0.0	[109]
R28	CH_4+C_2H_4=>CH_3+C_2H_5	3.0000E13	0.0	62000.00	[109]
R29	C_2H_2+C_2H_4=2C_2H_3	2.4000E13	0.0	68360.00	[109]
R30	2C_2H_4=C_2H_3+C_2H_5	4.8000E14	0.0	71500.00	[109]
R31	C_2H_3+SC_4H_7=>C_2H_4+C_4H_6	2.0000E12	0.0	0.0	[109]
R32	C_2H_2+H(+M)=C_2H_3(+M)	5.8800E12	0.0	2770.00	[109]
	/LOW/ 2.29E16 0.000 -560.0/				
	/TROE/ 0.5000 675.0 675.0 1.000E30/				
	/M/H_2O/ 5.00/ CO/ 2.00/ CO_2/ 3.00/ H_2/ 2.00/				

R33	$C_2H_4+H(+M)=C_2H_5(+M)$	1.7700E13	0.0	2110.0	[109]
	/LOW/ 4.60E18 0.000 1070.0/				
	/TROE/ 1.000 1.000e-15 95.00 200.0/				
	/M/ H_2O/ 5.00/ CO_2/ 3.00/ H_2/ 2.00/ CO/ 2.00/				
R34	$NC_3H_7=C_2H_4+CH_3$	1.0000e13	0.0	32000.00	[109]
R35	$SC_4H_7=C_4H_6+H$	2.0000E14	0.0	51000.00	[109]
R36	$2CH_3=H+C_2H_5$	1.4000E14	0.0	14000.00	[109]
R37	$C_4H_6+C_2H_5=>C_2H_4+SC_4H_7$	1.0000E10	0.0	5000.00	[109]
R38	$CH_2O+M=H_2+CO+M$	8.3000E15	0.0	70000.00	[109]
	/M/H_2O/ 16.00/ CO_2/ 3.80/ H_2/ 2.50/ CO/ 1.90/				
R39	$CH_2O+M=H+HCO+M$	2.0000E16	0.0	75600.00	[109]
	/M/H_2O/ 16.00/ CO_2/ 3.80/ H_2/ 2.50/ CO/ 1.90/				
R40	$CH_3CHO=HCO+CH_3$	1.5000E16	0.0	85000.00	[109]
R41	$CH_3CHO=H_2+CH_2CO$	4.0000E13	0.0	80500.00	[109]
R42	$CH_3CHO=CO+CH_4$	1.0000E14	0.0	79000.00	[109]
R43	$H+CH_3CO=CH_3CHO$	1.3000E13	0.0	0.0	[109]
R44	$O_2+C_2H_2=OH+HCCO$	2.0000E07	1.500	30000.00	[109]
R45	$CH_4+O_2=CH_3+HO_2$	3.98E13	0.0	56855.5	[90]
R46	$O_2+CH_2O=HO_2+HCO$	1.3000E14	0.0	41000.00	[109]
R47	$O_2+C_2H_4=HO_2+C_2H_3$	1.0000E14	0.0	60000.00	[109]
R48	$O_2+CH_3CHO=HO_2+CH_3CO$	3.0000E13	0.0	39200.00	[109]
R49	HCO+M=CO+H+M	0.1200E18	-1.00	17000.0	[109]
	/M/H_2O/5.00/ CO_2/3.00/ H_2/1.90/ CO/1.90/				
R50	$CH_3O(+M)=CH_2O+H(+M)$	6.0000E11	0.0	18000.00	[109]
	/LOW/ 1.20E25 -2.700 30600.0/				
R51	$CH_3CO=CH_2CO+H$	1.0000E14	0.0	49000.00	[109]
R52	$CH_3CO+M=CO+CH_3+M$	2.5000E15	0.0	14400.00	[109]
R53	$CH_2CO+H=>CO+CH_3$	1.0000E06	2.000	2000.00	[109]
R54	$CH_2CO+H=H_2+HCCO$	3.6000E14	0.0	8600.00	[109]

R55	$CH_2CO+CH_3=CH_4+HCCO$	3.7500E12	0.0	13000.00	[109]
R56	$C_2H_2+O=>CH_2CO$	1.0000E13	0.0	15000.00	[109]
R57	$C_2H_4+O=>CH_3CHO$	1.0000E09	0.0	5000.00	[109]
R58	$C_2H_4+O=HCO+CH_3$	5.0000E06	1.880	200.00	[109]
R59	$CH_2O+O=>CO_2+{}_2H$	2.0000E13	0.0	5000.00	[109]
R60	$CH_3CHO+O=>CO_2+H+CH_3$	2.0000E13	0.0	3000.00	[109]
R61	$CH_2CO+O=>2HCO$	2.0000E13	0.0	2300.00	[109]
R62	$CH_2CO+O=>CO+CH_2O$	1.0000E12	0.0	5000.00	[109]
R63	$C_2H_2+OH=>CO+CH_3$	1.5000E11	0.0	0.0	[109]
R64	$CH_2O+OH=>H_2+CO_2+H$	1.0000E11	0.0	0.0	[109]
R65	$CH_2CO+OH=>CH_2O+HCO$	1.5000E13	0.0	0.0	[109]
R66	$CH_2CO+OH=>CO_2+CH_3$	3.0000E12	0.0	0.0	[109]
R67	$CH_3CHO+OH=>H_2+CO_2+CH_3$	2.0000E11	0.0	0.0	[109]
R68	$C_2H_2+HO_2=>CH_2O+HCO$	5.0000E12	0.0	15000.00	[109]
R69	$C_2H_2+HCO=>CO+C_2H_3$	5.0000E11	0.0	6000.00	[109]
R70	$C_4H_6+HCO=>CO+SC_4H_7$	5.0000E11	0.0	6000.00	[109]
R71	$CH_2O+HCO=CO_2+CH_3$	5.0000E11	0.0	6000.00	[109]
R72	$CH_3CHO+HCO=>CO_2+C_2H_5$	3.0000E11	0.0	6000.00	[109]
R73	$CO+CH_3O=CO_2+CH_3$	5.0000E11	0.0	6500.00	[109]
R74	$O_2+C_2H_2=>CO+CH_2O$	3.0000E11	0.0	26000.00	[109]
R75	$O_2+C_2H_4=>{}_2CH_2O$	1.0000E14	0.0	48000.00	[109]
R76	$O_2+CH_2CO=>CO_2+CH_2O$	1.0000E14	0.0	37000.00	[109]
R77	$O_2+CH_2CO=>CO+OH+HCO$	3.0000E14	0.0	40000.00	[109]
R78	$O_2+C_2H_2=>2HCO$	3.0000E11	0.0	27000.00	[109]
R79	$O_2+C_2H_4=>HCO+CH_3O$	1.0000E14	0.0	43000.00	[109]
R80	$O_2+C_4H_6=>O_2+C_2H_2+C_2H_4$	4.0000E14	0.0	40000.00	[109]
R81	$O_2+CH_3O=>CH_2O+HO_2$	6.0000E11	0.0	6500.00	[109]
R82	$O_2+C_2H_5=>C_2H_4+HO_2$	1.0000E12	0.0	3000.00	[109]
R83	$O_2+SC_4H_7=>C_4H_6+HO_2$	3.0000E10	0.0	8000.00	[109]

R84	$O_2+CH_3=O+CH_3O$	4.0000E12	0.0	27000.00	[109]
R85	$O_2+C_2H_3=>CH_2O+HCO$	1.0000E12	0.0	4000.00	[109]
R86	$O_2+C_2H_3=>CH_2CO+OH$	6.0000E11	0.0	1000.00	[109]
R87	$_{O2}+C_2H_3=C_2H_2+HO_2$	6.0000E09	0.0	0.0	[109]
R88	$O_2+C_2H_5=>CH_2O+O+CH_3$	1.0000E13	0.0	27000.00	[109]
R89	$O_2+C_2H_5=>CH_2O+CH_3O$	1.0000E14	0.0	24000.00	[109]
R90	$O+CH_3+M=>CH_3O+M$	5.0000E16	0.0	0.0	[109]
R91	$O+NC_3H_7=>CH_2O+C_2H_5$	2.0000E13	0.0	0.0	[109]
R92	$OH+CH_3=H+CH_3O$	5.1000E11	0.0	13500.00	[109]
R93	$OH+CH_3=H_2+CH_2O$	6.0000E12	0.0	0.0	[109]
R94	$OH+CH_3=CH_4+O$	2.0000E12	0.0	8000.00	[109]
R95	$OH+C_2H_3=>CH_3CHO$	5.0000E12	0.0	0.0	[109]
R96	$OH+C_2H_3=H_2O+C_2H_2$	4.0000E12	0.0	0.0	[109]
R97	$OH+SC_4H_7=>C_2H_4+CH_3CHO$	2.0000E12	0.0	0.0	[109]
R98	$OH+CH_3CO=>H_2O+CH_2CO$	3.0000E12	0.0	0.0	[109]
R99	$HO_2+CH_3=OH+CH_3O$	6.0000E12	0.0	0.0	[109]
R100	$HO_2+C_2H_5=>CH_2O+OH+CH_3$	5.0000E12	0.0	0.0	[109]
R101	$O+HCO=CO_2+H$	3.0000E13	0.0	0.0	[191]
R102	$HCO+H=H_2+CO$	0.1000E15	0.0	0.0	[191]
R103	$OH+HCO=H_2O+CO$	5.0000E13	0.0	0.0	[191]
R104	$HO_2+HCO=H_2O_2+CO$	4.0000E11	0.0	0.0	[191]
R105	$HO_2+HCO=>CO_2+H+OH$	3.0000E13	0.0	0.0	[191]
R106	$_2HCO=CO+CH_2O$	6.0000E11	0.0	0.0	[109]
R107	$HCO+CH_3=CO+CH_4$	1.0000E13	0.0	0.0	[109]
R108	$H+CH_3O=>H_2+CH_2O$	2.0000E13	0.0	0.0	[109]
R109	$OH+CH_3O=>H_2O+CH_2O$	1.5000E13	0.0	0.0	[109]
R110	$HO_2+CH_3O=>H_2O_2+CH_2O$	1.5000E12	0.0	0.0	[109]
R111	$HCO+CH_3O=2CH_2O$	1.0000E13	0.0	0.0	[109]
R112	$CH_3+CH_3O=>CH_2O+CH_4$	1.0000E13	0.0	0.0	[109]

R113	$CH_2CO+HO_2=>CO+CH_2O+OH$	1.0000E10	0.0	5000.00	[109]
R114	$CH_4+CH_2=2CH_3$	4.3000E12	0.0	10034.00	[109]
R115	$CH_4+CH_2S=2CH_3$	4.3000E13	0.0	0.0	[109]
R116	$CH_3+M=H+CH_2+M$	1.0000E16	0.0	90600.00	[109]
R117	$H_2+CH_2S=H+CH_3$	7.2000E13	0.0	0.0	[109]
R118	$OH+CH_3=H_2O+CH_2S$	2.0000E13	0.0	0.0	[109]
R119	$CH_2+CH_3=C_2H_4+H$	4.2000E13	0.0	0.0	[109]
R120	$CH_2S+CH_3=C_2H_4+H$	2.0000E13	0.0	0.0	[109]
R121	$CH_2O+CH_3=CH_3CHO+H$	2.0000E11	0.0	7600.00	[109]
R122	$HCO+CH_2=CO+CH_3$	2.0000E13	0.0	0.0	[109]
R123	$O+CH_2=CO+2H$	7.0000E13	0.0	0.0	[109]
R124	$O+CH_2=H_2+CO$	5.0000E13	0.0	0.0	[109]
R125	$2CH_2=C_2H_2+2H$	1.2000E14	0.0	0.0	[109]
R126	$CH_2S+M=CH_2+M$	1.0000E13	0.0	0.0	[109]
	/M/H/ 20.00/ H_2O/ 3.00/ C_2H_2/ 4.00/				
R127	$O+CH_2S=CO+2H$	3.0000E13	0.0	0.0	[109]
R128	$OH+CH_2S=CH_2O+H$	3.0000E13	0.0	0.0	[109]
R129	$O_2+CH_2S=CO+H+OH$	3.1000E13	0.0	0.0	[109]
R130	$C_2H_2+O=CO+CH_2$	3.5000E03	2.8	500.00	[109]
R131	$C_2H_2+O=H+HCCO$	5.0000E06	2.0	1900.00	[109]
R132	$CH_2CO(+M)=CO+CH_2(+M)$	1.5000E14	0.0	76000.00	[109]
	/LOW/ 5.50E15 0.0 59270.0/				
R133	$2CH_2CO=HCCO+CH_3CO$	1.5000E13	0.0	60500.0	[109]
R134	$2CH_2CO=>2CO+C_2H_4$	7.5000E10	0.0	40000.0	[109]
R135	$CH_2CO=>H+HCCO$	1.5000E14	0.0	102400.0	[109]
R136	$CH_2CO+O=CO_2+CH_2$	1.5000E12	0.0	1350.00	[109]
R137	$CH2CO+CH2=CO+C_2H_4$	7.0000E11	0.0	2000.00	[109]
R138	$CH_2CO+CH_2=CH_3+HCCO$	3.6000E13	0.0	11000.00	[109]
R139	$CH_2CO+CH_3=CO+C_2H_5$	1.5000E11	0.0	7600.00	[109]

R140	H+HCCO=CO+CH_2S	1.5000E14	0.0	0.0	[109]
R141	O+HCCO=2CO+H	9.6000E13	0.0	600.00	[109]
R142	OH+HCCO=CO+H+HCO	1.0000E13	0.0	0.0	[109]
R143	CH_2+HCCO=CO+C_2H_3	3.0000E13	0.0	0.0	[109]
R144	2HCCO=2CO+C_2H_2	1.0000E13	0.0	0.0	[109]
R145	C_2H_4+OH=H_2O+C_2H_3	2.0000E13	0.0	6000.00	[109]
R146	CH_2O+H=H_2+HCO	4.5000E14	0.0	7500.00	[109]
R147	CH_3CHO+H=H_2+CH_3CO	4.5000E14	0.0	7500.00	[109]
R148	H_2+OH=H_2O+H	1.17E9	1.3	0.0	[194]
R149	H_2O_2+H=H_2+HO_2	1.70E12	0.0	3755.00	[73]
R150	CH_2O+HO_2=>H_2O_2+HCO	5.2000E12	0.0	13000.00	[109]
R151	O_2+CH_3=CH_3OO	2.0000E12	0.0	0.0	[109]
R152	O_2+C_2H_5=C_2H_5OO	1.0000E12	0.0	0.0	[109]
R153	CH_3OO=CH_2O+OH	1.5000E13	0.0	47000.0	[109]
R154	OH+CH_3OO=>HO_2+CH_3O	3.0000E12	0.0	0.0	[109]
R155	CH_3+CH_3OO=>2CH_3O	3.0000E13	0.0	1200.00	[109]
R156	HO_2+CH_3OO=>O_2+H_2O+CH_2O	5.0000E10	0.0	0.0	[109]
R157	2CH_3OO=>O_2+2CH_3O	2.0000E11	0.0	0.0	[109]
R158	CH_3+C2H_5OO=>CH_2O+CH_3+CH_3O	2.0000E12	0.0	-1200.00	[109]
R159	CH_3OO+C_2H_5OO=>O_2+CH_2O+CH_3+CH_3O	2.0000E11	0.0	0.0	[109]
R160	2C_2H_5OO=>O_2+2CH_2O+2CH_3	2.0000E11	0.0	0.0	[109]
R161	CH_2O+CH_3OO=>H_2+CO+CH_2O+OH	2.0000E11	0.0	11000.00	[109]
R162	CO+CH_3OO=>CO_2+CH_3O	1.0000E14	0.0	24000.00	[109]
R163	CO+C_2H_5OO=>CO_2+CH_2O+CH_3	1.0000E14	0.0	24000.00	[109]
R164	CH_3COCH_2=CH_2CO+CH_3	1.0000E14	0.0	31000.00	[109]
R165	O_2+CH_3COCH_2=>CH_2O+CH_2CO+OH	8.0000E11	0.0	0.0	[109]
R166	HO_2+CH_3COCH_2=>CH_2O+OH+CH_3CO	1.0000E11	0.0	0.0	[109]
R167	O_2+C_4H_6=>CO+HCO+C_2H_5	5.0000E13	0.0	41000.00	[109]
R168	NC_7H_{14}+H=NC_7H_{15}	2.5000E13	0.0	2500.00	[109]

R169	$O_2+NC_7H_{15}=>NC_7H_{14}+HO_2$	5.0000E11	0.0	3500.00	[109]
R170	$NC_7H_{14}+HO_2=>NC_7$-QOOH	8.0000E11	0.0	15000.00	[109]
R171	$O_2+NC_7H_{15}=>NC_7H_{15}$-OO	2.0000E12	0.0	0.0	[109]
R172	NC_7H_{15}-OO=>$O_2+NC_7H_{15}$	5.0000E12	0.0	30900.00	[109]
R173	NC_7H_{15}-OO=>NC_7-QOOH	3.0000E11	0.0	25100.00	[109]
R174	NC_7-QOOH=>NC_7H_{15}-OO	2.0000E10	0.0	16100.00	[109]
R175	NC_7-QOOH=>$NC7H_{14}+H_{O2}$	2.0000E12	0.0	24000	[109]
R176	O_2+NC_7-QOOH=>NC_7-OOQOOH	2.0000E12	0.0	0.0	[109]
R177	NC_7-OOQOOH=>O_2+NC_7-QOOH	2.0000E14	0.0	28400.0	[109]
R178	NC_7-OOQOOH=>NC_7-OQOOH+OH	1.0000E12	0.0	25000.00	[109]
R179	NC_7-OQOOH=>$CH_2O+NC_4H_8$+OH+CH_3CO	8.5000E13	0.0	39400.00	[109]
R180	NC_7-OQOOH=>$C_2H_4+C_2H_5CHO$+OH+CH_3CO	8.5000E13	0.0	39400.00	[109]
R181	NC_7-OQOOH=>$H_2+C_3H6O2+C_3H_5CHO$	1.0000E14	0.0	39400.00	[109]
R182	NC_7-OQOOH=O+$C2H_5+CH_3COCH_2$	1.90E13	0.0	39400.00	[109]
R183	HO_2+NC_7-OOQOOH=>$O_2+H_2O+NC_7$-OQOOH	1.0000E11	0.0	1200.00	[109]
R184	O_2+CH_2CO=>HO_2+HCCO	5.1110E06	2.0	38570.96	[109]
R185	CH_2CO+OH=>H_2O+HCCO	1.1980E06	2.0	3529.84	[109]
R186	CH_2CO+CH_3CO=>CH_3CHO+HCCO	4.0600E05	2.0	12609.32	[109]
R187	CH_2CO+HCO=>CH_2O+HCCO	3.7890E05	2.0	10951.12	[109]
R188	$CH_2CO+C_2H_3$=>C_2H_4+HCCO	2.0350E05	2.0	3378.60	[109]
R189	CH_2CO+O=>OH+HCCO	4.0600E06	2.0	1356.53	[109]
R190	CH_2CO+HO_2=>H_2O_2+HCCO	1.6160E05	2.0	10613.33	[109]
R191	$CH_2CO+NC_7H_{13}$=>NC_7H_{14}+HCCO	8.1010E04	2.0	9510.67	[109]
R192	$H_2+C_2H_3$=>C_2H_4+H	9.4960E05	2.0	8459.77	[109]
R193	$H_2+NC_7H_{13}$=>NC_7H_{14}+H	3.7800E05	2.0	15736.4	[109]
R194	CH_4+CH_3CO=>$CH_3CHO+CH_3$	9.4730E05	2.0	22216.4	[109]
R195	CH_4+HCO=>CH_2O+CH_3	8.8410E05	2.0	20281.3	[109]

R196	$CH_4+C_2H_3=>C_2H_4+CH_3$	4.7480E05	2.0	11093.6	[109]
R197	$CH_4+HO_2=CH_3+H_2O_2$	9.04E12	0.0	24629.4	[90]
R198	$CH_4+NC_7H_{13}=>NC_7H_{14}+CH_3$	1.8900E05	2.0	18573.86	[109]
R199	$C_2H_4+H=>H_2+C_2H_3$	1.9250E07	2.0	10409.77	[109]
R200	$C_2H_4+CH_3=>CH_4+C_2H_3$	3.1220E05	2.0	11393.6	[109]
R201	$C_2H_4+CH_3CO=>CH_3CHO+C_2H_3$	1.0830E06	2.0	22565.6	[109]
R202	$C_2H_4+HCO=>CH_2O+C_2H_3$	1.0100E06	2.0	20620.5	[109]
R203	$C_2H_4+HCCO=>CH_2CO+C_2H_3$	3.4240E05	2.0	12378.6	[109]
R204	$C_2H_4+O=>OH+C_2H_3$	1.0830E07	2.0	8781.96	[109]
R205	$C_2H_4+HO_2=>H_2O_2+C_2H_3$	4.3100E05	2.0	20242.5	[109]
R206	$C_2H_4+NC_7H_{13}=>NC_7H_{14}+C_2H_3$	2.1600E05	2.0	18904.0	[109]
R207	$CH_4+OH=CH_3+H_2O$	1.60E07	1.83	2771.1	[192]
R208	$H_2O+CH_3CO=>CH_3CHO+OH$	1.3530E06	2.0	30365.0	[109]
R209	$CH_2O+OH=HCO+H_2O$	3.90E10	0.89	406.1	[90]
R210	$H_2O+HCCO=>CH_2CO+OH$	4.2800E05	2.000	18970.16	[109]
R211	$OH+H_2O_2=HO_2+H_2O$	2.000E12	0.0	427.00	[109]
R212	$OH+H_2O_2=HO_2+H_2O$	1.700E18	0.0	29410.00	[109]
R213	$H_2O+NC_7H_{13}=>NC_7H_{14}+OH$	2.7000E05	2.0	25826.46	[109]
R214	$H_2O_2+CH_3CO=>CH_3CHO+HO_2$	1.0830E05	2.0	7876.73	[109]
R215	$H_2O_2+HCO=>CH_2O+HO_2$	1.0100E05	2.0	6335.02	[109]
R216	$H_2O_2+HCCO=>CH_2CO+HO_2$	3.4240E04	2.0	163.33	[109]
R217	$H_2O_2+C_2H_3=>C_2H_4+HO_2$	5.4260E04	2.0	792.54	[109]
R218	$H_2O_2+O=>OH+HO_2$	1.0830E06	2.0	1657.32	[109]
R219	$H_2O_2+NC_7H_{13}=>NC_7H_{14}+HO_2$	2.1600E04	2.0	5267.81	[109]
R220	$CH_2O+CH_3=>CH_4+HCO$	3.1220E05	2.0	3781.38	[109]
R221	$CH_2O+CH_3CO=>CH_3CHO+HCO$	1.0830E06	2.0	11500.00	[109]
R222	$CH_2O+HCCO=>CH_2CO+HCO$	3.4240E05	2.0	3151.12	[109]
R223	$CH_2O+C_2H_3=>C_2H_4+HCO$	5.4260E05	2.0	3820.50	[109]
R224	$CH_2O+O=>OH+HCO$	1.0830E07	2.0	1094.46	[109]

R225	$CH_2O+NC_7H_{13}=>NC_7H_{14}+HCO$	2.1600E05	2.0	8707.55	[109]
R226	$CH_3CHO+OH=>H_2O+CH_3CO$	2.3960E06	2.0	1734.99	[109]
R227	$CH_3CHO+CH_3=>CH_4+CH_3CO$	2.3420E05	2.0	3916.44	[109]
R228	$CH_3CHO+HCO=>CH_2O+CH_3CO$	7.5780E05	2.0	9700.00	[109]
R229	$CH_3CHO+HCCO=>CH_2CO+CH_3CO$	2.5680E05	2.0	3009.32	[109]
R230	$CH_3CHO+C_2H_3=>C_2H_4+CH_3CO$	4.0700E05	2.0	3965.69	[109]
R231	$CH_3CHO+O=>OH+CH_3CO$	8.1200E06	2.0	1094.46	[109]
R232	$CH_3CHO+HO_2=>H_2O_2+CH_3CO$	3.2330E05	2.0	8726.73	[109]
R233	$CH_3CHO+NC_7H_{13}=>NC_7H_{14}+CH_3CO$	1.6200E05	2.0	8613.01	[109]
R234	$O_2+NC_7H_{16}=>HO_2+NC_7H_{15}$	2.0450E07	2.0	40722.49	[109]
R235	$NC_7H_{16}+OH=>H_2O+NC_7H_{15}$	1.80E07	2.0	2259.83	[109]
R236	$NC_7H_{16}+H=>H_2+NC_7H_{15}$	2.8880E07	2.0	3950.57	[109]
R237	$NC_7H_{16}+CH_3=>CH_4+NC_7H_{15}$	4.6840E05	2.0	4871.29	[109]
R238	$NC_7H_{16}+CH_3CO=>CH_3CHO+NC_7H_{15}$	1.6240E06	2.0	14065.90	[109]
R239	$NC_7H_{16}+HCO=>CH_2O+NC_7H_{15}$	1.5160E06	2.0	12360.44	[109]
R240	$NC_7H_{16}+HCCO=>CH_2CO+NC_7H_{15}$	5.1360E05	2.0	5333.37	[109]
R241	$NC_7H_{16}+C_2H_3=>C_2H_4+NC_7H_{15}$	8.1390E05	2.0	4871.29	[109]
R242	$NC_7H_{16}+O=>OH+NC_7H_{15}$	1.6240E07	2.0	2579.54	[109]
R243	$NC_7H_{16}+HO_2=H_2O_2+NC_7H_{15}$	1.76E04	2.5	14860.0	[109]
R244	$NC_7H_{16}+NC_7H_{13}=>NC_7H_{14}+NC_7H_{15}$	3.2400E05	2.0	10943.77	[109]
R245	$O_2+NC_7H_{14}=>HO_2+NC_7H_{13}$	2.2150E07	2.0	40722.49	[109]
R246	$NC_7H_{14}+OH=>H_2O+NC_7H_{13}$	5.1920E06	2.0	1273.54	[109]
R247	$NC_7H_{14}+H=>H_2+NC_7H_{13}$	3.1290E07	2.0	4086.44	[109]
R248	$NC_7H_{14}+CH_3=>CH_4+NC_7H_{13}$	5.0740E05	2.0	5273.86	[109]
R249	$NC_7H_{14}+CH_3CO=>CH_3CHO+NC_7H_{13}$	1.7590E06	2.0	13613.01	[109]
R250	$NC_7H_{14}+HCO=>CH_2O+NC_7H_{13}$	1.6420E06	2.0	11907.55	[109]
R251	$NC_7H_{14}+HCCO=>CH_2CO+NC_7H_{13}$	5.5640E05	2.0	4910.67	[109]
R252	$NC_7H_{14}+C_2H_3=>C_2H_4+NC_7H_{13}$	8.8180E05	2.0	5304.06	[109]
R253	$NC_7H_{14}+O=>OH+NC_7H_{13}$	1.7590E07	2.0	2579.54	[109]

R254	$NC_7H_{14}+HO_2=>H_2O_2+NC_7H_{13}$	7.0040E05	2.0	11117.81	[109]
R255	$CH_3+O_2=CH_2O+OH$	3.30E11	0.0	8934.4	[191]
R256	$NC_7H_{16}(+M)<=>C_6H_{13-1}+CH_3(+M)$	4.32E24	-2.1	89900.0	[109]
	/LOW /0.49630E43 -0.77800E01 0.42800E05/				
	/TROE /0.89200E00 0.10000E11 0.22280E01 0.17980E10/				
R257	$C_7H_{14-1}+OH<=>CH_2O+C6H_{13-1}$	1.00E11	0.0	-4000.0	[109]
	REV /1.00E11 0.0 11900.0 /				
R258	$C_7H_{15}O_{-2}<=>CH_2O+C_6H_{13-1}$	1.35E21	-2.3	24780.0	[109]
	REV /1.00E11 0.0 11900.0 /				
R259	$C_7H_{15}O_{2-2+}CH_3O_2<=>C_7H_{15}O_{-2}+CH_3O+O_2$	7.00E15	-1.6	1860.0	[109]
	REV / 0.00E00 0.0 0.0/				
R260	$C_7H_{15-2}+HO_2<=>C_7H_{15}O_{-2}+OH$	7.00E12	0.0	-1000.0	[109]
	REV/ 3.08E17 -1.1 28070.0 /				
R261	C_7H_{15}-2=C_7H_{14-1}+H	3.155E12	0.09	36820.0	[109]
R262	$C_7H_{15-2}+O_2<=>C_7H_{14-1}+HO_2$	4.50E-09	0.0	5002.0	[109]
	REV /1.53E-08 -0.2 18270.0/				
R263	$C_7H_{15}O_{2-2}<=>C_7H_{14-1+}HO_2$	5.75E41	-9.4	42490.0	[109]
	REV / 9.60E32 -7.2 17070.0/				
R264	$C_7H_{14}+HO_2<=>C_7H_{14}OOH$	1.35E03	2.5	10500.0	[109]
NOx Reactions					
R265	$N+NO=N_2+O$	3.5E13	0.0	330.0	[154]
R266	$N+O_2=NO+O$	2.65E12	0.0	6400	[154]
R267	N+OH=NO+H	7.3E13	0.0	1120	[154]
R268	$N_2O+O=N_2+O_2$	1.4E12	0.0	10810	[26]
R269	$N_2O+O=2NO$	2.9E13	0.0	23150	[26]
R270	$N_2O+H=N_2+OH$	4.4E14	0.0	18880	[154]
R271	$N_2O+OH=N_2+HO_2$	2.0E12	0.0	21060	[26]
R272	$N_2O(+M)=N_2+O(+M)$	1.3E11	0.0	59620	[154]
	/LOW/ 6.2E14 0.0 56100				

	/M/ H_2/2.0/ H_2O/6.0/ CH_4=2.0/ CO/1.5/ CO_2/2.0/				
R273	HO_2+NO=NO_2+OH	2.11E12	0.0	-480.0	[26]
R274	NO+O(+M)=NO_2(+M)	1.06E20	-1.41	0.0	[26]
	/M/ H_2/2.0/ H_2O/6.0/ CH_4/2.0/ CO/1.5/ CO_2/2.0/				
R275	NO_2+O=NO+O_2	3.9E12	0.0	-240.0	[26]
R276	NO_2+H=NO+OH	1.32E14	0.0	360.0	[26]

6.3 Validation

The final n-heptane/syngas/NOx mechanism UNN-2, including the adjustment rate constants and the additional reactions, was validated against different experimental measurements from the literature and numerical results by using well-validated mechanisms in terms of ignition delay time, LFS and species concentration profiles. A variety of mixtures were used in order to validate the performance of the proposed mechanism to predict a) n-heptane oxidation ,b) syngas combustion, c) syngas/n-heptane co-oxidation and finally d)NOx formation during syngas combustion. Moreover, a multidimensional CFD analysis was performed, to predict the combustion of syngas in a micro-pilot-ignited supercharged dual-fuel engine.

6.3.1 N-heptane oxidation

To evaluate the performance of the final mechanism UNN-2 for predicting the ignition delay time of n-heptane/air mixture, three different sets of experimental data from the literature were used. Heufer et al. [186] measured experimentally the ignition delay times of n-heptane/air mixture, Fuel 19, at equivalence ratio 1,0, pressure 13.5 bar and a range of temperatures 757-1265K. The second set of experimental data was obtained from Zhang et al. [187], Fuel 20. In this study the authors measured the ignition delay times at equivalence ratio 1.0, pressure 20 bar and temperatures 750-1430 K. The final set of experimental ignition delay for n-heptane/air mixture was taken from Gauthier et al [188], Fuel 21. Their experiments were conducted at equivalence ratio 1.0, pressures 20 bar and 55 bar and temperatures 813-1250 K. Additionally, the calculated results by using the original n-heptane mechanism from Creck modelling group [109] were used for the validation procedure.. According to the comparison between the experimental and simulated results presented in Figure 6-14, the UNN-2 mechanism is in a good agreement with both the numerical results by using the original Creck mechanism [109] and the experimental results at pressure 13.5 bar (Figure 6-14a), pressure 20 bar (Figure 6-14b), and pressure 55 bar (Figure 6-14c).

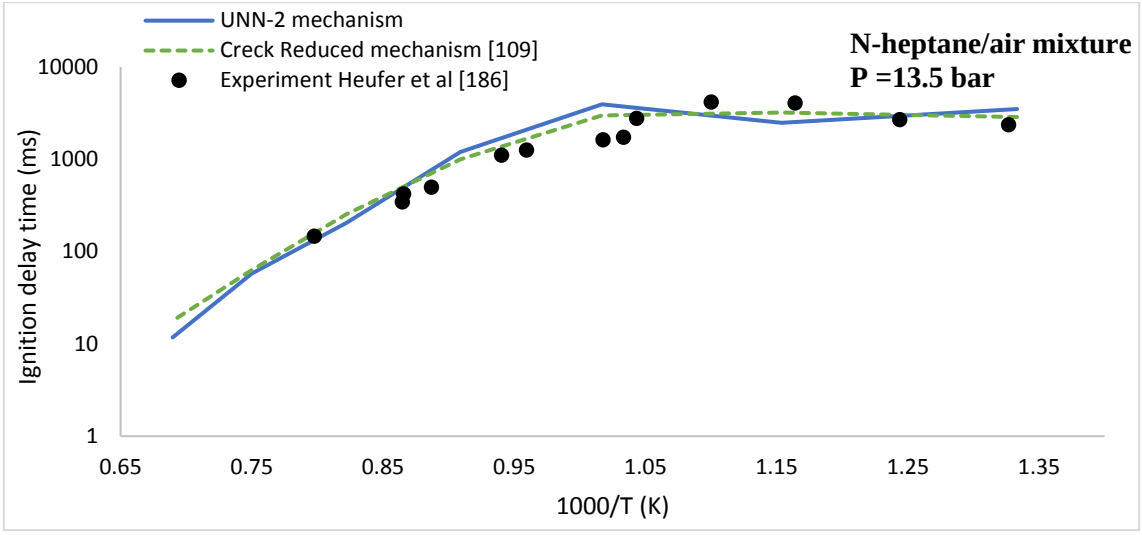

a)

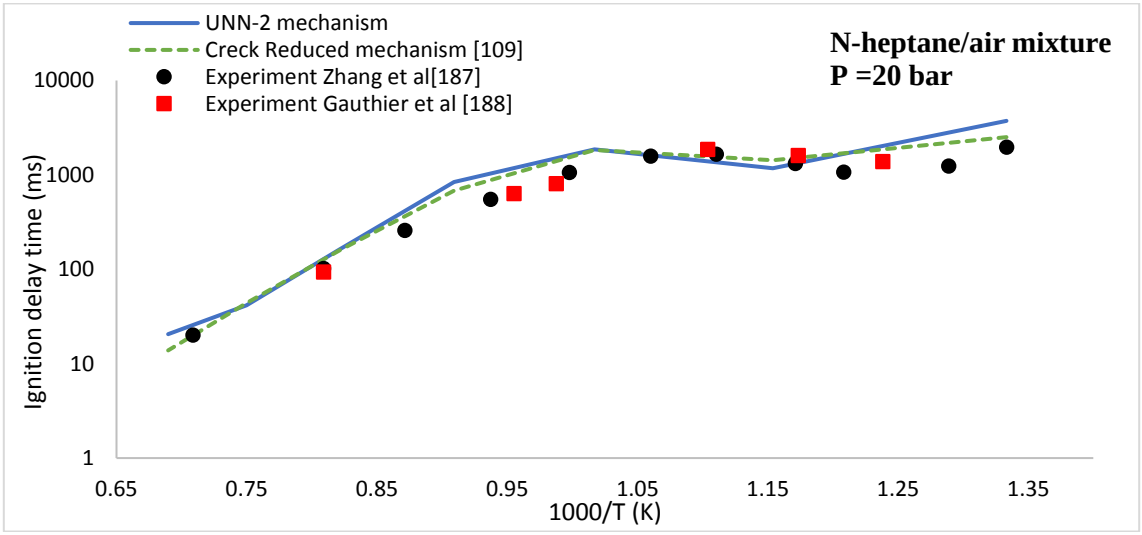

b)

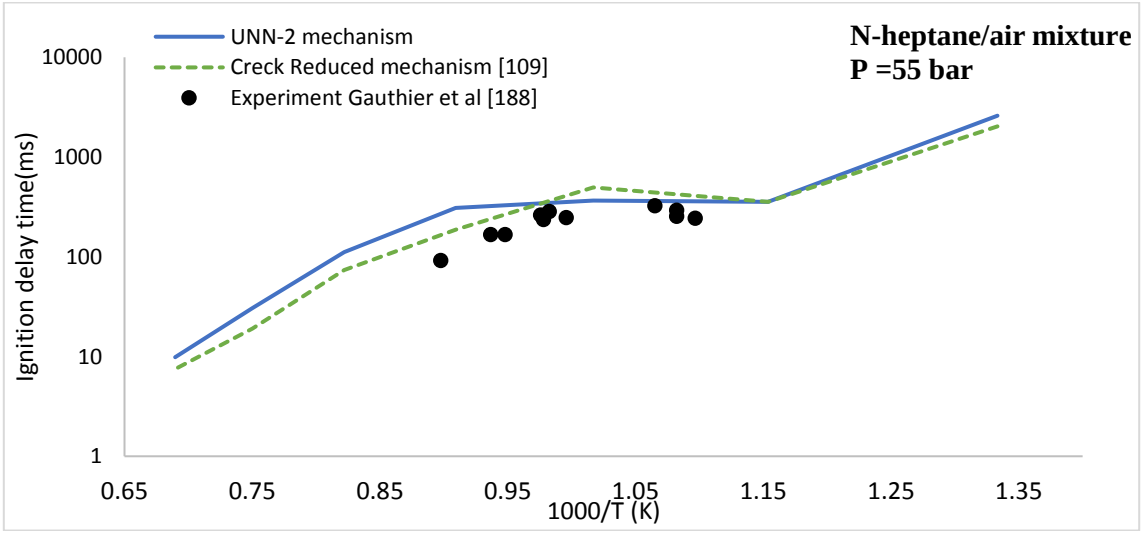

c)

Figure 6-14 Comparison of the calculated ignition delay time by using UNN-2 mechanism, n-heptane Creck reduced mechanism and the experimental measurements obtained from [186-188] for n-heptane/air mixtures at a)13.5 bar, b)20 bar and c) 55 bar.

6.3.2. Syngas combustion

In order to evaluate the performance of the UNN-2 mechanism on predicting syngas combustion, experimental measurements for LFS and ignition delay time were used as quantitative measurements. For LFS, three different fuel mixtures were used and the developed mechanism was compared with experimental measurements as well as simulated results obtained by using well-validated mechanisms. Moreover, for the ignition delay time analysis, two different sets of experimental data were used, each one having different syngas composition and different initial combustion parameters, in order to test the mechanism in a wide range of conditions. Furthermore, the developed mechanism was again compared with simulated results using other chemical kinetics mechanisms.

LFS

$H_2/CO/CO_2/CH_4/N_2$ mixture

To evaluate the performance of the developed UNN-2 mechanism on predicting LFS during multicomponent syngas combustion, the simulated LFS was compared with that obtained with the detail GRI Mech. 3.0 [26] and the original n-heptane mechanism from Creck modelling group [109]. GRI Mech. 3.0 is a detail mechanism that contains full H_2,CO and CH_4 chemistry as well as NOx chemistry. Therefore, it was used as a validation point during this comparison. For this comparison, Fuel 24 Type 1 and Fuel 24 Type 5 were used at pressures 20 and 40 bar, temperature 450 K and equivalence ratios 0.2-1. Fuel 24 Type 1 contains 13.4% H_2, while Fuel 24 Type 5 contains 58% H_2, Table 3-3. The results are presented in Figure 6-15 for Fuel 24 Type 1 and Figure 6-16 for Fuel 24 Type 5. According to the comparison the developed mechanism UNN-2 is close to GRI Mech. 3.0 for all of the conditions, while the mechanism from Creck modelling group over-predicts the LFS, especially at equivalence ratios higher than 0.5. This is because the n-heptane mechanism from Creck modelling group was developed to simulated mainly n-heptane and in general oxidation of large hydrocarbons. Moreover, it can be seen that the reduced UNN-2 mechanism captures accurately the effect of H_2 on the LFS: The LFS for syngas Type 5 is higher than for syngas Type 1 due to the higher H_2 concentration. The higher the H_2 concentration in the fuel mixture, the higher is the reactivity of the mixture and therefore the higher is the LFS.

By summarizing the results of this comparison, it can be said that the developed UNN-2 mechanism, can be used accurately for the simulation of LFS during syngas combustion even if it contains not only syngas chemistry but also n-heptane and NOx chemical pathways. On the other hand, the original n-heptane Creck mechanism [109] shows a significant deviation and over predicts LFS.

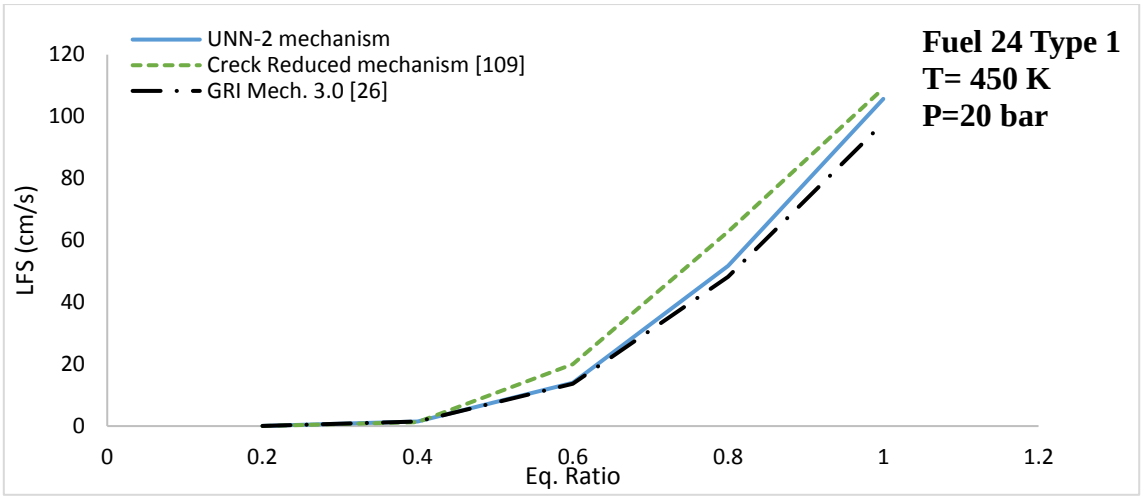

a)

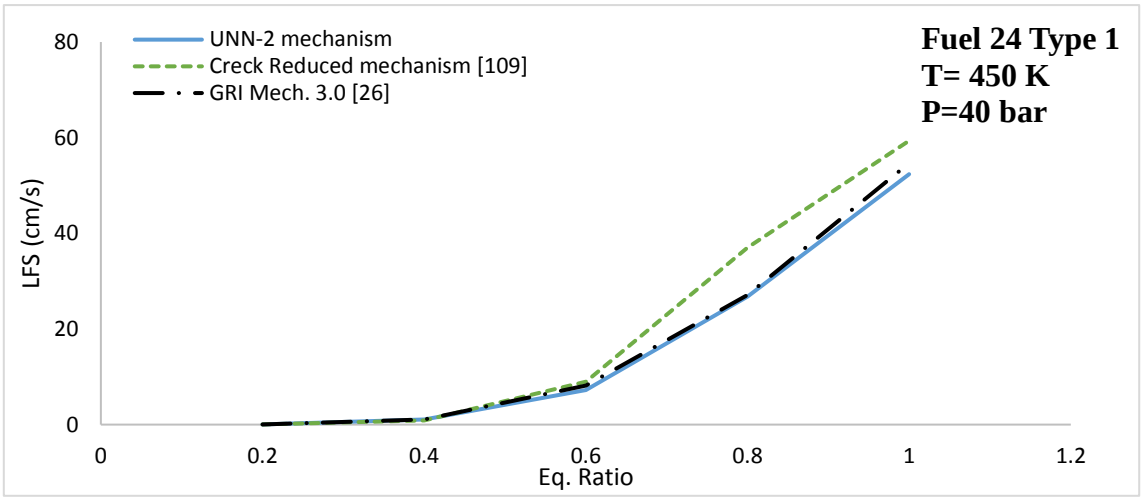

b)

Figure 6-15 Comparison of the LFS by using UNN-2 mechanism, n-heptane Creck reduced mechanism and GRI Mech. 3.0 for Fuel 24 Type 1 at a) P=20 bar and b) P=40 bar.

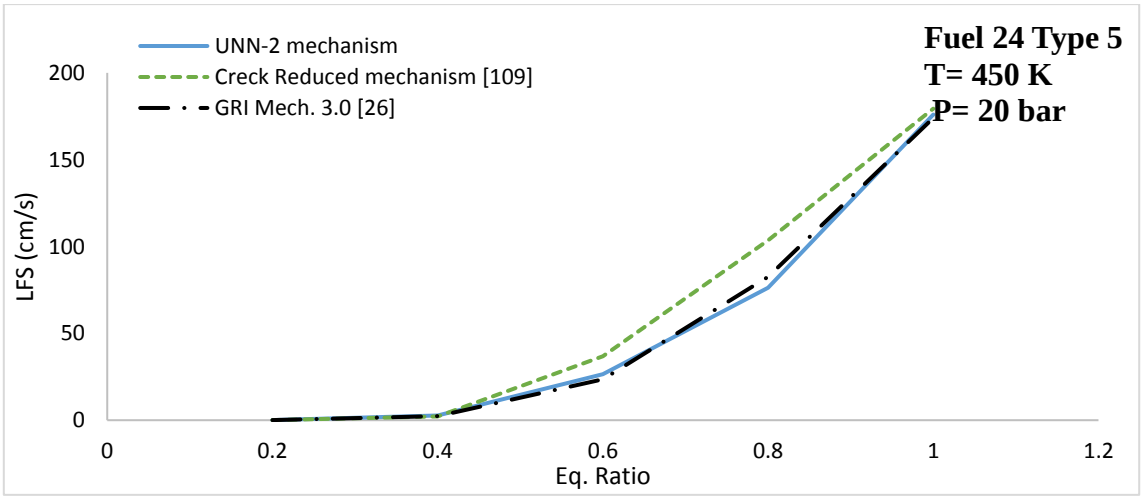

a)

Figure 6-16 Comparison of the LFS by using UNN-2 mechanism, n-heptane Creck reduced mechanism and GRI Mech. 3.0 for Fuel 24 Type 5 at a) P=20 bar and b) P=40 bar

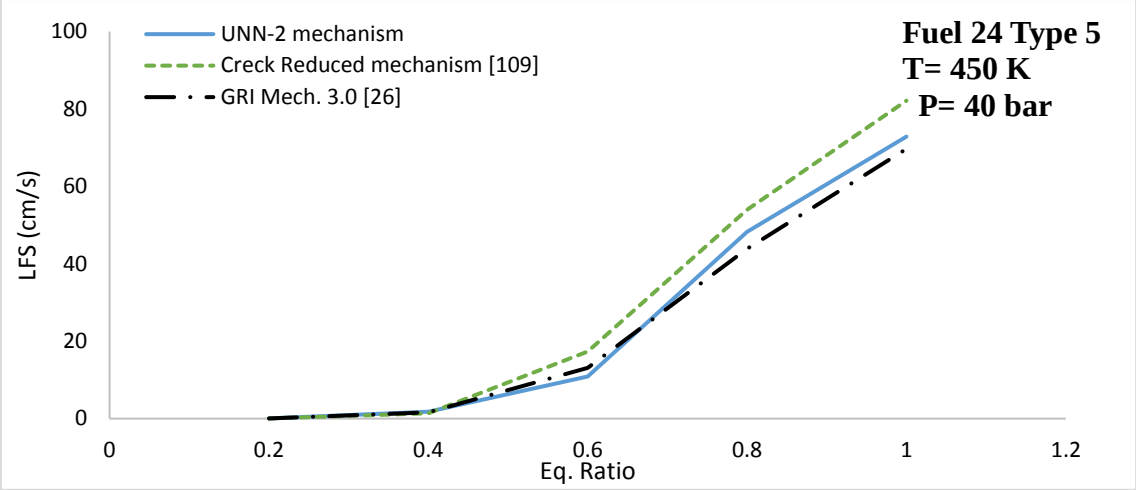

b)

Figure 6-16 (cont.) Comparison of the LFS by using UNN-2 mechanism, n-heptane Creck reduced mechanism and GRI Mech. 3.0 for Fuel 24 Type 5 at a) P=20 bar and b) P=40 bar

H_2/CH_4 mixture

The comparison between the calculated and experimental LFS for different H_2/CH_4 mixtures is presented in Figure 6-17. The experimental results were obtained from Donohoe et al. [175]. The authors measured the LFS for three different H_2/CH_4 ratios, 20/80%, 50/50% and 90/10%, Fuel 10 Table 3-3, at pressure 1.01 bar, a range of equivalence ratios 0.4-2.2 and temperature 298 K. It can be seen that at all of the tested conditions for all of the fuel mixture ratios, the UNN-2 mechanism is very close to the experimental results. Additionally, the UNN-2 mechanism accurately captures the effects of the H_2 and CH_4 addition on the LFS. The LFS by using high CH_4 (Figure6-17a), is very low in comparison to the LFS calculated for CH_4 at only 10% (Figure 6-17c). This is because CH_4 works as an absorber and requires a higher amount of thermal energy to be activated. Therefore, the reactivity of the fuel mixture is reduced and so is the LFS. On the other hand, the higher the amount of H2 in the mixture, the more reactive it is. This is obvious from the comparison of the SLmax between Figure 7-17a and 6-17c. For Figure 6-17a, in which H_2 is just 20%, SL max is approximately 50 cm/s. In contrary, the SLmax in Figure 6-17c, 90% H_2 content, is higher and close to 350 cm/s. Moreover, GRI Mech. 3.0 shows a good match with the experimental results for fuels with high CH_4, while as the amount of H_2 increased and CH_4 reduced, the deviation with the experimental results increased significantly. This is because GRI Mech. 3.0 was originally constructed for the simulation of natural gas (CH_4>80%).

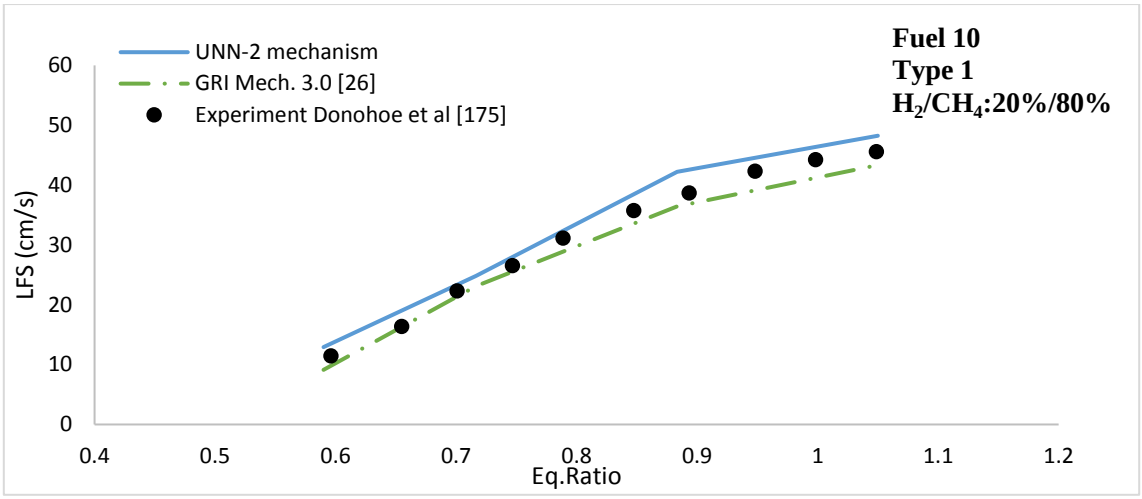

a)

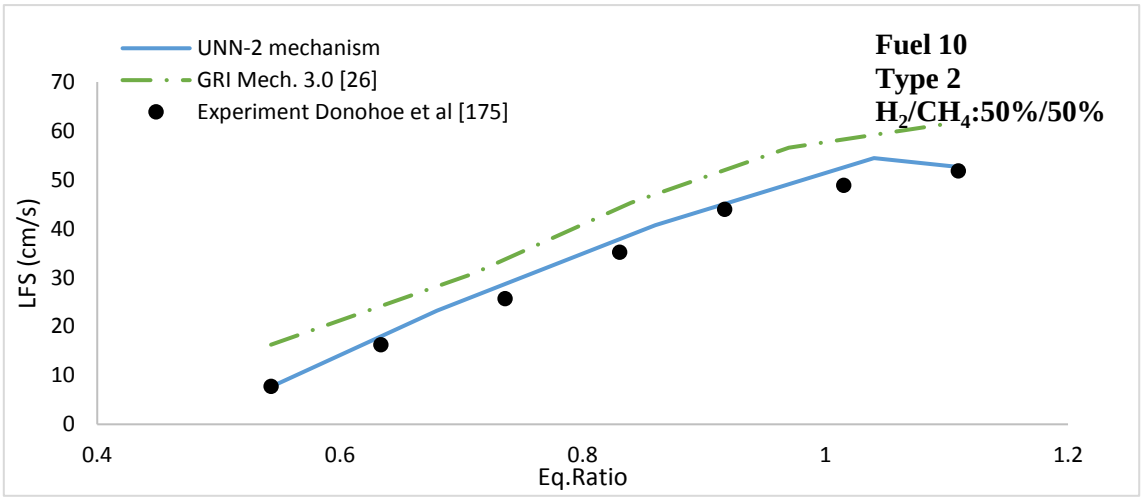

b)

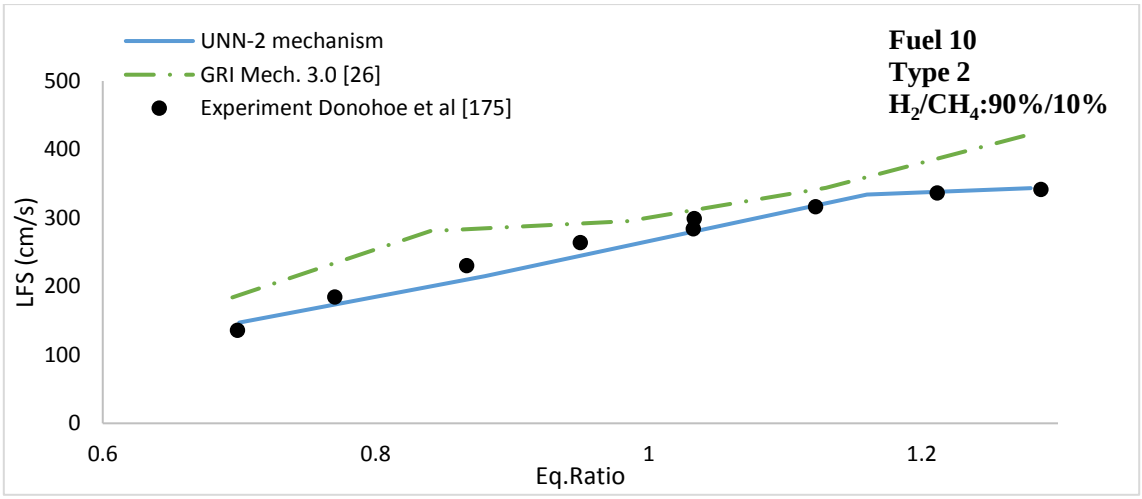

c)

Figure 6-17 Comparison of the calculated LFS by using UNN-2 mechanism, GRI Mech. 3.0 and the experimental measurements obtained from [175] for a) H_2/CH_4:20%/80% b) H_2/CH_4:50%/50% and c) H_2/CH_4:90%/10%, Fuel 10 Table 3-3.

$H_2/CO/CH_4$ mixture

For further validation of the UNN-2 mechanism on predicting the LFS of syngas mixtures, the experimental results from Lapalme et al. [173] were used. The authors measured the LFS of three different $H_2/CO/CH_4$ mixtures, Fuel 8 Table 3-3, at pressure 1.01 bar, temperature 295 K and a range of equivalence rations 0.2-2.5. Figure 6-18 shows the comparison between the experimental and numerical results by using the UNN-2 mechanism and GRI mech. 3.0. For all of the conditions, the UNN-2 mechanism is in a very good agreement with the experimental results while GRI mech. 3.0 slightly under-predicts the experimental measurements, especially for rich mixtures (high equivalence ratios).

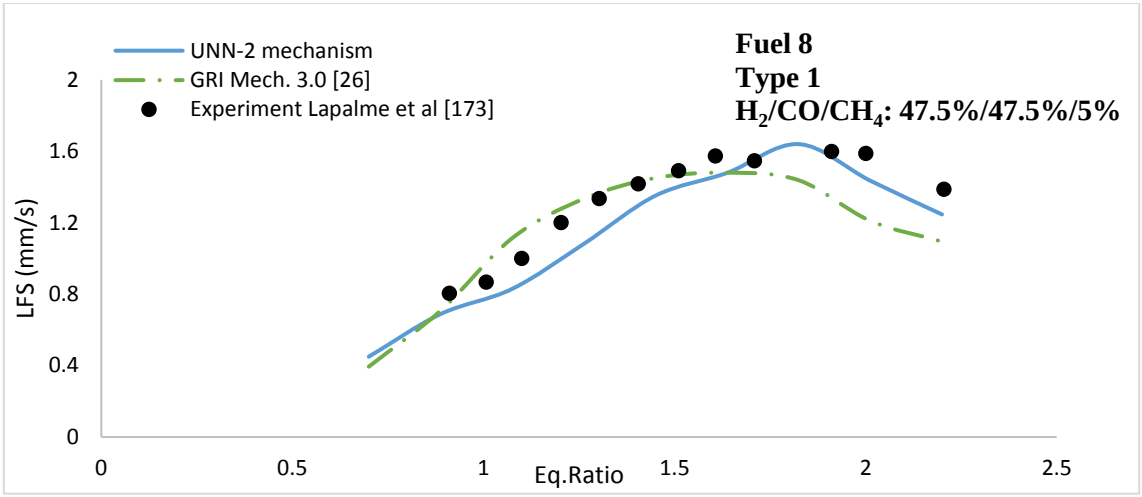

a)

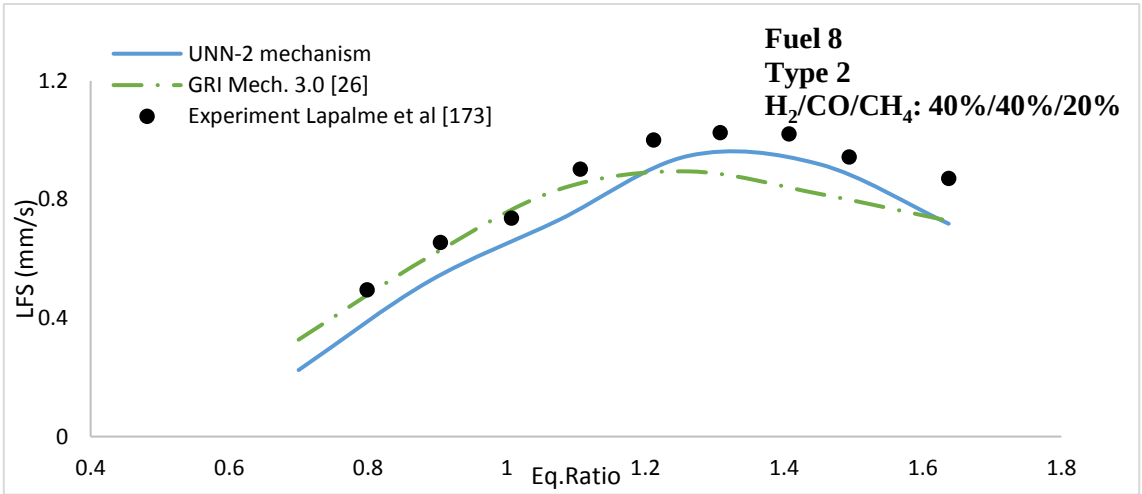

b)

Figure 6-18 Comparison of the calculated LFS by using UNN-2 mechanism, GRI Mech. 3.0 and the experimental measurements obtained from [173], Fuel 8 for a) $H_2/CO/CH_4$: 47.5%/47.5%/5% b) $H_2/CO/CH_4$: 40%/40%/20% and c) $H_2/CO/CH_4$: 30%/30%/40%.

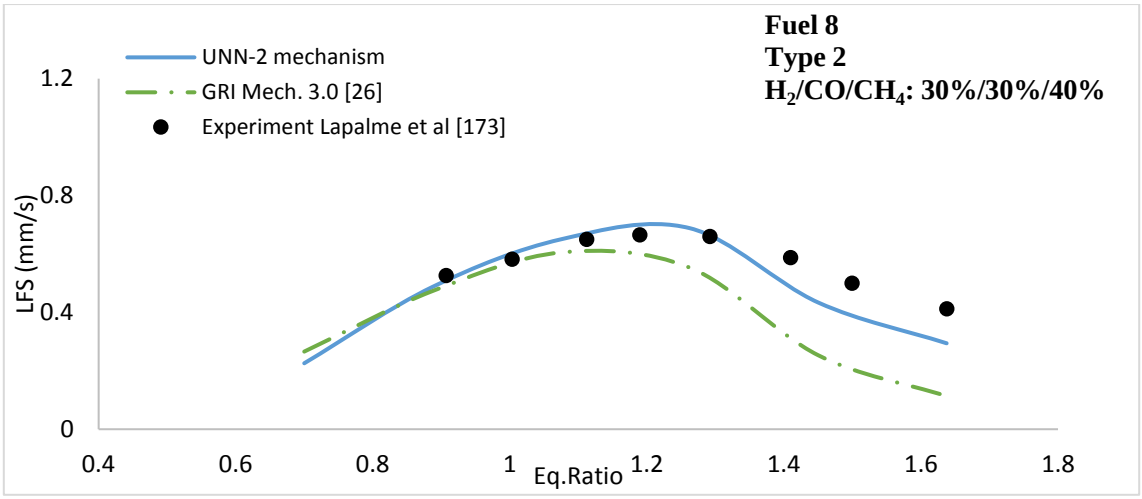

c)

Figure 6-18 (cont.) Comparison of the calculated LFS by using UNN-2 mechanism, GRI Mech. 3.0 and the experimental measurements obtained from [173], Fuel 8 for a) $H_2/CO/CH_4$: 47.5%/47.5%/5% b) $H_2/CO/CH_4$: 40%/40%/20% and c) $H_2/CO/CH_4$: 30%/30%/40%.

Ignition delay time

$H_2/CO/CO_2/CH_4/N_2$ mixture

Similar, to LFS simulations, the performance of the constructed UNN-2 mechanism on predicting the syngas ignition delay time was evaluated by using three sets of different fuel mixtures. First, the ignition delay time using the developed mechanism UNN-2, was compared with that obtained by using GRI Mech. 3.0 [26] and the n-heptane mechanism from Creck modelling group [109]. Fuel mixture 24 Type 1 and Type 5 were used at T= 1063-1162, P= 20 and 40 bar and equivalence ratios 0.2 and 0.4.

The comparisons are presented in Figure 6-19 for Fuel 24 Type 1 and Figure 6-20 for Fuel 24 Type 5. According to the comparison, GRI Mech. 3.0 and the developed UNN-2 mechanism are in a good agreement at all of the tested conditions. On the other hand, the mechanism from Creck modelling group, slightly overpredicts the ignition delay time, especially at 0.2 equivalence ratio and high pressure (40 bar) conditions.

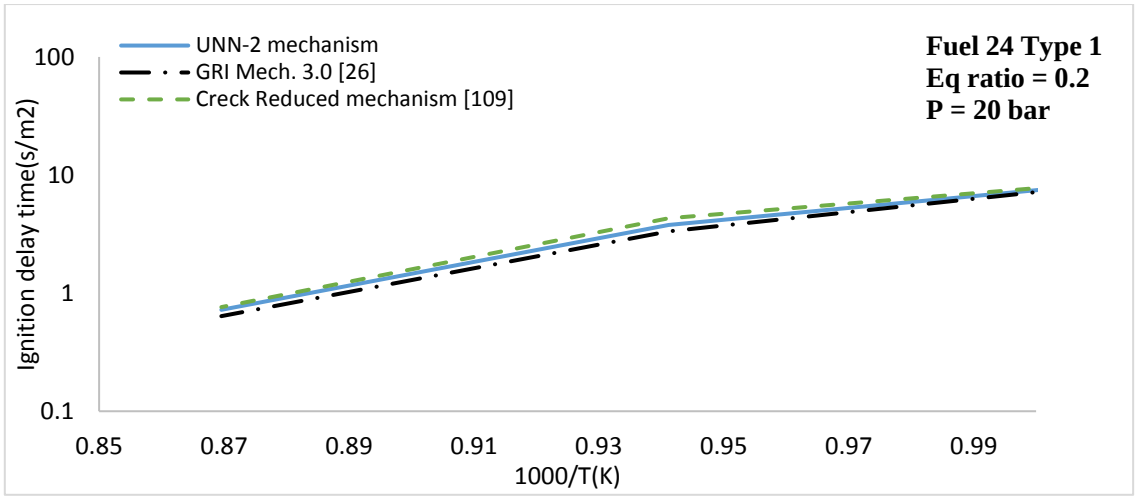

a)

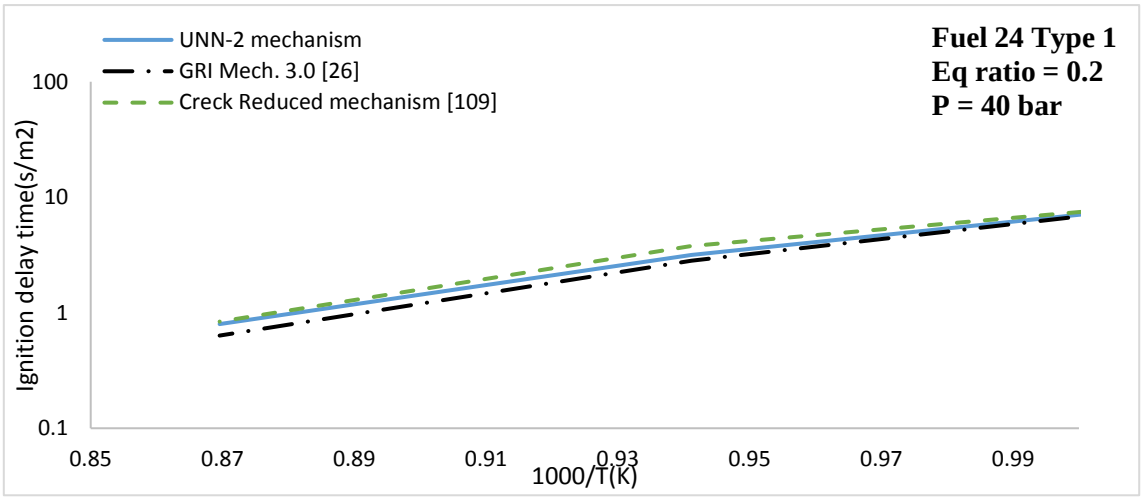

b)

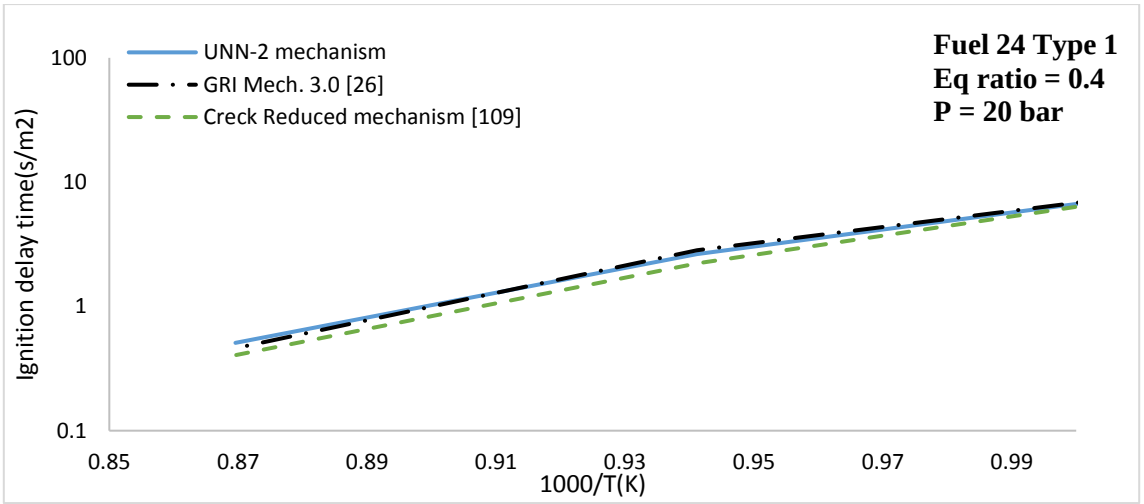

c)

Figure 6-19 Comparison of the ignition delay time obtained by using UNN-2 mechanism, n-heptane Creck reduced mechanism [109] and GRI Mech. 3.0 [26] for Fuel 24 Type 1, at a) Eq. ratio 0.2 and P=20 bar, b) Eq. ratio 0.2 and P= 40 bar, c) eq. ratio 0.4 and P= 20 bar and d) Eq. ratio 0.4 and P =40 bar.

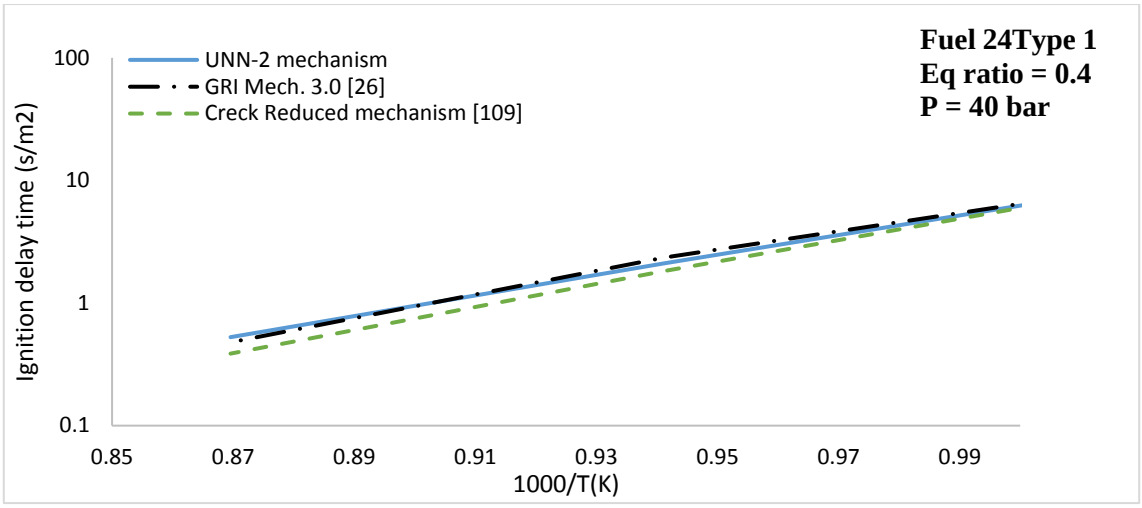

d)

Figure 6-19 (cont.) Comparison of the ignition delay time obtained by using UNN-2 mechanism, n-heptane Creck reduced mechanism [109] and GRI Mech. 3.0 [26] for Fuel 24 Type 1, at a) Eq. ratio 0.2 and P=20 bar, b) Eq. ratio 0.2 and P= 40 bar, c) eq. ratio 0.4 and P= 20 bar and d) Eq. ratio 0.4 and P =40 bar.

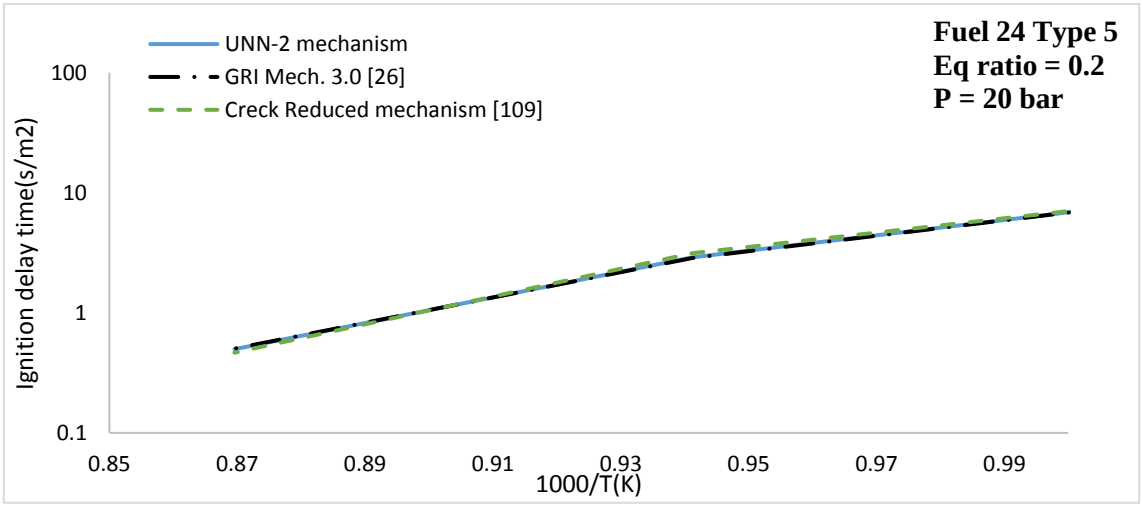

a)

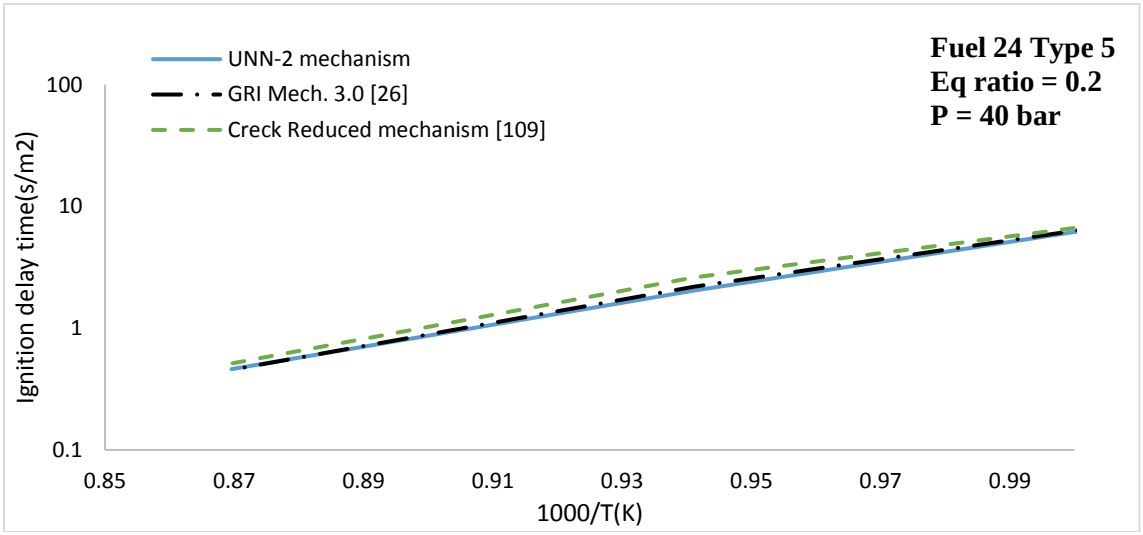

b)

Figure 6-20 Comparison of the ignition delay time obtained by using UNN-2 mechanism, n-heptane Creck reduced mechanism [109] and GRI Mech. 3.0 [26] for Fuel 24 Type 5, at a) Eq. ratio 0.2 and P=20 bar, b) Eq. ratio 0.2 and P= 40 bar, c) eq. ratio 0.4 and P= 20 bar and d) Eq. ratio 0.4 and P =40 bar.

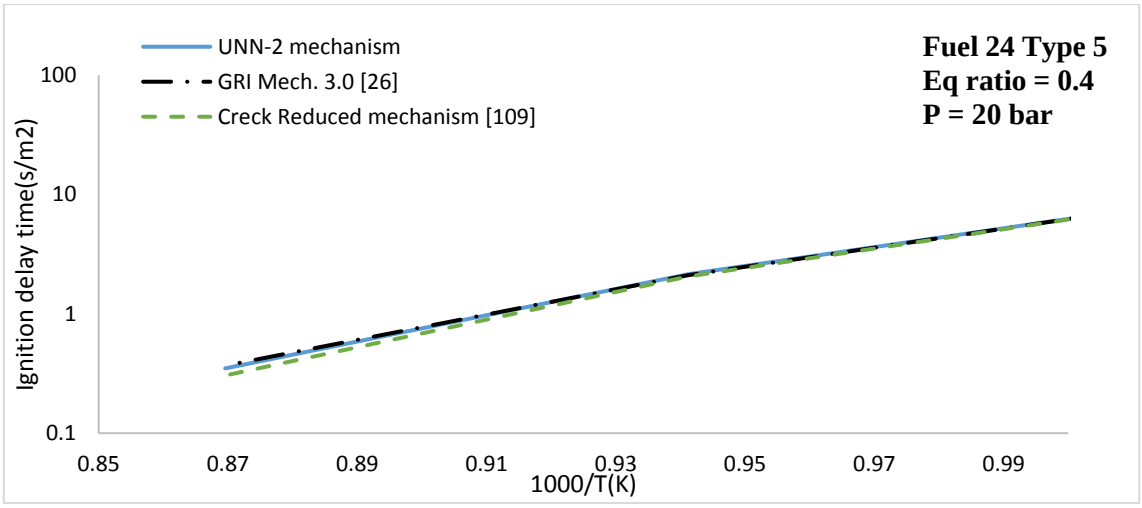

c)

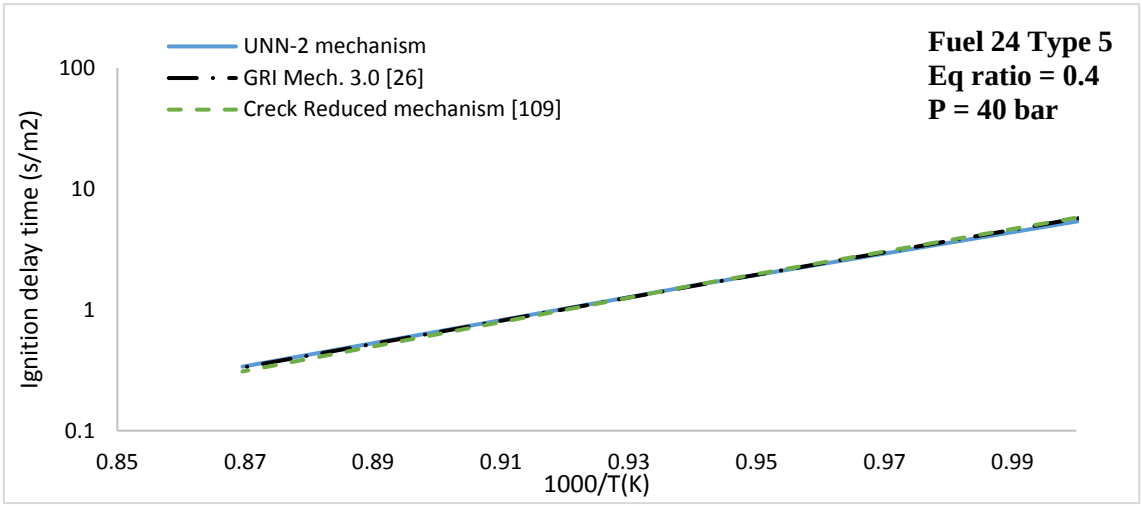

d)

Figure 6-20 (cont.) Comparison of the ignition delay time obtained by using UNN-2 mechanism, n-heptane Creck reduced mechanism [109] and GRI Mech. 3.0 [26] for Fuel 24 Type 5, at a) Eq. ratio 0.2 and P=20 bar, b) Eq. ratio 0.2 and P= 40 bar, c) eq. ratio 0.4 and P= 20 bar and d) Eq. ratio 0.4 and P =40 bar.

H_2/CH_4 mixture

For further validation, the experimental results from Zhang et al. [11], for different H_2/CH_4 mixtures, Fuel 3 Type 3 and Type 4, were used. The authors studied experimentally the ignition delay of different H_2/CH_4 mixtures at equivalence ratio 0.5, pressures 5 ,10 and 20 bar and temperature range 1050-1850 K. The comparison between the calculated results by using the UNN-2 mechanism and GRI Mech. 3.0 and the experimental data is presented in Figure 6-21 for Fuel 3 Type 3 and Figure 6-22 for Fuel 3 Type 4. It can be seen that the UNN-2 mechanism is in a good agreement with the experimental results at both conditions. GRI Mech. 3.0 on the other hand, shows a good match with the experimental results at high methane condition, CH_4=80%, Figure 6-22, while it over predicts the experimental measurements at high hydrogen conditions, Figure 6-21.

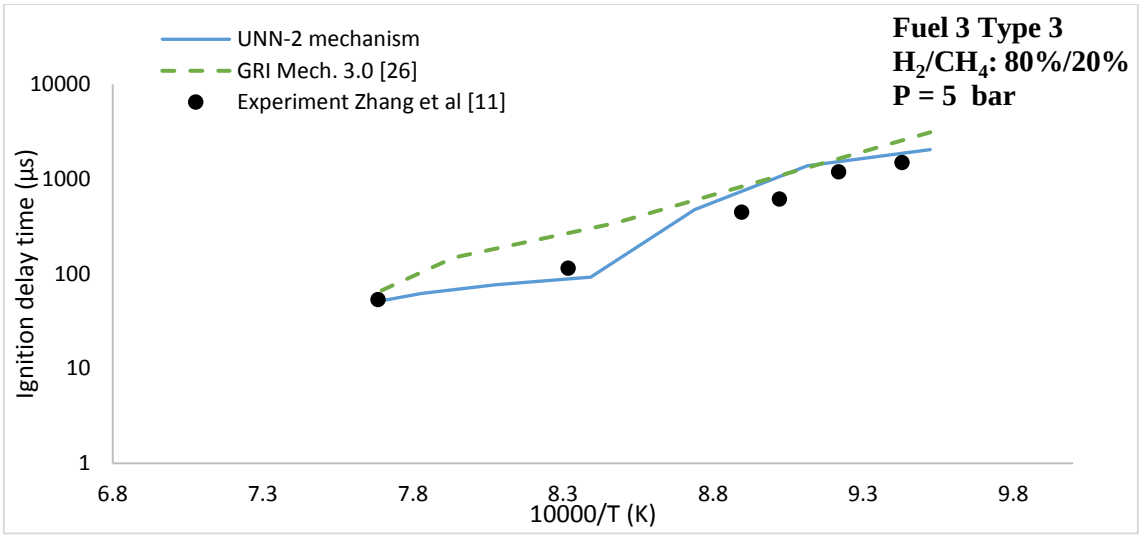

a)

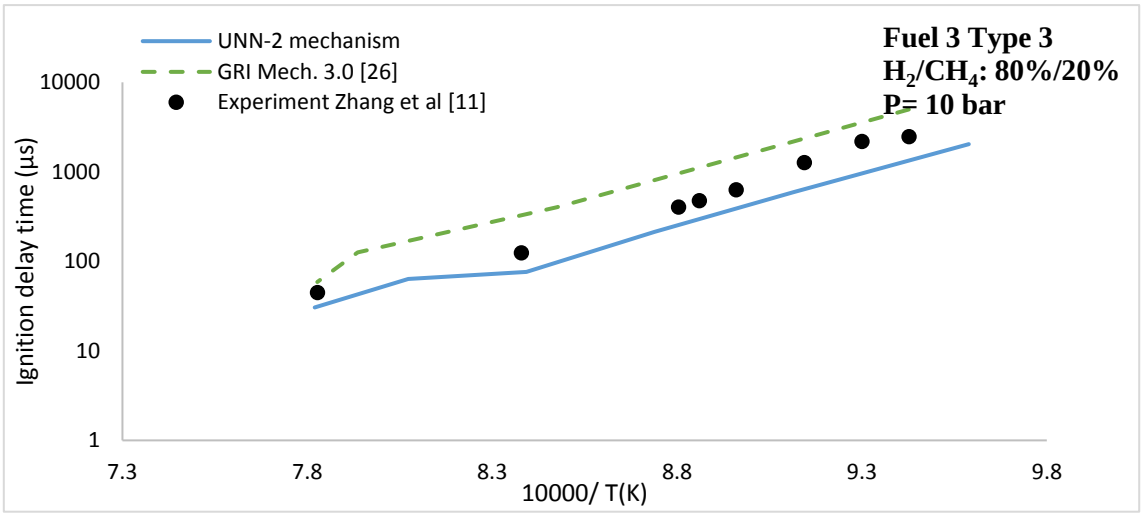

b)

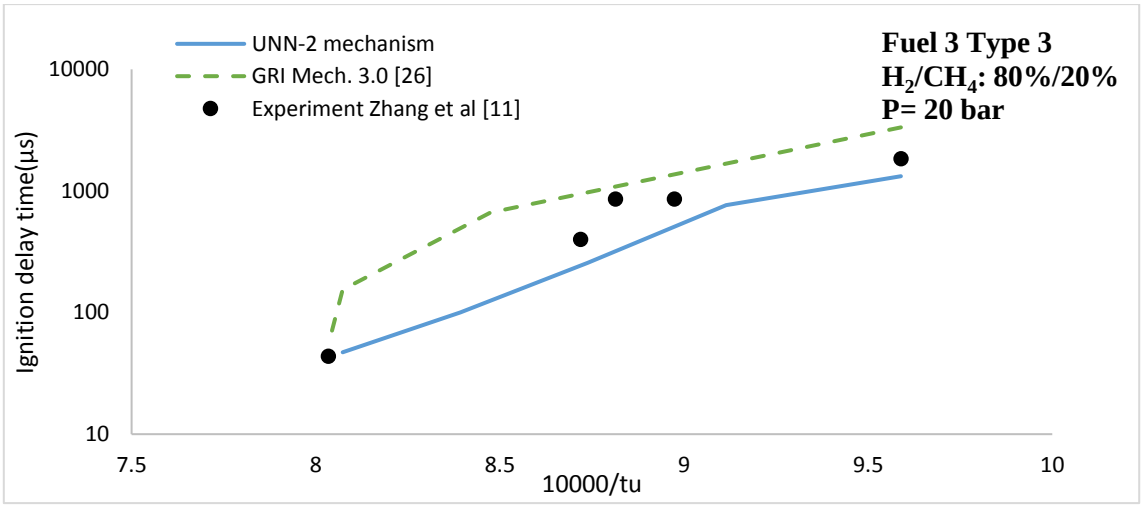

c)

Figure 6-21 Comparison of the calculated ignition delay time by using UNN-2 mechanism, GRI Mech. 3.0 [26] and the experimental measurements obtained from [11] for Fuel 3 Type 3 H_2/CH_4:80%/20% at a)5 atm b)10 atm and c)20 atm.

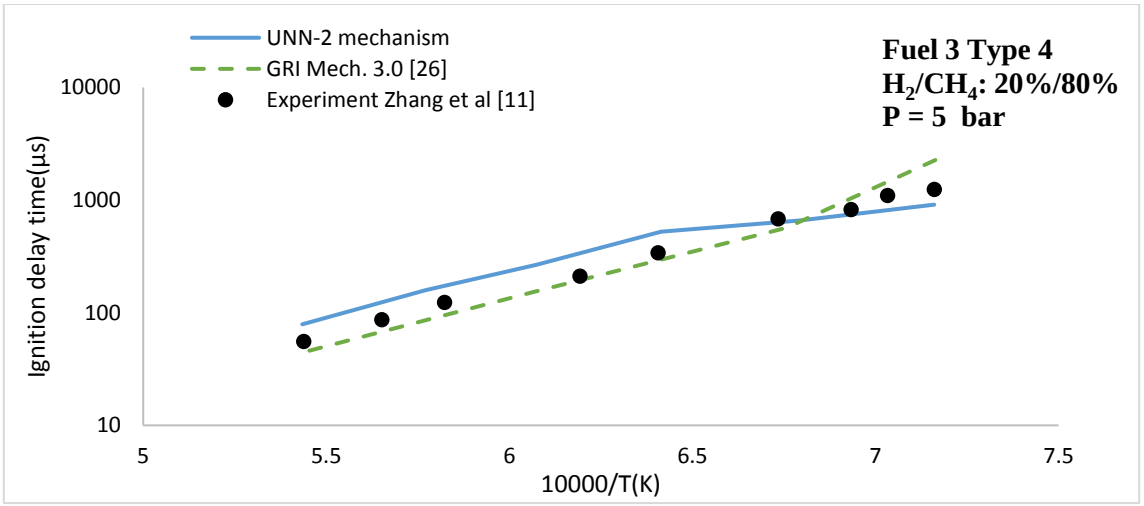

a)

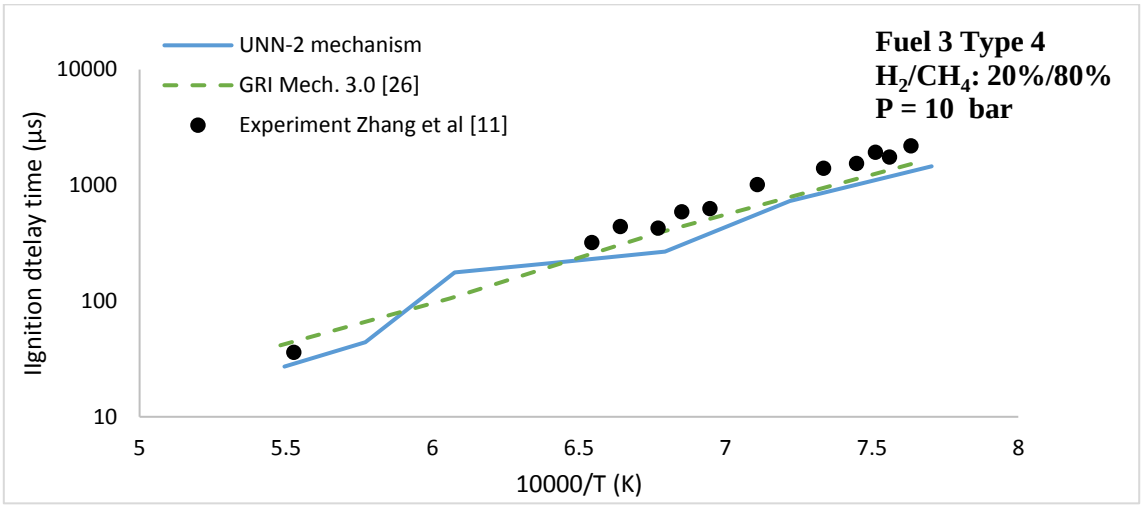

b)

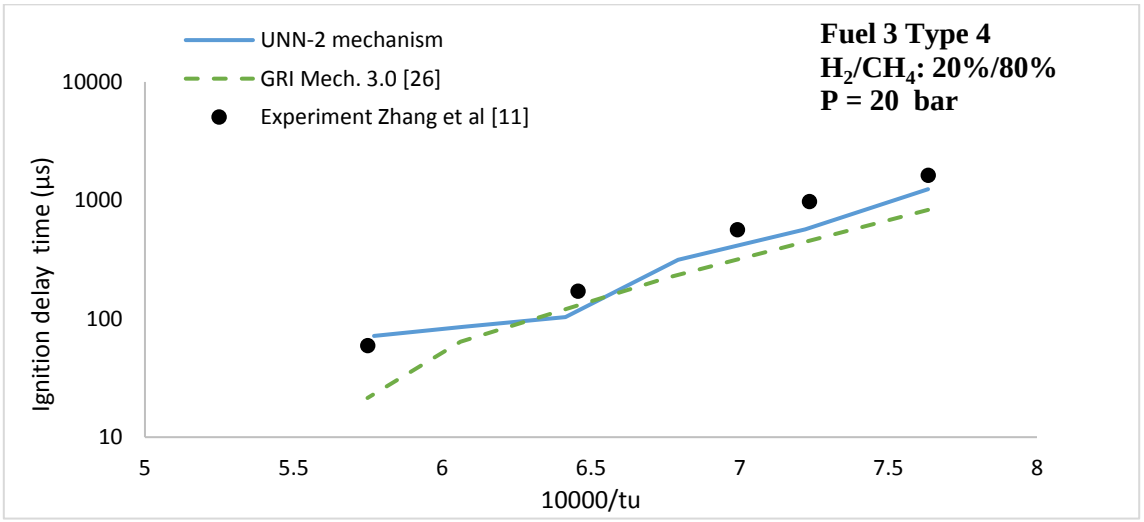

c)

Figure 6-22 Comparison of the calculated ignition delay time by using UNN-2 mechanism, GRI Mech. 3.0 [26] and the experimental measurements obtained from [11] for Fuel 3 Type 4 H_2/CH_4:20%/80% at a)5 bar b)10 bar and c)20 bar.

$H_2/CO/CO_2$ mixture

The last set of experimental syngas ignition delay time data that was used for the validation was taken from Luong et al. [171]. The authors measured the ignition delay times for two different $H_2/CO/CO_2/N_2$ syngas mixtures, Fuel 5 Table 3-3, at equivalence ratios 0.3, 1.0 and 1.5, atmospheric pressure(1.01 bar) and a range of temperatures from 850-1250 K. The comparison between the calculated and experimental results is presented in Figure 6-23 for Fuel 5 Type 1 and in Figure 6-24 for Fuel 5 Type 2.

For both Fuel 5 types, the UNN-2 mechanism accurately simulates the experimental results at all of the tested equivalence ratios, while GRI Mech. 3.0 shows a good agreement with the experiments for Fuel 5 Type 1, Figure 6-23 but deviates for Fuel 5 Type 2, Figure 6-24, especially at equivalence ratios 0.3 and 1.

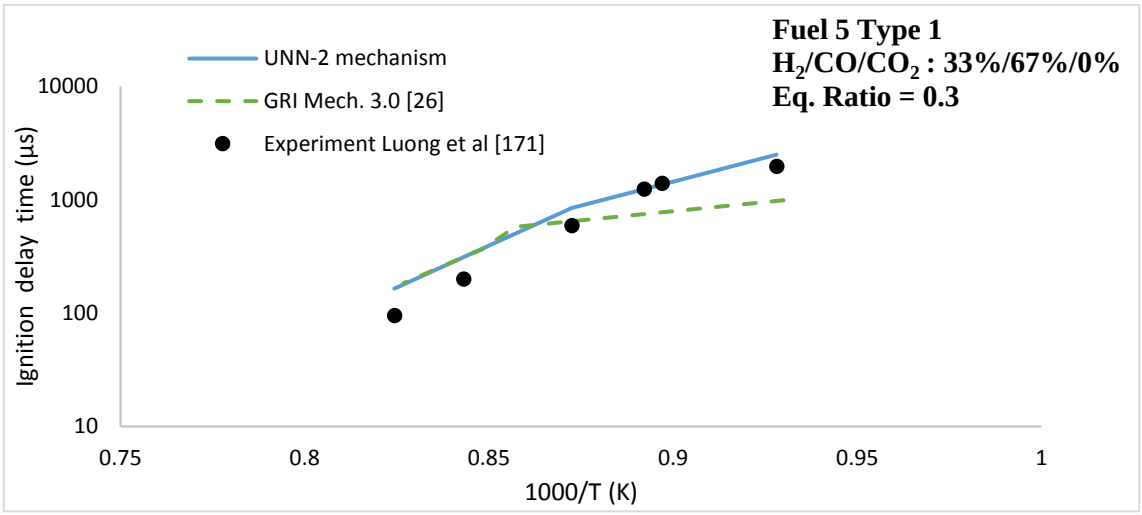

a)

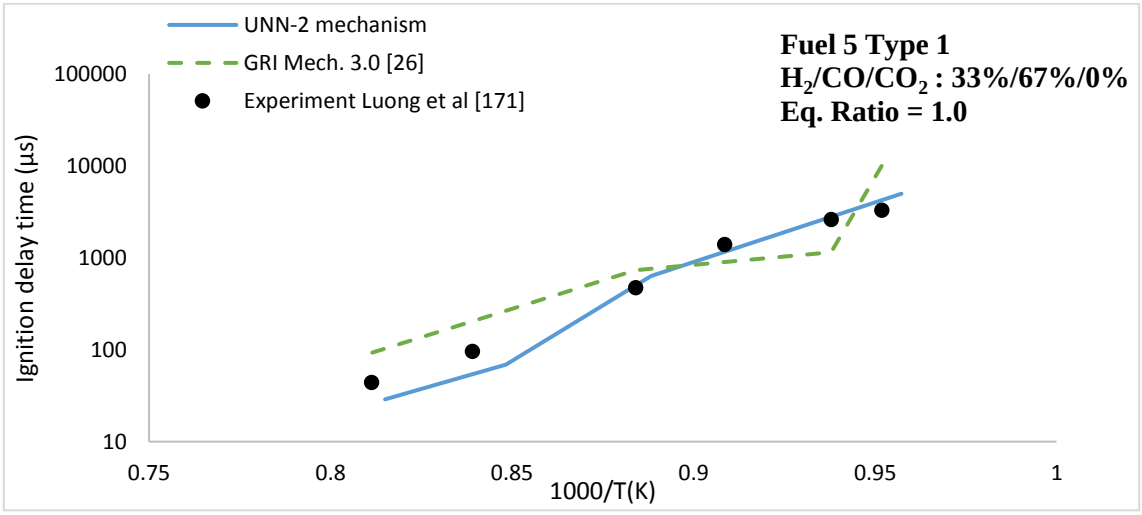

b)

Figure 6-23 Comparison of the calculated ignition delay time by using UNN-2 mechanism, GRI Mech. 3.0 [26] and the experimental measurements obtained from [171] for $H_2/CO/CO_2$:33%/67/0% ,Fuel 5 Type 1, at a) eq. ratio 0.3 b) eq. ratio 1.0 and c) eq. ratio 1.5.

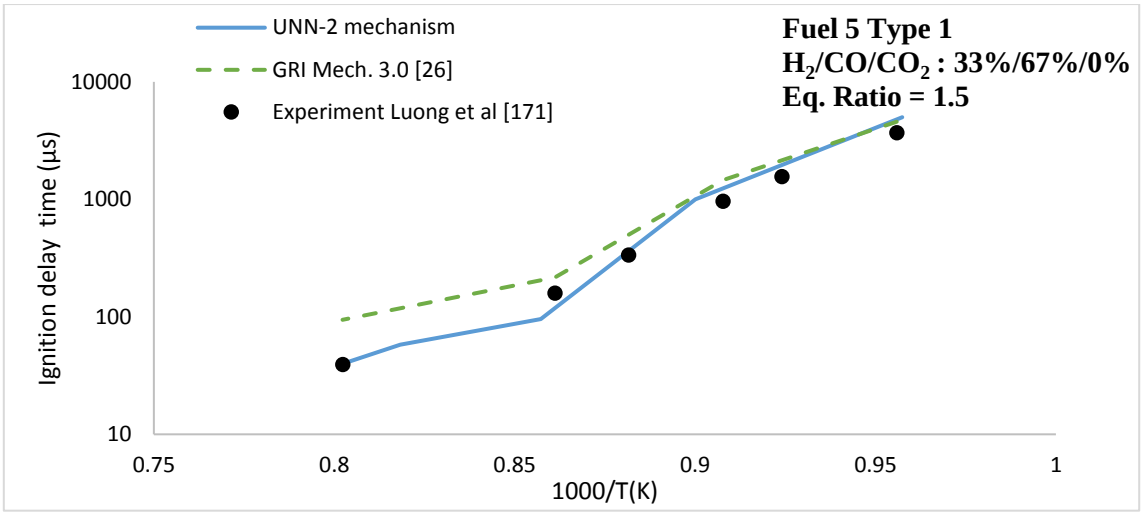

c)

Figure 6-23 (cont.) Comparison of the calculated ignition delay time by using UNN-2 mechanism, GRI Mech. 3.0 [26] and the experimental measurements obtained from [171] for $H_2/CO/CO_2$:33%/67/0% ,Fuel 5 Type 1, at a) eq. ratio 0.3 b) eq. ratio 1.0 and c) eq. ratio 1.5.

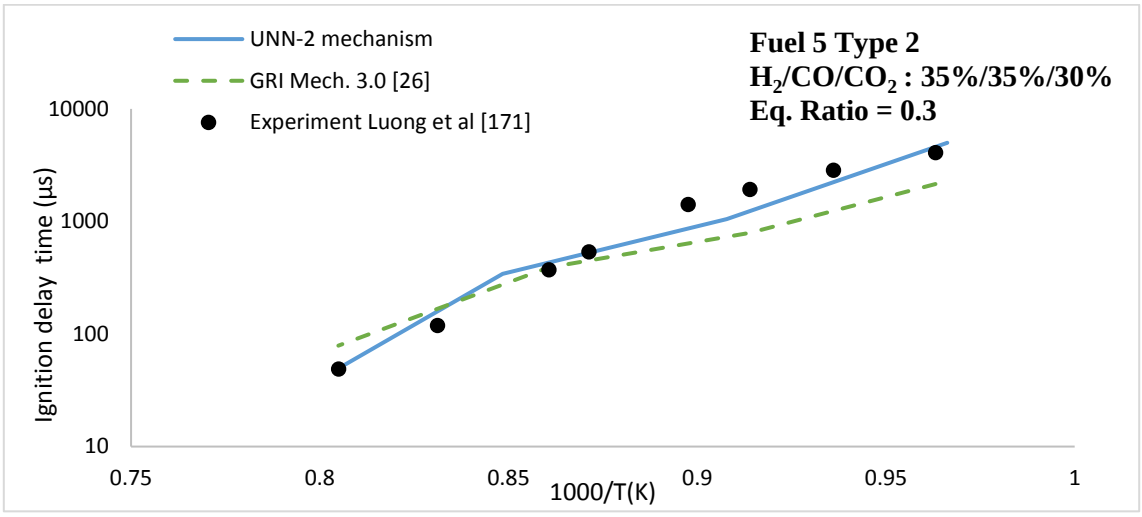

a)

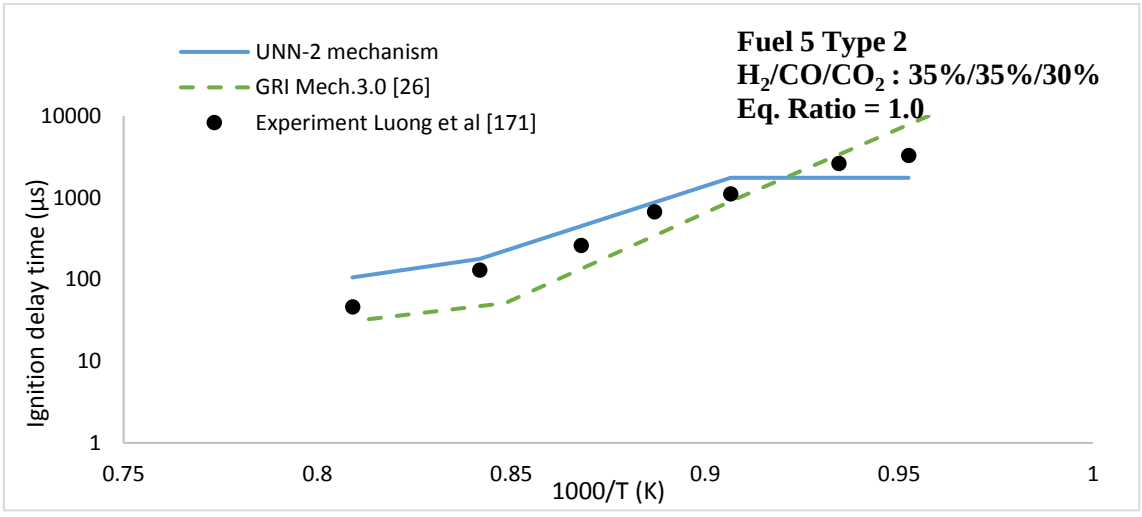

b)

Figure 6-24 Comparison of the calculated ignition delay time by using UNN-2 mechanism, GRI Mech. 3.0 [26] and the experimental measurements obtained from [171] for $H_2/CO/CO_2$:35%/35%/30% ,Fuel 5 Type 2, at a) eq. ratio 0.3 b) eq. ratio 1.0 and c) eq. ratio 1.5.

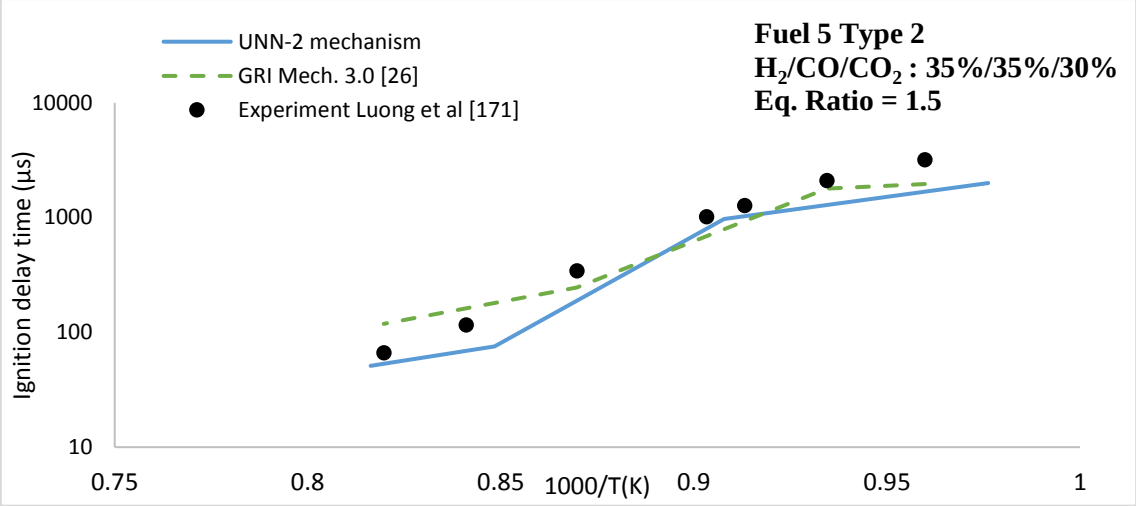

c)

Figure 6-24 (cont.) Comparison of the calculated ignition delay time by using UNN-2 mechanism, GRI Mech. 3.0 [26] and the experimental measurements obtained from [171] for $H_2/CO/CO_2$:35%/35%/30% ,Fuel 5 Type 2, at a) eq. ratio 0.3 b) eq. ratio 1.0 and c) eq. ratio 1.5.

6.3.3 NOx formation

One of the most important factors promoting the replacement of fossil fuels such as gasoline and diesel by syngas fuels is the fact that they produce low NOx emissions during their combustion [69]. During this research, the performance of the constructed UNN-2 mechanism on predicting NO formation was validated by using two different sets of experimental data.

$H_2/CO/CO_2/CH_4$ mixture

Watson et al. [13], performed an experimental study to investigate the NOx formation during the combustion of $H_2/CO/CO_2/CH_4$ syngas mixtures in jet wall stagnation flames, Fuel 12 Table 3-3. The experiments were conducted at temperature 300 K, atmospheric pressure (1.01 bar) and equivalence ratios 0.71, 1.03 and 1.34. The comparison between the calculated and measured axial concentration of NO along the combustion chamber is presented in Figure 6-25. The constructed UNN-2 mechanism shows a good match with the experimental results and accurately captures the effect of the equivalence ratio on the formation of NO. The higher is the equivalence ratio, the richer is the mixture and therefore the higher is the concentration of NO. GRI Mech. 3.0 [26], on the other hand, accurately reproduces the results at low equivalence ratios, but as the equivalence ratio increased the deviation from the experimental results increases.

$H_2/O_2/N_2$ mixture

The second set of experimental results were obtained from Homer and Sutton [177]. The authors analyse experimentally the formation of NO for three different $N_2/H_2/O_2$ fuel compositions at atmospheric pressures (1.01 bar), temperature 298 K and equivalence ratio 0.71. The fuel composition by volume is $2H_2+1.4O_2+5.3N_2$, $2H_2+1.4O_2+4.6N_2$ and

$2H_2+1.4O_2+6.1N_2$, while the O_2/N_2 ratio was 19/81%, Fuel 13 Table 3-3 [243]. The results of the comparison between the calculated and experimental NO concentration profiles are presented in Figure 6-26. The constructed UNN-2 mechanism predicts very well the NO concentration profiles at all of the tested mixtures. GRI Mech. 3.0 on the other hand, is close to the experimental measurements for Fuel mixture 13 Type 1 and Type 2 but deviates significantly from the experimental data for Fuel mixture 13 Type 3.

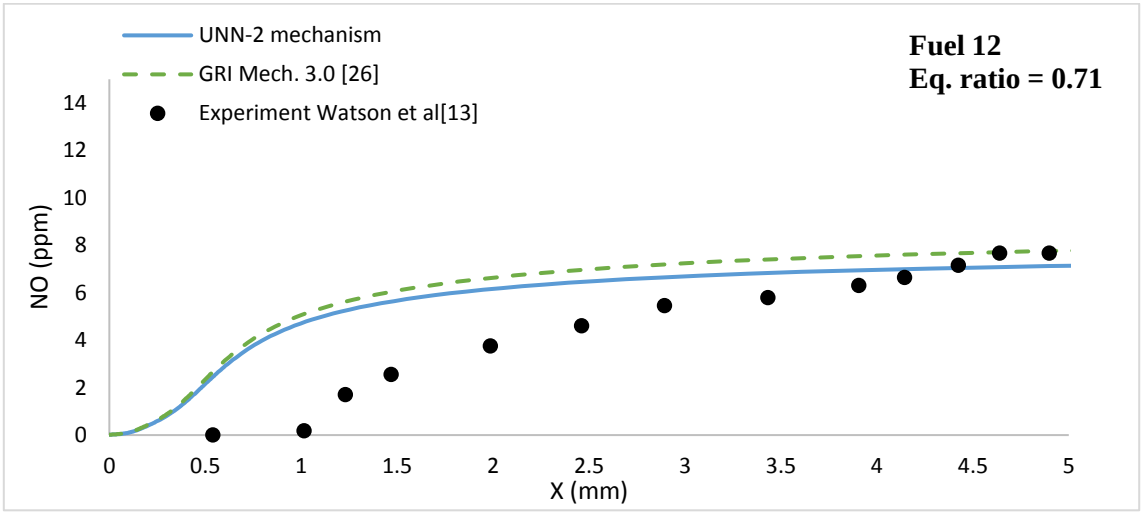

a)

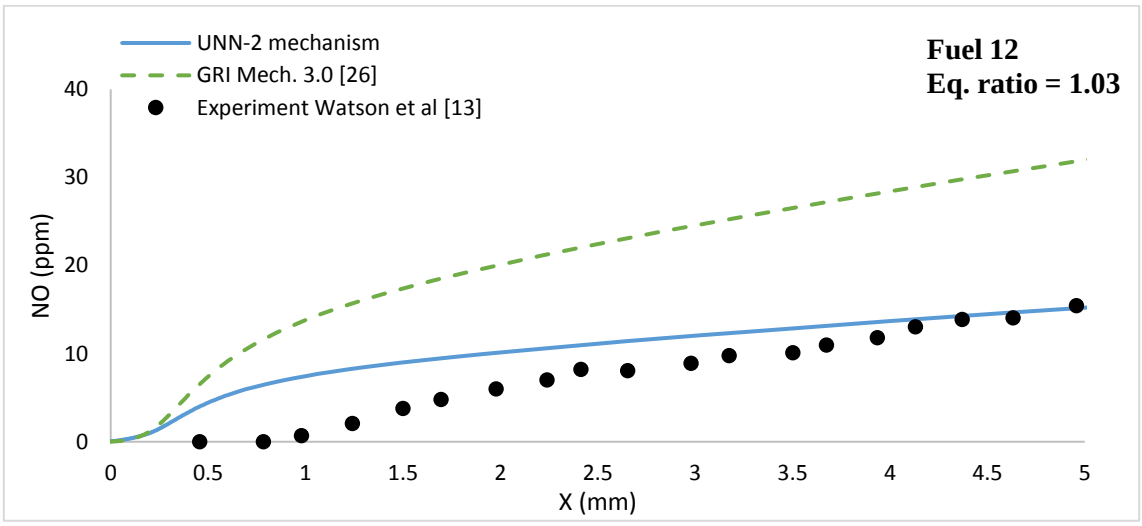

b)

Figure 6-25 Comparison of the simulated NO concentration profiles by using UNN-2 mechanism, GRI Mech. 3.0 [26] and the experimental measurements obtained from [13] for Fuel 13 Table 3-3, at pressure 1 bar, temperature 300 K and equivalence ratios a) 0.71 b) 1.03 and c) 1.34.

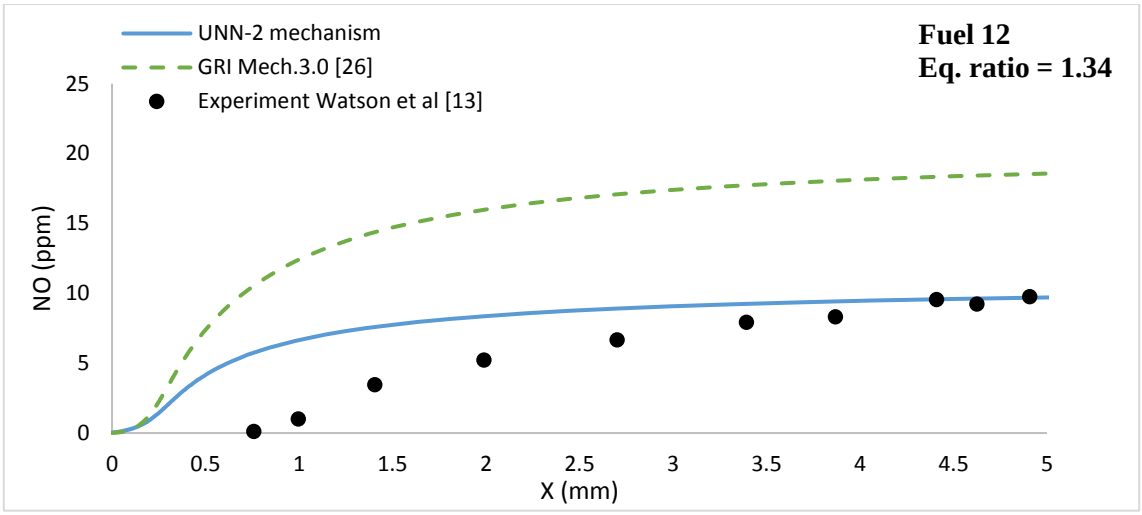

c)

Figure 6-25 (cont.) Comparison of the simulated NO concentration profiles by using UNN-2 mechanism, GRI Mech. 3.0 [26] and the experimental measurements obtained from [13] for Fuel 13 Table 3-3, at pressure 1 bar, temperature 300 K and equivalence ratios a) 0.71 b) 1.03 and c) 1.34.

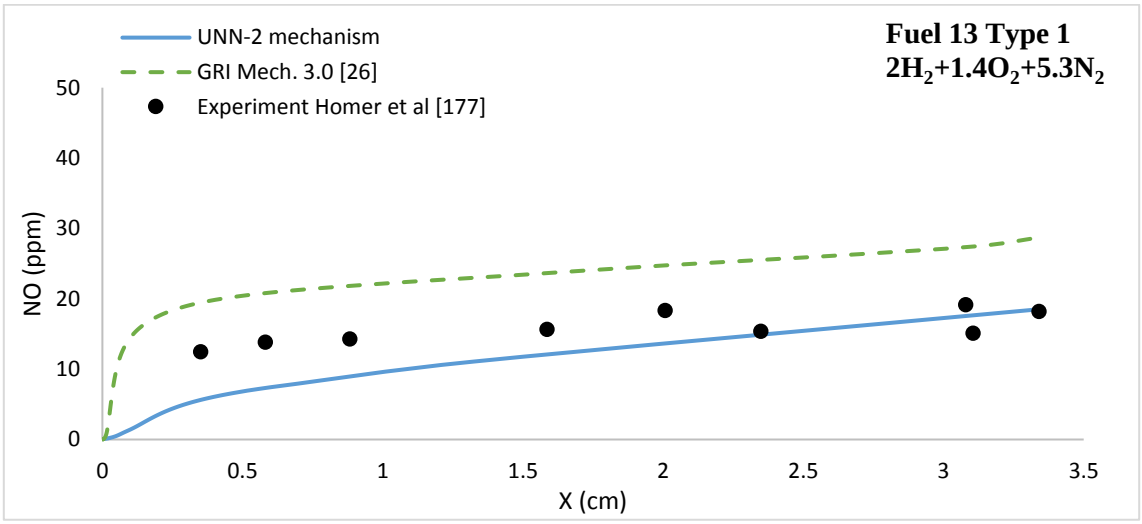

a)

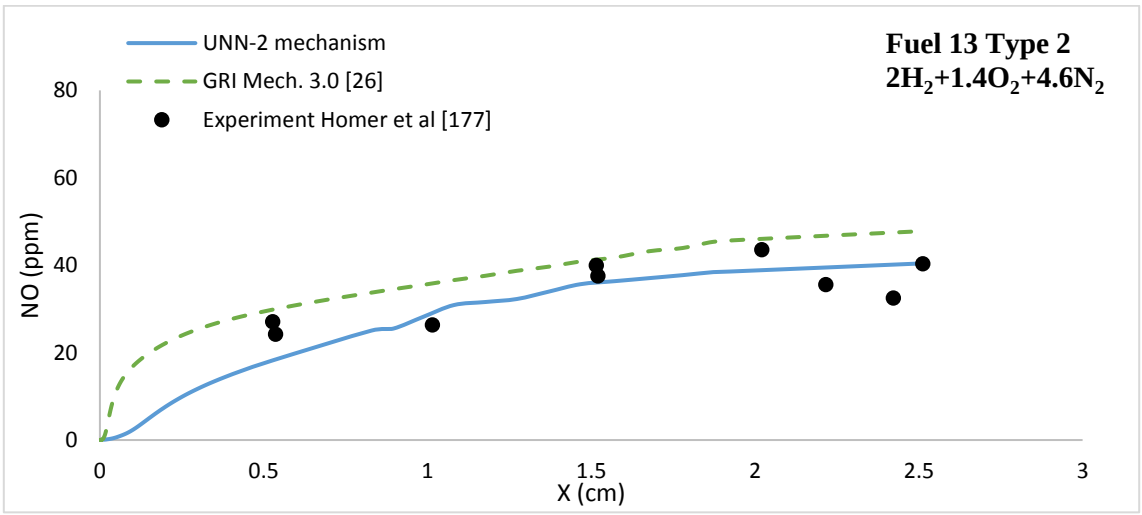

b)

Figure 6-26 Comparison of the simulated NO concentration profiles by using UNN-2 mechanism, GRI Mech. 3.0 [26] and the experimental measurements obtained from [177] for a) Fuel 13 Type1, b)Fuel 13 Type 2 and c) Fuel 13 Type 3(see Table 3-3) at pressure 1.01 bar, temperature 300 K and equivalence ratio 0.71

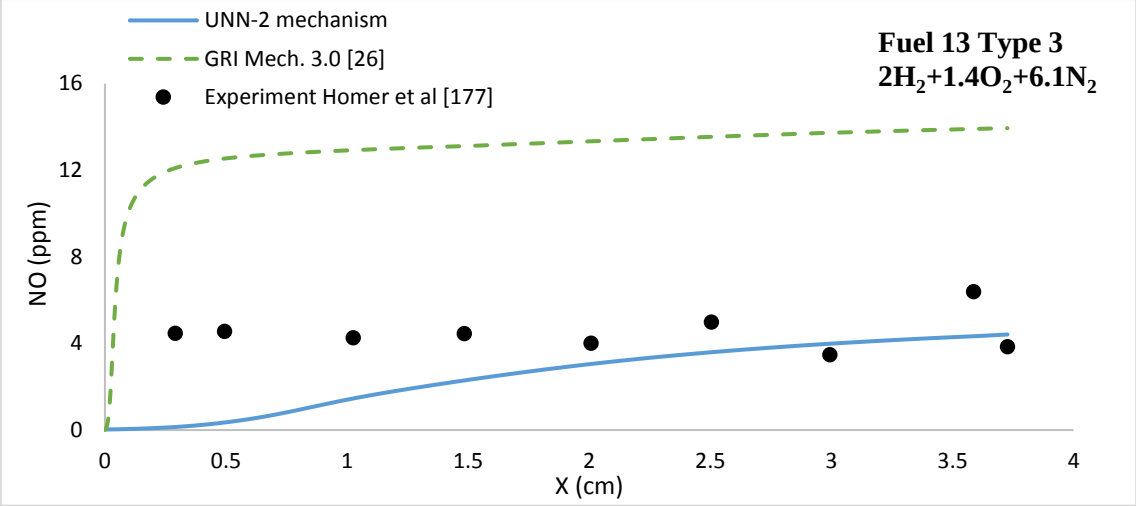

c)

Figure 6-26 (cont.) Comparison of the simulated NO concentration profiles by using UNN-2 mechanism, GRI Mech. 3.0 [26] and the experimental measurements obtained from [177] for a) Fuel 13 Type1, b)Fuel 13 Type 2 and c) Fuel 13 Type 3(see Table 3-3) at pressure 1.01 bar, temperature 300 K and equivalence ratio 0.71

6.3.4 N-heptane/syngas co-oxidation

Few experimental studies have been conducted for the individual investigation of n-heptane oxidation and syngas combustion. However, to date, there is no experimental data available for the co-oxidation of n-heptane and syngas. Due to the lack of experimental measurements, the performance of the developed mechanism on simulating accurately the co-oxidation of n-heptane and syngas was validated by using numerical results obtained by [189] using the reduced mechanism proposed by Chalmers University [251]. The authors investigated numerically the ignition of n-C_7H_{16}/H_2 and n-C_7H_{16}/CH_4 blends at conditions relevant to diesel and HCCI engines [252]. The reduced Chalmers mechanism for n-heptane oxidation consists of 168 reactions. However, the mechanism was designed specifically for low temperature combustion simulations and therefore includes the core reactions required to simulate the combustion characteristics under specific conditions. Moreover, the reduced Chalmers University mechanism does not include NOx chemistry [253, 254].

N-C_7H_{16}/H_2 mixture

For N-C_7H_{16}/H_2 mixture, Fuel 22 Table 3-3, the ignition delay times were calculated for two different blends: a) Fuel 22 Type 1 20% H2 by volume and b) Fuel 22 Type 2 80% H2 by volume , at pressures 30 and 55 bar, equivalence ratios 1 and 2 and temperature range 800-1400 K. The comparison between the numerical results by using the developed UNN-2 mechanism, the Chalmers University reduced mechanism [251] and the Creck n-heptane mechanism [109] are presented in Figure 6-27 for 80% C_7H_{16}/ 20% H_2 and in Figure 6-28 for 20% C_7H_{16} /80% H_2. According to the comparison, the UNN-2 and Chalmers mechanisms are

in a good agreement at all of the tested conditions, while the Creck mechanism deviates, especially at high pressures (55 bar). Moreover, the UNN-2 mechanism accurately captures the effect of H_2 and NC_7H_{16} addition on the ignition delay time. By increasing the H_2 content up to 80%, the ignition delay time reduced slightly at temperatures above 1000 K. Moreover, the addition of N-C_7H_{16} slightly reduces the ignition delay time of N-C_7H_{16}/H_2 mixtures for temperatures below 1000 K. At temperatures close to 1000 K the NTC event occurs [189, 255].

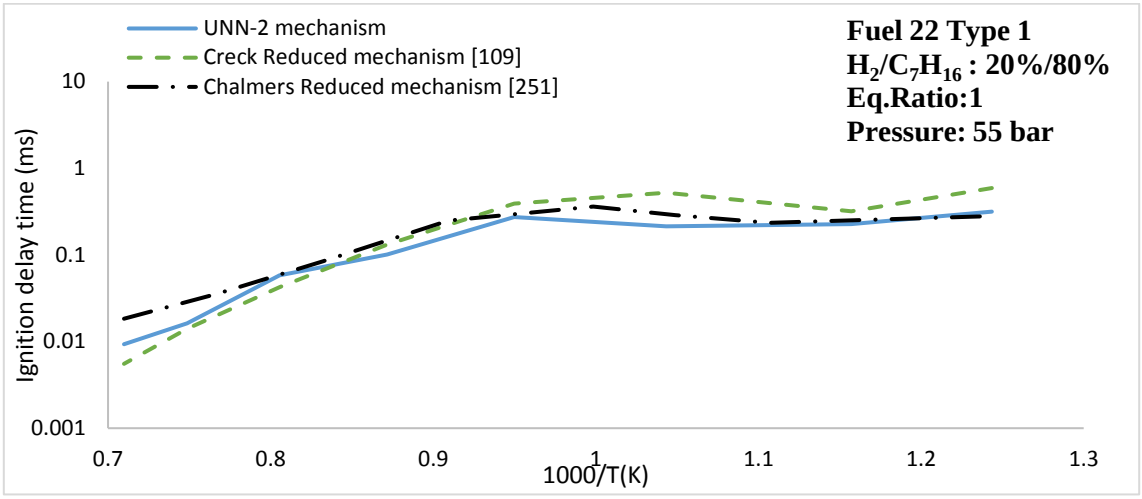

a)

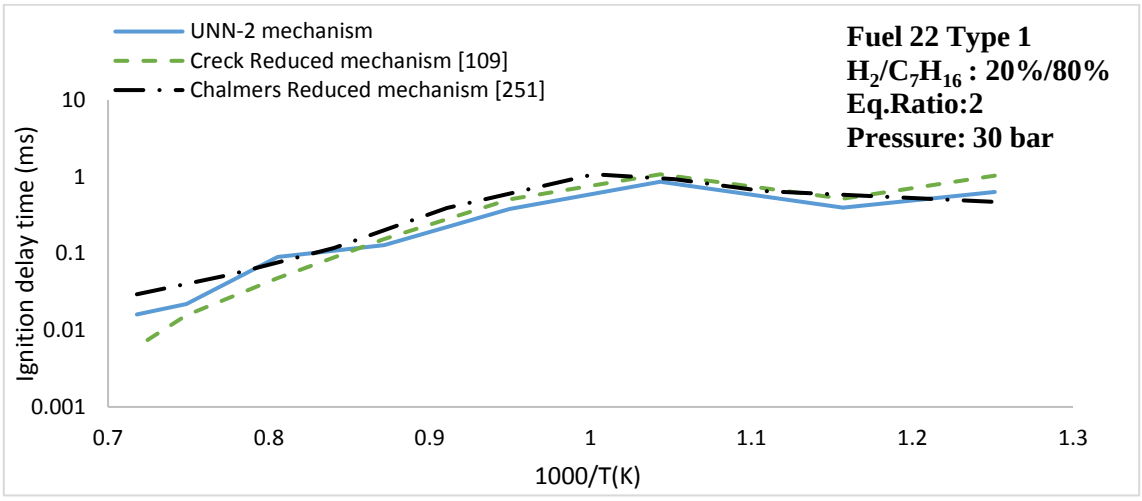

b)

Figure 6-27 Comparison of the simulated ignition delay times by using UNN-2 mechanism, Creck reduced mechanism [109] and Chalmers mechanism [251] for Fuel 22 Type 1 H_2/C_7H_{16}:20%/80% at a) P= 55 bar and eq. ratio 1.0 b)P=30 bar and equivalence ratio 2 and c) P=55 bar and equivalence ratio 2.

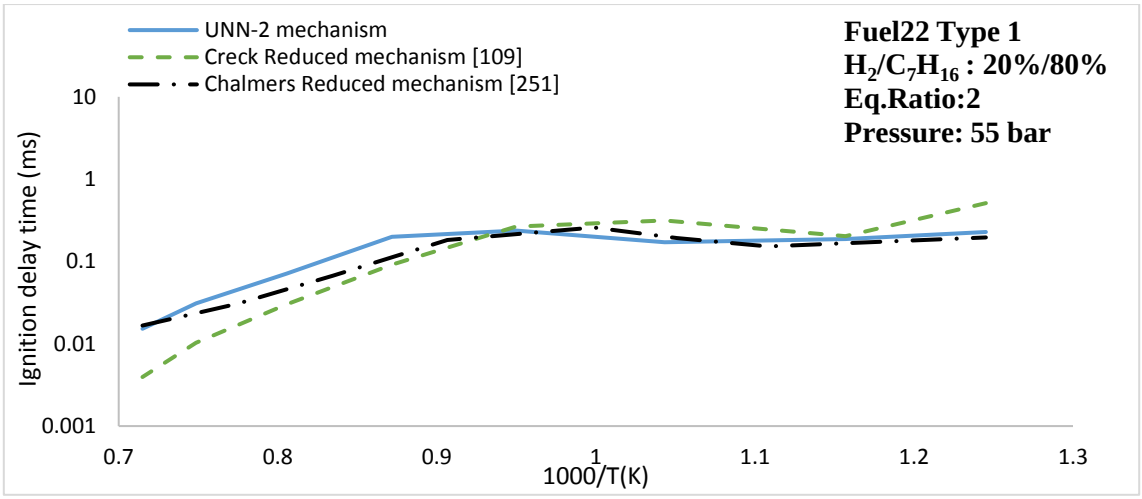

c)

Figure 6-27(cont.) Comparison of the simulated ignition delay times by using UNN-2 mechanism, Creck reduced mechanism [109] and Chalmers mechanism [251] for Fuel 22 Type 1 H_2/C_7H_{16}:20%/80% at a) P= 55 bar and eq. ratio 1.0 b)P=30 bar and equivalence ratio 2 and c) P=55 bar and equivalence ratio 2.

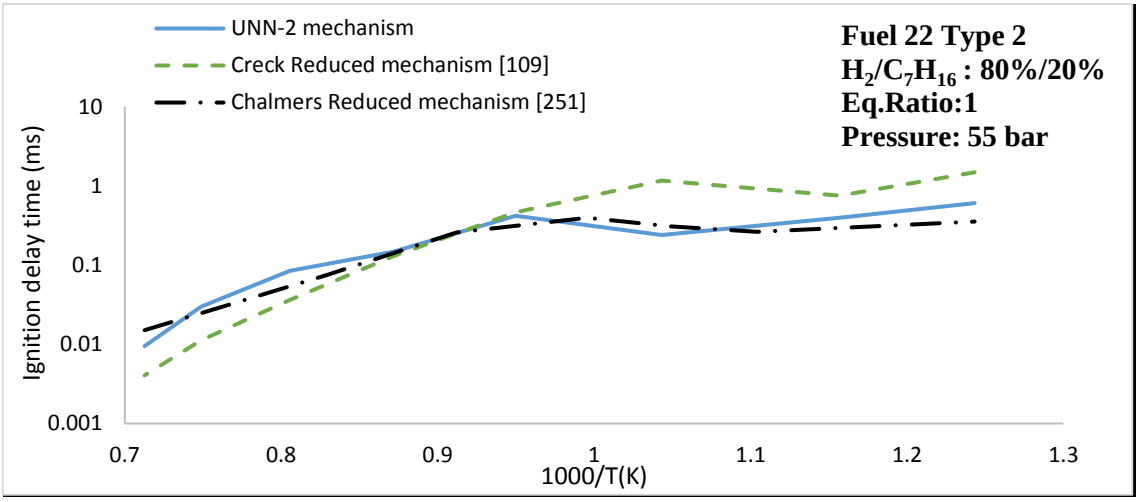

a)

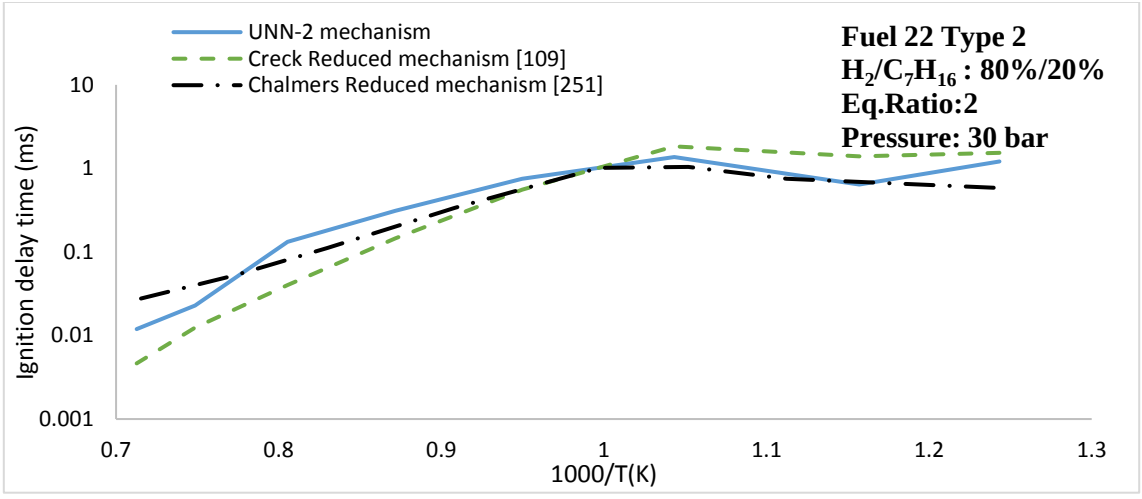

b)

Figure 6-28 Comparison of the simulated ignition delay times by using UNN-2 mechanism, Creck reduced mechanism [109] and Chalmers mechanism [251] for Fuel 22 Type 2 H_2/C_7H_{16}:80%/20% at a) P= 55 bar and eq. ratio 1.0 b)P=30 bar and equivalence ratio 2 and c) P=55 bar and equivalence ratio 2.

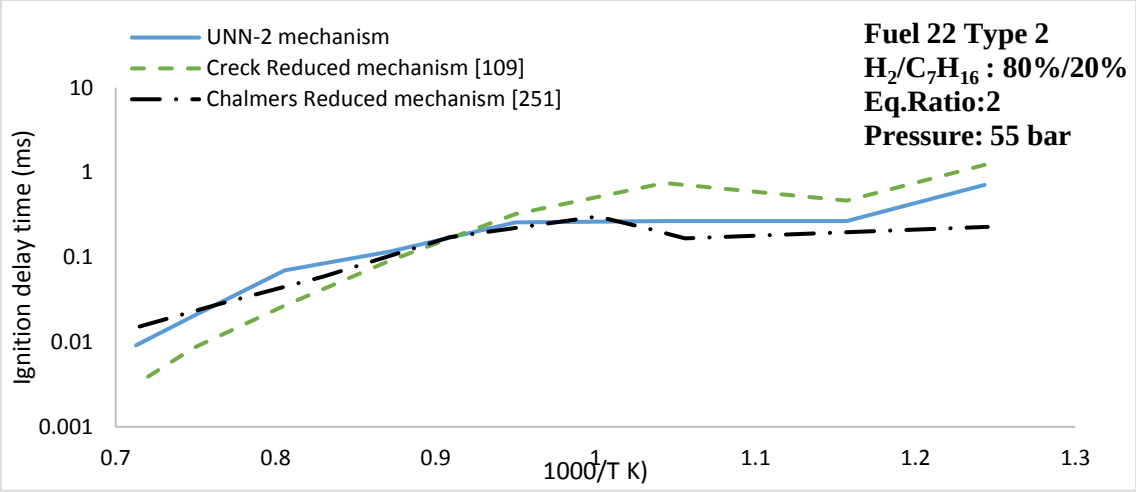

c)

Figure 6-28 Comparison of the simulated ignition delay times by using UNN-2 mechanism, Creck reduced mechanism [109] and Chalmers mechanism [251] for Fuel 22 Type 2 H_2/C_7H_{16}:80%/20% at a) P= 55 bar and eq. ratio 1.0 b)P=30 bar and equivalence ratio 2 and c) P=55 bar and equivalence ratio 2.

N-C_7H_{16}/CH_4 mixture

For further validation of the developed mechanism, the ignition delay times for three different NC_7H_{16}/CH_4 blends: a) Fuel 23 Type 1 80/20%, Fuel 23 Type 2 20/80% and Fuel 23 Type 3 5/95% at pressures 30 and 55 bar, equivalence ratios 0.5 and 1 and temperature range 800-1400 K were used. The results of the comparison between the numerical results of the UNN-2 mechanism, the Chalmers university mechanism [251] and the Creck n-heptane mechanism [109] are presented in Figure 6-29 for Fuel 23 Type 1, Figure 6-30 for Fuel 23 Type 2 and Figure 6-31 for Fuel 23 Type 3. Similar to the comparison of NC_7H_{16}/H_2 ignition delay times, UNN-2 and Chalmers mechanisms are in a good agreement at all of the tested conditions, while Creck mechanism is higher, especially during low to mid temperatures. Moreover, the UNN-2 mechanism accurately reproduces the effect of CH_4 and n-heptane addition on the ignition delay times; the higher the amount of CH_4 the higher is the ignition delay time, while the higher is the n-heptane, the lower is the ignition delay time at all of the pressures. This is due to the fact that the ignition or pyrolysis/oxidation chemistry of methane is slower compared to the heavy hydrocarbon fuels (e.g n-heptane) and therefore the ignition delay time required for fuels with higher amounts of CH_4 is larger [256, 257].

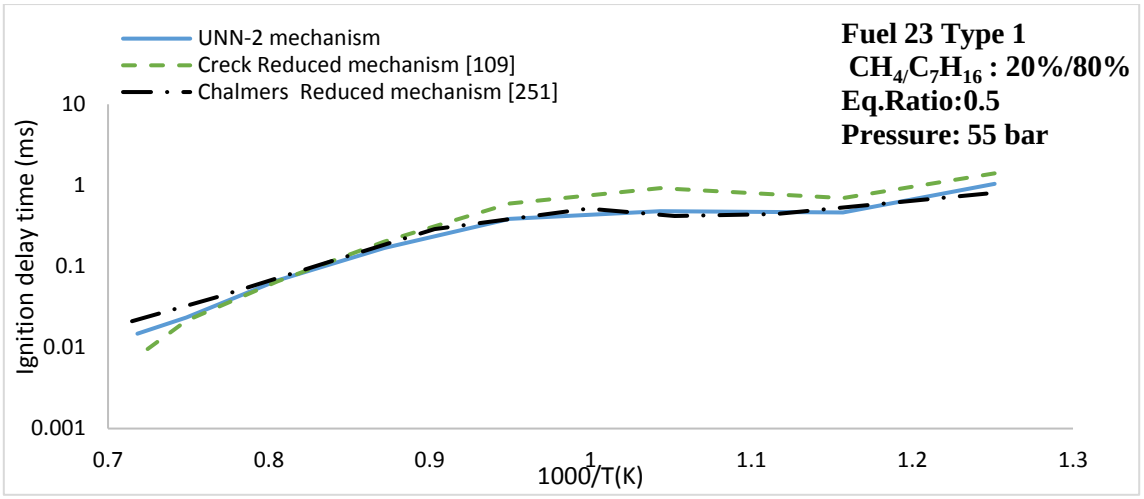

a)

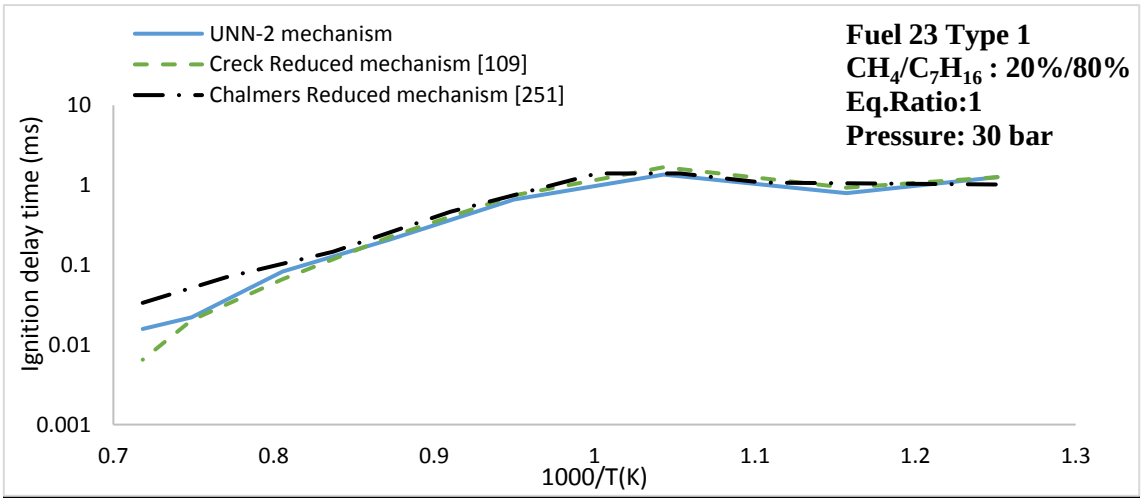

b)

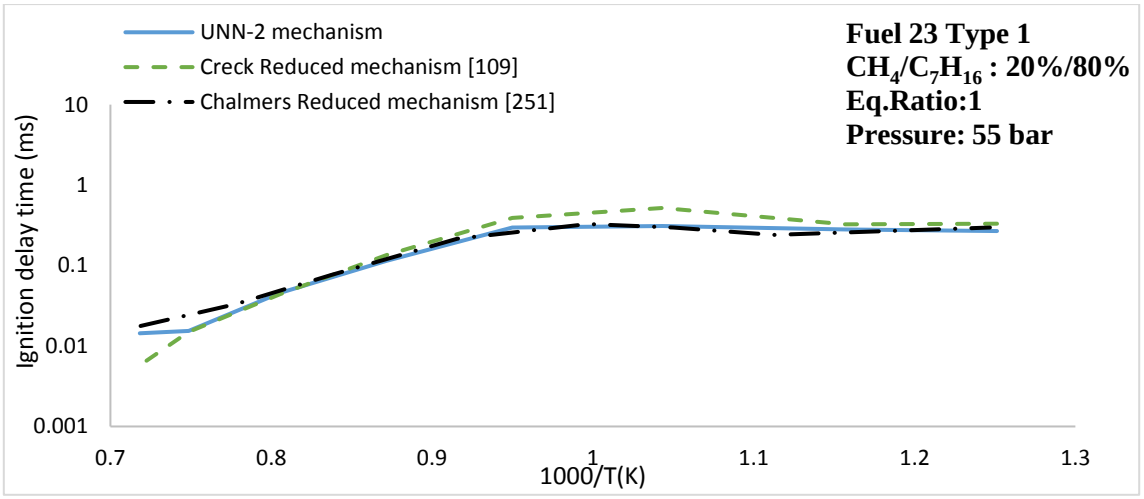

c)

Figure 6-29 Comparison of the simulated ignition delay times by using UNN-2 mechanism, Creck reduced mechanism [109] and Chalmers mechanism [251] for Fuel 23 Type 1, CH_4/C_7H_{16}:20%/80% ,at a) P= 55 bar and eq. ratio 0.5 b) P=30 bar and equivalence ratio 1 and c) P=55 bar and equivalence ratio 1.

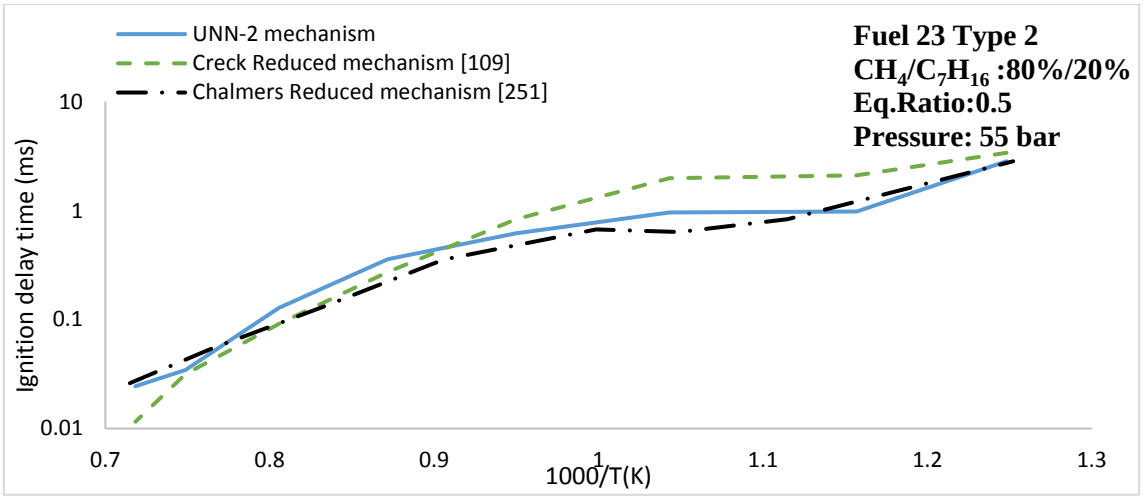

a)

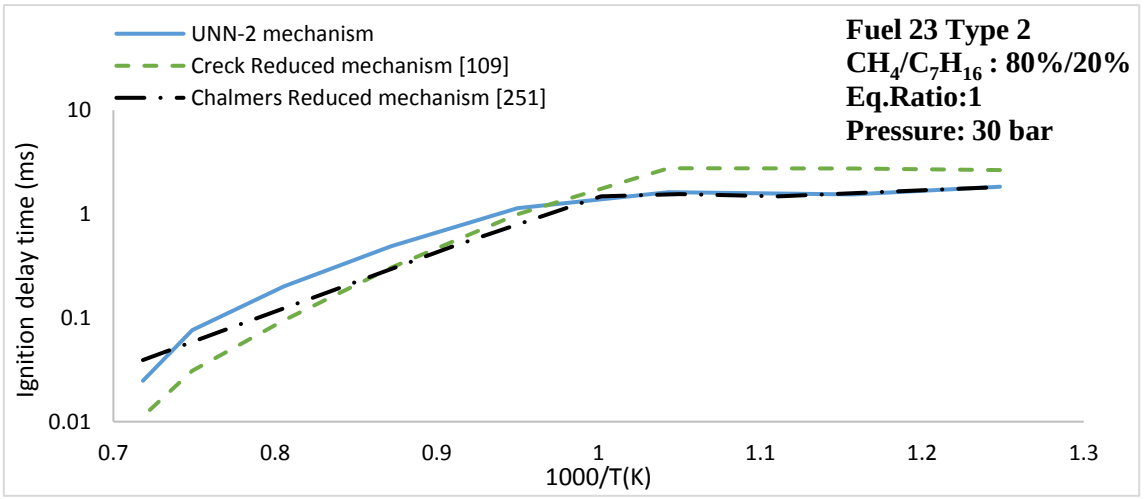

b)

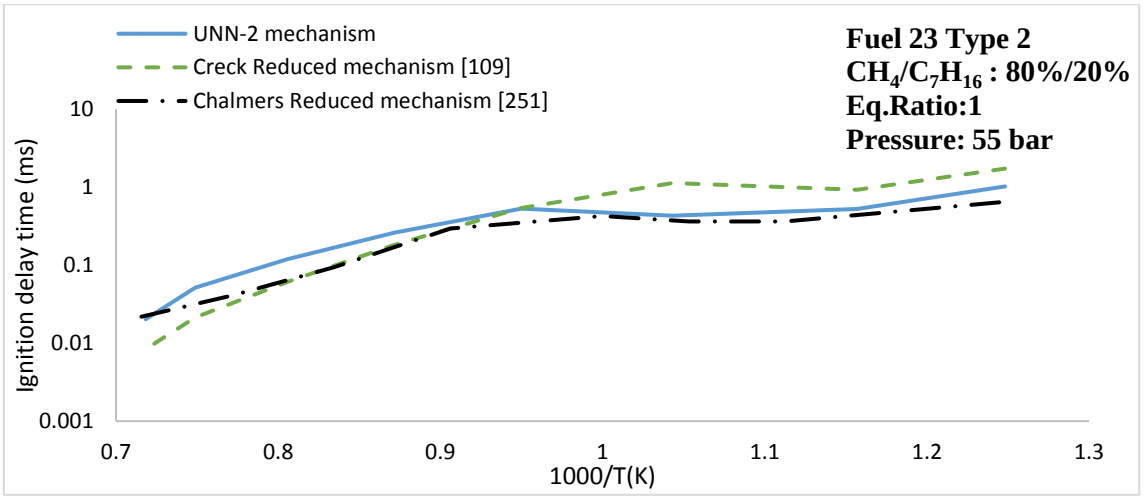

c)

Figure 6-30 Comparison of the simulated ignition delay times by using UNN-2 mechanism, Creck reduced mechanism [109] and Chalmers mechanism [251] for Fuel 23 Type 2, CH_4/C_7H_{16}:80%/20% at a) P= 55 bar and eq. ratio 0.5 b) P=30 bar and equivalence ratio 1 and c) P=55 bar and equivalence ratio 1.

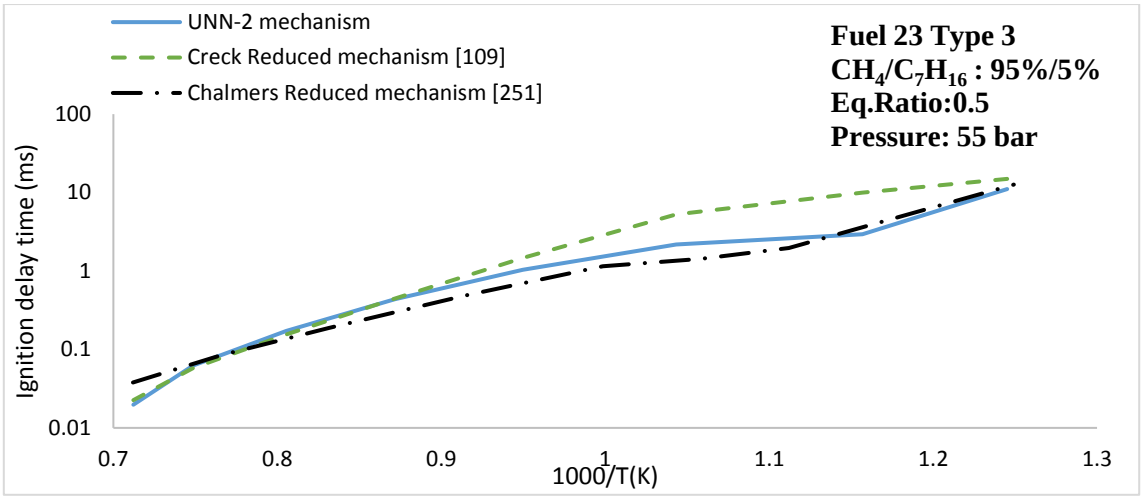

a)

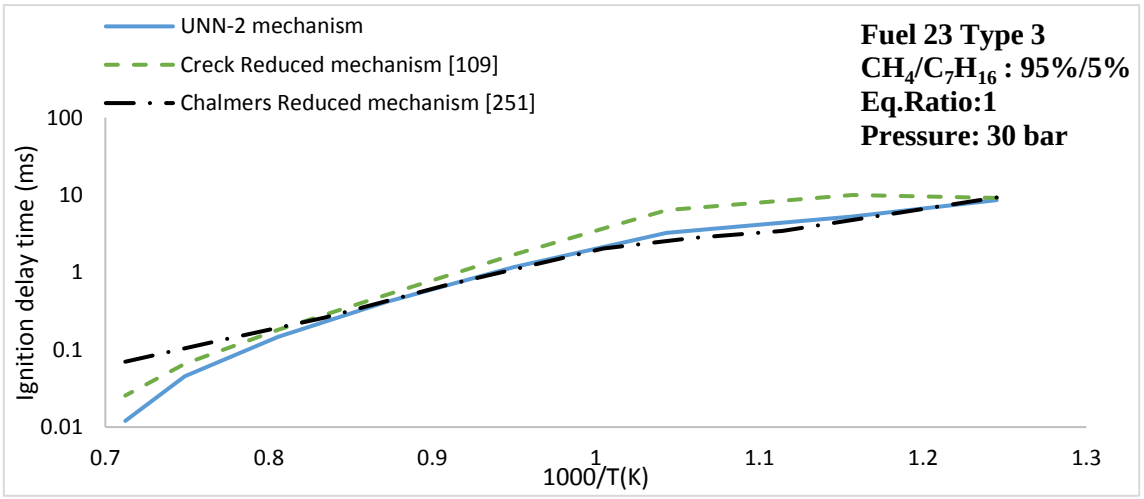

b)

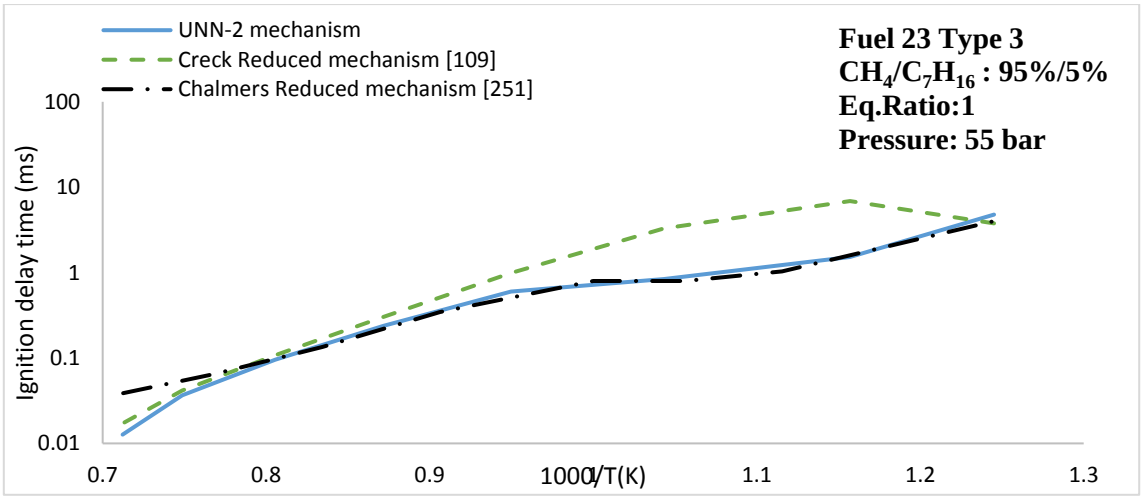

c)

Figure 6-31 Comparison of the simulated ignition delay times by using UNN-2 mechanism, Creck reduced mechanism [109] and Chalmers mechanism [251] for Fuel 23 Type 3, CH_4/C_7H_{16}:95%/5%, at a) P= 55 bar and eq. ratio 0.5 b) P=30 bar and equivalence ratio 1 and c) P=55 bar and equivalence ratio 1.

6.3.5 In-cylinder 3D combustion analysis

In this Chapter, for the modelling of the pilot-injected diesel spray, the ignition and the turbulent mixing representation, a combination of both the single-step global reaction based on the EBU mixing representation model and the n-heptane chemistry incorporated into the developed mechanism were used. First, for the n-heptane injection and the initial ignition, the single-step global reaction based on the EBU mixing was used. Then, the low and high temperature oxidation of the remaining amount of n-heptane during the combustion process and the co-oxidation with the premixed syngas fuel were simulated by using the developed chemical kinetics mechanism. Details about the spray model can be found in Chapter 3.

To validate performance of the developed UNN-2 mechanism to simulate the combustion of syngas derived from biomass and coke-oven solid feedstock in a micro-pilot ignited dual-fuel engine, a multidimensional computational fluid dynamic analysis (CFD) was performed. Six different types of syngas mixtures were used, Fuel 24 Types 1, 2, 3, 5, 6 and 7 presented in Table 3-3, each one was simulated by using different equivalence ratio and injection time. Moreover, the amount of injected n-heptane was 1.2 mg/cycle for mixtures Type 1, 2 and 3, and 3.0 mg/cycle for mixtures Type 5, 6 and 7.

In-cylinder pressure tracers and ROHR were used as quantitative measurements for the comparison between the simulated and experimental results, which are presented in Figures 6-32 to 6-37. The developed UNN-2 mechanism shows a good match with the experimental results at all of the equivalence ratios and injection times. However, for pure hydrogen (100%) Fuel 24 Type 7, Figure 6-37, the numerical ROHR increased very sharply and deviates from the experimental results, while the in-cylinder pressure tracers are in a good agreement in both of the conditions. Fuels with high hydrogen concentration tend to be more reactive especially at high temperature and pressure conditions in which more OH reactive radicals are formed. In order to investigate the reasons for the deviation between the simulated and experimental ROHR, ignition delay time and LFS simulations were performed for Fuel mixture 24 Type 7 (100% hydrogen), by using the RCM model in DARS. Simulated results by using the UNN-2 mechanism were compared with that obtained by using the mechanisms from O Connaire et al. [195] , Li et al. [232] and GRI Mech. 3.0 [26]. It is important to mention that both O Connaire et al. and Li et al. mechanisms were constructed for the simulation of pure hydrogen mixtures. The ignition delay time simulations were conducted at P= 20 and 40 bar, T=980-1162K and equivalence ratios 0.2 and 0.4. Ignition delay time comparisons are presented in Figure 6-38 for Fuel 24 Type 7 at equivalence ratio 0.2 and Figure 6-39 for Fuel 24 Type 7 at equivalence

ratio 0.4. Moreover, the LFS simulations were conducted at pressures 20 and 40 bar, temperature 450 K and equivalence ratios 0.2-1, and the comparisons are presented in Figure 6-40. The trend is similar for both ignition delay time and LFS simulations. The O Connaire et al. and Li et al. mechanisms show an identical trend while the UNN-2 mechanism and GRI Mech. 3.0 deviate. The deviation between the numerical results probably depends on the rate constants of specific hydrogen based reactions that were found to increase the reactivity of the mixture and control the formation of OH reactive radicals at high temperatures and pressure conditions. Such reactions are $H_2O_2+M=OH+OH$, $H_2+HO_2=H_2O_2+H$ and $HO_2+OH=>H_2O+O_2$, which were tested earlier in this study, showing very high sensitivity, especially at high pressure and temperature conditions. Moreover, the UNN-2 mechanism and GRI mech.3.0 include, not only hydrogen chemistry but also CO, CH_4 and NOx chemical pathways that affect the thermal stability of the mechanism. Further study is required for the investigation of the specific reactions that are responsible for that deviation and the optimization of their rate constants, in order to accurately simulate not only multicomponent syngas fuels but also pure hydrogen.

Although the reduced mechanism deviates from the experimental ROHR for pure hydrogen mixtures, the rest of the tested conditions were simulated very well for both in-cylinder pressure and ROHR.

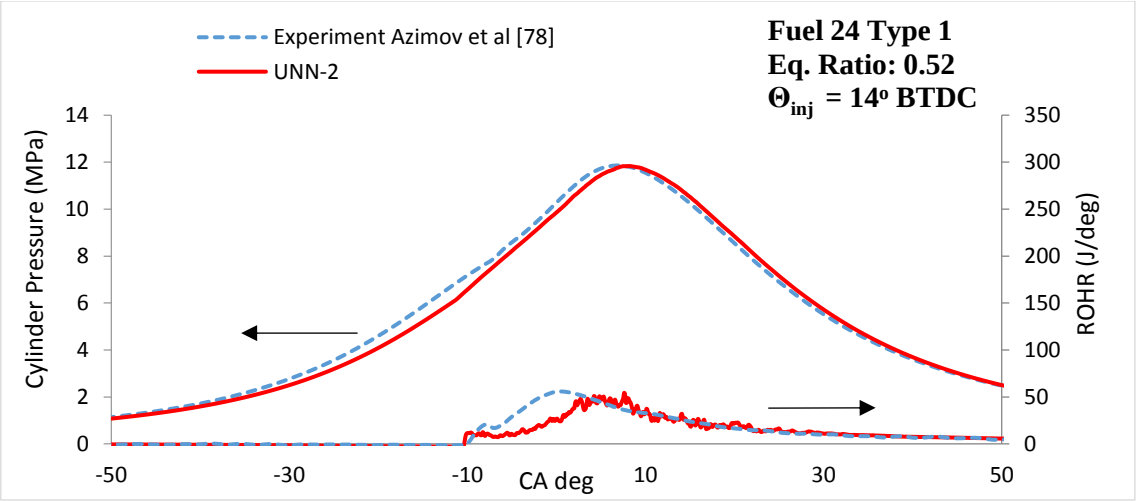

a)

Figure 6-32 Comparison of experimental and simulated in-cylinder pressure and heat release rate of dual-fuel micro-pilot ignited syngas combustion for Fuel 24 Type 1, Table 3-3

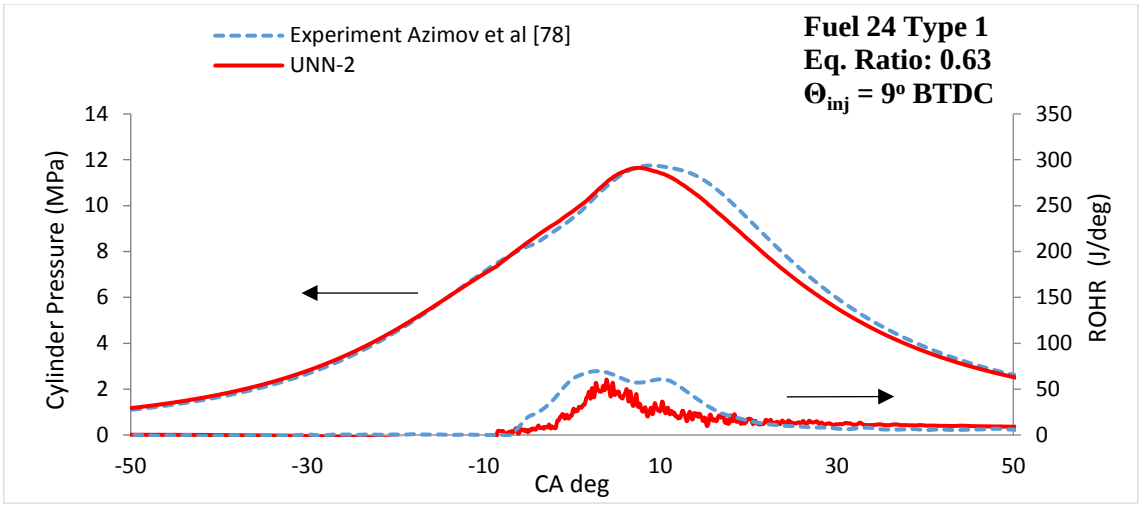

b)

Figure 6-32 (cont.) Comparison of experimental and simulated in-cylinder pressure and heat release rate of dual-fuel micro-pilot ignited syngas combustion for Fuel 24 Type 1, Table 3-3

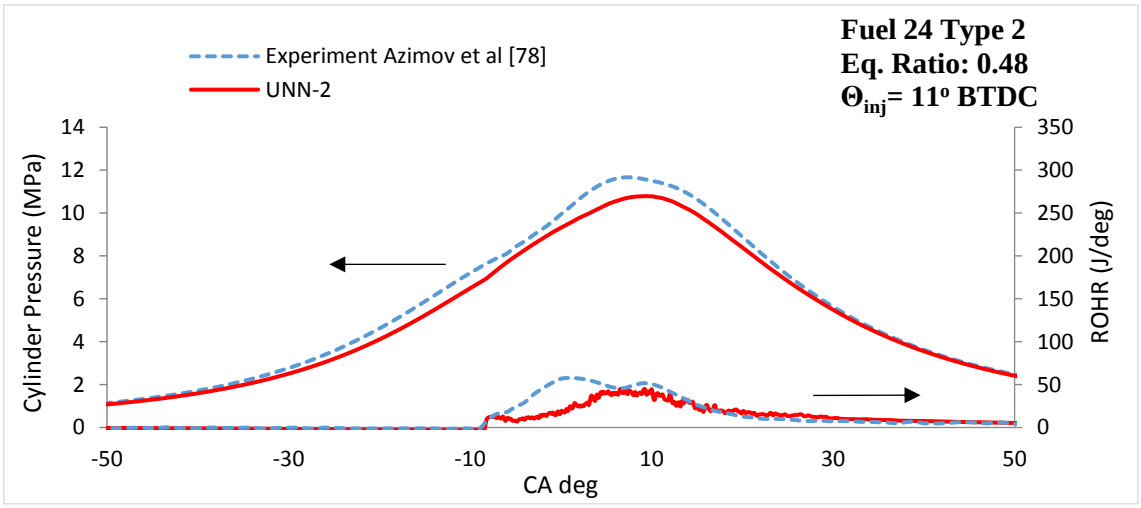

a)

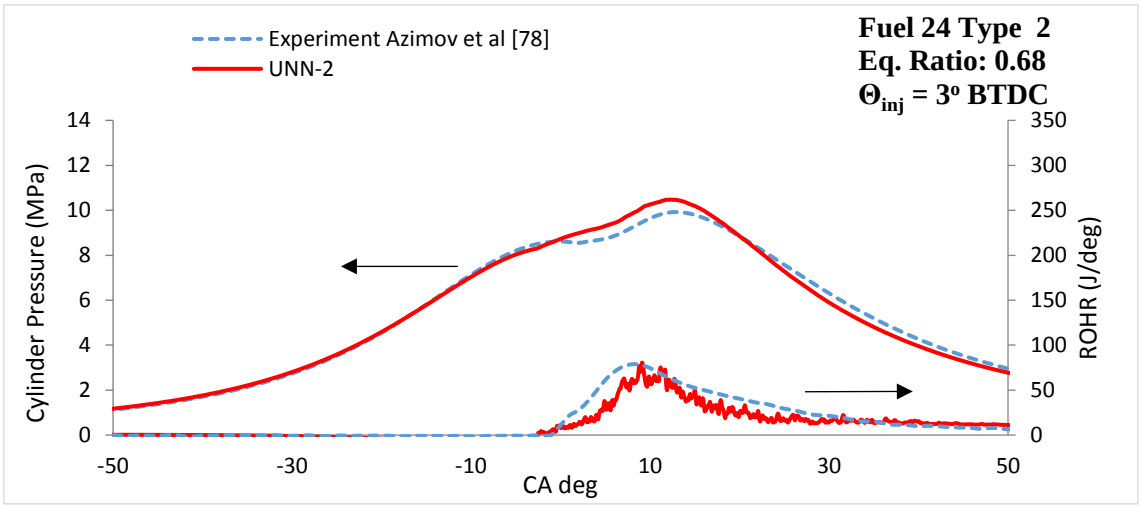

b)

Figure 6-33 Comparison of experimental and simulated in-cylinder pressure and heat release rate of dual-fuel micro-pilot ignited syngas combustion for Fuel 24 Type 2, Table 3-3

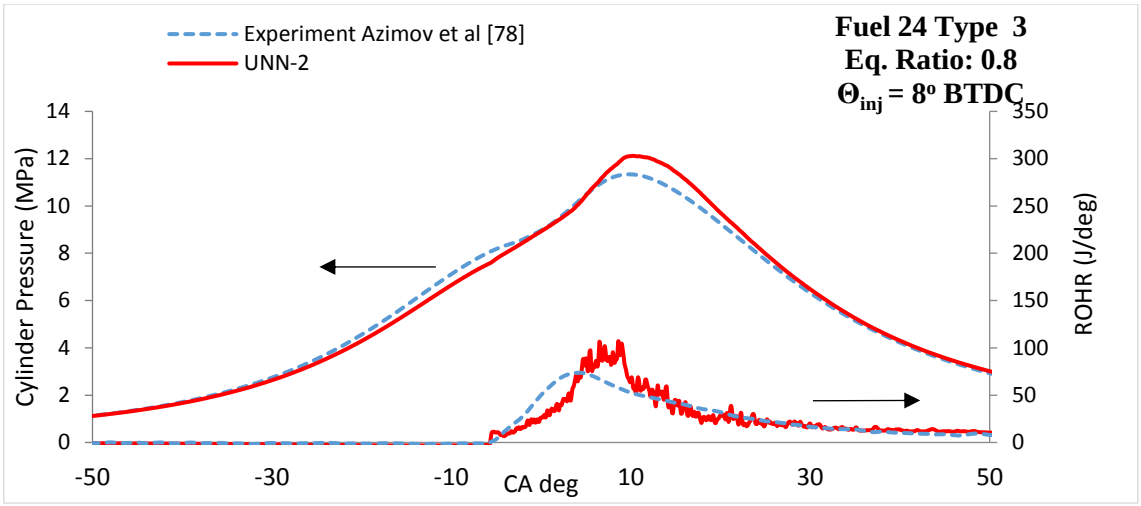

a)

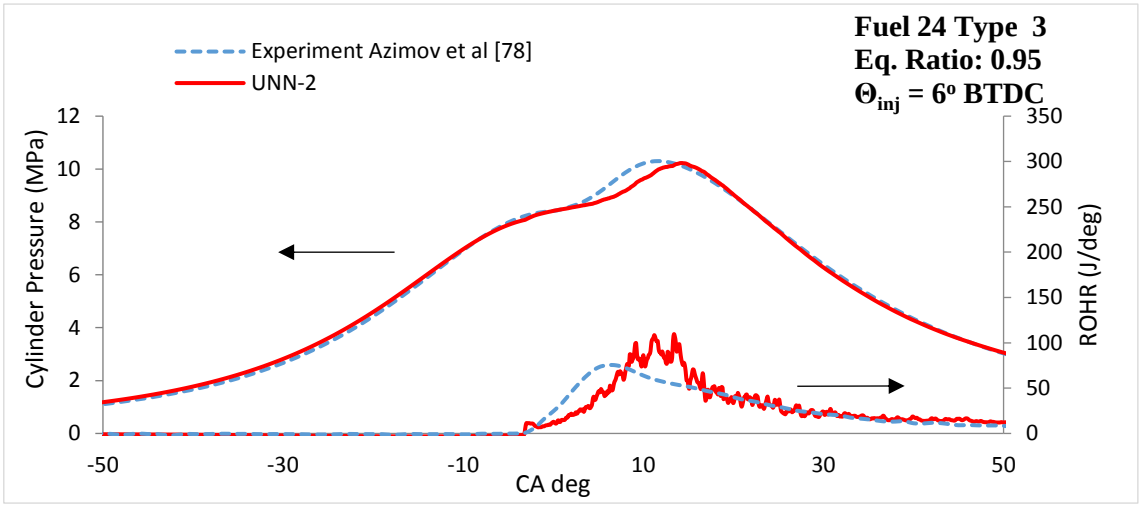

b)

Figure 6-34 Comparison of experimental and simulated in-cylinder pressure and heat release rate of dual-fuel micro-pilot ignited syngas combustion for Fuel 24 Type 3, Table 3-3.

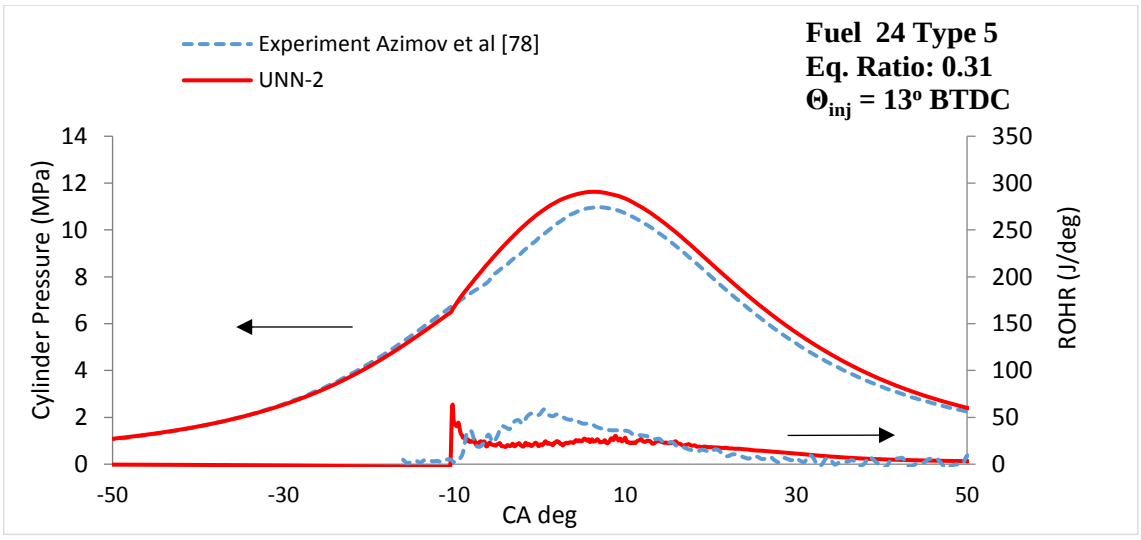

a)

Figure 6-35 Comparison of experimental and simulated in-cylinder pressure and heat release rate of dual-fuel micro-pilot ignited syngas combustion for Fuel 24 Type 5, Table 3-3

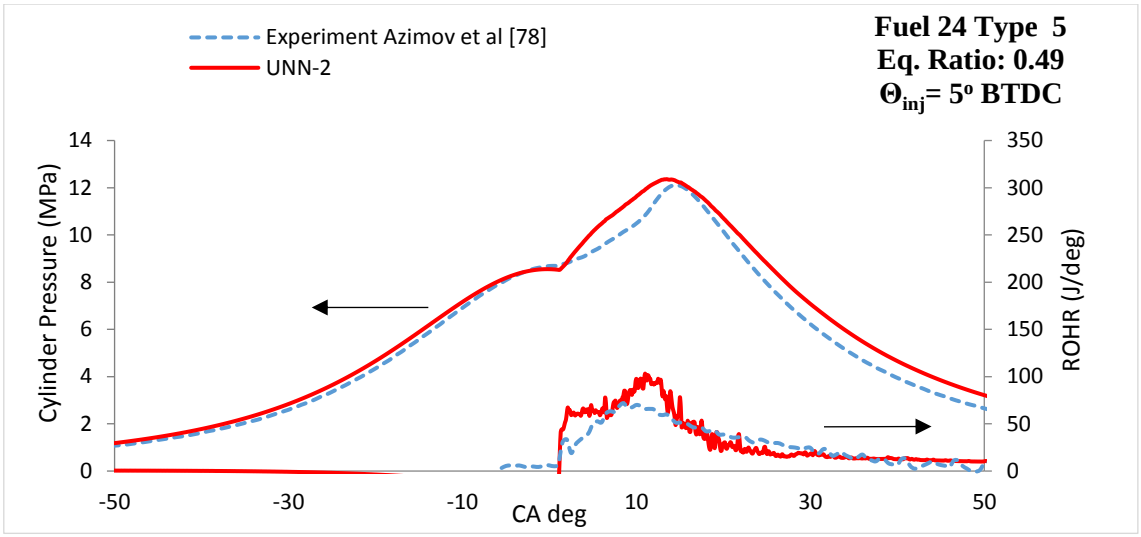

b)

Figure 6-35 (cont.) Comparison of experimental and simulated in-cylinder pressure and heat release rate of dual-fuel micro-pilot ignited syngas combustion for Fuel 24 Type 5, Table 3-3.

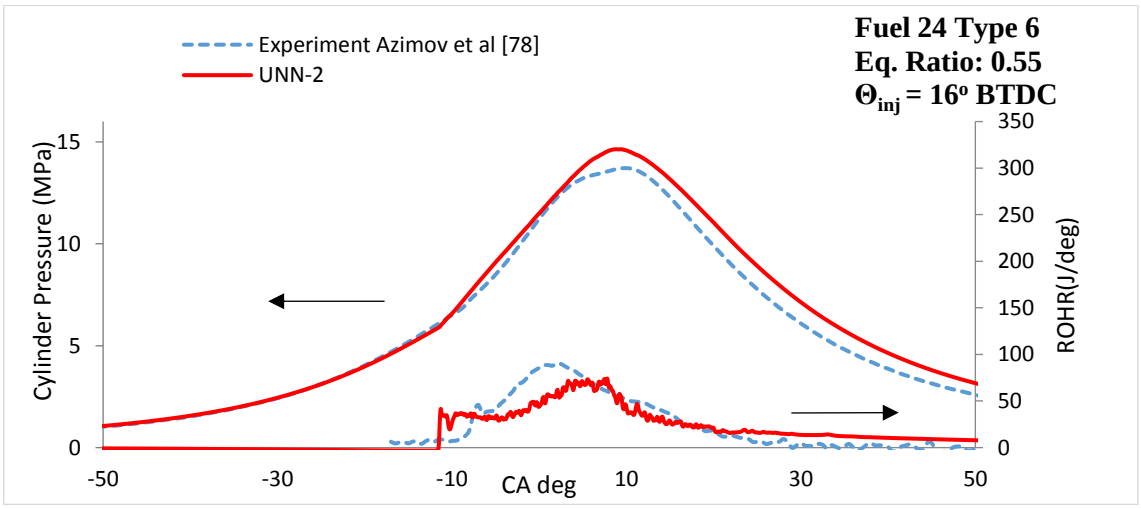

a)

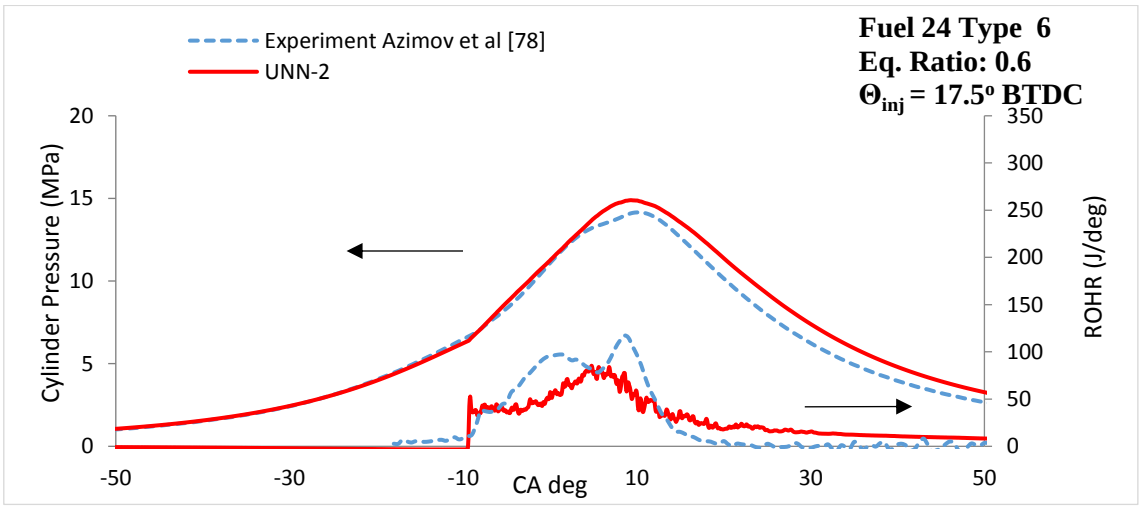

b)

Figure 6-36 Comparison of experimental and simulated in-cylinder pressure and heat release rate of dual-fuel micro-pilot ignited syngas combustion for Fuel 24 Type 6, Table 3-3.

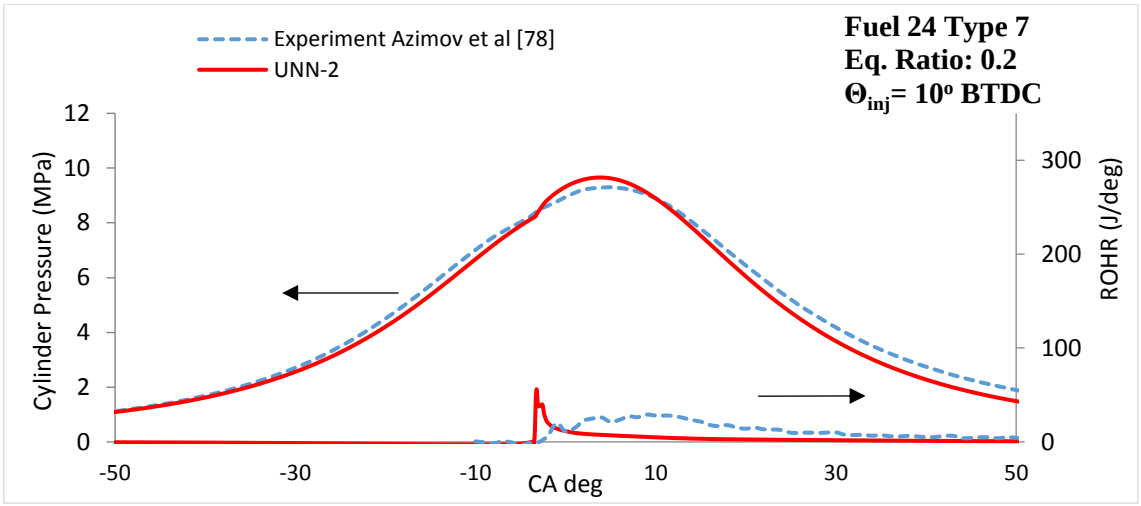

a)

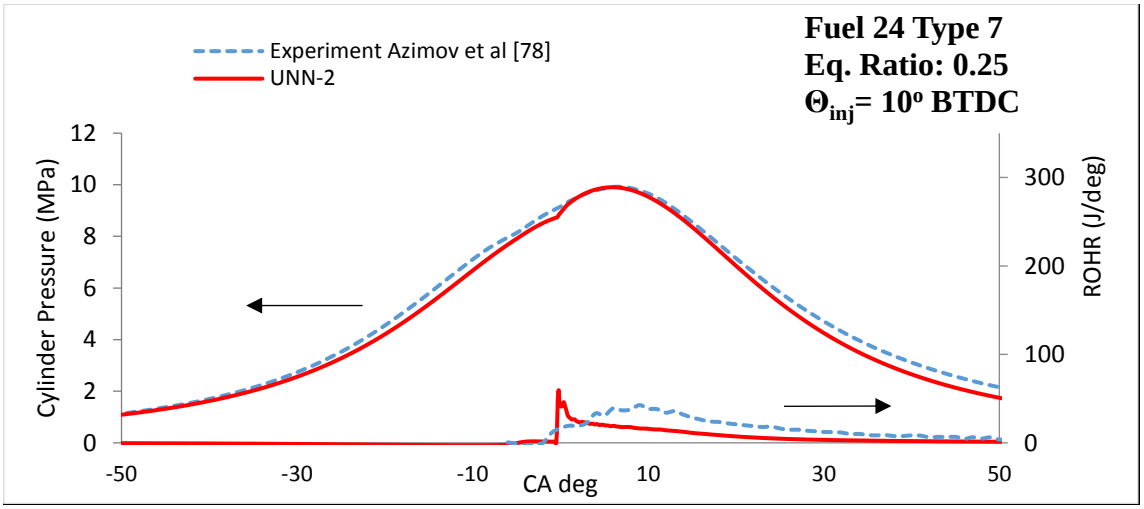

b)

Figure 6-37 Comparison of experimental and simulated in-cylinder pressure and heat release rate of dual-fuel micro-pilot ignited syngas combustion for Fuel 24 Type 7, Table 3-3.

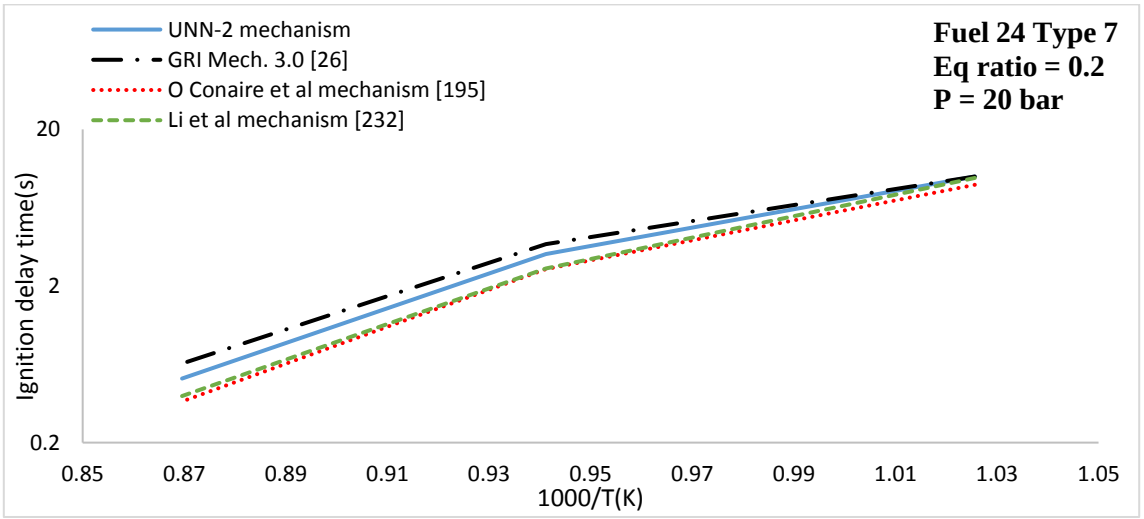

a)

Figure 6-38 Comparison of the simulated ignition delay times by using UNN-2 mechanism, GRI Mech. 3.0 [26], O Conaire mechanism [195] and Li mechanism [232] for Fuel 24 Type 7 at a) P= 20 bar and eq. ratio 0.2 and b)P=40 bar and equivalence ratio 0.2.

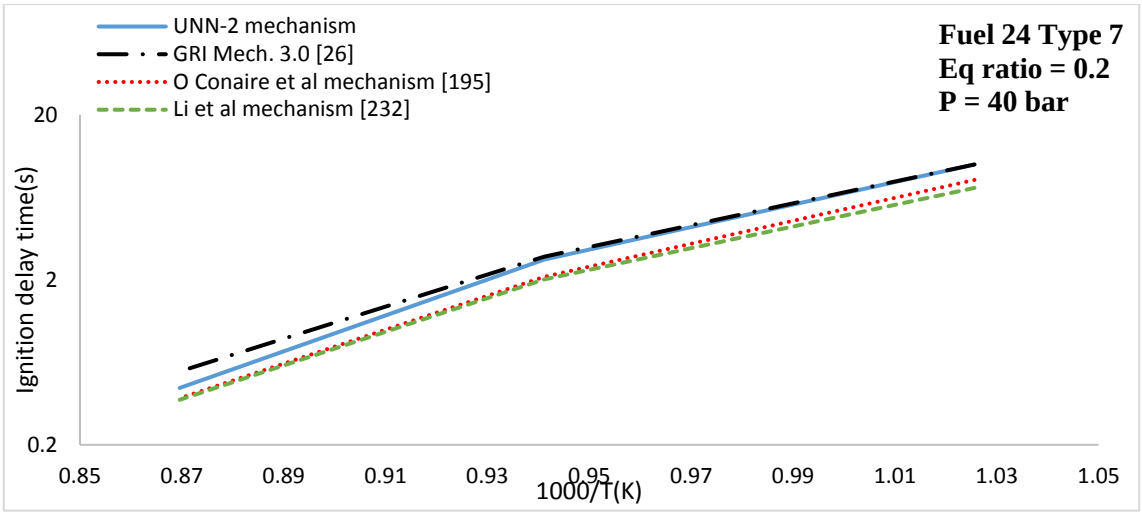

b)

Figure 6-38 (cont.) Comparison of the simulated ignition delay times by using UNN-2 mechanism, GRI Mech. 3.0 [26], O Conaire mechanism [195] and Li mechanism [232] for Fuel 24 Type 7 at a) P= 20 bar and eq. ratio 0.2 and b)P=40 bar and equivalence ratio 0.2.

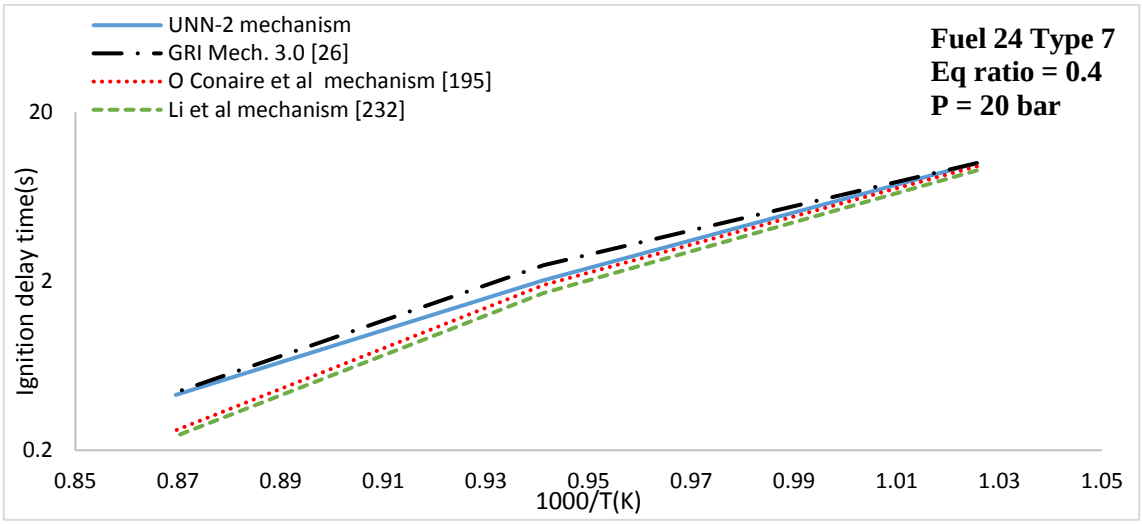

a)

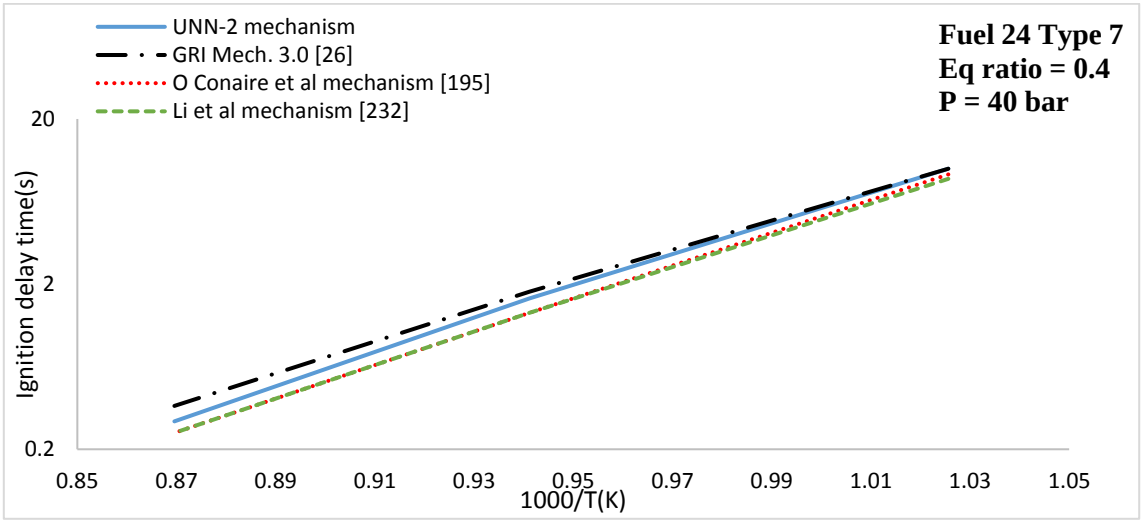

b)

Figure 6-39 Comparison of the simulated ignition delay times by using UNN-2 mechanism, GRI Mech. 3.0 [26] , O Conaire mechanism [195] and Li mechanism [232] for Fuel 24 Type 7 at a) P= 20 bar and eq. ratio 0.4 and b)P=40 bar and equivalence ratio 0.4.

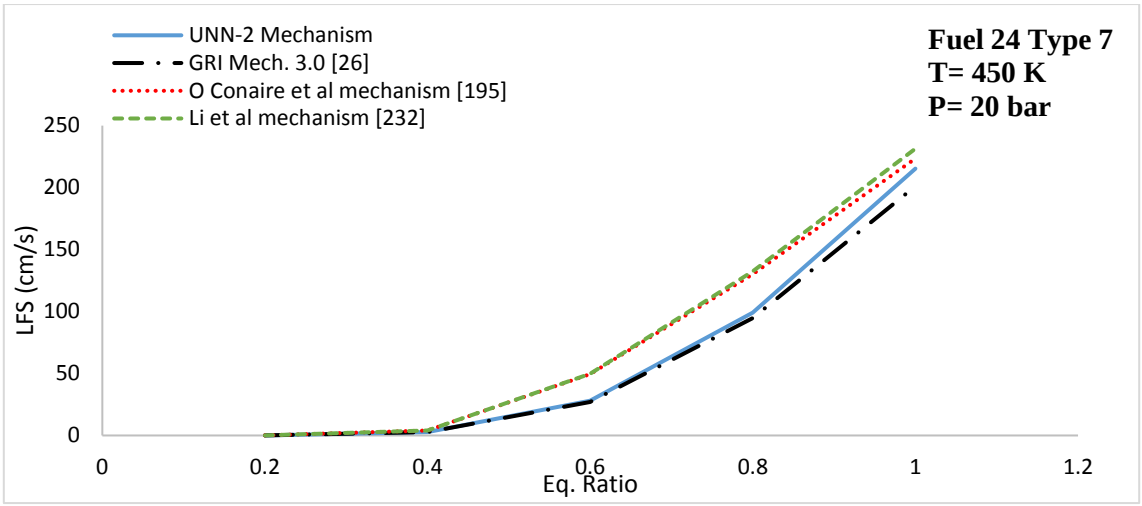

a)

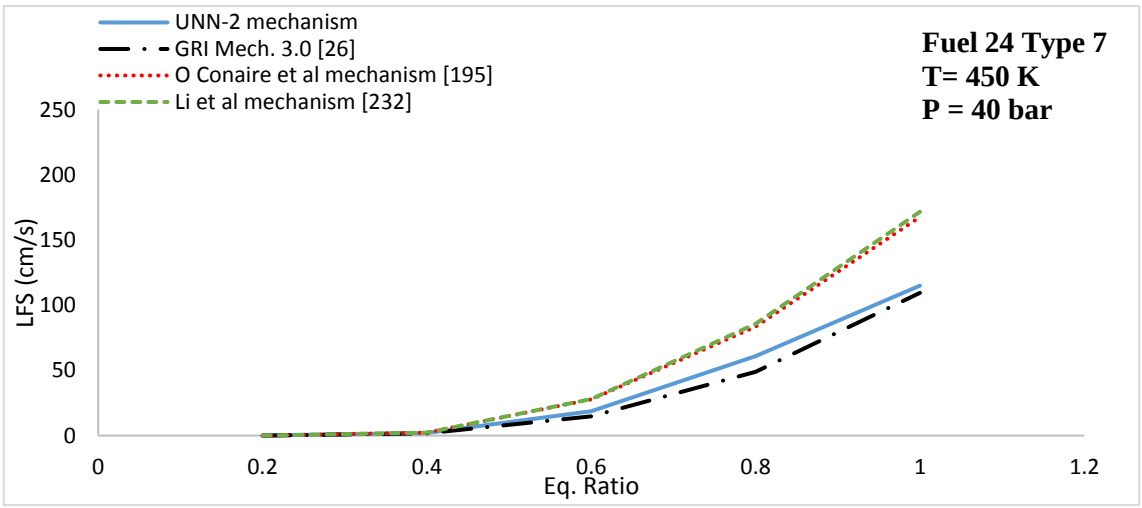

b)

Figure 6-40 Comparison of the simulated LFS by using UNN-2 mechanism, GRI Mech. 3.0 [26], O Conaire mechanism [195] and Li mechanism [232] for Fuel 24 Type 7 at a) P= 20 bar and T=450 K and b)P=40 bar and T= 450 K

The crank angle resolved in-cylinder spray and temperature distribution for syngas Fuel 24 Type 3 and Type 6 are shown in Figure 6-41 and Figure 6-42 respectively. The images show micro-pilot injected n-heptane spray development with further ignition and combustion of syngas. The maximum in-cylinder spatial temperature reached about 2200 K and it is seen that the flame front propagates towards the cylinder wall gradually consuming the unburned in-cylinder mixture and the fuel is fully burned.

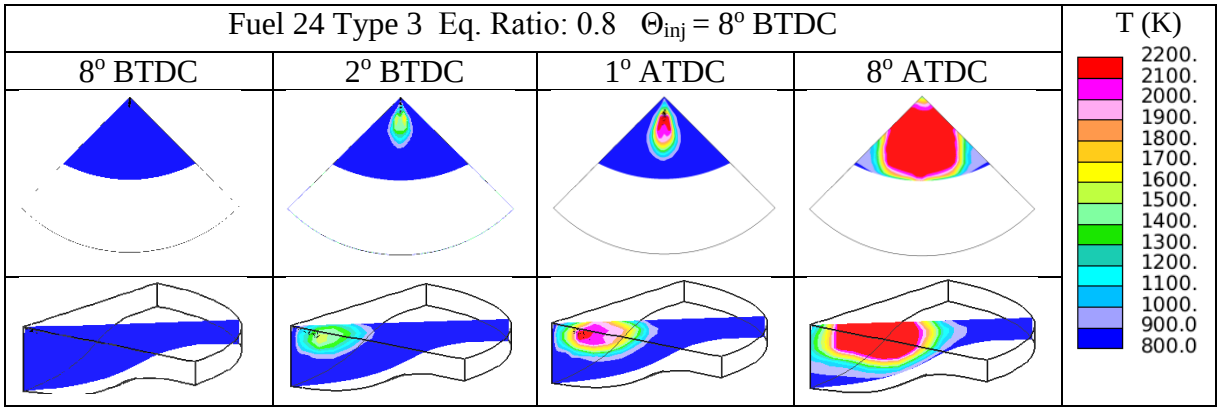

Figure 6-41 Sequential images of dual-fuel micro-pilot ignited syngas combustion with new kinetics mechanism. Fuel 24 Type 3 eq. ratio 0.8, Θinj = 8° BTDC

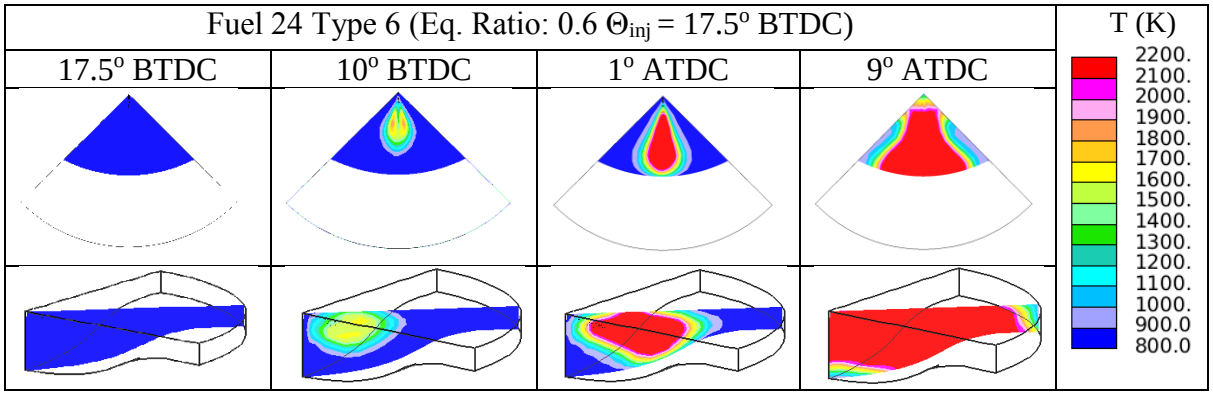

Figure 6-42 Sequential images of dual-fuel micro-pilot ignited syngas combustion with new kinetics mechanism. Fuel 24 Type 6 eq. ratio 0.6, Θinj 17.5° BTDC.

6.4 Summary

In this chapter, a reduced n-heptane/syngas /NOx mechanism has been developed for modelling n-heptane/syngas co-oxidation, syngas combustion and NOx formation in a micro-pilot injected dual-fuel engine. For n-heptane chemistry, the comprehensive Creck modelling n-heptane mechanism was selected and reduced by using necessity analysis. Moreover, the sensitivity of the ignition delay times of pure n-heptane and syngas mixtures on important hydrogen based, methane based and n-heptane based reactions was investigated. Reactions such as $H_2O_2+M=OH+OH$, $H_2+HO_2=H_2O_2+H$ and $HO_2+OH=>H_2O+O_2$ were found to affect not only the ignition delay times by using syngas as a fuel but also the n-heptane ignition delay times. Moreover, CH_4 based reactions were found to affect both n-heptane oxidation and syngas combustion. This is an indicator that CH_4 chemistry should be taken into account even if the amount of CH_4 in the mixture is very low. On the other hand, n-heptane reactions are very important for n-heptane oxidation but they have negligible effect on syngas combustion. Due to the fact that syngas reactions were already validated and tested, the rate constants of only the n-heptane based reactions were modified and adjusted in the developed mechanism.

The developed mechanism was validated in terms of ignition delay times, LFS and NO concentration profiles for three different types of fuel mixtures; a) pure n-heptane, b) n-heptane/syngas and c) syngas, showing a good agreement at all of the tested conditions. Moreover, the mechanism was shown to accurately capture the effect of the pressure, temperature and equivalence ratio on the tested combustion parameters. Finally, a multidimensional analysis study was performed to evaluate the performance of the developed mechanism on modelling n-heptane/syngas co-oxidation and syngas combustion in a micro-pilot injected a dual-fuel engine. The mechanism shows a good agreement with the experimental in-cylinder pressure and ROHR data for all of the tested syngas mixtures. However, when using pure hydrogen as the mixture, the UNN-2 mechanism shows a rapid and sudden increase of the ROHR and deviates from the experimental data at both of the tested equivalence ratios. Further analysis has been performed to understand the reasons for this deviation by comparing the ignition delay time and LFS of pure hydrogen obtained by using the UNN-2 mechanism and different hydrogen chemical kinetics mechanisms. It was found that due to the higher mixture reactivity, the rate constants of the reactions responsible for the formation of OH radicals (e.g $H_2O_2+M=OH+OH$, $H_2+HO_2=H_2O_2+H$ and $HO_2+OH=>H_2O+O_2$) should be optimized.

Although the reduced mechanism shows relative high deviation with the experimental results for pure hydrogen mixtures, the rest of the tested conditions were simulated very well for both in-cylinder pressure and ROHR.

Therefore, it can be concluded that the developed mechanism offers an accurate, robust and computational efficient solution for the simulation of multicomponent syngas mixtures, NOx formation and n-heptane/syngas co-oxidation, while further study is required for the simulation of pure hydrogen mixtures.

Chapter 7: Conclusions and future work

7.1 Conclusions

The overall aim of this project was the development of an up-to date, robust and reduced chemical kinetics mechanism for the simulation of the co-oxidation of syngas and n-heptane and NOx formation in a micro-pilot ignited dual-fuel engine. During this project, three different chemical kinetics mechanisms were developed; a) a reduced syngas mechanism consisting of 32 reactions (Chapter 4), b) a reduced syngas/NOx mechanism consisting of 44 reactions (Chapter 5) and c) a reduced n-heptane/syngas/NOx mechanism consisting of 276 reactions (Chapter 6). For reasons of simplicity, the key conclusions obtained from each Chapter of this thesis are summarized and presented in different paragraphs.

The key conclusions obtained during the development of the reduced syngas mechanism, Chapter 4: Development of a reduced chemical kinetics mechanism for syngas combustion in a micro-pilot ignited dual-fuel engine.

- For the analysis of the combustion chemistry and the identification of the important reactions affecting the combustion process, a sensitivity analysis study was conducted. According to this analysis, syngas combustion is driven mostly by hydrogen chemistry with significant contribution from carbon and methane chemistry.
- The developed reduced syngas mechanism was validated against various experimental data and different chemical kinetics mechanisms developed by other researchers.
- The effect of CO and H_2 concentration on the ignition delay times of syngas is captured accurately by the reduced mechanism; The results show that the higher the concentration of CO in the syngas, the higher the ignition delay time while the higher is the concentration of H_2 the lower is the ignition delay time.
- The reduced mechanism predicts well the effect of the methane concentration on the reactivity of the mixture and on the development of LFS; The higher the concentration of methane, the lower the reactivity of the mixture and therefore the lower the LFS.
- Multidimensional CFD analysis was performed for the simulation of syngas combustion in a micro-pilot ignited dual-fuel engine. The developed mechanism accurately predicted the experimental ROHR and in-cylinder pressure for hydrogen concentrations lower than 50%vol and required the lowest CPU time

for a complete CFD simulation compared to similar mechanisms developed by other authors.

- For H_2 higher than 50%vol (syngas produced from coke oven feedstock), the developed mechanism over-predicts the experimental data. Therefore, for the accurate simulation of the combustion of this type of syngas, the rate constant of reaction $H_2O_2+H=H_2+HO_2$ was modified.

Chapter 5: Development of an updated chemical kinetics mechanism for syngas combustion and NOx formation in a micro pilot ignited dual fuel engine.

- For the development of the reduced syngas/NOx mechanism, mechanism for lower hydrogen concentrations developed in Chapter 4 was optimized by incorporating a 12-step NOx sub-mechanism and by updating the rate constants of reactions $H_2O_2(+M)=OH+OH(+M)$ and $H_2O_2+H=H_2+HO_2$, that were found to be very sensitive during high pressure conditions.
- Important species affecting NOx formation were investigated by conducting a species sensitivity analysis with respect to NOx. According to this analysis, hydrogen, oxygen, nitrogen and carbon based species were identified to be critical for NOx formation. Interestingly, CH4 was also found to be important for NOx formation, even in trace amounts (>2%vol).
- The proposed mechanism was validated against experimental measurements and against modeling results obtained by other researchers. This mechanism showed high level of accuracy and low deviation for ignition delay time, laminar flame speed and NO concentration profiles.
- The syngas/NOx mechanism was applied to a multidimensional CFD simulation for the prediction of syngas combustion in a micro-pilot-ignited supercharged dual-fuel engine. For all of the conditions, the reduced syngas/NOx mechanism showed very good agreement with the experimental in-cylinder pressure and ROHR.
- The developed reduced syngas/NOx mechanism required the lowest CPU time (only 2.5 hours) compared to Keromnes mechanism [21] (3 hours). The mechanisms developed by Frassoldati et al [207] and by Gas Research Institute (GRI Mech. 3.0) [26] required 16.5 hours and 24 hours respectively.

Chapter 6: Development of a reduced n-heptane/syngas/NOx mechanism for syngas combustion, n-heptane/syngas co-oxidation and NOx formation in a micro-pilot ignited dual-fuel engine.

- For n-heptane chemistry, different n-heptane mechanisms from the literature were numerically tested and the mechanism proposed by Creck modelling group showed the highest accuracy and therefore was chosen for further reduction.
- The reduction was achieved by using necessity analysis. The new skeletal mechanism generated from the necessity analysis was then coupled with the reduced syngas/NOx mechanism proposed in Chapter 5
- In order to improve the performance of the new coupled reduced mechanism, the rate constants of important n-heptane based reactions such as $NC_7H_{16}+OH=C_7H_{15}+H_2O$, $NC_7H_{16}+HO_2=C_7H_{15}+H_2O_2$ and $NC_7H_{15}+O_2=C_7H_{15}O_2$ were modified based on the approach proposed by Ra and Reitz et al [100].
- Various experimental measurements, which were collected from the literature, for syngas combustion, n-heptane oxidation, syngas/n-heptane co-oxidation and NOx formation were used for validation purposes. In addition, modelling results obtained by other authors, were used. The comparisons between the simulated and experimental results show that the proposed mechanism simulates accurately the experimental and modeled results.
- The new reduced n-heptane/syngas/NOx mechanism was used in a multidimensional CFD code for the simulation of syngas combustion in a micro-pilot ignited dual-fuel engine. In contrast to the CFD simulations conducted in Chapters 4 and 5, the amount of the injected n-heptane was not only 1.2 mg/cycle but also 3.0 mg/cycle. The mechanism accurately predicts the experimental in-cylinder pressure and ROHR for all of the conditions investigated in this thesis. However, when pure hydrogen mixtures are used, the mechanism shows a significant deviation from the experiments. The deviation mainly depends on hydrogen based reactions and especially on the reactions producing high reactive OH radicals.

Each mechanism developed during this research can be used as a standalone tool for the simulation of the combustion processes, combustion chemistry and its interactions with the turbulence. The low number of reactions, robustness and the high level of accuracy of the developed mechanisms make them powerful tools for engine developers.

The reduced n-heptane/syngas/NOx mechanism can be used successfully for the simulation of not only syngas combustion, NOx formation and n-heptane/syngas co-oxidation during dual fuel combustion, but also for the simulation of LTC, NTC and high temperature oxidation of n-heptane. As it was already mentioned in this thesis, detailed n-heptane mechanisms developed by other authors include high number of reactions, have high level of complexity and require large amount of time for a complete simulation. Therefore, it can be concluded that the developed reduced mechanism offers computational efficiency, lower complexity and accuracy.

7.2 Future work

As mentioned in Chapter 6, the reduced n-heptane/syngas/NOx mechanism deviates from the experimental ROHR for pure hydrogen mixtures when used in multidimensional CFD simulations. The deviation is mainly due to the value of rate constants of important hydrogen-based reactions responsible for the formation and consumption of highly reactive OH radicals. Therefore, investigation of the combustion chemistry during pure hydrogen combustion and optimization of the rate constants of reactions are highly recommended to improve the performance of the constructed mechanism in predicting combustion in micro-pilot ignited dual-fuel engines.

In addition, during the CFD simulations, for all of the three mechanisms the range of equivalence ratios was kept below 1.0. For a future work, it would be beneficial to test the combustion and emission performance of the reduced mechanism using richer syngas mixtures (eq. ratio >1.0. Despite the progress that has been made throughout the years in the sector, more experimental studies are needed to validate the proposed mechanisms at different equivalence ratios and richer conditions.

Furthermore, there is a need for more experimental measurements of different n-heptane/syngas and multicomponent syngas mixtures. At the moment no experimental studies for n-heptane/syngas co-oxidation can be found and therefore the developed mechanisms was validated only against available numerical results. During this thesis laminar flame speed, in-cylinder pressure, ignition delay time and NO concentration were used as quantitative metrics for the validation of the developed mechanisms. However, in order to improve further the

performance of the mechanisms and analyse in detail the combustion chemistry and NOx formation, more experimental measurements are needed for the in-cylinder temperature and individual species profiles.

References

1. Shilling, N.Z. and Lee, D.T., IGCC-clean power generation alternative for solid fuels. PowerGen Asia, Ho Chi Minh City, Vietnam, September, 2003: p. 23-25.
2. Azimov, U., Okuno, M., Tsuboi, K., Kawahara, N., and Tomita, E., Multidimensional CFD simulation of syngas combustion in a micro-pilot-ignited dual-fuel engine using a constructed chemical kinetics mechanism. international journal of hydrogen energy, 2011. 36(21): p. 13793-13807.
3. Nikolaou, Z.M., Chen, J.-Y., and Swaminathan, N., A 5-step reduced mechanism for combustion of CO/H 2/H 2 O/CH 4/CO 2 mixtures with low hydrogen/methane and high H 2 O content. Combustion and flame, 2013. 160(1): p. 56-75.
4. Raibhole, V.N. and Sapali, S., Simulation and parametric analysis of cryogenic oxygen plant for biomass gasification. Mechanical Engineering Research, 2012. 2(2): p. 97.
5. Chaos, M. and Dryer, F.L., Syngas combustion kinetics and applications. Combustion Science and Technology, 2008. 180(6): p. 1053-1096.
6. Azimov, U., Tomita, E., Kawahara, N., and Harada, Y., Premixed mixture ignition in the end-gas region (PREMIER) combustion in a natural gas dual-fuel engine: operating range and exhaust emissions. International Journal of Engine Research, 2011. 12(5): p. 484-497.
7. Sahoo, B.B., Saha, U.K., and Sahoo, N., Theoretical performance limits of a syngas–diesel fueled compression ignition engine from second law analysis. Energy, 2011. 36(2): p. 760-769.
8. Sahoo, B.B., Sahoo, N., and Saha, U.K., Effect of H 2: CO ratio in syngas on the performance of a dual fuel diesel engine operation. Applied Thermal Engineering, 2012. 49: p. 139-146.
9. Shudo, T. and Takahashi, T., Influence of Reformed Gas Composition on HCCI Combustion Engine System fueled with DME and H 2-CO-CO 2 which are Onboard-reformed from Methanol Utilizing Engine Exhaust Heat. Nippon Kikai Gakkai Ronbunshu B Hen(Transactions of the Japan Society of Mechanical Engineers Part B)(Japan), 2004. 16(10): p. 2657-2662.
10. Shudo, T., An HCCI combustion engine system using on-board reformed gases of methanol with waste heat recovery: ignition control by hydrogen. International journal of vehicle design, 2006. 41(1-4): p. 206-226.
11. Zhang, Y., Huang, Z., Wei, L., Zhang, J., and Law, C.K., Experimental and modeling study on ignition delays of lean mixtures of methane, hydrogen, oxygen, and argon at elevated pressures. Combustion and Flame, 2012. 159(3): p. 918-931.
12. Tomita, E. Combustion characteristics and performance of supercharged pyrolysis gas engine with micro-pilot ignition. in Proc. of 25th CIMAC World Congress on Combustion Engine Technology (CIMAC 2007). 2007.
13. Watson, G.M., Munzar, J.D., and Bergthorson, J.M., NO formation in model syngas and biogas blends. Fuel, 2014. 124: p. 113-124.
14. Li, H. and Karim, G.A., Exhaust emissions from an SI engine operating on gaseous fuel mixtures containing hydrogen. International journal of hydrogen energy, 2005. 30(13): p. 1491-1499.
15. Zhao, F., Asmus, T.N., Assanis, D.N., Dec, J.E., Eng, J.A., and Najt, P.M., Homogeneous charge compression ignition (HCCI) engines. 2003, SAE Technical Paper.
16. Olsson, J.-O., Tunestål, P., and Johansson, B., Closed-loop control of an HCCI engine. 2001, SAE Technical Paper.
17. Tanaka, S., Ayala, F., Keck, J.C., and Heywood, J.B., Two-stage ignition in HCCI combustion and HCCI control by fuels and additives. Combustion and flame, 2003. 132(1): p. 219-239.
18. Poonia, M., Ramesh, A., and Gaur, R., Effect of intake air temperature and pilot fuel quantity on the combustion characteristics of a LPG diesel dual fuel engine. 1998, SAE Technical Paper.
19. Liu, Z. and Karim, G., Simulation of combustion processes in gas-fuelled diesel engines. Proceedings of the Institution of Mechanical Engineers, Part A: Journal of Power and Energy, 1997. 211(2): p. 159-169.

20. Sun, H., Yang, S., Jomaas, G., and Law, C., High-pressure laminar flame speeds and kinetic modeling of carbon monoxide/hydrogen combustion. Proceedings of the Combustion Institute, 2007. 31(1): p. 439-446.
21. Kéromnès, A., Metcalfe, W.K., Heufer, K.A., Donohoe, N., Das, A.K., Sung, C.-J., Herzler, J., Naumann, C., Griebel, P., and Mathieu, O., An experimental and detailed chemical kinetic modeling study of hydrogen and syngas mixture oxidation at elevated pressures. Combustion and Flame, 2013. 160(6): p. 995-1011.
22. Cuoci, A., Frassoldati, A., Faravelli, T., and Ranzi, E., Formation of soot and nitrogen oxides in unsteady counterflow diffusion flames. Combustion and Flame, 2009. 156(10): p. 2010-2022.
23. Cuoci, A., Frassoldati, A., Faravelli, T., and Ranzi, E. Formation of soot and nitrogen oxides in unsteady counterflow diffusion flames. Combustion and Flame 2009. 156(10):p.2010-2022. Available from: http://creckmodeling.chem.polimi.it/index.php/menu-kinetics/menu-kinetics-detailed-mechanisms/menu-kinetics-h2-co-mechanism.
24. Glarborg, P., Hidden interactions—Trace species governing combustion and emissions. Proceedings of the combustion institute, 2007. 31(1): p. 77-98.
25. Mathieu, O., Kopp, M., and Petersen, E., Shock-tube study of the ignition of multi-component syngas mixtures with and without ammonia impurities. Proceedings of the Combustion Institute, 2013. 34(2): p. 3211-3218.
26. Smith, G.P., Golden, D.M., Frenklach, M., Moriarty, N.W., Eiteneer, B., Goldenberg, M., Bowman, C.T., Hanson, R.K., and Song, S. WCG Jr., et al. 1999; Available from: http://www.me.berkeley.edu/gri_mech/.
27. Mehl, M., Pitz, W.J., Westbrook, C.K., and Curran, H.J., Kinetic modeling of gasoline surrogate components and mixtures under engine conditions. Proceedings of the Combustion Institute, 2011. 33(1): p. 193-200.
28. Ra, Y., Chuahy, F., and Kokjohn, S., Development and validation of a reduced reaction mechanism with a focus on diesel fuel/syngas co-oxidation. Fuel, 2016. 185: p. 663-683.
29. Türe, S., Uzun, D., and Türe, I.E., The potential use of sweet sorghum as a non-polluting source of energy. Energy, 1997. 22(1): p. 17-19.
30. Finley, M., BP statistical review of world energy. 2018.
31. Administration, U.S.E.I. Primary energy consumption by source and sector in 2017. 2017; Available from: https://www.eia.gov/energyexplained/.
32. Puhan, S., Vedaraman, N., Rambrahamam, B., and Nagarajan, G., Mahua (Madhuca indica) seed oil: a source of renewable energy in India. 2005.
33. Hagos, F.Y., Aziz, A.R.A., and Sulaiman, S.A., Trends of syngas as a fuel in internal combustion engines. Advances in Mechanical Engineering, 2014. 6: p. 401587.
34. Richards, G.A. and Casleton, K.H., Gasification technology to produce synthesis gas. Synthesis Gas Combustion: Fundamentals and Applications, 2009: p. 403.
35. Ry, S.E. History: Milestones of wood fumigation. 2012; Available from: http://www.ekoautoilijat.fi/tekstit/historiaa.htm.
36. Decker, K.D. "Wood gas vehicles: firewood in the fuel tank,". 2010; Available from: http://www.lowtechmagazine.com/2010/01/woodgas-cars.html.
37. Sridhar, G., Paul, P., and Mukunda, H., Biomass derived producer gas as a reciprocating engine fuel—an experimental analysis. Biomass and Bioenergy, 2001. 21(1): p. 61-72.
38. Basu, P., Biomass gasification and pyrolysis: practical design and theory. 2010: Academic press.
39. Couto, N., Rouboa, A., Silva, V., Monteiro, E., and Bouziane, K., Influence of the biomass gasification processes on the final composition of syngas. Energy Procedia, 2013. 36: p. 596-606.
40. Ahmad, A.A., Zawawi, N.A., Kasim, F.H., Inayat, A., and Khasri, A., Assessing the gasification performance of biomass: A review on biomass gasification process conditions, optimization and economic evaluation. Renewable and Sustainable Energy Reviews, 2016. 53: p. 1333-1347.

41. Ciferno, J.P. and Marano, J.J., Benchmarking biomass gasification technologies for fuels, chemicals and hydrogen production. US Department of Energy. National Energy Technology Laboratory, 2002.
42. Luo, S., Xiao, B., Guo, X., Hu, Z., Liu, S., and He, M., Hydrogen-rich gas from catalytic steam gasification of biomass in a fixed bed reactor: influence of particle size on gasification performance. International Journal of Hydrogen Energy, 2009. 34(3): p. 1260-1264.
43. Kumar, A., Jones, D.D., and Hanna, M.A., Thermochemical biomass gasification: a review of the current status of the technology. Energies, 2009. 2(3): p. 556-581.
44. Panda, C., Aspen plus simulation and experimental studies on biomass gasification. 2012.
45. Gañan, J., Abdulla, A.A.-K., Miranda, A., Turegano, J., Correia, S., and Cuerda, E., Energy production by means of gasification process of residuals sourced in Extremadura (Spain). Renewable Energy, 2005. 30(11): p. 1759-1769.
46. González, J.F., Encinar, J.M., Canito, J.L., Sabio, E., and Chacón, M., Pyrolysis of cherry stones: energy uses of the different fractions and kinetic study. Journal of analytical and applied pyrolysis, 2003. 67(1): p. 165-190.
47. Dean, J., Properties of atoms, radicals, and bonds. Lange's handbook of chemistry, 1999. 15: p. 4.1-4.84.
48. Luo, Y.-R., Handbook of bond dissociation energies in organic compounds. 2002: CRC press.
49. de Bruijn, F., The current status of fuel cell technology for mobile and stationary applications. Green Chemistry, 2005. 7(3): p. 132-150.
50. Ganesan, V., Internal combustion engines: McGraw Hill Education (India) Pvt Ltd.2012.
51. Stone, R., Introduction to internal combustion engines. 2012: Palgrave Macmillan.
52. Ferguson, C.R. and Kirkpatrick, A.T., Internal combustion engines: applied thermosciences. 2015.
53. Bargigli, S., Raugei, M., and Ulgiati, S., Comparison of thermodynamic and environmental indexes of natural gas, syngas and hydrogen production processes. Energy, 2004. 29(12): p. 2145-2159.
54. Cho, H.M. and He, B.-Q., Spark ignition natural gas engines—A review. Energy Conversion and Management, 2007. 48(2): p. 608-618.
55. Hagos, F.Y., Aziz, A.R.A., and Sulaiman, S.A., Methane enrichment of syngas (H 2/CO) in a spark-ignition direct-injection engine: combustion, performance and emissions comparison with syngas and compressed natural gas. Energy, 2015. 90: p. 2006-2015.
56. Hagos, F.Y., Aziz, A.R.A., and Sulaiman, S.A., Syngas (H 2/CO) in a spark-ignition direct-injection engine. Part 1: Combustion, performance and emissions comparison with CNG. International journal of hydrogen energy, 2014. 39(31): p. 17884-17895.
57. Boehman, A.L. and Corre, O.L., Combustion of syngas in internal combustion engines. Combustion Science and Technology, 2008. 180(6): p. 1193-1206.
58. Bae, C. and Kim, J., Alternative fuels for internal combustion engines. Proceedings of the Combustion Institute, 2017. 36(3): p. 3389-3413.
59. Qian, Y., Zhang, Y., Wang, X., and Lu, X., Experimental investigation of the combustion characteristics and the emission characteristics of biogas–diesel dual fuel in a common-rail diesel engine. Proceedings of the Institution of Mechanical Engineers, Part D: Journal of Automobile Engineering, 2017: p. 9-13.
60. Pitz, W.J. and Mueller, C.J., Recent progress in the development of diesel surrogate fuels. Progress in Energy and Combustion Science, 2011. 37(3): p. 330-350.
61. Donkerbroek, A., Van Vliet, A., Somers, L., Frijters, P., Klein-Douwel, R., Dam, N., Meerts, W., and ter Meulen, J., Time-and space-resolved quantitative LIF measurements of formaldehyde in a heavy-duty diesel engine. Combustion and Flame, 2010. 157(1): p. 155-166.
62. Roy, M.M., Tomita, E., Kawahara, N., Harada, Y., and Sakane, A., Performance and emission comparison of a supercharged dual-fuel engine fueled by producer gases with varying hydrogen content. International Journal of Hydrogen Energy, 2009. 34(18): p. 7811-7822.
63. Roy, M.M., Tomita, E., Kawahara, N., Harada, Y., and Sakane, A., Performance and emissions of a supercharged dual-fuel engine fueled by hydrogen-rich coke oven gas. International journal of hydrogen energy, 2009. 34(23): p. 9628-9638.

64. Garnier, C., Bilcan, A., Le Corre, O., and Rahmouni, C., Characterisation of a syngas-diesel fuelled CI engine. 2005, SAE Technical Paper.
65. Costa, M., La Villetta, M., Massarotti, N., Piazzullo, D., and Rocco, V., Numerical analysis of a compression ignition engine powered in the dual-fuel mode with syngas and biodiesel. Energy, 2017. 137: p. 969-979.
66. Dec, J.E., Advanced compression-ignition engines—understanding the in-cylinder processes. Proceedings of the combustion institute, 2009. 32(2): p. 2727-2742.
67. Stanglmaier, R.H. and Roberts, C.E., Homogeneous charge compression ignition (HCCI): benefits, compromises, and future engine applications. 1999, SAE Technical Paper.
68. Whitty, K.J., Zhang, H.R., and Eddings, E.G., Emissions from syngas combustion. Combustion Science and Technology, 2008. 180(6): p. 1117-1136.
69. Van Huynh, C. and Kong, S.-C., Combustion and NOx emissions of biomass-derived syngas under various gasification conditions utilizing oxygen-enriched-air and steam. Fuel, 2013. 107: p. 455-464.
70. Law, C.K., Combustion physics. 2010: Cambridge university press.
71. No, S., Gu, J., Moon, H., Lee, C., and Jo, Y., An Introduction to Combustion Concepts and Applications. McGraw-Hill Korea,2015.
72. Konnov, A., Detailed reaction mechanism for small hydrocarbons combustion, Release 0.5, 2000. Citée aux pages: 105, 109 et, 2011. 131.
73. Konnov, A., Remaining uncertainties in the kinetic mechanism of hydrogen combustion. Combustion and flame, 2008. 152(4): p. 507-528.
74. Hong, Z., Cook, R.D., Davidson, D.F., and Hanson, R.K., A shock tube study of OH+ H2O2→ H2O+ HO2 and H2O2+ M→ 2OH+ M using laser absorption of H2O and OH. The Journal of Physical Chemistry A, 2010. 114(18): p. 5718-5727.
75. Hong, Z., Farooq, A., Barbour, E.A., Davidson, D.F., and Hanson, R.K., Hydrogen peroxide decomposition rate: a shock tube study using tunable laser absorption of H2O near 2.5 μm. The Journal of Physical Chemistry A, 2009. 113(46): p. 12919-12925.
76. Frassoldati, A., Faravelli, T., and Ranzi, E., A wide range modeling study of NOx formation and nitrogen chemistry in hydrogen combustion. International Journal of Hydrogen Energy, 2006. 31(15): p. 2310-2328.
77. Lieuwen, T., Yang, V., and Yetter, R., Synthesis gas combustion: fundamentals and applications. CRC Press,2009.
78. Azimov, U., Tomita, E., Kawahara, N., and Harada, Y., Effect of syngas composition on combustion and exhaust emission characteristics in a pilot-ignited dual-fuel engine operated in PREMIER combustion mode. international journal of hydrogen energy, 2011. 36(18): p. 11985-11996.
79. Miller, C., Cicero, D., and Ackiewicz, M., Hydrogen from coal program: research development and demonstration plan for the period 2007 through 2016. The United States Department of Energy, National Energy Technology Laboratory, 2007.
80. Rasi, S., Lehtinen, J., and Rintala, J., Determination of organic silicon compounds in biogas from wastewater treatments plants, landfills, and co-digestion plants. Renewable Energy, 2010. 35(12): p. 2666-2673.
81. Gersen, S., Darmeveil, H., and Levinsky, H., The effects of CO addition on the autoignition of H 2, CH 4 and CH 4/H 2 fuels at high pressure in an RCM. Combustion and Flame, 2012. 159(12): p. 3472-3475.
82. Rauch, R., Hrbek, J., and Hofbauer, H., Biomass gasification for synthesis gas production and applications of the syngas. Wiley Interdisciplinary Reviews: Energy and Environment, 2014. 3(4): p. 343-362.
83. Saxena, P. and Williams, F.A., Testing a small detailed chemical-kinetic mechanism for the combustion of hydrogen and carbon monoxide. Combustion and Flame, 2006. 145(1): p. 316-323.
84. Dowdy, D.R., Smith, D.B., Taylor, S.C., and Williams, A. The use of expanding spherical flames to determine burning velocities and stretch effects in hydrogen/air mixtures. in Symposium (International) on Combustion. Elsevier.1991.

85. Egolfopoulos, F. and Law, C. An experimental and computational study of the burning rates of ultra-lean to moderately-rich H2/O2/N2 laminar flames with pressure variations. in Symposium (international) on combustion. Elsevier.1991.
86. Tse, S., Zhu, D., and Law, C., Morphology and burning rates of expanding spherical flames in H2/O2/inert mixtures up to 60 atmospheres. Proceedings of the Combustion Institute, 2000. 28(2): p. 1793-1800.
87. Kwon, O. and Faeth, G., Flame/stretch interactions of premixed hydrogen-fueled flames: measurements and predictions. Combustion and Flame, 2001. 124(4): p. 590-610.
88. Li, J., Zhao, Z., Kazakov, A., Chaos, M., Dryer, F.L., and Scire, J.J., A comprehensive kinetic mechanism for CO, CH2O, and CH3OH combustion. International Journal of Chemical Kinetics, 2007. 39(3): p. 109-136.
89. Held, T.J. and Dryer, F.L., A comprehensive mechanism for methanol oxidation. International Journal of Chemical Kinetics, 1998. 30(11): p. 805-830.
90. Li, S.-C., Williams, F.A., and Gebert, K., A reduced reaction mechanism for predicting knock in dual-fuel engines. 2000, SAE Technical Paper.
91. Glarborg, P., Kubel, D., Kristensen, P.G., Hansen, J., and Dam-Johansen, K., Interactions of CO, NOx and H2O under post-flame conditions. Combustion science and technology, 1995. 110(1): p. 461-485.
92. Tsang, W. and Herron, J.T., Chemical kinetic data base for propellant combustion I. Reactions involving NO, NO2, HNO, HNO2, HCN and N2O. Journal of Physical and Chemical Reference Data, 1991. 20(4): p. 609-663.
93. Zhang, Y., Mathieu, O., Petersen, E.L., Bourque, G., and Curran, H.J., Assessing the predictions of a NOx kinetic mechanism on recent hydrogen and syngas experimental data. Combustion and Flame, 2017. 182: p. 122-141.
94. Konnov, A. and Ruyck, J.D.,A possivble new route for NO formation via N2H3. Combustion science and technology, 2001. 168(1): p. 1-46.
95. Konnov, A., Colson, G., and De Ruyck, J., NO formation rates for hydrogen combustion in stirred reactors. Fuel, 2001. 80(1): p. 49-65.
96. Dayma, G. and Dagaut, P., Effects of air contamination on the combustion of hydrogen—effect of NO and NO2 addition on hydrogen ignition and oxidation kinetics. Combustion science and technology, 2006. 178(10-11): p. 1999-2024.
97. Rasmussen, C.L., Hansen, J., Marshall, P., and Glarborg, P., Experimental measurements and kinetic modeling of CO/H2/O2/NOx conversion at high pressure. International Journal of Chemical Kinetics, 2008. 40(8): p. 454-480.
98. Pan, L., Kokjohn, S., and Huang, Z., Development and validation of a reduced chemical kinetic model for dimethyl ether combustion. Fuel, 2015. 160: p. 165-177.
99. Yoshikawa, T. and Reitz, R.D., Development of an improved NOx reaction mechanism for low temperature diesel combustion modeling. SAE International Journal of Engines, 2008. 1(2008-01-2413): p. 1105-1117.
100. Ra, Y. and Reitz, R.D., A reduced chemical kinetic model for IC engine combustion simulations with primary reference fuels. Combustion and Flame, 2008. 155(4): p. 713-738.
101. Curran, H.J., Gaffuri, P., Pitz, W.J., and Westbrook, C.K., A comprehensive modeling study of n-heptane oxidation. Combustion and flame, 1998. 114(1): p. 149-177.
102. Curran, H.J., Gaffuri, P., Pitz, W.J., and Westbrook, C.K., A comprehensive modeling study of iso-octane oxidation. Combustion and flame, 2002. 129(3): p. 253-280.
103. Mehl, M., Pitz, W., Sjöberg, M., and Dec, J.E., Detailed kinetic modeling of low-temperature heat release for PRF fuels in an HCCI engine. 2009, SAE Technical Paper.
104. Stagni, A., Cuoci, A., Frassoldati, A., Faravelli, T., and Ranzi, E., Lumping and reduction of detailed kinetic schemes: an effective coupling. Industrial & Engineering Chemistry Research, 2013. 53(22): p. 9004-9016.
105. Seshadri, K., Bollig, M., and Peters, N., Numerical and asymptotic studies of the structure of stoichiometric and lean premixed heptane flames. Combustion and flame, 1997. 108(4): p. 518-536.

106. Tanaka, S., Ayala, F., and Keck, J.C., A reduced chemical kinetic model for HCCI combustion of primary reference fuels in a rapid compression machine. Combustion and flame, 2003. 133(4): p. 467-481.
107. CD-Adapco Inc. Methodology, Star-CD V4.6. 2017.
108. Chemical-Kinetic Mechanisms for Combustion Applications, Mechanical and Aerospace Engineering (Combustion Research), University of California at San Diego 2011.
109. Ranzi, E., Frassoldati, A., Stagni, A., Pelucchi, M., Cuoci, A., and Faravelli, T., Reduced kinetic schemes of complex reaction systems: fossil and biomass-derived transportation fuels. International Journal of Chemical Kinetics, 2014. 46(9): p. 512-542.
110. Løvås, T., Model reduction techniques for chemical mechanisms, in Chemical Kinetics. InTech.2012.
111. CD-Adapco Inc., DARS Manual, Book5: Mechanism Reduction 2005.
112. Kee, R.J., Rupley, F.M., and Miller, J.A., Chemkin-II: A Fortran chemical kinetics package for the analysis of gas-phase chemical kinetics.Sandia National Labs., Livermore.1989.
113. MathWorks, MathWorks. Bioinformatics Toolbox: User's Guide (R2012a), 2012.
114. Nilsson, D., Automatic analysis and reduction of reaction mechanisms for complex fuel combustion. Lund reports on combustion physics, 2001.
115. Tomlin, A.S., Turányi, T., and Pilling, M.J., Mathematical tools for the construction, investigation and reduction of combustion mechanisms. Comprehensive chemical kinetics, 1997. 35: p. 293-437.
116. Karadeniz, H., Soyhan, H.S., and Sorusbay, C., Reduction of large kinetic mechanisms with a new approach to the necessity analysis method. Combustion and Flame, 2012. 159(4): p. 1467-1480.
117. Lu, T. and Law, C.K., A directed relation graph method for mechanism reduction. Proceedings of the Combustion Institute, 2005. 30(1): p. 1333-1341.
118. Lu, T. and Law, C.K., Linear time reduction of large kinetic mechanisms with directed relation graph: n-Heptane and iso-octane. Combustion and Flame, 2006. 144(1): p. 24-36.
119. Løvs, T., Nilsson, D., and Mauss, F., Automatic reduction procedure for chemical mechanisms applied to premixed methane/air flames. Proceedings of the Combustion Institute, 2000. 28(2): p. 1809-1815.
120. Massias, A., Diamantis, D., Mastorakos, E., and Goussis, D., An algorithm for the construction of global reduced mechanisms with CSP data. Combustion and Flame, 1999. 117(4): p. 685-708.
121. Maas, U., Efficient calculation of intrinsic low-dimensional manifolds for the simplification of chemical kinetics. Computing and Visualization in Science, 1998. 1(2): p. 69-81.
122. Schmidt, D., Blasenbrey, T., and Maas, U., Intrinsic low-dimensional manifolds of strained and unstrained flames. Combustion Theory and Modelling, 1998. 2(2): p. 135-152.
123. CD-Adapco Inc., DARS Basic 2.10. 2015.
124. Lakshminarayanan, P. and Aghav, Y.V., Ignition Delay in a Diesel Engine. Modelling Diesel Combustion, 2010: p. 59-78.
125. Collin, R., Nygren, J., Richter, M., Aldén, M., Hildingsson, L., and Johansson, B., Simultaneous OH-and formaldehyde-LIF measurements in an HCCI engine. 2003, SAE Technical paper.
126. Zhou, A., Dong, T., and Akih-Kumgeh, B., Simplifying ignition delay prediction for homogeneous charge compression ignition engine design and control. International Journal of Engine Research, 2016. 17(9): p. 957-968.
127. Muharam, Y., Mahendra, M., Gayatri, D., and Kartohardjono, S., Simulation of ignition delay time of compressed natural gas combustion. International Journal of Automotive and Mechanical Engineering, 2015. 12: p. 3125.
128. Lee, H., Jiang, L., and Mohamad, A., A review on the laminar flame speed and ignition delay time of Syngas mixtures. International Journal of Hydrogen Energy, 2014. 39(2): p. 1105-1121.
129. Melguizo-Gavilanes, J. and Bauwens, L. On the validity of the constant volume assumption in shock tube experiments. in 28th International Symposium on Shock Waves.Springer, Berlin, Heidelberg.2012.

130. Lee, H.C., Mohamad, A.A., and Jiang, L.-Y., Comprehensive comparison of chemical kinetics mechanisms for syngas/biogas mixtures. Energy & Fuels, 2015. 29(9): p. 6126-6145.
131. Natarajan, J., Lieuwen, T., and Seitzman, J., Laminar flame speeds of H 2/CO mixtures: effect of CO 2 dilution, preheat temperature, and pressure. Combustion and flame, 2007. 151(1): p. 104-119.
132. Lee, H.C., A Detailed Chemical Kinetics Mechanism for Biogas and Syngas Combustion. University of Calgary.2016.
133. CD-Adapco Inc. DARS Manual, Book4: Flames. 2015.
134. Santner, J., Haas, F.M., Ju, Y., and Dryer, F.L., Uncertainties in interpretation of high pressure spherical flame propagation rates due to thermal radiation. Combustion and Flame, 2014. 161(1): p. 147-153.
135. Mazas, A., Lacoste, D., and Schuller, T. Experimental and numerical investigation on the laminar flame speed of CH4/O2 mixtures diluted with CO2 and H2O. in ASME Turbo Expo. 2010.
136. Turanyi, T., Applications of sensitivity analysis to combustion chemistry. Reliability Engineering & System Safety, 1997. 57(1): p. 41-48.
137. Soyhan, H.S., Amnéus, P., Løvås, T., Nilsson, D., Maigaard, P., Mauss, F., and Sorusbay, C., Automatic Reduction of Detailed Chemical Reaction Mechanisms for Autoignition Under SI Engine Conditions. 2000, SAE Technical Paper.
138. Hu, Y., Naito, S., Kobayashi, N., and Hasatani, M., CO 2, NO x and SO 2 emissions from the combustion of coal with high oxygen concentration gases. Fuel, 2000. 79(15): p. 1925-1932.
139. Shudo, T., Omori, K., and Hiyama, O., NOx reduction and NO 2 emission characteristics in rich-lean combustion of hydrogen. International journal of hydrogen energy, 2008. 33(17): p. 4689-4693.
140. Asgari, N., Ahmed, S.F., Farouk, T.I., and Padak, B., NOx formation in post-flame gases from syngas/air combustion at atmospheric pressure. International Journal of Hydrogen Energy, 2017. 42(38): p. 24569-24579.
141. Choudhuri, A.R. and Gollahalli, S., Combustion characteristics of hydrogen–hydrocarbon hybrid fuels. International journal of hydrogen energy, 2000. 25(5): p. 451-462.
142. Correa, S.M., A review of NOx formation under gas-turbine combustion conditions. Combustion science and technology, 1993. 87(1-6): p. 329-362.
143. Filippov, P., Khudyakov, P., and Ryzhkov, A. Validation of the thermal NOx emissions model from a gas fuel combustor under atmospheric pressure. in Journal of Physics: Conference Series. 2017.
144. Bugge, M., Skreiberg, Ø., Haugen, N.E.L., Carlsson, P., Houshfar, E., and Løvås, T., Numerical simulations of staged biomass grate fired combustion with an emphasis on NOx emissions. Energy Procedia, 2015. 75: p. 156-161.
145. Vedeshkin, G., Sverdlov, E., and Dubovitsky, A., Experimental Investigations of a Low-Emission Combustor Designed for Mid Power Gas Turbines. AerospaceLab, 2016(11): p. 8.
146. Strakey, P., Weiland, N., and Richards, G., Combustion Strategies for Syngas and High-Hydrogen Fuel. The Gas Turbine Handbook, 2006.
147. Schwerdt, C., Modelling NOx-formation in combustion processes. MSc Theses, 2006.
148. STAR-CD, Methodology V.4.22. 2015.
149. Fernando, S., Hall, C., and Jha, S., NO x reduction from biodiesel fuels. Energy & Fuels, 2006. 20(1): p. 376-382.
150. Pershing, D. and Wendt, J. Pulverized coal combustion: The influence of flame temperature and coal composition on thermal and fuel NOx. in Symposium (International) on Combustion. Elsevier.1977.
151. Chacartegui, R., Torres, M., Sánchez, D., Jiménez, F., Munoz, A. and Sánchez, T. Analysis of main gaseous emissions of heavy duty gas turbines burning several syngas fuels. Fuel Processing Technology, 2011. 92(2), pp.213-220
152. Williams, A., Pourkashanian, M., Jones, J., and Rowlands, L., A review of NOx formation and reduction mechanisms in combustion systems, with particular reference to coal. Journal of the Institute of Energy, 1997. 70(484): p. 102-113.

153. Fackler, K.B., Karalus, M.F., Novosselov, I.V., Kramlich, J.C., and Malte, P.C., Experimental and numerical study of NOx formation from the lean premixed combustion of CH4 mixed with CO2 and N2. Journal of Engineering for Gas Turbines and Power, 2011. 133(12): p. 121502.
154. Han, Z. and Reitz, R.D., Turbulence modeling of internal combustion engines using RNG κ-ε models. Combustion science and technology, 1995. 106(4-6): p. 267-295.
155. Reitz, R.D. and Diwakar, R., Effect of drop breakup on fuel sprays. 1986, SAE Technical Paper.
156. Reitz, R.D. and Diwakar, R., Structure of high-pressure fuel sprays. 1987, SAE Technical Paper.
157. Westbrook, C.K. and Dryer, F.L., Chemical kinetic modeling of hydrocarbon combustion. Progress in Energy and Combustion Science, 1984. 10(1): p. 1-57.
158. McDonald, H., Combustion modeling in two and three dimensions—some numerical considerations. Progress in Energy and Combustion Science, 1979. 5(2): p. 97-122.
159. Sarathy, S.M., Chemical kinetic modeling of biofuel combustion. 2010.
160. Jones, W. and Whitelaw, J., Calculation methods for reacting turbulent flows: a review. Combustion and flame, 1982. 48: p. 1-26.
161. McBride, B.J., Gordon, S., and Reno, M.A., Coefficients for calculating thermodynamic and transport properties of individual species. 1993.
162. Kee, R.J., Dixon-Lewis, G., Warnatz, J., Coltrin, M.E., and Miller, J.A., A Fortran computer code package for the evaluation of gas-phase multicomponent transport properties. Sandia National Laboratories Report SAND86-8246, 1986. 13: p. 80401-1887.
163. Jayashankara, B. and Ganesan, V., Effect of fuel injection timing and intake pressure on the performance of a DI diesel engine–A parametric study using CFD. Energy Conversion and Management, 2010. 51(10): p. 1835-1848.
164. Nicholls, J., Stream and droplet breakup by shock waves. Nasa Sp-194, 1972: p. 126-128.
165. Magnussen, B.F. and Hjertager, B. On the structure of turbulence and a generalized eddy dissipation concept for chemical reaction in turbulent flow. in 19th AIAA aerospace meeting, St. Louis, USA. 1981.
166. CD-Adapco Inc. Methodology, Star-CCM+. 2017.
167. Zhang, Z., Zhang, W., Zhai, Z.J., and Chen, Q.Y., Evaluation of various turbulence models in predicting airflow and turbulence in enclosed environments by CFD: Part 2—Comparison with experimental data from literature. Hvac&R Research, 2007. 13(6): p. 871-886.
168. Liu, C., Shy, S., Chiu, C., Peng, M., and Chung, H., Hydrogen/carbon monoxide syngas burning rates measurements in high-pressure quiescent and turbulent environment. international journal of hydrogen energy, 2011. 36(14): p. 8595-8603.
169. Ponzio, A., Thermally homogenous gasification of biomass/coal/waste for medium or high calorific value syngas production.KTH.2008.
170. Chmielniak, T. and Sciazko, M., Co-gasification of biomass and coal for methanol synthesis. Applied energy, 2003. 74(3): p. 393-403.
171. Thi, L.D., Zhang, Y., and Huang, Z., Shock tube study on ignition delay of multi-component syngas mixtures–Effect of equivalence ratio. international journal of hydrogen energy, 2014. 39(11): p. 6034-6043.
172. Hu, E., Fu, J., Pan, L., Jiang, X., Huang, Z., and Zhang, Y., Experimental and numerical study on the effect of composition on laminar burning velocities of H 2/CO/N 2/CO 2/air mixtures. international journal of hydrogen energy, 2012. 37(23): p. 18509-18519.
173. Lapalme, D. and Seers, P., Influence of CO 2, CH 4, and initial temperature on H 2/CO laminar flame speed. International Journal of Hydrogen Energy, 2014. 39(7): p. 3477-3486.
174. Park, O., Veloo, P.S., Liu, N., and Egolfopoulos, F.N., Combustion characteristics of alternative gaseous fuels. Proceedings of the Combustion Institute, 2011. 33(1): p. 887-894.
175. Donohoe, N., Heufer, A., Metcalfe, W.K., Curran, H.J., Davis, M.L., Mathieu, O., Plichta, D., Morones, A., Petersen, E.L., and Güthe, F., Ignition delay times, laminar flame speeds, and mechanism validation for natural gas/hydrogen blends at elevated pressures. Combustion and Flame, 2014. 161(6): p. 1432-1443.
176. Charlston–Goch, D., Chadwick, B., Morrison, R., Campisi, A., Thomsen, D., and Laurendeau, N., Laser-Induced fluorescence measurements and modeling of nitric oxide in premixed flames

of CO+ H 2+ CH 4 and air at high pressures: I. Nitrogen fixation. Combustion and flame, 2001. 125(1): p. 729-743.
177. Homer, J. and Sutton, M., Nitric oxide formation and radical overshoot in premixed hydrogen flames. Combustion and Flame, 1973. 20(1): p. 71-76.
178. Sahu, A. and Ravikrishna, R., A detailed numerical study of NO x kinetics in low calorific value H 2/CO syngas flames. International Journal of Hydrogen Energy, 2014. 39(30): p. 17358-17370.
179. Ciezki, H. and Adomeit, G., Shock-tube investigation of self-ignition of n-heptane-air mixtures under engine relevant conditions. Combustion and flame, 1993. 93(4): p. 421-433.
180. Fieweger, K., Blumenthal, R., and Adomeit, G., Self-ignition of SI engine model fuels: a shock tube investigation at high pressure. Combustion and Flame, 1997. 109(4): p. 599-619.
181. Shen, H.-P.S., Steinberg, J., Vanderover, J., and Oehlschlaeger, M.A., A shock tube study of the ignition of n-heptane, n-decane, n-dodecane, and n-tetradecane at elevated pressures. Energy & Fuels, 2009. 23(5): p. 2482-2489.
182. Herzler, J., Jerig, L., and Roth, P., Shock tube study of the ignition of lean n-heptane/air mixtures at intermediate temperatures and high pressures. Proceedings of the Combustion Institute, 2005. 30(1): p. 1147-1153.
183. Hartmann, M., Gushterova, I., Fikri, M., Schulz, C., Schießl, R., and Maas, U., Auto-ignition of toluene-doped n-heptane and iso-octane/air mixtures: High-pressure shock-tube experiments and kinetics modeling. Combustion and Flame, 2011. 158(1): p. 172-178.
184. Sileghem, L., Alekseev, V., Vancoillie, J., Van Geem, K., Nilsson, E., Verhelst, S., and Konnov, A., Laminar burning velocity of gasoline and the gasoline surrogate components iso-octane, n-heptane and toluene. Fuel, 2013. 112: p. 355-365.
185. Dirrenberger, P., Glaude, P.-A., Bounaceur, R., Le Gall, H., da Cruz, A.P., Konnov, A., and Battin-Leclerc, F., Laminar burning velocity of gasolines with addition of ethanol. Fuel, 2014. 115: p. 162-169.
186. Heufer, K. and Olivier, H., Determination of ignition delay times of different hydrocarbons in a new high pressure shock tube. Shock Waves, 2010. 20(4): p. 307-316.
187. Zhang, K., Banyon, C., Bugler, J., Curran, H.J., Rodriguez, A., Herbinet, O., Battin-Leclerc, F., B'Chir, C., and Heufer, K.A., An updated experimental and kinetic modeling study of n-heptane oxidation. Combustion and Flame, 2016. 172: p. 116-135.
188. Gauthier, B., Davidson, D., and Hanson, R., Shock tube determination of ignition delay times in full-blend and surrogate fuel mixtures. Combustion and Flame, 2004. 139(4): p. 300-311.
189. Aggarwal, S., Awomolo, O., and Akber, K., Ignition characteristics of heptane–hydrogen and heptane–methane fuel blends at elevated pressures. international journal of hydrogen energy, 2011. 36(23): p. 15392-15402.
190. Stylianidis, N., Azimov, U., Maheri, A., Tomita, E., and Kawahara, N., Chemical kinetics and CFD analysis of supercharged micro-pilot ignited dual-fuel engine combustion of syngas. Fuel, 2017. 203: p. 591-606.
191. Frassoldati, A., Faravelli, T., and Ranzi, E., The ignition, combustion and flame structure of carbon monoxide/hydrogen mixtures. Note 1: Detailed kinetic modeling of syngas combustion also in presence of nitrogen compounds. International Journal of Hydrogen Energy, 2007. 32(15): p. 3471-3485.
192. Li, S. and Williams, F. Reaction mechanisms for methane ignition. in ASME Turbo Expo 2000: Power for Land, Sea, and Air. American Society of Mechanical Engineers.2000.
193. Fernández-Galisteo, D., del Alamo, G., Sánchez, A.L., and Linán, A. Zeldovich analysis of hydrogen-air premixed flames. in Third European combustion Meeting, Crete, Greece. 2007.
194. Sutherland, J., Michael, J., Pirraglia, A., Nesbitt, F., and Klemm, R. Rate constant for the reaction of O (3P) with H2 by the flash photolysis—shock tube and flash photolysis—resonance fluorescence techniques; 504K≤ T≤ 2495K. in Symposium (International) on Combustion. Elsevier.1988.
195. Ó Conaire, M., Curran, H.J., Simmie, J.M., Pitz, W.J., and Westbrook, C.K., A comprehensive modeling study of hydrogen oxidation. International journal of chemical kinetics, 2004. 36(11): p. 603-622.

196. Hong, Z., Davidson, D.F., and Hanson, R.K., An improved H 2/O 2 mechanism based on recent shock tube/laser absorption measurements. Combustion and Flame, 2011. 158(4): p. 633-644.
197. Westbrook, C.K., Chemical kinetics of hydrocarbon ignition in practical combustion systems. Proceedings of the Combustion Institute, 2000. 28(2): p. 1563-1577.
198. Kappel, C., Luther, K., and Troe, J., Shock wave study of the unimolecular dissociation of H 2 O 2 in its falloff range and of its secondary reactions. Physical Chemistry Chemical Physics, 2002. 4(18): p. 4392-4398.
199. Sellevåg, S.R., Georgievskii, Y., and Miller, J.A., Kinetics of the gas-phase recombination reaction of hydroxyl radicals to form hydrogen peroxide. The Journal of Physical Chemistry A, 2009. 113(16): p. 4457-4467.
200. Troe, J., The thermal dissociation/recombination reaction of hydrogen peroxide H2O2 (+ M)⇔ 2OH (+ M) III.: Analysis and representation of the temperature and pressure dependence over wide ranges. Combustion and Flame, 2011. 158(4): p. 594-601.
201. Fernandes, R., Luther, K., Troe, J., and Ushakov, V., Experimental and modelling study of the recombination reaction H+ O 2 (+ M)→ HO 2 (+ M) between 300 and 900 K, 1.5 and 950 bar, and in the bath gases M= He, Ar, and N 2. Physical Chemistry Chemical Physics, 2008. 10(29): p. 4313-4321.
202. Bates, R.W., Golden, D.M., Hanson, R.K., and Bowman, C.T., Experimental Study and Modeling of the Reaction H+ O2+ M yields HO2+ M (M= Ar, N2, H2O) at Elevated Pressures and Temperatures Between 1050-1250K. Physical Chemistry , Chemical Physics, 2001. 3 (12):p. 2337-2342..
203. Pirraglia, A., Michael, J., Sutherland, J., and Klemm, R., A flash photolysis-shock tube kinetic study of the H atom reaction with O sub 2: H+ O sub 2 rightleftharpoons OH+ O (962 K le T le 1705 K) and H+ O sub 2+ Ar yields HO sub 2+ Ar (746 K le T le 987 K). Journal of Physical Chemistry, 1989. 93(1): p. 282-29
204. Mueller, M., Kim, T., Yetter, R., and Dryer, F., Flow reactor studies and kinetic modeling of the H2/O2 reaction. International Journal of Chemical Kinetics, 1999. 31(2): p. 113-125.
205. Hong, Z., Davidson, D., Barbour, E., and Hanson, R., A new shock tube study of the H+ O 2→ OH+ O reaction rate using tunable diode laser absorption of H 2 O near 2.5 μm. Proceedings of the Combustion Institute, 2011. 33(1): p. 309-316.
206. Baulch, D., Bowman, C.T., Cobos, C., Cox, R., Just, T., Kerr, J., Pilling, M., Stocker, D., Troe, J., and Tsang, W., Evaluated kinetic data for combustion modeling: supplement II. Journal of physical and chemical reference data, 2005. 34(3): p. 757-1397.
207. Tsang, W. and Hampson, R., Chemical kinetic data base for combustion chemistry. Part I. Methane and related compounds. Journal of Physical and Chemical Reference Data, 1986. 15(3): p. 1087-1279.
208. Ellingson, B.A., Theis, D.P., Tishchenko, O., Zheng, J., and Truhlar, D.G., Reactions of hydrogen atom with hydrogen peroxide. The Journal of Physical Chemistry A, 2007. 111(51): p. 13554-13566.
209. Mittal, G., Sung, C.J., and Yetter, R.A., Autoignition of H2/CO at elevated pressures in a rapid compression machine. International Journal of Chemical Kinetics, 2006. 38(8): p. 516-529.
210. Zhao, Z., Li, J., Kazakov, A., and Dryer, F.L., Temperature-dependent feature sensitivity analysis for combustion modeling. International journal of chemical kinetics, 2005. 37(5): p. 282-295.
211. Davis, S.G., Joshi, A.V., Wang, H., and Egolfopoulos, F., An optimized kinetic model of H 2/CO combustion. Proceedings of the Combustion Institute, 2005. 30(1): p. 1283-1292.
212. Cohen, N., Are reaction rate coefficients additive? Revised transition state theory calculations for OH+ alkane reactions. International Journal of Chemical Kinetics, 1991. 23(5): p. 397-417.
213. Baulch, D., Cobos, C., Cox, R., Frank, P., Hayman, G., Just, T., Kerr, J., Murrells, T., Pilling, M., and Troe, J., Evaluated kinetic data for combustion modeling. Supplement I. Journal of Physical and Chemical Reference Data, 1994. 23(6): p. 847-848.
214. Madronich, S. and Felder, W. Direct measurements of the rate coefficient for the reaction OH+ CH4→ CH3+ H2O over 300-1500 K. in Symposium (International) on Combustion. Elsevier.1985.

215. Srinivasan, N., Su, M.-C., Sutherland, J., and Michael, J., Reflected shock tube studies of high-temperature rate constants for OH+ CH4→ CH3+ H2O and CH3+ NO2→ CH3O+ NO. The Journal of Physical Chemistry A, 2005. 109(9): p. 1857-1863.
216. Aul, C.J., Metcalfe, W.K., Burke, S.M., Curran, H.J., and Petersen, E.L., Ignition and kinetic modeling of methane and ethane fuel blends with oxygen: A design of experiments approach. Combustion and Flame, 2013. 160(7): p. 1153-1167.
217. Giménez-López, J., Millera, A., Bilbao, R., and Alzueta, M.U., Experimental and kinetic modeling study of the oxy-fuel oxidation of natural gas, CH4 and C2H6. Fuel, 2015. 160: p. 404-412.
218. Srinivasan, N., Su, M.-C., Sutherland, J., and Michael, J., Reflected shock tube studies of high-temperature rate constants for CH3+ O2, H2CO+ O2, and OH+ O2. The Journal of Physical Chemistry A, 2005. 109(35): p. 7902-7914.
219. Herbon, J.T., Hanson, R.K., Bowman, C.T., and Golden, D.M., The reaction of CH 3+ O 2: experimental determination of the rate coefficients for the product channels at high temperatures. Proceedings of the Combustion Institute, 2005. 30(1): p. 955-963.
220. Maghbouli, A., Shafee, S., Saray, R.K., Yang, W., Hosseini, V., and An, H., A multi-dimensional CFD-chemical kinetics approach in detection and reduction of knocking combustion in diesel-natural gas dual-fuel engines using local heat release analysis. SAE International Journal of Engines, 2013. 6(2): p. 777-787.
221. Gharehghani, A., Mirsalim, S., and Jazayeri, S., Numerical and experimental investigation of combustion and knock in a dual fuel gas/diesel compression ignition engine. Journal of Combustion, 2012.
222. Baulch, D., Cobos, C., Cox, R., Frank, P., Hayman, G., Just, T., Kerr, J., Murrells, T., Pilling, M., and Troe, J., Summary table of evaluated kinetic data for combustion modeling: Supplement 1. Combustion and flame, 1994. 98(1-2): p. 59-79.
223. Natarajan, K. and Roth, P., High temperature rate coefficient for the reaction of O (3P) with H2 obtained by the resonance absorption of O and H atoms. Combustion and flame, 1987. 70(3): p. 267-279.
224. Davidson, D. and Hanson, R., A direct comparison of shock tube photolysis and pyrolysis methods in the determination of the rate coefficient for O+ H2→ OH+ H. Combustion and Flame, 1990. 82(3-4): p. 445-447.
225. Javoy, S., Naudet, V., Abid, S., and Paillard, C., Rate constant for the reaction of O with H2 at high temperature by resonance absorption measurements of O atoms. International Journal of Chemical Kinetics, 2000. 32(11): p. 686-695.
226. Smith, I.W. and Crim, F.F., The chemical kinetics and dynamics of the prototypical reaction: OH+ H 2→ H2O+ H. Physical Chemistry Chemical Physics, 2002. 4(15): p. 3543-3551.
227. Konnov AA. Detailed reaction mechanism for small hydrocarbons combustion, Release 0.5, 2000.
228. Krasnoperov, L. and Michael, J., Shock tube studies using a novel multipass absorption cell: rate constant results for OH+ H2 and OH+ C2H6. The Journal of Physical Chemistry A, 2004. 108(26): p. 5643-5648.
229. Oldenborg, R., Loge, G., Harradine, D., and Winn, K., Kinetic study of the hydrogel+ hydrogen reaction from 800 to 1550 K. The Journal of Physical Chemistry, 1992. 96(21): p. 8426-8430.
230. Kim, T.J., Yetter, R.A., and Dryer, F.L. New results on moist CO oxidation: high pressure, high temperature experiments and comprehensive kinetic modeling. in Symposium (international) on combustion. Elsevier.1994.
231. Lindstedt, R. and Skevis, G., Chemistry of acetylene flames. Combustion Science and Technology, 1997. 125(1-6): p. 73-137.
232. Li, J., Zhao, Z., Kazakov, A., and Dryer, F.L., An updated comprehensive kinetic model of hydrogen combustion. International journal of chemical kinetics, 2004. 36(10): p. 566-575.
233. Mittal, G. and SUNG*, C.-J., A rapid compression machine for chemical kinetics studies at elevated pressures and temperatures. Combustion Science and Technology, 2007. 179(3): p. 497-530.

234. Hippler, H., Neunaber, H., and Troe, J., Shock wave studies of the reactions HO+ H2O2→ H2O+ HO2 and HO+ HO2→ H2O+ O2 between 930 and 1680 K. The Journal of chemical physics, 1995. 103(9): p. 3510-3516.
235. Hong, Z., Vasu, S.S., Davidson, D.F., and Hanson, R.K., Experimental study of the rate of OH+ HO2→ H2O+ O2 at high temperatures using the reverse reaction. The Journal of Physical Chemistry A, 2010. 114(17): p. 5520-5525.
236. Burke, M.P., Chaos, M., Ju, Y., Dryer, F.L., and Klippenstein, S.J., Comprehensive H2/O2 kinetic model for high-pressure combustion. International Journal of Chemical Kinetics, 2012. 44(7): p. 444-474.
237. Keyser, L.F., Kinetics of the reaction hydroxyl+ hydroperoxo. fwdarw. water+ oxygen from 254 to 382 K. The Journal of Physical Chemistry, 1988. 92(5): p. 1193-1200.
238. Slavinskaya, N., Braun-Unkhoff, M., and Frank, P., Reduced reaction mechanisms for methane and syngas combustion in gas turbines. Journal of Engineering for Gas Turbines and Power, 2008. 130(2): p. 021504.
239. Mallard, W., Westley, F., Herron, J., and Hanson, R., NIST Standard Reference Database 17 2Q98. NIST Standard Reference Data: Gaithersburg, MD, 1994.
240. Hippler, H., Troe, J., and Willner, J., Shock wave study of the reaction HO2+ HO2→ H2O2+ O2: Confirmation of a rate constant minimum near 700 K. The Journal of chemical physics, 1990. 93(3): p. 1755-1760.
241. Stylianidis, N., Azimov, U., Kawahara, N., and Tomita, E., Chemical Kinetics and Computational Fluid-Dynamics Analysis of H 2/CO/CO 2/CH 4 Syngas Combustion and NOx Formation in a Micro-Pilot-Ignited Supercharged Dual Fuel Engine. 2017, SAE Technical Paper.
242. Miller, R., Davis, G., Lavoie, G., Newman, C., and Gardner, T., A super-extended Zel'dovich mechanism for NOx modeling and engine calibration. 1998, SAE Technical Paper.
243. Goswami, M., Volkov, E.N., Konnov, A.A., Bastiaans, R., and de Goey, L., Updated kinetic mechanism for NOx prediction and hydrogen combustion. Technische Universiteit Eindhoven, Eindhoven, The Netherlands, Technical Report, 2008.
244. Svoboda, K., Cermak, J., and Hartman, M., Chemistry and Emissions of Nitrogen Oxides (NO, NO~ 2, N~ 2O) in Combustion of Solid Fuels. II. Heterogeneous Reactions-N~ 2O. Chemical papers-Slovak Academy of Sciences, 2000. 54(2): p. 118-130.
245. Miller, I.M., A High-pressure Premixed Flat-flame Burner for Chemical Process Studies. Vol. 1318. 1978: National Aeronautics and Space Administration.
246. Lu, T. and Law, C.K., Diffusion coefficient reduction through species bundling. Combustion and flame, 2007. 148(3): p. 117-126.
247. Yoo, C.S., Lu, T., Chen, J.H., and Law, C.K., Direct numerical simulations of ignition of a lean n-heptane/air mixture with temperature inhomogeneities at constant volume: Parametric study. Combustion and Flame, 2011. 158(9): p. 1727-1741.
248. Patel, A., Kong, S.-C., and Reitz, R.D., Development and validation of a reduced reaction mechanism for HCCI engine simulations. 2004, SAE Technical Paper.
249. Ra, Y. and Reitz, R.D., A combustion model for IC engine combustion simulations with multi-component fuels. Combustion and flame, 2011. 158(1): p. 69-90.
250. Diamantis, D., Kyritsis, D., and Goussis, D.A. Two stage ignition of n-heptane: identifying the chemistry setting the explosive time scales. in 2nd Intl. Conference in Model Reduction in Reacting Flows. 2009.
251. Golovitchev, V. Semi -detailed mechanism for n-heptane oxidation. Combsution Chemistry. 2004. Available from: http://www.tfd.chalmers.se/~valeri/MECH.html.
252. Pang, K.M., Ng, H.K., and Gan, S., Development of an integrated reduced fuel oxidation and soot precursor formation mechanism for CFD simulations of diesel combustion. Fuel, 2011. 90(9): p. 2902-2914.
253. Machrafi, H., Lombaert, K., Cavadias, S., Guibert, P., and Amouroux, J., Reduced chemical reaction mechanisms: experimental and HCCI modelling investigations of autoignition processes of iso-octane in internal combustion engines. Fuel, 2005. 84(18): p. 2330-2340.
254. Shi, Y., Ge, H.-W., and Reitz, R.D., Computational optimization of internal combustion engines. Springer Science & Business Media.,2011.

255. Zheng, X. and Law, C., Ignition of premixed hydrogen/air by heated counterflow under reduced and elevated pressures. Combustion and flame, 2004. 136(1): p. 168-179.
256. Horning, D.C., Davidson, D., and Hanson, R., Study of the high-temperature autoignition of n-alkane/O/Ar mixtures. Journal of Propulsion and Power, 2002. 18(2): p. 363-371.
257. Hidaka, Y., Sato, K., Henmi, Y., Tanaka, H., and Inami, K., Shock-tube and modeling study of methane pyrolysis and oxidation. Combustion and flame, 1999. 118(3): p. 340-358.

Appendix A

Table A-1. Thermal properties of all the species included in the developed mechanisms

Species Name	Elemental Composition	Phase	Temperature K (Min/Max)	T min Coefficients	T max coefficients
AR	AR 1	G	300/4000	.250000000E+01	.250000000E+0
				.000000000E+00	.000000000E+00
				.000000000E+00	.000000000E+00
				.000000000E+00	.000000000E+00
				.000000000E+00	.000000000E+00
				-.745375000E+03	-.745375000E+03
				.436600000E+01	.436600000E+01
N_2	N 2	G	300/4000	.292663788E+01	.329867700E+01
				.148797700E-02	.140823990E-02
				-.568476030E-06	-.396322180E-05
				.100970400E-09	.564151480E-08
				-.675335090E-14	-.244485400E-11
				-.922795384E+03	-.102090000E+04
				.598054018E+01	.395037200E+01
O_2	O 2	G	300/4000	.369757685E+01	.321293600E+01
				.613519690E-03	.112748610E-02
				-.125884200E-06	-.575614990E-06
				.177528100E-10	.131387700E-08
				-.113643500E-14	-.876855390E-12
				-.123392966E+04	-.100524900E+04
				.318917125E+01	.603473900E+01
H_2	H 2	G	300/4000	.299142220E+01	.329812400E+01
				.700064410E-03	.824944120E-03
				-.563382800E-07	-.814301470E-06
				-.923157820E-11	-.947543430E-10
				.158275200E-14	.413487200E-12
				-.835033546E+03	-.101252100E+04
				-.135510641E+01	-.329409400E+01
H_2O	H 2O 1	G	300/4000	.267214569E+01	.338684200E+01
				.305629290E-02	.347498200E-02
				-.873026070E-06	-.635469590E-05
				.120099600E-09	.696858040E-08
				-.639161790E-14	-.250658800E-11
				-.298992115E+05	-.302081100E+05
				.686281125E+01	.259023200E+01
H_2O_2	H 2O 2	G	300/40000	.457316594E+01	.338875300E+01
				.433613590E-02	.656922580E-02
				-.147468900E-05	-.148501200E-06
				.234890300E-09	-.462580510E-08
				-.143165410E-13	.247151410E-11
				-.180069531E+05	-.176631400E+05
				.501137915E+00	.678536300E+01
CO	C 1O 1	G	300/4000	.302507617E+01	.326245100E+01
				.144268900E-02	.151194100E-02
				-.563082720E-06	-.388175520E-05

				.101858100E-09	.558194380E-08
				-.691095110E-14	-.247495100E-11
				-.142683499E+05	-.143105400E+05
				.610822521E+01	.484889700E+01
CO_2	C 1O 2	G	300/4000	.445362582E+01	.227572400E+01
				.314016800E-02	.992207230E-02
				-.127841100E-0	-.104091100E-04
				.239399610E-09	.686668590E-08
				-.166903300E-13	-.211728010E-11
				-.489669524E+05	-.483731400E+05
				-.955420007E+00	.101884900E+02
CH_2O	C 1H 2O 1	G	300/4000	.299560858E+01	.165273100E+01
				.668132120E-02	.126314400E-01
				-.262895400E-05	-.188816790E-04
				.473715290E-09	.205003110E-07
				-.321251710E-13	-.841323710E-11
				-.153203666E+05	-.148654000E+05
				.691256052E+01	.137848200E+02
N	N 1	G	200/6000	0.24159429E+01	0.25000000E+01
				0.17489065E-03	0.00000000E+00
				-0.11902369E-06	0.00000000E+00
				0.30226245E-10	0.00000000E+00
				-0.20360982E-14	0.00000000E+00
				0.56133773E+05	0.56104637E+05
				0.46496096E+01	0.41939087E+01
NO	N 1O 1	G	200/6000	0.32606056E+01	0.42184763E+01
				0.11911043E-02	-0.46389760E-02
				-0.42917048E-06	0.11041022E-04
				0.69457669E-10	-0.93361354E-08
				-0.40336099E-14	0.28035770E-11
				0.99209746E+04	0.98446230E+04
				0.63693027E+01	0.22808464E+01
NO_2	N 1O 2	G	200/6000	0.48847542E+01	0.39440312E+01
				0.21723956E-02	-0.15854290E-02
				-0.82806906E-06	0.16657812E-04
				0.15747510E-09	-0.20475426E-07
				-0.10510895E-13	0.78350564E-11
				0.23164983E+04	0.28966179E+04
				-0.11741695E+00	0.63119917E+01
N_2O	N 2O 1	G	200/6000	0.48230729E+01	0.22571502E+01
				0.26270251E-02	0.11304728E-01
				-0.95850874E-06	-0.13671319E-04
				0.16000712E-09	0.96819806E-08
				-0.97752303E-14	-0.29307182E-11
				0.80734048E+04	0.87417744E+04
				-0.22017207E+01	0.10757992E+02
$C_7H_{14}OOH_{2-4}$	C 7H 15O 2	0g	300/5000	2.73843966e+01	1.62083964e+00
				3.17800796e-02	8.83636215e-02
				-1.07557689e-05	-5.64527235e-05
				1.65881427e-09	1.76325999e-08
				-9.58200506e-14	-2.10369342e-12
				-2.49404488e+04	-1.57072842e+04
				-1.09739277e+02	2.97815441e+01

C_6H_{13-1}	C 6H 13 0	0g	300/5000	1.85219223e+01	-7.62937152e-01
				2.82755903e-02	7.18105209e-02
				-9.62785872e-06	-4.71329725e-05
				1.49000931e-09	1.62249790e-08
				-8.62480621e-14	-2.32087543e-12
				-5.00124444e+03	1.89021556e+03
				-7.06345855e+01	3.35439856e+01
C_7H_{14}-1	C 7H 14 0	0g	300/5000	2.10898039e+01	-1.67720549e+00
				3.10607878e-02	8.24611601e-02
				-1.05644793e-05	-5.46504108e-05
				1.63405780e-09	1.87862303e-08
				-9.45598219e-14	-2.65737983e-12
				-1.83260065e+04	-1.02168601e+04
				-8.44391108e+01	3.85068032e+01
$C_7H_{15}O_{2-2}$	C 7H 15O 2	0g	300/5000	2.52622017e+01	1.51378168e+00
				3.46652053e-02	8.85572745e-02
				-1.18812593e-05	-5.92457147e-05
				1.84687322e-09	2.11801862e-08
				-1.07234165e-13	-3.20741722e-12
				-3.05051074e+04	-2.19818400e+04
				-1.00675588e+02	2.76255370e+01
$C_7H_{15}O_{-2}$	C 7H 15O 1	0g	300/5000	2.43070968e+01	-1.09087925e+00
				3.31267815e-02	9.23217022e-02
				-1.13034023e-05	-6.44477835e-05
				1.75198875e-09	2.36808474e-08
				-1.01526943e-13	-3.61067567e-12
				-2.88623481e+04	-1.99926675e+04
				-9.87360860e+01	3.77738325e+01
CH_3O_2	C 1H 3O 2	0g	300/5000	5.95787891e+00	4.26146906e+00
				7.90728626e-03	1.00873599e-02
				-2.68246234e-06	-3.21506184e-06
				4.13891337e-10	2.09409267e-10
				-2.39007330e-14	4.18339103e-14
				-1.53574838e+03	-6.84394259e+02
				-4.71963886e+00	5.16330320e+00
C_7H_{15-2}	C 7H 15	0g	300/5000	2.16368842e+01	-3.79155767e-02
				3.23324804e-02	7.56726570e-02
				-1.09273807e-05	-4.07473634e-05
				1.68357060e-09	9.32678943e-09
				-9.71774091e-14	-4.92360745e-13
				-1.05873616e+04	-2.35605303e+03
				-8.52209653e+01	3.37321506e+01
C_3H_6	C 3H 6	G	300/4000	.673231663E+01	.149330700E+01
				.149083400E-01	.209251700E-01
				-.494989900E-05	.448679380E-05
				.721202210E-09	-.166891190E-07
				-.376620390E-13	.715814600E-11
				-.923623057E+03	.107482600E+04
				-.133137684E+02	.161453400E+02
CH_4	C 1H 4	G	300/4000	.168346564E+01	.778741700E+00
				.102372400E-01	.174766800E-01
				-.387512820E-05	-.278340900E-04
				.678558490E-09	.304970800E-07

				-.450342310E-13	-.122393100E-10
				-.100807773E+05	-.982522800E+04
				.962347575E+01	.137221900E+02
C_2H_2	C 2H 2	G	300/4000	.443677300E+01	.201356200E+01
				.537603910E-02	.151904500E-01
				-.191281610E-05	-.161631910E-04
				.328637890E-09	.907899180E-08
				-.215670900E-13	-.191274600E-11
				.256676622E+05	.261244400E+05
				-.280035722E+01	.880537800E+01
CH_2CO	C 2H 2O 1	G	300/4000	.603885318E+01	.297497100E+01
				.580484000E-02	.121187100E-01
				-.192095400E-05	-.234504600E-05
				.279448500E-09	-.646668500E-08
				-.145886800E-13	.390564900E-11
				-.858343402E+04	-.763263700E+04
				-.765782305E+01	.867355300E+01
C_2H_4	C 2H 4	G	300/4000	.352841648E+01	-.861487900E+00
				.114851800E-01	.279616190E-01
				-.441838480E-05	-.338867690E-04
				.784460000E-09	.278515200E-07
				-.526684780E-13	-.973787890E-11
				.442829030E+0	.557304700E+04
				.223039249E+01	.242114800E+02
CH_3CHO	C 2H 4O	G	300/4000	.586869116E+01	.250569500E+01
				.107942400E-01	.133699100E-01
				-.364552990E-05	.467195290E-05
				.541291180E-09	-.112814000E-07
				-.289684390E-13	.426356610E-11
				-.226457128E+05	-.212458800E+05
				-.601321650E+01	.133508900E+02
C_4H_6	C 4H 6	G	300/4000	.823794980E+01	.112443850E+00
				.173695890E-01	.343711770E-01
				-.615923200E-05	-.111106630E-04
				.979908060E-09	-.921096660E-08
				-.578075590E-13	.620841700E-11
				.923259930E+04	.118022620E+05
				-.203418190E+02	.230917180E+02
C_3H_5CHO	C 4H 6O 1	G	300/4000	.121670926E+02	-.227554121E-01
				.150749706E-01	.441176181E-01
				-.518640017E-05	-.322046234E-04
				.808302587E-09	.124986163E-07
				-.470194864E-13	-.202269249E-11
				-.156762389E+05	-.114618192E+05
				-.365095664E+02	.288193193E+02
C_3H_5CHO	C 4H 6O 1	G	300/4000	.121670926E+02	-.227554121E-01
				.150749706E-01	.441176181E-01
				-.518640017E-05	-.322046234E-04
				.808302587E-09	.124986163E-07
				.470194864E-13	-.202269249E-11
				-.156762389E+05	-.114618192E+05
				-.365095664E+02	.288193193E+02
NC_7H_{14}	C 7H 14	G	300/4000	.206190401E+02	-.116533279E+01

				.314852991E-01	.790439806E-01
				-.107162057E-04	-.496101666E-04
				.165827662E-08	.158569009E-07
				-.959911785E-13	-.205346433E-11
				-.196710875E+05	-.117362359E+05
				-.822507478E+02	.359871070E+02
NC_4H_8	C 4H 8	G	300/4000	.205358410E+01	.118113800E+01
				.343505070E-01	.308533800E-01
				-.158831970E-04	.508652470E-05
				.330896620E-08	-.246548880E-07
				-.253610450E-12	.111101930E-10
				-.213972310E+04	-.179040040E+04
				.155432010E+02	.210624690E+02
C_2H_5CHO	C 3H 6O 1	G	300/4000	.872954858E+01	.441647615E+01
				.199253945E-01	.159069417E-01
				-.785642340E-05	.990305472E-05
				.132736406E-08	-.119062354E-07
				-.812865962E-13	.290135824E-11
				-.281462888E+05	-.249124705E+05
				-.222846545E+02	.642168604E+01
$C_3H_6O_2$	C 3H 6O 2	G	300/4000	.118936666E+02	.266613285E+01
				.144153203E-01	.346302298E-01
				-.477525443E-05	-.214380719E-04
				.726036430E-09	690469334E-08
				-.415285995E-13	-.916939105E-12
				-.459271652E+05	-.425706030E+05
				-.327285750E+02	.173358364E+02
NC_7-OQOOH	C 7H 14O 3	G	300/4000	.288332529E+02	.152936692E+01
				.320168096E-01	.958173466E-01
				-.111508456E-04	-.696688520E-04
				.175226159E-08	.269540382E-07
				-.102520451E-12	-.438728126E-11
				-.622309509E+05	-.526003608E+05
				-.116187714E+03	.306986714E+02
NC_7H_{16}	C 7H 16	G	300/4000	.205103125E+02	-.679531340E+00
				.346389640E-01	.810756760E-01
				-.107743740E-04	-.423279310E-04
				.160399760E-08	.697965770E-08
				-.937017530E-13	.837326950E-12
				-.326499224E+05	-.256907030E+05
				-.807081180E+02	.329815600E+02
O	O 1	G	300/4000	.254205876E+01	.294642800E+01
				-.275506100E-04	-.163816600E-02
				-.310280290E-08	.242103100E-05
				.455106700E-11	-.160284300E-08
				-.436805100E-15	.389069610E-12
				.292307989E+05	.291476400E+05
				.492030884E+01	.296399500E+01
H	H 1	G	300/4000	.250000000E+01	.250000000E+01
				.000000000E+00	.000000000E+00
				.000000000E+00	.000000000E+00
				.000000000E+00	.000000000E+00
				.000000000E+00	.000000000E+00

				.254716200E+05	.254716200E+05
				-.460117600E+00	-.460117600E+00
OH	H 1O 1	G	300/4000	.285376040E+01	.341896226E+01
				.102994334E-02	.319255801E-03
				-.232666477E-06	-.308292717E-06
				.193750704E-10	.364407494E-09
				-.315759847E-15	-.100195479E-12
				.369949720E+04	.345264448E+04
				.578756825E+01	.254433372E+01
HO_2	H 1O 2	G	300/4000	.401721090E+01	.430179801E+01
				.223982013E-02	-.474912051E-02
				-.633658150E-06	.211582891E-04
				.114246370E-09	-.242763894E-07
				-.107908535E-13	.929225124E-11
				.111856713E+03	.294808040E+03
				.378510215E+01	.371666245E+01
HCO	C 1H 1O 1	G	300/4000	.355727119E+01	.289832900E+01
				.334557190E-02	.619914620E-02
				-.133500600E-05	-.962308420E-05
				.247057210E-09	.108982500E-07
				-.171385000E-13	-.457488520E-11
				.391632208E+04	.415992100E+04
				.555229973E+01	.898361500E+01
CH_2S	C 1H 2	G	300/4000	.355288641E+01	.397126500E+01
				.206678800E-02	-.169908800E-03
				-.191411600E-06	.102536900E-05
				-.110467300E-09	.249254990E-08
				.202134890E-13	-.198126610E-11
				.498497521E+05	498936700E+05
				.168658499E+01	.575320760E-01
CH_2	C 1H 2	G	300/4000	.363640757E+01	.376223700E+01
				.193305600E-02	.115981900E-02
				-.168701600E-06	.248958490E-06
				-.100989900E-09	.880083620E-09
				.180825510E-13	-.733243490E-12
				.453413341E+05	.453679000E+05
				.215656196E+01	171257700E+01
CH_3	C 1H 3	G	300/4000	.284405718E+01	.243044200E+01
				.613797410E-02	.111241000E-01
				-.223034500E-05	-.168022000E-04
				.378516110E-09	.162182910E-07
				-.245215900E-13	-.586495220E-11
				.164378004E+05	.164237800E+05
				.545265727E+01	.678979400E+01
CH_3O	C 1H 3O 1	G	300/4000	.377081447E+01	.210620400E+01
				.787149740E-02	.721659510E-02
				.265638390E-05	-.211261600E-13
				.394443090E-09	-.737763630E-08
				-.211261600E-13	.207561010E-1
				.127818951E+03	978601200E+03
				.292947482E+01	.131521800E+02
CH_3OO	C 1H 3O 2	G	300/4000	.595784570E+01	.426146906E+01
				.790728626E-02	.100873599E-01

				-.268246234E-05	-.321506184E-05
				.413891337E-09	.209409267E-09
				-.239007330E-13	.418339103E-13
				-.378178515E+03	.473129653E+03
				-.353671121E+01	.634599067E+01
HCCO	C 2H 1O 1	G	300/4000	.675807437E+01	.504796600E+01
				.200040010E-02	.445347790E-02
				-.202760700E-06	.226828210E-06
				-.104113200E-09	-.148209400E-08
				.196516400E-13	.225074100E-12
				.190151261E+05	.196589100E+05
				-.907126528E+01	.481843900E+00
C_2H_3	C 2H 3	G	300/4000	.593346697E+01	.245927600E+01
				.401774510E-02	.737147590E-02
				-.396673900E-06	.210987200E-05
				-.144126700E-09	-.132164200E-08
				.237864300E-13	-.118478400E-11
				.318543468E+05	.333522500E+05
				-.853030497E+01	.115562000E+02
CH_3CO	C 2H 3O 1	G	300/4000	.561230883E+01	.312527800E+01
				.844988600E-02	.977822020E-02
				-.285414690E-05	.452144790E-05
				.423837600E-09	-.900946160E-08
				-.226840300E-13	.319371700E-11
				-.518788372E+04	-.410850700E+04
				-.327515155E+01	.112288500E+02
C_2H_5	C 2H 5	G	300/4000	.719047846E+01	.269070100E+01
				.648407680E-02	.871913320E-02
				-.642806410E-06	.441983820E-05
				-.234787910E-09	.933870310E-09
				.388087690E-13	-.392777300E-11
				.106745471E+05	.128704000E+05
				-.147808755E+02	.121382000E+02
C_2H_5OO	C 2H 5O 2	G	300/4000	.951115499E+01	.177950508E+01
				.122676900E-01	.304938087E-01
				-.422364452E-05	-.216376209E-04
				.658474989E-09	.868906296E-08
				-.383095208E-13	-.151788464E-11
				-.676067578E+04	-.399101974E+04
				.223427083E+02	.192919501E+02
CH_3COCH_2	C 3H 5O 1	G	300/4000	.102303674E+02	.180339187E+01
				.116494161E-01	.301407085E-01
				-.401005537E-05	-.193505552E-04
				.625205246E-09	.638199034E-08
				-.363784362E-13	-.866103180E-12
				-.844376284E+04	-.537233261E+04
				-.279195044E+02	.178046408E+02
NC_3H_7	C 3H 7	G	300/4000	.722715260E+01	.192253600E+01
				.172648710E-01	.247892700E-01
				-.588880490E-05	.181024900E-05
				.669183600E-09	-.178326490E-07
				.000000000E+00	.858299630E-11
				.782835831E+04	.971328300E+0

				-.127978858E+02	.164927100E+02
SC_4H_7	C 4H 7	G	300/4000	.714879043E+01	-.442598200E+00
				.219663880E-01	.422160100E-01
				-.774471300E-05	-.254697900E-04
				.907477370E-09	.597432100E-08
				.000000000E+00	.000000000E+00
				.124589843E+05	.145672100E+05
				-.117547735E+02	.276086500E+02
NC_7H_{13}	C 7H 13	G	300/4000	.140838604E+02	-.697079542E+00
				.208584950E-01	.514354766E-01
				-.722620456E-05	-.304500502E-04
				.113154433E-08	.880925852E-08
				-.660424465E-13	-.994458078E-12
				.542225436E+04	.110172568E+05
				-.515371079E+02	.293601364E+02
NC_7H_{15}	C 7H 15	G	300/4000	.216371448E+02	-.379155767E-01
				.323324804E-01	.756726570E-01
				-.109273807E-04	-.407473634E-04
				.168357060E-08	.932678943E-08
				-.971774091E-13	-.492360745E-12
				-.105877217E+05	-.235605303E+04
				-.852228493E+02	.337321506E+02
NC_7-QOOH	C 7H 15O 2	G	300/4000	.449365222E+02	.169959950E+01
				.384325070E-02	.943723540E-01
				-.181753210E-06	-.755904260E-04
				-.116055420E-10	.401131540E-07
				.168632530E-14	-.120065810E-10
				-.301866739E+05	-.147076150E+05
				-.207157897E+03	.283145640E+02
NC_7H_{15}-OO	C 7H 15O 2	G	300/4000	.272928290E+02	.137396160E+0
				.327034748E-01	.925294066E-01
				-.112483701E-04	-.644403647E-04
				.175282538E-08	.235223293E-07
				-.101955579E-12	-.356678305E-11
				-.235449480E+05	-.144154775E+05
				-.109307876E+03	.302419431E+02
NC_7-OOQOOH	C 7H 15O 4	G	300/4000	.269436049E+02	.234060326E+01
				.351661203E-01	.923428863E-01
				-.120111248E-04	-.637138459E-04
				.186268617E-08	.236026902E-07
				-.107974911E-12	-.368902757E-11
				-.478858130E+05	-.392112217E+05
				-.104588181E+03	.278171493E+02

Table A-2. Transport properties of all the species included in the developed mechanisms

Species Name	**Geometrical Configuration (0,1 OR 2)**	**Lennard Jones potential well depth**	**Lennard Jones collision Diameter**	**Dipole Moment**	**Polarizability**	**Rotational Relaxation collision number**
AR	0	136.500	3.330	0.000	0.000	0.000
N_2	1	97.530	3.621	0.000	1.760	4.000
O_2	1	107.400	3.621	0.000	1.600	3.800
H_2	1	38.000	2.920	0.000	0.790	280.000
H_2O	2	572.400	2.605	1.844	0.000	4.000
H_2O_2	2	107.400	3.458	0.000	0.000	3.800
CH_4	2	141.400	3.746	0.000	2.600	13.000
CO	1	98.100	3.650	0.000	1.950	1.800
CO_2	1	244.000	3.763	0.000	2.650	2.100
CH_2O	2	498.000	3.590	0.000	0.000	2.100
N	0	71.400	3.298	0.000	0.000	0.000
N_2O	1	232.400	3.828	0.000	0.000	1.000
NO_2	2	200.000	3.500	0.000	0.000	1.000
NO	1	97.530	3.621	0.000	1.760	4.000
$C_7H_{14}OOH_{2\text{-}4}$	2	561.0	6.317	1.7	0.0	1.000
$C_6H_{13\text{-}1}$	2	489.224	5.349	0.000	0.000	0.000
$C_7H_{14\text{-}1}$	2	457.8	6.173	0.3	0.0	1.000
$C_7H_{15}O_{\text{-}2}$	2	561.0	6.317	1.7	0.0	1.000
$C_7H_{15}O_{2\text{-}2}$	2	561.0	6.317	1.7	0.0	1.000
CH_3O_2	2	481.800	3.626	0.000	0.000	1.000
$C_7H_{15\text{-}2}$	2	459.6	6.253	0.00	0.00	1.000
C_3H_6	2	307.800	4.140	0.000	0.000	1.000
C_2H_2	1	209.00	4.100	0.000	0.000	2.500
C_2H_4	2	289.800	3.971	0.000	0.000	1.500
CH_2CO	2	436.000	3.970	0.000	0.000	2.000
CH_3CHO	2	436.000	3.970	0.000	0.000	2.000
C_4H_6	2	357.000	5.180	0.000	0.000	1.000
NC_7H_{14}	2	459.980	6.310	0.000	0.000	1.000
NC_4H_8	2	355.000	4.650	0.000	0.000	1.000
C_2H_5CHO	2	411.000	4.820	0.000	0.000	1.000
$C_3H_6O_2$	2	503.072	5.339	1.670	7.016	1.000
C_3H_5CHO	2	332.713	5.642	0.000	0.000	1.000
NC_7-OQOOH	2	559.980	6.310	0.000	0.000	1.000
NC_7H_{16}	2	459.980	6.310	0.000	0.000	1.000
O	0	80.000	2.750	0.000	0.000	0.000
H	O	145.000	2.050	0.000	0.000	0.000
OH	1	80.000	2.750	0.000	0.000	0.000
HO_2	2	107.400	3.458	0.000	0.000	1.000
HCO	2	489.999	3.590	0.000	0.000	0.000
CH_2	1	144.000	3.800	0.000	0.000	0.000
CH_2S	1	144.000	3.800	0.000	0.000	0.000
CH_3	1	144.000	3.800	0.000	0.000	0.000
CH_3CO	2	436.000	3.970	0.000	0.000	2.000
CH_3O	2	417.000	3.690	1.700	0.000	2.000

CH_3OO	2	417.000	3.690	1.700	0.000	2.000
HCCO	2	150.000	2.500	0.000	0.000	1.000
C_2H_3	2	209.000	4.100	0.000	0.000	1.000
C_2H_5	2	252.300	4.302	0.000	0.000	1.500
C_2H_5OO	2	362.600	4.530	0.000	0.000	1.500
CH_3COCH_2	2	424.600	4.820	0.000	0.000	1.000
NC_3H_7	2	303.400	4.810	0.000	0.000	1.000
SC_4H_7	2	355.000	4L650	0.000	0.000	1.000
NC_7H_{13}	2	559.980	6.310	0.000	0.000	1.000
NC_7H_{15}	2	459.980	6.310	0.000	0.000	1.000
NC_7-QOOH	2	559.980	6.310	0.000	0.000	1.000
NC_7H_{15}-OO	2	559.980	6.310	0.000	0.000	1.000
NC_7-OOQOOH	2	559.980	6.310	0.000	0.000	1.000

Appendix B

Table B-1. Calculated overall mean error, $\bar{\bar{\varepsilon}}$, and the grand mean error , $\bar{\bar{\Psi}}$

No.	Fuel Mixture	Composition in (%vol)		Equivalence ratio	Initial Pressure	Initial Temperature	Model	Overall absolute mean error value (%)					
								Reduced Mechanism	Takashi et al	Super Extended	Keromnes et al	Frassoldati et al	GRI mech. 3.0
LFS													
Fuel 8	$H_2/CO/CH_4$	Type1	47.5/47.5/5	0.2-2.5	1 atm	295 K	LFS	0.83	-	-	1.54	1.9	1.3
		Type2	40/40/20					3.6	-	-	29.3	33.8	12.5
		Type3	30/30/40					3.2	-	-	27.9	29.9	17.4
Fuel 9	$H_2/CO/CO_2/CH_4$	Type1	54/11/25/10	0.4-0.9	1 atm	298 K	LFS	0.9	-	-	3.2	6.5	2.3
		Type2	60/10/0/30					1.1	-	-	4.1	7.4	2.5
		Type3	32/58/0/10					2.3	-	-	4.5	7.5	3.7
Grand mean error of LFS (%)								1.9	-	-	11.7	14.5	6.6
Ignition delay time													
Fuel 2	$H_2/CO/CH_4/O_2/AR$	0.406/0.406/0.075/1.113/98		0.5	1.6 atm	1010-1920 K	Shock Tube/Constant Volume	4.4	-	-	5.1	9.6	19.3
					12.0 atm			2.5	-	-	36.0	40.2	21.3
					32.0 atm			2.7	-	-	8.4	6.7	6.1
Grand mean error of ignition delay time (%)								3.2	-	-	16.5	18.8	15.5
NOx													
Fuel 12	$H_2/CO/CO_2/CH_4$	37.5/37.5/20/5.0		0.72	1 atm	300 K	Premixed Laminar flame NOx	5.2	-	-	25.5	7.0	60.2
				1.03				5.9	-	-	50.2	13.8	64.2
				1.34				5.8	-	-	9.2	32.9	76.0
Fuel 11	$H_2/CO/CO_2/N_2/CH_4$	16.99/20.58/11.84/47.67/2.8		0.8	1atm	300 K	Premixed Laminar Flame-NOx	3.5	-	-	8.7	2.3	26.4
					3.05 atm			1.3	-	-	8.8	1.4	5.3
					9.15 atm			0.46	-	-	7.3	1.0	4.4
Fuel 13	$H_2/O_2/N_2$	$2H_2+1.4O_2+5.3N_2$		0.71	1 atm	300 K	Premixed Laminar flame NOx	3.8	4.0	13.5	-	-	-
		$2H_2+1.4O_2+4.6N_2$						2.4	3.0	8.1	-	-	-
		$2H_2+1.4O_2+6.1N_2$						2.2	3.0	47.1	-	-	-
Grand mean error of NOx (%)- NOx selection (only Fuel 10)								2.8	3.3	22.9	-	-	-
Grand mean error of NOx (%)- Fuel 11 and Fuel 12								3.6	-	-	18.28	9.73	39.4

Individual error analysis

$H_2/O_2/N_2$ mixture- Selection of NOx sub-mechanism

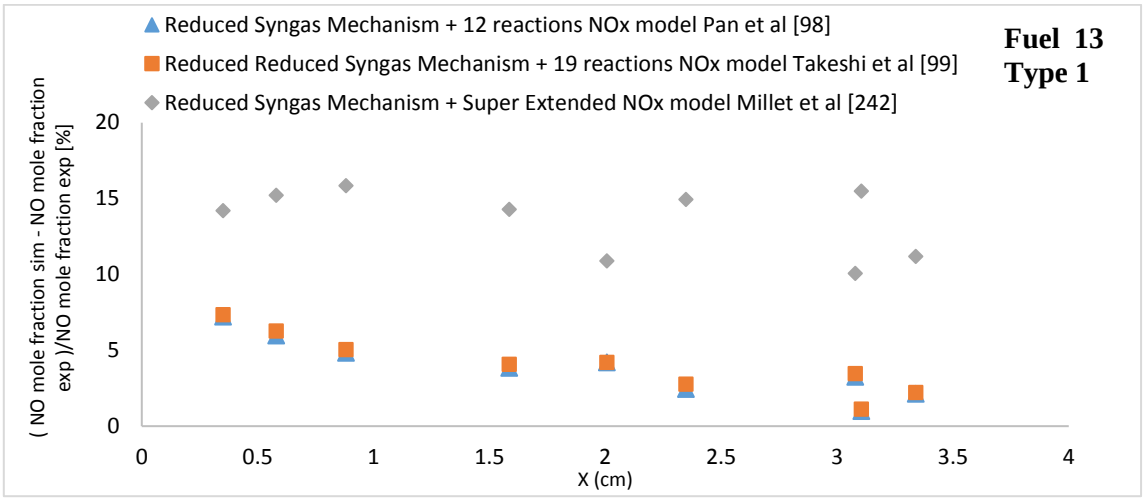

a)

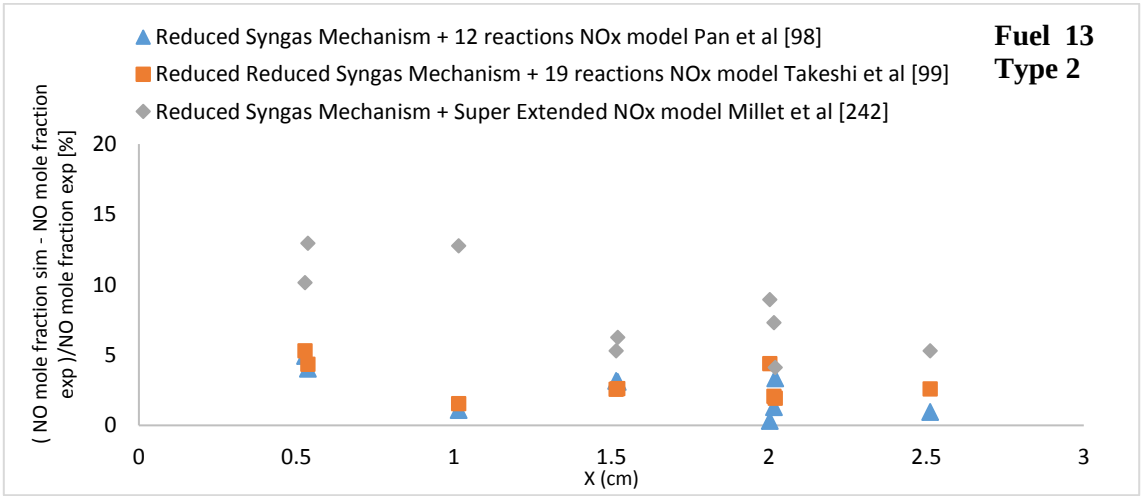

b)

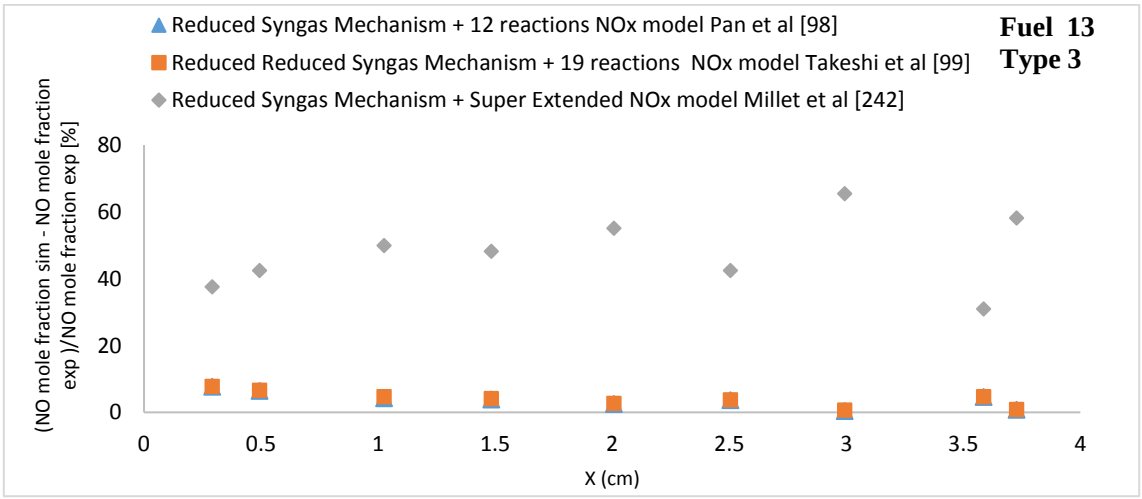

c)

Figure B-1 Absolute error calculation for NO mole fractions calculations using Fuel 13, Figure 5-1

LFS

H_2/CO/CH_4 syngas mixture

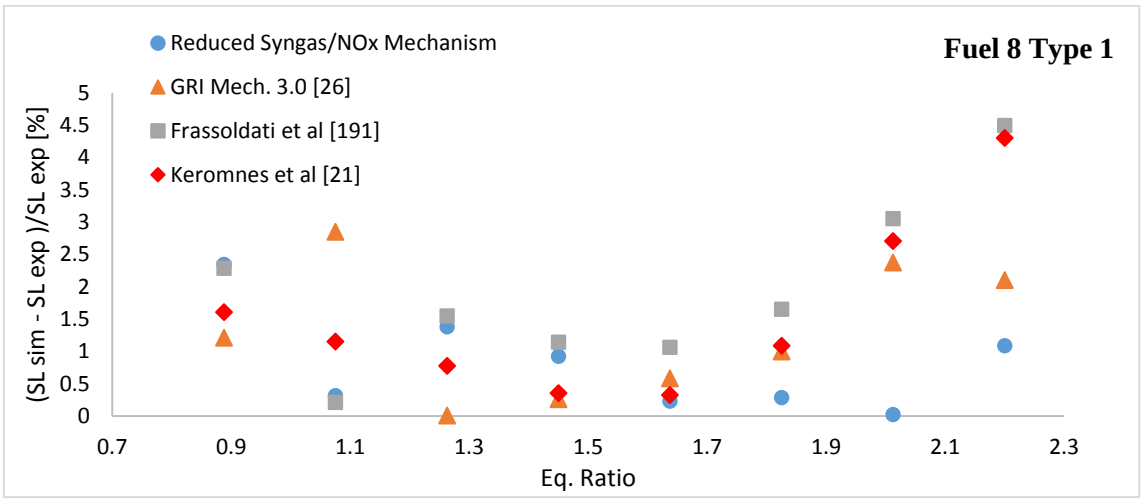

a)

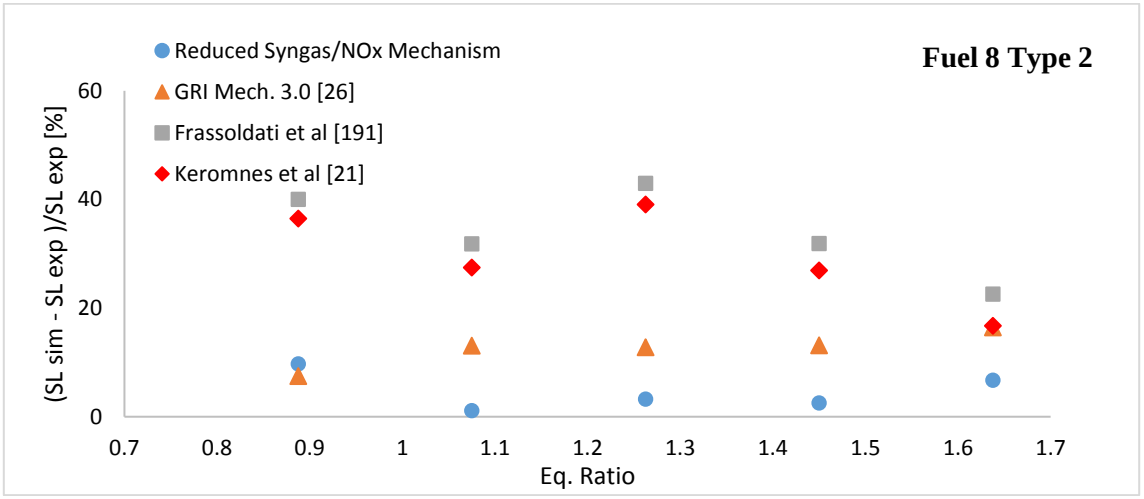

b)

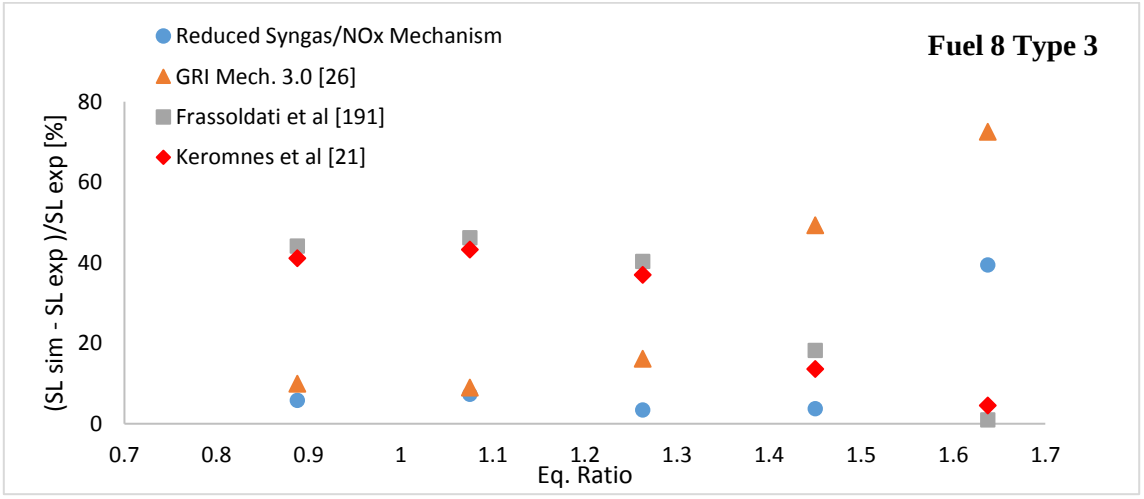

c)

Figure B-2. Absolute error calculation for LFS using Fuel 8, Figure 5-7.

$H_2/CO/CO_2/CH_4$ syngas mixture

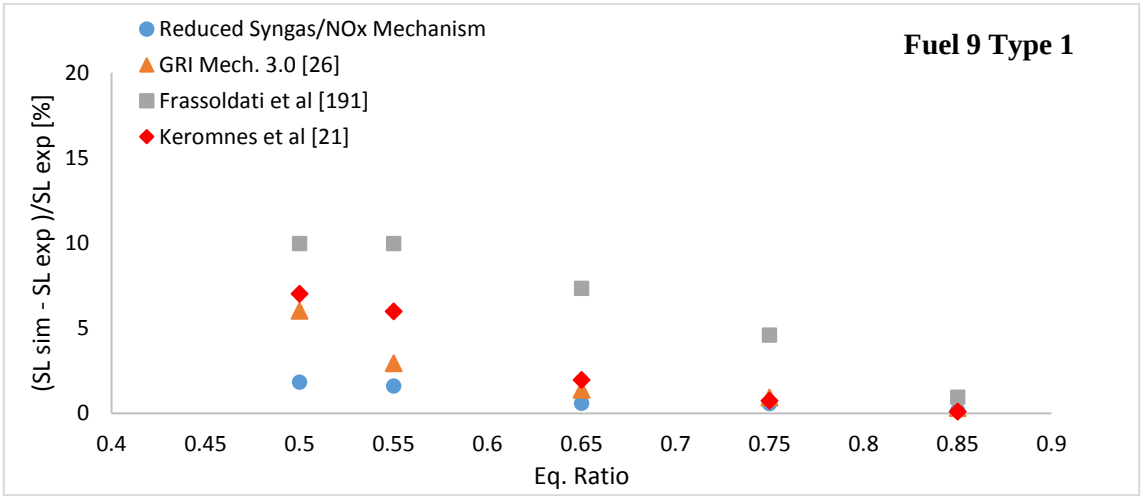

a)

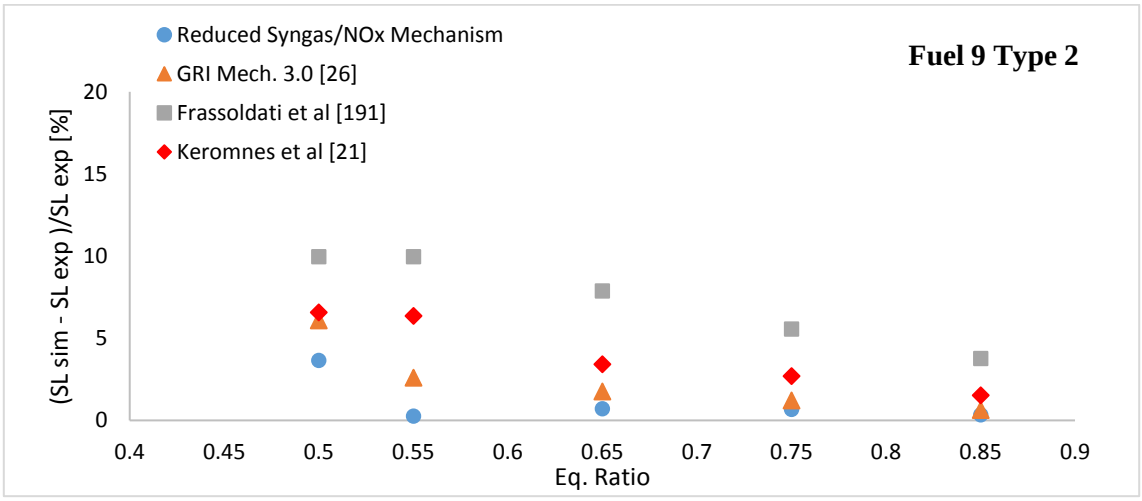

b)

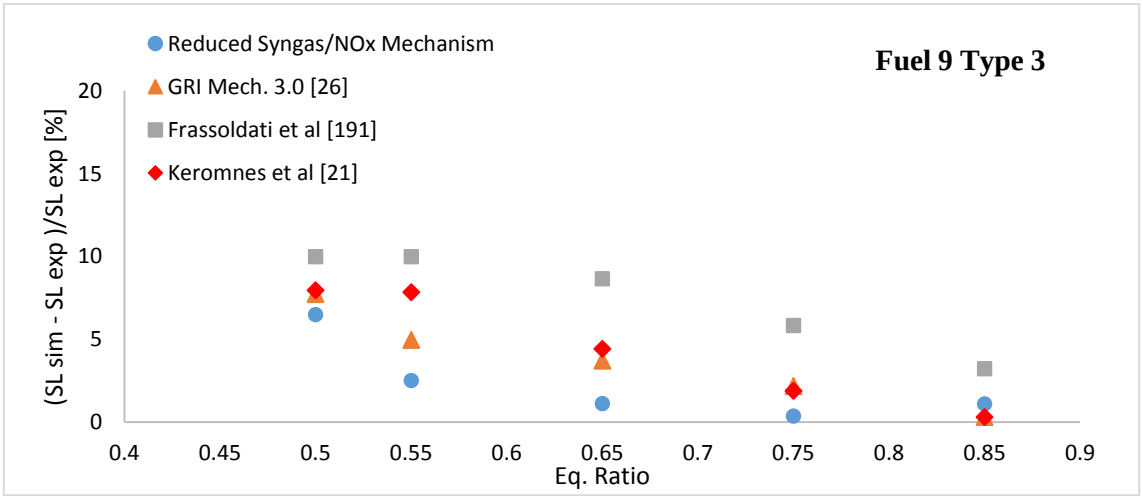

c)

Figure B-3. Absolute error calculation for LFS using Fuel 9, Figure 5-8.

Ignition delay time

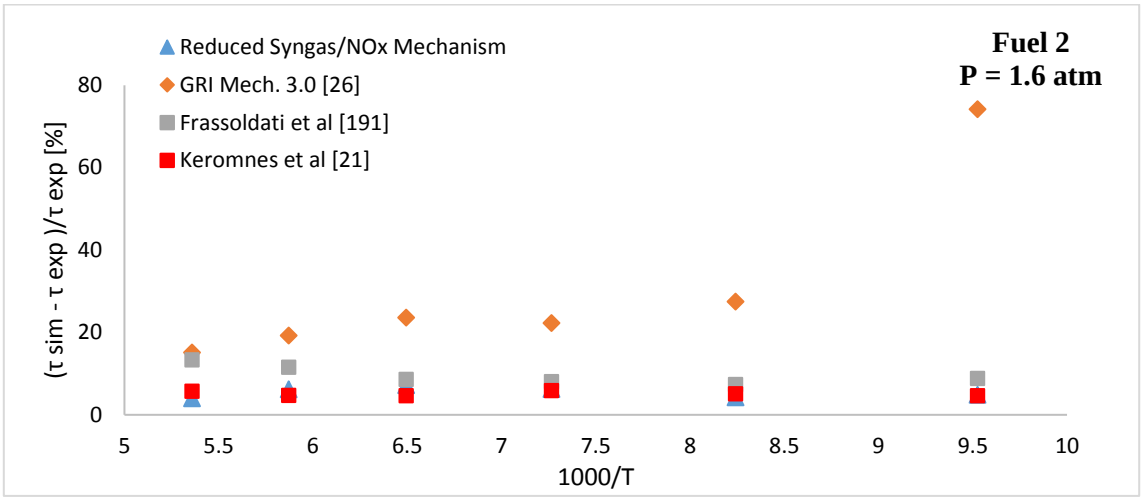

a)

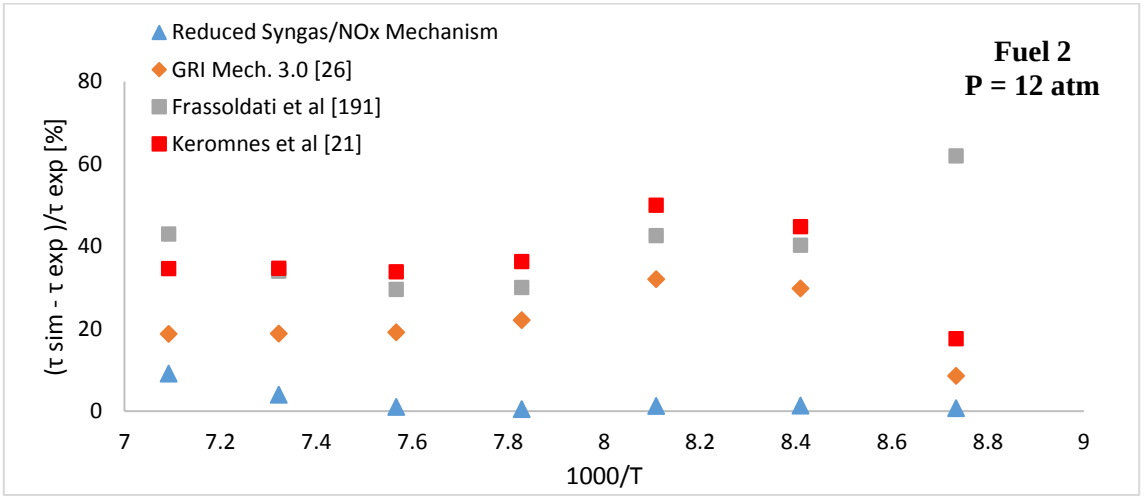

b)

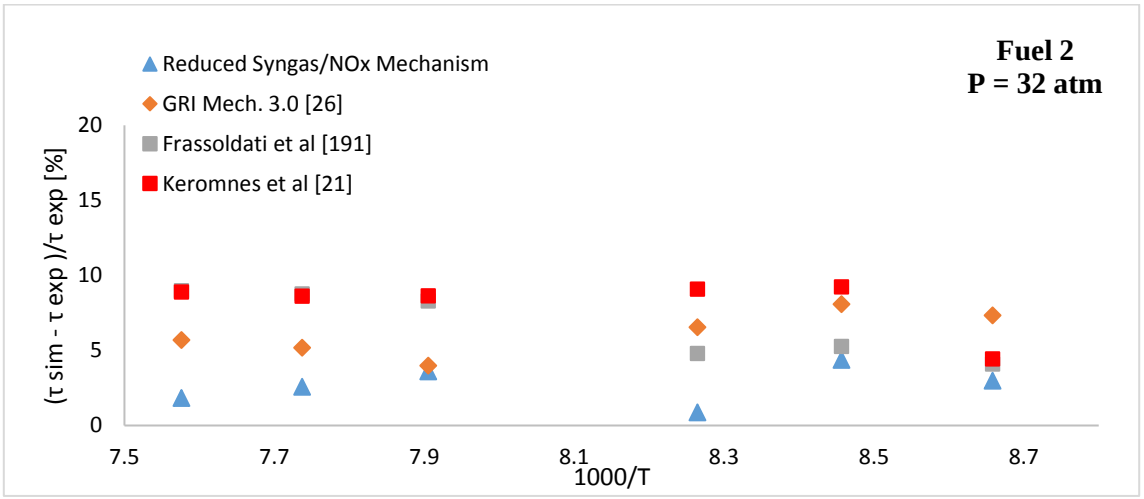

c)

Figure B-4. Absolute error calculation for ignition delay time using Fuel 2, Figure 5-9.

NOx comparison

$H_2/CO/CO_2/CH_4/N_2$ mixture

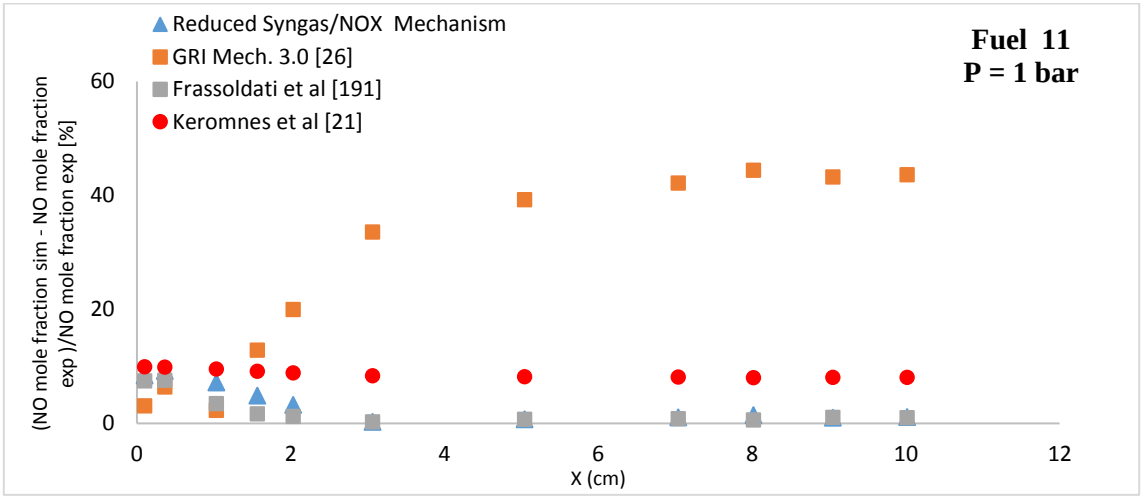

a)

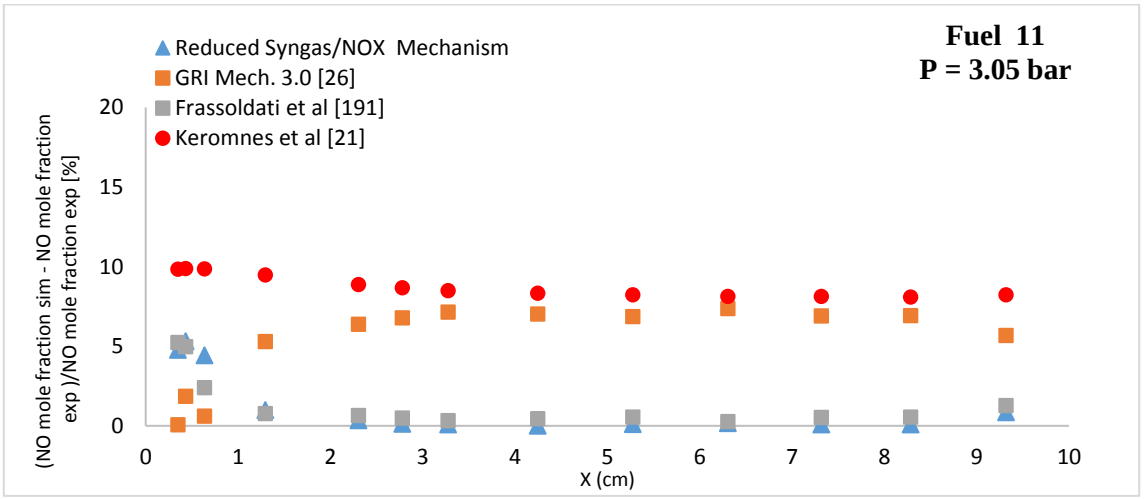

b)

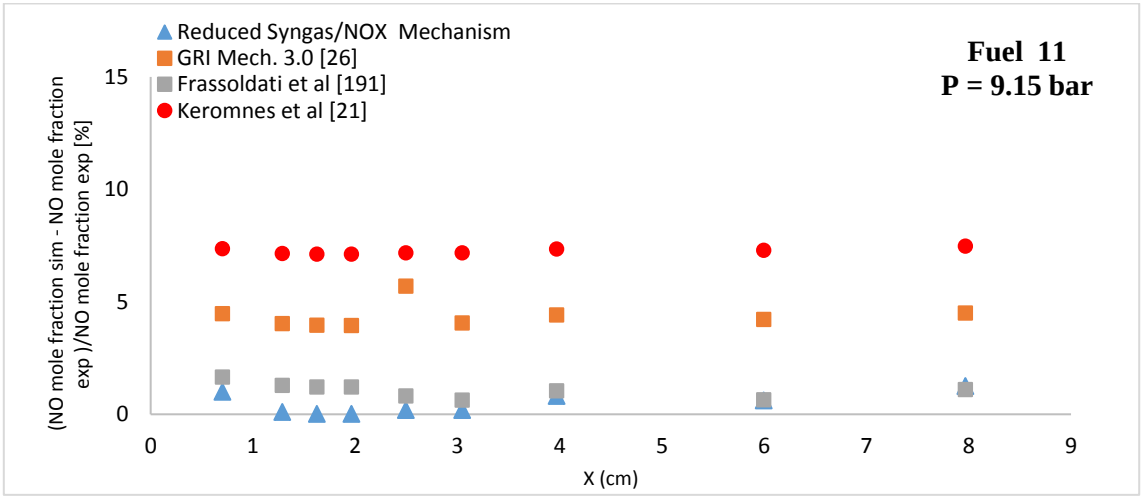

c)

Figure B-5. Absolute error calculation for NO mole fractions calculations using Fuel 11, Figure 5-10.

$H_2/CH_4/CO/CO_2$ mixture

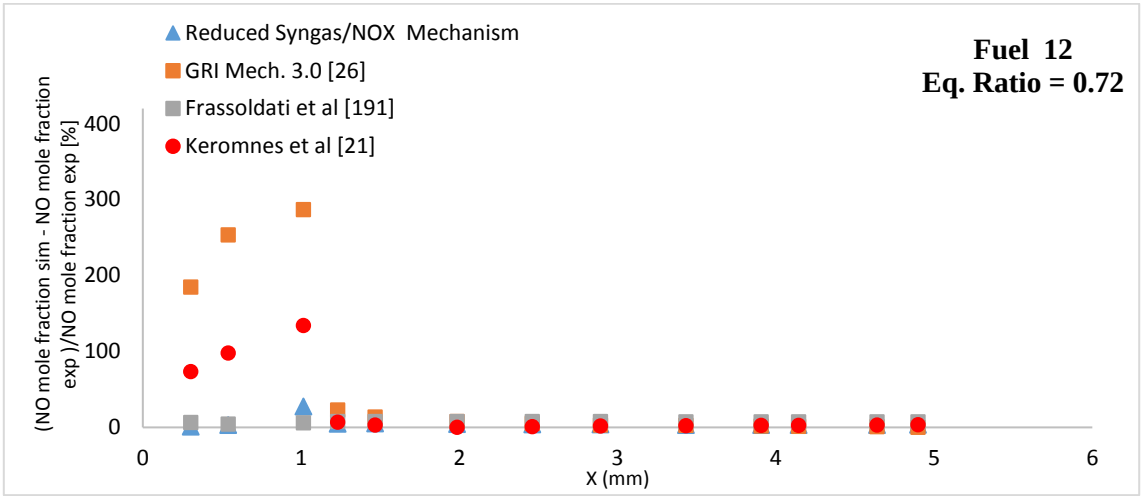

a)

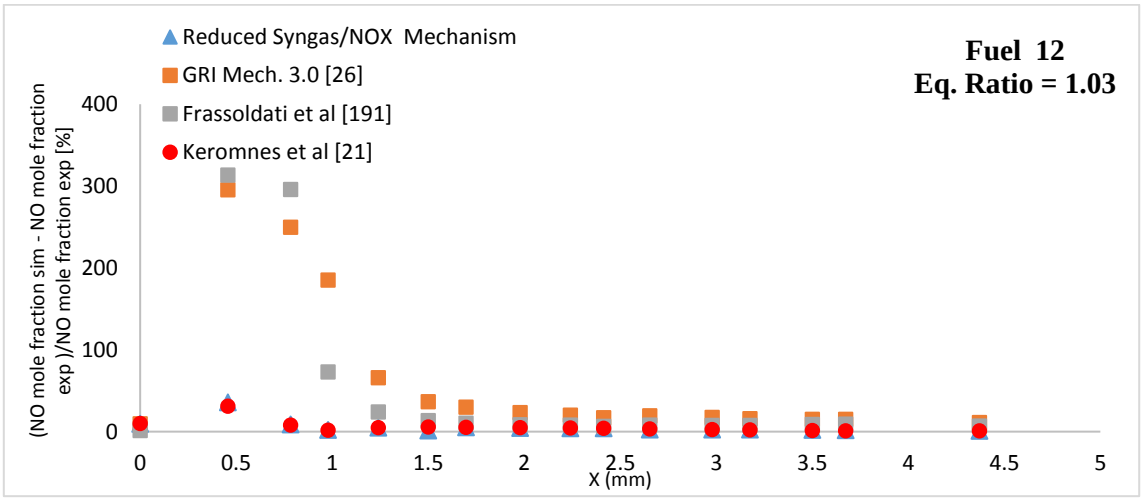

b)

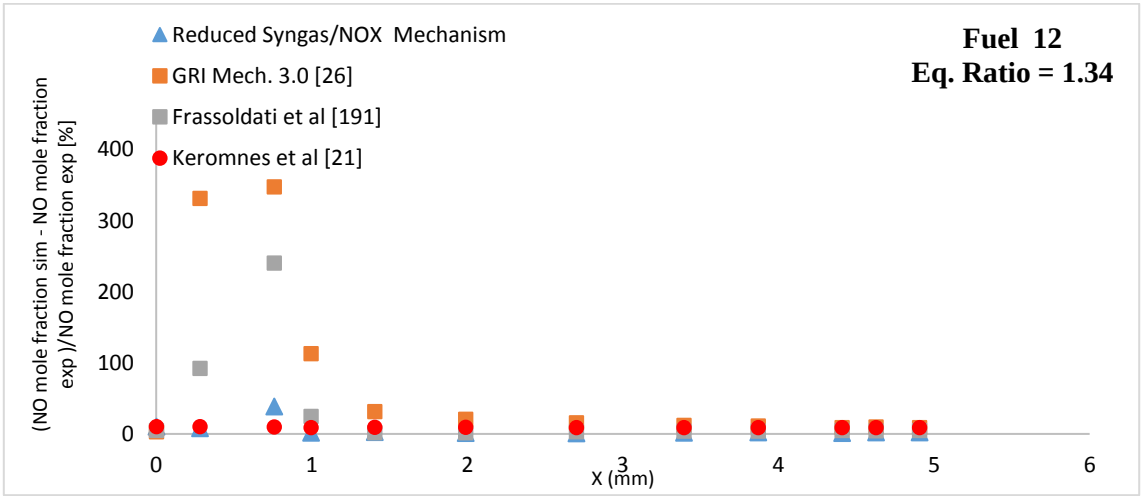

c)

Figure B-6. Absolute error calculation for NO mole fractions calculations using Fuel 12, Figure 5-11.

Appendix C

Table C-1 Skeletal mechanisms created during the reduction of the original (Generation 0) mechanism.

Skeletal Mechanism	Number of Reactions
Generation 0 (Original Mech.)	1791
Generation 1	1710
Generation 2	1635
Generation 3	1535
Generation 4	1425
Generation 5	1340
Generation 6	1188
Generation 7	1142
Generation 8	971
Generation 9	944
Generation 10	934
Generation 11	903
Generation 12	828
Generation 13	798
Generation 14	539
Generation 15	522
Generation 16	494
Generation 17	488
Generation 18	405
Generation 19	372
Generation 20	291
Generation 21	274
Generation 22	264
Generation 23	255
Generation 24	248